Mitochondrial haemoglobin and ATP synthase – molecular interactions in health and disease

Brad Ebanks BSc (Hons)

Thesis submitted to the University of Nottingham for the degree of Doctor of Philosophy (PhD)

Abstract

The mitochondrial ATP synthase is a fundamental enzyme to multicellular life, as it is responsible for producing the vast majority of cellular adenosine triphosphate (ATP). Its molecular structure and enzymatic function have been widely studied to date. Here I have investigated the broader range of interactions that the enzyme participates in, including with mitochondrial haemoglobin, across a range of different species and under hypoxic conditions. I have also sought to understand potential changes in the activity and expression of mitochondrial ATP synthase in the skeletal muscle mitochondria of humans with chronic obstructive pulmonary disease (COPD) in response to exercise, as well as broader changes to the mitochondrial proteome.

Within this thesis I present data that demonstrate that the interactome of mitochondrial ATP synthase is associated with the translational silencing of the iron oxidase enzyme ceruloplasmin. I also present evidence of a molecular interaction with mitochondrial haemoglobin, and that this interaction may be part of a broader hypoxic response within the mitochondria. I show that the expression and activity of ATP synthase does not change in response to the studied exercise conditions in COPD, but that the expression of proteins associated with mitochondrial structure and morphology do change.

List of Publications

The following list contains published manuscripts that I have authored or co-authored throughout my PhD but, with the exception to manuscript numbers 8 and 11, have not included as chapters within this thesis. These manuscripts are included in Appendix C.

1. **Ebanks, B.**, Ingram, T. L., & Chakrabarti, L. (2020). ATP synthase and Alzheimer's disease: putting a spin on the mitochondrial hypothesis. Aging, 12(16), 1–16. https://doi.org/10.18632/aging.103867
2. Sargent, C., **Ebanks, B.**, Hardy, I. C. W., Davies, T. G. E., Chakrabarti, L., & Stöger, R. (2021). Acute Imidacloprid Exposure Alters Mitochondrial Function in Bumblebee Flight Muscle and Brain. Frontiers in Insect Science, 1(December), 1–8. https://doi.org/10.3389/finsc.2021.765179
3. **Ebanks, B.**, Ingram, T. L., Katyal, G., Ingram, J. R., Moisoi, N., & Chakrabarti, L. (2021). The dysregulated Pink1 - drosophila mitochondrial proteome is partially corrected with exercise. Aging, 13(11), 14709–14728. https://doi.org/10.18632/aging.203128
4. Katyal, G., **Ebanks, B.**, Lucassen, M., Papetti, C., & Chakrabarti, L. (2021). Sequence and structure comparison of ATP synthase F0 subunits 6 and 8 in notothenioid fish. PLOS ONE, 16(10), e0245822. https://doi.org/10.1371/journal.pone.0245822
5. Krako Jakovljevic, N., **Ebanks, B.**, Katyal, G., Chakrabarti, L., Markovic, I., & Moisoi, N. (2021). Mitochondrial homeostasis in cellular models of Parkinson's disease. Bioenergetics Communications, 2021(2), 1–31. https://doi.org/https://doi.org/10.26124/bec:2021-0002
6. **Ebanks, B.**, Wang, Y., Katyal, G., Sargent, C., Ingram, T. L., Bowman, A., Moisoi, N., & Chakrabarti, L. (2021). Exercising D. melanogaster Modulates the Mitochondrial Proteome and Physiology. The Effect on Lifespan Depends upon Age and Sex. International Journal of Molecular Sciences, 22(21), 11606. https://doi.org/10.3390/ijms222111606

7. **Ebanks, B.**, & Chakrabarti, L. (2022). Mitochondrial ATP Synthase is a Target of Oxidative Stress in Neurodegenerative Diseases. Frontiers in Molecular Biosciences, 9(February), 1–7. https://doi.org/10.3389/fmolb.2022.854321
8. **Ebanks, B.**, Katyal, G., Lucassen, M., Papetti, C., & Chakrabarti, L. (2022). Proteomic analysis of the ATP synthase interactome in notothenioids highlights a pathway that inhibits ceruloplasmin production. American Journal of Physiology-Regulatory, Integrative and Comparative Physiology, 323(2), 181-192. https://doi.org/10.1152/ajpregu.00069.2022
9. Katyal, G., **Ebanks, B.**, Dowle, A., Shephard, F., Papetti, C., Lucassen, M., & Chakrabarti, L. (2022). Quantitative Proteomics and Network Analysis of Differentially Expressed Proteins in Proteomes of Icefish Muscle Mitochondria Compared with Closely Related Red-Blooded Species. *Biology*, *11*(8), 1118. https://doi.org/10.3390/biology11081118
10. Barnes, M.; **Ebanks, B**.; MacColl, A.; Chakrabarti, L. (2023) A Common Anaesthetic, MS-222, Alters Measurements Made Using High-Resolution Respirometry in the Three-Spined Stickleback (*Gasterosteus aculeatus*). *Fishes*, *8*, 42. https://doi.org/10.3390/fishes8010042
11. **Ebanks, B**.; Katyal, G.; Taylor, C.; Dowle, A.; Papetti, C.; Lucassen, M.; Moisoi, N.; Chakrabarti, L. (2023). Mitochondrial Haemoglobin Is Upregulated with Hypoxia in Skeletal Muscle and Has a Conserved Interaction with ATP Synthase and Inhibitory Factor 1. *Cells*, *12*, 912. https://doi.org/10.3390/cells12060912

External Poster Presentations

1. Carbonic anhydrase inhibitors are an anti-ageing drug candidate in glaucoma patient. Drugs Repurposing II, London, 2022.
2. Exercise alters mitochondrial physiology and has age-specific impacts on the fitness and lifespan of *D. melanogaster*. Bioblast 2022: BEC Inaugural Conference, Innsbruck, 2022.
3. Exercise alters mitochondrial physiology and has age-specific impacts on the fitness and lifespan of *D. melanogaster*. Mitochondria and Chloroplasts Gordon Research Conference, Vermont, 2022.

Acknowledgements

I would first like to express my gratitude to the Biotechnology and Biosciences Research Council for providing the funding that made this PhD possible. The importance of publicly funded research cannot be understated, especially when events across the last three years are considered.

I would also like to acknowledge the University of Nottingham. I arrived as an undergraduate in September 2016, and now nearly 7 years later I will leave with two degrees and wonderful memories.

I would like to thank Professor Peijun Zhang and Dr David Scott for agreeing to co-supervise me during this PhD, and for hosting me as a rotation student in their laboratories at Harwell Campus in the beginning of 2020. This experience of structural biology was limited but insightful, and I am sure that I would have had great experiences under their supervision if not for the COVID-19 pandemic. In addition, I would also like to thank Dr Nicoleta Moisoi for her support across the last three years, especially with respect to the fly research that I have completed.

My most sincere thanks go to Donna Molloy (of the Early Intervention Foundation) and Katy Ball (of Nottingham City Council). Donna has been immeasurably generous with her time and knowledge as I have sought to turn my interest in policymaking into a career beyond this PhD. Katy was an incredibly kind and constructive supervisor during my Professional Internship for PhD students at Nottingham City Council. The opportunities that both Donna and Katy have offered have significantly shaped my thinking.

To my friends, you have all helped to make this possible, offering both encouragement and distraction (when necessary). I apologise for my intermittent absences in this time, it turns out that a PhD can be quite time-consuming.

While I would love to thank everyone in the lab that I have worked with over the years, this would then become a chapter in itself. However, I would like to thank Tom for his great mentorship, Gunjan for being a model of resilience

and determination, Zubair for your infectious enthusiasm, Nial for your excellent stories and dad-jokes, and Chloe for always bringing fun to the lab.

To my family, I could not have done this without you all. I hope you're all suitably proud.

At this point I would like to express my gratitude to my supervisor Professor Lisa Chakrabarti. Having first emailed Lisa as a second-year undergraduate with an interest in mitochondria, Lisa brought me in as a summer student that year, and then as a PhD student a year later. Lisa has been a thoughtful, inspiring, reassuring, imaginative, kind, funny, and constructive mentor. Myself, her students before me, and those that will follow are all incredibly fortunate.

Finally, I would like to thank Lucy. I could never explain how grateful that I am for your limitless patience and support. The things that you have achieved inspire me to do more, and this has undoubtedly pushed me over the finish line of this PhD.

Thesis statement and contributions

The work presented in this thesis is mine (Brad Ebanks), unless otherwise declared.

In chapter 3 (Mitochondrial haemoglobin is upregulated with hypoxia and has a conserved interaction with ATP synthase), the data contained within figures 3.1, 3.2, 3.3 and 3.4, the figures themselves, and the data contained within tables 3.2 and 3.3, were generated by Dr Gunjan Katyal.

Abbreviations

ADP – adenosine diphosphate

AFGP – antifreeze glycoprotein

AFPP – antifreeze potentiating protein

AMP – adenosine monophosphate

ANOVA – analysis of variance

ATP – Adenosine Triphosphate

BMI – body mass index

CA – carbonic anhydrase

CETF – electron-transferring flavoprotein complex

COPD – Chronic Obstructive Pulmonary Disease

CR – caloric restriction

Cryo-EM – cryo-electron microscopy

DMEM – Dulbecco's modified eagle medium

DNA – deoxyribonucleic acid

DTT - Dithiothreitol

ECL - Enhanced Chemiluminescence

EI – external intercostals

ETC – electron transfer chain

ETS – electron transfer system

$FADH_2$ – Dihydroflavine-adenine dinucleotide

FDR – false discovery rate

GAPDH – glyceraldehyde phosphate dehydrogenase

GOLD – global initiative for chronic obstructive lung disease

GPI – glycosylphosphatidylinositol

GWAS – genome wide association study

HIF – hypoxia inducible factor

HRP – horseradish peroxidase

IF1 – inhibitory factor 1

KEGG – Kyoto encyclopaedia of genes and genomes

LDS - Lithium diisopropylamide

LIP – labile iron pool

MALDI-TOF - Matrix-assisted laser desorption/ionization-time of flight

MDA - malondialdehyde

MPTP - 1-methyl-4-phenyl-1,2,3,6-tetrahydropyridine

MS – mass spectrometry

MTT - 3-(4,5-dimethylthiazol-2-yl)-2,5-diphenyl-2H-tetrazolium bromide

NADH - Nicotinamide adenine dinucleotide hydrogen

NBIA – neurodegeneration with brain iron accumulation

NO – nitric oxide

OSCP – oligomycin sensitivity conferring protein

P_i – inorganic phosphate

PBS – phosphate buffered saline

PCR – polymerase chain reaction

PMF – proton motive force

PPI – protein-protein interaction

RBC – red blood cells

RNA – ribonucleic acid

ROS – reactive oxygen species

RT – room temperature

SOD – superoxide dismutase

SNP – single nucleotide polymorphism

SUIT – substrate, uncoupler, inhibitor titration

TBS-T – tris buffered saline tween

TCA – tricarboxlic acid

UPR – unfolded protein response

VL – vastus lateralis

Table of contents

1 General Introduction and Methods Background

1.1 Mitochondrial evolution and function

The mitochondrion is a subcellular organelle that is found in nearly every cell of eukaryotes. First observed through early microscopy methods by Albert von Kolliker in 1857, they were later termed bioblasts by Richard Altman in 1886, and finally named mitochondria by Carl Benda in 1898[1]. Our understanding of the fundamental role played by mitochondria in cellular biogenetics and the production of adenosine triphosphate (ATP) was driven throughout the 20th century by Nobel prize winning research by Peter Mitchell, Hans Krebs, and John Walker[2–5].

It is widely accepted that the evolutionary lineage of mitochondria-containing eukaryotes can be traced back to an event in which a host cell (likely an archaeon) engulfed an α-protobacterium, and from this, an endosymbiotic relationship between the two organisms evolved[6,7]. The origins of endosymbiotic theory are well-reviewed, including the historical origins of the theory, the early alternative proposals of non-endosymbiotic evolution of mitochondria that placed intracellular compartmentalisation at the apex of their arguments, and the current outstanding questions around eukaryogenesis[8].

Throughout the evolution of this endosymbiotic relationship, there was a consistent transfer of genetic material from the mitochondrial genome to the nuclear genome[9–12]. As a result of this unilateral transfer of genetic material from the mitochondrial to nuclear genome, the human mitochondrial genome now contains just 13 protein coding genes, 22 tRNAs, and 2 rRNAs[13].

Beyond their role as bioenergetic hubs and gene-encoding organelles, mitochondria have dynamic internal and ultrastructural features; they can import proteins post-translationally to their different compartments through a collection of outer and inner membrane translocase complexes[14–20]. They can also undergo fusion events, mediated by mitofusin to increase rates of oxidative phosphorylation[21,22], as well as being able to undergo fission to facilitate mitochondrial turnover[23].

Mitochondria are important mediators of metabolic signalling. This can be through metabolites such as acetyl-coA, which has previously been described as a metabolic node due to its high levels of connectivity in carbon metabolism[24], and metals such as iron[25] and calcium[26]. Mitochondrial calcium signalling is important to neuromuscular function, and its sequestration within the mitochondria can also promote mitochondrial ATP synthesis via activation of dehydrogenase enzymes[27,28]. The mitochondrial calcium uniporter (MCU) is the key protein that enables the uptake of Ca^{2+} into the mitochondrial matrix[29], and this imported calcium then stimulates the activity of three dehydrogenase enzymes of the TCA cycle: pyruvate dehydrogenase, isocitrate dehydrogenase, and alpha-ketoglutarate dehydrogenase[30]. The mammalian mitochondrial electron transfer enzyme glycerophosphate dehydrogenase also has activity that is dependent on local calcium concentrations.

Mitochondria play roles in cell-autonomous immune signalling, through recruitment of adaptors such as STING and TRAF3 that subsequently activate transcription factors of pro-inflammatory pathways, such as NF-κβ[31,32]. Mitochondria are a major regulator of apoptosis, as they release pro-apoptotic factors such as cytochrome c in response to extreme physiological insult[33–35].

The physiological functions of mitochondria are varied, and mitochondria lie at the heart of many physiological processes as a major signalling hub. They are able to integrate numerous different forms of signalling, and communicate this via mito-nuclear interactions that lead to whole cell responses[36,37]. However, their most important function is within cellular bioenergetics, specifically the synthesis of ATP.

1.1.1 Bioenergetics

The first key stage within the mitochondria in the process of ATP synthesis is the tricarboxylic acid (TCA) cycle. Acetyl-CoA derived from aerobic glycolysis via the pyruvate dehydrogenase enzyme is funnelled into the cycle through the citrate synthase enzyme, a widely used marker for mitochondrial viability[38]. As acetyl-CoA is a metabolic node it can also be produced via other

metabolic pathways, such as β-oxidation of fatty acids and ketolysis. Acetyl-CoA then provides the carbon required by the TCA cycle to supplement mitochondrial respiration, or it can act as a biosynthetic precursor for anabolic pathways in the cytosol[39]. However, when acetyl-CoA is directed into the TCA cycle, carbon, electrons, and protons are stripped from the TCA metabolites to produce CO_2 and NADH, the major electron source for the electron transfer system (ETS).

The NADH produced in the TCA cycle provides electrons for mitochondrial complex I to feed into coenzyme Q (the Q-junction) (**Figure 1.1**), as well as protons used to maintain the mitochondrial membrane potential[40]. Other sources of electrons that feed into the Q-junction include succinate at complex II, $FADH_2$ at the electron-transferring flavoprotein complex (CETF)[41,42], and in a species- and tissue-specific manner by mitochondrial glycerol-3-phosphate through glycerophosphate dehydrogenase complex[43] and proline through proline dehydrogenase[44].

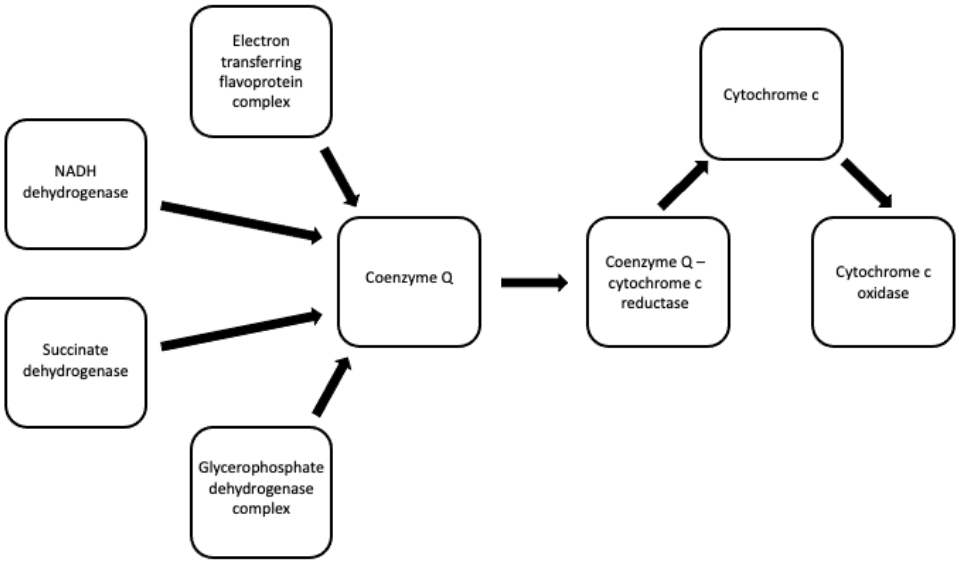

Figure 1.1 – The convergence of electrons at coenzyme Q – the Q-junction. Oxidation of metabolites by electron transferring flavoprotein complex, NADH dehydrogenase, succinate dehydrogenase, and glycerophosphate dehydrogenase leads to the reduction of coenzyme Q. This figure is adapted from Gnaiger (2020)[45].

Electrons then progress from coenzyme Q, through to complex III, to cytochrome c, before arriving at complex IV where they are used to reduce molecular oxygen into water by the catalytic activity of the complex[46,47]. The continued transport of electrons is coupled to the pumping of protons across the membrane by complexes I, III and IV to further maintain the proton motive force (PMF). The PMF is harnessed by ATP synthase, as protons diffuse back into the mitochondrial matrix through the ATP synthase enzyme, driving its catalytic activity and producing ATP[48–51].

An important point to consider in bioenergetics is the role of mitochondria as metabolic signal integrators. As the site where acetyl-CoA is produced from glycolysis, β-oxidation, and amino acid metabolism, the bioenergetic environment of the cell then determines whether that acetyl-CoA is to be exported to the cytosol for synthetic purposes or fed into the TCA cycle so that ATP can ultimately be produced[39]. Additionally, an important pathway that relates indirectly to mitochondrial metabolism is the pentose phosphate pathway, a key anabolic pathway that produces NADPH in its oxidative phase that is then used to protect the cell against mitochondrial oxidative stress[52,53].

In this model, acetyl-CoA is a metabolic junction, acting as an intermediate metabolite between carbohydrate and fatty acid metabolism. This is distinct from other metabolic state markers such as AMP levels, and the NAD+/NADH ratio, where adenylate kinase forms AMP and ATP from two ADP molecules; an accumulation of AMP triggers the key metabolic switch enzyme AMP kinase, leading to promoted catabolism and inhibited anabolism[54,55].

1.1.2 Mitochondria, ageing and diseases of ageing

The dysfunction of mitochondria is one of the key hallmarks of ageing, as defined by López-Otin, with evidence of substantial and progressive dysfunction throughout the ageing process[56]. One major change to mitochondrial function in the ageing process is disrupted bioenergetics[57–59], which can lead to the production of reactive oxygen species (ROS) via electron leak from the ETS complexes[60]. ROS can then cause damage to mtDNA,

mitochondrial proteins, and lipids, that leads to more widespread dysfunction. Decreased mitochondrial biogenesis and the accumulation of mtDNA point mutations are also observed during the ageing process and contribute to the increased ROS output[61–65].

The main sites of ROS production within the mitochondria are the enzyme complexes of the ETS, with superoxide being the predominant ROS produced. Complex I is the primary producer of superoxide, particularly when there is a low demand for ATP and abundant NADH, leading to an elevated proton motive force and a saturated co-enzyme Q pool[66]. Complex III is the other major source of superoxide generation, during the auto-oxidation of unisemiquinone[60].

The increased production of ROS observed during the ageing process helps to underpin the free radical theory of ageing, first proposed by Denham Harman in 1956 before being developed further throughout the late 20th century[67–69]. The principle of this theory is the accumulation of damage, or the 'damage maintenance paradigm', which is one of the two dominant theories of ageing.

However, we now have a greater understanding of the role of free radicals in biology, and this helped lead to the development of the mitohormesis theory that healthy levels of free radicals are required for physiological functions and signalling[70–72]. There has been an increased focus on the impact of accumulated mtDNA polymorphisms because of replication errors during ageing, albeit with mixed results in terms of understanding the contribution of the accumulated mutations to the ageing process[62,73–77].

Another leading theory in the field of ageing is that of genetic pleiotropy, whereby genes that confer survival and reproductive advantage in early life continue to be highly expressed later in life, to the physical detriment of the organism in question[78]. This theory does not hold the mitochondrion quite so centrally as does the accumulated damage theory of ageing. However, the genes of complex I might be pleiotropic, as it is possible that the administration of the complex I inhibitor metformin in later life may promote longevity[79].

Interventions to promote the activity and turnover of mitochondria as a means of facilitating healthy ageing are a major focus of current research. There are many studies that suggest exercise induces changes to physiology at the molecular level that in turn promote healthy mitochondrial function[80–84]. However, beyond increasing the expression levels of ETS complex proteins and their enzymatic activity, there is a limited understanding of how changes at the molecular level in response to ageing, increase longevity. The other major lifestyle intervention that impacts the ageing phenotype is caloric restriction (CR), which has been shown to maintain mitochondrial function and protect against oxidative stress, but there have been contradictory results about the rates of mitochondrial biogenesis[85–89].

Dysfunction of mitochondria is often a key part of the pathophysiology of many diseases of ageing. This has been reviewed in detail for cancer[90], Alzheimer's disease[91], and Parkinson's disease[92]. In Alzheimer's disease the mitochondrial cascade hypothesis describes mitochondrial dysfunction and production of reactive oxygen species as a major driver of disease. This could be either as a primary cascade that supersedes amyloid beta plaque formation, or as a secondary cascade that arises because of the accumulation of amyloid beta plaques[93].

The molecular contributions of dysfunctional mitochondria in different forms of parkinsonism are better understood. Mutations to the PINK1 and Parkin encoding genes have negative consequences for mitophagy (a form of mitochondria specific autophagy that is important for mitochondrial turnover), that lead to accumulation of dysfunctional mitochondria and the degeneration of muscle and neuronal cells[94–98]. This can lead to juvenile onset Parkinson's disease[99]. Xenotoxic forms of Parkinsonism also arise because of toxic action on mitochondrial function, which includes rotenone inhibition of complex I activity[100] and 6-hydroxydopamine inhibition of complex I and IV[101].

1.1.3 ATP synthase structure and function

The mitochondrial ATP synthase is a dual-component enzyme complex that synthesises ATP using energy derived from aerobic metabolism. Tens of kilos of ATP is synthesised per person per day[102]. To do this, the F_O component harnesses the energy potential of the PMF to drive its membrane bound turbine capacity[51], which in turn stimulates the catalytic activity of its aqueous F_1 component, the site of ATP synthesis (**Figure 1.2**)[103].

The F_O component of mammalian mitochondrial ATP synthase is the hydrophobic, inner mitochondrial membrane-bound domain of the enzyme. It is composed of a c-ring, a multimeric cylindrical structure composed of a species-dependent number of c-subunits (10 in *H. sapiens*)[104], and other core subunits ATP6, b, e, f, g, and ATP8[105]. The primary purpose of the F_O component of ATP synthase is to harness the PMF by funnelling protons from the intermembrane space back into the mitochondrial matrix, where the translocation of protons drives the turbine function of the c-ring, the rotation of which was first reported in a classic study by Noji *et al*[106]. The movement of these protons is facilitated by four horizontal membrane-intrinsic α-helices from subunit a[107].

The protons travel through an aqueous half-channel in subunit a to the c-ring of the F_O complex where they bind to conserved acidic c-ring residues (aspartate or glutamate) in the second transmembrane helix of subunit-c[107]. The subsequent rotation of the α-helices in c subunits is suggested to conceal the charged proton binding sites, which leads to c-ring to rotation along with the central rotary stalk γ-subunit. The rotating F_O component transports protons into the matrix through a second aqueous half channel on the matrix side of the membrane and the asymmetric rotor stalk causes conformational changes in F1 which drive the catalytic activity of the β subunits.

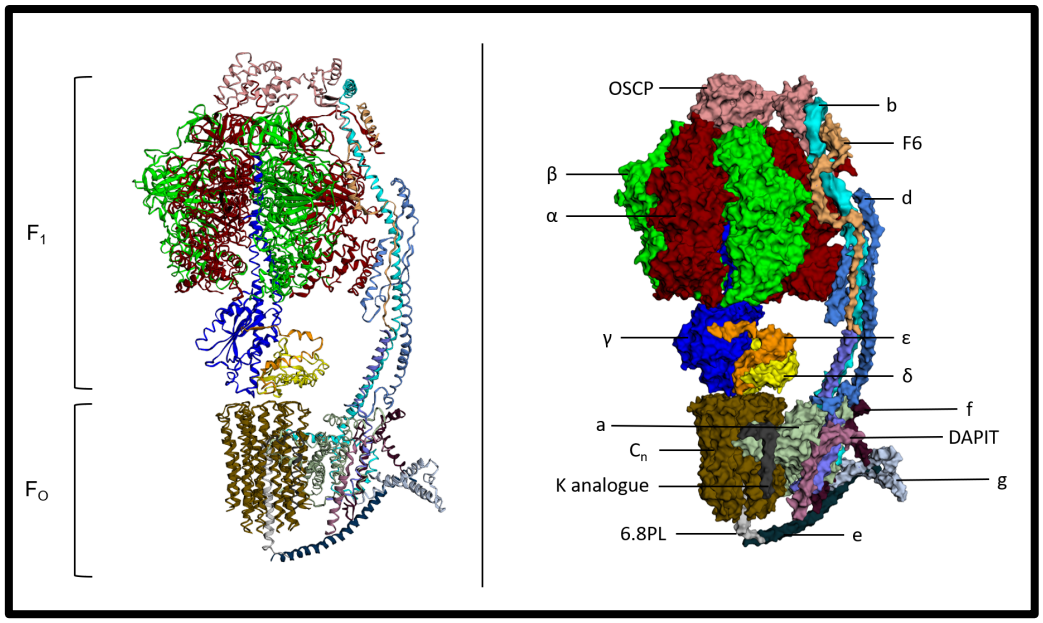

Figure 1.2 – Structure of the mammalian ATP synthase enzyme. *The F_1 and F_O components of the mammalian (S. scrofa) ATP synthase enzyme, with individual subunits labelled in the space-fill model of the enzyme. Figure adapted from Ebanks et al., 2020*[108].

The aqueous F_1 component of ATP synthase, with its well defined $\alpha_3\beta_3\gamma\delta\varepsilon$ structure, couples the turbine function of the F_O component with its own catalytic capacity via the asymmetrical central stalk, which is mounted onto the c-ring and protrudes through the core of the F_1 domain[5]. The β-subunits contain the catalytic sites of ATP synthase and operate with corresponding α-subunits adjacent from each catalytic site. The central stalk effectively rotates in 120° steps, triggering conformational changes at the catalytic site that lead to the synthesis of ATP from ADP and P_i, as was deduced from a combination of structural[5,109–111], biochemical[112,113] and molecular dynamics[103] studies. The asymmetry of the central stalk means the three catalytic sites have different conformations to each other at any given moment, which results in one site being occupied by ATP (β_{TP}), another by ADP (β_{DP}), and the third is empty (β_E). It is now understood that each 120° step is actually composed of 80° substrate binding sub-step, and a catalytic 40° sub-step[114–116]. Studies showing nucleotides bound to the asymmetrical catalytic sites have revealed potential

intermediate catalytic stages[117–119]. Magnesium is also an important co-factor for the catalytic cycle.

The final, integral structural element of the mitochondrial ATP synthase is the peripheral stalk, composed of the subunits b, d, OSCP, and F_6, spans the length of the enzyme complex acting as the stator to its motor function[120,121]. A cryo-EM study of yeast ATP synthase has reported that there is a high degree of flexibility in the peripheral stalk, allowing for the temporary storage of energy whilst under strain, which is thought necessary due to the symmetry mismatch of the F_O and F_1 components[122].

An important feature of ATPase enzymes is the regulation of their function, and it varies between the F-type ATPases of bacteria, yeast, and metazoans. The metazoan mitochondrial ATP synthase is in part regulated by the ATP inhibitory factor 1 (IF1). The metazoan IF1 is in its active dimer state at lower pH, and an inactive tetrameric state at higher pH values, sensitivity to pH is modulated by five conserved histidine residues that can be readily protonated or deprotonated[123]. The binding of IF1 to ATP synthase was first shown to take place at the β_{DP}-α_{DP} catalytic interface[124], however it has recently been observed that IF1 is also capable of binding to the OSCP subunit under oxidative phosphorylation conditions[125]. While IF1 is capable of inhibiting both the hydrolytic and synthetic functions of ATP synthase, it is widely suggested that the main physiological purpose of IF1 is to prevent the hydrolytic activities of the enzyme that would lead to a depletion of ATP levels[124].

IF1 has also been reported as a regulator of mitochondrial haem synthesis[126], as a potential target for ETS dysfunction in disease pathology[127], and as a phosphorylation target for protein kinase A in a pathway of metabolic regulation[128]. A cryo-EM study of ATP synthase observed that IF1 plays an important role in the structure of the type III ATP synthase dimer[129]. It is clear that IF1 has a diversity of physiological roles, which can be tissue specific, and some of which have been recently reviewed for neuronal cells[130].

1.1.4 ATP synthase in disease

As the physiological function and chemical mechanism of ATP synthase has become increasingly well-defined since the 1970s, its potential role in the pathophysiology of diseases has also been scrutinised more deeply in the last two decades. I have previously reviewed the broad dysfunction of ATP synthase in Alzheimer's disease, including changes in expression, changes to activity levels, and post-translational modifications[108]. I have also reviewed the evidence of oxidative modifications of ATP synthase in different neurodegenerative diseases, including Alzheimer's disease, Parkinson's disease, and Huntington's disease[131].

Mitochondrial dysfunction is widely observed in a range of different neurodegenerative diseases, so it follows that ATP synthase dysfunction could be observed in tandem, and possibly be directly implicated with disease incidence and progression. In particular, the redox stress that is observed with neurodegenerative disease may be a causative factor for the oxidative modifications of ATP synthase. The dysfunction of ATP synthase in certain cancers is also being investigated, with ATP synthase as a potential pharmacological target being brought forward for consideration[132].

1.2 Haemoglobin structure and erythroid function

Haemoglobin is observed within the red blood cells (RBCs) of nearly every species of vertebrate, and in many invertebrate species. The protein is responsible for the delivery of oxygen to respiring tissues, and subsequent return of carbon dioxide to the lungs. The publication of its resolved structure, alongside that of myoglobin, was the first of any protein and led to the awarding of the Nobel Prize in Chemistry to Max Perutz and John Kendrew in 1962[133–135].

Haemoglobin is composed of four polypeptide chains, with a subunit stoichiometry of $\alpha_2\beta_2$ in human adults. Within each polypeptide chain is a prosthetic haem group, composed of one iron atom within a porphyrin ring. It

is the reversible oxidation of the iron atom from the Fe (II) to the Fe (III) state that allows for the binding of oxygen to haemoglobin. Within RBCs, the delivery of oxygen to tissues is explained by the Bohr effect; the respiratory by-product carbon dioxide forms carbonic acid, and the acidification of the tissue microenvironment decreases haemoglobin's affinity for oxygen. This mechanism has become a model for describing allosteric protein interactions[136,137].

1.2.1 Globin superfamily

Haemoglobin exists as part of a larger family of structurally similar globin proteins. Some of members of this protein family, such as myoglobin, are well defined in structure[134,135], and have a widely understood and reviewed function[138]. However, other globin proteins are now being studied for their diverse non-erythroid functions, including cytoglobin, neuroglobin, and globin x[139].

There is an increased understanding of the tissue-specific expression and functionality of these globin proteins. Cytoglobin is expressed ubiquitously in human tissues[140,141], is upregulated in expression in response to hypoxia[142], and helps to regulate levels of NO[143]. While progress has been made, there is less that is understood about the physiological function of globin X. It is known to be present in vertebrate RBCs where it reduces nitrite to nitric oxide[144], that it is found in a wide variety of species[145,146], and that it is membrane bound and protective against ROS[147].

Of the novel proteins in the globin superfamily that have been identified since haemoglobin and myoglobin, neuroglobin has been implicated most directly in the function of mitochondria. Primary mouse cortical neurons that overexpressed neuroglobin and were exposed to hypoxia and reoxygenation were found to have higher levels of ATP, reduced mitochondrial membrane depolarisation, and higher levels of MTT reduction (to assess mitochondrial viability) than control cells[148]. Neuroglobin was later shown to be localised to the mitochondria in primary mouse cortical neurons, and the relative

mitochondrial content of neuroglobin increased in response to oxygen-glucose deprivation[149]. Neuroglobin knockdown in primary cultures of rat retinal cells found that the enzymatic activity of respiratory complexes I and III were both significantly reduced, implicating neuroglobin respiratory chain function[150].

1.2.2 Non-erythroid haemoglobin

In addition to the globin superfamily of proteins, there is a growing body of evidence that haemoglobin has an important physiological purpose in a variety of non-erythroid tissues and cells. Its observed presence in mesangial and hepatic cells has been suggested to be as part of a protective mechanism against oxidative stress[151,152]. Its expression at non-variable levels throughout the menstrual cycle of human endometrium tissue has been reported as a possible regulator of haem, iron, and oxygen bioavailability[153]. Its presence has also been reported in neuronal cells, in its tetrameric $\alpha_2\beta_2$ form[154].

Other studies of neuronal haemoglobin have placed its physiological role at the mitochondrion. Studies of dopaminergic cell lines that overexpress haemoglobin α and haemoglobin β have reported decreased expression of the major hypoxia regulator gene Hif1α and upregulation of oxidative phosphorylation genes[155]. It was found that increased haemoglobin conferred the cells susceptibility to apoptosis in response to MPTP and rotenone treatment[156]. Another study of nigral dopaminergic cells reported that rotenone administration caused a decrease in the expression of haemoglobin α and haemoglobin β transcripts[157]. In a review of non-erythroid haemoglobin, Saha *et al.* discuss its potential significance, as well as the varied expression patterns of the α and β chains, as well as questions around its specific structure and the potential for cytotoxicity from cell-free haemoglobin[158].

1.2.3 Mitochondrial haemoglobin

Studies of neuroglobin and neuronal haemoglobin demonstrate the physiological importance of globin proteins for mitochondrial function, and this is further highlighted by the recent observation of mitochondrial haemoglobin. The presence of yeast flavohaemoglobins within the mitochondrial fractions of cells has previously been reported, with the distribution between the cytosol and mitochondria increasing in favour of the latter in response to anaerobic culture conditions[159].

It is important to study mitochondrial haemoglobin in the context of human health and disease, as in mammalian brains it has been shown that haemoglobin localises to the inner mitochondrial membrane and in the intermembrane space, that its intracellular distribution is age and tissue specific, and that in Parkinson's disease its mitochondrial/cytoplasmic ratio is reduced[160]. Additional evidence to link mitochondrial haemoglobin with Parkinson's disease has also been reported, including its immunoprecipitation with α-synuclein protein from mitochondrial fractions[161], and a redistribution of haemoglobin α from the inter membrane space to the outer mitochondrial membrane in male Parkinson's disease cerebellum samples[162]. This variable distribution of mitochondrial haemoglobin, and association with α-synuclein, in the context of Parkinson's disease might play a mechanistic role in disease progression or serve as a potential biological marker.

Co-immunoprecipitation with an anti-haemoglobin β antibody found that haemoglobin complexes with ATP synthase subunits α and β, ADP/ATP translocase 4, and the mitochondrial phosphate carrier[163]. In addition, U937 cells that were treated with varied concentrations of haemoglobin showed that intracellular haemoglobin co-localises with mitochondrial complex I, stimulates mitochondrial respiration, and led to increased mRNA expression of hypoxia-associated transcription factors HIF1α and Nrf2[164]. These two studies directly link mitochondrial haemoglobin with ATP synthase and electron transport chain activity.

1.2.4 Comparative physiology of mammalian and Drosophila haemoglobin

Comparative physiology is still currently understood to be the "exploration of physiological principles through examination of the functional diversity among animal species"[165]. In this, it has not moved far from the Krogh Principle that was first defined in 1929, "For a large number of problems there will be some animal of choice or a few such animals on which it can be most conveniently studied"[166]. A particular animal of choice that has been studied in order to solve a large number of problems is the fruit fly, *Drosophila melanogaster (Drosophila).*

Despite the clear distinctions between the physiology of *Drosophila* and mammalian species, *Drosophila* express three increasingly well-characterised haemoglobin proteins. The first of these is globin-1, which is largely associated with the tracheal system and fat body[167,168]. Globin-2 and globin-3 are the additional globin proteins, they are less well-studied, but are expressed exclusively, and in limited quantities, in the testes of male *Drosophila* during spermatogenesis[169,170]. Knockdown and over-expression studies of globin-1, as well as over-expression studies of globin-2 and globin-3, under hypoxic conditions have suggested that globin-1 is likely associated with oxygen homeostasis and supply, while globin-2 is protective against ROS during spermatogenesis[171,172]. As such, globin-1 in *Drosophila* is a useful candidate for studying the non-erythroid function of haemoglobin in vertebrate and mammalian species.

1.2.5 Notothenioids as a null mutant

Genetic manipulation in the form of knockdowns or knockouts of specific genes is a classical method of producing a model that allows for the increased understanding of a protein's function. However, haemoglobin is fundamental to the viability of vertebrates, and is expressed in nearly every known species of vertebrate. The exception to this rule is the Channichthyidae family of the suborder notothenioid, species of which are found in the Southern Ocean of Antarctica[173]. All species within the Channichthyidae family lack

haemoglobin, and some species also lack myoglobin too[174]. This absence of the proteins is due to mutations to haemoglobin and myoglobin genes, that has resulted in transcriptionally inactive haemoglobin genes[175,176], species-dependent transcriptional and translational failure in myoglobin protein expression[177–179].

The selective pressure that allowed for these different mutations to radiate through the Channichthyidae family is still undetermined, however a recent theory suggested that a period of low iron levels in the Southern Ocean of Antarctica may have conferred an advantage to species with a lower iron dependence[180]. The inverse relationship between water temperature and oxygen solubility is another key environmental consideration that may have allowed for the persistence of this phenotype, as it leads to high levels of oxygen saturation in the sub-zero temperatures of the Southern Ocean.

Other key adaptions to this sub-zero environment include the evolution and expression of antifreeze glycopeptides[181,182], an increase in mitochondrial density[183], and shorter oxygen diffusion distances within ventricular tissues[184]. Studying the physiology of these haemoglobin-less icefish, and comparing it to closely related red-blooded notothenioid fish, allows for a deeper understanding of the role of non-erythroid and mitochondrial haemoglobin.

1.3 Ceruloplasmin and iron metabolism

Iron metabolism is a fundamental process for vertebrate species. Iron is incorporated into a porphyrin ring to make haem, which is the oxygen binding co-factor of haemoglobin[185,186]. Due to its redox capacities, iron is also an important element of many electron transporting proteins and enzymes, present in the form of iron-sulphur clusters[187,188]. However, iron can be toxic due to its potential redox activity, and subsequent capacity to produce harmful ROS through the Fenton reaction[189], so homeostatic mechanisms are vital.

Iron metabolism can be divided into two different categories: systemic and intracellular[190]. Both are crucial to mitochondrial function, as systemic iron

homeostasis ensures the delivery of oxygen to metabolically active cells and tissues, while intracellular iron homeostasis is important to the intramitochondrial synthesis of haem and of the iron-sulphur clusters contained within electron transport chain proteins.

For intracellular iron metabolism, the maintenance of iron levels and detoxification of redox active Fe (II) are key. While the vast majority of cellular iron is contained with proteins and prosthetic groups such as haem, the cell maintains a small, chelatable reservoir of redox active iron referred to as the labile iron pool[191,192]. The labile iron pool has been described as the 'metabolically active and regulatory forms of cellular iron', and the intracellular iron binding protein ferritin is an important regulator of this cellular source of iron[193]. For extracellular iron, transferrin is the key transporter[194].

1.3.1 Ceruloplasmin as an iron oxidase

Ceruloplasmin is a multi-functional copper-binding protein, predominantly synthesised in the liver for its role as a copper-transport protein in the blood. However early studies of rodent models reported expression in a range of tissues, including mammary gland and the central nervous system[195,196]. A pathophysiological deficiency in the protein is categorised as aceruloplasminemia, a rare autosomal recessive disorder in which there is an accumulation of iron in the brain[197]. The distinction in the two functions of the protein is explained by its expression as two different isoforms, due to alternative splicing downstream of exon 18[198]. The soluble isoform is predominantly synthesised in the liver and is responsible for the copper transport function in the blood. The second isoform is GPI-anchored to the plasma membrane, is observed in the non-liver tissues, and plays a key role in the iron efflux function of ceruloplasmin[199].

The role of ceruloplasmin in iron metabolism was first described in 1970 by Roeser *et al.*, where copper-deficiency led to ceruloplasmin deficiency and decreased blood-iron levels[200]. Injection with inorganic copper resulted in

elevated ceruloplasmin expression, and increased blood-iron levels subsequently followed. Roeser *et al*. proposed that the oxidation of Fe (II) to Fe (III) by ceruloplasmin was essential to the export of iron from cells to the blood, where it would then be bound by transferrin.

Inflammation has also been shown to increase hepatic ceruloplasmin transcription[201], while hyperoxia and inflammation have been shown to increase pulmonary ceruloplasmin transcription[202]. It has been demonstrated that the iron oxidase capacity of ceruloplasmin enabled the export of iron from the labile iron pool (LIP) of macrophages under hypoxic conditions[203]. These studies suggest that ceruloplasmin is an iron oxidase enzyme that is fundamental to iron metabolism, and particularly iron efflux, with potential tissue-specific patterns of expression and activity. This is further reinforced by the proposal that ceruloplasmin has an important role to play in the import of iron by brain neuronal cells[204].

More recently it has been demonstrated that cultured retinal pigmented epithelial cells treated with exogenous ceruloplasmin have increased levels of ferritin, which would indicate an increased iron availability in the cytoplasmic labile iron pool (LIP)[205]. However, the same study also reported increased expression of the transferrin receptor protein and increased nuclear content of the hypoxia transcription factor HIF1α, which the authors of the study interpreted as signs of a contradictory decrease in iron availability. A mechanism of action for the binding of Fe (II) and its oxidation to Fe (III) by ceruloplasmin, before its subsequent uptake by transferrin has also been described[206].

1.3.2 Aceruloplasminemia

The important iron efflux function of cellular ceruloplasmin places it at the interface of systemic and intracellular iron metabolism[207]. The inability to express a functional GPI-anchored isoform of ceruloplasmin results in the brain iron accumulation that is observed in aceruloplasminemia. It is suggested

that the brain iron accumulation drives the neurodegenerative component of the disease.

Aceruloplasminemias arise from mutations to the *CP* gene and are associated with neurodegeneration, diabetes[208], retinal degeneration[209], and anaemia[210]. While aceruloplasminemia is a rare disease, it is suggested to be underdiagnosed, and efforts are being made to identify both clinical and biochemical hallmarks that might allow for earlier diagnosis and therefore more effective therapies[210,211].

1.3.3 Ceruloplasmin and mitochondrial function

The links between mitochondrial function and the iron oxidase ceruloplasmin include the report of a mammalian mitochondrial ceruloplasmin protein, where an immunoreactive 30 kDa CP polypeptide was identified and suggested to be a product of the CP pseudogene that contains a potential signal peptide for mitochondrial import[212]. In addition, a study of brain tissue from aceruloplasminemia patients reported a significant decrease in mitochondrial complexes I and IV activity in the frontal cortex, cerebellar cortex and putamen[213].

Mitochondria play an important role in the metabolism of iron[25], and it is therefore plausible that excessive brain iron accumulation would have an impact on their metabolic function, in part due to the production of ROS by the Fenton reaction. Other neurodegenerative diseases that exhibit brain iron accumulation[214–216], while not being classical neurodegeneration with brain iron accumulation (NBIA) disorders, are also associated with decreased electron transport chain function[217–219].

Copper is also a key cofactor for mitochondrial respiratory complex IV and the antioxidant enzyme superoxide dismutase (SOD). While copper metabolism is not as widely considered as other metals in the context of mitochondria, the importance of copper metabolism to mitochondrial function has recently been reviewed, and highlights the importance of copper to assembly of these two

enzymes, cell fate, and the potential role of copper in cancer[220]. Copper metabolism should be further considered when ceruloplasmin is studied in the context of mitochondria, as well as for the observed mitochondrial ceruloplasmin pseudogene.

1.4 Chronic obstructive pulmonary disease

Chronic obstructive pulmonary disease (COPD) is estimated to impact close to 400 million people across the globe[221]. The primary cause of the disease is environmental exposure to cigarette smoke[222], however there are also several other known environmental risk factors that include, but are not limited to, low BMI, advancing age, and a history of obstructive lung diseases[221]. A family history of COPD has also been shown to be a risk factor[223], and a growing number of genome wide association studies (GWAS) have identified single nucleotide polymorphisms (SNPs) with genes that associate with lung function[224]. The biggest genetic risk factor identified so far is homozygosity for the Z mutation in the alpha-1 antitrypsin gene, resulting in deficiency of the protein, but this only accounts for up to 2% of all COPD cases[225]. While anti-smoking campaigns have resulted in reduced COPD mortality rates in higher income countries, global cases of COPD are expected to continue to rise due to high smoking rates and high levels of air pollution in certain African and Asian countries[226,227].

COPD is characterised by a limitation of the airflow into the lungs. The primary cause of this airflow limitation is damage caused by the immune response to inhaled toxic particles and gases, leading to a thickening and narrowing of the bronchioles, increased mucus content in the airway lumen, and emphysema that results in a loss of elasticity[228]. The most widely recognised symptom of COPD is dyspnoea, and other symptoms of the disease include persistent coughing, increased sputum, and chest tightness[229]. Acute exacerbation of the disease can result in respiratory failure, a common but important medical emergency[230].

1.4.1 Dysfunction of pulmonary mitochondria in COPD

The bioenergetic function of mitochondria is heavily dependent on a ready supply of oxygen. A failure to achieve physiological levels of gas exchange in the lungs is shown to lead to a localised hypoxia in the alveoli[231]. Dysfunction of pulmonary mitochondria has been reported in cells cultured from COPD patient airway smooth muscle tissue, with the cells having reduced respiratory capacity, ATP output, and membrane potential, while the mitochondrial ROS levels were significantly increased[232].

A study of cultured senescent pulmonary fibroblasts from COPD patients had reduced respiratory capacity and ATP content, and elevated levels of ROS[233]. In addition, human lung tissue samples from COPD patients were found to express the short isoform of the mitochondrial fusion protein OPA1 (S-OPA1) at significantly elevated levels[234], where S-OPA1 expression has previously been observed during physiological stress and is followed by a collapse in mitochondrial fusion networks[235]. Decreased mitochondrial membrane potential and elevated mitochondrial ROS levels have been reported in bronchial biopsies of COPD patients[236].

1.4.2 Skeletal muscle mitochondrial dysfunction in COPD

Mitochondrial dysfunction in peripheral tissue such as skeletal muscle has also been reported in COPD. One suggested potential mechanism for skeletal muscle dysfunction in COPD is a failure to deliver sufficient oxygen to these sites, leading to systemic hypoxia[237]. With respect to mitochondrial dysfunction in COPD patient skeletal muscle, patients with low BMI had decreased mitochondrial respiratory function when compared to those with a normal BMI as well as healthy age-matched control patient tissue[238].

Mitochondrial measurements of biopsies taken from the vastus lateralis (VL) and external intercostals (EI) of COPD patients reported increased complex IV activity and ROS output in both muscles, while complex I-III activity was increased in EI and ATP output was decreased in VL, while state 3 respiratory

activity was decreased in both muscles[239]. Increased levels of mitochondrial ROS were reported in Global Initiative For Chronic Obstructive Lung Disease (GOLD) grade 2 and grade 3/4 COPD patient quadriceps biopsies, with grade 3/4 patients also having decreased ETC complex proteins I, II, III and V expression[236].

1.5 Methods

In undertaking the research contained within this thesis, I used a combination of both *in vitro* and *in silico* methods on samples from a range of different biological systems. This includes human skeletal muscle tissue biopsies, mouse and rat liver and skeletal muscle tissue, fruit-fly (*Drosophila melanogaster*), and notothenioid fish liver tissue. This comparative physiology approach allows insight into whether our observations are conserved across species or not, and more likely to be important biological life.

1.5.1 High-resolution respirometry

The measurement of oxygen consumption by living organisms and biological samples has long been possible using Clark electrodes[240], with a series of classical studies published in the 1950s by Chance and Williams demonstrating the utility of this method for assessing mitochondrial oxygen consumption and going on to define mitochondrial respiratory states with respect to oxygen, ADP, and substrate availability[241–244]. The Clark electrode method of measuring oxygen consumption has endured as a highly reliable method into the 21st century, with some adaptation since its first inception[245]. Other methods to assess the oxygen consumption of a given biological sample now include higher-throughput, plate-based, fluorescence measurements[246–248].

The current gold standard for respirometry that utilises Clark electrode technology is the Oroboros Oxygraph-O2k[249]. In contrast to the other respirometry systems used, the substrate, uncoupler, inhibitor titration (SUIT) protocols are highly dynamic and the instrument measures the oxygen consumption of tissues, cells, and isolated mitochondria with high-resolution. Studies that have used the Oroboros instrument have offered insights into physiology and the pathophysiology of a range of diseases, including cancers[250], neurodegenerative disease[251], and the biology of ageing[252]. In addition, there have been numerous studies of non-model species, including insects such as *Aeges aegypti*[253] and marine species such as *Clupea harengus*[254].

1.5.2 In vitro methods

The *in vitro* methods that I have utilised to produce the research contained within this thesis contain a combination of classical biochemical approaches, as well as using more contemporary technologies. Classical methods used have included harnessing the utility of antibodies to measure relative protein expression levels by western blot[255], and to analyse protein-protein interactions by co-immunoprecipitation[256]. Optimisation of antibodies was also required throughout this research. Polyclonal antibodies were used extensively, and exclusively with species without commercially available antibodies (Notothenioidei), and all antibodies were validated by western blot (with reference against molecular weight markers) before being used in immunoprecipitation experiments. In addition, I have also used colorimetric assays to determine rates of enzyme activity and to quantify the presence of specific biomolecules.

In combination with these approaches, my samples have also been subject to proteomic analysis via label-free mass spectrometry. This method produces large protein expression quantification datasets, which can be used to build a picture of proteins contained within a complex or interactome[257], an organelle[84], a whole cell or tissue[258]. When produced with biological replicates, we can compare how a given proteome changes in response to system perturbation, such as in disease or an intervention such as exercise[83].

1.5.3 In silico methods

The large proteomic datasets generated from the label-free mass spectrometry methods can be studied using *in silico* approaches. This can be through enrichment analysis of pathways and ontologies, and through the production of protein-protein interaction networks using tools such as STRING-db[259]. These methods highlight biologically relevant proteins, pathways and processes that can then be used a springboard for further *in vitro* and *in vivo* exploration. Additionally, molecular docking data that was produced using a combination of PatchDock and FireDock is included in the second results chapter. The

structures are ranked by their global energy, which is the global minimum binding energy, and lower values being indicative of more viable binding interactions.

1.6 Research aims and objectives

In this thesis I have sought to explore the potential interaction between the mitochondrial ATP synthase and mitochondrial haemoglobin, as well as to understand the broader molecular interactions of mitochondrial ATP synthase. Mitochondrial ATP synthase allows for sufficient production of ATP to sustain multicellular life, and while there is a significant body of research on the structure and function of the enzyme, there is still much that we do not know about its interactions and activity in health and disease.

As previously discussed, mitochondrial haemoglobin is an exciting observation but there are still many outstanding questions about its physiological purpose. The essential role that haemoglobin plays in animal physiology at whole organism and cellular level, means that to produce a knockout model is unfeasible. In consideration of this, I worked with four different species of notothenioid fish, two of which had red blood (*N. rossii* and *T. bernacchii*), one which does not express haemoglobin (*C. rastrospinosus*) and another which does not express haemoglobin or myoglobin (*C. gunnarii*). The first results chapter manuscript contained within this thesis compared the interactome of the mitochondrial ATP synthase subunit α across the four species of notothenioid.

The second study contained within this thesis used a combination of *in* vitro and *in* silico approaches to describe and characterise the molecular interaction between mitochondrial haemoglobin and ATP synthase. Notothenioid, *D. melanogaster*, mouse and rat models were used in this work to assess the conservation of the interaction across vertebrate and invertebrate species. *D. melanogaster* and rodent models exposed to hypoxia were also used to further study the physiological role of mitochondrial haemoglobin.

To follow the work on hypoxia exposed rodent tissue and *D. melanogaster* throughout this research, I have also explored the changes to ATP synthase activity and the broader mitochondrial physiology in human COPD patient skeletal muscle in response to exercise. Hypoxemia is a defining characteristic of COPD, and it is suggested that many of the alterations to skeletal muscle physiology in COPD are due to tissue hypoxia. A proteomic analysis of mitochondria from male and female COPD patient skeletal muscle biopsies pre- and post-concentric and eccentric exercise was undertaken, with complementary laboratory experiments used to follow up the bioinformatic results.

The final study presented in this thesis demonstrates a replicable methodology to measure the activity of mitochondrial electron transfer complexes I and II as a function of oxygen consumption, using the Oroboros Oxygraph-O2k, from previously cryopreserved rodent skeletal muscle and frozen *D. melanogaster*. A limitation of assessing the oxygen flux of the electron transfer system is the requirement for fresh tissue or cells, as typical methods of cryopreservation inactivate the TCA cycle and disrupt the outer mitochondrial membrane, leading to uncoupling of the mitochondria. The simple method outlined in this study demonstrates how activity as a function of oxygen consumption by the ETS for two complexes can be readily measured, with scope for extending the study to assess the activity for other ETS complexes including proline dehydrogenase and the electron-transferring flavoprotein complex.

In summary, the studies that are presented within this thesis offer deeper insights into the interactions and function of mitochondrial ATP synthase across different systems biological systems, as well as in COPD pathophysiology, and they describe a novel method to assess the activity of associated respiratory enzymes.

1.7 Hypothesis

Based upon the published literature that guided the experimental design for the data presented in this thesis, I hypothesise that mitochondrial haemoglobin

may play a role within mitochondrial bioenergetics, specifically, as a potential sensor of ATP levels within the mitochondria. This is due to the observation that mitochondrial haemoglobin localises to the inner mitochondrial membrane and binds to the ATP synthesis machinery[160,163], haemoglobin binds to organophosphates including ATP[260], cellular expression of haemoglobin has been shown to vary with ATP availability[261], overexpression of haemoglobin drives OXPHOS gene expression[155], and the expression of haemoglobin is dependent upon the ATPIF1-regulated pH of the mitochondrial matrix[126]. The data presented in this study, particularly those in chapter 3, aim to assess the validity of this hypothesis.

2 Proteomic analysis of the ATP synthase interactome in notothenioids highlights a pathway that inhibits ceruloplasmin production

Brad Ebanks[1], Gunjan Katyal[1], Magnus Lucassen[2], Chiara Papetti[3], Lisa Chakrabarti[1,4]

Published: *American Journal of Physiology – Regulatory, Integrative and Comparative Physiology (2022)* ***323(2):*** *181-192 (https://doi.org/10.1152/ajpregu.00069.2022)*

[1] School of Veterinary Medicine and Science, University of Nottingham, Nottingham NG7 2RD, UK

[2] Alfred Wegener Institute, Bremerhaven, Germany

[3] Biology Department, University of Padova, Padova, Italy

[4] MRC Versus Arthritis Centre for Musculoskeletal Ageing Research, UK

2.1 Abstract

Antarctic notothenioids have unique adaptations that allow them to thrive in sub-zero Antarctic waters. Within the suborder Notothenioidei, species of the family Channichthyidae (icefish) lack haemoglobin and in some instances myoglobin too. In studies of mitochondrial function of notothenioids, few have focussed specifically on ATP synthase. In this study, we find that the icefish *Champsocephalus gunnari* has a significantly higher level of ATP synthase subunit α expression than in red-blooded *Notothenia rossii*, but a much smaller interactome than the other species. We characterise the interactome of ATP synthase subunit a in two red-blooded species *Trematomus bernacchii, N. rossii,* and in the icefish *Chionodraco rastrospinosus, and C. gunnari* and find that in comparison with the other species, reactome enrichment for *C. gunnari* lacks chaperonin-mediated protein folding, and fewer oxidative-stress-associated proteins are present in the identified interactome of *C. gunnari*. Reactome enrichment analysis also identifies a transcript-specific translational silencing pathway for the iron oxidase protein ceruloplasmin, which has previously been reported in studies of icefish as distinct from other red-blooded fish and vertebrates in its activity and RNA transcript expression. Ceruloplasmin protein expression is detected by Western blot in the liver of *T. bernacchii*, but not in *N. rossii, C. rastrospinosus,* and *C. gunnari.* We suggest that the translation of ceruloplasmin transcripts is silenced by the identified pathway in icefish notothenioids, which is indicative of altered iron metabolism and Fe(II) detoxification.

2.2 Introduction

Antarctic notothenioid fishes are a exemplars of marine adaptive radiation and they evolved unique adaptations to the sub-zero temperatures of the Southern Ocean[262,263] that still contribute to opening new avenues for research in organismal biology[264,265]. One example of the key adaptations seen across the suborder is the ability to produce antifreeze glycoproteins (AFGP) and antifreeze-potentiating proteins (AFPP)[266].

The Channichthyidae family, within the notothenioid suborder, are widely studied as they express no haemoglobin, and in some cases, no myoglobin either[173,267]. It is thought that the high oxygen solubility in the sub-zero waters of Antarctica allowed for the loss haemoglobin in a common ancestor to spread throughout the subsequent radiation of the family[268]. The absence of globin proteins in Channichthyidae make them, and other closely related red-blooded notothenioids an ideal model for understanding the broader physiological purpose of globin proteins and the mechanisms of iron metabolism. Globin proteins are important in the context of mitochondrial biology due to their role as oxygen transporters that facilitate the aerobic respiration of the mitochondria. Further, globin proteins have been observed within the mitochondria suggesting a possible functional role within the organelle[160,162].

While many studies of notothenioids have considered the adaptations of their mitochondria[183,269–271], due to the oxygen dependence of the electron transport chain, few have directly studied the ATP synthase enzyme in these fish. ATP synthase utilises the potential difference across the inner mitochondrial membrane by channelling protons from the intermembrane space into the mitochondrial matrix through its rotating, membrane-bound F_O component, with energy from this process being harnessed to synthesise ATP from ADP and P_i by the F_1 component of the enzyme[5,48,103,106]. As the movement of protons across the inner mitochondrial membrane and into the intermembrane space is dependent upon oxygen acting as the terminal electron acceptor of the electron transport chain (ETC), any adaptations to oxygen metabolism will likely impact the metabolism of ATP synthase.

Co-immunoprecipitation is a biochemical method that is used to study protein-protein interactions (interactome), including those of mitochondrial proteins[256,272]. Mass spectrometry is widely used for the identification of proteins that interact with the protein of interest, with chemical cross-linking acting as an intermediate step in some circumstances[273,274]. Label-free mass spectrometry is a powerful quantitative method used in proteomics to make comparisons across different sample types[275].

In this study, we sought to study the interactome of ATP synthase in both red-blooded and icefish notothenioid species through coupling co-immunoprecipitation with label-free mass spectrometry to investigate what pathways are impacted by the loss of haemoglobin and, more specifically, whether these may have any relation to the metabolism of iron. We first compared the relative expression of the ATP synthase subunit α in liver tissue between red-blooded notothenioids (*Trematomus bernacchii* and *Notothenia rossii*) and the icefish *Chionodraco rastrospinosus* (haemoglobin-less) and *Champsocephalus gunnari* (haemoglobin and myoglobin-less). The same anti-ATP synthase subunit α antibody was used in co-immunoprecipitation reactions with same notothenioid species liver tissue to investigate the protein-protein interactions of the ATP synthase enzyme. The proteins identified by label-free mass spectrometry were analysed through KEGG and reactome-enrichment before protein-protein interaction (PPI) networks were produced using local network clusters in STRING-db[259]. Following the enrichment analysis of the label-free mass spectrometry, we sought to detect the expression of the liver protein ceruloplasmin, an iron oxidase enzyme and copper transporter.

2.3 Methods

2.3.1 Fish tissue samples

SVMS Clinical Ethical Review, University of Nottingham, (ref # 2744 190509). Liver tissue samples of Antarctic notothenioid fish were collected for: *N. rossii*, *T. bernacchii* (Cruise PS112, Weddell Sea in 2013-2014), *C. gunnari* and *C. rastrospinosus* (Cruise ANTXXVIII (PS79), Antarctic Peninsula in 2012).

2.3.2 Fish liver lysate preparation for SDS-PAGE and Western Blot

1 mg of liver tissue from the notothenioid species (*C. rastrospinosus, T. bernacchii, N. rossii* and *C. gunnari*) was added to 100 µL of PBS and mechanically homogenised for 1 minute with a 1.2-2.0 mL Eppendorf micro-pestle (Sigma-Aldrich) at room temperature (N=3 for each species).

2.3.3 Fish liver lysate preparation for co-IP

10 mg of liver tissue from the fish species (*C. rastrospinosus, T. bernacchii, N. rossii* and *C. gunnari*) was added to 100 µL of extraction buffer (1X IP, Dynabeads™ Co-Immunoprecipitation Kit (ThermoFisher)) and mechanically homogenised for 1 minute with a 1.2-2.0 mL Eppendorf micro-pestle (Sigma-Aldrich). The homogenate was left on ice for 15 minutes, before centrifugation at 15,000 g for 5 minutes to pellet the insoluble fraction. The supernatant was collected, to be used in the co-immunoprecipitation reaction, and the pellet discarded.

2.3.4 Co-immunoprecipitation

10 µg of antibody (anti-HbB, ab227552) was bound to 2 mg of Dynabeads™ M-270 Epoxy (ThermoFisher) Dynabeads™ M-270 Epoxy (ThermoFisher), as

per manufacturer's instructions, and the antibody-bound Dynabeads were incubated overnight, (18 hours, 4°C) with the notothenioid liver lysate. The following day the Dynabeads were washed, and the antibody-antigen complex was eluted and stored at -80°C.

2.3.5 SDS-PAGE

1 µL of sample was added to 5 µL of PBS, 3 µL LDS and 3µL DTT for ATP5A expression measurements, and 6 µL of sample, 3 µL LDS and 3µL DTT for ceruloplasmin expression measurements. The solution was boiled and then loaded onto polyacrylamide pre-cast gels (NuPAGE™ 4 to 12%, Bis-Tris, 1.0 mm, Mini Protein Gel, 12-well). For the co-IP fractions to be analysed by label-free mass spectrometry, a fixed voltage (200V) was applied until the dye front had run 2 cm into the gel. The gel was then removed from the casing and stained overnight (18 hours, RT) with ProtoBlue Safe Coomassie G-250. For Western Blots, the fixed voltage (200V) was applied for 35 minutes, before continuation of the Western Blot procedure. Overnight Coomassie stained gels were destained with three 10-minute-long washes of dH_2O. The Coomassie stained section of the gel lanes were excised, and they were then stored in 1.5 mL Eppendorf tubes (4°C), until ready to be sent for mass spectrometry analysis.

2.3.6 Western Blot

The proteins within the gels were transferred to a nitrocellulose membrane at 30 V for 60 minutes. The membrane was blocked with 3% (w/v) milk powder in TBS-T for 60 minutes with gentle agitation (RT). The membrane was then probed overnight (18 hours, 4°C) with the primary antibody (anti-ATP5A, ab245580; anti-ceruloplasmin, ab48614; anti-GAPDH, ab9485), at a 1:5000 dilution in 3% (w/v) milk powder in TBS-T. The membrane was then washed three times with TBS-T before incubation with secondary antibody (goat anti-rabbit HRP conjugate, ab6721), at a 1:5000 dilution in 5% (w/v) milk powder

in TBS-T. The membrane was again washed three times with TBS-T before a five-minute incubation with ECL substrate and chemiluminescence measurement. Band densities were measured using Image J and samples were normalised to appropriate loading controls[276]. Statistical analysis was performed using GraphPad Prism version 9.3.1.

2.3.7 Mass spectrometry

Samples were analysed by the Centre of Excellence in Mass Spectrometry at University of York[277]. Protein was in-gel digested post reduction and alkylation. Resulting extracted peptides were analysed over 1 h LC-MS acquisitions with elution from a 50 cm, C18 PepMap column onto a Thermo Orbitrap Fusion Tribrid mass spectrometer using a Waters mClass UPLC. Data analysis was performed using PEAKS StudioX-Pro, employing the Spider search function to include single amino acid point mutations as variable modifications, allowing for better matching to more divergent sequence data.

NCBI entries for *Trematomus bernacchii* (41,453), *Notothenia rossii* (94), and due to the lack of NCBI entries for the other species, *Ommatophoca rossii* (65), *Erebia rossii* (27), *Fannyella rossii* (17), *Anser rossii* (12), Other *rossii* (50), *Chionodraco rastrospinosus* (174) and *Chaenocephalus aceratus* (224) were downloaded into a concatenated database for searching within PEAKS. To qualitatively determine presence of a protein, protein identities were filtered to achieve <1% false discovery rate (FDR) as assessed against a reverse database. Identities were further filtered to require a minimum of two unique peptides per protein group. For quantitative analysis of protein abundance between species, the mapped peptide ion areas were tested using a multi-way ANOVA.

Heatmaps and graphs were produced using GraphPad Prism version 9.3.1.

2.3.8 STRING enrichment and network analysis

Proteins that had a spectral match for the co-IP reaction with given species were compiled into a list, thus one list of co-immunoprecipitated proteins per species, and the lists were then separately uploaded as FASTA (extracted from NCBI's batch entrez) sequences to the STRING-DB.

The top five KEGG and reactome enrichment pathways were extracted according to the lowest FDR values (p-values corrected for multiple testing within each category using the Benjamini–Hochberg procedure), and then the strength (Log10(observed / expected)) score for each pathway was used to analyse the data in GraphPad Prism version 9.3.1. PPI networks were produced in STRING-db.

2.4 Results

2.4.1 The ATP synthase subunit α has higher relative expression in Champsocephalus gunnari when compared with Notothenia rossii

The expression of the ATP synthase F_1 subunit ATP5A was measured, relative to the expression of GAPDH across the four species of fish. A significant increase in the relative expression was observed between the icefish *C. gunnari* and red-blooded *N. rossii* (**Figure 2.1, * p < 0.05)**.

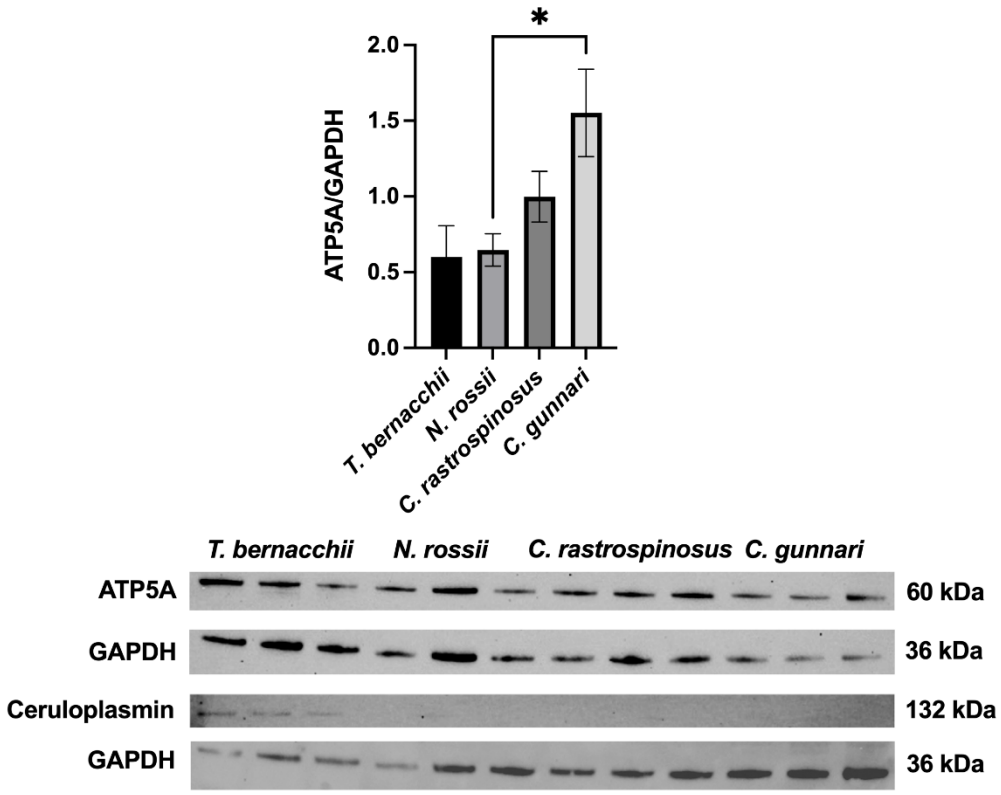

Figure 2.1 – Western blot to measure the expression of ATP5A and ceruloplasmin. *ATP5A in C. gunnari has significantly higher relative expression (ATP5A/GAPDH) than in N. rossii. Traces of ceruloplasmin expression were detected in T. bernacchii, but not in N. rossii, C. rastrospinosus, or C. gunnari. GAPDH present as a loading control. Error bars = SEM, students unpaired t test * = p < 0.05, N=3. Samples are biological replicates.*

2.4.2 C. gunnari has greatly reduced ATP synthase subunit α interactome

The co-immunoprecipitation reaction pulled down 362 proteins for *T. bernacchii*, 105 for *C. gunnari*, 329 for *C. rastrospinosus*, and 309 for *N. rossii*, according to spectral matches. The proteins identified across all four species are presented as a relative expression heatmap in **Figure 2.2A**. The proteins with significant variance ($q < 0.01$, multi-way ANOVA) in expression across the four species are largely absent in *C. gunnari* (**Figure 2.2B**) when compared with the other three species of notothenioid.

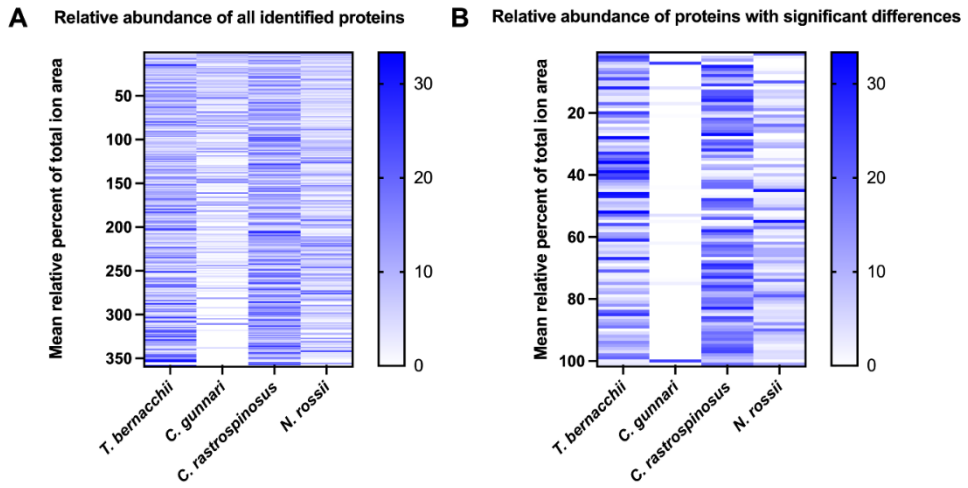

Figure 2.2 – Heatmaps of proteins detected by label-free mass spectrometry from co-immunoprecipitation samples. *Samples are presented as mean relative percentage of total ion areas, an intensity-based quantification of relative protein abundance, from N=3 biological replicates.* ***A)*** *Relative percentage of total ion areas for all proteins identified across the four notothenioid species;* ***B)*** *Proteins identified across all four species of notothenioid with $q < 0.01$ following multi-way ANOVA analysis.*

2.4.3 The four fish species show KEGG enrichment for the same terms

Proteins with spectral matches for each species were uploaded to the STRING-DB and KEGG enrichment was presented. The KEGG enriched pathways were then ranked according to the lowest FDR values, and the five pathways with the lowest FDRs were then scored according to the strength of the enrichment effect (Log10(observed / expected)) (**Figure 2.3**).

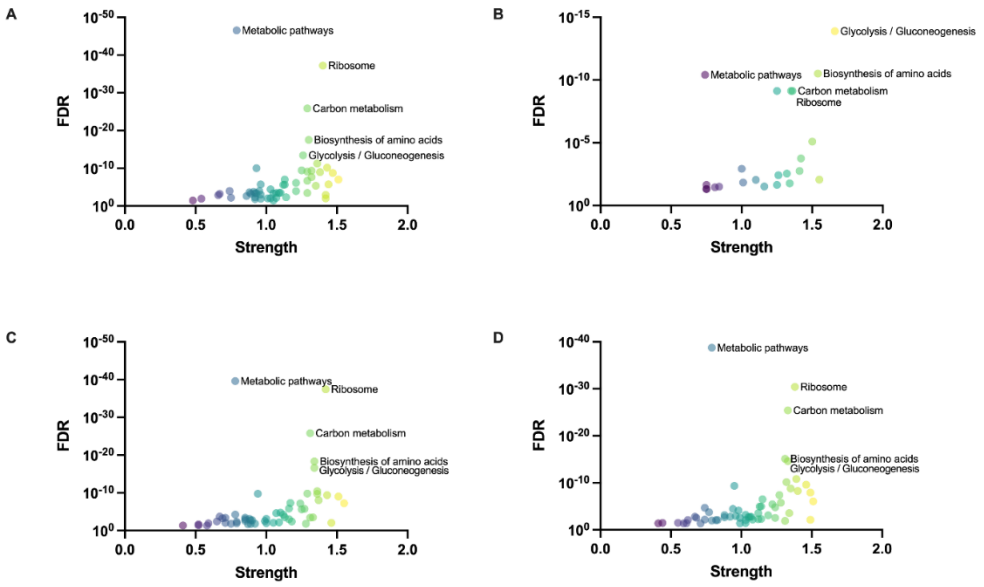

Figure 2.3 – KEGG enrichment of the co-immunoprecipitated proteins for each of the four fish species. ***A)*** *T. bernacchii,* ***B)*** *C. gunnari,* ***C)*** *C. rastrospinosus,* ***D)*** *N. rossii. The five KEGG enriched terms with the lowest FDRs are the same for the four species: glycolysis / gluconeogenesis, biosynthesis of amino acids, carbon metabolism, ribosome, and metabolic pathways. The five pathways with the lowest FDRs within each species are scored according to strength of the enrichment effect (Log10(observed/expected)).*

The four species had the lowest FDR values for the same five pathways, with the strength of the enrichment effect varying to a small degree within each species. This indicates a consistency in the function of the proteins that co-immunoprecipitated with anti-ATP5A. In all four species, 'Metabolic pathways' scored the lowest for the strength of the enrichment effect, while in

all species except *C. gunnari*, 'Ribosome' scored the highest for strength of the enrichment effect.

2.4.4 Reactome enrichment for L13a-mediated translational silencing of ceruloplasmin expression

As with the KEGG enrichment, the reactome pathways identified as enriched from the protein lists uploaded to the STRING-DB were first ranked by the lowest FDR values. The strength of the enrichment effect was again used to score the pathways (**Figure 2.4**).

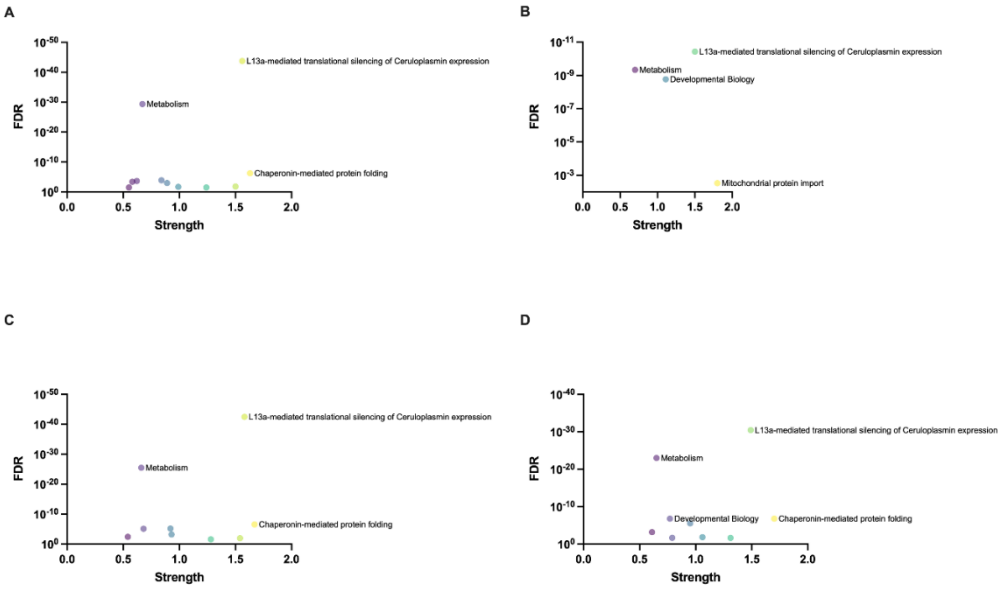

Figure 2.4 - Reactome enrichment of the proteins that co-immunoprecipitated with anti-ATP5A for each of the four notothenioid species. ***A)*** *T. bernacchii,* ***B)*** *C. gunnari,* ***C)*** *C. rastrospinosus,* ***D)*** *N. rossii. The reactome enrichment terms with the lowest FDRs are varied between the four species, with only Metabolism and L13a-mediated translational silencing of ceruloplasmin expression common to all four species. The five pathways with the lowest FDRs within each species are scored according to strength of the enrichment effect (Log10(observed/expected)).*

There is again a significant overlap between the pathways with the lowest FDRs across the four species. 'Metabolism' was enriched across all four

species, and perhaps most notably, ‘L13a-mediated translational silencing of ceruloplasmin expression’. ‘Developmental biology’ was reactome pathways enriched across all species except *T. bernacchii*, while ‘Chaperonin-mediated protein folding’ was enriched across all species except for *C. gunnari.*

The interactomes of the different notothenioids also had a varied presence of redox stress proteins (**Table 2.1**). *C. gunnari* had the fewest spectral matches for the five identified proteins, with only carbonyl reductase 1 and peroxiredoxin 4 identified in the co-immunoprecipitated proteins.

Table 2.1 - Mean spectral matches of redox stress associated proteins in notothenioids*. Carbonyl reductase, catalase, glutathione peroxidase, peroxiredoxin 4, and peroxiredoxin 6 were identified in the ATP synthase subunit α interactome of T. bernacchii, C. rastrospinosus, and N. rossii. Few spectral matches for these proteins were identified in C. gunnari. Spectral matches identified using PEAKS StudioX-Pro. Values are calculated from N=3 biological replicates.*

	Mean relative spectral matches			
Oxidative stress response proteins	***T. bernacchii***	***C. gunnari***	***C. rastrospinosus***	***N. rossii***
Carbonyl reductase 1	4.5	1.5	12.1	6.1
Catalase	6.1	0	9.1	10.1
Glutathione peroxidase	10	0	5	6.7
Peroxiredoxin 4	9.7	1.4	11.1	4.2
Peroxiredoxin 6	9.5	0	7.6	5.7

2.4.5 PPI networks of co-immunoprecipitated proteins

FASTA sequences of proteins that were co-immunoprecipitated within each species were used to produce protein-protein interaction (PPI) networks using STRING-DB. A highest confidence interaction score was used (0.900) in all species, and disconnected nodes were hidden due to the large number of nodes within each network.

The *T. bernacchii* PPI network consisted of 337 nodes, 1580 edges, an average node degree of 9.38 and a PPI enrichment p-value of < 1.0e-16 (**Figure 2.5**). The highlighted local network clusters are: 'Mixed, incl. cap-dependent translation initiation, and groEL-like equatorial domain superfamily' (observed gene count 59, strength 1.46, FDR 4.27E-55), 'Cytoplasmic ribosomal proteins' (observed gene count 40, strength 1.55, FDR 1.06E-38), 'Carbon metabolism, and 'Phosphoglycerate/bisphosphoglycerate mutase, active site' (observed gene count 22, strength 1.18, FDR 1.24E-12), 'Mixed, incl. biosynthesis of amino acids, and alanine, aspartate and glutamate metabolism' (observed gene count 20, strength 1.1, FDR 6.77E-10), and 'Pentose phosphate pathway, and Glycolysis' (observed gene count 15, strength 1.36, FDR 8.13E-10).

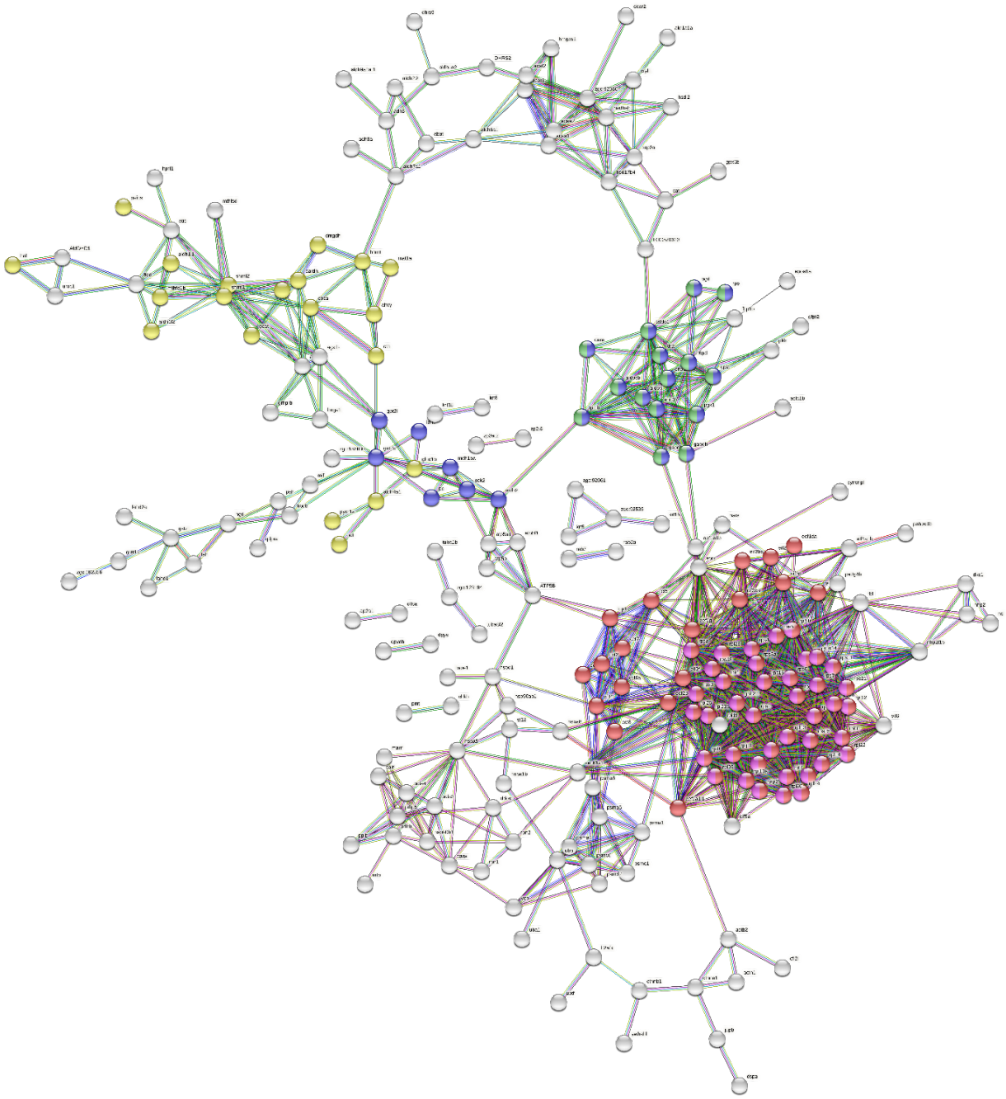

Figure 2.5 – PPI network of co-immunoprecipitated proteins in Trematomus bernacchii*. Colour of edges shows type of interactions. Colour of nodes represents local network clusters. Cytoplasmic ribosomal proteins are red, Carbon metabolism, and Phosphoglycerate/bisphosphoglycerate mutase, and active site proteins are blue, Mixed, incl. biosynthesis of amino acids, and one carbon pool by folate proteins are green, Pentose phosphate pathway, and Glycolysis proteins are yellow, Mixed, incl. fatty acid degradation, and valine, leucine and isoleucine degradation proteins are pink.*

The *C. gunnari* PPI network consisted of 93 nodes, 138 edges, an average node degree of 2.95 and a PPI enrichment p-value of < 1.0e-16 (**Figure 2.6**). The highlighted local network clusters are: 'Glycolysis, and Enolase, conserved site' (observed gene count 9, strength 2.03, FDR 9.47E-09), 'Cytoplasmic ribosomal proteins, and Elongation factor' (observed gene count 12, strength 1.53, FDR 1.34E-08), and 'Carbon metabolism, and Phosphoglycerate/bisphosphoglycerate mutase, active site' (observed gene count 10, strength 1.39, FDR 6.35E-06).

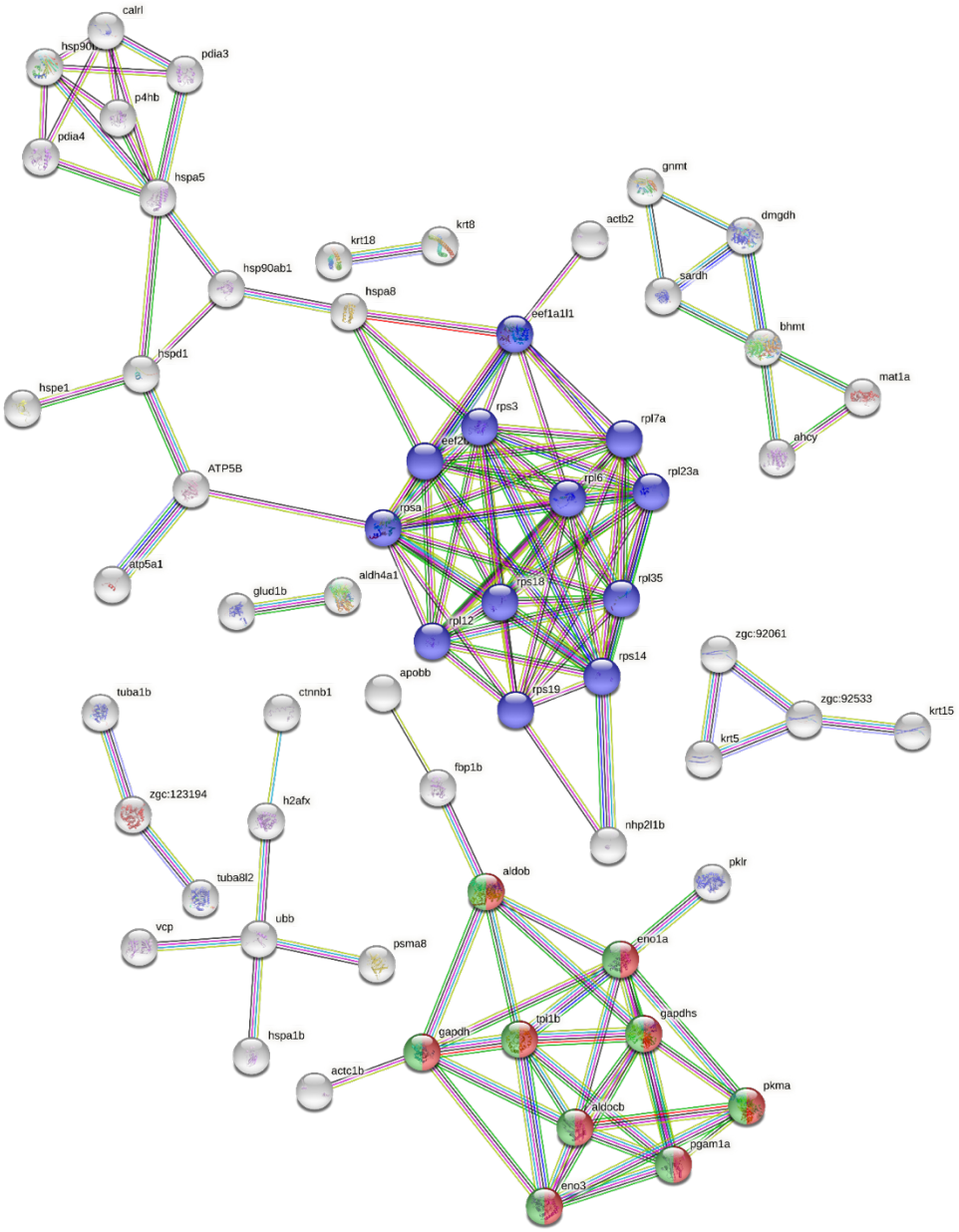

Figure 2.6 – PPI network of co-immunoprecipitated proteins in Champsocephalus gunnari*. Colour of edges shows type of interactions. Colour of nodes represents local network clusters. Glycolysis, and Enolase, conserved site proteins are red, Cytoplasmic ribosomal proteins, and Elongation factor proteins are blue, and Carbon metabolism, and Phosphoglycerate/bisphosphoglycerate mutase, active site proteins are green.*

The *C. rastrospinosus* PPI network consisted of 308 nodes, 1502 edges, an average node degree of 9.75 and a PPI enrichment value of < 1.0e-16 (**Figure 2.7**). The highlighted local network clusters are: 'Cytoplasmic ribosomal proteins' (observed gene count 38, strength 1.59, FDR 2.48E-38), 'Carbon metabolism, and Phosphoglycerate/bisphosphoglycerate mutase, active site' (observed gene count 22, strength 1.22, FDR 1.85E-13), 'Mixed, incl. biosynthesis of amino acids, and one carbon pool by folate' (observed gene count 22, strength 1.15, FDR 2.50E-12), 'Pentose phosphate pathway, and Glycolysis' (observed gene count 15, strength 1.4, FDR 2.42E-10), and 'Mixed, incl. fatty acid degradation, and valine, leucine and isoleucine degradation' (observed gene count 21, strength 1.02, FDR 2.58E-09).

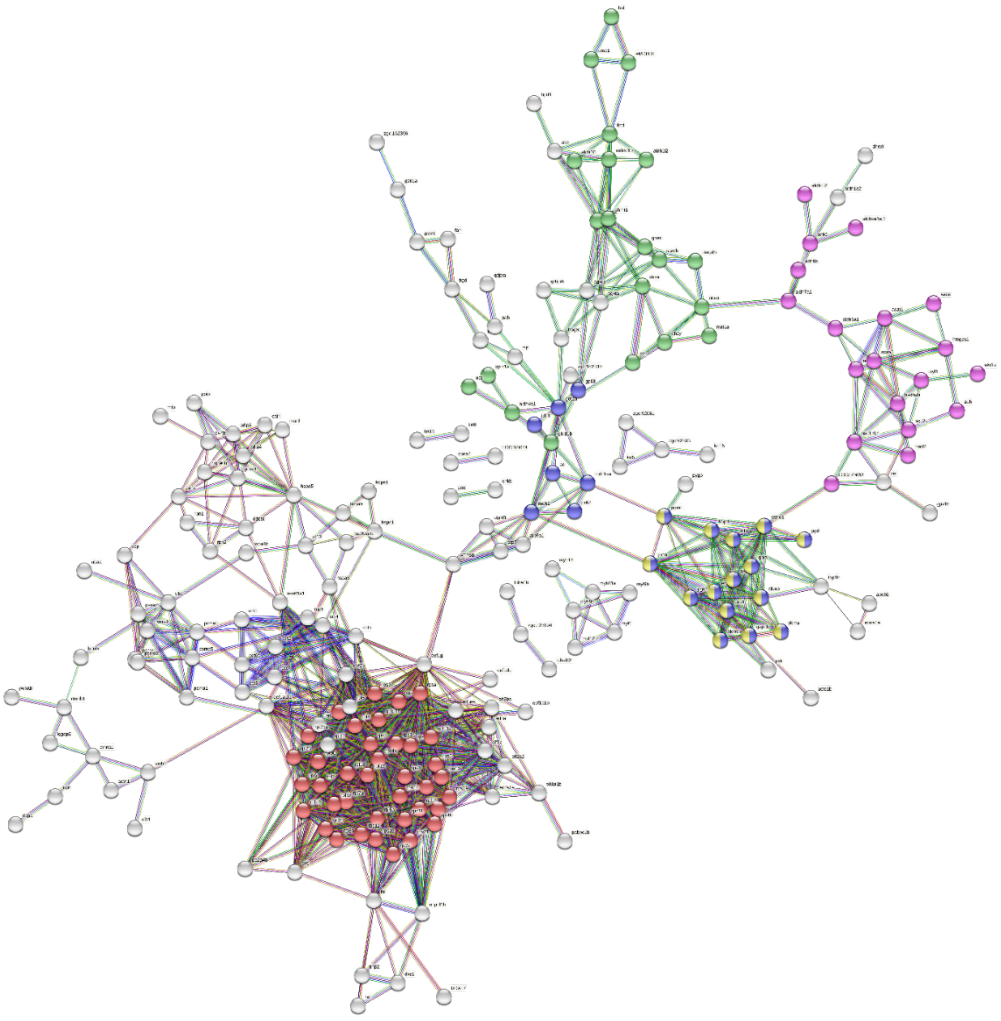

Figure 2.7 – PPI network of co-immunoprecipitated proteins in Chionodraco rastrospinosus*. Colour of edges shows type of interactions. Colour of nodes represents local network clusters. Cytoplasmic ribosomal proteins are red, Carbon metabolism, and Phosphoglycerate/bisphosphoglycerate mutase, active site proteins are blue, Mixed, incl. biosynthesis of amino acids, and one carbon pool by folate proteins are green, Pentose phosphate pathway, and Glycolysis proteins are yellow, and Mixed, incl. fatty acid degradation, and valine, leucine and isoleucine degradation proteins are pink.*

The *N. rossii* PPI network consisted of 287 nodes, 1010 edges, an average node degree of 7.04 and a PPI enrichment value of < 1.0e-16 (**Figure 2.8**). The highlighted local network clusters are: 'Cytoplasmic ribosomal proteins' (observed gene count 32, strength 1.52, FDR 1.11E-29), 'Pentose phosphate pathway, and Glycolysis' (observed gene count 15, strength 1.43, FDR 1.09E-10), 'Mixed, incl. biosynthesis of amino acids, and one carbon pool by folate' (observed gene count 18, strength 1.1, FDR 1.46E-08), and 'Mixed, incl. one-carbon metabolism, and glycine, serine and threonine metabolism' (observed gene count 12, strength 1.33, FDR 7.33E-07).

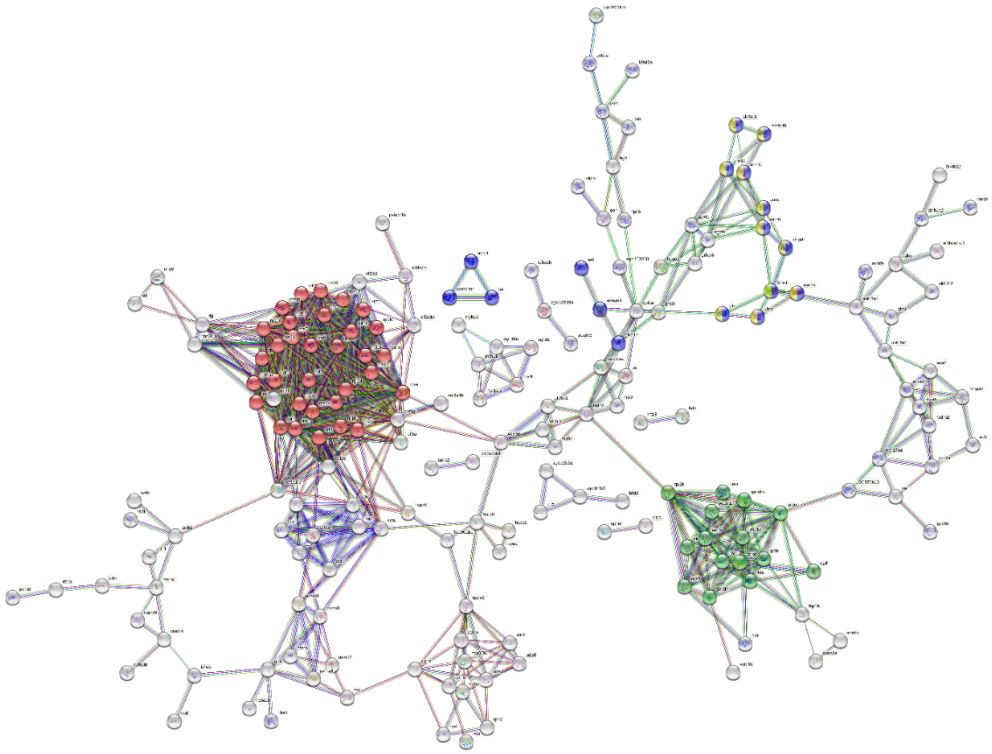

Figure 2.8 – PPI network of co-immunoprecipitated proteins in Notothenia rossii*. Colour of edges shows type of interactions. Colour of nodes represents local network clusters. Cytoplasmic ribosomal proteins are red, Pentose phosphate pathway, and Glycolysis proteins are green, Mixed, incl. biosynthesis of amino acids, and one carbon pool by folate proteins are green, Mixed, incl. one-carbon metabolism, and glycine, serine and threonine metabolism proteins are yellow.*

2.4.6 Absence of ceruloplasmin protein expression in Chionodraco rastrospinosus and Champsocephalus gunnari

Following the reactome enrichment for the L13a-mediated translational silencing of ceruloplasmin expression (**Figure 2.4**) in the four notothenioid species, Western blot was used to detect the presence of ceruloplasmin in the liver of the four species (**Figure 2.1**). Only *T. bernacchii* had bands that

indicated the presence of ceruloplasmin, while the red-blooded *N.* rossii and the icefish *C. rastrospinosus* and *C. gunnari* had no bands present for ceruloplasmin.

2.5 Discussion

2.5.1 Champsocephalus gunnari has a higher level of relative ATP synthase subunit α expression than Notothenia rossii

We found a significant increase in the relative expression levels of the ATP synthase subunit α between the liver tissue of *C. gunnari* and *N. rossii* (**Figure 2.1**). Limited research has so far been presented on the ATP synthase enzyme in notothenioids; however, a comparative study between the icefish *C. aceratus* and the red-blooded *Notothenia coriiceps* reported that there was no difference in the enzyme activity in cardiac tissue between the species at either ambient temperatures or at CT_{max}[278]. The same study did report that cardiac ATP levels declined at higher temperatures in both species but remained higher at all temperatures (mitochondrial respiration rates were measured at 2 and 10°C) in *N. coriiceps.*

We reported amino acid sequence differences between Antarctic fish species and other vertebrates in the ATP6 gene, with *C. gunnari* having a small non-polar alanine residue at residue 35, where other studied Antarctic fish species, including the icefish *Chaenocephalus aceratus,* had a serine residue in the same position[279]. These studies would suggest that there are significant differences in ATP metabolism between notothenioid species, but these not necessarily depend on the haemoglobin trait.

2.5.2 Champsocephalus gunnari has a comparatively smaller ATP synthase subunit α interactome than other studied notothenioid species

Despite *C. gunnari* having a significantly higher level of ATP synthase α-subunit expression than *N. rossii*, the interactome of the α-subunit contained far fewer proteins (105), compared with *C. rastrospinosus* (329), *T. bernacchii* (362), and *N. rossii* (309) (**Figure 2.2**). Given the relatively similar number of proteins contained with the α-subunit interactome of the haemoglobin-less *C. rastrospinosus* and the two red-blooded species, this would suggest that the absence of myoglobin in *C. gunnari* has a significant impact on the

metabolism of the α-subunit and the larger ATP synthase complex within the liver.

The intracellular myoglobin is associated with the delivery of oxygen to the mitochondria, with its expression correlated with cytochrome c oxidase activity in cultured myoblasts[280], and a physical interaction between myoglobin and cytochrome c oxidase being reported in rats[281]. However, studies of the haemoglobin- and myoglobin-less *C. aceratus* have reported no difference in the maximal activities of both cytochrome c oxidase[282] and ATP synthase[278], when compared with red-blooded species. The authors of the study with ATP synthase maximal activity also reported a significantly increased citrate synthase activity and ATP content in the red-blooded *N. coriiceps* in comparison with *C. aceratus*, which they suggest is indicative of higher aerobic metabolic capacity.

That ATP synthase forms large supramolecular complexes is well reported and reviewed, both in a physiological and pathophysiological context[283,284]. Previous studies of mitochondria have coupled chemical cross-linking methods with mass spectrometry to understand the mitochondrial interactome, and this has provided evidence of the large respirasome complexes and interaction between ATP synthase and mitochondrial contact site and cristae organizing system (MICOS) proteins that influence the structure of the cristae[285,286].

When considered alongside other published data that highlights differences in icefish ATP metabolism[278] and the structure of *C. gunnari* ATP synthase subunits[279], this offers further evidence of icefish ATP synthase functionality being distinct from other red-blooded notothenioid, and vertebrate species. However, these differences appear to correlate more closely with the myoglobin-less trait than the haemoglobin-less trait.

2.5.3 *The ATP synthase subunit α interactome of Champsocephalus gunnari lacks redox stress associated proteins and reactome enrichment for chaperonin-mediated protein folding*

The ATP synthase subunit α interactomes of *T. bernacchii*, *C. rastrospinosus*, *N. rossii* were all reactome enriched for chaperonin mediated protein folding (**Figure 2.4**) and contained a greater array of oxidative stress response proteins (**Table 2.1**) when compared with *C. gunnari*. Heat shock proteins are known to play a role in the physiological response to oxidative stress[287,288], while ATP synthase has previously been discussed as a location of oxidative stress[289,290]. Additionally, previous research into the notothenioid oxidative stress response has reported in some instances that icefishes are more vulnerable to temperature induced oxidative stress[291,292], however this effect was not observed at more modest temperature increases[293]. Levels of oxidised proteins and lipids and capacities for antioxidant activity have been compared between icefish and red-blooded fish, and while differences between icefish and red-blooded fish were tissue dependent, a particularly high level of oxidative damage was observed in the liver of *C. gunnari*[294].

2.5.4 *All four species show reactome enrichment for L13a-mediated translational silencing of ceruloplasmin expression*

The four notothenioid species studied were strongly reactome-enriched for the L13a-mediated translational silencing of ceruloplasmin expression pathway (**Figure 2.4**) identified by Mazumder *et al*. in a study of transcript-specific translational control[295]. Ceruloplasmin is a polyfunctional protein that is synthesised in the liver and acts as the main transporter of copper in the blood, as well as functioning as an iron oxidase, and antioxidant[296]. A mitochondrial ceruloplasmin has also been previously identified and characterised in mammals[212]. The iron oxidase capacity of ceruloplasmin was suggested to be important for mitochondrial ferritin and the formation of Fe-S clusters.

A previous study of iron metabolism in notothenioids reported that the ceruloplasmin of haemoglobin-less *C. rastrospinosus* had altered codons at the

Cu5 binding site when compared with *Homo sapiens* and *Danio rerio*[297]. The authors also demonstrated a small but significant increase in the levels of ceruloplasmin mRNA transcripts in the liver of *C. rastrospinosus* when compared with red-blooded *T. bernacchii* which they interpreted as a compensatory mechanism to remove ferrous iron. However, a more recent study reported a significantly lower levels of oxidase activity in icefish species (*C. aceratus* and *C. gunnari*) when compared with red-blooded species (*N. coriiceps* and *Gobionotothen gibberifrons*)[298]. We suggest that these two seemingly contrasting data points can be explained by the translational silencing of ceruloplasmin, where mRNA for ceruloplasmin can be detected but measured activity of the enzyme is near-zero.

2.5.5 Ceruloplasmin protein expression was not detected by Western blot in N. rossii, C. rastrospinosus and C. gunnari

Western blot was used to detect the presence of ceruloplasmin protein in the liver tissue of the four species but was below levels of detection in *N. rossii* and the two icefish species (**Figure 2.1**). While it has previously been reported that *C. rastrospinosus* has upregulated levels of liver ceruloplasmin mRNA when compared with red-blooded *T. bernacchii,* the expression of the protein itself was not measured[297]. Additionally, the levels of ceruloplasmin iron oxidase activity in the serum of *C. gunnari* have been previously reported as close to zero[298]. It is therefore possible that while the gene is being transcribed as reported, the translation of the protein from these mRNA transcripts could be limited, which would support the previously described observation of minimal iron oxidase activity in certain notothenioid species.

2.6 Perspectives and significance

While the mitochondria of notothenioids have been widely studied, few have specifically considered the functionality of ATP synthase. Given the importance of ATP synthase in aerobic respiration, the absence of haemoglobin and myoglobin is likely to cause alterations to its physiological function and interactions. Our co-immunoprecipitation and proteomics study presents an overview of the ATP synthase interactome and identifies a translational silencing pathway of the iron oxidase enzyme ceruloplasmin. Levels of ceruloplasmin protein expression were below levels of detection by Western blot in all but one of the species considered, the red-blooded species *T. bernacchii*. This observation fits with previous studies of notothenioid ceruloplasmin and points toward an altered metabolism of iron, specifically the detoxification of Fe(II), in the notothenioid suborder.

2.7 Author contributions

BE performed experimental work, data analysis and wrote the manuscript; GK aided with data analysis; ML generated the samples; CP generated the samples and helped to write the manuscript; LC directed the research, supervised experiments, provided reagents and helped to write the manuscript.

2.8 Funding

BE is supported by the Biotechnology and Biological Sciences Research Council [grant number BB/J014508/1]. GK is supported by a University of Nottingham Vice- Chancellors International Scholarship award.

2.9 Acknowledgements

The York Centre of Excellence in Mass Spectrometry was created thanks to a major capital investment through Science City York, supported by Yorkshire Forward with funds from the Northern Way Initiative, and subsequent support from EPSRC (EP/K039660/1; EP/M028127/1).

We would also like to thank the crew and scientists from the expeditions in which the samples used in this study were collected.

3 Mitochondrial haemoglobin is upregulated with hypoxia and has a conserved interaction with ATP synthase and inhibitory factor 1.

Brad Ebanks*[1], Gunjan Katyal*[1], Adam Dowle[2], Chiara Papetti[3], Magnus Lucassen[4], Nicoleta Moisoi[5], Lisa Chakrabarti[1,6]

Published: *Cells (2023)* ***12(6):*** *912 (https://doi.org/10.3390/cells12060912)*

[1] School of Veterinary Medicine and Science, University of Nottingham, Nottingham NG7 2RD, UK

[2] Department of Biology, Bioscience Technology Facility, University of York, York YO10 5DD, UK

[3] Biology Department, University of Padova, Padova, Italy

[4] Alfred Wegener Institute, Bremerhaven, Germany

[5] Leicester School of Pharmacy, Leicester Institute for Pharmaceutical Innovation, De Montfort University, The Gateway, Leicester LE1 9BH

[6] MRC Versus Arthritis Centre for Musculoskeletal Ageing Research, UK

3.1 Abstract

The globin protein superfamily has diverse functions. Haemoglobin has been found in non-erythroid locations, including within the mitochondria. Using co-immunoprecipitation and in silico methods, we investigated the interaction of mitochondrial haemoglobin with ATP synthase and its associated proteins, including inhibitory factor 1 (IF1). We measured the expression of mitochondrial haemoglobin in response to hypoxia. In vitro and in silico evidence of interactions between mitochondrial haemoglobin and ATP synthase were found, and we report upregulated mitochondrial haemoglobin expression in response to hypoxia within skeletal muscle tissue. Our observations indicate that mitochondrial pH and ATP synthase activity are implicated in the mitochondrial haemoglobin response to hypoxia.

3.2 Introduction

Haemoglobin has a physiological role within red-blood cells as the protein that binds to both oxygen and carbon dioxide. This function of haemoglobin allows the controlled delivery of oxygen to tissues to meet metabolic demand. Its structure was first characterised in the 1960s[133], shortly after it was demonstrated that its function could be modulated by pH and the allosteric binding of organic phosphates[299–301]. The tetrameric $\alpha_2\beta_2$ structure, with a prosthetic haem group located within each subunit, allows for a co-operative oxygen binding mechanism that results in oxyhaemoglobin having a substantially different structure to deoxyhaemoglobin[186].

In the last two decades, myoglobin and haemoglobin have been grouped with novel globin proteins such as cytoglobin[302], neuroglobin[303] and globin X[144]. While the precise physiological purpose of this expanded globin family is yet to be fully understood, it is suggested they may have signalling functions and the capacity to buffer against oxidative stress[304], while their dysfunction is implicated in disease pathologies[305]. Alongside an expanded family of globin proteins, there has also been an increased understanding of non-erythroid haemoglobin. Haemoglobin has been located in neuronal cells[155,157,306], and within the mitochondria[160]. Both neuronal haemoglobin and mitochondrial haemoglobin have been suggested to be dysfunctional in the pathophysiology of Parkinson's disease[161,162,307,308]. Despite this, the intracellular physiological role of these haemoglobin proteins remains undefined.

Comparative physiology can be used to understand the functionality of non-erythroid haemoglobin. The function and expression of haemoglobin varies across species. *D. melanogaster* possess three globin genes; a haemoglobin, Glob1, that is widely expressed across the tracheal system and fat body of the *D. melanogaster* and is thought to play an important role in O_2 homeostasis[167,171], while Glob2 and Glob3 show exclusive and limited expression in the testes of male *D. melanogaster*[172].

When using a comparative physiology approach to study haemoglobin, the Channichthyidae family of fishes from the Notothenioid suborder offer a

unique advantage. This is because Channichthyidae fishes are unique among vertebrates in their absence of haemoglobin expression, and in some species, their myoglobin is at low levels or not expressed[173,174]. It has been suggested that the sub-zero temperatures in the Southern Ocean of Antarctica, that allow for high oxygen saturation, may have contributed to the loss of haemoglobin mutation being spread throughout the Channichthyidae family. A period with low levels of iron in thew Southern Ocean has also been suggested as an additional selective pressure for this mutation to thrive[180]. Meanwhile, numerous physiological adaptations have been reported in both Channichthyidae and red-blooded members of the Notothenioids, including altered mitochondrial structure and function[183,267,270,271,291], and the expression of antifreeze glycopeptides[182,309–312].

Due to the mitochondrial dependence on oxygen for aerobic respiration, and the oxygen-binding properties of haemoglobin, hypoxia is an important condition to consider when studying mitochondrial haemoglobin. Hypoxia occurs when the demand for oxygen exceeds supply, resulting in decreased partial pressures of oxygen within tissues that can ultimately lead to impaired physiological function[313]. The lack of oxygen available for complex IV of the mitochondrial electron transport chain impairs the function of the system, leading to a reduced output of ATP[314]. In order to adapt to this low oxygen and low bioenergetic state, cells undergo metabolic reprogramming, including a reduction in the activity of ATP-consuming processes and a switch to anaerobic ATP production[313,315]. The main driver of the eukaryotic response is the well characterised hypoxia inducible factor (HIF) response, while other pathways such as the unfolded protein response (UPR) and the mechanistic target of rapamycin (mTOR) are also implicated[316].

Studies of mitochondrial haemoglobin have reported its localisation to the inner mitochondrial membrane[160], and that overexpression of haemoglobin in MN9D cells causes changes to the expression of oxygen homeostasis and mitochondrial oxidative phosphorylation genes[155]. A mechanism by which the ATP synthase regulatory protein inhibitory factor 1 (IF1) controls the synthesis of haemoglobin, due to the pH-dependence of the haem synthesis pathway, has

also been reported[126]. In this study we therefore sought to investigate the physiological role of mitochondrial haemoglobin, including in bioenergetics and oxygen homeostasis. Through investigations across multiple species, using both molecular and bioinformatic methods, we have examined the conserved role of this novel haemoglobin protein.

3.3 Methods

3.3.1 Rat and mouse hypoxia

The samples used to study the impact of hypoxia on mitochondria haemoglobin in rodents were kindly provided by Andrew Murray (University of Cambridge, UK). Rat liver, mouse liver, and mouse quadriceps were collected from animals exposed to hypoxia as described in detail previously by Murray and colleagues[317–319]. Briefly, rats and mice were housed in conventional cages in a temperature (23 °C) and humidity-controlled environment with a 12 h/12 h light/dark cycle. They were fed a standard diet and had access to water ad libitum. For the experiment, the rodents either remained under normoxic conditions (21% O2) or were housed in hypoxic conditions (10% O2) in a flexible-film chamber (PFI Systems Ltd., Milton Keynes, UK). The rats were housed under hypoxic conditions for 14 days, and the mice for 28 days, with 20 air changes/h.

3.3.2 D. melanogaster hypoxia

Mixed populations of wild type flies were subjected to the following conditions: 2.5% O_2 for 30 minutes at 25°C followed by normoxia for 30 minutes at 25 °C, then either stored frozen at -80°C or subjected to a second cycle of 2.5% O_2 30 minutes at 25°C followed by normoxia for 30 minutes at 25°C, before freezing at -80°C.

3.3.3 Fish liver lysate preparation

First, 10 mg of liver tissue from each of the fish species (C. rastrospinosus, T. bernacchii, N. rossii and C. gunnari) was added to 100 µL of extraction buffer (1X IP, Dynabeads™ Co-Immunoprecipitation Kit (ThermoFisher, Waltham, Mass., USA)) and mechanically homogenised for 1 min with a 1.2–2.0 mL Eppendorf micro-pestle (Sig-ma-Aldrich, St. Louis, Missouri, USA). The homogenate was cooled on ice for 15 min before centrifugation at 15,000× g

for 5 min to pellet the insoluble fraction. The supernatant was collected to be used in the co-immunoprecipitation reaction, and the pellet was discarded.

3.3.4 HEPG2 treatment with atractyloside

HEPG2 cells were seeded in T175 flasks (DMEM, 10% FCS, L-glutamine). After 24 hours, cells were treated with 8 μM atractyloside for 24 hours, following previous literature[320]. After 24 hours of treatment, cells were trypsinised and frozen at -80°C until use.

3.3.5 HEPG2 mitochondrial isolation

Cells were resuspended in mitochondrial extraction buffer, and then passed 10 times through a 1 mL syringe with a 26-gauge needle for lysis, as per published protocols[321]. The homogenate was centrifuged at 2000 g for 10 minutes to clear debris. This step was repeated to clear any remaining nuclear material. The post-nuclear supernatant was then centrifuged at 14,000 g for 30 minutes, and the subsequent supernatant was removed leaving the mitochondrial pellet.

3.3.6 Rat and mouse tissue lysate preparation

10 mg of either liver or quadriceps tissue was added to 100 μL of extraction buffer (1X IP, Dynabeads™ Co-Immunoprecipitation Kit (ThermoFisher)) and mechanically homogenised for 1 minute with a 1.2-2.0 mL Eppendorf micro-pestle (Sigma-Aldrich). The homogenate was cooled on ice for 15 minutes, before centrifugation at 15,000 g for 5 minutes to pellet the insoluble fraction. The supernatant was collected, to be used in the co-immunoprecipitation reaction, and the pellet discarded.

3.3.7 D. melanogaster mitochondrial isolation

100 frozen *D. melanogaster* were added to 500 μL of mitochondrial extraction buffer, and mechanically homogenised for 1 minute with a 1.2-2.0 mL

Eppendorf micro-pestle (Sigma-Aldrich). The homogenate was spun at 850 g for 10 minutes to clear debris, and the supernatant was extracted and spun again at 1000 g for a further 10 minutes to produce a nuclear pellet. The subsequent supernatant was taken and a final spin done at 12,000 g for 30 minutes to produce a mitochondrial pellet and cytoplasmic supernatant, which were extracted and stored.

3.3.8 Co-immunoprecipitation (Dynabeads™ Co-Immunoprecipitation Kit (ThermoFisher))

10 µg of antibody (anti-HbB, ab227552) was bound to 2 mg of Dynabeads, as per manufacturer's instructions. The antibody-conjugated Dynabeads were incubated overnight, (18 hours, 4°C) with Notothenioid liver lysate. The following day the Dynabeads were washed, and the antibody-antigen complex was eluted and stored at -80°C.

3.3.9 SDS-PAGE

1 µL of protein sample was added to 5µL of PBS, 3 µL LDS and 3µL DTT. The solution was boiled at 100 degrees C for 10 minutes and loaded onto SDS-polyacrylamide pre-cast gels (NuPAGE™ 4 to 12%, Bis-Tris, 1.0 mm, Mini Protein Gel, 12-well). In preparation for label-free mass spectrometry of co-IP fractions, a fixed voltage (200V) was applied until the dye front had run 2cm into the gel. The gel was then removed from the casing and stained overnight (18 hours, RT) with ProtoBlue Safe Coomassie G-250. For Western Blots or MALDI-TOF-MS, the fixed voltage (200V) was applied for 35 minutes, before continuation of the Western Blot procedure or Coomassie staining. Coomassie stained gels were destained with three 10-minute-long washes of deionised H_2O. The Coomassie stained section of the gel lanes were excised, and they were then stored in 1.5 mL Eppendorf tubes (4°C), until ready to be sent for mass spectrometry analysis.

3.3.10 Western Blot

Proteins were transferred to a nitrocellulose membrane at 30 V for 60 minutes. The membrane was blocked with 5 mL 3% (w/v) milk powder (Marvel) in TBS-T for 60 minutes with gentle agitation (RT). The membrane was then probed overnight (18 hours, 4°C) with the primary antibody (anti-HbA, ab82871; anti-HbB, ab227552; anti-Beta actin, ab8227; anti-ATP5A, ab245580; anti-ATPIF1, SAB2100188; anti-GAPDH, ab9485), at a 1:5000 dilution in 3% (w/v) milk powder in TBS-T. The membrane was then washed three times with TBS-T before incubation with secondary antibody (goat anti-rabbit HRP conjugate, ab6721), at a 1:5000 dilution in 5% (w/v) milk powder in TBS-T. The membrane was again washed three times with TBS-T before a five-minute incubation with ECL substrate and chemiluminescence measurement. Band densities were measured using Image J and samples normalised to appropriate loading controls. Statistical analysis was performed using GraphPad Prism.

3.3.11 Label-free mass spectrometry

Samples were analysed by the Centre of Excellence in Mass Spectrometry at the University of York. Protein was in-gel digested post reduction and alkylation. Extracted peptides were analysed over 1 h LC-MS acquisitions with elution from a 50 cm, C18 PepMap column onto a Thermo Orbitrap Fusion Tribrid mass spectrometer using a Waters mClass UPLC. Data analysis was performed using PEAKS StudioX-Pro, employing the Spider search function to include single amino acid point mutations as variable modifications, allowing for better matching to more divergent sequence data[322].

NCBI entries for Trematomus bernacchii (41,453), Notothenia rossii (94), Ommatophoca rossii (65), Erebia rossii (27), Fannyella rossii (17), Anser rossii (12), rossii (50), Chionodraco rastrospinosus (174) and Chaenocephalus

aceratus (224) were downloaded into a concatenated database for searching within PEAKS. To qualitatively determine presence of a protein, protein identities were filtered to achieve <1% false discovery rate (FDR) as assessed against a reverse database. Identities were further filtered to require a minimum of two unique peptides per protein group. For quantitative analysis of protein abundance between species, the mapped peptide ion areas were tested using a multi-way ANOVA.

3.3.12 Co-immunoprecipitation (Invitrogen™ Dynabeads™ Protein G Immunoprecipitation Kit)

10 µg of antibody (anti-HbB, ab227552) was conjugated to 2 mg of Dynabeads (Invitrogen™ Dynabeads™ Protein G Immunoprecipitation Kit), as per manufacturer's instructions. The antibody-conjugated Dynabeads were incubated overnight, (18 hours, 4°C) with the *D. melanogaster* mitochondrial fraction. The following day the Dynabeads were washed, and the antibody-antigen complex was eluted and stored at -80°C.

3.3.13 MALDI-TOF-MS

Samples were analysed by the Centre of Excellence in Mass Spectrometry at the University of York. Following in-gel digestion, peptides were analysed over 20 min acquisitions with elution from a 10 cm Waters T3 nano C18 column onto a Bruker maXis qTOF operated in DDA mode. Resulting peptide spectra were searched against provided sequences and the appropriate species-specific entries in the SwissProt protein database using Mascot.

3.3.14 ATPase assay

5 mg of rat liver tissue was mechanically homogenised with a 1.2-2.0 mL Eppendorf micro-pestle (Sigma-Aldrich), and the lysate cleared by centrifugation (10,000 g, 10 minutes). Co-immunoprecipitation reactions with

anti-haemoglobin beta and non-specific anti-IgG were completed with the Invitrogen™ Dynabeads™ Protein G Immunoprecipitation Kit. The ATPase Assay Kit (Colorimetric) (ab234055) was then used as per the manufacturer's instructions to assess the ATPase activity of the immunoprecipitated protein eluates.

3.3.15 Molecular docking

The IF1 3D structure was extracted from its X-ray resolved complex with ATP synthase complex from *B. taurus* (cow) (PDB ID:1OHH) and was used for docking simulations (*B. taurus* is the only verified structure from mammals available). The haemoglobin structure was taken from 3D structure of haemoglobin from *B. taurus*, to keep the consistency in the choice of organism and was prepared for docking as tetrameric, dimeric, and monomeric forms (only HbA). All protein structures were minimised before proceeding with docking using Chimera[323].

Patch dock protein-protein docking[324] (bioinfo3d.cs.tau.ac.il/ PatchDock/) server was used for different dockings a) IF1 to ATPase complex. B) IF1 monomer to haemoglobin tetramer no ligands. C) IF1 dimer to haemoglobin tetramer no ligands. D) IF1 monomer with haemoglobin dimer E) IF1 dimer to haemoglobin dimer. F) IF1 with HbA chains A and C. G) Voxelotor inhibitor for haemoglobin. The results obtained from this server were further improved with submission to associate refinement server FireDock[325]. The poses were selected based on Global energy.

The PDBsum was used to analyse interacting residues in the docked proteins (residue colours based on their properties and the coloured lines joining these residues representing the type of interaction)[326]. The docked proteins were analysed and visualised using ChimeraPyMOL (Version 1.2r3pre.) and UCSF Chimera[323]. The proteins were docked using different webservers for comparison, HDOCK[327] and ClusPro[328] (**Supplementary Figure 1.3**).

3.3.16 Molecular dynamics of protein–protein complexes

Protein–protein complexes were subsequently prepared for MD simulation with GROMACS ('S2352711015000059', version2021.5 /11/2021) by generating topology files and coordinate files. Simulation boxes of 11.88 × 11.88 × 11.88 nm (haemoglobin tetramer- IF1), 11.89× 11.89 × 11.89 nm (HbA – IF1), were initially set, with the protein complex centred inside. spc216.gro solvent configuration was used to add water molecules together with the addition of NaCl to neutralize the entire system. The resulting models were parametrised using AMBER99SB-ILDNP Force Field[329,330] implemented in the GROMACS 5.0 software package.

A robust energy minimization protocol was applied consisting of 50 000 cycles with the Steepest Descent minimization algorithm. Velocity was generated using a V-rescale thermostat,48 according to a Maxwell distribution at 310 K, with a short 200 ps run in the NVT ensemble. Position restraints were applied to the protein with a force constant of 1000 kJ mol−1, for the whole NVT run. The accurate leap-frog algorithm was used as the MD integrator for the whole dynamics using 0.002 fs as the time step for integration. Periodic boundary conditions were applied in all directions (pbc = XYZ). The LINCS algorithm was used to constrain the stretching of all bonds.

Electrostatic interactions were calculated applying the Particle Mesh Ewald (PME) algorithm and a cut-off at 1.2 nm.49 The same cut-off (1.2 nm) was also chosen for switching off the van der Waals potential. Changing the ensemble to the NPT one required an 8 ns equilibration run with the Parrinello–Rahman algorithm for pressure coupling under isotropic conditions and V-rescale was still used for temperature coupling. MD analysis was mostly performed using Pymol[331] and CHIMERA[323]. We used a similar approach to the docking as described in the protein-protein interaction of human glyoxalase II paper[332].

3.3.17 Structure and sequence alignment

Sequence alignment was completed with T-Coffee[333]. Structural alignment was completed with UCSF ChimeraX[334], with structures downloaded from PDB for *H. sapiens* haemoglobin b[335] and *D. melanogaster* globin 1[336].

3.4 Results

3.4.1 Co-immunoprecipitation of haemoglobin with ATP synthase and IF1

We first sought to understand the different interaction partners of haemoglobin that are found within the mitochondria through immunoprecipitation studies. A previous immunogold labelling transmission electron microscopy study has shown haemoglobin to be present in proximity to the inner mitochondrial membrane, and its presence was detected by Western blot of the inner mitochondrial membrane subfraction. Others suggest that its presence within certain cell types is physiologically linked to oxidative phosphorylation, and we used anti-ATP5A antibodies to co-immunoprecipitate proteins from homogenised Notothenioid liver tissue lysates. Label-free mass spectrometry analysis of the eluted fractions showed that haemoglobin subunits were precipitated in the red-blooded Notothenioid species N. rossii and T. bernacchii (**Table 3.1**). We then investigated this potential interaction in mammals (rats) and observed that haemoglobin beta co-immunoprecipitated with anti-ATP5A antibodies, which were incubated with mitochondria isolated from rat liver tissue (**Table 3.1, Supplementary Figure 1.1**).

***Table 3.1 - Co-immunoprecipitation of haemoglobin and ATP synthase proteins**. Haemoglobin subunits co-immunoprecipitate with ATP synthase subunit a in rat liver lysates and notothenioid liver lysates. Haemoglobin a co-immunoprecipitates with IF1 in notothenioid liver lysates. Multiple ATP subunits immunoprecipitate with haemoglobin in D. melanogaster.*

Purification method	**Antibody**	**Sample**	**Detection method**	**Identified proteins**
Dynabeads™ Co-Immunoprecipitation Kit	Anti-ATP5A	Rat liver lysate	Western Blot	Haemoglobin beta
		Notothenioid liver lysate	Label-free mass spectrometry	Haemoglobin alpha, haemoglobin beta
	Anti-IF1	Notothenioid liver lysate	Western Blot	Haemoglobin alpha
Invitrogen™ Dynabeads™ Protein G Immunoprecipitation Kit	Anti-HbB	Drosophila mitochondria	MALDI-TOF/MS	ATP synthase subunit alpha, ATP synthase subunit beta, ADP/ATP carrier protein, ATP synthase subunit d, ATP synthase subunit gamma, ATP synthase subunit b, putative ATP synthase subunit f

To confirm whether this interaction was also conserved in non-vertebrates that express haemoglobin, we used an anti-haemoglobin beta antibody in a co-immunoprecipitation reaction with mitochondria isolated from D.

melanogaster. MALDI-TOF/MS analysis of the co-immunoprecipitation elution revealed that several ATP synthase proteins, as well as the ADP/ATP carrier protein, immunoprecipitated with the anti-HbB antibody (**Table 3.1**). Based upon structural and sequence alignment analyses (**Supplementary Figure 1.1**), as well as the highly limited tissue- and sex-specific ex-pression of Glob2 and Glob3 in D. melanogaster, we concluded that the anti-HbB antibody was binding to Glob1.

3.4.2 In silico interaction between ATPIF1 and haemoglobin α2β2

IF1 has previously been reported to regulate haem synthesis[126], and thus haemoglobin levels, so we sought to investigate any potential interaction between the two proteins. As haemoglobin alpha immunoprecipitated with anti-IF1 in red-blooded notothenioid liver tissue (**Table 3.1**), we modelled the potential physical interaction between mitochondrial haemoglobin and IF1 through simulating molecular docking interactions (using a combination of Patchdock and then Firedock for refinement).

Table 3.2 contains the geometric score, interface area size and normalised desolvation energy from PatchDock, and subsequent FireDock refinement for the docking of IF1 with tetrameric haemoglobin. The tetrameric haemoglobin docking simulation used a minimised structure of haemoglobin with all chains and no ligands, and the docking simulation with haemoglobin alpha used chain C. The docking of the known haemoglobin inhibitor, Voxelotor, was also simulated with PatchDock to compare it to the docking with IF1.

Table 3.2 - Docking scores from PatchDock and FireDock for tetrameric haemoglobin and IF1. *Binding affinity (score) and binding energy (global energy) of the solution in kcal/mol, attractive and repulsive Van der Waals forces (kJ/mol) and atomic contact energy (kcal/mol).*

S. No. (FireDock)	Solution Number (PatchDock)	Global Energy (kcal/mol)	Attractive VdW (kcal/mol)	Repulsive VdW (kcal/mol)	ACE (kcal/mol)	Score	Area
1	8	-37.84	-27.85	13.77	3.13	11588	1356.50
2	3	-20.75	-18.22	6.18	2.50	11988	1706.30
3	34	-19.64	-33.34	24.33	10.24	10584	1428.20
4	25	-10.15	-28.12	15.34	6.04	10824	1323.70
5	43	-5.36	-37.07	30.53	18.52	10296	1449.80
6	31	-5.14	-27.18	7.12	12.45	10608	1849.70
7	2	-3.89	-28.98	7.95	5.50	12304	1659.30
8	5	-2.64	-18.48	2.52	6.48	11966	1606.50

For docking the IF1 monomer to haemoglobin tetramer, we chose 50 docking conformations ranked based on their PatchDock scores and then submitted these to Firedock refinement. The top ten were selected based on global energy (**Supplementary Figure 1.2**). After assessing the structures using Ramachandran plot to validate the docking pose, we chose FireDock solution number 1 (solution 8 of PatchDock), this conformation had high global energy, attractive van der Waals and low repulsive van der Waals (**Table 3.2**).

The possible interaction of monomeric IF1 with tetrameric haemoglobin, according to PatchDock solution 8 was assessed, with all simulations at a constant pH of 7.4 (**Figure 3.1**). The energy stable computational structures produced by PatchDock showed residues 35-60 of IF1 interacting with tetrameric haemoglobin residues.

Figure 3.1 – Molecular docking of IF1 and tetrameric haemoglobin, and a visualisation of interacting residues. *A) docking of tetrameric haemoglobin (red) with a single chain of IF1;* ***B****) the interacting residues of IF1 in haemoglobin docking simulation;* ***C****) schematic representation of interacting residues between haemoglobin chain A and IF1 chain;* ***D****) positioning of IF1 in proximity to interacting haemoglobin chains A and C, where different coloured lines represent different interactions between amino acids, specifically: red—salt bridges, yellow—disulphide bonds, blue—hydrogen bonds, and orange—non-bonded contacts;* ***E****) schematic representation of the interacting residues between haemoglobin chain C and IF1 chain.*

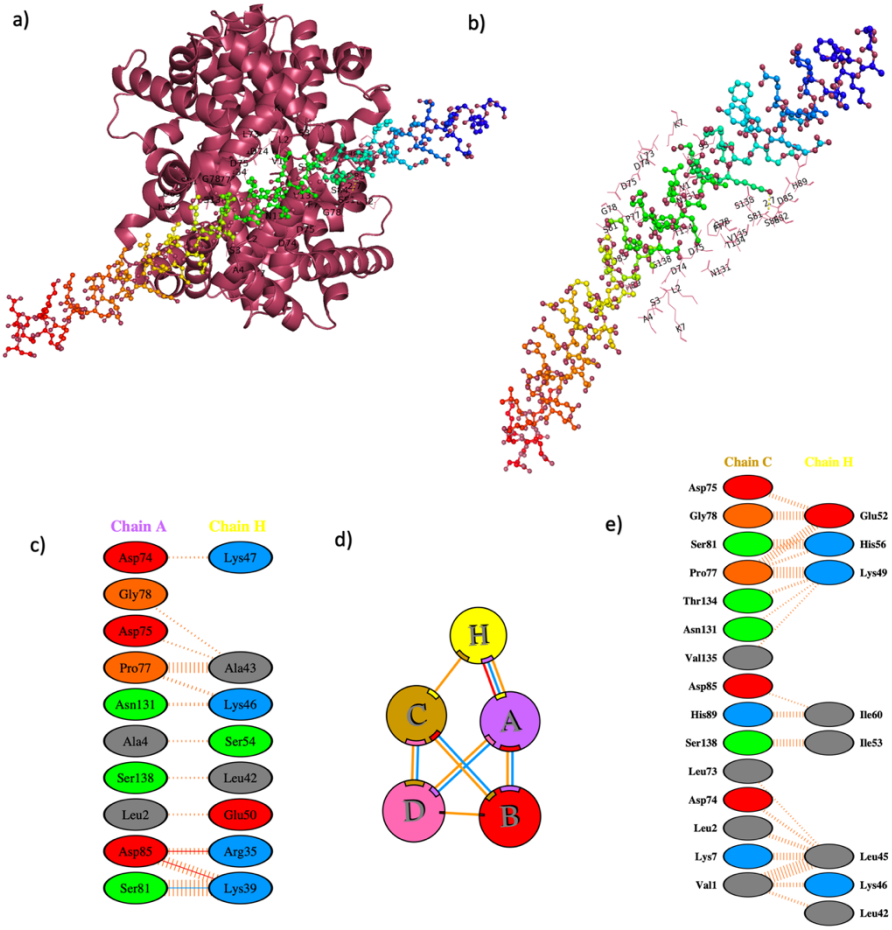

3.4.3 In silico interaction between IF1 and haemoglobin α

When docking only the alpha globin peptide of haemoglobin (Chain C) with IF1 (Chain A) (**Table 3.3**), it showed two polar contacts between the two molecules (5 Å); between residues Glu66 of IF1 protein and Lys99 of haemoglobin α (bond length 2.7 Å), and between His56 of IF1 and Ser138 of haemoglobin α (bond length 3.5 Å) (**Figure 3.2**). The isolated haemoglobin alpha chain interacted with residues 52-74 (C-terminal end) of IF1. The interacting residues common to both haemoglobin $\alpha_2\beta_2$ and haemoglobin α were Val1, Leu2, Asn131, Thr134, Thr137, Ser 138 (**Supplementary Table 1.1**). This interaction was confirmed experimentally by co-immunoprecipitation of haemoglobin α with IF1 in *N. rossii* (**Table 3.1**).

Table 3.3 - Docking scores from PatchDock and FireDock for monomeric haemoglobin alpha and IF1. Binding affinity (score) and binding energy (global energy) of the solution in kcal/mol, attractive and repulsive Van der Waals forces (kJ/mol) and atomic contact energy (kcal/mol).

S. No. (FireDock)	Solution Number (PatchDock)	Global Energy (kcal/mol)	Attractive VdW (kcal/mol)	Repulsive VdW (kcal/mol)	ACE (kcal/mol)	Score	Area
1	30	-27.01	29.93	11.49	7.74	8696	1125.90
2	19	-16.10	-25.88	13.35	11.48	8852	1081.70
3	44	-15.84	-28.74	26.23	5.54	8340	1267.10
4	15	-12.18	-29.70	13.98	8.57	9022	1087.50
5	38	-8.08	-18.35	14.55	5.09	8464	1444.70
6	7	-6.67	-33.25	18.06	15.48	9368	1154.40
7	11	-4.14	-6.10	2.72	4.76	9132	1123.70
8	25	-0.54	-26.40	13.84	10.61	8814	1202.00
9	36	-0.33	-19.90	7.34	4.43	8502	1368.90

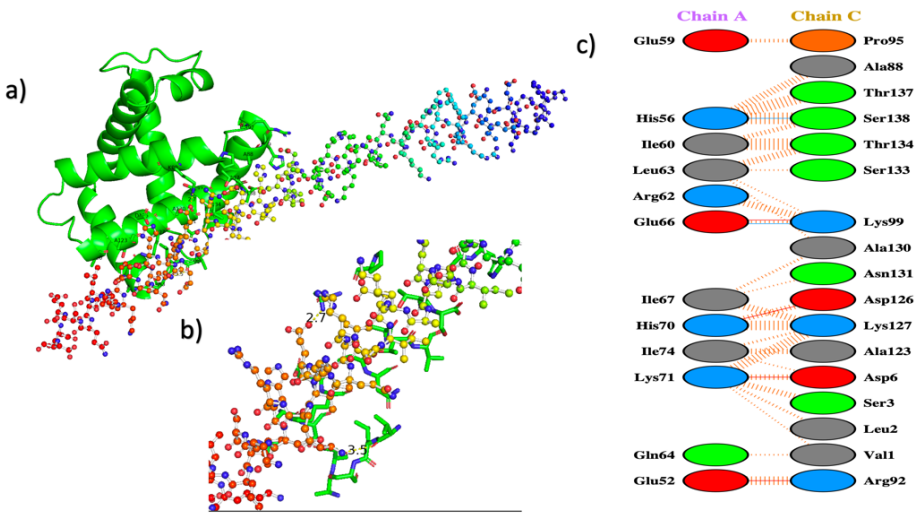

Figure 3.2 – Molecular docking of IF1 and monomeric haemoglobin alpha, and a visualisation of interacting residues. *A) docking of monomeric haemoglobin alpha (green) with a single chain of IF1;* ***B****) the monomeric haemoglobin alpha interaction site of IF1 chain;* ***C****) schematic representation of the interacting residues between monomeric haemoglobin alpha and IF1.*

3.4.4 Molecular docking simulation of IF1 and haemoglobin α2β2

The best docked conformation for haemoglobin $\alpha_2\beta_2$ was chosen according to the global energy of the docked compound (**Table 3.2**), and a molecular docking interaction was simulated (**Figure 3.3**). The docked protein was prepared creating a topology file that contains all the information of the structure, and AMBER99SB-ILDN (Lindorff-Larsen) forcefield was applied on the complex[337].

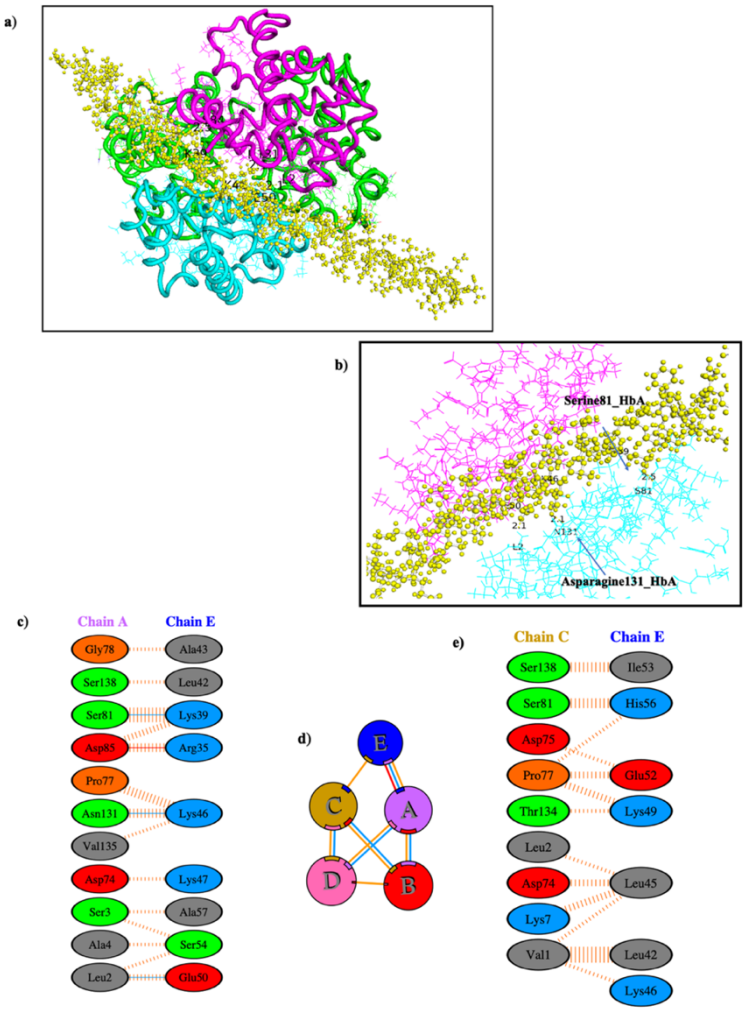

Figure 3.3 - Hb-IF1 association after 8 ns MD simulation. ***A)*** *IF1 docked in the cleft of two alpha chains of Hb (Pink- Chain A, light blue- Chain C, yellow-IF1);* ***B)*** *Shows interaction of Hb residues with IF1 residues - Serine 84 and Asparagine 131 of HbA. Interacting residues;* ***C)*** *Schematic representation of interacting residues between tetrameric haemoglobin chain A and ATPIF1 after 8 ns MD simulation ;* ***D)*** *Positioning of IF1 in proximity to interacting haemoglobin chains A and C after 8 ns MD simulation, where different coloured lines represent different interactions between amino acids, specifically: red—salt bridges, yellow—disulphide bonds, blue—hydrogen bonds, and orange—non-bonded contacts;* ***E)*** *Schematic representation of interacting residues between tetrameric haemoglobin chain C and IF1 after 8 ns MD simulation.*

The system was equilibrated at 305K constant temperature, density, and pressure; the structure was relaxed using energy minimisation (**Supplementary Figure 1.3**). The quality of simulated structure was checked using root-mean-square deviation over the simulation time (8 ns) a common technique to verify the stability of MD simulation. The system was stable between 4 and 7 ns (**Figure 3.4**).

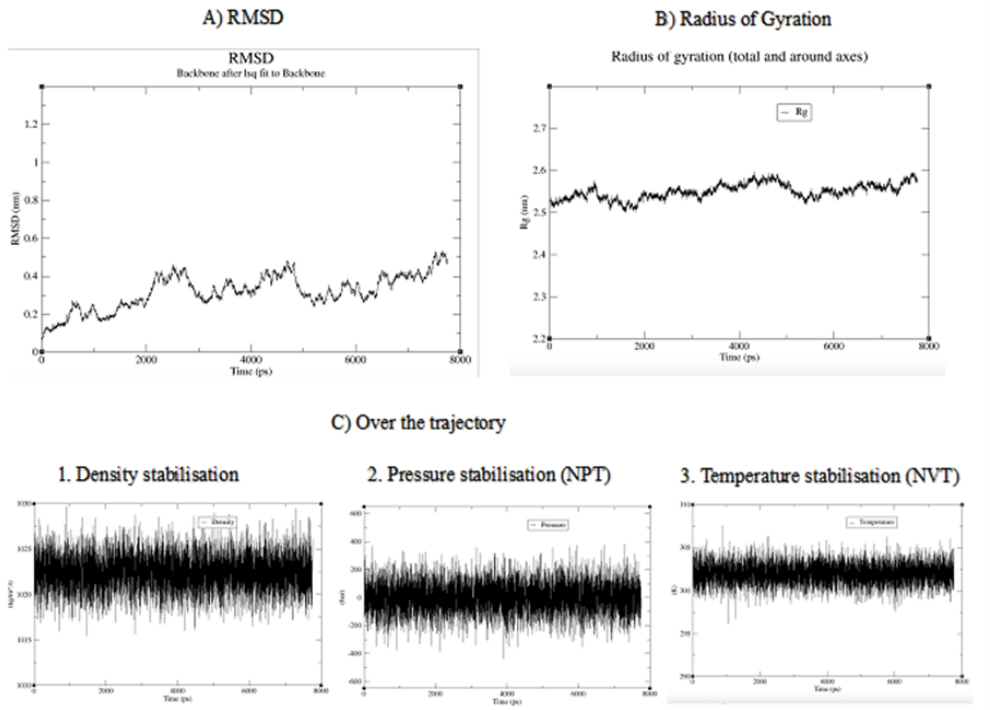

Figure 3.4 - Quantitative quality check for the MD run. *A) Root-mean-square deviation (RMSD);* ***B****) Radius of gyration shows a reasonable invariant Rg values across the MD run of 8 ns indicating the protein remains very stable;* ***C****) The thermodynamic factors of density, pressure and temperature are stable across the MD run.*

IF1 bound to haemoglobin after the MD simulation run of 8 ns (**Figure 3.4**). Most of the interactions that were present at the start of the MD simulation were observed at the end of the MD stabilisation (**Supplementary Table 1.1**). An additional hydrogen bond was seen between Asn131 and Lys46, with a measured distance of 2.1 Å. Ser81 of haemoglobin was seen to form a hydrogen bond with Lys39 both before and after MD stabilisation. Another polar contact was observed between Leu2 of haemoglobin with Glu50 of IF1, a measured distance of 2.1 Å.

3.4.5 Mitochondrial haemoglobin, ATP5A and ATPIF1 expression in rodents exposed to chronic hypoxia

As a previous study of non-erythroid haemoglobin linked its expression with mitochondrial function, via modulation of oxidative phosphorylation and oxygen homeostasis genes[155], we characterised the expression of mitochondrial haemoglobin subunits alpha and beta, ATP5A of the ATP synthase enzyme, and IF1, in response to hypoxia. The expression varied according to species, tissue type, and hypoxia conditions (**Figure 3.5, Supplementary Figure 1.4**). No significant changes in expression were observed in rat liver in response to hypoxia, while in mouse liver only IF1 showed a significant increase in expression in response to hypoxia. However, in mouse quadriceps muscle, haemoglobin alpha expression was only detected after exposure to hypoxia, haemoglobin beta expression was significantly increased above normoxic levels in response to hypoxia.

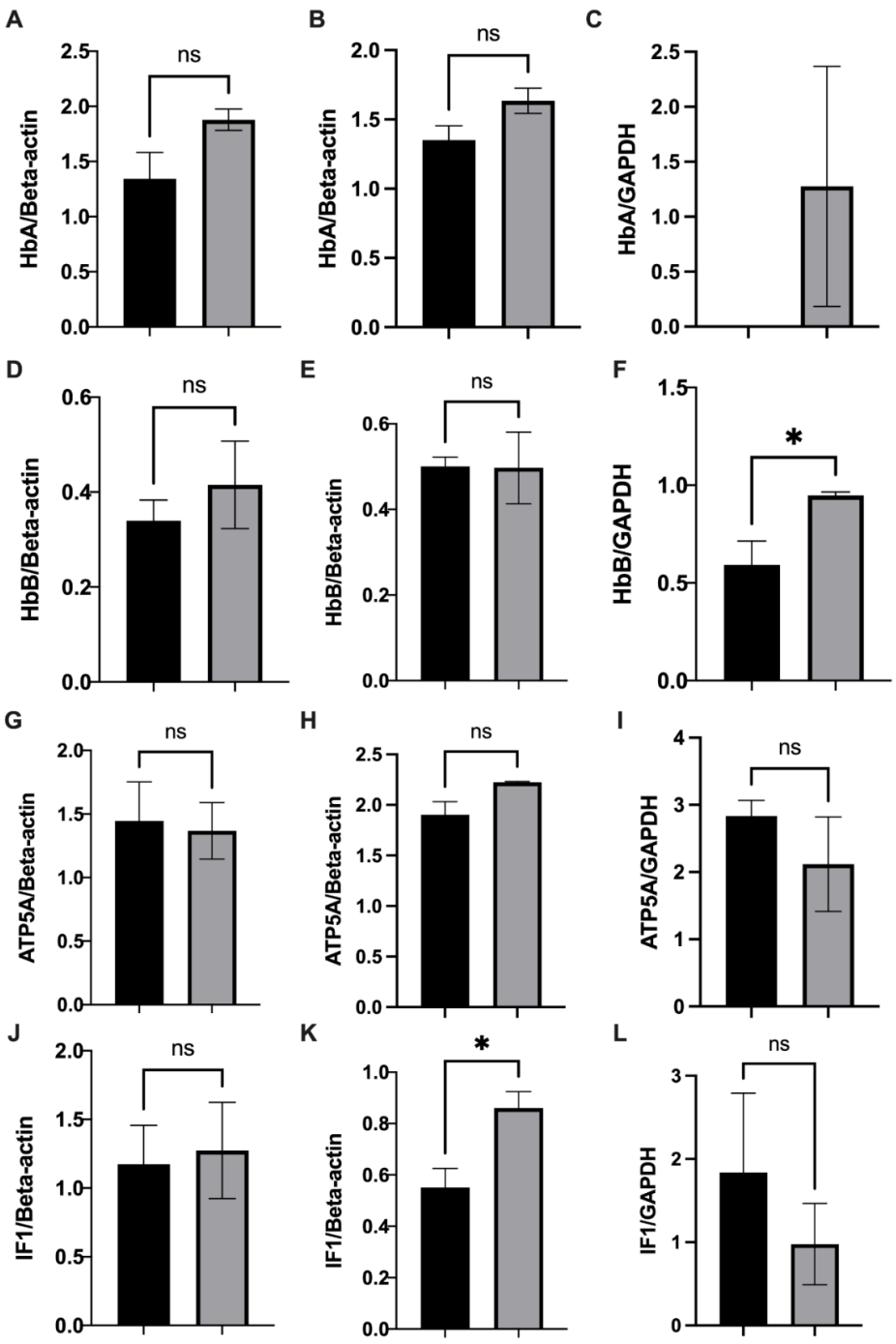

Figure 3.5 – Relative mitochondrial protein expression in normoxic (black) and hypoxic (grey) rat liver (A, D, G, J), mouse liver (B, E, H, K), and mouse quadriceps muscle (C, F, I, L). A-C) *haemoglobin a;* ***D-F)*** *haemoglobin b;* ***G-I)*** *ATP5A;* ***J-L)*** *ATPIF1. Liver mitochondria protein expression normalised to b-actin and quadriceps muscle mitochondria protein expression normalised to GAPDH (see* ***Supplementary Figure 1.4****). Data presented as mean with SEM, * $p < 0.05$, N=3, Student's unpaired t-test.*

3.4.6 Mitochondrial haemoglobin, ATP5A and ATPIF1 expression in D. melanogaster exposed to acute hypoxia cycles

To then investigate the impact of hypoxia on mitochondrial haemoglobin and the ATP synthase machinery in an invertebrate species, *D. melanogaster* were exposed to acute cycles of hypoxia and mitochondria were then isolated from them. The expression of their mitochondrial haemoglobin, ATP5A, and IF1 was measured (**Figure 3.6, Supplementary Figure 1.5**). After two cycles of hypoxia and recovery, mitochondrial haemoglobin, IF1 and ATP5A expression were found to be expressed at significantly higher levels.

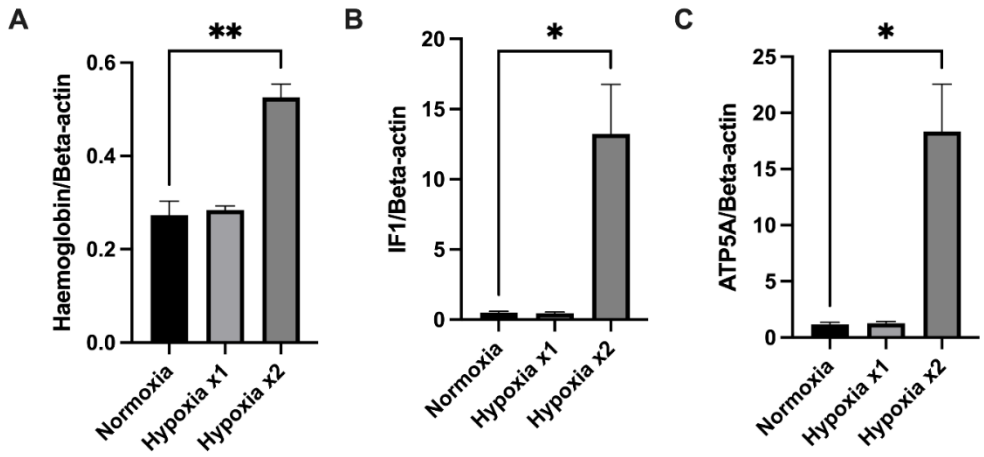

Figure 3.6 – Relative expression of mitochondrial proteins in normoxic and hypoxic D. melanogaster. ***A****) haemoglobin;* ***B****) ATPIF1;* ***C****) ATP5A. Protein expression normalised to b-actin (see* ***Supplementary Figure 1.5****). Data are presented as mean with SEM, * p < 0.05, ** p < 0.005, N=3, Student's unpaired t-test.*

3.4.7 HEPG2 cells treated with atractyloside show an increase in haemoglobin α and β expression

To investigate whether the dependence of mitochondrial haemoglobin expression was dependent on oxygen availability or ATP levels, HEPG2 cells were treated were for 24 hours with atractyloside, an inhibitor of the ADP/ATP translocase which causes a reduction in mitochondrial ATP synthesis. We observed an increase in the expression of both haemoglobin α and β subunits (**Figure 3.7, Supplementary Figure 1.6**).

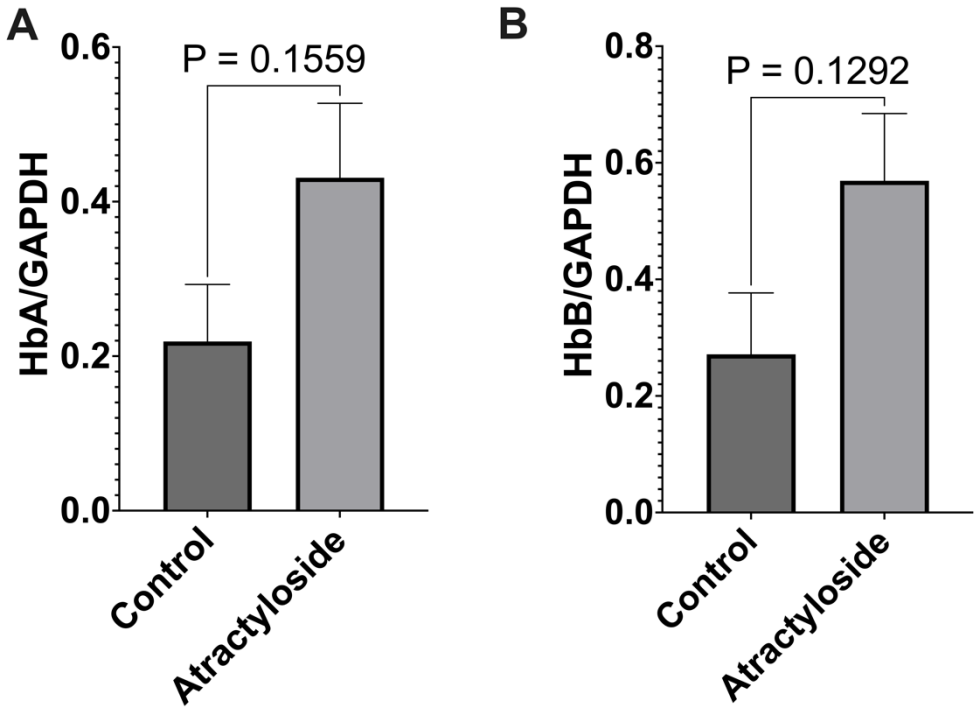

Figure 3.7 – Atractyloside treated HEPG2 cells show a trend toward increased expression of mitochondrial haemoglobin. ***A)*** *Relative expression of haemoglobin α in mitochondria isolated from atractyloside treated HEPG2 cells;* ***B)*** *Relative expression of haemoglobin β in mitochondria isolated from atractyloside treated HEPG2 cells. Data are presented as mean with SEM, N=3, student's unpaired t test.*

3.5 Discussion

3.5.1 Haemoglobin binds to ATP synthase and associated proteins

We have found evidence of interactions between mitochondrial haemoglobin and ATP synthase, ADP/ATP translocase and IF1 that are conserved across different species. Using *in silico* methods, we have described a binding interaction between haemoglobin and IF1. Our findings concur with previous observations of haemoglobin being localised to the inner mitochondrial membrane by Shephard *et al.*[160]. Also a co-immunoprecipitation reaction using an anti-haemoglobin beta antibody with total cell extracts from MS patient motor cortices pulled down ATP synthase subunits alpha and beta, ADP/ATP translocase 4, and the mitochondrial phosphate carrier[163]. Beyond binding to the ATP associated proteins of the mitochondria, the binding interaction of haemoglobin and organic phosphates (such as ATP and ADP) is a well characterised phenomenon[260,299–301].

3.5.2 ATP synthase activity and haemoglobin

A study of barley aleurone tissue investigated the effects of different respiratory inhibitors on whole cell haemoglobin expression, and found that in response to inhibitors that reduced oxygen consumption, as well as to uncouplers that increased oxygen consumption, haemoglobin expression was upregulated[261]. The authors suggested that haemoglobin expression was not directly responsive to oxygen usage, but to ATP availability in the tissue. To understand whether mitochondrial haemoglobin was subject to the same trend, we treated HEPG2 cells with atractyloside, an inhibitor of the ADP/ATP translocase that leads to reduced mitochondrial ATP synthesis. We observed in increase in the expression of mitochondrial haemoglobin α and β. Like the work of Nie *et al*., this suggests that the expression of mitochondrial haemoglobin could be responsive to ATP levels, not oxygen availability.

Previously, it has been reported that IF1 deficient zebrafish exhibit profound anaemia[126]. The absence of the IF1 allows for the reverse hydrolytic function

of ATP synthase to occur, increasing the pH within the mitochondrial matrix, which in turn causes the inhibition of the haem synthetic pathway enzyme ferrochelatase. The absence of haem leads to a reduced transcription of the globin genes, and thus anaemia. This suggests there is a potential mechanism for the modulation of haemoglobin synthesis in response to the bioenergetic state of the mitochondria.

Hypoxia is characterised by low ATP and acidosis, which alters mitochondrial structure and function[338–340]. Our observed localisation of mitochondrial haemoglobin to the ATP synthase machinery and associated proteins, suggests that the link between mitochondrial haemoglobin and ATP synthase may be involved in the hypoxia response.

3.5.3 Mitochondrial haemoglobin abundance is responsive to hypoxia

We observed that mitochondrial haemoglobin was upregulated in response to hypoxia in the skeletal muscle of mice and in *D. melanogaster*. Exercise leads to a drop in oxygen concentration in skeletal muscle[341,342], and thus hypoxia, and so we see a different specific response in skeletal muscle compared with the liver with hypoxia. The consistent expression levels of mitochondrial haemoglobin in the liver tissue in response to hypoxia might suggest that the hepatic mitochondrial hypoxia response does not require upregulated haemoglobin, perhaps due to other tissue-specific mechanisms[317]. *D. melanogaster* have a well-described tolerance to hypoxia[343,344], and the modulation of mitochondrial haemoglobin content appears to be a part of this response.

Functional studies of mitochondrial haemoglobin include the NO-consuming yeast flavohaemoglobin (YHb), where it has been reported that YHb is distributed between the cytosol and the mitochondria, whereas all of the YHb was located in the mitochondrial fraction of JM43 cells grown in anaerobic conditions[159]. A study of U937 cells treated with differing concentrations of haemoglobin found that intracellular haemoglobin co-localises with mitochondrial complex I, stimulates mitochondrial respiration, and led to

increased expression of HIF1a and Nrf2 mRNA[164]. Treatment of nigral dopaminergic neurons with the complex I inhibitor rotenone led to a significant decrease in haemoglobin a and b mRNA levels[157]. When viewed in the context of the data we report here, this would indicate that the presence of mitochondrial haemoglobin is not dependent upon electron transport chain activity.

3.6 Conclusion

The role of mitochondrial haemoglobin is not yet known, though there is a suggestion that it may provide a protective response against oxidative stress. We present evidence of the interaction between mitochondrial haemoglobin and ATP synthase proteins, as well as showing that it has a modulated expression in response to hypoxia. Moreover, our observations fit in with previously described mechanisms that have shown that hypoxia alters mitochondrial function via acidosis, also we provide evidence to support the link between haemoglobin expression and ATP availability. We have modelled a mechanism by which the IF1-regulated pH of the mitochondrial matrix regulates haemoglobin synthesis. The studies we present here directly link the activity of mitochondrial ATP synthase with the key protein for oxygen delivery in metazoans.

3.7 Author contributions

BE wrote the manuscript, completed *in vitro* experiments and analysed the data. GK co-wrote the manuscript, completed *in silico* experiments, and analysed the data. AD completed mass spectrometry experiments and analysis. CP and ML provided notothenioid expertise and samples. NM provided *D. melanogaster* expertise and samples. LC co-wrote the manuscript, provided all materials and facilities, and directed the research.

3.8 Funding

BE is funded by the Biotechnology and Biological Sciences Research Council (grant number BB/J014508/1). GK is supported by a University of Nottingham Vice Chancellor's International Scholarship award.

3.9 Acknowledgements

The York Centre of Excellence in Mass Spectrometry was created thanks to a major capital investment through Science City York, supported by Yorkshire Forward with funds from the Northern Way Initiative, and subsequent support from EPSRC (EP/K039660/1; EP/M028127/1).

We would like to thank Andrew Murray and his group (University of Cambridge, UK) for providing the rat and mouse tissue samples used for this study.

3.10 Appendix A: Chapter 3

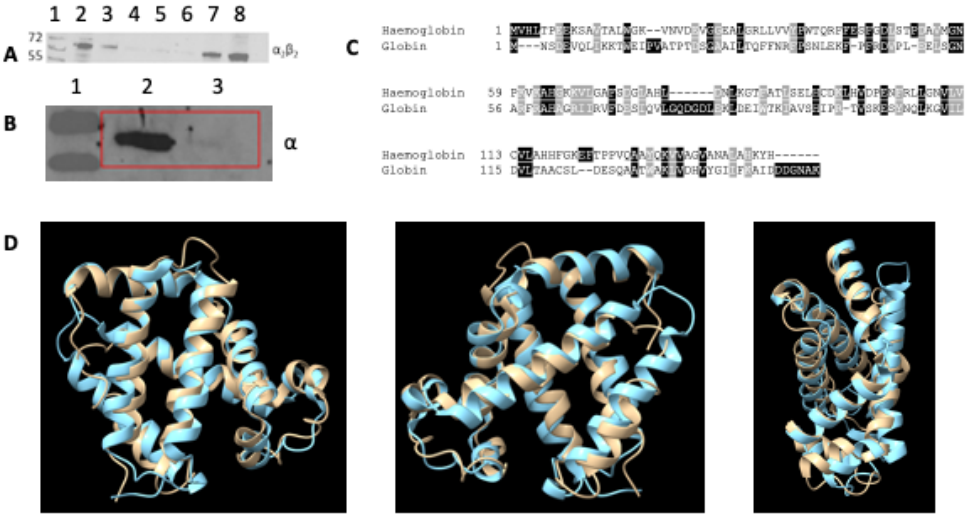

Supplementary Figure 1.1 *– A) Co-IP of haemoglobin subunits in rat liver, 1 = molecular weight marker, 2 = rat liver lysate, 3 = unbound lysate proteins, 4 = extraction buffer 1, 5 = extraction buffer 2, 6 = extraction buffer 3, 7 = last wash buffer, 8 = elution buffer; B) Co-IP of haemoglobin alpha in Notothenioids with ATPIF1, 1 = molecular weight marker, 2 = unbound lysate protein, 3 = elution buffer; C) Sequence homology of H. sapiens haemoglobin β and D. melanogaster globin 1; D) Structural alignment of H. sapiens haemoglobin β (brown) and D. melanogaster globin 1 (blue).*

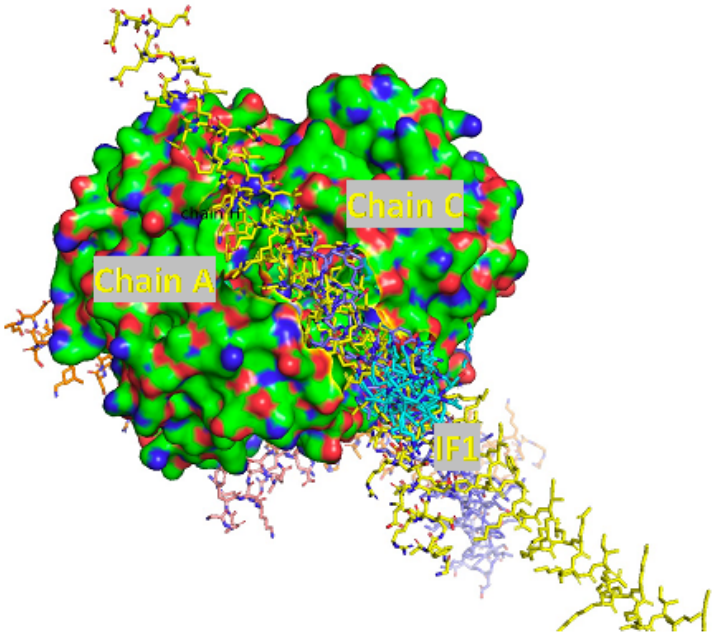

Supplementary Figure 1.2 *- Top 10 best ranked Docking results for Hb-all chains and IF1. Hb is represented by a molecular green surface, the IF1 structures are represented by different colours.*

Supplementary Table 1.1 *– IF1 interacting residues with Hb. The first part of the table shows residues interacting between IF1 and HbA, and IF1 and Hb all chains from the FireDock best docking pose. Second half of the table shows stable interacting residues that remained through the MD trajectory.*

Before simulation				
IF1	**HbA**	**Hb-all chains**		**IF1**
	Chain C	Chain A	Chain C	
Arg35		Asp85		Arg35
Lys39		Asp85, Ser81		Lys39
Leu42		Ser138	Val1	Leu42
Ala43		Gly78, Asp75, Pro77		Ala43
Leu45			Leu73, Asp74, Leu2, Lys7, Val1	Leu45
Lys46		Pro77, Asn131	Val1	Lys46
Lys47		Asp74		Lys47
Lys49			Pro77, Thr134, Asn131, Val135	Lys49
Glu50		Leu2		Glu50
Glu52	Arg92		Asp75, Gly78, Pro77	Glu52
Ile53			Ser138	Ile53
Ser54		Ala4		Ser54
His56	Ala88, Thr137, Ser138		Ser81, Pro77	His56
Ala57				Ala57
Glu59	Pro95			Glu59
Ile60	Thr134, Ser138		His89, Asp85	Ile60
Arg62	Lys99			Arg62
Leu63	Lys99, Thr134, Ser133, Ala130			Leu63
Gln64	Val1			Gln64
Glu66	Lys99			Glu66
Ile67	Ala130, Asn131, Lys127			Ile67
His70	Asp126, Lys127			His70
Lys71	Lys127, Asp6, Ser3, Leu2			Lys71
Ile74	Lys127, Ala123, Asp6			Ile74

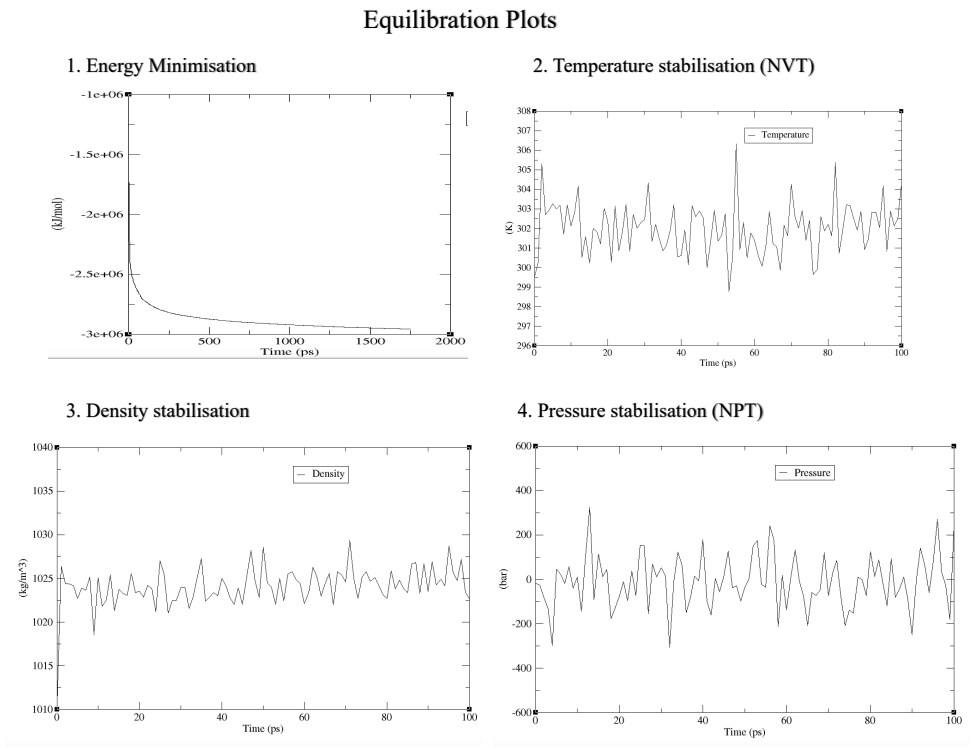

Supplementary Figure 1.3 *- MD Simulation for Hb and IF1. a) Energy Minimisation of the system, demonstrating a nice steady convergence of potential energy. b) Temperature equilibration (NVT), the plot shows that temperature ranges 302-306 K (average temperature 305 K). c) Pressure equilibration, the pressure fluctuates but in the expected range maintaining the average value. d) Density equilibration, the density plot is very close to the expected values and is stable over time.*

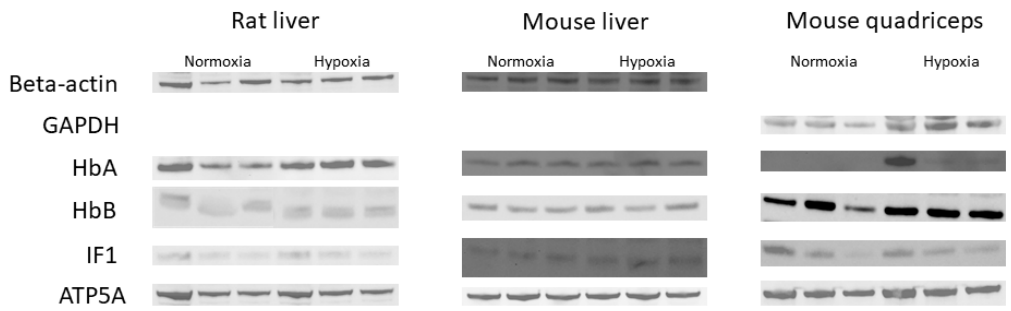

Supplementary Figure 1.4 *– Western blot relative expression bands for rodent hypoxia tissues (N=3). Beta actin is a loading control in rat liver mitochondria and mouse liver mitochondria samples, GAPDH is a loading control in mouse quadriceps mitochondria samples.*

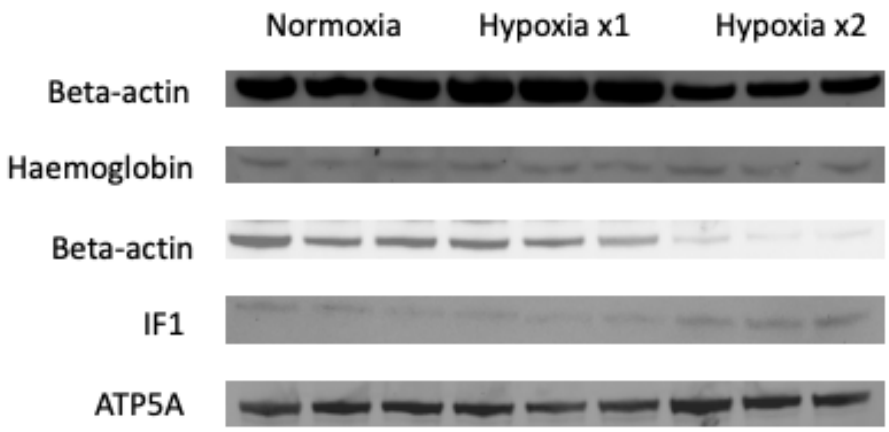

Supplementary Figure 1.5 *– Western blot relative expression bands for hypoxia exposed D. melanogaster mitochondrial isolates (N=3). Beta actin is a loading control.*

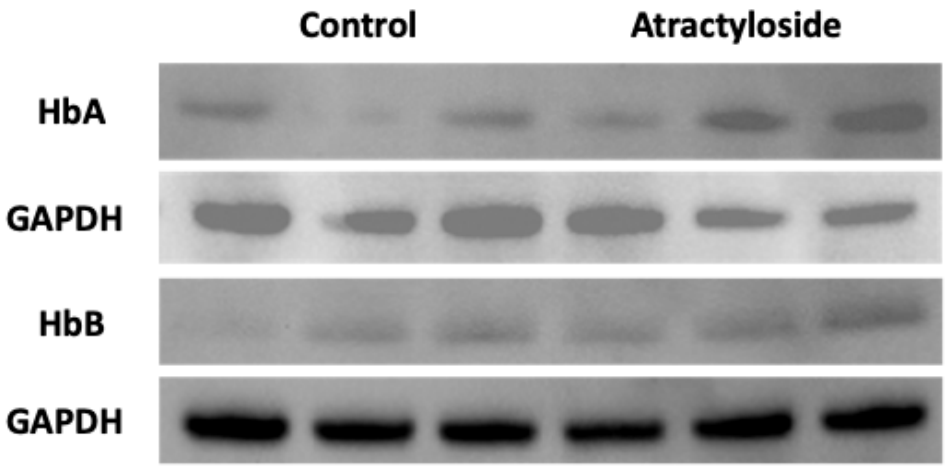

Supplementary Figure 1.6 – *Western blot relative expression bands for haemoglobin α, haemoglobin β, and GAPDH in mitochondria isolated from control and atractyloside treated HEPG2 cells.*

Ethics statement

Animal work was carried out in accordance with United Kingdom Home Office regulations under the Animals in Scientific Procedures Act, and underwent review by the University of Cambridge Animal Welfare and Ethical Review Committee. Procedures involving live animals were carried out by a license holder in accordance with these regulations.

This study was granted specific ethical approval by the School of Veterinary Medicine and Science Local Ethics Committee at the University of Nottingham.

4 Eccentric and concentric cycling induce alterations in the expression of mitochondrial structure-associated proteins in COPD skeletal muscle

Brad Ebanks*[1], Adam Dowle[2], Thomas Ward[3,4,5], Martin Lindley[5,6], Reinhard Stoeger[7], Lisa Chakrabarti[1,8]

This manuscript is currently undergoing peer review.

[1] School of Veterinary Medicine and Science, University of Nottingham, Nottingham, UK
[2] Department of Biology, Bioscience Technology Facility, University of York, York, UK
[3] Centre for Exercise & Rehabilitation Science, Leicester Biomedical Research Centre-Respiratory, Glenfield Hospital, Leicester, UK
[4] Department of Respiratory Medicine, Glenfield Hospital, University Hospitals of Leicester NHS Trust, Leicester, UK
[5] National Centre for Sport and Exercise Medicine, Loughborough University, Loughborough, UK
[6] Translational Chemical Biology Research Group, SSHES, Loughborough University, Loughborough, UK
[7] School of Biosciences, Sutton Bonington Campus, University of Nottingham, Loughborough, UK
[8] MRC Versus Arthritis Centre for Musculoskeletal Ageing Research, UK

4.1 Abstract

Chronic obstructive pulmonary disease (COPD) is an inflammatory lung condition that is characterised by obstructed airflow from the lungs. Around 390 million people are affected across the globe, with exposure to environmental tobacco smoke being the greatest risk factor. While it is described as a chronic disease, complications can lead to acute respiratory failure. Different types of physical exercise may have a potential therapeutic benefit, but COPD can coincidentally limit such activities in affected people. Here we explore differences that eccentric and concentric cycling induce in the proteome of mitochondria isolated from skeletal muscle of COPD individuals. We report changes in the abundance of proteins that have been associated with mitochondrial ultrastructure and morphology, with some sex-specific changes, while others are common to both male and female participants. As the changes in protein expression that we observe are distinct between the two different types of cycling, and there are more proteins with significantly altered abundance in response to both types of exercise in males, this should be considered carefully for studies of exercise in COPD.

4.2 Introduction

Chronic obstructive pulmonary disease (COPD) is a global disease that is estimated to impact 10.3% of people aged 30 to 79 years old, which amounts to over 390 million people[221]. The 2022 report published by the Global Initiative for Chronic Obstructive Lung Disease (GOLD) define COPD as a "common, preventable, and treatable disease that is characterized by persistent respiratory symptoms and airflow limitation"[345]. The most significant risk factor for COPD is exposure to environmental tobacco smoke[222]. The major pathophysiology of COPD is the narrowing of the bronchioles in the lungs, due to inflammation and fibrosis, resulting in impaired airflow and gas exchange[346]. The impaired airflow leads to the characteristic symptom of dyspnoea, while acute respiratory failure is a common event associated with severe exacerbation of the disease[230].

Hypoxia of the alveoli in the lungs is understood to contribute to the hypoxemia observed in COPD patients[231], which has been suggested to contribute to the muscle dysfunction and wasting observed in COPD[347]. This is significant with respect to bioenergetic function of the mitochondria, as it is dependent upon the availability of molecular oxygen for ATP production by oxidative phosphorylation. COPD patients with a low BMI have reduced respiratory chain function in the vastus lateralis when compared with COPD patients with a normal BMI, as well as healthy control trial participants[238]. Rabinovich and colleagues speculate that this could be associated with abnormal mitochondrial adaptation to episodes of cell hypoxia. Mitochondrial oxygen consumption and ATP production in state 3 respiration were both decreased in the vastus lateralis and the external intercostalis of mild to moderate COPD patients undergoing surgery for lung cancer, while cytochrome c oxidase activity showed a significant negative relationship with arterial oxygen tension[239].

Beyond respiratory enzyme activity, other COPD-associated perturbations have been reported in mitochondrial function. This includes increased levels of uncoupling protein 3 (UCP3) transcription[238], increased ROS in both skeletal muscle and bronchial tissue[236,239], decreased mitochondrial membrane potential

in bronchial tissue of Global Initiative For Chronic Obstructive Lung Disease (GOLD) grade 2 COPD patient bronchial tissue, and decreased expression of respiratory complex proteins in the bronchial tissue mitochondria of both GOLD grade 2 COPD patients and GOLD grade 3/4 skeletal muscle mitochondria[236]. The role of the inner mitochondrial fusion protein OPA1 has also been studied with respect to the pathophysiology of COPD; short OPA1 isoforms maintain mitochondrial bioenergetic function and cristae structure and appear to be significantly elevated in COPD patient lung tissue[234,348].

While COPD limits the capacity for exercise of those living with the disease[349], exercise therapy has long been considered for both physical and psychosocial wellbeing of patients with this condition[350]. Contemporary studies with exercise regimes that have a low cardiorespiratory demand also demonstrate the benefits of exercise as a therapeutic intervention for COPD[351]. The effectiveness of exercise therapy for other chronic respiratory diseases, including for both cystic fibrosis and asthma in children, has also been reviewed [352]. However, changes to molecular physiology associated with improved skeletal muscle function in response to exercise remains largely undefined in individuals with respiratory disease, and COPD in particular.

Muscle contraction can either be isometric, where length does not change during contraction, or isotonic, where muscle can become either shorter or longer while tension is constant[353]. Isotonic contraction can either be defined as concentric, where muscle becomes shorter while producing force, or eccentric, when it becomes longer. As eccentric cycling has been shown to have a lower cardiopulmonary demand than concentric exercise when mechanical loads are matched[354], studies have sought to understand the safety of this form of exercise for COPD patients, who suffer from muscle weakness and lower ventilation capacity[355].

Due to the description of eccentric exercise as having the highest forces with the lowest energy requirement[356], when compared with concentric exercise, studies have sought to understand the impact of eccentric exercise on mitochondria in both animal and human. The results have been mixed, where mitochondrial calcium content has been shown to be elevated, which leads to

increased mitochondrial permeability transition pore (MPTP) sensitivity[357]. However other aspects of mitochondrial physiology remain unaltered, including respiratory chain activity of skeletal muscle from participants with COPD[358], despite suggestions that the high levels of muscle damage associated with eccentric exercise might lead to significant changes[359]. This is in comparison to the impact of concentric exercise on mitochondrial physiology, where a study of rats found that 20 days of concentric exercise training increased maximal respiration in gastrocnemius and soleus muscles but eccentric training did not, and eccentric training caused an increase in H_2O_2 output in vastus intermedius muscle[360].

Proteomic profiling has been used in studies of COPD, both to develop a deeper understanding of the pathophysiological changes in disease relevant tissues[361–363], and as a potential diagnostic tool from minimally invasive sample collection procedures[364]. The mitochondrial proteome has also been widely studied across a range of model organisms[82,84,365,366], as well as different states of human health and disease[83,367,368]. Contemporary methods of label-free mass spectrometry are increasingly used for quantitative proteomic studies in place of more expensive and often time-consuming sample labelling methods[275]. Orbitrap technology has been widely adopted in proteomic studies since the early 2000s and has allowed for high-sensitivity, high-resolution studies of biological samples[369,370]. The acquired datasets can be analysed downstream using bioinformatics tools such as STRING-db and KEGG, offering novel biological insights based on the proteomic profile of the sample in question[259,371]. These bioinformatics data can then be pursued further by classical molecular biology and biochemical experimentation.

Here we sought to study potential changes in the physiology of skeletal muscle mitochondria in response to cycling, and to quantify any potential differences in response to i) eccentric or concentric exercise, and ii) sex of the participant. Label-free mass spectrometry and western blot were used to study the proteome of isolated mitochondria. Additional biochemical assays, including ATPase activity and lipid peroxidation (MDA), were employed to characterise change in response to the exercise.

4.3 Methods

4.3.1 COPD patient exercise and tissue sampling

COPD patient quadriceps biopsy samples were used in a previous study[351]. The protocol was approved by the Leicestershire South Regional Ethics Committee (Identifier: IRAS 214536). All participants gave informed written consent before taking part. Separate informed written consent was obtained for biopsy sampling.

In brief, participants performed 20-minute bouts of eccentric and concentric exercise at 65% peak workload. Biopsies were obtained at rest and 60 s after exercise cessation from incisions at least 2 cm apart. Biopsies for eccentric exercise and concentric exercise were obtained from opposite legs. Approximately 100 mg of tissue was removed under local anaesthetic using the modified Bergstrom technique. Tissue was frozen immediately in liquid nitrogen and stored at -80°C until analysis.

4.3.2 Mitochondrial isolation

Mitochondria were isolated from 25 mg of tissue per biopsy sample via differential centrifugation, using previously described methods[160]. Male and female samples for pre- and post-exercise condition were chosen (N=3 biological replicates, 24 samples in total). In brief, tissue was lysed in mitochondrial isolation buffer with a Dounce homogeniser. The lysate was centrifuged at 850 g for 10 mins to remove insoluble material. The supernatant was centrifuged at 1050 g for 10 mins, and the supernatant collected before centrifugation at 10,000 g for 15 mins to generate the mitochondrial pellet, and subsequent supernatant was discarded.

4.3.3 SDS-PAGE

The mitochondrial pellet generated from each 25 mg tissue sample was subject to SDS-PAGE. The pellet was resuspended in 5 µL PBS, 3 µL DTT, and 3 µL LDS. The resuspended sample was loaded onto polyacrylamide pre-cast gels (NuPAGE™ 4 to 12%, Bis-Tris, 1.0 mm, Mini Protein Gel, 12-well). A fixed voltage (200 V) was applied to the gel until the dye front reached 2 cm into the gel and the gel was then stained with ProtoBlue Safe Coomassie G-250. The gels were de-stained with deionised water, and stained protein bands were excised from the gel and added to 1.5 mL microfuge tubes.

4.3.4 Label-free mass spectrometry

The mitochondrial protein samples were sent to the Centre of Excellence for Mass Spectrometry at the University of York for analysis. Protein was in-gel digested overnight at 37ºC with 0.2 □g sequencing grade trypsin and Lys-C protease mixture (Promega V5073), following reduction 10 mM dithioerythritol and *S*-carbamidomethylation with 50 mM iodoacetamide.

Extracted peptides were loaded onto an mClass nanoflow UPLC system (Waters) equipped with a nanoEaze M/Z Symmetry 100 Å C_{18}, 5 µm trap column (180 µm x 20 mm, Waters) and a PepMap, 2 µm, 100 Å, C_{18} EasyNano nanocapillary column (75 µm x 500 mm, Thermo). The trap wash solvent was aqueous 0.05% (v:v) trifluoroacetic acid and the trapping flow rate was 15 µL/min. The trap was washed for 5 min before switching flow to the capillary column. Separation used gradient elution of two solvents: solvent A, aqueous 0.1% (v:v) formic acid; solvent B, acetonitrile containing 0.1% (v:v) formic acid. The flow rate for the capillary column was 330 nL/min and the column temperature was 40°C. The linear multi-step gradient profile was: 3-10% B over 7 mins, 10-35% B over 30 mins, 35-99% B over 5 mins and then proceeded to wash with 99% solvent B for 4 min. The column was returned to initial conditions and re-equilibrated for 15 min before subsequent injections.

The nanoLC system was interfaced with an Orbitrap Fusion Tribrid mass spectrometer (Thermo) with an EasyNano ionisation source (Thermo). Positive ESI-MS and MS^2 spectra were acquired using Xcalibur software (version 4.0,

Thermo). Instrument source settings were: ion spray voltage, 1,900 V; sweep gas, 0 Arb; ion transfer tube temperature; 275°C. MS^1 spectra were acquired in the Orbitrap with: 120,000 resolution, scan range: *m/z* 375-1,500; AGC target, $4e^5$; max fill time, 100 ms. Data dependant acquisition was performed in top speed mode using a 1 s cycle, selecting the most intense precursors with charge states >1. Easy-IC was used for internal calibration. Dynamic exclusion was performed for 50 s post precursor selection and a minimum threshold for fragmentation was set at $5e^3$. MS^2 spectra were acquired in the linear ion trap with: scan rate, turbo; quadrupole isolation, 1.6 *m/z*; activation type, HCD; activation energy: 32%; AGC target, $5e^3$; first mass, 110 *m/z*; max fill time, 100 ms. Acquisitions were arranged by Xcalibur to inject ions for all available parallelizable time.

Peaklists in .raw format were loaded into PEAKS Studio X Pro (Version 10.6, Bioinformatics Solutions Inc.) for peptide identification and peak area-based label-free relative quantification. Database searching was performed against the human subset of the UniProt database (20476 sequences), specifying: Enzyme, trypsin; Max missed cleavages, 2; Fixed modifications, Carbamidomethyl (C); Variable modifications, Oxidation (M); Peptide tolerance, 3 ppm; MS/MS tolerance, 0.5 Da. Subsequent PEAKS-PTM searching was used to consider all Unimod listed modifications for PEAKS-DB identified proteins. Peptide identifications were filtered to 1% false discovery rate as assessed empirically against a decoy database. Protein quantification was performed using MS1 precursor ion areas following LC-MS chromatogram alignment. Protein quantifications were set to require a minimum of two unique peptides to be considered quantifiable. 727 proteins were accepted as quantifiable among samples. MS intensity was normalized between samples by total MS1 ion signal. An ANOVA comparison was applied for significance testing with the null hypothesis that proteins are of equal abundance between sample groups tested. The Hochberg and Benjamini multiple test correction was used to convert p-values to q-values. For pairwise comparisons multiple unpaired t tests were applied in GraphPad Prism.

4.3.5 Enrichment analysis and hierarchical clustering

Protein accession numbers were uploaded to STRING-db for enrichment analysis, and additional analysis of results was completed in GraphPad Prism. Hierarchical clustering analysis was completed using Morpheus (https://software.broadinstitute.org/morpheus). Data presented with average-linkage and one minus Pearson correlation distance.

4.3.6 ATPase assay

The ATPase activity of tissue lysates from patient tissue samples was measured using the ab234055 ATPase Assay Kit (Colorimetric), according to the manufacturer's instructions. Briefly, 10 mg of quadriceps tissue sample was homogenised with a Dounce homogeniser in ATPase assay buffer, before centrifugation (10,000 g, 4°C, 10 mins) to pellet insoluble material. Ammonium sulphate method was used to remove endogenous phosphate. Samples were added to a 96 well plate and activity was measured in endpoint mode at 650 nm.

4.3.7 Lipid peroxidation assay

The lipid peroxidation levels (malondialdehyde) of tissue samples was quantified using the Lipid Peroxidation (MDA) Assay Kit (ab118970) according to the manufacturer's instructions. Briefly, 10 mg of tissue was washed with cold PBS, homogenised in MDA Lysis Buffer with a Dounce homogeniser, then centrifuged (13,000 g, 4°C, 10 mins). The supernatants were mixed with thiobarbituric acid (TBA) that was suspended in glacial acetic acid, then incubated at 95°C (10 mins). Samples were added to a 96 well plate and MDA content was measured in endpoint mode at 532 nm.

4.3.8 Western Blot

The proteins within the gels were transferred to a nitrocellulose membrane at 30 V for 60 minutes. The membrane was blocked with 3% (w/v) milk powder in TBS-T for 60 minutes with gentle agitation (RT). The membranes were then probed overnight (18 hours, 4°C) with the primary antibody (anti-plectin, ab229467; anti-annexin 6, ab196942; anti-annexin 11, ab137424; anti-GLO2, ab154108; anti-ALDH4A1, ab181256), at a 1:5000 dilution in 3% (w/v) milk powder in TBS-T. The membrane was then washed three times with TBS-T before incubation with secondary antibody (goat anti-rabbit HRP conjugate, ab6721), at a 1:5000 dilution in 5% (w/v) milk powder in TBS-T. The membrane was again washed three times with TBS-T before a five-minute incubation with ECL substrate and chemiluminescence measurement. Band densities were measured using Image J and samples were normalised to appropriate loading controls[276].

Statistical analysis was performed using GraphPad Prism version 9.3.1.

4.3.9 P5cDH gene methylation

Pre-concentric and post-concentric exercise samples were assessed for methylation of the P5cDH encoding gene *ALDH4A1* by the Genome Centre (Blizard Institute, Queen Mary University of London). Briefly, DNA was extracted from the tissue using the Qiagen DNeasy Blood & Tissue kit. DNA was quantified with NanoDrop QC, and double stranded DNA was then quantified with Qubit 2.0 Fluorometer. Agilent 4200 Tapestation was then used to assess the quantity and quality of the extracted DNA.

Primers were designed to cover 500 bp upstream and 400 bp downstream of exon 1, *ALDH4A1* (chr1:18,901,960-18,902,956 997 bp). PCR optimisation was completed with Roche High-Fidelity PCR system. The amplified PCR products were barcoded and then validated with Agilent 4200 Tapestation. Bisulphite conversion of the DNA (200 – 500 ng) was completed with the

Zymo EZ DNA Methylation Kit, and samples quantified with the Roche High-Fidelity PCR System.

DNA pools were quantified with Qubit 2.0 Fluorometer and determination of average product size with Agilent 4200 Tapestation. Illumina MiSeq was used for DNA denaturation and loading before Illumina sequencing. Bismarck mapping was used to determine methylated and unmethylated DNA[372].

4.4 Results

4.4.1 Isolated mitochondrial fractions were enriched with mitochondrial proteins

We first confirmed that mitochondrial-enriched fractions had been analysed following our label-free mass spectrometry procedure. That is, we would expect a disproportionate number of mitochondrial proteins in the list of 'hits'. A cellular compartment (GO) enrichment analysis as performed (**Figure 4.1**) and the returned terms were ranked by lowest false discovery rate (FDR), and the five terms with the lowest FDR were then presented based on strength of the enrichment effect. The term 'Mitochondrion' was highly enriched in both the total protein list and in the list of proteins with significant variance (ANOVA) across the eight conditions (pre-/post-eccentric/concentric, male/female), indicating that mitochondrial enrichment was successful.

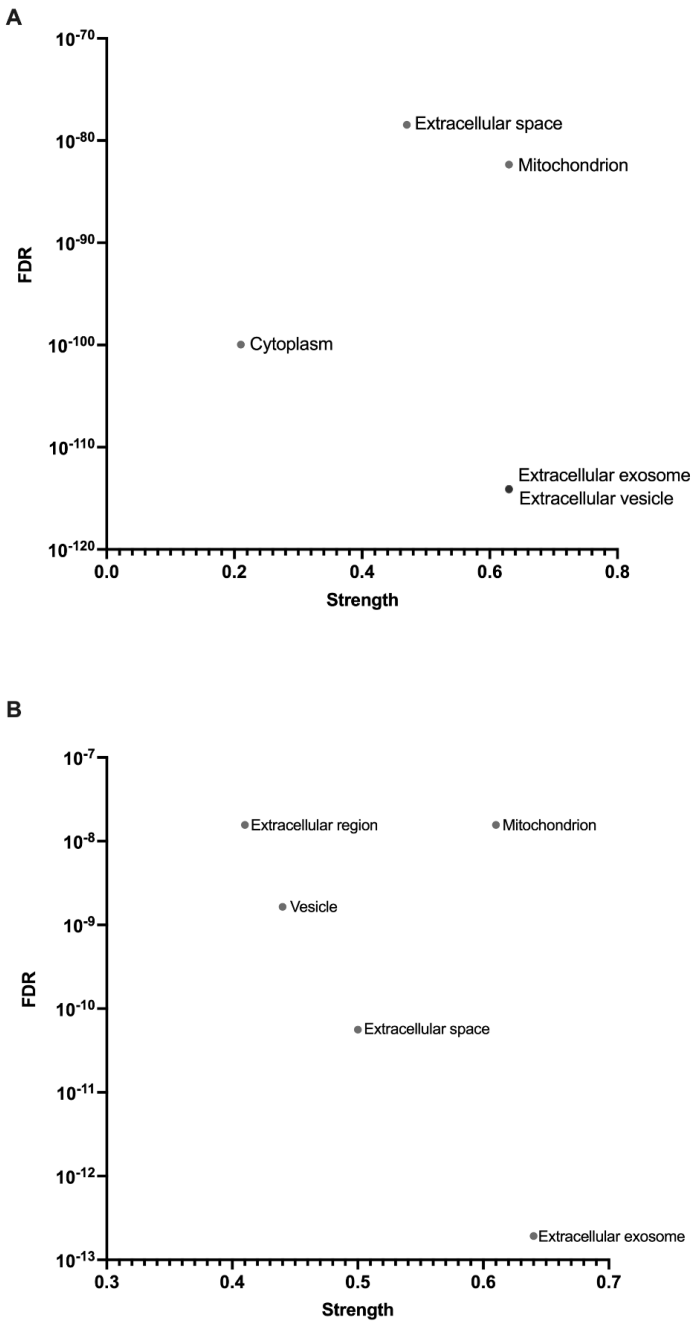

Figure 4.1 – Cellular compartment (GO) enriched terms for mitochondrial isolates. ***A)*** *Cellular compartment (GO) enriched terms for all proteins identified across both sexes and exercise conditions;* ***B)*** *all proteins with significant ANOVA variation identified across both sexes and conditions. Enrichment analysis in STRING-db. The five pathways with the lowest false discovery rates (FDR) are scored according to strength of the enrichment effect (Log10(observed/expected)).*

4.4.2 Changes to protein expression in response to concentric and eccentric exercise

Hierarchical clustering was then used to compare the individual samples of We then used hierarchical clustering to compare the individual samples of males and females for pre- and post- concentric and eccentric exercise (**Figure 4.2**). There were 36 proteins identified with significant changes in abundance across the four pairwise comparisons (**Table 4.1**).

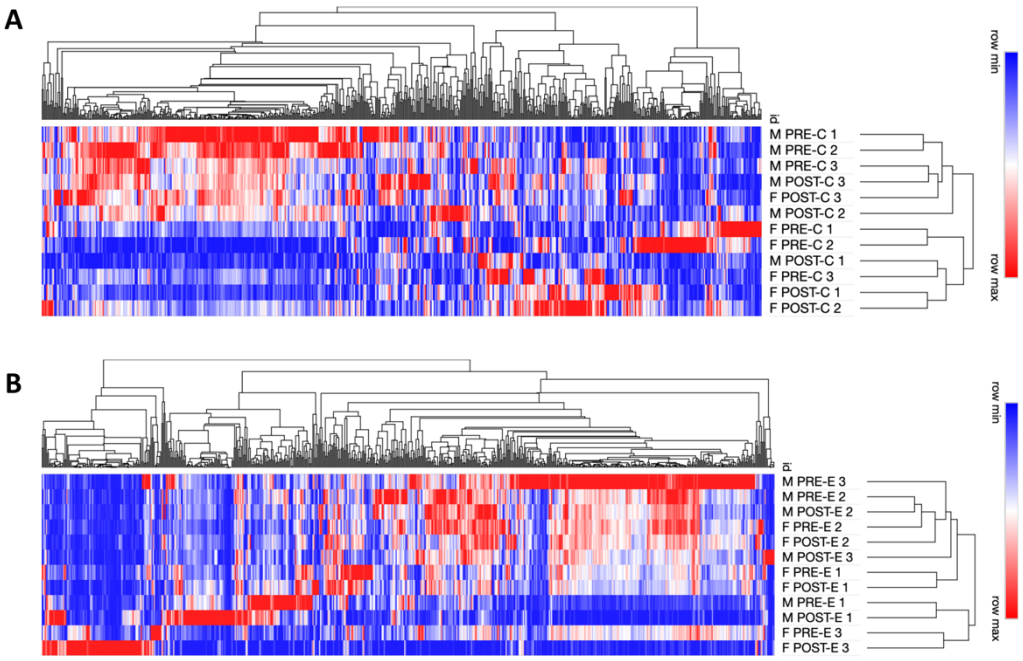

Figure 4.2– Hierarchical clustering heatmap of protein expression for concentric and eccentric exercise. *M = male, F = female, C = concentric, E = eccentric.* ***A)*** *Hierarchical clustering of identified protein expression in pre-concentric and post-concentric exercise for male and female participants, measured by relative peak areas;* ***B)*** *Hierarchical clustering of identified protein expression in pre-eccentric and post-eccentric exercise for male and female participants, measured by relative peak areas. Clustering performed with Morpheus (https://software.broadinstitute.org/morpheus), average linkage, one minus Pearson correlation. Red = increased expression, blue = decreased expression.*

In response to concentric exercise plectin expression was upregulated in both male and female participants, while annexin A11 was upregulated in males and annexin A6 was upregulated in females. Notable hits of canonical mitochondrial proteins identified as having altered expression in the mitochondrial fractions include MICOS complex subunit MIC27 and Delta-1-pyrroline-5-carboxylate dehydrogenase mitochondrial (P5cDH), also known as Aldehyde Dehydrogenase 4 Family Member A1 (ALDH4A1); levels for both of these proteins were decreased in male concentric exercise. Post-eccentric exercise, hydroxyacylglutathione hydrolase mitochondrial (HAGH) had upregulated expression in males, and MICOS complex subunit MIC13 had decreased expression in females.

Table 4.1 – Proteins with significantly altered expression in pairwise comparisons of concentric and eccentric exercise conditions for male and female participants. *18 proteins had altered abundance in response to concentric exercise in males, and 8 proteins had altered abundance in response to concentric exercise in females. 7 proteins had altered abundance in response to eccentric exercise in males, and 3 proteins had altered abundance in response to eccentric exercise in females. M= male, F = female. Mean values of relative peak areas, unpaired t test, * $P < 0.05$.*

Sex	Exercise condition	Protein	Fold change	P value
M	**Concentric**	Plectin	1.971	0.000
		60S ribosomal protein L7	0.099	0.002
		60S acidic ribosomal protein P0	0.370	0.010
		Peptidyl-prolyl cis-trans isomerase FKBP3	0.316	0.012
		60S acidic ribosomal protein P1	0.449	0.015
		Collagen alpha-1(I) chain	0.000	0.018

		Isochorismatase domain-containing protein 2	0.333	0.026
		Elongation factor 1-gamma	1.590	0.030
		60S ribosomal protein L6	0.250	0.032
		Vesicle-associated membrane protein-associated protein A	0.316	0.037
		60S ribosomal protein L18	0.253	0.038
		Protein cordon-bleu	0.394	0.038
		Elongation factor 1-delta	5.666	0.039
		MICOS complex subunit MIC27	0.515	0.042
		Delta-1-pyrroline-5-carboxylate dehydrogenase mitochondrial	0.375	0.042
		Annexin A11	3.166	0.045
		OCIA domain-containing protein 1	0.449	0.048
		Collagen alpha-2(I) chain	0.176	0.049
	Eccentric	Alpha-1-acid glycoprotein 1	3.166	0.012
		Calpain-1 catalytic subunit	0.578	0.015
		Cytosol aminopeptidase	0.282	0.024
		Hydroxyacylglutathione hydrolase mitochondrial	1.631	0.033
		Complement C4-B	0.408	0.033
		Myosin-9	0.429	0.043
		Kelch-like protein 41	0.597	0.046
F	**Concentric**	Collagen alpha-3(VI) chain	3.166	0.000
		Collagen alpha-1(VI) chain	4.263	0.013
		Alpha-1-syntrophin	3.949	0.022
		Myosin regulatory light chain 2 ventricular/cardiac muscle isoform	2.961	0.028
		Vitronectin	0.282	0.032

		Annexin A6	1.564	0.038
		Plectin	2.333	0.041
		Heat shock protein beta-7	2.667	0.049
	Eccentric	Ryanodine receptor 1	0.190	0.023
		MICOS complex subunit MIC13	0.000	0.033
		T-complex protein 1 subunit delta	0.754	0.049

We used western blot to confirm the proteomics results and measure the relative expression in additional samples that had not already been analysed by mass spectrometry. We measured plectin in eccentric exercise males and concentric exercise males and females, GLO2 in eccentric males, annexin A11 and P5cDH in concentric males, and annexin A6 in concentric females. The expression of P5cDH in concentric exercise males and plectin in concentric exercise females matched the trends observed within the mass spectrometry proteomic data (**Figure 4.3**), while heterogenous levels of expression relative to GAPDH were observed for the other proteins (**Supplementary Figure 2.1**).

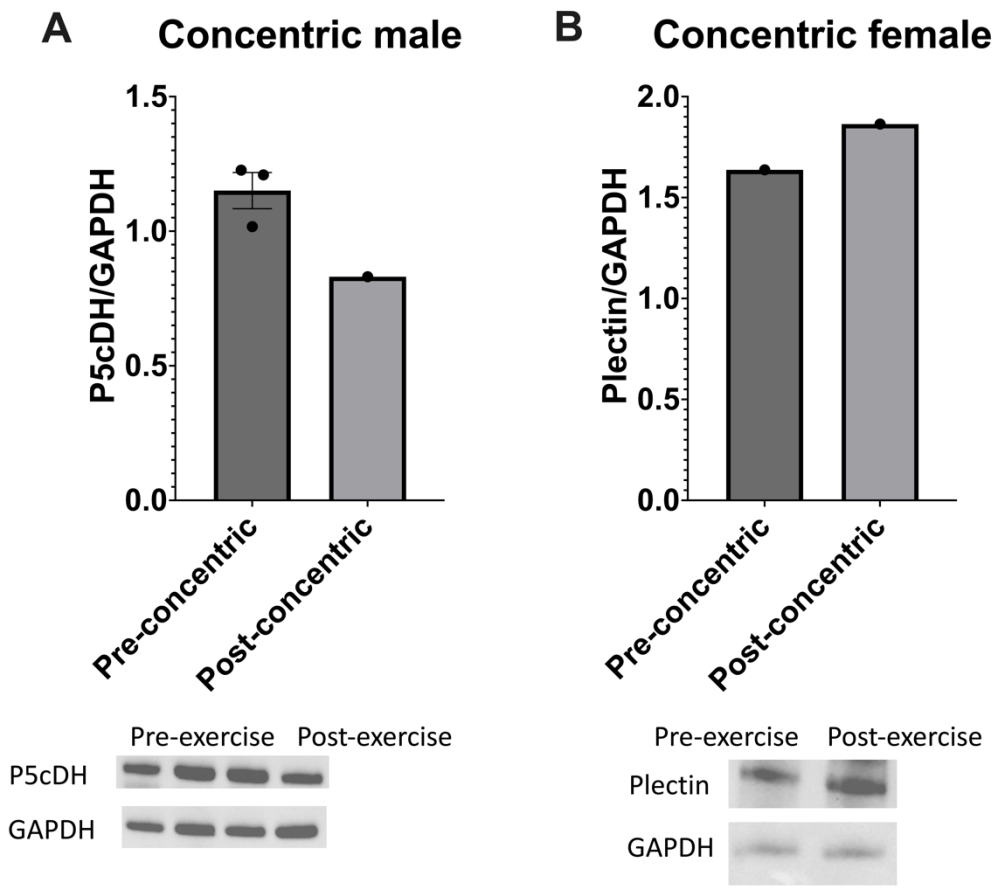

Figure 4.3 – Western blot assessments of the relative expression of P5cDH in concentric male and of plectin in concentric female skeletal muscle samples matches the trend reported by mass spectrometry proteomics. A) *mitochondrial relative expression of P5cDH in concentric male skeletal muscle, normalised to GAPDH (pre-concentric exercise N=3, post concentric exercise N=1);* ***B)*** *mitochondrial relative expression of plectin in concentric female skeletal muscle, normalised to GAPDH (N=1).*

4.4.3 P5cDH gene is unmethylated in response to concentric exercise

Post-exercise alterations of epigenetic states in skeletal muscle have been repeatedly documented [373,374]. As P5cDH was down-regulated following concentric exercise, we sought to determine DNA methylation levels within a regulatory region of this gene. The *P5cDH* promoter is located within a CpG

island containing 75 CpG sites on chromosome 1p36.13. Bisulfite sequencing showed that *ALDH4A1* is almost completely unmethylated in all human skeletal muscle tissue samples tested (N=3), and that concentric exercise does not influence this epigenetic state at the time when tissue samples were collected (**Figure 4.4**).

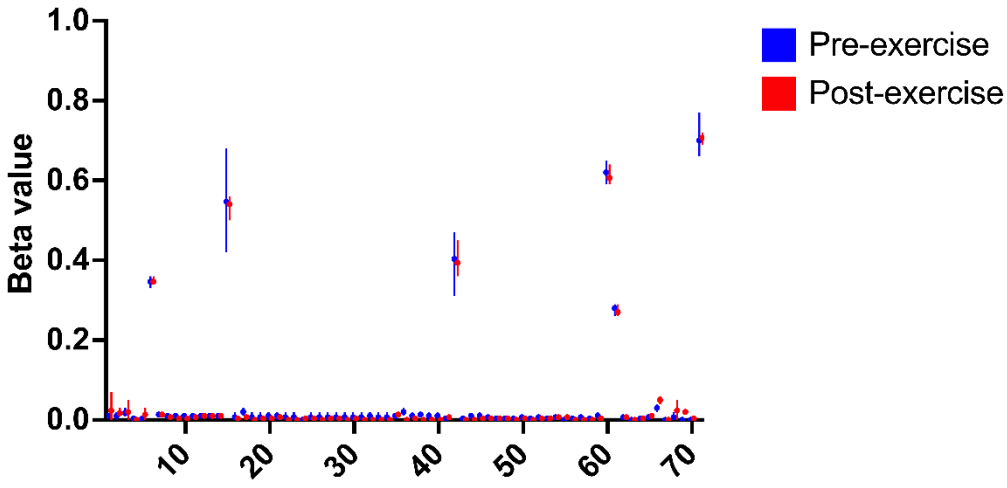

Figure 4.4 – the CpG island upstream of the P5cDH gene (ALDH4A1) is unmethylated in human skeletal muscle and remains unmethylated post-concentric exercise. *The beta value (number of methylated reads/total number of reads) was not significantly different for any of the CpG sites (numbered on x-axis) located on chromosome 1: 18902000 – 18903000 (multiple unpaired t tests, error bars = SEM, N=3 biological replicates).*

4.4.4 Concentric exercise in COPD males: enrichment for translation elongation factors

Enrichment analysis of proteins with altered abundance in each of the four pairwise comparisons (**Table 4.1**) revealed that the proteins associated with male concentric exercise were significantly enriched for factors operating in the 'eukaryotic translation elongation' network (**Figure 4.5**). For example, the tRNA delivery proteins elongation factor 1-delta (EEF1D) and elongation factor 1-gamma (EEF1G), are both present in the enrichment cluster and are upregulated. In contrast, five ribosomal subunit proteins, also present in this cluster, are all downregulated (**Figure 4.5**).

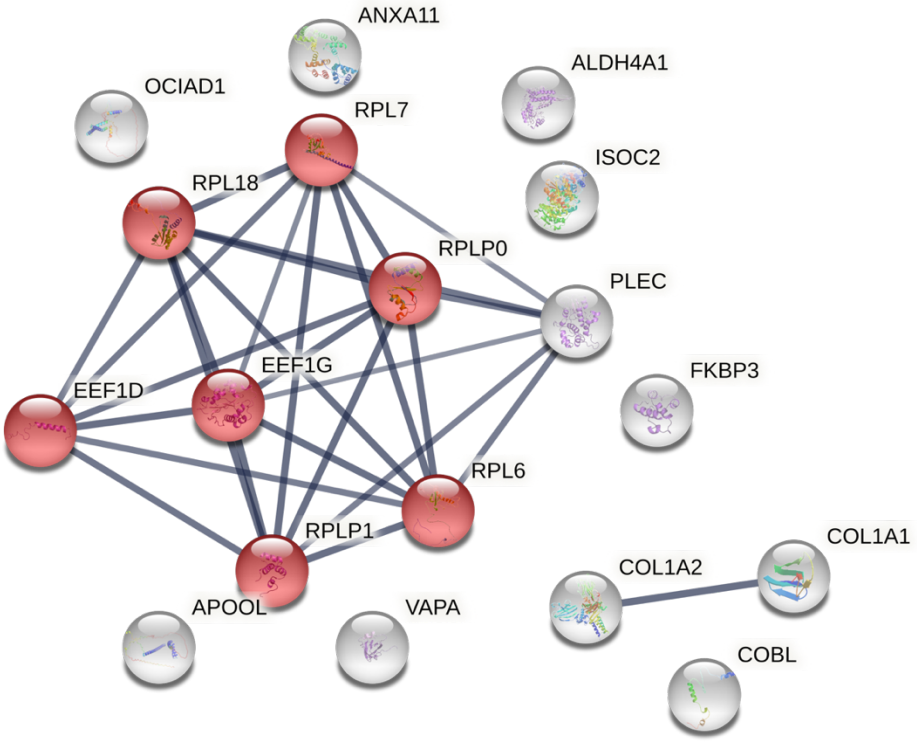

Figure 4.5 – Protein-protein interaction network of proteins with significantly altered expression in concentric exercise male participants. *Nodes are proteins, and edges indicate functional and physical interactions, with edge thickness indicative of the strength of supporting data. Red nodes show local network cluster enrichment for the term 'eukaryotic translation elongation'. The minimum required interaction score was 0.700 (high confidence), and the PPI enrichment p-value < 1.0e-16.*

4.4.5 Carbonic anhydrases I-III, haemoglobin subunits, and haemoglobin associated proteins are present in COPD skeletal muscle mitochondria

We sought to identify novel protein hits from the identified protein lists from both concentric and eccentric exercise samples, and we have previously reported on mitochondrial haemoglobin and carbonic anhydrase II (CA-II) from mitochondrial samples[160,162,375]. We identified haemoglobin subunit α, haemoglobin subunit β, and haemoglobin subunit δ within all the studied samples, without significant variation (**Figure 4.6**). Further, hemopexin and haptoglobin were also present in the mitochondrial samples, as were CA-I, CA-II, and CA-III.

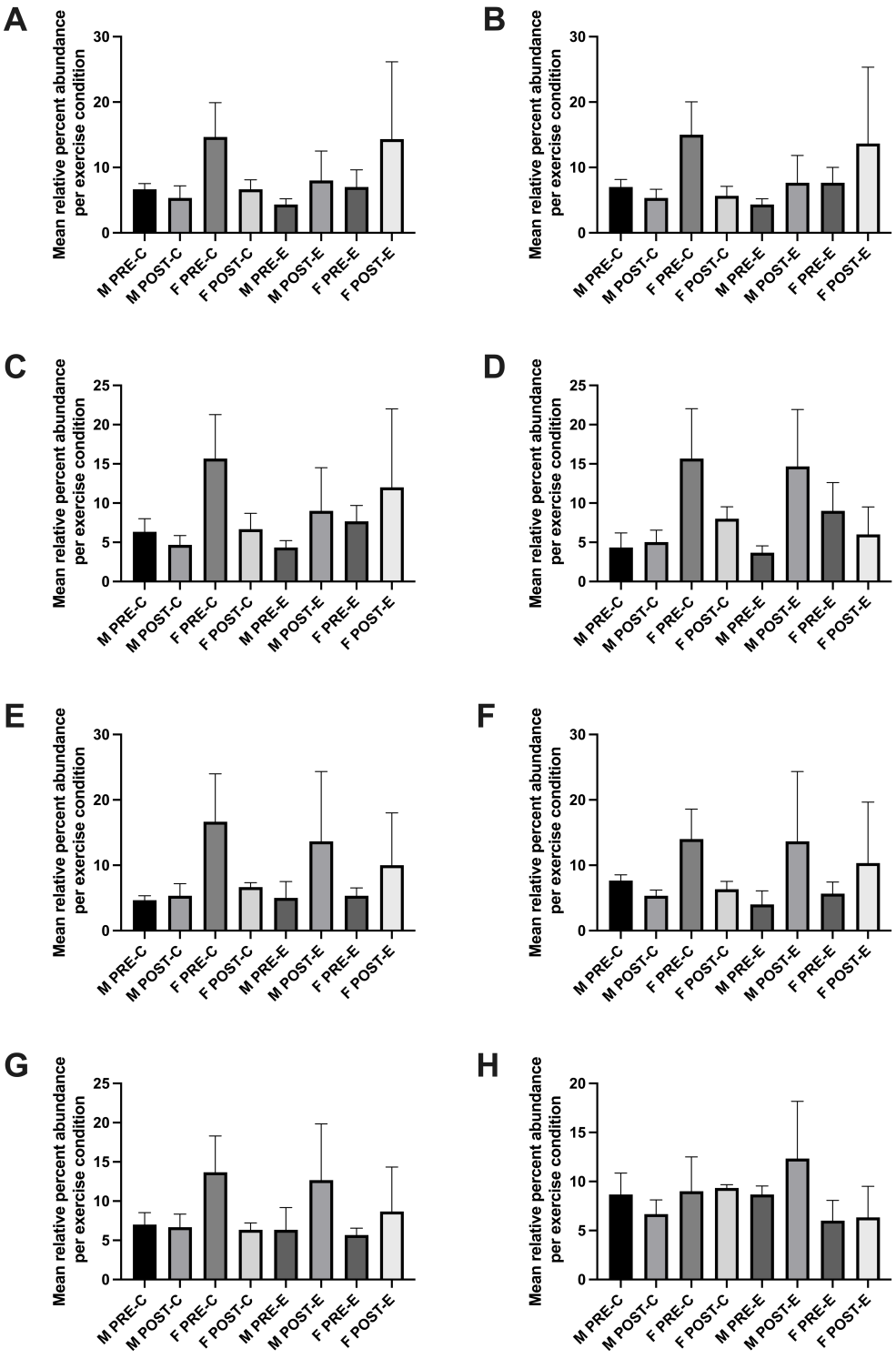

Figure 4.6 – Expression of haemoglobin subunits, haptoglobin, hemopexin, and carbonic anhydrase I, II and III across both sexes and exercise conditions. *Relative percentage abundance of* ***A)*** *haemoglobin subunit α;* ***B)*** *haemoglobin subunit β;* ***C)*** *haemoglobin subunit δ;* ***D)*** *haptoglobin;* ***E)*** *hemopexin;* ***F)*** *carbonic anhydrase I;* ***G)*** *carbonic anhydrase II;* ***H)*** *carbonic*

*anhydrase III. Data presented as mean of relative percentage abundance within concentric exercise samples and eccentric exercise samples, N=3 biological replicates, SEM, one-way ANOVA P * < 0.05. All pre- and post-exercise pairwise comparisons showed no significant difference in expression.*

4.4.6 ATPase activity and levels of lipid peroxidation are unchanged in COPD skeletal muscle in response to concentric or eccentric exercise

A notable, but non-significant decrease in the ATPase activity of the post-concentric exercise samples (unpaired t test, P = 0.095) was observed (**Figure 4.7**). Lipid peroxidation (MDA) levels in the same quadriceps samples were also measured; neither concentric or eccentric exercise induced a significant difference in lipid peroxidation (MDA) levels.

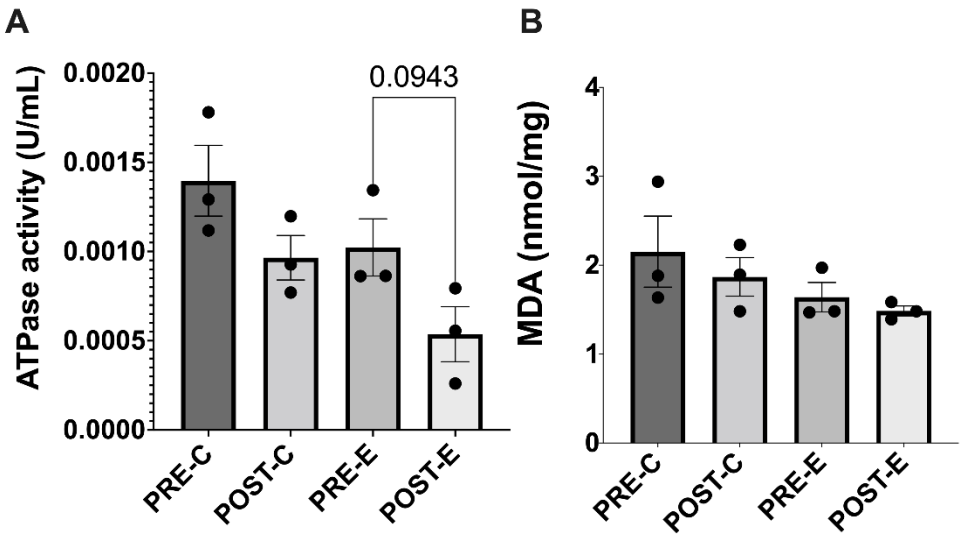

Figure 4.7 – ATPase activity and lipid peroxidation levels of quadricep samples pre- and post-concentric and eccentric exercise. A) *Exercise caused a slight, but not significant decrease in ATPase activity (U/mL) of COPD patient quadriceps tissue;* ***B)*** *Exercise caused no significant difference the level of lipid peroxidation (MDA) in the tissue samples post-concentric and*

*eccentric exercise. N=3 biological replicates, error bars = SEM, unpaired t test, P * = 0.05.*

4.5 Discussion

This is the first study in which sex-specific alterations to the mitochondrial proteome in response to eccentric and concentric exercise have been explored, we followed this up with an investigation of potential epigenetic modulation of the P5cDH gene expression. We were able to identify the presence of proteins not normally associated with this organelle in the mitochondrial proteome of individuals with COPD. To get a better overall picture of exercise induced cellular physiology ATPase activity and lipid peroxidation levels in the skeletal muscle samples were measured.

4.5.1 Concentric exercise upregulates plectin and annexin proteins in male and female participants

Sex specific adaptations of the mitochondrial proteome in response to the concentric and eccentric cycling is one of the key findings of this study. The numbers of proteins with altered abundance, and the specific proteins that were identified were changed in muscle samples with respect to sex (**Table 4.1**). Male and female muscle samples after concentric cycling had significant upregulation of plectin and annexin proteins (annexin A11 in males, annexin A6 in females). Plectin is a member of the plakin family of cytolinker proteins, and is a major component of intermediate filament networks of muscle tissue[376,377]. Beyond its role in cellular structure, multiple studies have shown plectin to be an important modulator of mitochondrial morphology and function, particularly in the structural organisation of mitochondria within muscle tissue[378,379].

The plectin 1b isoform has been shown to bind to the outer mitochondrial membrane, where it links mitochondria to intermediate filaments, and deficiency of the plectin 1b isoform results in elongated mitochondria in primary fibroblast cells[380]. In addition, plectin 1b isoform deficiency in mice has been shown to reduce the mitochondrial respiratory capacity in heart, soleus, and gastrocnemius tissue[381]. It is possible that the upregulation of

plectin in the mitochondrial fraction of skeletal muscle in response to concentric exercise is a positive response to higher bioenergetic demand.

Annexin A6 has been shown to be an important calcium channel in the inner mitochondrial membrane[382]. Fibroblasts derived from annexin A6 knockout mice have been shown to be highly fragmented, as Chlystun and colleagues reported that annexin A6 inhibits Drp1 mediated mitochondrial fission[383]. The authors of that study go on to demonstrate that Ca^{2+}-binding with annexin A6 disrupts the interaction between anneixin A6 and Drp1, which allows for mitochondrial fission to occur.

4.5.2 Alterations in mitochondrial protein abundance are sex-specific in response to concentric and eccentric exercise

In male participants, concentric exercise led to decreased expression of several proteins (**Table 4.1**). These included the MICOS complex subunit MIC27 (MIC27) and Delta-1-pyrroline-5-carboxylate dehydrogenase (P5cDH). The mitochondrial contact site and cristae organizing system (MICOS) complex is one of the key inner membrane organisation structures, as well as being a hub for protein-protein interactions[384]. A double knockout study of MIC26 and MIC27 in HAP1 cells reported that the two subunits have a cooperative role in maintaining the integrity of respiratory super-complex and ATP synthase structures, through modulation of cardiolipin levels[385]. P5cDH is responsible for the second step in the degradation of proline which is interesting since a homozygous mutant of the *D. melanogaster* orthologue (*CG7145*^{f04633}/*CG7145*^{f04633}) has elevated proline levels and swollen mitochondrial morphology[386].

After eccentric exercise, muscle from males contained significantly increased amounts of hydroxyacylglutathione hydrolase mitochondrial (GLO2) protein, while in female participants the MICOS complex subunit MIC13 (MIC13) protein could no longer be detected post-eccentric exercise. MIC13 knockout cells have been shown to have impaired cristae junction formation and decreased basal and maximal respiratory capacity. MIC13 is also considered

necessary for the integration of MIC26 and MIC27 into the MICOS complex structure[387].

4.5.3 Measurement of additional muscle samples confirmed specific proteomic changes

Human studies are complicated by the heterogeneity of the samples in older cohorts, these cannot be controlled for the variety of lifestyle factors encountered over many decades. Western blot was used to prioritise the proteins that most consistently changed quantity in larger numbers of individuals muscle samples. This approach highlighted a trend toward decreased expression of the P5cDH protein (**Figure 4.3**). Previous studies that show epigenetic changes in response to exercise have been reviewed, and we sought to determine whether methylation of the gene that encodes P5cDH takes place in response to exercise[373]. However, using targeted bisulfite sequencing, we did not find any significant differences in the levels of methylation at the CpG island we interrogated directly upstream of the gene (**Figure 4.4**).

4.5.4 Concentric exercise in males is associated with increases in protein translation and elongation factors in muscle

Proteins that had significantly altered abundance in male muscle post-concentric exercise had local network enrichment for the term ‘eukaryotic translation elongation’ (**Figure 4.5**). Specifically, the tRNA delivery proteins elongation factor 1-gamma and elongation factor 1-delta were upregulated in expression. Conversely, ribosomal proteins 60S ribosomal protein L6, 60S ribosomal protein L7, 60S ribosomal protein L18, 60S acidic ribosomal protein P0, and 60S acidic ribosomal protein P0 were all downregulated in expression (**Table 4.1**).

It has previously been reported that the expression of ribosomal proteins is highly differentiated according to tissue type[388]. The elongation factor 1 complex has been shown to have a range of functions beyond protein translation[389], which may help to explain the contradictory nature of the translation elongation protein expression patterns observed in response to exercise.

The presence of cytosolic ribosomal subunits in the mitochondrial fraction of skeletal muscle supports the observation by Gold *et al*. that cytosolic ribosomes can localise to the surface of the mitochondria through the TOM complex[390]. A decrease in the levels of association between the cytosolic ribosomes associated with the surface of the mitochondria may be indicative of a decreased rate of synthesis and or import of nuclear-encoded mitochondrial proteins.

4.5.5 Haemoglobin subunits, haptoglobin, hemopexin, and carbonic anhydrases I, II and III are present in the mitochondrial proteome of COPD skeletal muscle

We have previously reported the presence of both haemoglobin and carbonic anhydrase II within the mitochondria, showing relevance to Parkinson's disease and ageing[160,162,375]. One of the outstanding questions that has been raised about non-erythroid haemoglobin is its potential cytotoxicity[158]. The presence of the cell-free haemoglobin detoxifying protein haptoglobin and the haem detoxifying protein hemopexin in the mitochondrial fraction of these muscle tissue samples offers a potential insight into the physiology of mitochondrial haemoglobin (**Figure 4.6**).

Carbonic anhydrases VA and VB are the isozymes known to be associated with mitochondria[391,392], we have made repeated observations of carbonic anhydrases II and III in the mitochondrial proteome, and found that increased levels of carbonic anhydrase II is associated with decreased longevity[375].

Now we find that the isozyme carbonic anhydrase I is also present in the mitochondrial fraction of COPD skeletal muscle. This isozyme is considered to be a cytosolic protein, and a study by Torella *et al.* reported that its increased myocardial expression in the ischemic myocardium of type 2 diabetes increases rates of endothelial cell death[393]. It would be pertinent to consider a dynamic intracellular distribution of the different carbonic anhydrase isozymes. Their increased levels of expression in the context of cell and organism dysfunction could be linked to mitochondrial pathways.

4.5.6 Concentric and eccentric exercise did not alter ATPase activity and levels of lipid peroxidation in the muscle biopsies

To better understand any changes in mitochondrial physiology in response to concentric and eccentric exercise, we measured the ATPase activity from pre- and post-exercise tissue lysates and observed a trend toward decreased ATPase activity (**Figure 4.7A**). Mitochondria are a major source of endogenous ROS and COPD is associated with oxidative stress[394], exercise is recognised as promoting healthy levels of oxidative stress that ameliorate insulin resistance[395]. However, we also found that there were no changes in the MDA content of the samples pre- and post-concentric and eccentric cycling (**Figure 4.7B**), which suggests the exercise did not promote significant oxidative stress in the participants' skeletal muscle.

4.6 Conclusion

Eccentric and concentric exercise in people with COPD induces changes in the expression profile of the muscle mitochondrial proteome. Proteins with altered abundance in response to both exercise conditions include those that have previously been associated with regulating mitochondrial morphology and ultrastructure. Some changes in protein expression were specific to whether the muscle was rested or exercised. However, some changes were peculiar to the type of exercise loading or the sex of the participant. Changes to mitochondrial morphology may be a positive adaptation to exercise in COPD.

4.7 Author Contributions

BE wrote the manuscript, completed experiments, and analysed the data. AD completed mass spectrometry experiments and analysis. TW and ML conducted exercise experiments and provided samples. RS provided DNA methylation expertise and analysis. LC co-wrote the manuscript, provided all materials and facilities, and directed the research.

4.8 Funding

BE is funded by the Biotechnology and Biological Sciences Research Council (grant number BB/J014508/1).

4.9 Acknowledgements

The York Centre of Excellence in Mass Spectrometry was created thanks to a major capital investment through Science City York, supported by Yorkshire Forward with funds from the Northern Way Initiative, and subsequent support from EPSRC (EP/K039660/1; EP/M028127/1).

4.10 Appendix B: Chapter 4

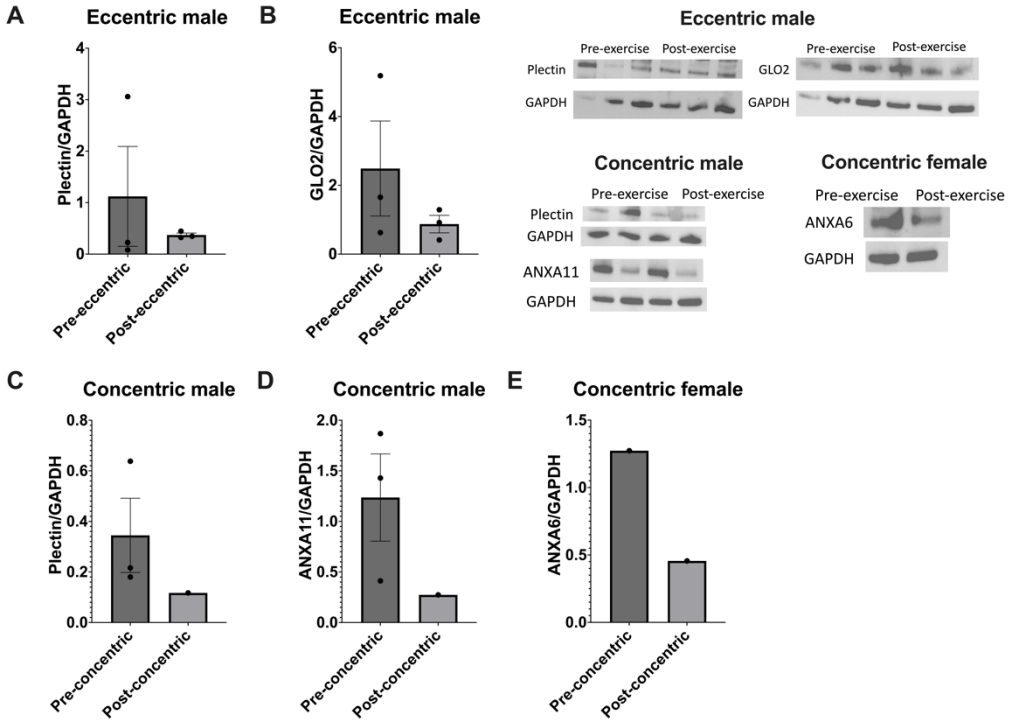

Supplementary Figure 2.1 – Western blot assessment of relative mitochondrial protein expression in skeletal muscle samples of eccentric males and concentric males and females. *Relative mitochondrial protein expression normalised to GAPDH of* ***A)*** *plectin in eccentric exercise males (N=3);* ***B)*** *GLO2 in eccentric exercise males (N=3);* ***C)*** *plectin in concentric exercise males (pre-concentric exercise N=3, post-concentric exercise N=1);* ***D)*** *ANXA11 in concentric exercise males (pre-concentric exercise N=3, post-concentric exercise N=1);* ***E)*** *ANXA6 in concentric exercise females (N=1).*

5 A method to assess the mitochondrial respiratory capacity of complexes I and II from frozen tissue using the Oroboros O2k-FluoRespirometer

Brad Ebanks[1], Pola Kwiecinska[1], Nicoleta Moisoi[2] and Lisa Chakrabarti[1,3]

This manuscript is currently undergoing peer review.

[1] School of Veterinary Medicine and Science, University of Nottingham, Nottingham NG7 2RD, UK

[2] Leicester School of Pharmacy, Leicester Institute for Pharmaceutical Innovation, De Montfort University, The Gateway, Leicester LE1 9BH

[3] MRC Versus Arthritis Centre for Musculoskeletal Ageing Research, Nottingham NG7 2RD, UK

5.1 Abstract

High-resolution respirometry methods allow for the assessment of oxygen consumption by the electron transfer systems within cells, tissue samples, and isolated mitochondrial preparations. As mitochondrial integrity is compromised by the process of cryopreservation, these methods have been limited to fresh samples. Here we present a simple method to assess the activity of mitochondria respiratory complexes I and II in previously cryopreserved murine skeletal muscle tissue homogenates, as well as previously frozen *D. melanogaster*, as a function of oxygen consumption.

5.2 Introduction

As the field of biomedical research continues to expand throughout the 21st century, the use of frozen tissue in research laboratories will continue to expand. This increases the accessibility of clinically relevant samples to researchers and institutions where fresh samples might not be available. Sample freezing has consistently proven to be effective when making assessments of genomes, transcriptomes and proteomes of a given sample[396].

However, sample freezing is not always compatible with certain research interests, including mitochondrial respiration. Mitochondria are a fundamental organelle in eukaryotic organisms, where they are responsible for a wide range of biosynthetic and metabolic processes. This includes haem biosynthesis[397], calcium signalling[26], and apoptosis regulation[398]. However, they are most widely studied for the capacity to produce the biological energy currency of ATP, through the coupling of oxidative phosphorylation with the electron transfer system.

The electron transfer system is composed of a series of enzyme complexes in the inner mitochondrial membrane that oxidise a range of metabolites, including NADH derived from the TCA cycle[40], fatty acids via beta-oxidation[42], succinate[399], proline[44], and glycerol-3-phosphate in mammals[43]. Electrons derived from these species are funnelled into the Q-junction (co-enzyme Q), before the sequential movement through complex III, cytochrome c and finally respiratory complex IV, where they reduce molecular oxygen in a system that has been well-reviewed[45]. As a part of this process, complexes I, III, and IV pump protons across the inner mitochondrial membrane to generate the proton motive force that drives ATP synthesis via ATP synthase[400].

Classical studies by Chance and Williams in the 1950s used platinum microelectrode chemistry to assess oxygen consumption, with simultaneous spectrophotometric assays to assays ATP production via DNPH oxidation[244]. The current leading instruments for assessing mitochondrial oxygen consumption are based on either fluorometric measurement of oxygen (SeaHorse)[246,248], or Clark electrodes within polarographic oxygen sensors

(Oroboros Oxygraph-O2k)[401]. In particular the Oroboros Oxygraph-O2k allows for dynamic high-resolution respirometry assessments across tissues, cells, and mitochondrial isolates in response to titrations of substrates, uncouplers, and inhibitors of mitochondrial respiratory function (SUIT protocols)[402].

One limiting factor of existing SUIT protocols for the Oroboros Oxygraph-O2k, and respirometry assessments made with other instruments, is the inability to assess the respiratory profile or frozen tissue samples. This is due to the inactivation of the TCA cycle and the rupturing of the mitochondrial outer membrane during the process of sample freezing[403–405]. However, there are established enzyme assays that can measure the activity of mitochondrial enzyme complexes[406].

Recent studies have described methods to assess mitochondrial oxygen consumption in cryopreserved samples[407], alongside new respirometry protocols in different instruments[408]. Therefore, we sought to establish a method to measure the activity of mitochondrial respiratory complexes I and II as a function of oxygen consumption, in the Oroboros Oxygraph-O2k. NADH is directly oxidised by complex I, and succinate is commonly used in respirometry to assess complex II activity, so we tested these substrates in homogenates of previously frozen mouse tissue and *Drosophila*.

5.3 Methods

5.3.1 Mouse husbandry

Skeletal muscle sourced from 71-week-old female C57BL/6J mice was sourced from Charles River. Samples were snap frozen and stored at -80°C.

Animals were bred and housed in accordance with strict Home Office stipulated conditions. The overall programme of work (in respect to the original UK Home Office Project Licence application) is reviewed by the Animal Welfare and Ethical Review Body at the University of Nottingham and then scrutinised by the UK Home Office Inspectorate before approval by the Secretary of State. Individual study protocols link to the overarching Home Office Project Licence and are made available to the Named Animal Care and Welfare Officer, the Named Veterinary Surgeon (both are members of the AWERB), the animal care staff and the research group. The Project Licence Number for the breeding and maintenance of this genetically altered line of mice is PPL 40/3576. The mice are typically group housed and maintained within solid floor cages containing bedding and nesting material with additional environmental enrichment including chew blocks and hiding tubes. Cages are Individually Ventilated Cage Units within a barrier SPF unit to maintain biosecurity. Animals are checked daily by a competent and trained animal technician. Any animal giving cause for concern such as subdued behaviour, staring coat, loss of weight or loss of condition will be humanely killed using a Home Office approved Schedule 1 method of killing.

5.3.2 Drosophila husbandry

Drosophila melanogaster strain w1118 (males) were used in this study, housed in glass vials Fly food (Quick Mix Medium, Blades Biological) was added to the vial, to a depth of 1 cm, and 3 mL of distilled water was added; it was left for one minute, and then a small sprinkle of yeast was added. The *Drosophila* were maintained at 25°C, and the food was rehydrated with 150 uL of H2O every 24 hours. Flies were either frozen at -20 or -80. The study was reviewed

and approved by the University of Nottingham SVMS local area ethics committee (#3091 200203 10 February 2020).

5.3.3 Skeletal muscle sample preparation

1, 5, 10, and 25 mg of skeletal muscle tissue from 71-week-old female mice was mechanically homogenised in 300 µL of MiRO5 buffer (Oroboros Instruments; 0.5 mM EGTA, 3 mM MgCl2, 60 mM lactobionic acid, 20 mM taurine, 10 mMKH2PO4, 20 mM HEPES, 110 mM D-sucrose, 1 g/L BSA, pH 7.1). The homogenate was spun down at 850 g (10 mins, 4°C) to remove the insoluble fraction. The subsequent lysate was added to 2ml volume chambers in the Oroboros O2k-FluoRespirometer. Technical replicates were used for this study (N=5).

5.3.4 Drosophila sample preparation

Five flies were mechanically homogenised in 500 µL of MiR05 buffer. The homogenate was spun at 850 g (10 mins, 4°C) to clear insoluble material. The supernatant was added to the O2k-FluoRespirometer. Biological replicates were used for this study, with samples frozen at -20 (n=3) or -80 (n=6) used in this study.

5.3.5 High-resolution respirometry

A substrate, uncoupler, inhibitor, titration (SUIT) protocol was used to assess the uncoupled mitochondrial oxygen consumption capacity[402]. Briefly, 5 µL of cytochrome c was titrated into each chamber and a baseline value was reached, this was followed by a titration of 10 µL of NADH (10 mM) and the peak specific flux value was marked, then 20 µL of succinate (1 M), 1 µL of rotenone (1 mM), and 1 µL of antimycin A (5 mM) which is used for background correction.

Data analyses were performed in GraphPad Prism version 9.3.1.

5.4 Results

5.4.1 The mitochondrial respiratory capacity of frozen mouse skeletal muscle homogenate

Different masses of skeletal muscle tissue were homogenised before being assessed for their mitochondrial respiratory capacity in response to NADH and succinate titrations (**Figure 5.1, Figure 5.2**). All tissues masses that we assessed (1, 5, 10, and 25 mg) showed oxygen consumption in response to substrate titration, and the 5 mg tissue sample lysate produced the strongest oxygen consumption signal (**Table 5.1**).

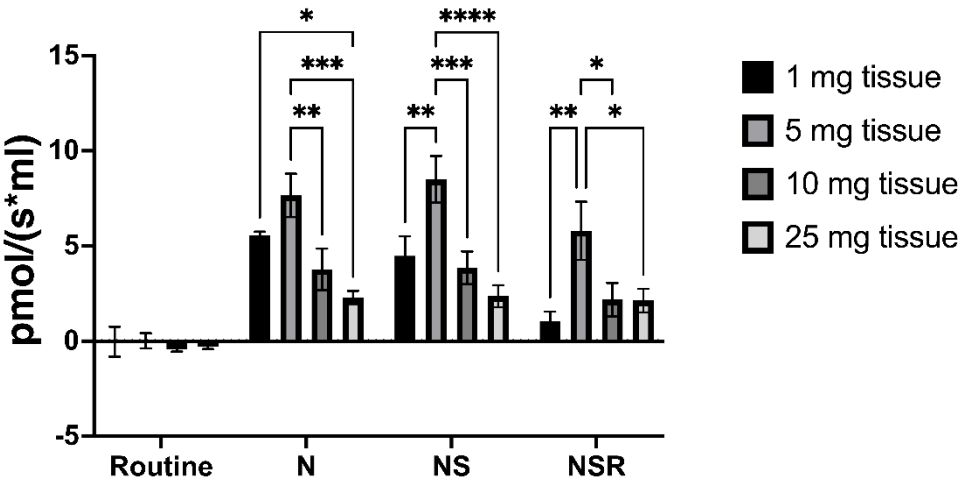

Figure 5.1 – Complex I and complex II-linked mitochondrial oxygen consumption of frozen mouse skeletal muscle. *Mitochondrial respiration was stimulated in either 1, 5, 10, or 25 mg mouse skeletal muscle tissue homogenates with titrations of NADH (N) and succinate (S), before being inhibited by rotenone (R), and antimycin A for background correction. Technical replicates, N = 5, 2-way ANOVA, Turkey's multiple comparison test, * P = 0.033, ** P = 0.002, *** P < 0.001.*

Table 5.1 – Specific flux values of mouse skeletal muscle oxygen consumption. *Mean specific flux values (pmol/(s*mL)) in 1, 5, 10, and 25 mg lysates of skeletal mouse muscle tissue in response to sequential titrations of substrates (NADH, succinate) and inhibitors (rotenone). N=5, (SEM).*

Specific flux of substrate and inhibitor titrations (pmol/(s*mL))	**Mouse skeletal muscle**			
	1 mg	**5 mg**	**10 mg**	**25 mg**
Routine	-0.029 (0.784)	0.016 (0.396)	-0.415 (0.136)	-0.281 (0.135)
NADH	5.565 (0.181)	7.659 (1.139)	3.769 (1.097)	2.304 (0.345)
NADH, succinate	4.475 (1.032)	8.501 (1.228)	3.852 (0.863)	2.358 (0.579)
NADH, succinate, rotenone	1.046 (0.508)	5.795 (1.527)	2.181 (0.876)	2.13 (0.618)

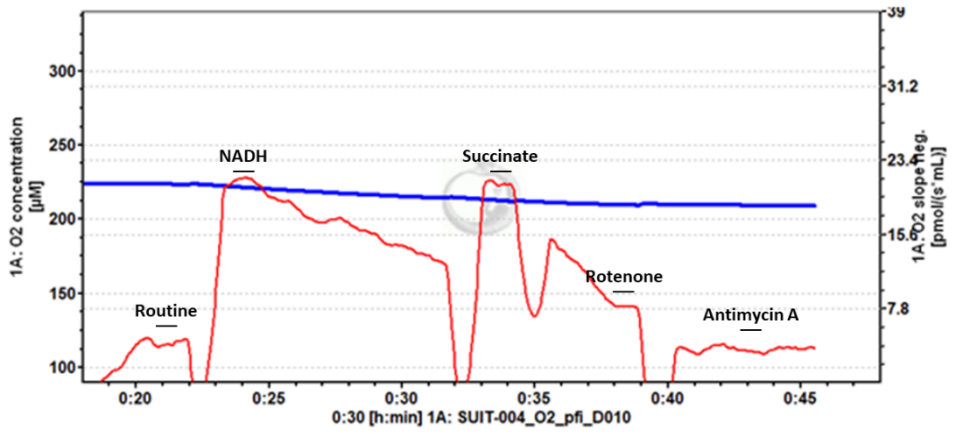

Figure 5.2 – Example trace of frozen mouse skeletal muscle. *Stepwise titrations of NADH and succinate stimulate oxygen flux, which is inhibited by rotenone and antimycin A titrations. Titration of NADH leads to a peak of oxygen flux before progressive decrease.*

5.4.2 *The mitochondrial respiratory capacity of frozen Drosophila (flies) after homogenisation*

Using the same protocol, we assessed the activity of complex I and complex II as a function of oxygen consumption in *D. melanogaster* that had previously been frozen at either -20°C or -80°C (**Figure 5.3, Figure 5.4**). We report that oxygen consumption in *D. melanogaster* frozen at -20 °C is limited for titrations of both NADH and succinate (**Table 5.2**), but a strong signal is detected in *D. melanogaster* that had previously been frozen at -80°C.

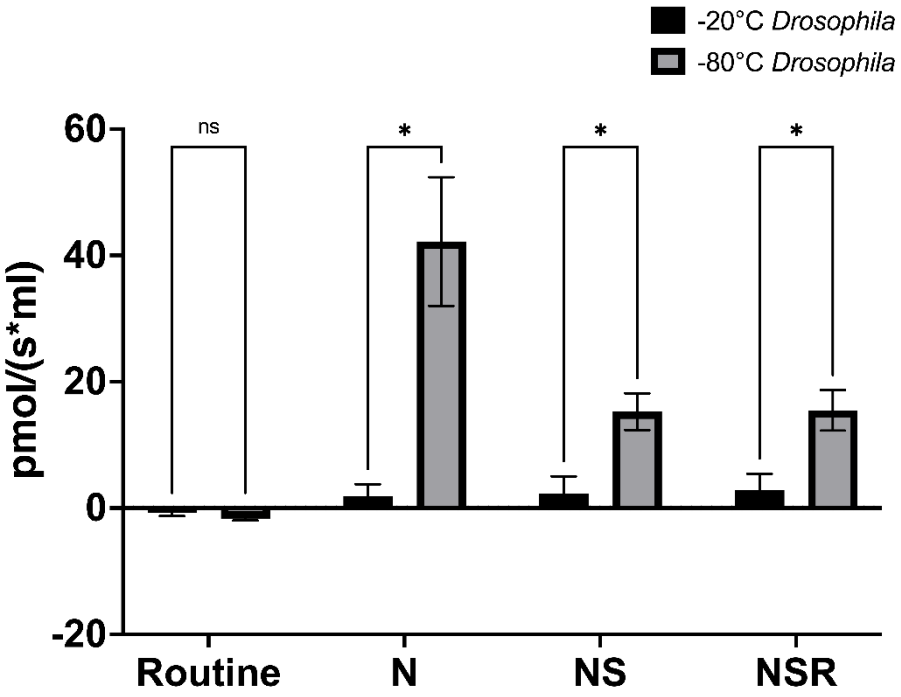

Figure 5.3 – Complex I and complex II-linked mitochondrial oxygen consumption of D. melanogaster frozen at -20℃ and -80 ℃. *The specific oxygen flux (pmol/(s*mL)) of D. melanogaster was assessed in samples that had been frozen at either -20℃ (black) or -80℃ (grey) in response to stepwise titrations of NADH (N), succinate (S), and rotenone (R), followed by antimycin A for background correction. D melanogaster -20℃ (N=3), D. melanogaster -80℃ (N=6). Error bars = SEM, * $p < 0.05$.*

Table 5.2 – Specific flux values of oxygen consumption from previously frozen D. melanogaster. *Mean specific flux values (pmol/(s*mL)) in homogenates of D. melanogaster previously frozen at -20 ℃ and -80 ℃, in response to sequential titrations of substrates (NADH, succinate) and inhibitors (rotenone). D melanogaster -20 ℃ (N=3), D. melanogaster -80 ℃ (N=6), (SEM).*

Specific flux of substrate and inhibitor titrations (pmol/(s*mL))	***D. melanogaster***	
	-20	***-80***
Routine	*-0.745 (0.499)*	*-1.658 (0.310)*
NADH	*1.847 (1.928)*	*42.19 (10.176)*
NADH, succinate	*2.334 (2.679)*	*15.26 (2.915)*
NADH, succinate, rotenone	*2.825 (2.608)*	*15.48 (3.205)*

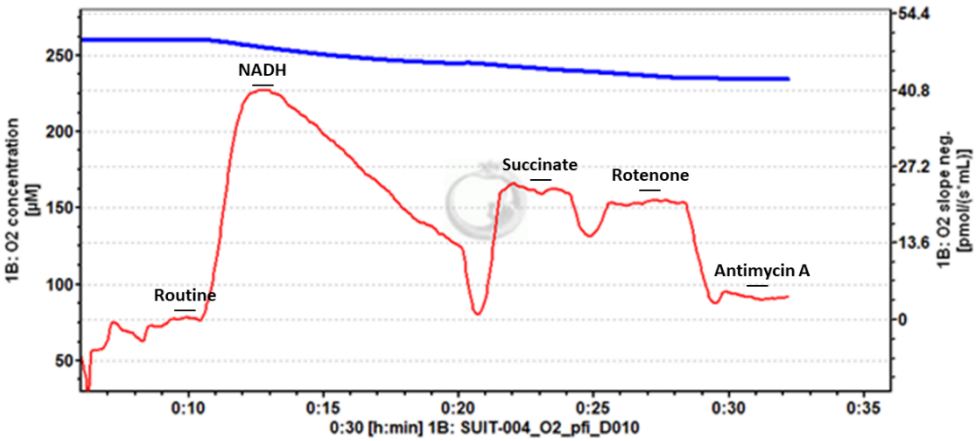

Figure 5.4 – Example trace of -80 ℃ frozen Drosophila. *Stepwise titration of NADH and succinate stimulate oxygen flux, that is then inhibited by titrations of rotenone and antimycin A. Titration of NADH leads to a peak of oxygen flux, before progressive decrease.*

5.5 Discussion

We have demonstrated a simple method to assess the activity of mitochondrial electron transport complexes I and II as a function of mitochondrial oxygen consumption using the Oroboros Oxygraph-O2k. We demonstrated the feasibility of this protocol using lysates of different masses from mouse skeletal muscle, as well as comparing the values between *D. melanogaster* that had previously been frozen at either -20°C or -80°C.

We report that when the 2ml volume chambers are used the smallest mass tested of mouse skeletal muscle homogenate, 5 mg, gives the strongest signals in response to the substrate and inhibitor titrations (**Figure 5.1**). The observation of a stronger signal being observed for this mass of tissue compared with 10 mg and 25 mg could be due to an excess of tissue obscuring the oxygen flux detection by the instrument and warrants additional investigation. For the *D. melanogaster*, those that had been frozen at -80°C gave a significantly stronger signal than those frozen at -20°C (**Figure 5.2**), which is understandable due to the colder temperatures better maintaining the structural integrity of the relevant biomolecules.

While freezing of samples is known to compromise the integrity of the outer mitochondrial membrane[409,410], thus preventing the study of coupled respiratory capacity and oxidative phosphorylation[411], this study shows that the electron transfer system is maintained in such a way that the activity of constituent enzymes can be assessed as a function of oxygen consumption by the system. This is in contrast with static assays which measure the specific activity of the single enzyme in isolation[406,412].

Previous studies, including in the Oroboros Oxygraph-O2k[413], have presented methods to assess the oxygen consumption of the electron transfer system from cryopreserved samples[407,408]. Through consideration of these studies, we have developed the methods reported in this study.

We also believe that this protocol is highly useful for assessing the activities of respiratory complexes in samples that have previously been archived at -80°C,

including valuable clinical samples. It may also be considered for use by research groups that are based in laboratories and institutions where access to high-quality fresh samples is a particular logistical challenge.

Further work using the principles outlined in this pilot study could be undertaken to explore the feasibility of assessing the activity of other electron transfer system enzymes, including proline dehydrogenase, the electron-transferring flavoprotein complex (cETF), and the mitochondrial glycerol-3-phosphate dehydrogenase in mammalian systems.

5.6 Acknowledgments

We would like to thank Deniz Akbulut for his efforts in the laboratory during this time, and the interest that he displayed in this project.

5.7 Author Contributions

B.E. performed the experiments, completed the data analysis, and wrote the manuscript. P.K. assisted with the experiments. N.M. bred and provided *D. melanogaster.* L.C. directed the research, supervised experiments, provided reagents, and prepared the manuscript.

5.8 Funding

This work was supported by the Biotechnology and Biological Sciences Research Council (grant number BB/J014508/1), via an award to B.E.

6 General Discussion

6.1 The interactome of ATP synthase in red-blooded and icefish notothenioid fish

The mitochondrial ATP synthase has been considered as a key enzyme to be studied since the work of Peter Mitchell and the publication of his 'grey book', which presented the idea of the proton motive force[2,48]. However, it was not until 1994 that the structure of its F_1 component was solved[5], and in 1999 a structure of the F_O component was presented[104], with high-resolution structures of the entire F_1F_O structure now published for different species[414–416]. Since the first original structures were published, additional supernumerary subunits in mammals have been reported, subunits j and k[417,418], and their place and potential function in the enzyme's structure have been determined[419]. Novel insights are still be made about the relationship between the enzyme's structure and function, including on how protons are pumped through the F_O component via the horizontal helices of subunit a[107].

Alongside this, many studies have sought also to characterise the activity of the enzyme, through *in vitro* assays of its hydrolytic and synthetic function[50,106,112,117,420]. In combination these structural and mechanistic studies have allowed novel insights into the function of the enzyme to be developed.

Due to the dependency of mitochondrial function and ATP production on the availability of molecular oxygen, many studies of the haemoglobin-less Channichthyidae fish have sought to investigate how the absence of haemoglobin might affect the organelle. With respect to the structure and morphology of the mitochondria , icefish have been reported to have a higher density of mitochondria in the slow muscle fibres[183], with a suggestion that this facilitates more efficient cellular transport and utilisation of oxygen. Shorter oxygen diffusion distances between cardiac mitochondria of icefishes has also been reported, as another adaptation that might increase oxygen availability in Channichthyidae[184]. Changes to respiratory function have also been reported, with implications for thermal tolerance of the haemoglobin-less species[278].

A small number of studies have investigated the function of the ATP synthase enzyme in Channichthyidae, in comparison to red-blooded notothenioid fish. A comparision of the activity of ATP synthase in red-blooded *N. coriiceps* and the icefish *C. aceratus* found no difference in its activity at ambient temperatures (0°C) or at CT_{max}[278], however changes to the mtDNA sequence that encodes the ATP6/8 subunits of the enzyme have also been reported[279].

In the first study presented in this thesis, the interactome of ATP synthase in different species of Channichthyidae and notothenioid fish (*T. bernacchii*, *N. rossii*, *C. rastrospinosus*, and *C. gunnari*) is investigated. I sought to understand how the absence of haemoglobin, and in the case of *C. gunnari* myoglobin, has impacted the enzyme's function, given the fundamental need for oxygen in order for the mitochondria to produce ATP.

The study contains data that show *N. rossii* has significantly lower levels of relative ATP synthase subunit α expression than the haemoglobin- and myoglobin-less *C. gunnari*. However, the co-immunoprecipitation and label-free mass spectrometry study of the interactome of the four different species reported that *C. gunnari* had a significantly smaller protein interactome than the other three species. This would suggest either that the absence of myoglobin has a more significant physiological impact with respect to ATP synthase function than the absence of haemoglobin, or that an additive effect is taking place. Given that myoglobin is responsible for the storage and delivery of oxygen to the mitochondria within cells, it follows that the absence of myoglobin would require physiological adaptation[421].

Despite the differences in the sizes of interactomes across the different species, enrichment analyses of the protein interactomes found that many of the pathways identified were similar across the species studied. One such pathway that was identified in all four species via reactome enrichment analysis was for the post-transcriptional silencing of the iron oxidase enzyme ceruloplasmin[295]. Previous studies of notothenioid ceruloplasmin have reported that ceruloplasmin mRNA is transcribed at higher levels in the icefish *C. rastrospinosus* than in red-blooded *T. bernacchii*[297], but that the two icefish species *C. aceratus* and *C. gunnari* had near-zero levels of ceruloplasmin iron

oxidase activity in comparison with the red-blooded *N. coriiceps* and *Gobionotothen gibberifrons*[298]. This observation of potential post-transcriptional silencing may reconcile the contradiction between mRNA expression but lack of enzymatic activity.

Given that ceruloplasmin is physiologically important for the export of cellular iron and for the transport of copper in the blood, this has important implications for transition metal-based metabolic processes of notothenioid fish. Iron metabolism has already been widely studied in these species, and new insights continue to be presented[180,298,422].

In addition, aceruloplasminemias are a rare but severe genetic disease, which lead to neurodegeneration with brain iron accumulation[423]. A link between the interactome of ATP synthase and the regulation of the expression of the ceruloplasmin protein from its mRNA transcripts may therefore have important implications for human medicine. It should be noted that the original study by Mazumder *et al*. that reported the post-transcriptional silencing of ceruloplasmin studied the human L13a ribosomal subunit, which highlights the importance of further understanding this mechanism and its potential relationship with ATP synthase.

The key limitation of this particular study is that it is observational, and the noteworthy finding of the enriched ceruloplasmin silencing pathway has not undergone a mechanistic investigation in this context. The non-specific interaction of proteins with antibodies can also be problematic in co-immunoprecipitation studies, and so the results could have been complimented by methods such as a protein pull-down assay, or a chemical cross-linking study.

6.2 A role for mitochondrial haemoglobin and its interaction with ATP synthase

The presence of haemoglobin in non-erythroid locations has been reported repeatedly across the last two decades, and the list of non-erythroid locations

where haemoglobin has been observed is still continuing to expand[158]. Largely, studies that have reported its presence in atypical tissues and cells, such as neurons[155], mesangial cells[151], the endometrium[153], and epithelial cells[424], but do not specify a subcellular location for the protein.

However, the first comprehensive evidence of haemoglobin's presence specifically within the mitochondria was first reported by Shephard *et al*. in human cortex tissue, mouse skeletal muscle, and mouse brain[160]. Following this, other studies also reported the presence of haemoglobin in the mitochondria of leukocytes[164], human cerebellum and substantia nigra[162], human multiple sclerosis cortex[163], cultured MES23.5 dopaminergic cells[161], and whole *D. melanogaster*[162].

In line with this, the second study contained within this thesis sought to understand whether mitochondrial haemoglobin is present in a range of different species and tissues, to understand its potential interaction partners, how physiological hypoxia might impact the expression patterns of the protein, and whether any of the patterns of observed are common across species and tissues. It has previously been suggested that the non-erythroid role of haemoglobin may be to protect against oxidative stress[164], a characteristic of hypoxia[425], and that the oxygen binding capacity of haemoglobin might also enable it to act as an oxygen reservoir during the hypoxia response of neuronal cells[155].

This study presents evidence of a physical interaction between haemoglobin and the mitochondrial ATP synthase in *D. melanogaster*, red-blooded species of notothenioid fish, and in the liver tissue of rats. In addition to this, molecular docking and molecular dynamics simulations provide *in silico* evidence for a binding interaction between ATPIF1 and both tetrameric haemoglobin and the haemoglobin alpha subunit. The study also presents evidence of a dynamic response in the expression patterns of mitochondrial haemoglobin in response to acute hypoxia treatments in both rats, mice, and *D. melanogaster*.

When these different pieces of evidence are considered collectively, it points toward mitochondrial haemoglobin being a part of the mitochondrial response to hypoxia, as others have previously suggested[155], with potential implications for the metabolism of ATP under this condition, where ATP content has also previously been linked with levels of cellular haemoglobin[261].

A dynamic expression profile for mitochondrial haemoglobin has previously been reported in the brain tissue of Parkinson's disease patients[160,162]. Mitochondrial oxidative stress is a well-recognised feature in physiologically relevant tissues in Parkinson's disease[426], and when considered with the upregulation of expression we presented in response to hypoxia, the commonality between these two conditions is oxidative stress. The study by Shephard *et al.* from 2014 also reported the localisation of haemoglobin to the inner mitochondrial membrane in a distinctive rosette-like structure, that is reminiscent of the structure of the F_1 component of ATP synthase.

The relationship between mitochondrial haemoglobin and ATP synthase is highly interesting, due to the fundamental nature of these two proteins to eukaryotic biology. Haemoglobin has the capacity to bind to certain organophosphates, including both ADP and ATP[301], and as previously discussed, cellular expression has also previously been correlated with ATP availability[261].

When this information is viewed alongside the evidence presented in the second study of this thesis, we now understand that haemoglobin binds to ATP, ADP, ATP synthase subunit alpha, and the major physiological inhibitor of ATP synthase, ATPIF1. In addition, we can see that the expression of mitochondrial haemoglobin is upregulated in response to hypoxia in skeletal muscle of mice and in whole *D. melanogaster*. It is plausible that this is related to the availability of ATP, based on the dependency of ATP production on oxygen availability, the association between haemoglobin and ATP associated proteins, and the previously mentioned literature which has reported this relationship on a cellular level in barley aleurone[261].

With respect to the potential role of mitochondrial haemoglobin as a defence mechanism against oxidative stress, mitochondrial ATP synthase has also been shown to be a target to various different forms of redox active species, which I have previously reviewed[131]. This includes in different disease states, such as Alzheimer's[427], Parkinson's[428], and Huntington's diseases[429]. It is therefore possible that the association of mitochondrial haemoglobin with ATP synthase is as a mechanism to protect the enzyme against attack from oxidative stress associated species.

This study would have been improved by the inclusion of structural biology data (cryo-electron microscopy or x-ray crystallography), to validate the *in silico* predicted interaction between IF1 and haemoglobin, and to understand the potential direct interaction between haemoglobin and ATP synthase. Additionally, to better understand the tissue-specific responses of mitochondrial haemoglobin, treatment of a muscle cell line with atractyloside (alongside the liver cell line HEPG2) would have better enhanced our understanding.

6.3 The proteomic profile of COPD muscle mitochondria is modulated by eccentric and concentric exercise

Concentric and eccentric exercise are both isotonic forms of exercise, but eccentric exercise has a much lower cardiopulmonary demand. Eccentric exercise has therefore been considered for its potential therapeutic effects for people living with respiratory conditions, including COPD[351,355]. In this study, we profiled mitochondria from the skeletal muscle of humans with COPD before and after eccentric or concentric cycling exercise.

Through proteomic analysis of the enriched mitochondrial fraction from skeletal muscle biopsies, we observed that both forms have exercise caused changes to the mitochondrial proteome, with sex-specific effects also observed. Alongside the proteomic data, western blot experiments on additional samples similarly identified the protein P5cDH as downregulated in male skeletal muscle samples in response to concentric exercise, however this could not be

explained by gene methylation in response to the exercise. We also reported that there was no significant difference in the activity of the ATPase enzyme or in the levels of lipid peroxidation (MDA) in response to either eccentric or concentric exercise.

Notably, many of the proteins with altered abundance post-eccentric and post-concentric exercise have previously been associated with alterations with mitochondrial ultrastructure. These include P5CDH, plectin, annexin A6 and A11, MIC27 and MIC13. It is plausible that the two different forms of exercise trigger adaptations in the mitochondrial structure of skeletal muscle cells, which should be further investigated in microscopy studies.

Given that COPD results in impaired pulmonary function, it is important to consider its impact on mitochondrial function, as well as the impact of any possible therapeutic interventions on the mitochondria also. It is also important to consider potential sex-differences in the pathology of a disease, and in any response to proposed therapeutic interventions. Our data highlighted the differences in the mitochondrial proteome both pre- and post- the two different exercise conditions in males and females.

It would have been advantageous to include non-COPD age-matched controls in this study, to better understand how the applied exercise condition impacts the mitochondrial proteome, and whether it might cause it to resemble a non-COPD profile. This would have allowed the study to determine any potential therapeutic benefits of the applied exercise condition more definitively, with respect to mitochondrial activity in skeletal muscle.

6.4 The respiratory capacity of complexes I and II can be assessed in frozen tissue samples with high-resolution respirometry

High-resolution respirometry conducted using instruments such as the Oroboros O2k-oxygraph provides detailed insights into the metabolism and respiratory function of the mitochondria in a given sample. Different respiratory enzyme complexes can be targeted through use of specific

substrates, and different respiratory states can also be assessed through targeted use of uncouplers and inhibitors[430].

Despite the rich information that can be gathered through use of high-resolution respirometers, one of the limits is the requirement for live cells or tissue samples. This is due to the inactivation of the TCA cycle and disruption of the outer mitochondrial membrane that is caused by the freezing process[403–405]. This limits the use of these instruments when considering the activity of respiratory complexes in precious samples that require frozen storage, or for laboratories in locations that have limited access to such samples.

In this study we therefore sought to develop a protocol in which the activity of mitochondrial respiratory complexes could be assessed as a function of mitochondrial oxygen consumption. Recently studies have also outlined methods by which the respiratory activity of previously frozen samples could be assessed, including through developing new methods of sample freezing and the use of alternative substrates[407,408,413].

In previously frozen mouse skeletal muscle and whole *D. melanogaster* we used NADH and succinate to directly drive the enzymatic activities of mitochondrial respiratory complexes I and II, respectively. With the protocol that we developed, it was possible to measure the activity of the two enzymes as a function of oxygen consumption by respiratory complex IV, downstream of complexes I and II in the ETS. In addition, we compared different masses of the mouse skeletal muscle as well as *D. melanogaster* that had been frozen at two different temperatures, demonstrating that this protocol can be used to make comparisons between different samples.

There is scope to build upon this protocol, including through use of different substrates to assess the activity of different enzyme complexes, and optimisation of the protocol for different sample, including variations in tissue type and sample mass. In developing this protocol, we see that it will be useful for research groups with high-resolution respirometers that are seeking to make assessments of mitochondrial respiratory enzyme activities from previously

frozen samples they currently have catalogued, as well as for laboratories based in locations where reliable access to live or fresh samples is limited.

To fully determine the utility of the method that is presented in this study, additional experiments need to be undertaken in which fresh samples are matched with frozen samples. This will allow us to see whether the activity observed in the frozen samples is representative of the activity of fresh, and therefore most physiologically relevant, samples. Combinations of additional ETS substrates could also be investigated, including for complexes III and IV, proline dehydrogenase, electron-transferring flavoprotein complex, and glyceraldehyde-3-phosphate dehydrogenase.

Further, as NADH could be being consumed by glycerol-3-phosphate dehydrogenase on the outer surface of the inner membrane, rotenone normalisation of complex I-linked oxygen consumption should be considered. Permeabilisation of the inner mitochondrial membrane should also be considered to determine whether incomplete permeability of the membrane is kinetically limiting NADH and substrate access to complexes I and II, respectively.

6.5 General Conclusions

The research that has been presented within this thesis demonstrates that the mitochondrial ATP synthase has a varied protein-protein interactome, and that this has implications for its function beyond being the primary producer of molecular ATP. Within the interactome of ATP synthase, this thesis contains data on its relationship with mitochondrial haemoglobin. Mitochondrial haemoglobin also binds to ATPIF1, and its expression is responsive to hypoxia. This has potential implications for the hypoxic response, antioxidant defences, and bioenergetics. Finally, the mitochondrial proteome of COPD skeletal muscle is responsive to concentric and eccentric exercise, but the expression and activity of ATP synthase did not change under the conditions studied. Therefore, despite the potential bioenergetic demands of exercise, adaptations in the expression and activity of ATP synthase may not be a primary response in many conditions.

6.6 Future Direction and Perspectives

The work contained within this thesis lays a foundation for studies that can explore the presented ideas in greater depth. Firstly, there is opportunity to develop a greater understanding of the protein-protein interactome of ATP synthase beyond respiratory super-complexes and supernumerary subunits. A comparative approach can be applied to this work, across a range of different species as well as in varying states of human health and disease. As ATP synthase dysfunction has been linked to a range of different human diseases, including neurodegenerative diseases and cancer, it is important to understand how the interactomes of its key subunits change in the context of those diseases. Additionally, methods such as protein pull-down assays and chemical cross-linking could be used as complimentary approaches.

With respect to mitochondrial haemoglobin and its interaction with ATP synthase, there are a number of outstanding questions that are key to developing our understanding of that relationship. This includes how haemoglobin is imported into the mitochondria and whether the canonical haemoglobin folding chaperone AHSP is needed, or whether a novel mitochondrial import sequence is contained with the subunit amino acid sequences; what the structural basis for the interaction between haemoglobin and ATP synthase is and whether other bridging proteins are necessary; whether the potential link between mitochondrial haemoglobin levels and ATP availability can be explicitly described.

In the context of health and disease, mitochondrial haemoglobin has already been demonstrated to have a disease-specific distribution within the mitochondria in Parkinson's disease. For the mitochondrial haemoglobin that is present in proximity to the inner mitochondrial membrane, it will be important to consider how the interaction between haemoglobin and ATP synthase and IF1 changes, and whether there is an increased are decreased level of protein-protein interaction. This should be considered for diseases where hypoxia is a characteristic component, such as COPD.

6.7 Appendix C: Papers Resulting from the PhD Study

www.aging-us.com AGING 2020, Vol. 12, No. 16

Review

ATP synthase and Alzheimer's disease: putting a spin on the mitochondrial hypothesis

Brad Ebanks[1], Thomas L Ingram[1], Lisa Chakrabarti[1,2]

[1]School of Veterinary Medicine and Science, University of Nottingham, Sutton Bonington LE12 5RD, UK
[2]MRC Versus Arthritis Centre for Musculoskeletal Ageing Research, Chesterfield, UK

Correspondence to: Lisa Chakrabarti; **email:** lisa.chakrabarti@nottingham.ac.uk
Keywords: Alzheimer's disease, mitochondria, ATP synthase
Received: June 4, 2020 **Accepted:** July 21, 2020 **Published:** August 27, 2020

ABSTRACT

It is estimated that over 44 million people across the globe have dementia, and half of these cases are believed to be Alzheimer's disease (AD). As the proportion of the global population which is over the age 60 increases so will the number of individuals living with AD. This will result in ever-increasing demands on healthcare systems and the economy. AD can be either sporadic or familial, but both present with similar pathobiology and symptoms. Three prominent theories about the cause of AD are the amyloid, tau and mitochondrial hypotheses. The mitochondrial hypothesis focuses on mitochondrial dysfunction in AD, however little attention has been given to the potential dysfunction of the mitochondrial ATP synthase in AD. ATP synthase is a proton pump which harnesses the chemical potential energy of the proton gradient across the inner mitochondrial membrane (IMM), generated by the electron transport chain (ETC), in order to produce the cellular energy currency ATP. This review presents the evidence accumulated so far that demonstrates dysfunction of ATP synthase in AD, before highlighting two potential pharmacological interventions which may modulate ATP synthase.

INTRODUCTION

AD is a progressive, irreversible neurodegenerative disease that accounts for more than half of the 44 million cases of dementia globally [1]. AD can be either sporadic or familial (inherited). The greatest risk factor for the onset of AD is ageing, and the World Health Organization predicts that by 2050 the number of people over the age of 60 will have increased to 2 billion [2]. With that, the number of people living with AD will increase as well as the economic costs of supporting and treating AD patients.

Symptomatically, AD is initially recognised by mild cognitive impairment (MCI) and problems with short- and long-term memory. As the disease progresses neuropsychiatric symptoms can develop including affective, psychomotor, psychotic and manic syndromes [3]. There are two distinct biomolecular markers within the brain that have long been known to characterise AD, amyloid plaques composed of the amyloid-β (Aβ) peptide and neurofibrillary tangles (NFTs) composed of hyperphosphorylated tau proteins [4]. However, due to their location AD can only be diagnosed using these markers post-mortem.

Mitochondria are also widely observed as dysfunctional in AD, which has resulted in the development of the mitochondrial cascade hypothesis [5, 6]. The dysfunction of mitochondria, and in particular the ETC, has been coupled with the oxidative stress observed in AD [7, 8]. It has been widely debated as to whether amyloid plaques, NFTs or dysfunctional mitochondria play the primary role in the aetiology of AD. We now understand that interactions actually take place between these different biomolecular markers contributing to disease progression [9, 10].

When considering the role of mitochondria in AD, ATP synthase has not been widely discussed. ATPases are present across eukaryotes, prokaryotes and archaea. They can be placed into one of three different classes: F-type, V-type or A-type, similar in structure but differing in function [11, 12]. Mitochondrial ATP synthase is an F-type ATPase and is the final ETC complex of the IMM. It is responsible for the pumping of protons from the inter-membrane space into the matrix while harnessing the chemical energy from this process. The chemical energy is converted into mechanical energy that allows the complex to behave as a molecular motor. Rotation of the motor triggers conformational changes in the catalytic domain of the enzyme that enables the production of ATP, the cellular energy currency of which an estimated 50kg a day is required by the body, from ADP and P_i[13]. In medical research, ATP synthase has been more widely studied in classic mitochondria disorders such as Leigh Syndrome [14, 15].

This review is a synthesis of the data which implicate ATP synthase in the pathology of AD. It then considers ways in which ATP synthase can be therapeutically targeted in order to try and prevent disease onset or to alleviate symptoms.

ATP synthase

What is ATP synthase

F-type ATP synthase is the fifth and final ETC complex of the IMM. It has a large structure with a molecular weight of around 600 kDa and is composed of up to 20 different subunits in mammals [16]. ATP synthase is responsible for the production of the cellular energy carrier ATP from ADP and P_i. This process is driven by the chemiosmotic potential across the IMM first described by Peter Mitchell in the 1960s [17–19]. While F-type ATP synthase is predominantly housed within mitochondria, data have shown that F-type ATP synthase is present at plasma membranes of different cell types both physiologically and pathophysiologically [20, 21].

After ATP synthase's function was described *in vitro*, landmark measurements including the kinetic parameters of its three-site cooperative-binding catalytic mechanism and the discovery that protein conformational changes would facilitate the release of tightly bound ATP were reported [22, 23]. The atomic structure of the complex was resolved to 2.8 Å in 1994, revealing a structure which supported the mechanism of rotary catalysis [24]. Since 1994, multiple atomic structures of both eukaryotic and prokaryotic ATP synthase structures have been published, with a recent cryo-EM structure of ATP synthase from *S. scrofa* shown in Figure 1 [25–28]. ATP synthase consists of two distinct components; a membrane bound F_O component and a matrix exposed F_1 component. They function cooperatively through a central rotor stalk and a peripheral stator stalk.

F_O

The F_O component of ATP synthase is an insoluble structure that is primarily composed of a ring of varying numbers of c-subunits called the c-ring and has a size that appears to be species dependent [29]. Other F_O proteins include subunit a and subunit b as well as others with less well understood roles including subunits d, e, f, g, F6 and 8 (A6L). DAPIT and 6.8PL are present in vertebrates and assist in the assembly of the F_O component of ATP synthase [30, 31]. An additional subunit called the oligomycin sensitivity conferring protein (OSCP) is located at the top of the F_1 component of ATP synthase. It couples the F_O component with the F_1 component through its interaction with the peripheral stalk of F_O and central stalk of F_1 [32]. Protons from the intermembrane space of the mitochondria travel through an aqueous half-channel in subunit a to the c-ring of the F_O complex where they bind to conserved acidic c-ring residues, aspartate or glutamate, in the second transmembrane helix of subunit-c [13, 33–35]. These charged proton binding sites are then suggested to be concealed by rotation of α-helices in c subunits which leads to c-ring to rotation along with the central rotary stalk γ-subunit [36, 37]. The rotating F_O component transports protons into the matrix through a second aqueous half channel on the matrix side of the membrane and the asymmetric rotor stalk causes conformational changes in F_1 which drive the catalytic activity of the β subunits [13].

The role of OSCP

The oligomycin sensitivity conferring protein (OSCP) is part of the peripheral stalk of the F_O component of ATP synthase and physically couples the two enzyme components together through its interaction with the central stalk of the F_1 component. It is encoded by the *ATP5O* gene on the long arm of the nuclear chromosome 21. Structurally, OSCP has an N-terminal domain which contains six α-helices and a C-terminal domain consisting of a β-hairpin and two α-helices [32, 38]. While oligomycin does not bind to OSCP, OSCP confers the enzyme's sensitivity to the antibiotic as it is OSCP that couples the F_1 component to the F_O component that is bound and inhibited by oligomycin [39].

F_1

The F_1 component is solvent exposed and far more about its activity and structure is understood than its F_O

counterpart. Its subunit composition is $\alpha_3\beta_3\gamma\delta\varepsilon$, with its structure being a six part barrel of alternating α and β subunits, a central asymmetric γ subunit (the afore-mentioned rotor stalk) protruding through the centre of the barrel while the δ and ε subunits are found at the matrix exposed surface of the F_O c-ring [24]. The site of catalysis is located at the interface of the α and β subunits, both of which have nucleotide binding sites and multiple studies of atomic structures have shown nucleotides bound at this interface [40–42]. Interestingly, both α and β subunits possess the same folds despite only sharing around 20% sequence homology [16]. The structural similarities are presented in Figure 2 using the atomic structures of ATP synthase in *S. scrofa* [27, 43]. Despite the similarity, only the β-subunit possesses catalytic activity due to its ability to form an open conformation as well as possessing a catalytic base for the reverse ATP hydrolysis reaction [44, 45].

The role of the α-subunit

The α-subunit of the F-type ATP synthase is located in the F_1 solvent exposed component of ATP synthase, facing the mitochondrial matrix [24]. It functions as part of a six-part barrel structure ($\alpha_3\beta_3$), and the catalytic nucleotide binding site is located at its interface with the β-subunit [40]. However, the α-subunit displays regulatory activity when compared with the β-subunit which exhibits the catalytic activity of the enzyme [44, 45]. Like its β-subunit counterpart, the α-subunit can be divided into three different domains: a small N-terminal domain, a nucleotide binding domain and a helical C-terminal domain.

The role of the β-subunit

The β-subunit is also located in the solvent exposed F_1 component of ATP synthase and it has a largely similar structure to the α-subunit. Its interface with the α-subunit forms the nucleotide binding site and it is the β-subunit that possesses the catalytic activity required for both the synthesis and hydrolysis of ATP. The β-subunit is able to undergo conformational changes to form three distinct conformations in response to the rotation of the γ-subunit in 120° increments [46]. This, coupled with critical arginine, lysine and glutamate residues is what enables β-subunit to catalyse the synthesis and hydrolysis of ATP [47]. For well-illustrated figures of this mechanism, see Feniouk et al., 2008 and Okuno et al., 2011 [48, 49].

ATP synthase in Alzheimer's Disease (AD)

Mitochondria are known to be dysfunctional in AD patients and this has resulted in the development of the mitochondrial cascade hypothesis [5]. This hypothesis has been developed and revisited several times across

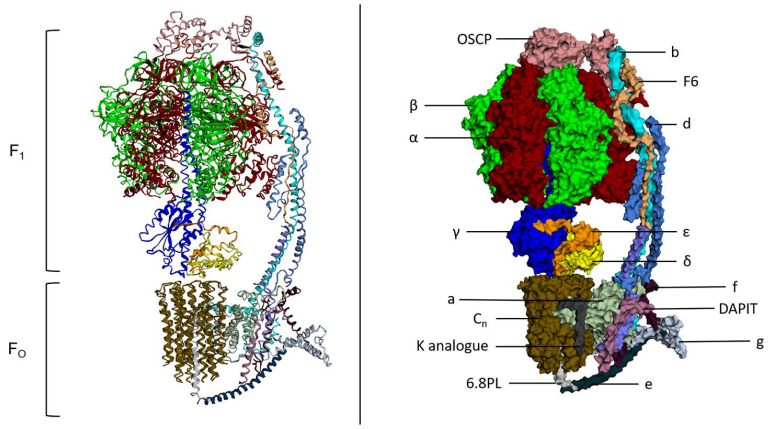

Figure 1. Atomic structure and labelled space fill model of ATP Synthase (S. scrofa). F_O and F_1 components of the complex both labelled. Individual subunits labelled on the space fill model. This figure was created using image 6J5J from PDB (http://doi.org/10.2210/pdb6J5J/pdb https://www.rcsb.org/structure/6J5J) and processed using http://www.sbg.bio.ic.ac.uk/ezmol/.

the last two decades, serving as a viable alternative to the predominant amyloid hypothesis [6, 50–52]. Much of the focus of the research has been based on the oxidation levels found in the brains of AD patients, and how this observation can be synthesised with the mitochondrial theory of ageing [4, 53]. Despite its physiological relevance to both mitochondrial activity and structure, little attention has been paid to ATP synthase in the formation and development of this theory [54].

The first study implicating ATP synthase in AD aetiology found, through BN-PAGE analysis, decreased expression of the whole complex in the hippocampal tissue of AD patients [55]. Since then, multiple studies have pointed to a decrease in the expression of ATP synthase subunits and they are addressed in this review. There was decreased expression in several of the nuclear encoded ATP synthase genes in the posterior cingulate cortex (11), hippocampal field CA1 (10), middle temporal gyrus (9) and entorhinal cortex (5) [56]. Adult neurogenesis defects are common in AD and it has been suggested that this arises from impaired function of hippocampal neuronal stem cells (NSCs). A study using iPSC-derived NSCs, with familial AD (FAD) associated PS1 mutation M146L, observed a decreased expression of the ATP synthase complex while PS1 expression was kept at physiological levels [57]. In a study with implications for sporadic AD, N2a neuroblastoma cells expressing the ApoE4 allele of the

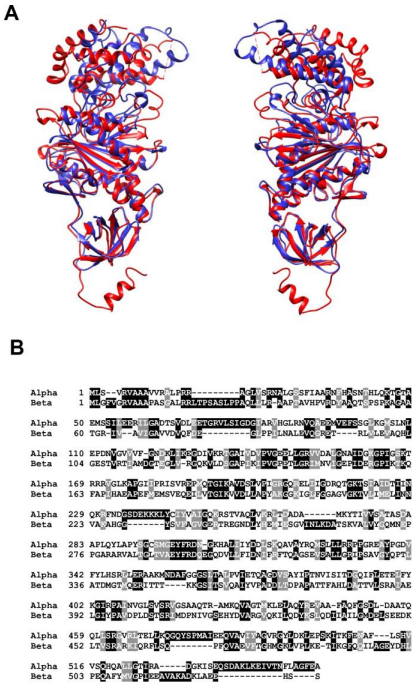

Figure 2. (**A**) Structural alignment of the alpha (red) and beta (blue) subunits of mitochondrial ATP synthase in S. scrofa. Both subunits are reproduced from image 6J5J in PDB (https://www.rcsb.org/structure/3ZIA http://doi.org/10.2210/pdb3ZIA/pdb) and processed using http://www.cgl.ucsf.edu/chimera/. (**B**) BLAST alignment of the primary amino acid sequences of H. sapiens alpha (UniProt P25705) and beta (UniProt P06576) subunits performed using https://blast.ncbi.nlm.nih.gov/Blast.cgi?PAGE=Proteins.

ApoE gene, the major genetic risk factor for sporadic AD, showed a reduction in the levels of all ATP synthase subunits they detected in comparison to ApoE3 controls [58].

Considering ATP synthase activity instead of protein expression, an early study investigating AD and ATP synthase found no significant decrease in the enzyme's catalytic activity when studying the isolated mitochondria from AD patient hippocampal tissue, motor cortex and platelets [59]. However, since this study was published there have been data published that are contradictory to this observation and these are discussed in the following sections of this review.

The α-subunit in AD

ATP synthase subunit α, Amyloid β and NFTs

Transgenic Swedish APP mice (Tg2576) had increased levels of amyloid plaque formation in the brain as they aged, compared with controls. Proteomic analysis of the brains from the Tg2576 mice found that the increase in amyloid plaque deposition with age correlated with an increase in the expression of the α-subunit [60].

An N-glycosylated form of the α-subunit has been shown to act as a binding partner of the extracellular domain of APP and Aβ, with Aβ being the primary component of the AD hallmark amyloid plaques. The α-subunit reaches the membrane via the secretory pathway and it is during this process that it becomes N-glycosylated. Schmidt et al. also demonstrated the localisation of the whole ATP synthase complex at the neuronal membrane and that its extracellular ATPase activity is inhibited by both APP and Aβ. This is especially noteworthy as APP and Aβ share sequence homology with the native ATPase inhibitory factor IF1 [61]. The inhibition was shown to downregulate long-term potentiation (LTP) at the synapses, that Aβ oligomers have since been shown to inhibit alongside the upregulation of long-term depression (LTD) via the NMDA receptors [62].

A study that builds upon the work of Schmidt et al. found that in the cortex and hippocampus of Tg APP PS1 mice, the α-subunit co-localises with insoluble plaques of Aβ – not just the soluble monomeric form of the peptide [63]. Moreover, the authors showed that this interaction occurs at the plasma membrane of neuronal cells, causes inhibition of enzymatic activity and a decrease in the levels of extracellular ATP. These decreases of extracellular ATP may be critical in the cognitive defects which arise in AD due to disruptions in synaptic plasticity, given the important role extracellular ATP plays in LTP [64, 65].

The α-subunit has been observed as part of the NFTs in human AD patient brain samples, one of the characteristic observations in AD patient brains. Monoclonal antibodies that target the insoluble brain lesions in AD found that the α-subunit acted as an antigen to one of the antibodies (AD46). Immunohistochemistry and electron microscopy confirmed the co-localisation of the α-subunit with the NFTs in the cytosol of a degenerating AD neuron [66].

ATP synthase subunit α and oxidative stress

Oxidative stress is a frequently observed phenomenon of AD. *C. elegans* that over-expressed green fluorescent protein (GFP) as a means of studying the oxidative stress caused by protein aggregation presented carbonylation of the α-subunit [67]. In the hippocampus of AD patients the α-subunit was also shown to be excessively nitrated in comparison to age-matched control brains, as well as having significantly increased protein levels [68].

Another marker of oxidative stress is the level of lipid peroxidation, that arises from the reaction of oxygen radicals with lipids to produce reactive aldehydes. One such example of this is 4-hydroxy-2-nonenal (4-HNE), that covalently attaches to proteins in a Michael addition reaction [69]. The α-subunit of ATP synthase was shown to be HNE modified in the hippocampal tissue of individuals with mild cognitive impairment (MCI), which is symptomatic of early stage AD [70, 71]. The same study also showed that, in the same tissue from MCI patients, ATP synthase had a 35% decrease in activity compared to age-matched controls when measured as a function of ADP production.

A study investigating oxidative stress in the early stages of AD (Braak stages I and II, prior to the onset of MCI) found that the α-subunit of mitochondrial ATP synthase is HNE modified in the entorhinal cortex and that ATP synthase has a decrease in activity of around 30% [72, 73]. The authors chose to use the entorhinal cortex tissue for this study as it is the location of NFTs used to track AD progression during Braak stages I and II. When these data are taken with those from Reed et al. showing 4-HNE modification of the α-subunit and decreased ATP synthase activity, there appears to be correlation between disease progression as measured by the presence of NFTs and the lipoxidation of the α-subunit resulting in reduced ATP synthase activity. Further, the presence of oxidative stress and diminished ATP synthase activity from the earliest stages of AD onset may prove critical to the pathology of the disease. If this oxidative stress precedes the presence of Aβ in the affected tissue, it raises additional questions about the primacy of the amyloid pathology in the aetiology of AD.

Whether or not the α-subunit is oxidised may be dependent upon the tissue that it is found in and the stage of AD pathology in which it is being considered. A line of transgenic mice (J20 Tg) expressing a mutant form of APP that corresponds to the Swedish and Indiana familial forms of AD had a 12.2-fold increase in the expression of the α-subunit in a whole mouse brain homogenate compared with non-Tg mouse brain homogenate [74]. However, there was no indication of oxidation when measured as a function of 3-nitrotyrosine (3-NT) modification of the protein. The authors suggest that this significant increase in the expression of the protein could be a related to cellular stress responses by the brain to maintain energy production. Future studies should look to measure the α-subunit expression of early, middle and late Braak stages of AD in brain tissues shown to have reduced ATP synthase activity as a way to try and validate their suggestion.

Post-translational modification of the α-subunit

Glycosylation of proteins with O-linked β-N-acetylglucosamine (O-GlcNAc) is a widely observed post-translational modification that regulates intra-cellular events [75]. The α-subunit can be O-GlcNAcylated on the Thr432 residue. However, this modification is reduced in the brains of AD patients, Tg AD mice and in Aβ treated mammalian cell cultures – which resulted in reduced ATP levels [76]. Molecular modelling and co-IP experiments with deletion mutants of the α- and β-subunits with no pocket site showed that Aβ directly blocks the O-GlcNAcylation of the Thr432 residue by mitochondrial O-GlcNAc transferase. Interestingly, the O-GlcNAcylation of Thr432 that had been inhibited by Aβ was rescued by treatment with O-GlcNAcase inhibitor. These findings are particularly noteworthy as they demonstrate a chemical mechanism for the interaction of the Aβ peptide with mitochondrial ATP synthase, and as a result could offer a potential therapeutic target for AD.

The β-subunit in AD

Downregulation of the β-subunit

Several studies have found changes in the expression of the β-subunit of ATP synthase in AD tissue samples and models of AD, and in particular reductions in its expression. Table 1 lists changes in protein expression of ATP synthase subunits, including the β-subunit, that are presented in this review. An early observed instance of reduced expression is the reduction of β-subunit mRNA levels by over 50% in the midtemporal cortex of AD patient brains compared with age-matched controls [77]. In another study, that linked Aβ peptides with ATP synthase in AD, rats that received a bilateral intrahippocampal injection of Aβ showed a significant decrease in the levels of β-subunit compared with controls [78]. Gene expression analysis of the entorhinal cortex of AD patient brains showed reduced expression of *ATP5C1* (γ-subunit), *ATP5D* (δ-subunit), *ATP5G1* (subunit c) and *ATP5B* (β-subunit) [79]. This strengthens the argument that ATP synthase dysfunction plays a role in the disrupted glycometabolism of AD. It must be noted that these studies do not provide a mechanism of how the expression of the β-subunit is downregulated, but early gene mapping studies of the β-subunit reported that ETS domain transcription factors and redox sensitive OXBOX and REBOX transcription factors regulate gene expression [80–82].

Autoimmune response to the β-subunit

Autoimmunity is now thought to play a role in the onset of AD [83, 84]. While this hypothesis has not been developed to the same extent as the amyloid, tau and mitochondrial hypotheses, the idea is grounded in the fact that anti-neuronal antibodies have been found in the sera of AD patients. Notably, it was found that the brain of AD patients contains antibodies which target the c-terminal domain of the β-subunit [85]. In neuroblastoma cell lines these antibodies caused a dose dependent decrease in the activity of the ATP synthase complex, and then most strikingly, apoptosis. The apoptotic event was preceded by IMM hyperpolarization and then depolarization.

A study that followed this showed that mice injected into their right cerebral ventricle with anti-β-subunit antibodies isolated from AD patient sera had reduced memory retention [86]. Additionally, an increased rate of apoptosis was detected in the dorsal hippocampal regions of their brains, post-mortem. Taken together, these two studies show a mechanism for the antibodies detected in the brain sera of AD patients to cause neuronal apoptosis and cognitive impairment, both of which are classical symptoms of AD.

Excitotoxicity and cyclin-B1 accumulation

Excitotoxicity is common to neurons in AD and may be mediated by the action of glutamate on the NMDA receptors of excitatory post-synaptic neurons [87]. Interestingly, a mechanism of ATP synthase inhibition via action on the β-subunit has been elucidated in rat cortical neurons and HEK293T cells using glutamate induced excitotoxicity [88]. Cell cultures of rat cortical neurons were treated with glutamate which resulted in an accumulation of cyclin-B1, the cyclin-B1 was shown to form complexes with Cdk1 which accumulated in mitochondria resulting in superoxide production.

Table 1. Regulation of individual ATP synthase subunit protein expression levels across different tissue samples from different AD models, summarising data presented in this review.

Model	Tissue	α-subunit	β-subunit	OSCP	Subunit d	δ-subunit	Reference
Aβ injected rat	Hippocampus		Down				Shi, X. et al., 2011
SweAPP Tg mice	Whole brain homogenate	Up					Carrette, O. et al., 2006
4 months old 5xFAD mice	Synaptic mitochondria			Down			Beck, S. J. et al., 2016
	Synaptic mitochondria			Down			Beck, S. J. et al., 2016
	Non-synaptic mitochondria			Down			Beck, S. J. et al., 2016
3x Tg AD mouse	Hippocampus				Down		Yu, H. et al., 2018
	Temporal lobe			Down			Beck, S. J. et al., 2016
	Medial frontal gyrus				Down		Adav, S. S. et al., 2019
	Temporal cortex				Down		Mukherjee, S. et al., 2017
	Frontal cortex					Up	Manczak, M. et al., 2004

HEK293T cells were then used in the study to demonstrate that the cyclin-B1-Cdk1 complex phosphorylates Bcl-xL causing its dissociation from the β-subunit of the ATP synthase, a reduction in the enzyme's catalytic activity and increased oxidative stress. Bcl-xL is a transmembrane mitochondrial protein that acts as a regulator of cell death through its action on proapoptotic factors [89]. Bcl-xL has also been shown to improve the efficiency of neuronal metabolism through its interaction with ATP synthase which decreases membrane-ion leakage [90]. From these data it is clear that a disruption of the interaction between the β-subunit and Bcl-xL could contribute to AD pathology.

OSCP in AD

OSCP downregulation in AD

In 2016 a comprehensive study was published investigating changes in expression of OSCP in the brains of human AD patients, MCI patients and Tg AD mice brains (5xFAD mice) [91]. OSCP was shown to be significantly downregulated in the temporal lobe of AD patients compared to controls. There was also a significant decrease in OSCP expression between the synaptic mitochondria of young and old 5xFAD mice compared with controls as well as in the non-synaptic mitochondria of old 5xFAD mice. Primary cultured mice neurons with downregulated OSCP showed decreased membrane potential, reduced ATP synthesis and elevated levels of superoxide. Beck et al. also demonstrated that there is a physical interaction between Aβ and the OSCP in brain mitochondria which reduced ATP synthase activity, which is supported by evidence of Aβ localising to brain mitochondria [92, 93]. This study is notable as it provides mechanistic detail and also presents another case of Aβ peptides interacting with ATP synthase subunits in a detrimental fashion, as is the case with the α-subunit.

Interaction with Cyclophilin D (Ppif)

Cyclophilin D (CypD) is one of the only proteins which appears to be essential to the elusive molecular make-up of the mitochondrial permeability transition pore (mPTP) [94]. CypD has also been demonstrated to interact with ATP synthase, regulating the formation of the respiratory efficiency enhancing synthasome [95]. Of note, it was also shown that synthasome assembly and mPTP formation are inversely proportional. A study of mice in 2017 found that CypD levels increased with ageing, as did the physical interaction between OSCP and CypD, despite a decrease in the expression levels of OSCP [96]. These changes resulted in decreased ATP synthase activity and an increase in mitochondrial dysfunction, including a decreased ATP:oxygen ratio. A follow up study found that the temporal lobe of AD

patient brains and 5xFAD mice had increased formation of CypD-OSCP complexes, and that the presence of Aβ substantially decreased the K_D of this interaction [97]. The authors also showed that in 5xFAD mice CypD promotes the OSCP-Aβ interaction as well as the ubiquitin mediated degradation of OSCP. However, CypD deficient 5xFAD mice had improved cognitive function and attenuated ATP synthase deregulation compared to their 5xFAD littermates.

Subunit d in AD

Decreased expression and gene locus risk factor

Subunit d of mitochondrial ATP synthase is a component of the F_O peripheral stalk which is encoded by the *ATP5H* (*ATP5PD*) gene, located on the long arm of nuclear chromosome 17. A genome wide association study (GWAS) found that the shared locus of *ATP5H* and *KCTD2* could be a genetic risk factor for AD, where until a few years ago *APOE4* was thought to be the only instance of this [98]. A study of 3x Tg AD mice found significantly decreased expression of *ATP5H* in hippocampal tissue [99]. An LC-MS/MS-based iTRAQ quantitative proteomics study also demonstrated that multiple proteins from the mitochondrial proteome are under-expressed in the medial frontal gyrus of AD human patients including *ATP5H*, *ATP5B*, *ATP5I* and *ATP5J* compared with age-matched controls [100]. Perhaps most interestingly, another GWAS found the *ATP5H* gene to be a candidate gene of interest in late-onset AD (LOAD) and that its expression was decreased in the temporal cortex of AD patients [101]. An RNAi knockdown of *C. elegans* Tg for Aβ peptide proved to be protective against Aβ toxicity. From these data we can see that the *ATP5H* gene appears to be associated with LOAD, but any kind of molecular mechanism for this association is yet to be elucidated.

The δ-subunit in AD

Upregulation in AD

The δ-subunit of mitochondrial ATP synthase is part of the F_1 component and associates with the γ-subunit of the rotary stalk, in proximity of the F_0 c-ring. It is encoded by the *ATP5D* gene located on the short arm of nuclear chromosome 19. In 2004 a study from Manczak et al. showed increased mRNA levels for *ATP6* and *ATP8* genes in AD patient brains, while immunofluorescence analysis of the frontal cortex of AD patients found increased levels of the δ-subunit of ATP synthase [102]. While isolated, these data show yet another example of altered patterns of subunit expression across different tissues of the human AD brain.

ATP synthase therapeutics in AD

J147

J147 was identified in 2011 through a drug discovery scheme that sought to target age associated pathologies, as opposed to amyloid plaques, due to age being the greatest risk-factor in AD onset [103]. J147 is a neurotrophic compound that has proven safe to use in animal studies and has been shown to rescue cognitive defects in aged mouse models of AD [104]. The cognitive rescue effects seen in this study are shown to correlate with the induction of the neurotrophic factors NGF (nerve growth factor) and BDNF (brain derived neurotrophic factor). A later study from the same group demonstrated that the α-subunit is a molecular target of J147 and that J147 modulates ATP synthase activity [105]. The mild inhibition of ATP synthase by J147 may be neuroprotective. J147 also activates the canonical longevity pathway of AMPK/mTOR via CamKK2 and its administration was shown to extend the lifespan of *Drosophila*. This is noteworthy due to the fact that ageing is the biggest risk factor for the onset of AD.

Following this, a computational modelling paper of mitochondrial αβγ was published which demonstrated a mechanism of how J147 could bind to the α-subunit and modulate enzymatic activity [106]. Soliman et al. then used their per-residue energy decomposition (PRED) protocol to identify three compounds from a molecular library which could modulate ATP synthase activity in a similar manner to J147 [107]. The compounds which they identified had a higher binding propensity for the α-subunit than J147 and specifically targeted Arg1112 and Gln426 for binding.

While J147 may have potential as an effective treatment for AD, it is noteworthy that the mechanism of action is through an inhibition of ATP synthase activity given that ATP synthase activity inhibition has been observed as part of the pathophysiology of AD. It may be that there are subtle but significant differences in the decreased levels of enzymatic activity between those induced by J147 and those observed in studies of AD. We suggest that the stage of disease progression should also be considered with J147 administration, as it may be the case that the positive outcomes of J147 treatment may not be observed once pathological ATP synthase activity inhibition crosses a certain threshold.

Taken together, these data present J147 as a potentially suitable AD drug which alleviates cognitive symptoms after they have presented with a known mechanism of action. Currently J147 is undergoing clinical trials to assess its safety and efficacy as a treatment for AD.

Salvianolic acid B (SalB)

Salvianolic acid B (SalB) is a polyphenolic compound which possesses therapeutic potential as a treatment of AD. SalB has been suggested to act on multiple different pathologies present in various neurodegenerative diseases, and in particular mitochondrial dysfunction [108]. In both cellular and mouse models of AD it has been reported that SalB can inhibit Aβ generation and may help to prevent neuroinflammation [109–111]. Alongside mitochondrial dysfunction, these two phenomena are pathologies classically associated with AD.

With regards to ATP synthase and SalB, a study in 2018 showed that in mouse neuronal cell cultures treated with Aβ SalB was able suppress superoxide production, preserve mitochondrial dynamics and mitigate the decrease in ATP synthase activity [112]. While no mechanism is offered by the authors of the paper, this is a line of investigation that we believe should be further pursued.

CONCLUSION

AD is widely studied due to the hugely debilitating effects it exhibits on the individual, as well as its prevalence in countries with ageing populations. The dysfunction of mitochondria is heavily implicated in the aetiology of the sporadic and familial forms of AD. There is some debate about whether mitochondrial dysfunction is the primary lesion in the disease onset. Likely mitochondrial dysfunction is a convergence point for several concurrent lesions resulting in disease pathology and progression. However, little attention has so far been paid to the role that ATP synthase may play in AD. The data presented in this review suggest that this is an oversight and that the dysfunction of ATP synthase and its constituent components not only leads to disease onset, but that the enzyme complex can be targeted pharmacologically to treat the disease. In J147 there is a candidate drug currently undergoing clinical trials, and we follow these developments with cautious optimism. While only one study so far has investigated the efficacy of SalB as a potential therapeutic agent for AD, the data produced is encouraging and we hope to see this investigated further. Due to both the structural and functional complexity of ATP synthase, we see that its contribution to both disease pathology and its potential therapeutic targeting should be considered with enthusiasm and studied with intellectual nuance.

CONFLICTS OF INTEREST

The authors declare that they have no conflicts of interest.

FUNDING

This work was supported by the Biotechnology and Biological Sciences Research Council [grant number BB/J014508/1], via awards to BE and TLI.

REFERENCES

1. GBD 2016 Dementia Collaborators. Global, regional, and national burden of Alzheimer's disease and other dementias, 1990-2016: a systematic analysis for the global burden of disease study 2016. Lancet Neurol. 2019; 18:88–106. https://doi.org/10.1016/S1474-4422(18)30403-4 PMID:30497964
2. Mitchell E, Walker R. Global ageing: successes, challenges and opportunities. Br J Hosp Med (Lond). 2020; 81:1–9. https://doi.org/10.12968/hmed.2019.0377 PMID:32097073
3. Neugroschl J, Wang S. Alzheimer's disease: diagnosis and treatment across the spectrum of disease severity. Mt Sinai J Med. 2011; 78:596–612. https://doi.org/10.1002/msj.20279 PMID:21748748
4. Querfurth HW, LaFerla FM. Alzheimer's disease. N Engl J Med. 2010; 362:329–44. https://doi.org/10.1056/NEJMra0909142 PMID:20107219
5. Swerdlow RH, Khan SM. A "mitochondrial cascade hypothesis" for sporadic Alzheimer's disease. Med Hypotheses. 2004; 63:8–20. https://doi.org/10.1016/j.mehy.2003.12.045 PMID:15193340
6. Swerdlow RH. Mitochondria and mitochondrial cascades in Alzheimer's disease. J Alzheimers Dis. 2018; 62:1403–16. https://doi.org/10.3233/JAD-170585 PMID:29036828
7. Zhao Y, Zhao B. Oxidative stress and the pathogenesis of Alzheimer's disease. Oxid Med Cell Longev. 2013; 2013:316523. https://doi.org/10.1155/2013/316523 PMID:23983897
8. Wang X, Wang W, Li L, Perry G, Lee HG, Zhu X. Oxidative stress and mitochondrial dysfunction in Alzheimer's disease. Biochim Biophys Acta. 2014; 1842:1240–47. https://doi.org/10.1016/j.bbadis.2013.10.015 PMID:24189435
9. Chen JX, Yan SS. Role of mitochondrial amyloid-beta in Alzheimer's disease. J Alzheimers Dis. 2010 (Suppl 2); 20:S569–78. https://doi.org/10.3233/JAD-2010-100357 PMID:20463403

10. Cheng Y, Bai F. The association of tau with mitochondrial dysfunction in Alzheimer's disease. Front Neurosci. 2018; 12:163. https://doi.org/10.3389/fnins.2018.00163 PMID:29623026

11. Grüber G, Wieczorek H, Harvey WR, Müller V. Structure-function relationships of A-, F- and V-ATPases. J Exp Biol. 2001; 204:2597–605. PMID:11533110

12. Kühlbrandt W, Davies KM. Rotary ATPases: a new twist to an ancient machine. Trends Biochem Sci. 2016; 41:106–16. https://doi.org/10.1016/j.tibs.2015.10.006 PMID:26671611

13. von Ballmoos C, Wiedenmann A, Dimroth P. Essentials for ATP synthesis by F1F0 ATP synthases. Annu Rev Biochem. 2009; 78:649–72. https://doi.org/10.1146/annurev.biochem.78.081307.104803 PMID:19489730

14. Ruhoy IS, Saneto RP. The genetics of leigh syndrome and its implications for clinical practice and risk management. Appl Clin Genet. 2014; 7:221–34. https://doi.org/10.2147/TACG.S46176 PMID:25419155

15. Dautant A, Meier T, Hahn A, Tribouillard-Tanvier D, di Rago JP, Kucharczyk R. ATP synthase diseases of mitochondrial genetic origin. Front Physiol. 2018; 9:329. https://doi.org/10.3389/fphys.2018.00329 PMID:29670542

16. Xu T, Pagadala V, Mueller DM. Understanding structure, function, and mutations in the mitochondrial ATP synthase. Microb Cell. 2015; 2:105–25. https://doi.org/10.15698/mic2015.04.197 PMID:25938092

17. Mitchell P. Coupling of phosphorylation to electron and hydrogen transfer by a chemi-osmotic type of mechanism. Nature. 1961; 191:144–48. https://doi.org/10.1038/191144a0 PMID:13771349

18. Mitchell P. Chemiosmotic coupling in oxidative and photosynthetic phosphorylation. Biol Rev Camb Philos Soc. 1966; 41:445–502. https://doi.org/10.1111/j.1469-185x.1966.tb01501.x PMID:5329743

19. Walker JE. The ATP synthase: the understood, the uncertain and the unknown. Biochem Soc Trans. 2013; 41:1–16. https://doi.org/10.1042/BST20110773 PMID:23356252

20. Taurino F, Giannoccaro C, Sardanelli AM, Cavallo A, De Luca E, Santacroce S, Papa S, Zanotti F, Gnoni A. Function and expression study uncovered hepatocyte plasma membrane ecto-ATP synthase as a novel player in liver regeneration. Biochem J. 2016; 473:2519–30. https://doi.org/10.1042/BCJ20160065 PMID:27287557

21. Chang HY, Huang TC, Chen NN, Huang HC, Juan HF. Combination therapy targeting ectopic ATP synthase and 26S proteasome induces ER stress in breast cancer cells. Cell Death Dis. 2014; 5:e1540. https://doi.org/10.1038/cddis.2014.504 PMID:25429617

22. Boyer PD, Cross RL, Momsen W. A new concept for energy coupling in oxidative phosphorylation based on a molecular explanation of the oxygen exchange reactions. Proc Natl Acad Sci USA. 1973; 70:2837–39. https://doi.org/10.1073/pnas.70.10.2837 PMID:4517936

23. Gresser MJ, Myers JA, Boyer PD. Catalytic site cooperativity of beef heart mitochondrial F1 adenosine triphosphatase. Correlations of initial velocity, bound intermediate, and oxygen exchange measurements with an alternating three-site model. J Biol Chem. 1982; 257:12030–8. PMID:6214554

24. Abrahams JP, Leslie AG, Lutter R, Walker JE. Structure at 2.8 a resolution of F_1-ATPase from bovine heart mitochondria. Nature. 1994; 370:621–28. https://doi.org/10.1038/370621a0 PMID:8065448

25. Sobti M, Smits C, Wong AS, Ishmukhametov R, Stock D, Sandin S, Stewart AG. cryo-EM structures of the autoinhibited E. Coli ATP synthase in three rotational states. Elife. 2016; 5:e21598. https://doi.org/10.7554/eLife.21598 PMID:28001127

26. Stock D, Leslie AG, Walker JE. Molecular architecture of the rotary motor in ATP synthase. Science. 1999; 286:1700–05. https://doi.org/10.1126/science.286.5445.1700 PMID:10576729

27. Gu J, Zhang L, Zong S, Guo R, Liu T, Yi J, Wang P, Zhuo W, Yang M. cryo-EM structure of the mammalian ATP synthase tetramer bound with inhibitory protein IF1. Science. 2019; 364:1068–75. https://doi.org/10.1126/science.aaw4852 PMID:31197009

28. Reynolds CR, Islam SA, Sternberg MJ. EzMol: a web server wizard for the rapid visualization and image production of protein and nucleic acid structures. J Mol Biol. 2018; 430:2244–48. https://doi.org/10.1016/j.jmb.2018.01.013 PMID:29391170

29. Nesci S, Trombetti F, Ventrella V, Pagliarani A. The c-ring of the F1FO-ATP synthase: facts and perspectives. J Membr Biol. 2016; 249:11–21.

https://doi.org/10.1007/s00232-015-9860-3 PMID:26621635

30. Ohsakaya S, Fujikawa M, Hisabori T, Yoshida M. Knockdown of DAPIT (diabetes-associated protein in insulin-sensitive tissue) results in loss of ATP synthase in mitochondria. J Biol Chem. 2011; 286:20292–96. https://doi.org/10.1074/jbc.M110.198523 PMID:21345788

31. He J, Ford HC, Carroll J, Douglas C, Gonzales E, Ding S, Fearnley IM, Walker JE. Assembly of the membrane domain of ATP synthase in human mitochondria. Proc Natl Acad Sci USA. 2018; 115:2988–93. https://doi.org/10.1073/pnas.1722086115 PMID:29440398

32. Antoniel M, Giorgio V, Fogolari F, Glick GD, Bernardi P, Lippe G. The oligomycin-sensitivity conferring protein of mitochondrial ATP synthase: emerging new roles in mitochondrial pathophysiology. Int J Mol Sci. 2014; 15:7513–36. https://doi.org/10.3390/ijms15057513 PMID:24786291

33. Angevine CM, Fillingame RH. Aqueous access channels in subunit a of rotary ATP synthase. J Biol Chem. 2003; 278:6066–74. https://doi.org/10.1074/jbc.M210199200 PMID:12473663

34. Symersky J, Pagadala V, Osowski D, Krah A, Meier T, Faraldo-Gómez JD, Mueller DM. Structure of the c_{10} ring of the yeast mitochondrial ATP synthase in the open conformation. Nat Struct Mol Biol. 2012; 19:485–91. https://doi.org/10.1038/nsmb.2284 PMID:22504883

35. Allegretti M, Klusch N, Mills DJ, Vonck J, Kühlbrandt W, Davies KM. Horizontal membrane-intrinsic α-helices in the stator a-subunit of an f-type ATP synthase. Nature. 2015; 521:237–40. https://doi.org/10.1038/nature14185 PMID:25707805

36. Noji H, Yasuda R, Yoshida M, Kinosita K Jr. Direct observation of the rotation of F1-ATPase. Nature. 1997; 386:299–302. https://doi.org/10.1038/386299a0 PMID:9069291

37. Fillingame RH, Angevine CM, Dmitriev OY. Mechanics of coupling proton movements to c-ring rotation in ATP synthase. FEBS Lett. 2003; 555:29–34. https://doi.org/10.1016/s0014-5793(03)01101-3 PMID:14630314

38. Rees DM, Leslie AG, Walker JE. The structure of the membrane extrinsic region of bovine ATP synthase. Proc Natl Acad Sci USA. 2009; 106:21597–601. https://doi.org/10.1073/pnas.0910365106 PMID:19995987

39. Giorgio V, Fogolari F, Lippe G, Bernardi P. OSCP subunit of mitochondrial ATP synthase: role in regulation of enzyme function and of its transition to a pore. Br J Pharmacol. 2019; 176:4247–57. https://doi.org/10.1111/bph.14513 PMID:30291799

40. Menz RI, Walker JE, Leslie AG. Structure of bovine mitochondrial F_1-ATPase with nucleotide bound to all three catalytic sites: implications for the mechanism of rotary catalysis. Cell. 2001; 106:331–41. https://doi.org/10.1016/s0092-8674(01)00452-4 PMID:11509182

41. Braig K, Menz RI, Montgomery MG, Leslie AG, Walker JE. Structure of bovine mitochondrial F_1-ATPase inhibited by Mg^{2+}ADP and aluminium fluoride. Structure. 2000; 8:567–73. https://doi.org/10.1016/s0969-2126(00)00145-3 PMID:10873854

42. Kagawa R, Montgomery MG, Braig K, Leslie AG, Walker JE. The structure of bovine F_1-ATPase inhibited by ADP and beryllium fluoride. EMBO J. 2004; 23:2734–44. https://doi.org/10.1038/sj.emboj.7600293 PMID:15229653

43. Pettersen EF, Goddard TD, Huang CC, Couch GS, Greenblatt DM, Meng EC, Ferrin TE. UCSF chimera—a visualization system for exploratory research and analysis. J Comput Chem. 2004; 25:1605–12. https://doi.org/10.1002/jcc.20084 PMID:15264254

44. Dittrich M, Hayashi S, Schulten K. On the mechanism of ATP hydrolysis in F_1-ATPase. Biophys J. 2003; 85:2253–66. https://doi.org/10.1016/S0006-3495(03)74650-5 PMID:14507690

45. Sakamoto J. Identification of the nucleotide-binding site for ATP synthesis and hydrolysis in mitochondrial soluble F_1-ATPase. J Biochem. 1984; 96:475–81. https://doi.org/10.1093/oxfordjournals.jbchem.a134859 PMID:6238951

46. Ma J, Flynn TC, Cui Q, Leslie AG, Walker JE, Karplus M. A dynamic analysis of the rotation mechanism for conformational change in F_1-ATPase. Structure. 2002; 10:921–31. https://doi.org/10.1016/s0969-2126(02)00789-x PMID:12121647

47. Senior AE, Nadanaciva S, Weber J. The molecular mechanism of ATP synthesis by F1F0-ATP synthase. Biochim Biophys Acta. 2002; 1553:188–211. https://doi.org/10.1016/s0005-2728(02)00185-8 PMID:11997128

48. Feniouk BA, Yoshida M. Regulatory mechanisms of proton-translocating F_OF_1-ATP synthase. Results Probl Cell Differ. 2008; 45:279–308.

https://doi.org/10.1007/400_2007_043 PMID:18026702

49. Okuno D, Iino R, Noji H. Rotation and structure of F_oF_1-ATP synthase. J Biochem. 2011; 149:655–64. https://doi.org/10.1093/jb/mvr049 PMID:21524994

50. Swerdlow RH, Burns JM, Khan SM. The Alzheimer's disease mitochondrial cascade hypothesis. J Alzheimers Dis. 2010 (Suppl 2); 20:S265–79. https://doi.org/10.3233/JAD-2010-100339 PMID:20442494

51. Makin S. The amyloid hypothesis on trial. Nature. 2018; 559:S4–S7. https://doi.org/10.1038/d41586-018-05719-4 PMID:30046080

52. Kametani F, Hasegawa M. Reconsideration of amyloid hypothesis and tau hypothesis in Alzheimer's disease. Front Neurosci. 2018; 12:25. https://doi.org/10.3389/fnins.2018.00025 PMID:29440986

53. Sun N, Youle RJ, Finkel T. The Mitochondrial Basis of Aging. Mol Cell. 2016; 61:654–666. https://doi.org/10.1016/j.molcel.2016.01.028 PMID:26942670

54. Blum TB, Hahn A, Meier T, Davies KM, Kühlbrandt W. Dimers of mitochondrial ATP synthase induce membrane curvature and self-assemble into rows. Proc Natl Acad Sci USA. 2019; 116:4250–55. https://doi.org/10.1073/pnas.1816556116 PMID:30760595

55. Schägger H, Ohm TG. Human diseases with defects in oxidative phosphorylation. 2. F1F0 ATP-synthase defects in Alzheimer disease revealed by blue native polyacrylamide gel electrophoresis. Eur J Biochem. 1995; 227:916–21. https://doi.org/10.1111/j.1432-1033.1995.tb20219.x PMID:7867655

56. Liang WS, Reiman EM, Valla J, Dunckley T, Beach TG, Grover A, Niedzielko TL, Schneider LE, Mastroeni D, Caselli R, Kukull W, Morris JC, Hulette CM, et al. Alzheimer's disease is associated with reduced expression of energy metabolism genes in posterior cingulate neurons. Proc Natl Acad Sci USA. 2008; 105:4441–46. https://doi.org/10.1073/pnas.0709259105 PMID:18332434

57. Martín-Maestro P, Sproul A, Martinez H, Paquet D, Gerges M, Noggle S, Starkov AA. Autophagy induction by bexarotene promotes mitophagy in presenilin 1 familial Alzheimer's disease iPSC-derived neural stem cells. Mol Neurobiol. 2019; 56:8220–36. https://doi.org/10.1007/s12035-019-01665-y PMID:31203573

58. Orr AL, Kim C, Jimenez-Morales D, Newton BW, Johnson JR, Krogan NJ, Swaney DL, Mahley RW. Neuronal apolipoprotein E4 expression results in proteome-wide alterations and compromises bioenergetic capacity by disrupting mitochondrial function. J Alzheimers Dis. 2019; 68:991–1011. https://doi.org/10.3233/JAD-181184 PMID:30883359

59. Bosetti F, Brizzi F, Barogi S, Mancuso M, Siciliano G, Tendi EA, Murri L, Rapoport SI, Solaini G. Cytochrome c oxidase and mitochondrial F_1F_0-ATPase (ATP synthase) activities in platelets and brain from patients with Alzheimer's disease. Neurobiol Aging. 2002; 23:371–76. https://doi.org/10.1016/s0197-4580(01)00314-1 PMID:11959398

60. Carrette O, Burgess JA, Burkhard PR, Lang C, Côte M, Rodrigo N, Hochstrasser DF, Sanchez JC. Changes of the cortex proteome and apolipoprotein E in transgenic mouse models of Alzheimer's disease. J Chromatogr B Analyt Technol Biomed Life Sci. 2006; 840:1–9. https://doi.org/10.1016/j.jchromb.2006.05.019 PMID:16781898

61. Schmidt C, Lepsverdize E, Chi SL, Das AM, Pizzo SV, Dityatev A, Schachner M. Amyloid precursor protein and amyloid beta-peptide bind to ATP synthase and regulate its activity at the surface of neural cells. Mol Psychiatry. 2008; 13:953–69. https://doi.org/10.1038/sj.mp.4002077 PMID:17726461

62. Shankar GM, Li S, Mehta TH, Garcia-Munoz A, Shepardson NE, Smith I, Brett FM, Farrell MA, Rowan MJ, Lemere CA, Regan CM, Walsh DM, Sabatini BL, Selkoe DJ. Amyloid-beta protein dimers isolated directly from Alzheimer's brains impair synaptic plasticity and memory. Nat Med. 2008; 14:837–42. https://doi.org/10.1038/nm1782 PMID:18568035

63. Xing SL, Chen B, Shen DZ, Zhu CQ. B-amyloid peptide binds and regulates ectopic ATP synthase α-chain on neural surface. Int J Neurosci. 2012; 122:290–97. https://doi.org/10.3109/00207454.2011.649867 PMID:22185089

64. Fujii S. ATP- and adenosine-mediated signaling in the central nervous system: the role of extracellular ATP in hippocampal long-term potentiation. J Pharmacol Sci. 2004; 94:103–06. https://doi.org/10.1254/jphs.94.103 PMID:14978345

65. Yamazaki Y, Fujii S. Extracellular ATP modulates synaptic plasticity induced by activation of metabotropic glutamate receptors in the hippocampus. Biomed Res. 2015; 36:1–9.

https://doi.org/10.2220/biomedres.36.1
PMID:25749146

66. Sergeant N, Wattez A, Galván-valencia M, Ghestem A, David JP, Lemoine J, Sautiére PE, Dachary J, Mazat JP, Michalski JC, Velours J, Mena-López R, Delacourte A. Association of ATP synthase alpha-chain with neurofibrillary degeneration in Alzheimer's disease. Neuroscience. 2003; 117:293–303. https://doi.org/10.1016/s0306-4522(02)00747-9 PMID:12614671

67. Boyd-Kimball D, Poon HF, Lynn BC, Cai J, Pierce WM Jr, Klein JB, Ferguson J, Link CD, Butterfield DA. Proteomic identification of proteins specifically oxidized in caenorhabditis elegans expressing human Aβ(1-42): implications for Alzheimer's disease. Neurobiol Aging. 2006; 27:1239–49. https://doi.org/10.1016/j.neurobiolaging.2005.07.001 PMID:16099075

68. Sultana R, Poon HF, Cai J, Pierce WM, Merchant M, Klein JB, Markesbery WR, Butterfield DA. Identification of nitrated proteins in Alzheimer's disease brain using a redox proteomics approach. Neurobiol Dis. 2006; 22:76–87. https://doi.org/10.1016/j.nbd.2005.10.004 PMID:16378731

69. Reed TT. Lipid peroxidation and neurodegenerative disease. Free Radic Biol Med. 2011; 51:1302–19. https://doi.org/10.1016/j.freeradbiomed.2011.06.027 PMID:21782935

70. Reed T, Perluigi M, Sultana R, Pierce WM, Klein JB, Turner DM, Coccia R, Markesbery WR, Butterfield DA. Redox proteomic identification of 4-hydroxy-2-nonenal-modified brain proteins in amnestic mild cognitive impairment: insight into the role of lipid peroxidation in the progression and pathogenesis of Alzheimer's disease. Neurobiol Dis. 2008; 30:107–20. https://doi.org/10.1016/j.nbd.2007.12.007 PMID:18325775

71. Lindeboom J, Weinstein H. Neuropsychology of cognitive ageing, minimal cognitive impairment, Alzheimer's disease, and vascular cognitive impairment. Eur J Pharmacol. 2004; 490:83–86. https://doi.org/10.1016/j.ejphar.2004.02.046 PMID:15094075

72. Terni B, Boada J, Portero-Otin M, Pamplona R, Ferrer I. Mitochondrial ATP-synthase in the entorhinal cortex is a target of oxidative stress at stages I/II of Alzheimer's disease pathology. Brain Pathol. 2010; 20:222–33. https://doi.org/10.1111/j.1750-3639.2009.00266.x PMID:19298596

73. Braak H, Braak E. Neuropathological stageing of Alzheimer-related changes. Acta Neuropathol. 1991; 82:239–59. https://doi.org/10.1007/BF00308809 PMID:1759558

74. Robinson RA, Lange MB, Sultana R, Galvan V, Fombonne J, Gorostiza O, Zhang J, Warrier G, Cai J, Pierce WM, Bredesen DE, Butterfield DA. Differential expression and redox proteomics analyses of an Alzheimer disease transgenic mouse model: effects of the amyloid-β peptide of amyloid precursor protein. Neuroscience. 2011; 177:207–22. https://doi.org/10.1016/j.neuroscience.2011.01.005 PMID:21223993

75. Yang X, Qian K. Protein O-GlcNAcylation: emerging mechanisms and functions. Nat Rev Mol Cell Biol. 2017; 18:452–65. https://doi.org/10.1038/nrm.2017.22 PMID:28488703

76. Cha MY, Cho HJ, Kim C, Jung YO, Kang MJ, Murray ME, Hong HS, Choi YJ, Choi H, Kim DK, Choi H, Kim J, Dickson DW, et al. Mitochondrial ATP synthase activity is impaired by suppressed O-GlcNAcylation in Alzheimer's disease. Hum Mol Genet. 2015; 24:6492–504. https://doi.org/10.1093/hmg/ddv358 PMID:26358770

77. Chandrasekaran K, Hatanpää K, Rapoport SI, Brady DR. Decreased expression of nuclear and mitochondrial DNA-encoded genes of oxidative phosphorylation in association neocortex in Alzheimer disease. Brain Res Mol Brain Res. 1997; 44:99–104. https://doi.org/10.1016/s0169-328x(96)00191-x PMID:9030703

78. Shi X, Lu X, Zhan L, Liu L, Sun M, Gong X, Sui H, Niu X, Liu S, Zheng L, Chen J, Zhou Y. Rat hippocampal proteomic alterations following intrahippocampal injection of amyloid beta peptide (1-40). Neurosci Lett. 2011; 500:87–91. https://doi.org/10.1016/j.neulet.2011.06.009 PMID:21699958

79. Ding B, Xi Y, Gao M, Li Z, Xu C, Fan S, He W. Gene expression profiles of entorhinal cortex in Alzheimer's disease. Am J Alzheimers Dis Other Demen. 2014; 29:526–32. https://doi.org/10.1177/1533317514523487 PMID:24558171

80. Chung AB, Stepien G, Haraguchi Y, Li K, Wallace DC. Transcriptional control of nuclear genes for the mitochondrial muscle ADP/ATP translocator and the ATP synthase beta subunit. Multiple factors interact

with the OXBOX/REBOX promoter sequences. J Biol Chem. 1992; 267:21154–61. PMID:1400425

81. Haraguchi Y, Chung AB, Neill S, Wallace DC. OXBOX and REBOX, overlapping promoter elements of the mitochondrial F0F1-ATP synthase beta subunit gene. Oxbox/REBOX in the ATPsyn beta promoter. J Biol Chem. 1994; 269:9330–34. PMID:8132672

82. Villena JA, Martin I, Viñas O, Cormand B, Iglesias R, Mampel T, Giralt M, Villarroya F. ETS transcription factors regulate the expression of the gene for the human mitochondrial ATP synthase beta-subunit. J Biol Chem. 1994; 269:32649–54. PMID:7798271

83. D'Andrea MR. Add Alzheimer's disease to the list of autoimmune diseases. Med Hypotheses. 2005; 64:458–63. https://doi.org/10.1016/j.mehy.2004.08.024 PMID:15617848

84. Wotton CJ, Goldacre MJ. Associations between specific autoimmune diseases and subsequent dementia: retrospective record-linkage cohort study, UK. J Epidemiol Community Health. 2017; 71:576–83. https://doi.org/10.1136/jech-2016-207809 PMID:28249989

85. Vacirca D, Delunardo F, Matarrese P, Colasanti T, Margutti P, Siracusano A, Pontecorvo S, Capozzi A, Sorice M, Francia A, Malorni W, Ortona E. Autoantibodies to the adenosine triphosphate synthase play a pathogenetic role in Alzheimer's disease. Neurobiol Aging. 2012; 33:753–66. https://doi.org/10.1016/j.neurobiolaging.2010.05.013 PMID:20594618

86. Berry A, Vacirca D, Capoccia S, Bellisario V, Malorni W, Ortona E, Cirulli F. anti-ATP synthase autoantibodies induce neuronal death by apoptosis and impair cognitive performance in C57BL/6J mice. J Alzheimers Dis. 2013; 33:317–21. https://doi.org/10.3233/JAD-2012-121312 PMID:22954670

87. Hynd MR, Scott HL, Dodd PR. Glutamate-mediated excitotoxicity and neurodegeneration in Alzheimer's disease. Neurochem Int. 2004; 45:583–95. https://doi.org/10.1016/j.neuint.2004.03.007 PMID:15234100

88. Veas-Pérez de Tudela M, Delgado-Esteban M, Maestre C, Bobo-Jiménez V, Jiménez-Blasco D, Vecino R, Bolaños JP, Almeida A. Regulation of bcl-xL-ATP synthase interaction by mitochondrial cyclin B1-cyclin-dependent kinase-1 determines neuronal survival. J Neurosci. 2015; 35:9287–301. https://doi.org/10.1523/JNEUROSCI.4712-14.2015 PMID:26109654

89. Michels J, Kepp O, Senovilla L, Lissa D, Castedo M, Kroemer G, Galluzzi L. Functions of BCL-X L at the interface between cell death and metabolism. Int J Cell Biol. 2013; 2013:705294. https://doi.org/10.1155/2013/705294 PMID:23533418

90. Alavian KN, Li H, Collis L, Bonanni L, Zeng L, Sacchetti S, Lazrove E, Nabili P, Flaherty B, Graham M, Chen Y, Messerli SM, Mariggio MA, et al. bcl-xL regulates metabolic efficiency of neurons through interaction with the mitochondrial F1FO ATP synthase. Nat Cell Biol. 2011; 13:1224–33. https://doi.org/10.1038/ncb2330 PMID:21926988

91. Beck SJ, Guo L, Phensy A, Tian J, Wang L, Tandon N, Gauba E, Lu L, Pascual JM, Kroener S, Du H. Deregulation of mitochondrial F1FO-ATP synthase via OSCP in Alzheimer's disease. Nat Commun. 2016; 7:11483. https://doi.org/10.1038/ncomms11483 PMID:27151236

92. Caspersen C, Wang N, Yao J, Sosunov A, Chen X, Lustbader JW, Xu HW, Stern D, McKhann G, Yan SD. Mitochondrial abeta: a potential focal point for neuronal metabolic dysfunction in Alzheimer's disease. FASEB J. 2005; 19:2040–41. https://doi.org/10.1096/fj.05-3735fje PMID:16210396

93. Manczak M, Anekonda TS, Henson E, Park BS, Quinn J, Reddy PH. Mitochondria are a direct site of a beta accumulation in Alzheimer's disease neurons: implications for free radical generation and oxidative damage in disease progression. Hum Mol Genet. 2006; 15:1437–49. https://doi.org/10.1093/hmg/ddl066 PMID:16551656

94. Izzo V, Bravo-San Pedro JM, Sica V, Kroemer G, Galluzzi L. Mitochondrial permeability transition: new findings and persisting uncertainties. Trends Cell Biol. 2016; 26:655–67. https://doi.org/10.1016/j.tcb.2016.04.006 PMID:27161573

95. Beutner G, Alanzalon RE, Porter GA Jr. Cyclophilin D regulates the dynamic assembly of mitochondrial ATP synthase into synthasomes. Sci Rep. 2017; 7:14488. https://doi.org/10.1038/s41598-017-14795-x PMID:29101324

96. Gauba E, Guo L, Du H. Cyclophilin D promotes brain mitochondrial F1FO ATP synthase dysfunction in aging mice. J Alzheimers Dis. 2017; 55:1351–62. https://doi.org/10.3233/JAD-160822 PMID:27834780

97. Gauba E, Chen H, Guo L, Du H. Cyclophilin D deficiency attenuates mitochondrial F1Fo ATP synthase

dysfunction via OSCP in Alzheimer's disease. Neurobiol Dis. 2019; 121:138–47.
https://doi.org/10.1016/j.nbd.2018.09.020
PMID:30266287

98. Boada M, Antúnez C, Ramírez-Lorca R, DeStefano AL, González-Pérez A, Gayán J, López-Arrieta J, Ikram MA, Hernández I, Marín J, Galán JJ, Bis JC, Mauleón A, et al, and Alzheimer's Disease Neuroimaging Initiative. ATP5H/KCTD2 locus is associated with Alzheimer's disease risk. Mol Psychiatry. 2014; 19:682–87.
https://doi.org/10.1038/mp.2013.86
PMID:23857120

99. Yu H, Lin X, Wang D, Zhang Z, Guo Y, Ren X, Xu B, Yuan J, Liu J, Spencer PS, Wang JZ, Yang X. Mitochondrial molecular abnormalities revealed by proteomic analysis of hippocampal organelles of mice triple transgenic for Alzheimer disease. Front Mol Neurosci. 2018; 11:74.
https://doi.org/10.3389/fnmol.2018.00074
PMID:29593495

100. Adav SS, Park JE, Sze SK. Quantitative profiling brain proteomes revealed mitochondrial dysfunction in Alzheimer's disease. Mol Brain. 2019; 12:8.
https://doi.org/10.1186/s13041-019-0430-y
PMID:30691479

101. Mukherjee S, Russell JC, Carr DT, Burgess JD, Allen M, Serie DJ, Boehme KL, Kauwe JS, Naj AC, Fardo DW, Dickson DW, Montine TJ, Ertekin-Taner N, et al. Systems biology approach to late-onset Alzheimer's disease genome-wide association study identifies novel candidate genes validated using brain expression data and caenorhabditis elegans experiments. Alzheimers Dement. 2017; 13:1133–42.
https://doi.org/10.1016/j.jalz.2017.01.016
PMID:28242297

102. Manczak M, Park BS, Jung Y, Reddy PH. Differential expression of oxidative phosphorylation genes in patients with Alzheimer's disease: implications for early mitochondrial dysfunction and oxidative damage. Neuromolecular Med. 2004; 5:147–62.
https://doi.org/10.1385/NMM:5:2:147
PMID:15075441

103. Chen Q, Prior M, Dargusch R, Roberts A, Riek R, Eichmann C, Chiruta C, Akaishi T, Abe K, Maher P, Schubert D. A novel neurotrophic drug for cognitive enhancement and Alzheimer's disease. PLoS One. 2011; 6:e27865.
https://doi.org/10.1371/journal.pone.0027865
PMID:22194796

104. Prior M, Dargusch R, Ehren JL, Chiruta C, Schubert D. The neurotrophic compound J147 reverses cognitive impairment in aged Alzheimer's disease mice. Alzheimers Res Ther. 2013; 5:25.
https://doi.org/10.1186/alzrt179
PMID:23673233

105. Goldberg J, Currais A, Prior M, Fischer W, Chiruta C, Ratliff E, Daugherty D, Dargusch R, Finley K, Esparza-Moltó PB, Cuezva JM, Maher P, Petrascheck M, Schubert D. The mitochondrial ATP synthase is a shared drug target for aging and dementia. Aging Cell. 2018; 17:e12715.
https://doi.org/10.1111/acel.12715
PMID:29316249

106. Emmanuel IA, Olotu FA, Agoni C, Soliman ME. Deciphering the 'Elixir of life': dynamic perspectives into the allosteric modulation of mitochondrial ATP synthase by J147, a novel drug in the treatment of Alzheimer's disease. Chem Biodivers. 2019; 16:e1900085.
https://doi.org/10.1002/cbdv.201900085
PMID:30990952

107. Emmanuel IA, Olotu F, Agoni C, Soliman ME. Broadening the horizon: integrative pharmacophore-based and cheminformatics screening of novel chemical modulators of mitochondria ATP synthase towards interventive Alzheimer's disease therapy. Med Hypotheses. 2019; 130:109277.
https://doi.org/10.1016/j.mehy.2019.109277
PMID:31383337

108. Zhao R, Liu X, Zhang L, Yang H, Zhang Q. Current progress of research on neurodegenerative diseases of salvianolic acid B. Oxid Med Cell Longev. 2019; 2019:3281260.
https://doi.org/10.1155/2019/3281260
PMID:31341529

109. Lee YW, Kim DH, Jeon SJ, Park SJ, Kim JM, Jung JM, Lee HE, Bae SG, Oh HK, Son KH, Ryu JH. Neuroprotective effects of salvianolic acid B on an Aβ25-35 peptide-induced mouse model of Alzheimer's disease. Eur J Pharmacol. 2013; 704:70–77.
https://doi.org/10.1016/j.ejphar.2013.02.015
PMID:23461850

110. Tang Y, Huang D, Zhang MH, Zhang WS, Tang YX, Shi ZX, Deng L, Zhou DH, Lu XY. Salvianolic acid B inhibits Aβ generation by modulating BACE1 activity in SH-SY5Y-APPsw cells. Nutrients. 2016; 8:333.
https://doi.org/10.3390/nu8060333
PMID:27258307

111. Liu J, Wang Y, Guo J, Sun J, Sun Q. Salvianolic acid B improves cognitive impairment by inhibiting neuroinflammation and decreasing Aβ level in Porphyromonas gingivalis-infected mice. Aging (Albany NY). 2020; 12:10117–28.
https://doi.org/10.18632/aging.103306
PMID:32516126

112. He Y, Jia K, Li L, Wang Q, Zhang S, Du J, Du H. Salvianolic acid B attenuates mitochondrial stress against Aβ toxicity in primary cultured mouse neurons. Biochem Biophys Res Commun. 2018; 498:1066–72.
https://doi.org/10.1016/j.bbrc.2018.03.119
PMID:29551684

frontiers in Insect Science

ORIGINAL RESEARCH
published: 01 December 2021
doi: 10.3389/finsc.2021.765179

Acute Imidacloprid Exposure Alters Mitochondrial Function in Bumblebee Flight Muscle and Brain

Chloe Sargent[1*], *Brad Ebanks*[2], *Ian C. W. Hardy*[1,2,3], *T. G. Emyr Davies*[4], *Lisa Chakrabarti*[2,5] *and Reinhard Stöger*[1]

[1] School of Biosciences, Sutton Bonington Campus, University of Nottingham, Loughborough, United Kingdom, [2] School of Veterinary Medicine and Science, Sutton Bonington Campus, University of Nottingham, Loughborough, United Kingdom, [3] Department of Agricultural Sciences, University of Helsinki, Helsinki, Finland, [4] Department of Biointeractions and Crop Protection, Rothamsted Research, Harpenden, United Kingdom, [5] Medical Research Council Versus Arthritis Centre for Musculoskeletal Ageing Research, Birmingham, United Kingdom

Mitochondria are intracellular organelles responsible for cellular respiration with one of their major roles in the production of energy in the form of ATP. Activities with increased energetic demand are especially dependent on efficient ATP production, hence sufficient mitochondrial function is fundamental. In bees, flight muscle and the brain have particularly high densities of mitochondria to facilitate the substantial ATP production required for flight activity and neuronal signalling. Neonicotinoids are systemic synthetic insecticides that are widely utilised against crop herbivores but have been reported to cause, by unknown mechanisms, mitochondrial dysfunction, decreasing cognitive function and flight activity among pollinating bees. Here we explore, using high-resolution respirometry, how the neonicotinoid imidacloprid may affect oxidative phosphorylation in the brain and flight muscle of the buff-tailed bumblebee, *Bombus terrestris*. We find that acute exposure increases routine oxygen consumption in the flight muscle of worker bees. This provides a candidate explanation for prior reports of early declines in flight activity following acute exposure. We further find that imidacloprid increases the maximum electron transport capacity in the brain, with a trend towards increased overall oxygen consumption. However, intra-individual variability is high, limiting the extent to which apparent effects of imidacloprid on brain mitochondria are shown conclusively. Overall, our results highlight the necessity to examine tissue-specific effects of imidacloprid on respiration and energy production.

Keywords: ***Bombus terrestris*, mitochondria, imidacloprid, oxidative phosphorylation, high-resolution respirometry**

OPEN ACCESS

Edited by:
Léa Tison,
INRAE Nouvelle-Aquitaine Bordeaux, France

Reviewed by:
Michael B. Powner,
City University of London, United Kingdom
Harmen P. Hendriksma,
Julius Kühn-Institut-Braunschweig, Germany

Correspondence:
Chloe Sargent
Chloe.Sargent@nottingham.ac.uk

Specialty section:
This article was submitted to Insect Neurobiology, a section of the journal Frontiers in Insect Science

Received: *26 August 2021*
Accepted: *12 November 2021*
Published: *01 December 2021*

Citation:
Sargent C, Ebanks B, Hardy ICW, Davies TGE, Chakrabarti L and Stöger R (2021) Acute Imidacloprid Exposure Alters Mitochondrial Function in Bumblebee Flight Muscle and Brain.
Front. Insect Sci. 1:765179.
doi: 10.3389/finsc.2021.765179

INTRODUCTION

Intensification of agriculture has driven a global increase in pesticide use and fragmentation of pollinator habitats, often leading to a sparsity of resources within the foraging range of bees (1, 2). This requires bees to fly greater distances, thus increasing the energy demand of foraging. At the cellular level, energy is produced in the form of adenosine triphosphate (ATP) *via* oxidative phosphorylation (OXPHOS) within mitochondria (3). During OXPHOS, ATP is synthesised *via* the electron transport chain located in the inner mitochondrial membrane; electrons are transported *via* a series of carriers and protons are pumped into the intermembrane space producing a proton gradient which

drives ATP synthesis *via* ATP synthase (4). It has been reported that the rate of electron transfer between OXPHOS enzymes in bees are the highest measured in any animal (5).

Carbohydrate, predominately in the form of trehalose, is the main source of energy in the nervous system and flight muscles of bees, however tissue-specific differences have been shown (5, 6). In the brain, evidence of β-oxidation to metabolise fatty acids and contribute to the high energetic demands has been reported, however there is little evidence of fatty acids fuelling flight in the thoracic muscle (6). Furthermore, glycogen is stored in the flight muscles which may be utilised to extend flight duration (5). These differences reinforce the importance of looking at multiple tissue types when analysing the mitochondrial function in bees.

In bees and other hymenopterans, the brain and flight muscle have particularly high densities of mitochondria to facilitate the substantial energy demands of neuronal signalling and flight activity (3, 5, 7). There is increasing evidence of an association between brain mitochondrial OXPHOS and behaviour in bees, suggesting that alterations in brain mitochondrial function, such as those caused by neonicotinoids, could induce changes in behaviours, such as aggression (7). External factors that affect mitochondrial function may have the greatest impact within tissues with the highest energy demands.

Neonicotinoids are a widely used group of systemic insecticides which have been shown to affect pollinator learning, memory, homing, and flight capacity (8, 9). These compounds target nicotinic acetylcholine receptors (nAChRs); the most prevalent excitatory neurotransmitter in the central nervous system of insects (10, 11). Neonicotinoids impair mitochondrial function and structure in bumblebees and honeybees (12–14) and exposure to the neonicotinoid imidacloprid leads to premature flight exhaustion and altered cognitive performance (15, 16). This may be associated with a transient excitatory affect caused by the overstimulation of nAChRs by imidacloprid and potentially lead to a reduction in flight activity and foraging capacity (15). The decline in flight activity associated with pesticide exposure may be due to insufficient ATP production in the flight muscle leading to premature exhaustion and flight inactivity. As mitochondria are responsible for the majority of ATP production during insect flight, an imidacloprid-induced impairment of mitochondrial function may impact on flight performance and neuronal signalling (17).

Here we seek to determine if and how acute exposure to field-realistic doses of imidacloprid may affect mitochondrial function and OXPHOS in the bumblebee, *Bombus terrestris*. Using high-resolution respirometry we analyse mitochondrial respiration in the brain and flight muscle of female worker bees (18). We analyse the oxygen consumption of three different respiration states: (i) Routine—the rate at which OXPHOS occurs in cells in the physiological coupling state, where ATP synthesis is coupled with the electron transport chain (ii) LEAK—a non-phosphorylating resting state of uncoupled respiration by the inhibition of ATP synthase; hence, oxygen consumption is associated with proton leak through the inner mitochondrial membrane and not *via* ATP synthesis-linked respiration; and (iii) maximum electron transport capacity (ET capacity)—the maximum rate of the electron transport pathway when not coupled to ATP synthase and at an optimum concentration of uncoupler (18). By analysing these three states we aim to identify if and how imidacloprid may affect the OXPHOS system.

MATERIALS AND METHODS

Bee Husbandry

Commercial queen-right *B. terrestris audax* colony were obtained from Biobest® (Westerlo, Belgium) between November 2020 and June 2021, and maintained at 26°C and 33% relative humidity. We fed the colony and age-matched laboratory reared bees on 2.0M sucrose solution and pollen (purchased from Agralan, UK) provided *ad libitum*. To create cohorts of bees of a similar age, pupae were harvested and stored in a separate plastic container adjacent to the colony until eclosion. Once eclosed, bees were placed into cohorts of 1–3 bees and contained in plastic deli pots (115 × 75 mm) until used for high-resolution respirometry (HRR).

Imidacloprid Treatment

Individual bees were taken from their cohort and placed in a queen marker tube where they were starved for 1 h to increase the likelihood of feeding on the diet subsequently provided. For the insecticide exposed bees, a 2.92 M sucrose solution containing 10 ppb imidacloprid was then used to feed the bees. This field-realistic concentration was selected as it has been previously reported in pollen and nectar, foraging bees, and inside colonies (15). For the control bees, feeding was with 2.92 M sucrose solution only. Bees were allowed to feed for 10 mins and the quantify consumed was recorded. Any bees which did not feed during this period were excluded from the experiment. Thirty minutes after the end of feeding, bees were cold anesthetised (flight muscle $n = 4$, and brain $n = 7$; for both control and IMD groups).

Flight Muscle and Brain Tissue Dissection

Cold-anaesthetised bees were killed by decapitation. The thorax was photographed to later measure the inter-tegular distance (representing body size) for each bee using ImageJ software (32). The brain or a small section of flight muscle were removed, using a scalpel and forceps, and then individually weighed in 1.5 ml tubes. Individual bees representing biological replicates were used for each tissue type sample. Then 100 μl of MiR05 buffer (0.5 mM EGTA, 3 mM $MgCl_2$, 60 mM Lactobionic acid, 20 mM Taurine, 10 mM KH_2PO_4, 20 mM HEPES, 110 mM D-Sucrose, 1g/L BSA, pH 7.1) per 1 mg of muscle, or one whole brain, was added and the tissue mechanically homogenised. Then 100 μl (1 mg) of muscle tissue homogenate and all the brain homogenate were transferred into a high-resolution respirometry chamber for analysis.

High-Resolution Respirometry

High-resolution respirometry (HRR) was carried out using an Oroboros Oxygraph-2k (Oroboros® Instruments, Innsbruck, Austria). The respirometer electrodes were calibrated daily to ensure oxygen concentration remained consistent for the duration of the experiment. All respiratory analyses were

performed at 35°C as previous studies have reported this close to the average thoracic and head temperature of *B. terrestris* during flight (19, 20). Oxygen consumption of one brain and 1 mg flight muscle were analysed using the SUIT-003 protocol (18, 21). Routine respiration was measured followed by the addition of 1.0 µl of 5 µM oligomycin to determine LEAK state (inhibition of ATP synthase). Uncoupled maximal electron transport state was then measured by subsequent 10.0 µl titrations of 0.5 µM carbonyl cyanide m-chlorophenyl hydrazone (CCCP). Finally, 1 µl of 2.5 µM Antimycin A to determine the residual oxygen consumption (ROX) (**Figure 1**).

Data Analysis

Raw data outputs were acquired using the O2k-Software (DatLab v7.4.0.4, Oroboros), for data acquisition and analysis to determine instrumental background corrected oxygen flux values. Data were subsequently analysed using R Team (22). Unpaired Student's *t*-tests were performed to determine whether there were differences between the mean oxygen flux at routine, LEAK and maximum ET capacity states, as well as the mean FCRs for routine and LEAK. The FCR can be defined as the ratio of oxygen flux in the different respiration states (routine and LEAK) that are normalised to obtain lower [residual oxygen consumption (ROX)] and upper (maximum ET capacity) limits of 0–1 (23). Each of these tests used adopted a Type I error rate of $\alpha = 0.5$, with interpretations controlled for multiple comparisons as detailed in the supplementary materials. Oxygen consumption was also analysed in relation to the amount of sucrose consumed, bee age, and bee size (inter-tegular distance, ITD). There was no significant difference found in mean bee age or size between treatment groups in either tissue (**Supplementary Table 2**). However, as a range of ages check were used in both groups, one-way ANOVAs were used to check for potential age-related effects on mitochondrial function: age did not significantly affect any of the respiration states in the flight muscle or brain. To determine whether the amount of diet (sucrose solution with or without imidacloprid) consumed correlated with oxygen flux, Pearson's correlation coefficients were calculated; there was no effect in either the flight muscle or brain (**Supplementary Table 3**).

RESULTS

Flight Muscle

Acute oral exposure of imidacloprid in worker bees significantly increased routine respiration in flight muscle (Oxygen flux: $t_{df=6} = -3.58$, $p = 0.012$; FCR: $t_{df=6} = -2.50$, $p = 0.047$,

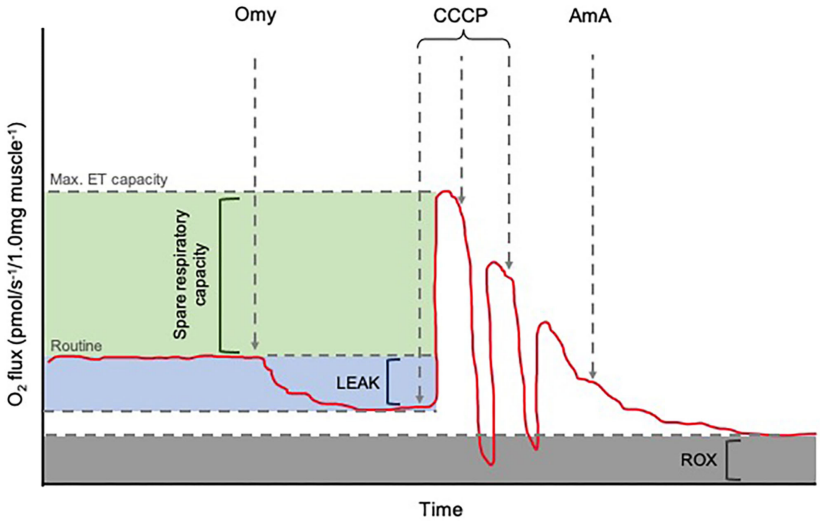

FIGURE 1 | Annotated representation of the O_2k oxygraph output. The red line is the oxygen flux. Routine is shown before the addition of Omy. LEAK state can be determined after the inhibition of ATP synthase by Omy. The maximum electron capacity is determined as the highest peak after CCCP titrations. The spare respiratory capacity and its relative value can be calculated *via* the calculation, [(ET capacity specific flux)/(Routine specific flux × 100)]. AmA, a complex III inhibitor, is added to determine the residual oxygen consumption (ROX) as the baseline state and allow for background correction. Abbreviations: Omy: oligomycin; CCCP: carbonyl cyanide m-chlorophenyl hydrazone; AmA: antimycin A.

Figure 2; **Table 1**, note that the difference in FCR did not remain significant after correction for multiple comparisons, **Supplementary Table 1**). There were no significant differences found between the LEAK and maximum ET capacity states when comparing exposed and control bees (LEAK: oxygen flux, $t_{df=6} = -0.96$, $p = 0.376$; FCR, $t_{df=6} = -1.45$, $p = 0.196$. Maximum ET capacity: oxygen flux, $t_{df=6} = 1.72$, $p = 0.136$, **Figure 2**; **Table 1**).

The spare respiratory capacity (SRC) was also calculated for the flight muscle. The SRC describes the mitochondrial capacity to reach additional ATP demands that are greater than routine respiration levels and can be expressed as a quantitative value using the formula, SRC = [(ET capacity specific flux)/(Routine specific flux × 100)] (24) (**Figure 1**). Hence, the mean SRCs were 0.069 and 0.035 for the control and imidacloprid groups respectively. This may be explained by the increase in routine respiration but not the maximum ET capacity by imidacloprid which would result in a lower SRC.

Brain

In brain tissue we found that the oxygen flux for imidacloprid fed bees had a significantly higher maximum ET capacity ($t_{df=12} = -2.76$, $p = 0.017$), but not in Routine and LEAK ($t_{df=12} = -2.08$, $p = 0.060$ and $t_{df=12} = -1.80$, $p = 0.097$, respectively) (**Figure 3**; **Table 1**). However, there were no significant differences between the treatment groups in terms of FCRs (Routine: $t_{df=12} = 0.48$, $p = 0.639$; LEAK: $t_{df=12} = 0.43$, $p = 0.674$). The SRC values were similar for both groups; 0.011 and 0.009 for control and imidacloprid treated bees, respectively.

DISCUSSION

Acute imidacloprid exposure at the established field-realistic concentration of 10 ppb has been previously shown to affect flight activity in *B. terrestris* by increasing short-term velocity and decreasing the overall duration and distance flown (15, 25, 26). This study has further shown that exposure to imidacloprid, at a concentration of 10 ppb, increases routine oxygen consumption in the flight muscles of workers. Imidacloprid targets acetylcholine receptors and can result in over-stimulation of the nervous system, initiating an excitatory response (10). We suggest that an increase in oxygen consumption and respiration initiated by this response enables the short-term increase in flight velocity that has been previously reported (15, 27). The enhanced flight velocity in turn may lead to premature exhaustion resulting in a shorter flight duration (15, 28, 29). Hyperactivity caused by neonicotinoids, such as imidacloprid, could also result in long-term muscle exhaustion and impaired energy metabolism as shown with thiamethoxam by Tosi et al. (27).

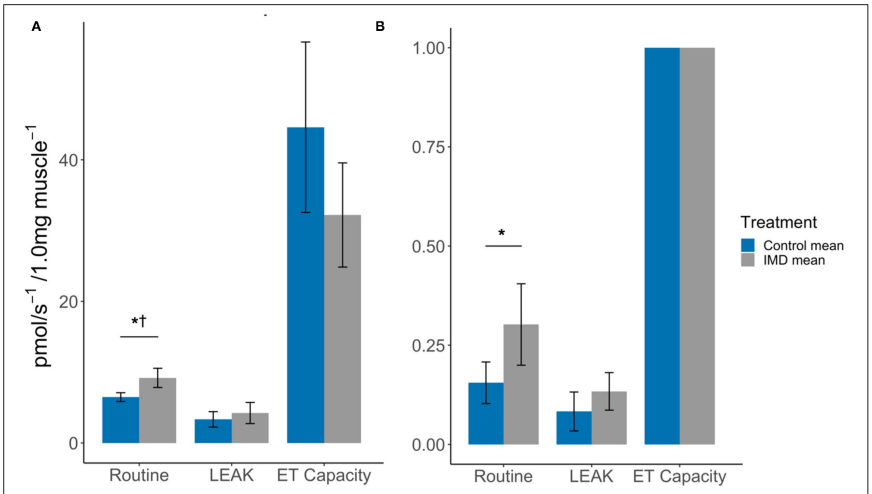

FIGURE 2 | Effects of imidacloprid on flight muscle mitochondria at Routine, LEAK, and maximum ET capacity. States **(A)** Mean oxygen flux; and **(B)** Mean FCR, in flight muscle of imidacloprid and control worker bees. An unpaired students *t*-test was performed to determine significance between treatment groups. *$p < 0.05$. *p*-values marked with † were also significant after controlling for Type I error rates. Error bars show 95% confidence interval. $n = 4$ for each of the control and imidacloprid groups. Routine: routine respiration rate; LEAK: electron/H^+ leak; ET capacity: maximum electron transport capacity.

TABLE 1 | Mean oxygen flux and flux control ratio values in the brain and flight muscle of imidacloprid and non-imidacloprid fed worker bees.

	Flight Muscle			Brain		
	Control $n = 4$	**IMD** $n = 4$	***p***	**Control** $n = 7$	**IMD** $n = 7$	***p***
Routine						
Oxygen flux						
Mean (s.e.)	6.48 (0.32)	9.20 (0.69)	**0.012*†**	2.75 (0.60)	7.23 (2.07)	0.060
Variance	0.40	1.91		2.54	30.02	
FCR						
Mean (s.e.)	0.16(0.03)	0.30(0.05)	**0.047***	1.18 (0.38)	0.99 (0.13)	0.639
LEAK						
Oxygen flux						
Mean (s.e.)	3.33 (0.56)	4.24 (0.76)	0.376	1.62 (0.37)	4.82 (1.74)	0.097
Variance	1.24	2.32		0.97	21.24	
FCR						
Mean (s.e.)	0.08(0.03)	0.13(0.02)	0.196	0.73 (0.26)	0.60 (0.15)	0.67
ET Capacity						
Oxygen flux						
Mean (s.e.)	44.60 (6.14)	32.21 (3.75)	0.136	3.11 (0.59)	6.59 (1.12)	**0.017*†**
Variance	150.83	56.38		2.42	8.76	

*No flux control ratio (FCR) data are provided for the maximum electron transport capacity (ET capacity) as this is set to 1 to obtain the FCR for the routine and electron/H⁺ leak (LEAK) states. p-values were obtained from unpaired Student's t-tests, with significance: *p < 0.05. p-values marked with † were also significant after controlling for Type I error rates (**Supplementary Table 1**). IMD: imidacloprid; s.e.: ±1 standard error.*

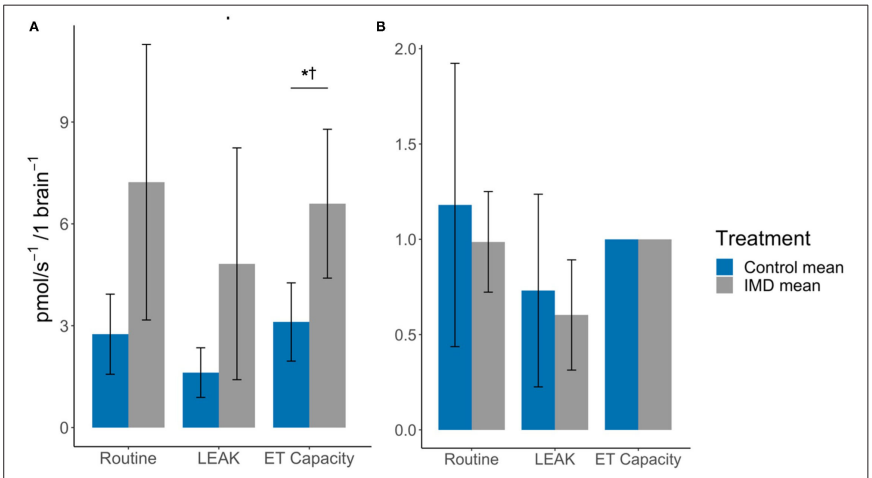

FIGURE 3 | Effects of imidacloprid on brain mitochondria at Routine, LEAK, and maximum ET capacity. **(A)** Mean oxygen flux; and **(B)** Mean FCR, in the brains of imidacloprid and control worker bees. An unpaired students *t*-test was performed to determine significance between treatment groups *$p < 0.05$. *p*-values marked with † were also significant after controlling for Type I error rates. Error bars show 95% confidence interval. $n = 7$ for control and IMD groups. Routine: routine respiration rate; LEAK: electron/H⁺ leak; ET capacity: maximum electron transport capacity.

The higher routine oxygen flux and low spare respiratory capacity detected in the flight muscle of bees exposed to imidacloprid may be further factors contributing to the negative effects on flight activity. The SRC is defined as the mitochondrial capacity to reach additional ATP demands that are greater than routine respiration levels, and to thus prevent ATP crisis (24). This is important in times of stress, exercise, and increased workload when the extra capacity is needed. Hence, the lower SRC in the imidacloprid-exposed bees, which was approximately half of the value for unexposed control bees, suggests a greater mitochondrial dysfunction during times of high ATP demand that is above the routine respiration rate, such as during flight. Imidacloprid increased routine respiration but did not affect the maximum ET capacity; the knock-on effect is likely a diminished SRC. We currently do not know for how long the effects of acute imidacloprid exposure on mitochondria functions last and if the resulting increases in routine respiration are transient. Therefore, the duration of lowered SRC will need to be determined in future follow-up studies.

In the brain, we detected no significant difference in routine and LEAK oxygen consumption between imidacloprid-exposed and control bees, however the maximum ET capacity in imidacloprid-exposed group showed a greater oxygen consumption. This indicates that acute imidacloprid-exposure results in elevated levels of oxygen consumption and thus, in higher maximum respiration rates. However, there was no detected difference in routine or LEAK FCRs, which are likely to be associated with the higher mean routine and LEAK oxygen consumption values. In addition, the FCR values suggest that the routine and LEAK values are in a similar ratio to the maximum ET capacity for both treatment groups. The similarity in the SRC values (0.011 for the control treatment and 0.009 for imidacloprid exposed bees) also illustrates this; these low values indicate that the routine respiration rate in the brain is at maximum ET capacity, as a SRC value of 0.01 represents that the oxygen consumption during routine and maximum ET capacity are equal. Therefore, it appears that imidacloprid increases overall oxygen consumption in the brain; however, due to high inter-individual variance, our results remain inconclusive. This high variability could be associated with the quantity of nAChRs in the brain, which is much greater than in the flight muscle and may therefore explain why there is lower variance among the flight muscles of imidacloprid-exposed bees and among control groups. Cognitive ability such as learning and memory varies among individual bees; this suggests that the brain is particularly susceptible to interspecific variation (30, 31). Hence, a possible variation in the number of neonicotinoid target sites among individual bees may lead to more variability in the response of imidacloprid on mitochondrial function.

Bees are exposed to imidacloprid both acutely and chronically, hence it is important to elucidate the mitochondiral function of both acute and chronic exposure. Chronic exposure of imidacloprid can lead to neuronal dysfunction (13). Neurons require high levels of ATP, and a stable mitochondiral membrane potentital is crucial to sustain ATP production at this level and thereby normal neuronal function (13). Moffat et al. (13) also reported that acute exposure of 10 nM (2.5 ppb) imidacloprid did not reach concentrations in the brain to induce membrane depolarisation. In contrast, 2 day chronic exposure of 1 nM led to an increased sensitivity of bumblebee neurones to acetylcholine, and elicited mitochondrial depolarisaiton of neurons (13). Our findings are in agreement with Nicodemo and colleagues (12), who reported tissue-specific sensitivity to acute imidacloprid exposure in the head and thorax of honeybees and negative effects on ATP synthesis. Our results will help resolve how acute imidacloprid exposure causes a different signature of mitochondiral activity compared to effects of chronic exposure. Moreover, it may now be possible to delineate where acute exposure ends and chronic effects begin.

An aspect of our study is that the worker bees were kept in an enclosed colony and were unable to fly. While this allowed a great deal of experimental control, it should be considered that exercise, such as foraging flights, can increase maximum ET capacity. Hence, mitochondrial function from laboratory-reared non-flying worker bees may vary from that of wild, free-flying and foraging worker bees. Another consideration is that social interactions may also impact brain energetics and mitochondrial function; all bees were kept in small cohorts within small containers from the time of adult eclosion, thus removing them from wider colony interactions and pheromones (7). This may impact brain mitochondrial respiration and behaviour, which may in turn not provide a true representation of *B. terrestris* in a natural or agricultural environment. The effects of acute imidacloprid were only analysed at one time point, shortly after exposure; potential long-term implications of acute exposure on the mitochondrial function in bees remain to be determined. For example, whether mitochondria exposed to imidacloprid return to pre-exposure functioning and, if so, how long such recovery may take.

In this study we have further scrutinised how imidacloprid affects the different mitochondrial respiration states. We found that imidacloprid did not affect LEAK, indicating an increase in oxygen consumption is not associated with proton leak and thus imidacloprid does not seem to have an inhibitory effect on ATP synthase. The increase in routine respiration in the muscle suggests imidacloprid may affect the rate at which electrons flow through the electron transport chain, and thereby increases the rate closer to the maximum ET capacity *via* utilisation of the SRC. A similar mechanism of increased electron transport rate could also explain how imidacloprid increased the maximum ET capacity in the brain. The SRC values were much lower in the brain compared to the flight muscle. This difference between the two tissues could explain how imidacloprid was able to increase the maximum ET capacity in the brain and not the flight muscle as only a slight increase in the rate would be capable of surpassing the maximum ET capacity. The exact mechanism by which imidacloprid affects the electron transport chain requires further investigation.

Overall, we found that acute exposure to imidacloprid, *via* feeding, increased the routine respiration rate in the flight muscle and showed a similar, marginally non-significant, trend towards higher respiration rates in the brain of workers. The higher routine respiration rates in the flight muscle may lead to short-term increases in oxygen consumption and potentially increase ATP production equating to a longer-term deprivation of energy. These results accord with those of previous studies which have shown flight duration and distance to be shorter in bumblebees exposed to imidacloprid. Negative impacts of flight activity will increase exhaustion and mortality of individual bees during flight and this reduced foraging capacity will lead to a reduction in pollination services within natural and agricultural landscapes. The broad range of responses in the brain by individual bees makes it difficult to draw clear conclusions from the measurements. Hence, more research is required to establish the impact of imidacloprid on the brain and elucidate possible explanations for the inconsistencies observed.

These results further contribute to our understanding of how sub-lethal levels of imidacloprid mediate tissue-specific effects on respiration and energy production and thereby impacts pollinator fitness. This study will provide a foundation for further research into the link between mitochondrial function and neonicotinoid exposure, as well as assist in the development and assessment of novel pesticides that minimise harmful effects on non-target species.

DATA AVAILABILITY STATEMENT

The original contributions presented in the study are included in the article/**Supplementary Material**, further inquiries can be directed to the corresponding author.

AUTHOR CONTRIBUTIONS

CS and RS designed the experiment with the additional support of LC and BE. Bee husbandry, laboratory work, and data collection were performed by CS. HRR was performed by CS with the support of LC and BE. Data analysis was performed by CS with supplementary analysis by CS and IH. Figures were prepared by CS. Paper was written by CS and RS with additional editorial assistance by LC, BE, IH, and TD. All authors contributed to the article and approved the submitted version.

FUNDING

CS is a PhD candidate funded by the Future Food Beacon/Graduate Centre for International Agriculture, University of Nottingham and Rothamsted Research and BE is a PhD candidate funded by the University of Nottingham Biotechnology and Biological Sciences Doctoral Training Programme (BBSRC-DTP).

ACKNOWLEDGMENTS

The authors would like to thank Peter Graystock, Daniel Kenna, and Richard Gill at Imperial College London for their previous support to the first author and their research which helped to guide this study.

SUPPLEMENTARY MATERIAL

The Supplementary Material for this article can be found online at: https://www.frontiersin.org/articles/10.3389/finsc.2021.765179/full#supplementary-material

REFERENCES

1. Kremen C, Williams NM, Thorp RW. Crop pollination from native bees at risk from agricultural intensification. *Proc Natl Acad Sci U S A.* (2002) 99:16812–6. doi: 10.1073/pnas.262413599
2. Gonzalez-Varo JP, Biesmeijer JC, Bommarco R, Potts SG, Schweiger O, Smith HG, et al. Combined effects of global change pressures on animal-mediated pollination. *Trends Ecol Evol.* (2013) 28:524–530. doi: 10.1016/j.tree.2013.05.008
3. Hedges CP, Wilkinson RT, Devaux JBL, Hickey AJR. Hymenoptera flight muscle mitochondrial function: Increasing metabolic power increases oxidative stress. *Comp Biochem Physiol A Mol Integr Physiol.* (2019) 230:115–21. doi: 10.1016/j.cbpa.2019.01.002
4. Chaban Y, Boekema EJ, Dudkina NV. Structures of mitochondrial oxidative phosphorylation supercomplexes and mechanisms for their stabilisation. *Biochim Biophys Acta Bioenerg.* (2014) 1837:418–26. doi: 10.1016/j.bbabio.2013.10.004
5. Suarez RK, Darveau CA, Welch KC, O'Brien DM, Roubik DW, Hochachka PW. Energy metabolism in orchid bee flight muscles: carbohydrate fuels all. *J Expl Biol.* (2005) 208:3573–79. doi: 10.1242/jeb.01775
6. Rittschof CC, Schirmeier S. Insect models of central nervous system energy metabolism and its links to behavior. *Glia.* (2018) 66:1160–75. doi: 10.1002/glia.23235
7. Rittschof CC, Vekaria HJ, Palmer JH, Sullivan PG. Brain mitochondrial bioenergetics change with rapid and prolonged shifts in aggression in the honey bee, Apis mellifera. *J Exp Biol.* (2018) 221:176917 doi: 10.1242/jeb.176917
8. Gill RJ, Raine NE. Chronic impairment of bumblebee natural foraging behaviour induced by sublethal pesticide exposure. *Funct Ecol.* (2014) 28:1459–71. doi: 10.1111/1365-2435.12292
9. Stanley DA, Smith KE, Raine NE. Bumblebee learning and memory is impaired by chronic exposure to a neonicotinoid pesticide. *Sci Rep.* (2015) 5:10. doi: 10.1038/srep16508
10. Buckingham SD, Lapied B, LeCorronc H, Grolleau F, Sattelle DB. Imidacloprid actions on insect neuronal acetylcholine receptors. *J Exp Biol.* (1997) 21:2685–92. doi: 10.1242/jeb.200.21.2685
11. Colgan TJ, Fletcher IK, Arce AN, Gill RJ, Ramos Rodrigues A, Stolle E, et al. Caste- and pesticide-specific effects of neonicotinoid pesticide exposure on gene expression in bumblebees. *Mol Ecol.* (2019) 28:1964–74. doi: 10.1111/mec.15047
12. Nicodemo D, Maioli MA, Medeiros HCD, Guelfi M, Balieira KVB, De Jong D, et al. Fipronil and imidacloprid reduce honeybee mitochondrial activity. *Environ Toxicol Chem.* (2014) 33:2070–5. doi: 10.1002/etc.2655
13. Moffat C, Pacheco JG, Sharp S, Samson AJ, Bollan KA, Huang J, et al. Chronic exposure to neonicotinoids increases neuronal vulnerability to mitochondrial dysfunction in the bumblebee (*Bombus terrestris*). (2015) *Faseb J.* 29:2112–9. doi: 10.1096/fj.14-267179
14. Friol PS, Catae AF, Tavares DA, Malaspina O, Roat TC. Can the exposure of Apis mellifera (Hymenoptera, Apiadae) larvae to a field concentration of thiamethoxam affect newly emerged bees? *Chemosphere.* (2017) 185:56–66. doi: 10.1016/j.chemosphere.2017.06.113

15. Kenna D, Cooley H, Pretelli I, Ramos Rodrigues A, Gill S, Gill R. Pesticide exposure affects flight dynamics and reduces flight endurance in bumblebees. *bioRxiv.* (2018) 449280. doi: 10.1101/449280
16. Schwartz KR, Minor H, Magro C, McConnell J, Capani J, Griffin J, et al. The neonicotinoid imidacloprid alone alters the cognitive behavior in Apis mellifera L. and the combined exposure of imidacloprid and Varroa destructor mites synergistically contributes to trial attrition. *J Apic Res.* (2020) 60:431–8. doi: 10.1080/00218839.2020.1866233
17. Thompson SN, Suare RK. "Metabolism," In: Resh VH, Cardé RT editors, *Encyclopedia of Insects*. New York, NY: Academic Press (2009), 623–627.
18. Gnaiger E. *Mitochondrial Pathways and Respiratory Control. An Introduction to OXPHOS* Ananlysis. 5th Ed. Bioenerg Commun (2020)
19. Reber T, Vahakainu A, Baird E, Weckstrom M, Warrant E, Dacke M. Effect of light intensity on flight control and temporal properties of photoreceptors in bumblebees. (2015) *J Exp Biol.* 218:1339–1346. doi: 10.1242/jeb.113886
20. Teulier L, Weber JM, Crevier J, Darveau CA. Proline as a fuel for insect flight: enhancing carbohydrate oxidation in hymenopterans. *Proc R Soc B.* (2016) 16:283. doi: 10.1098/rspb.2016.0333
21. Bioblast. *SUIT-003.* (2021). Available online at: https://wiki.oroboros.at/index.php/SUIT-003. Last. (accessed August 23, 2021).
22. R Core Team. R: A language and Environment for Statistical Computing. Version 3.6.2 (2020). Available online at: https://www.R-project.org.
23. Bioblast. Flux control ratio (2021). Available online at: https://wiki.oroboros.at/index.php/Flux_control_ratio. (accessed June 21, 2021).
24. Marchetti P, Fovez Q, Germain N, Khamari R, Kluza J. Mitochondrial spare respiratory capacity: Mechanisms, regulation, and significance in non-transformed and cancer cells. *FASEB J.* (2020) 34:13106–24. doi: 10.1096/fj.202000767R
25. Goulson D. REVIEW: An overview of the environmental risks posed by neonicotinoid insecticides. *J Appl Ecol.* (2013) 50:977–87. doi: 10.1111/1365-2664.12111
26. Botias C, David A, Hill EM, Goulson D. Contamination of wild plants near neonicotinoid seed-treated crops, and implications for non-target insects. *Sci Total Environ.* (2016) 566:269–78. doi: 10.1016/j.scitotenv.2016.05.065
27. Tosi S, Burgio G, Nieh JC. A common neonicotinoid pesticide, thiamethoxam, impairs honey bee flight ability. *Sci Rep.* (2017) 7:8. doi: 10.1038/s41598-017-01361-8
28. Smit WA, Becht G, Beenakkers AM. Structure fatigue and enzyme activities in fast insect muscles. *J Insect Physiol.* (1967) 13:12. doi: 10.1016/0022-1910(67)90022-4
29. Usherwood PN. Insect Neuromuscular Mechanisms. *Am Zoologist.* (1967) 7:553–82. doi: 10.1093/icb/7.3.553
30. Dyer AG. The mysterious cognitive abilities of bees: why models of visual processing need to consider experience and individual differences in animal performance. *J Exp Biol.* (2012) 215:387–95. doi: 10.1242/jeb.038190
31. Chittka L. Bee Cognition. *Curr Biol 27:19.* (2017) R1049–53. doi: 10.1016/j.cub.2017.08.008
32. Image J. *U. S. National Institutes of Health, Bethesda, Maryland, USA*. (2021). Available online at: https://imagej.nih.gov/ij/ 1997–2018

Conflict of Interest: The authors declare that the research was conducted in the absence of any commercial or financial relationships that could be construed as a potential conflict of interest.

Publisher's Note: All claims expressed in this article are solely those of the authors and do not necessarily represent those of their affiliated organizations, or those of the publisher, the editors and the reviewers. Any product that may be evaluated in this article, or claim that may be made by its manufacturer, is not guaranteed or endorsed by the publisher.

www.aging-us.com AGING 2021, Vol. 13, No. 11

Research Paper

The dysregulated *Pink1*$^{-}$ *Drosophila* mitochondrial proteome is partially corrected with exercise

Brad Ebanks[1,*], Thomas L. Ingram[1,*], Gunjan Katyal[1], John R. Ingram[1], Nicoleta Moisoi[2], Lisa Chakrabarti[1,3]

[1]School of Veterinary Medicine and Science, University of Nottingham, Sutton Bonington, LE12 5RD, UK
[2]Leicester School of Pharmacy, Leicester Institute for Pharmaceutical Innovation, De Montfort University, The Gateway, Leicester LE1 9BH, UK
[3]MRC Versus Arthritis Centre for Musculoskeletal Ageing Research, Birmingham, UK
*Equal contribution

Correspondence to: Lisa Chakrabarti; **email:** lisa.chakrabarti@nottingham.ac.uk
Keywords: PINK1, *Drosophila*, mitochondria, exercise, proteomics
Received: February 11, 2021 **Accepted:** May 20, 2021 **Published:** June 1, 2021

ABSTRACT

One of the genes which has been linked to the onset of juvenile/early onset Parkinson's disease (PD) is PINK1. There is evidence that supports the therapeutic potential of exercise in the alleviation of PD symptoms. It is possible that exercise may enhance synaptic plasticity, protect against neuro-inflammation and modulate L-Dopa regulated signalling pathways. We explored the effects of exercise on *Pink1* deficient *Drosophila melanogaster* which undergo neurodegeneration and muscle degeneration. We used a 'power-tower' type exercise platform to deliver exercise activity to *Pink1*$^{-}$ and age matched wild-type *Drosophila*. Mitochondrial proteomic profiles responding to exercise were obtained. Of the 516 proteins identified, 105 proteins had different levels between *Pink1*$^{-}$ and wild-type non-exercised *Drosophila*. Gene ontology enrichment analysis and STRING network analysis highlighted proteins and pathways with altered expression within the mitochondrial proteome. Comparison of the *Pink1*$^{-}$ exercised proteome to wild-type proteomes showed that exercising the *Pink1*$^{-}$ *Drosophila* caused their proteomic profile to return towards wild-type levels.

INTRODUCTION

Parkinson's disease (PD) is a progressive, irreversible neurodegenerative condition which affects over 6 million people across the globe [1]. The greatest risk factor for PD is advancing age, and with the number of people over the age of 60 expected to exceed 2 billion by the year 2050 (currently estimated to be over 900 million) there will soon be significantly higher numbers of people living with PD [2]. The classical physical symptoms are known to be resting tremor, rigidity and bradykinesia. It is now also known that symptoms of PD include reduced quality of sleep as well as both cognitive impairments and poor mental health. In terms of the pathophysiology of the disease, the death of pigmented dopaminergic neurons in the substantia nigra pars compacta in PD patients is critical [3]. Molecular characteristics of PD include the aggregation of α-synuclein leading to Lewy body formation, alongside mitochondrial dysfunction [4, 5].

Hereditary forms of PD can be either autosomal dominant or autosomal recessive, dependent upon the mutant gene involved. In both dominant and recessive forms of hereditary PD, autophagic and lysosomal pathways are both mechanistically implicated [6–8]. One of the critical pathways which has been linked to the onset of juvenile/early onset PD is the PINK1/

Parkin mitophagy pathway, a form of autophagy for the degradation of dysfunctional mitochondria. The role of mitophagy is to provide a quality control mechanism for the mitochondrial population within a cell, and this is a particularly crucial function in energetically demanding neuronal cells [9].

Mechanistically, PINK1 localizes with outer mitochondrial membrane (OMM) of depolarized mitochondria and then recruits and activates the E3 ubiquitin-ligase activity of Parkin via phosphorylation of its Ser65 residue [10, 11]. PINK1 has also been shown to phosphorylate the Ser65 residue of Ubiquitin, which aids in the activation of Parkin's E3 ligase activity [12, 13]. Ultimately these events lead to the ubiquitination of OMM proteins by Parkin, the autophagic machinery then degrades the ubiquitinated mitochondria [14]. Mutations in PINK1 (and Parkin) can result in autosomal recessive juvenile onset PD, with onset before the age of 40 years old [15]. While this form of PD is rare, a comprehensive understanding of it can improve the outcomes of patients with PINK1 mutations and also those with idiopathic PD due to their shared pathophysiology [16]. A recent publication by Sliter et al. reported that *Pink1* and *Parkin* mitigate STING induced inflammation, where both *Pink1*$^{-/-}$ *and Prkn*$^{-/-}$ mice under exhaustive exercise have a strong inflammatory phenotype that is rescued by the concurrent loss of the STING pathway [17]. In the same year, Zhong et al. reported that newly synthesised oxidised mitochondrial DNA is exported to the cytosol and stimulates another of the innate immune responses, the NLRP3 inflammasome [18].

Given the overlapping biology between PINK1 loss of function in PD and other forms of genetic and sporadic PD, PINK1 null mutants of animal models are hugely useful in studies of PD. *Pink1* loss of function *Drosophila* models were first developed in 2006, shortly after the first *parkin* loss of function mutant *Drosophila* models were being utilised in research [19–21]. These first studies found that *Pink1* loss of function resulted in mitochondrial dysfunction, compromised fertility in males, indirect flight muscle degeneration and associated locomotor defects, increased sensitivity to oxidative stress, and dopaminergic degeneration (Park et al., 2006) [19]. *Parkin* overexpression rescued many of the defects observed in the *Pink1* mutants, indicating the downstream function of Parkin in the now established PINK1/Parkin mitophagy pathway, reviewed here [22]. More recent studies using *Pink1* mutant *Drosophila* have found that their neurons exhibit decreased levels of synaptic transmission, defective fission and reduced ATP levels due to decreased COXI and COXIV activity as well as non-motor symptoms such as learning and memory deficits, weakened circadian rhythms and electrophysiological changes in clock-neurons [23–25].

It was first observed in 1992 that participation in exercise reduced the risk of the onset of PD in later years, while later data showed that this protection against PD risk is more obvious in males [26, 27]. Many groups have presented data that show the therapeutic potential of exercise in the alleviation of patient symptoms [28–30]. The biochemical mechanisms that would explain these observations are still unclear, but current evidence suggests that exercise may enhance synaptic plasticity, protect against neuroinflammation and modulate L-Dopa regulated signalling pathways [31–33].

In this study we aimed to analyse the biochemical changes induced by exercise in the mitochondrial proteome of the *Pink1* loss of function mutant (*Pink1*$^{-}$) *Drosophila*. As exercise is reported to both reduce the risk of onset and improve outcomes for Parkinson's disease patients, we sought to characterise the biochemical changes that could underpin this improvement in our model of Parkinson's disease. We focused on the mitochondria as their dysfunction is widely associated with Parkinson's disease, and the *Pink1*$^{-}$ genetic model has a disrupted mitophagy pathway due to the absence of a functional PINK1 protein.

MATERIALS AND METHODS

Drosophila stocks

Fly stocks were kindly provided to NM by Miguel Martins (MRC Toxicology Unit) and Alex Whitworth (MRC Mitochondrial Biology Unit). Fly stocks and crosses were maintained on standard cornmeal agar media at 25° C in a 12:12 light-dark cycle. The experiments were performed on males: wild type (genotype *w1118)* and *Pink1*$^{-}$ *(genotype Pink1B9/Y).*

Drosophila exercise

Approximately twenty wild-type control or *Pink1*$^{-}$ *Drosophila*, 1-4 days post-eclosion, were separated into glass vials filled with 5ml food. Exercised group vials were stoppered with cotton wool 6cm from the food; non-exercised group vials were stopped with cotton wool 1cm from the food, creating a physical barrier to activity. Both exercised and non-exercised groups were placed in racks on the ICE machine (Supplementary Material) for 30 minutes per day for 7 days. The *Drosophila* were exercised in the morning each day and were sacrificed by freezing at -80° C one hour after the final exercise bout. Comparison groups were exercised and non-exercised wild-type and *Pink1*$^{-}$ *Drosophila.*

Mitochondrial isolation

Groups of twenty wild-type or *Pink1*$^{-}$ *Drosophila* were homogenised in 100-200µl mitochondrial extraction buffer (50mM Tris-Cl pH 7.4, 100mM KCL, 1.5mM MgCl2, 1mM EGTA, 50mM HEPES and 100mM sucrose) by 5 minutes of manual homogenisation using a 1.2-2ml Eppendorf micro-pestle (Sigma-Aldrich). The homogenate was centrifuged at 800g for 10 minutes, at 4° C, to remove the insoluble fraction. Supernatants from the first centrifugation were centrifuged at 1,000g for 10 minutes at 4° C to pellet the nuclear fraction. Supernatants from the second centrifugation were centrifuged at 13,200g for 30 minutes at 4° C to pellet the mitochondrial fraction. The protein content was determined by Bradford assay (µg/µl) and mitochondrial fractions were stored at -80° C.

2D-gel electrophoresis

50µg of the mitochondrial fraction were added to rehydration solution (8M urea, 2% CHAPS, 2% IPG Buffer, 0.1% bromophenol blue). 20mM DTT was added to an aliquot of rehydration solution directly before use. The standard protocol according to manufacturer instructions was followed [34]. Briefly, sample was applied to rehydrate ZOOM IPG strips for an hour at room temperature followed by iso-electric focusing using the ZOOM IPG (Life Technologies) system and pH 3-10 (non-linear) ZOOM IPG strips. Gels were stained (SimplyBlue™ SafeStain, Life Technologies) and imaged (ImageQuant 300, GE Healthcare Life Sciences). Analyses were performed using SameSpots software (Totallab) (one-way ANOVA). Three pooled biological replicates were included for each of the four groups.

Samples were analysed by the Centre of Excellence in Mass Spectrometry at University of York [35]. Briefly, proteins were reduced and alkylated, followed by digestion in-gel with trypsin. Matrix Assisted Laser Desorption Ionization Tandem Time-of-Flight mass spectrometry (MALDI-TOF/MS) was used to analyse the samples. The generated tandem MS data was compared against the NCBI database using the MASCOT search programme to identify the proteins. De novo sequence interpretation for individual peptides were inferred from peptide matches.

Label-free proteomics

30µg/µl of each mitochondrial fraction was prepared with 4X LDS sample buffer and 4mM DTT. Samples were run in triplicate on a 4-12% Bis-Tris gel in 1X MES SDS running buffer for 40 minutes at 200V (all Invitrogen). Three biological replicates were run for each of the four groups. The whole, individual gel lanes were excised and placed into separate Eppendorf tubes.

Samples were analysed by the Centre of Excellence in Mass Spectrometry at University of York [35]. Briefly, protein was in-gel digested post-reduction and alkylation. The resulting extracted peptides were analysed over 1-hour LC-MS acquisitions with elution from a 50cm, C18 PepMap column onto a Thermo Orbitrap Fusion Tribrid mass spectrometer using a Waters mClass UPLC. Extracted tandem mass spectra were searched against the combined *Drosophila melanogaster* and *Saccharomyces cerevisiae* subsets of the UniProt database. Protein identifications were filtered to achieve <1% false discovery rate as assessed against a reverse database. Identifications were further filtered to require a minimum of two unique peptides per protein group.

For relative label-free quantification, extracted ion chromatograms for identified peptides were extracted and integrated for all samples. A maximum mass deviation of 3 ppm and retention time drift of 3 mins were set. Resulting quantifications were further filtered to an arbitrary PEAKS quality factor of 5 for feature mapping and required a minimum of two aligned features from a minimum of two unique peptides per protein quantification. Protein abundances were normalised between samples based on total identified peptide ion area.

Gene ontology enrichment analysis

gProfiler was used to undertake Gene Ontology (GO) enrichment analysis for the label-free mass spectrometry identified proteins with significant expression differences between each of the four experimental groups [36]. KEGG, Molecular Function (MF), Biological Process (BP) and Cellular Compartment (CC) enrichment analyses are generated by gProfiler are presented.

Protein-protein interaction network analysis

Differences in expression of proteins between groups were further analysed using the STRING database v.11.0 [37]. The platform was used to create protein-protein interaction (PPI) networks based upon the differentially expressed proteins (DEPs) observed between groups.

RESULTS AND DISCUSSION

We subjected male *Pink1*$^{-}$ and wild-type *Drosophila* to a seven-day exercise regimen, whilst maintaining groups of unexercised *Pink1*$^{-}$ and wild-type as controls. The

mitochondria of the four groups were then isolated and investigated using 2D gel electrophoresis and label-free mass spectrometry analyses to determine changes in their mitochondrial proteome. The 2D gel electrophoresis method allowed for a fast and simple separation of proteins, which served as a scoping method to identify some of the most significant changes in expression. Label-free mass spectrometry analyses generated proteomes that we used in network enrichment analysis. Previously we have used proteomic profiling to characterise mitochondrial populations in both mice and long-lived pipistrelle bats, and here we apply this to better understand the PD phenotype as well as possible changes due to exercise [38, 39].

2DE-MS identified a general reduction in protein expression post-exercise in the *Pink1* mutant *Drosophila*

We isolated mitochondria from exercised and non-exercised *Pink1*$^{-}$ *Drosophila* and performed 2DE-MS on these fractions (Supplementary Figure 1). All proteins that were identified as changed in expression after the exercise intervention were reduced in expression (Table 1). PINK1 is recognised as having a central role in mitophagy, ensuring a healthy pool of mitochondria are maintained [19, 20]. It has recently been recognised that the regulation of mitophagy by the PINK1 system is age-dependent, with the *Drosophila* dependency on this pathway increasing with age [40]. Further, it has also been reported that earlier in the lifespan of the *Drosophila* there is a basal level of mitophagy that is not disrupted by the loss of PINK1 [41].

It is therefore possible that alternate mitophagy pathways can compensate for the loss of PINK1 and are upregulated during exercise, and this could account for the sweeping reductions in protein levels via 2DE-MS (Table 1). Indeed, alternative proteins have been identified and a pathway described in which they promote PINK1/PARKIN-independent mitophagy: AMBRA1, HUWE1 and IKKα [42]. It is also notable that ATG8, the final mediator of the AMBRA1 PINK1/PARKIN-independent mitophagy pathway, has been reported to be upregulated in response to exercise as a part of a broader upregulated autophagic response to exercise [43]. However, it could also be suggested that the energetic demands of the exercise result in less energy available to protein synthesis pathways. In this instance, exercise would likely affect proteostasis more broadly, beyond just the mitochondrial proteome.

The specific proteins identified within the table include structural proteins such as tropomyosin which is associated with the intracellular transport of mitochondria as well as mitochondrial metabolic proteins from a variety of pathways, such as acyl co-enzyme A dehydrogenase from the β-oxidation pathway, isocitrate dehydrogenase from the TCA cycle, and the metabolic gatekeeper pyruvate dehydrogenase. Due to the varied function of the proteins in Table 1, it is likely that their downregulation is representative of a broader decrease in protein expression levels in Pink1 *Drosophila* in response to exercise.

We proceeded to pursue the directionally homologous 2DE-MS results by obtaining a global topology of the mitochondrial protein changes that occur to *Pink1*$^{-}$ *Drosophila* due to exercise intervention using a label-free proteomics method.

GO annotation of identified label-free proteins and proportion identified that are localised to mitochondria

Non-gel-based label-free proteomic analyses identified 516 proteins from the mitochondrial fractions of *Pink1*$^{-}$ and wild-type *Drosophila* (Supplementary Table 1). GO and KEGG analyses showed that these fractions were enriched for mitochondrial processes and pathways, confirming the efficacy of our fractionation methodology (Figure 1). The top term of the GO cellular compartment analysis was cytoplasm, followed by mitochondrion and sub-mitochondrial compartments, many mitochondrial proteins are known to also localise to the cytoplasm [44, 45].

Pink1*$^{-}$ *Drosophila* have decreased levels of proteins from energy metabolism pathways compared with wild-type *Drosophila

Label-free proteomics highlighted 105 differently expressed proteins between non-exercised wild-type *Drosophila* and non-exercised *Pink1*$^{-}$ *Drosophila* (Supplementary Table 2). Ten of the proteins were shown to be reduced in expression in *Pink1*$^{-}$ *Drosophila* compared to wild-type *Drosophila*. We found that *Pink1*$^{-}$ *Drosophila* have reductions in protein expression in proteins from mitochondrial processes associated with energy metabolism, with the top GO biological process terms being oxidative phosphorylation, electron transport chain, ATP metabolic process and oxidation-reduction process (Figure 2).

The deficiencies in mitochondrial oxidative phosphorylation, the electron transport chain and specifically in the activity of Complex I in Parkinson's disease are well established, and this aligns with our findings from the GO analysis of the proteomics data [46–49]. Specific subunits of complexes within the electron transport chain that decreased in expression include NADH dehydrogenase (ubiquinone) 75 kDa

Table 1. Expression changes between exercised *Pink1- Drosophila* and non-exercised *Pink1- Drosophila*.

***Pink1*- mitochondria - 2DE**			
Protein identity	**ANOVA (p)**	**Fold change**	**Exercise related change**
Tropomyosin-1, isoforms 33/34 Tropomyosin-2	0.022	1.4	↓
Acyl-coenzyme A dehydrogenase	0.015	1.4	↓
Isocitrate dehydrogenase	0.008	1.4	↓
Enolase	0.022	1.3	↓
Probable isocitrate dehydrogenase [NAD] subunit alpha Glycerol-3-phosphate dehydrogenase [NAD(+)] Pyruvate dehydrogenase E1 component subunit beta	0.015	1.5	↓
Pyruvate dehydrogenase E1 component subunit beta Aldo-keto reductase, isoform C	0.048	1.3	↓
Alcohol dehydrogenase CG9992, isoform A	0.024	1.3	↓

Changes in expression were determined by 2DE-MS.

subunit isoform B (complex I), GH01077p (complex III in *Drosophila*), HDC00331 (complex IV in *Drosophila*) and Levy isoform A (complex IV in *Drosophila*). While complex I and complex IV have been reported as dysfunctional in PD, reduced expression or decreased activity for complex III isn't well documented [47, 50, 51]. However, decreased Complex II/III activity has been shown in platelets of untreated Parkinson's disease patients [52].

It is interesting to note that most (95/105) of the differentially expressed proteins were more highly expressed in *Pink1- Drosophila* (Supplementary Table 2). GO biological process analysis showed these proteins to be enriched for redox processes, cytoplasmic translation, cellular amide metabolic processes and fatty acid derivative biosynthetic processes. GO cellular compartment analysis showed that the more highly expressed proteins in *Pink1-* were enriched for cytoplasmic ribosomes, organelle membranes and endoplasmic reticulum. KEGG pathway analysis paralleled these findings, highlighting the identified proteins as involved in fatty acid metabolism, ribosomes and one carbon pool by folate.

There is evidence linking fatty acid metabolism and function to Parkinson's disease, with proteins identified by GWAS studies, suppressed β-oxidation, and physical interaction between α-synuclein and fatty acids potential being key factors [53–57]. Early studies into the effect of α-synuclein (*SNCA*) gene deletion on lipid metabolism in mice reported reduced palmate uptake and altered palmate metabolism in the brain, reduced acyl-CoA Synthetase activity that resulted in reduced arachidonic acid uptake and turnover, and increased docosahexaenoic acid brain mass, incorporation and turnover [58–60]. Our own work shows differences in arachidonic acid derivatives in Parkinson's disease mitochondria [61].

The data presented here show an enrichment of the folate metabolic pathway, not reported previously. It may be that in *Pink1- Drosophila* this is a compensatory mechanism. KEGG analysis highlighted the metabolism of folate (vitamin B_9) as enriched in *Pink1- Drosophila*. B-vitamins, in particular folate, are well studied in the context of Parkinson's disease due to the observation of homocysteine (a methionine cycle metabolite) having neurotoxic effects [62–65]. It is hypothesised that the administration of B-vitamins can drive the synthesis of methionine, thus reducing intracellular homocysteine [66–68]. However, the relationship between B - vitamins, neurotoxicity and Parkinson's disease is complex and a consensus has yet to be established. Some data show either little correlation between homocysteine levels and B vitamins including B6, folate and B12 while others show contradictory results, including elevated homocysteine levels and decreased folate levels in Parkinson's disease patients [68–71].

Exercise reduces measured protein levels in *Pink1- Drosophila*

The 2DE-MS analysis of exercised and non-exercised *Pink1- Drosophila* revealed reductions in twelve proteins in response to exercise (Table 1). Label-free proteomics showed a similar pattern in *Pink1-* exercised *Drosophila* compared with non-exercised *Pink1- Drosophila;* of the fifty-seven protein expression differences, fifty-five were reductions of protein expression in response to

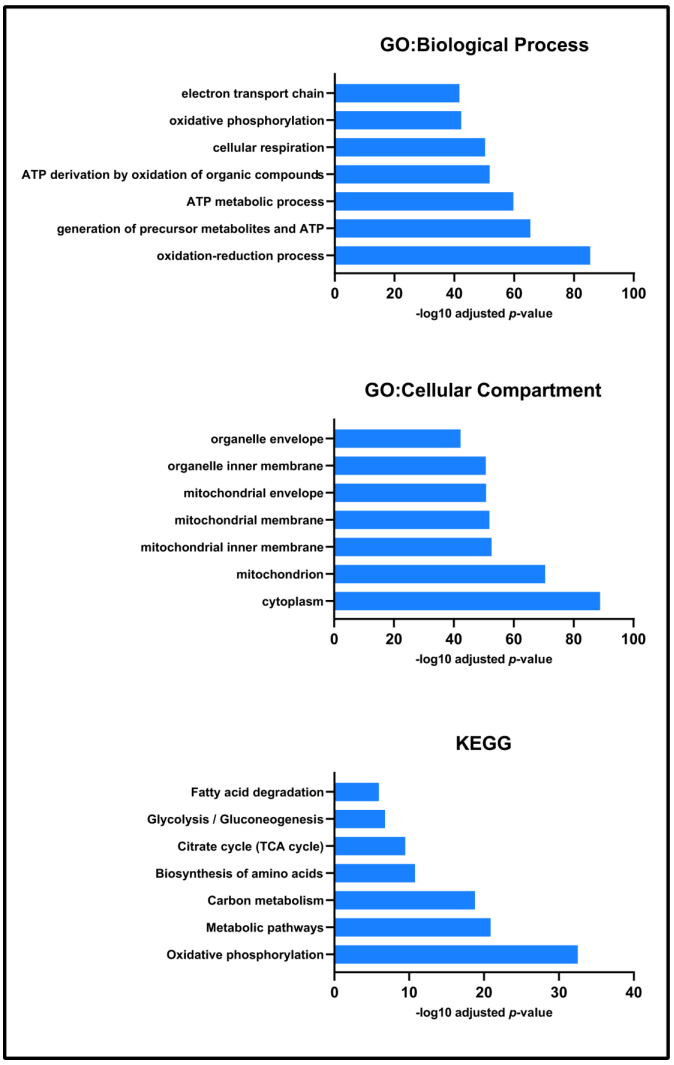

Figure 1. Enrichment analysis of all proteins identified by label-free proteomics. Biological process, cellular compartment and KEGG enrichment analysis each presented processes associated with mitochondrial function and physiology.

exercise (Supplementary Table 3). GO:MF and KEGG pathway analysis determined that the terms ribosomal and fatty acid metabolism were significantly represented in the proteins with reduced expression (Figure 3). Interestingly, these terms were shown to be increased in *Pink1*$^{-}$ *Drosophila* compared to wild-type *Drosophila* that had not been exercised. This suggests that in *Pink1*$^{-}$ *Drosophila* exercise returns levels of protein expression towards wild-type values.

It has been shown that PINK1 interacts with the protein translation pathway and that increased protein translation in *Pink1*$^{-}$ *Drosophila* causes an exacerbated *Pink1*$^{-}$ phenotype. Taking this a step further, it was shown that 40S ribosomal subunit S6 (RpS6) RNAi was able to mitigate the *Pink1*$^{-}$ phenotype [72]. These data suggest improper protein translation regulation is involved in the pathogenesis of PD and that inhibition of this pathway mitigates progression. Exercise appears to be able to reverse the upregulated protein translation pathways found in *Pink1*$^{-}$ *Drosophila*.

KEGG analysis identified fatty acid metabolism from proteins reduced in expression due to exercise, while GO:MF analysis highlighted CoA Carboxylase activity from the same protein data set. This reduction in the metabolism, and in particular the synthesis, of fatty acids can be contrasted with the KEGG analysis described earlier which identified elevated expression of fatty acid metabolism associated proteins in *Pink1*$^{-}$ *Drosophila* compared with wild-type *Drosophila*. It can be interpreted that exercise reverses the change in *Pink1*$^{-}$ *Drosophila* and returns the fatty acid metabolic profile back towards wild-type *Drosophila*.

The two proteins upregulated with exercise in *Pink1*$^{-}$ *Drosophila* were OCIA domain-containing protein 1 (OCIAD1) and dihydroorotate dehydrogenase (quinone) mitochondrial (DHODH), neither have previously been connected with exercise. OCIAD1 has been shown to localise to both endosomes and mitochondria and regulate pathways such as JAK/STAT, Notch and PI3K/AKT [73–75]. OCIAD1 has been shown to regulate mitochondrial ETC activity via control of complex I activity, which showed an inverse association with OCIAD1 overexpression [76]. Deregulated OCIAD1 levels have been linked to mitochondrial dysfunction, interaction with BCL-2 and Alzheimer's disease [75].

DHODH is an inner mitochondrial membrane enzyme that catalyses the fourth step in *de novo* synthesis of pyrimidines [77]. A link between pyrimidine synthesis and mitochondrial morphology was shown with the addition of the drug leflunomide to muscle cells [78]. The group showed that leflunomide inhibited DHODH by binding to its ubiquinone binding channel, thereby preventing the production of pyrimidine ribonucleotide uridine monophosphate (UMP). DHODH inhibition induced upregulation of mitochondrial fusion and subsequent mitochondrial elongation, by depleting the cellular pyrimidine pool. As ubiquinone is reduced to ubiquinol in the DHODH-mediated catalysis of dihydroorotate to orotate, and as ubiquinol is a substrate of respiratory complex III, DHODH is important for the

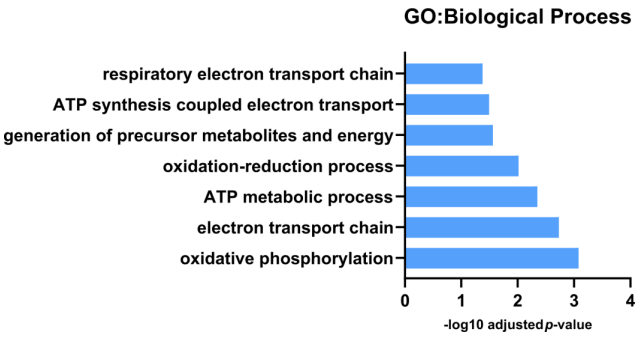

Figure 2. GO: Biological process analysis for downregulated protein expression differences between Pink1 non-exercised and wild-type non-exercised files. Pink1 files have reduced expression of proteins involved in mitochondrial respiration and oxidative phosphorylation.

ETS. DHODH deficiency has been reported to partially inhibit complex III and increase ROS generation [79].

The same *Pink1*- *Drosophila* strain has previously been reported to have upregulated genes involved in nucleotide metabolism, which is also the case in brains of PD patients with *PINK1* mutations [80]. Genetic and pharmacological upregulation of nucleotide metabolism and scavenging pathways restored mitochondrial function caused by *PINK1* loss. Therefore, DHODH upregulation by exercise may act in a compensatory manner to manage metabolic stress due to the *Pink1*- phenotype.

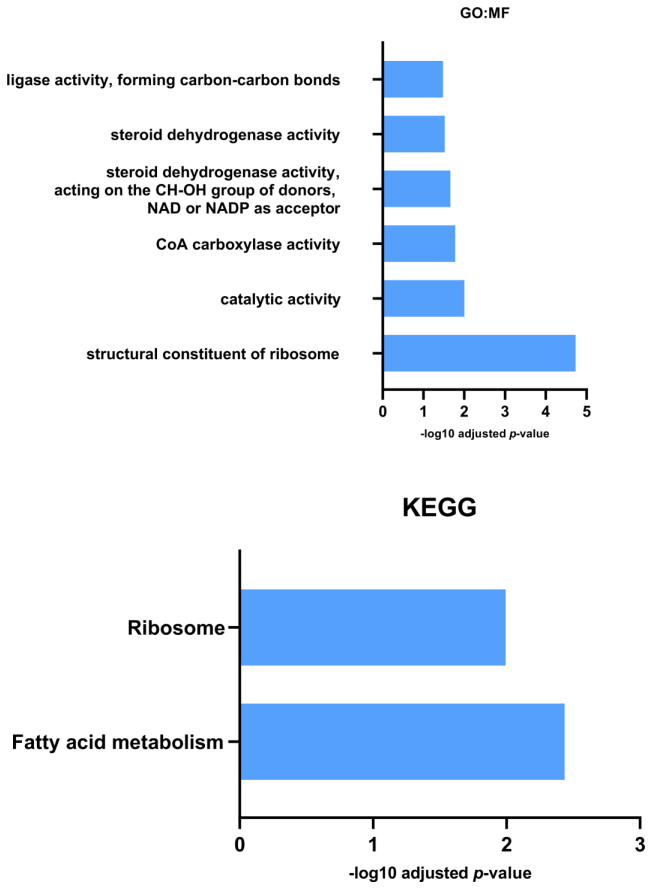

Figure 3. GO: Molecular Function and KEGG analysis for proteins reduced in expression in Pink1- exercised files compared with Pink1- non-exercised files. Both Molecular Function and KEGG enrichment analysis indicated a decrease in expression of fatty acid metabolic proteins in the exercised Pink1- files.

Exercise reduces the difference in levels of protein expression between *Pink1*- and wild-type *Drosophila*

Of the 516 proteins identified, 105 protein had different levels between non-exercised *Pink1*- *Drosophila* and non-exercised wild-type *Drosophila* (Supplementary Table 2). Comparing the exercised *Pink1*- *Drosophila* group to either non-exercised wild-type *Drosophila,* or exercised wild-type *Drosophila,* showed close to half the number of differentially expressed proteins (55 and 56 proteins, respectively) (Supplementary Tables 4, 5). Qualitatively the heatmap of protein expression for exercised *Pink1*- *Drosophila* more closely resembles wild-type *Drosophila* (Figure 4). This suggests exercise can ameliorate the aberrant protein profile of *Pink1*- *Drosophila* towards a more wild-type profile.

This is in agreement with findings from Cheedipudi et al. (2020) who reported gene expression data from an exercised mouse model of arrhythmogenic cardiomyopathy, that originally showed a dysregulation of near 800 genes, showed partial restoration of gene expression with regular exercise, with the greatest remedial effects on proteins involved in inflammation and oxidative phosphorylation [81].

Network analyses of differentially expressed proteins

STRING database network analysis complemented the results seen with gProfiler. The protein-protein interaction (PPI) networks were generated using STRING, and Figure 5A shows that exercised *Pink1*- *Drosophila*, compared with the exercised wild-type *Drosophila*, have a differentially expressed proteins (DEPs) network that consisted of 49 nodes and 200 edges with average node degree 8.16 and PPI enrichment p-value of (P < 1.0e-16).

Most of the proteins in the network have downregulated expression, with the following proteins found to be upregulated: endoplasmic reticulum chaperone BiP, enoyl-CoA hydratase short chain, glutamine synthetase, protein disulfide isomerase, methylmalonate-semialdehyde dehydrogenase, polyadenylate-binding protein, poly(U)-specific endoribonuclease, glutamine synthetase, flotillin-1, heat shock protein 22, phosphatidate cytidylyltransferase, fatty acyl-CoA reductase and dihydroorotate dehydrogenase.

The DEPs were found to be part of the ETC and OXPHOS processes, transmembrane transport and oxidative-reduction processes. The highly connected cluster in this network consisted of proteins from complex I: ND-18, ND-MLRQ, ND-ASHI, ND-B14.5B, ND-B14, ND-B16.6, ND-49, ND-51, ND-B17.2, ND-B14.7; complex IV: COX6B, COX4, mt: COII, COX5A; complex III: OX, and other proteins CYPE, UQCR-6.4, UQCR-14, levy and 40S ribosomal proteins S18. This cluster of proteins was downregulated in the exercised *Pink1*- *Drosophila*.

Figure 5B shows the non-exercised *Pink1*- *Drosophila* versus the non-exercised wild-type *Drosophila* PPI network, which consists of 86 nodes and 121 edges with average node degree 2.81 and PPI enrichment p-value (P < 1.0e-16). In contrast to exercised *Pink1*- *Drosophila* versus exercised wild-type *Drosophila,* all DEPs were upregulated, except for cytochrome c oxidase subunit 4, cyclope isoform A, flightin isoform B, cytochrome b-c1 complex subunit 7, NADH dehydrogenase 1 alpha subcomplex 12, Troponin 1, NADH dehydrogenase 18, cytochrome c oxidase subunit, cytochrome P450, NADH dehydrogenase 1 beta subcomplex subunit 8, cytochrome c oxidase subunit 5A, NADH dehydrogenase B14 and levy isoform A.

The DEPs were found to be a part of oxidation-reduction processes, fatty-acyl-CoA metabolic processes, translation and protein folding. The identification of DEPs from fatty-acyl-CoA metabolic process is concurrent with the enrichment analysis presented in Figure 3. The highly connected node in this network is that of upregulated ribosomal proteins RPS18, RPS23, RPS23, RPS7, RPS14b, RPL6, RPL5, RPL10AB and RPL9.

The DEPs were found to be a part of oxidation-reduction processes, fatty-acyl-CoA metabolic processes, translation and protein folding. The identification of DEPs from fatty-acyl-CoA metabolic process concurs with the enrichment analysis presented in Figure 3. The highly connected node in this network is that of upregulated ribosomal proteins RPS18, RPS23, RPS23, RPS7, RPS14b, RPL6, RPL5, RPL10AB and RPL9.

Similarly, for Figure 6A–6C, three additional PPI networks were generated for DEPs in pairwise group comparisons. For exercised *Pink1*- *Drosophila* compared with non-exercised *Pink1*- *Drosophila* the PPI network consisted of 43 nodes and 29 edges with average node degree 1.35 and PPI enrichment p-value <1.62e-06 (Figure 6A). All of the DEPs were downregulated except for OCIA domain containing protein 1 and dihydroorotate dehydrogenase. The DEPs were found to be involved in formation of 40S ribosomal subunit, oxidation reduction processes, synthesis of ketone bodies, translation and cellular lipid catabolic processes.

For non-exercised *Pink1*- *Drosophila* compared with exercised wild-type *Drosophila* the network has 107

nodes and 341 edges with average node degree 6.37 and PPI enrichment p-value (P <1.0e-16) (Figure 6B). The DEPs were found to be involved in ETC, translation, peroxisome, formation of 40S subunits and protein folding. The PPI network showed three highly connected clusters. Cluster 1 contained proteins from both complex I and complex IV, proteins that are downregulated like that of exercised *Pink1*$^{-}$ *Drosophila* compared with the exercised wild-type *Drosophila*. Cluster 2 contained ribosomal proteins that are upregulated, similar to that of non-exercised *Pink1*$^{-}$ *Drosophila* compared with the non-exercised wild-type *Drosophila* PPI network. Cluster 3 contains the proteins UGT, HSP22, HSP60C, CABP1, GP93, HSC70-5, HSC70Cb, HSP60A, RTNL1 and CNX99A. These proteins involved in proteostasis and protein folding and were found to be upregulated.

For the final PPI network, exercised *Pink1*$^{-}$ *Drosophila* compared with non-exercised wild-type *Drosophila*, there are 44 nodes and 40 edges with average node degree 1.82 and PPI enrichment p-value 6.79e-11 (Figure 6C). The exercised *Pink1*$^{-}$ *Drosophila* versus non-exercised wild-type *Drosophila* were involved in purine ribonucleotide triphosphate metabolic processes, ETC and peroxisomes.

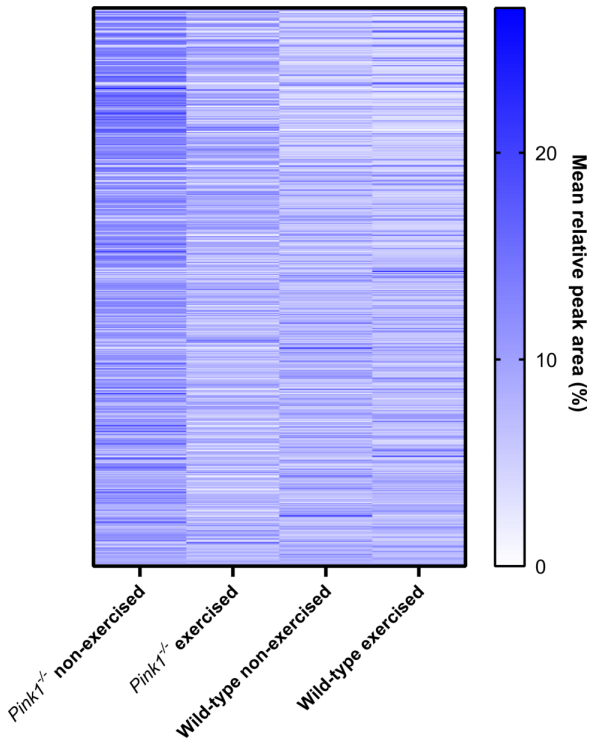

Figure 4. Heat map of protein expression levels (for proteins identified among all groups), determined by label-free mass spectrometry of mitochondrial fractions. Qualitatively, the identified Pink1^{-} exercised fly proteome more closely resembles the two WT fly proteomes than does the Pink1 non-exercised fly proteome.

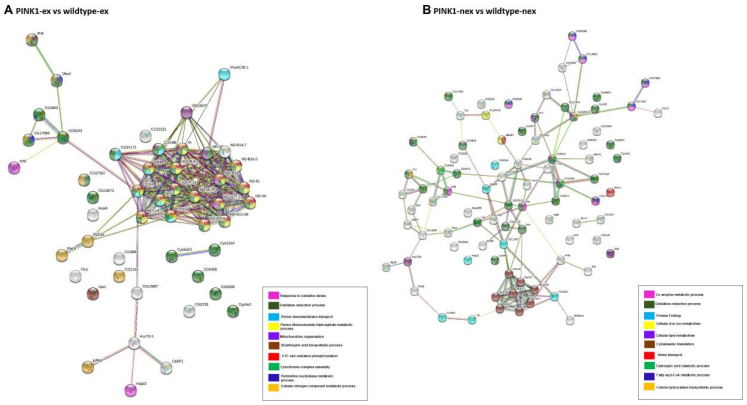

Figure 5. Network analysis of differentially expressed proteins. (**A**) Pink1^{-} exercised vs wild type exercised; (**B**) Pink1^{-} non-exercised vs wild type non-exercised. Networks analysed using STRINGdb. The nodes are coloured according to the processes (legend) that the proteins are involved in by using GO Terms for Biological Processes. The edge shows type of interactions, experimentally determined interactions are pink and those obtained from databases are sky blue. Predicted interactions such as gene neighbourhood are blue, green and red for gene co-occurrence, gene neighbourhood and gene fusions. Co-expression interactions are shown in black, text-mining interactions are shown in light green and protein homology edges are purple.

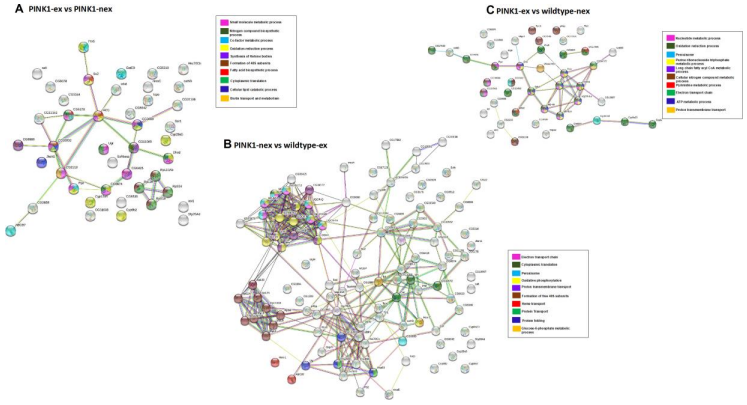

Figure 6. Network analysis of differentially expressed proteins. (**A**) Pink1^{-} exercised vs Pink1^{-} non-exercised; (**B**) Pink1^{-} non-exercised vs wild type exercised; (**C**) Pink1^{-} exercised vs wild type non-exercised. Networks analysed using STRINGdb. The nodes are coloured according to the processes (legend) that the proteins are involved in by using GO Terms for Biological Processes. The edge shows type of interactions, experimentally determined interactions are pink and the one obtained from databases are sky blue. Predicted interactions such as gene neighbourhood are blue, green and red for gene co-occurrence, gene neighbourhood and gene fusions. Co-expression interactions are shown in black, text-mining interactions are shown in light green and protein homology edges are purple.

For each of the three PPI networks, the number of edges is larger than expected and the nodes were more connected than for a random PPI network of the same size.

CONCLUSIONS

A picture of mitochondrial proteomic changes made in response to exercise was obtained by using two different mass spectrometry methodologies. We were able to measure changes in an organelle whose function in exercise, and dysfunction in Parkinson's disease, is crucial.

2D-GE MS data comparison between *Pink1*$^{-}$ exercised and *Pink1*$^{-}$ non-exercised *Drosophila* revealed several proteins with decreased levels of expression in response to exercise. These data were indicative of a generalised reduction of expression of the mitochondrial proteome in *Pink1*$^{-}$ *Drosophila* in response to exercise. This was investigated further in exercised and non-exercised *Drosophila*, both wild-type and *Pink1*$^{-}$, by label-free mass spectrometry.

GO and KEGG analyses of the label-free mass spectrometry proteomic data validated our mitochondrial isolation methodology by identifying the enrichment of mitochondrial processes and pathways. The comparison between non-exercised wild-type *Drosophila* and non-exercised *Pink1*$^{-}$ *Drosophila* revealed that proteins involved in bioenergetics had reduced expression in the mutant. Most strikingly, exercise of the *Pink1*$^{-}$ *Drosophila* caused a broad reduction in protein expression within the mitochondrial protein, resulting in the *Pink1*$^{-}$ *Drosophila* mitochondrial proteome to return to levels similar to the wild-type *Drosophila*.

GO, KEGG and STRING network analysis of the differentially expressed proteins from the mitochondrial proteome comparisons identified enrichment of bioenergetic pathways. The most significantly enriched pathways in the non-exercised *Pink1*$^{-}$ *Drosophila* included oxidation-reduction, fatty acid metabolism, and folate metabolism, all of which are associated with PD. Our data point to exercise aiding normalisation of these pathways. Specific proteins in the pathways may be candidates to develop therapeutic approaches in PD.

AUTHOR CONTRIBUTIONS

BE performed data analysis, assisted with experiments, and wrote the manuscript, TLI performed experimental work and helped prepare the manuscript, GK performed STRING analyses and helped prepare the manuscript, JRI developed and constructed the ICE machine for fly exercise, NM generated the *Drosophila* used for these experiments and was consulted on all aspects of the fly work, LC directed the research, supervised experiments, provided reagents and prepared the manuscript.

CONFLICTS OF INTEREST

The authors declare that they have no conflicts of interest.

FUNDING

This work was supported by the Biotechnology and Biological Sciences Research Council [grant number BB/J014508/1], via awards to BE and TLI. GK is supported by a University of Nottingham Vice-Chancellors International Scholarship award. NM and LC are funded by HEFCE.

REFERENCES

1. GBD 2016 Parkinson's Disease Collaborators. Global, regional, and national burden of Parkinson's disease, 1990-2016: a systematic analysis for the Global Burden of Disease Study 2016. Lancet Neurol. 2018; 17: 939–53. https://doi.org/10.1016/S1474-4422(18)30295-3 PMID:30287051

2. Storey A. Living longer - how our population is changing and why it matters. Off. Natl. Stat. 2018; 1–53.

3. Hirsch E, Graybiel AM, Agid YA. Melanized dopaminergic neurons are differentially susceptible to degeneration in Parkinson's disease. Nature. 1988; 334:345–48. https://doi.org/10.1038/334345a0 PMID:2899295

4. Schulz-Schaeffer WJ. The synaptic pathology of alpha-synuclein aggregation in dementia with Lewy bodies, Parkinson's disease and Parkinson's disease dementia. Acta Neuropathol. 2010; 120:131–43. https://doi.org/10.1007/s00401-010-0711-0 PMID:20563819

5. Park JS, Davis RL, Sue CM. Mitochondrial Dysfunction in Parkinson's Disease: New Mechanistic Insights and Therapeutic Perspectives. Curr Neurol Neurosci Rep. 2018; 18:21. https://doi.org/10.1007/s11910-018-0829-3 PMID:29616350

6. Alegre-Abarrategui J, Christian H, Lufino MM, Mutihac R, Venda LL, Ansorge O, Wade-Martins R. LRRK2 regulates autophagic activity and localizes to specific membrane microdomains in a novel human genomic reporter cellular model. Hum Mol Genet. 2009; 18:4022–34.

https://doi.org/10.1093/hmg/ddp346 PMID:19640926

7. Thomas KJ, McCoy MK, Blackinton J, Beilina A, van der Brug M, Sandebring A, Miller D, Maric D, Cedazo-Minguez A, Cookson MR. DJ-1 acts in parallel to the PINK1/parkin pathway to control mitochondrial function and autophagy. Hum Mol Genet. 2011; 20:40–50. https://doi.org/10.1093/hmg/ddq430 PMID:20940149

8. Zavodszky E, Seaman MN, Moreau K, Jimenez-Sanchez M, Breusegem SY, Harbour ME, Rubinsztein DC. Mutation in VPS35 associated with Parkinson's disease impairs WASH complex association and inhibits autophagy. Nat Commun. 2014; 5:3828. https://doi.org/10.1038/ncomms4828 PMID:24819384

9. Palikaras K, Lionaki E, Tavernarakis N. Mechanisms of mitophagy in cellular homeostasis, physiology and pathology. Nat Cell Biol. 2018; 20:1013–22. https://doi.org/10.1038/s41556-018-0176-2 PMID:30154567

10. Shiba-Fukushima K, Imai Y, Yoshida S, Ishihama Y, Kanao T, Sato S, Hattori N. PINK1-mediated phosphorylation of the Parkin ubiquitin-like domain primes mitochondrial translocation of Parkin and regulates mitophagy. Sci Rep. 2012; 2:1002. https://doi.org/10.1038/srep01002 PMID:23256036

11. Kondapalli C, Kazlauskaite A, Zhang N, Woodroof HI, Campbell DG, Gourlay R, Burchell L, Walden H, Macartney TJ, Deak M, Knebel A, Alessi DR, Muqit MM. PINK1 is activated by mitochondrial membrane potential depolarization and stimulates Parkin E3 ligase activity by phosphorylating Serine 65. Open Biol. 2012; 2:120080. https://doi.org/10.1098/rsob.120080 PMID:22724072

12. Koyano F, Okatsu K, Kosako H, Tamura Y, Go E, Kimura M, Kimura Y, Tsuchiya H, Yoshihara H, Hirokawa T, Endo T, Fon EA, Trempe JF, et al. Ubiquitin is phosphorylated by PINK1 to activate parkin. Nature. 2014; 510:162–66. https://doi.org/10.1038/nature13392 PMID:24784582

13. Kazlauskaite A, Kondapalli C, Gourlay R, Campbell DG, Ritorto MS, Hofmann K, Alessi DR, Knebel A, Trost M, Muqit MM. Parkin is activated by PINK1-dependent phosphorylation of ubiquitin at Ser65. Biochem J. 2014; 460:127–39. https://doi.org/10.1042/BJ20140334 PMID:24660806

14. Ordureau A, Sarraf SA, Duda DM, Heo JM, Jedrychowski MP, Sviderskiy VO, Olszewski JL, Koerber JT, Xie T, Beausoleil SA, Wells JA, Gygi SP, Schulman BA, Harper JW. Quantitative proteomics reveal a feedforward mechanism for mitochondrial PARKIN translocation and ubiquitin chain synthesis. Mol Cell. 2014; 56:360–75. https://doi.org/10.1016/j.molcel.2014.09.007 PMID:25284222

15. Cookson MR. Parkinsonism due to mutations in PINK1, parkin, and DJ-1 and oxidative stress and mitochondrial pathways. Cold Spring Harb Perspect Med. 2012; 2:a009415. https://doi.org/10.1101/cshperspect.a009415 PMID:22951446

16. Pankratz N, Foroud T. Genetics of Parkinson disease. Genet Med. 2007; 9:801–11. https://doi.org/10.1097/gim.0b013e31815bf97c PMID:18091429

17. Sliter DA, Martinez J, Hao L, Chen X, Sun N, Fischer TD, Burman JL, Li Y, Zhang Z, Narendra DP, Cai H, Borsche M, Klein C, Youle RJ. Parkin and PINK1 mitigate STING-induced inflammation. Nature. 2018; 561:258–62. https://doi.org/10.1038/s41586-018-0448-9 PMID:30135585

18. Zhong Z, Liang S, Sanchez-Lopez E, He F, Shalapour S, Lin XJ, Wong J, Ding S, Seki E, Schnabl B, Hevener AL, Greenberg HB, Kisseleva T, Karin M. New mitochondrial DNA synthesis enables NLRP3 inflammasome activation. Nature. 2018; 560:198–203. https://doi.org/10.1038/s41586-018-0372-z PMID:30046112

19. Park J, Lee SB, Lee S, Kim Y, Song S, Kim S, Bae E, Kim J, Shong M, Kim JM, Chung J. Mitochondrial dysfunction in Drosophila PINK1 mutants is complemented by parkin. Nature. 2006; 441:1157–61. https://doi.org/10.1038/nature04788 PMID:16672980

20. Clark IE, Dodson MW, Jiang C, Cao JH, Huh JR, Seol JH, Yoo SJ, Hay BA, Guo M. Drosophila pink1 is required for mitochondrial function and interacts genetically with parkin. Nature. 2006; 441:1162–66. https://doi.org/10.1038/nature04779 PMID:16672981

21. Greene JC, Whitworth AJ, Kuo I, Andrews LA, Feany MB, Pallanck LJ. Mitochondrial pathology and apoptotic muscle degeneration in Drosophila parkin mutants. Proc Natl Acad Sci USA. 2003; 100:4078–83. https://doi.org/10.1073/pnas.0737556100 PMID:12642658

22. Pickrell AM, Youle RJ. The roles of PINK1, parkin, and mitochondrial fidelity in Parkinson's disease. Neuron. 2015; 85:257–73. https://doi.org/10.1016/j.neuron.2014.12.007 PMID:25611507

23. Morais VA, Verstreken P, Roethig A, Smet J, Snellinx A, Vanbrabant M, Haddad D, Frezza C, Mandemakers W, Vogt-Weisenhorn D, Van Coster R, Wurst W, Scorrano L, De Strooper B. Parkinson's disease mutations in

PINK1 result in decreased Complex I activity and deficient synaptic function. EMBO Mol Med. 2009; 1:99–111. https://doi.org/10.1002/emmm.200900006 PMID:20049710

24. Liu W, Acín-Peréz R, Geghman KD, Manfredi G, Lu B, Li C. Pink1 regulates the oxidative phosphorylation machinery via mitochondrial fission. Proc Natl Acad Sci USA. 2011; 108:12920–24. https://doi.org/10.1073/pnas.1107332108 PMID:21768365

25. Julienne H, Buhl E, Leslie DS, Hodge JJ. Drosophila PINK1 and parkin loss-of-function mutants display a range of non-motor Parkinson's disease phenotypes. Neurobiol Dis. 2017; 104:15–23. https://doi.org/10.1016/j.nbd.2017.04.014 PMID:28435104

26. Sasco AJ, Paffenbarger RS Jr, Gendre I, Wing AL. The role of physical exercise in the occurrence of Parkinson's disease. Arch Neurol. 1992; 49:360–65. https://doi.org/10.1001/archneur.1992.00530280040020 PMID:1558515

27. Yang F, Trolle Lagerros Y, Bellocco R, Adami HO, Fang F, Pedersen NL, Wirdefeldt K. Physical activity and risk of Parkinson's disease in the Swedish National March Cohort. Brain. 2015; 138:269–75. https://doi.org/10.1093/brain/awu323 PMID:25410713

28. Ashburn A, Fazakarley L, Ballinger C, Pickering R, McLellan LD, Fitton C. A randomised controlled trial of a home based exercise programme to reduce the risk of falling among people with Parkinson's disease. J Neurol Neurosurg Psychiatry. 2007; 78:678–84. https://doi.org/10.1136/jnnp.2006.099333 PMID:17119004

29. Goodwin VA, Richards SH, Taylor RS, Taylor AH, Campbell JL. The effectiveness of exercise interventions for people with Parkinson's disease: a systematic review and meta-analysis. Mov Disord. 2008; 23:631–40. https://doi.org/10.1002/mds.21922 PMID:18181210

30. Murray DK, Sacheli MA, Eng JJ, Stoessl AJ. The effects of exercise on cognition in Parkinson's disease: a systematic review. Transl Neurodegener. 2014; 3:5. https://doi.org/10.1186/2047-9158-3-5 PMID:24559472

31. Shin MS, Jeong HY, An DI, Lee HY, Sung YH. Treadmill exercise facilitates synaptic plasticity on dopaminergic neurons and fibers in the mouse model with Parkinson's disease. Neurosci Lett. 2016; 621:28–33. https://doi.org/10.1016/j.neulet.2016.04.015 PMID:27080424

32. Jang Y, Koo JH, Kwon I, Kang EB, Um HS, Soya H, Lee Y, Cho JY. Neuroprotective effects of endurance exercise against neuroinflammation in MPTP-induced Parkinson's disease mice. Brain Res. 2017; 1655: 186–93. https://doi.org/10.1016/j.brainres.2016.10.029 PMID:27816415

33. Klemann CJ, Xicoy H, Poelmans G, Bloem BR, Martens GJ, Visser JE. Physical Exercise Modulates L-DOPA-Regulated Molecular Pathways in the MPTP Mouse Model of Parkinson's Disease. Mol Neurobiol. 2018; 55:5639–57. https://doi.org/10.1007/s12035-017-0775-0 PMID:29019056

34. Life Technologies. ZOOM ® IPGRunner TM System For isoelectric focusing of ZOOM ® Strips Catalog Numbers ZM0001, ZM0002, ZM0004. 2012.

35. Centre for Excellence in Mass Spectrometry. FAQs - Biology, The University of York. 2019.

36. Raudvere U, Kolberg L, Kuzmin I, Arak T, Adler P, Peterson H, Vilo J. g:Profiler: a web server for functional enrichment analysis and conversions of gene lists (2019 update). Nucleic Acids Res. 2019; 47:W191–98. https://doi.org/10.1093/nar/gkz369 PMID:31066453

37. Szklarczyk D, Gable AL, Lyon D, Junge A, Wyder S, Huerta-Cepas J, Simonovic M, Doncheva NT, Morris JH, Bork P, Jensen LJ, Mering CV. STRING v11: protein-protein association networks with increased coverage, supporting functional discovery in genome-wide experimental datasets. Nucleic Acids Res. 2019; 47:D607–13. https://doi.org/10.1093/nar/gky1131 PMID:30476243

38. Pollard A, Shephard F, Freed J, Liddell S, Chakrabarti L. Mitochondrial proteomic profiling reveals increased carbonic anhydrase II in aging and neurodegeneration. Aging (Albany NY). 2016; 8:2425–36. https://doi.org/10.18632/aging.101064 PMID:27743511

39. Pollard AK, Ingram TL, Ortori CA, Shephard F, Brown M, Liddell S, Barrett DA, Chakrabarti L. A comparison of the mitochondrial proteome and lipidome in the mouse and long-lived Pipistrelle bats. Aging (Albany NY). 2019; 11:1664–85. https://doi.org/10.18632/aging.101861 PMID:30892277

40. Cornelissen T, Vilain S, Vints K, Gounko N, Verstreken P, Vandenberghe W. Deficiency of parkin and PINK1 impairs age-dependent mitophagy in Drosophila. Elife. 2018; 7:e35878. https://doi.org/10.7554/eLife.35878 PMID:29809156

41. Lee JJ, Sanchez-Martinez A, Martinez Zarate A, Benincá C, Mayor U, Clague MJ, Whitworth AJ. Basal mitophagy is widespread in Drosophila but minimally affected by loss of Pink1 or parkin. J Cell Biol. 2018; 217:1613–22. https://doi.org/10.1083/jcb.201801044 PMID:29500189

42. Di Rita A, Peschiaroli A, D Acunzo P, Strobbe D, Hu Z, Gruber J, Nygaard M, Lambrughi M, Melino G, Papaleo E, Dengjel J, El Alaoui S, Campanella M, et al. HUWE1 E3 ligase promotes PINK1/PARKIN-independent mitophagy by regulating AMBRA1 activation via IKKα. Nat Commun. 2018; 9:3755. https://doi.org/10.1038/s41467-018-05722-3 PMID:30217973

43. Lira VA, Okutsu M, Zhang M, Greene NP, Laker RC, Breen DS, Hoehn KL, Yan Z. Autophagy is required for exercise training-induced skeletal muscle adaptation and improvement of physical performance. FASEB J. 2013; 27:4184–93. https://doi.org/10.1096/fj.13-228486 PMID:23825228

44. Yogev O, Pines O. Dual targeting of mitochondrial proteins: mechanism, regulation and function. Biochim Biophys Acta. 2011; 1808:1012–20. https://doi.org/10.1016/j.bbamem.2010.07.004 PMID:20637721

45. Ben-Menachem R, Tal M, Shadur T, Pines O. A third of the yeast mitochondrial proteome is dual localized: a question of evolution. Proteomics. 2011; 11:4468–76. https://doi.org/10.1002/pmic.201100199 PMID:21910249

46. Parker WD Jr, Boyson SJ, Parks JK. Abnormalities of the electron transport chain in idiopathic Parkinson's disease. Ann Neurol. 1989; 26:719–23. https://doi.org/10.1002/ana.410260606 PMID:2557792

47. Schapira AH, Cooper JM, Dexter D, Clark JB, Jenner P, Marsden CD. Mitochondrial complex I deficiency in Parkinson's disease. J Neurochem. 1990; 54:823–27. https://doi.org/10.1111/j.1471-4159.1990.tb02325.x PMID:2154550

48. Shoffner JM, Watts RL, Juncos JL, Torroni A, Wallace DC. Mitochondrial oxidative phosphorylation defects in Parkinson's disease. Ann Neurol. 1991; 30:332–39. https://doi.org/10.1002/ana.410300304 PMID:1952821

49. Finsterer J, Jarius C, Baumgartner M. Parkinson's disease associated with impaired oxidative phosphorylation. Neuroradiology. 2001; 43:997–1000. https://doi.org/10.1007/s002340100618 PMID:11760809

50. Keeney PM, Xie J, Capaldi RA, Bennett JP Jr. Parkinson's disease brain mitochondrial complex I has oxidatively damaged subunits and is functionally impaired and misassembled. J Neurosci. 2006; 26:5256–64. https://doi.org/10.1523/JNEUROSCI.0984-06.2006 PMID:16687518

51. Müftüoglu M, Elibol B, Dalmizrak O, Ercan A, Kulaksiz G, Ogüs H, Dalkara T, Ozer N. Mitochondrial complex I and IV activities in leukocytes from patients with parkin mutations. Mov Disord. 2004; 19:544–48. https://doi.org/10.1002/mds.10695 PMID:15133818

52. Haas RH, Nasirian F, Nakano K, Ward D, Pay M, Hill R, Shults CW. Low platelet mitochondrial complex I and complex II/III activity in early untreated Parkinson's disease. Ann Neurol. 1995; 37:714–22. https://doi.org/10.1002/ana.410370604 PMID:7778844

53. Chang D, Nalls MA, Hallgrímsdóttir IB, Hunkapiller J, van der Brug M, Cai F, Kerchner GA, Ayalon G, Bingol B, Sheng M, Hinds D, Behrens TW, Singleton AB, et al, International Parkinson's Disease Genomics Consortium, and 23andMe Research Team. A meta-analysis of genome-wide association studies identifies 17 new Parkinson's disease risk loci. Nat Genet. 2017; 49:1511–16. https://doi.org/10.1038/ng.3955 PMID:28892059

54. Li G, Cui S, Du J, Liu J, Zhang P, Fu Y, He Y, Zhou H, Ma J, Chen S. Association of GALC, ZNF184, IL1R2 and ELOVL7 With Parkinson's Disease in Southern Chinese. Front Aging Neurosci. 2018; 10:402. https://doi.org/10.3389/fnagi.2018.00402 PMID:30618709

55. Saiki S, Hatano T, Fujimaki M, Ishikawa KI, Mori A, Oji Y, Okuzumi A, Fukuhara T, Koinuma T, Imamichi Y, Nagumo M, Furuya N, Nojiri S, et al. Decreased long-chain acylcarnitines from insufficient β-oxidation as potential early diagnostic markers for Parkinson's disease. Sci Rep. 2017; 7:7328. https://doi.org/10.1038/s41598-017-06767-y PMID:28779141

56. Sharon R, Goldberg MS, Bar-Josef I, Betensky RA, Shen J, Selkoe DJ. alpha-Synuclein occurs in lipid-rich high molecular weight complexes, binds fatty acids, and shows homology to the fatty acid-binding proteins. Proc Natl Acad Sci USA. 2001; 98:9110–15. https://doi.org/10.1073/pnas.171300598 PMID:11481478

57. Karube H, Sakamoto M, Arawaka S, Hara S, Sato H, Ren CH, Goto S, Koyama S, Wada M, Kawanami T, Kurita K, Kato T. N-terminal region of alpha-synuclein is essential for the fatty acid-induced oligomerization of the molecules. FEBS Lett. 2008; 582:3693–700. https://doi.org/10.1016/j.febslet.2008.10.001 PMID:18848547

58. Golovko MY, Faergeman NJ, Cole NB, Castagnet PI, Nussbaum RL, Murphy EJ. Alpha-synuclein gene deletion decreases brain palmitate uptake and alters the palmitate metabolism in the absence of alpha-synuclein palmitate binding. Biochemistry. 2005; 44:8251–59. https://doi.org/10.1021/bi0502137 PMID:15938614

59. Golovko MY, Rosenberger TA, Faergeman NJ, Feddersen S, Cole NB, Pribill I, Berger J, Nussbaum RL, Murphy EJ. Acyl-CoA synthetase activity links wild-type but not mutant alpha-synuclein to brain arachidonate metabolism. Biochemistry. 2006; 45:6956–66. https://doi.org/10.1021/bi0600289 PMID:16734431

60. Golovko MY, Rosenberger TA, Feddersen S, Faergeman NJ, Murphy EJ. Alpha-synuclein gene ablation increases docosahexaenoic acid incorporation and turnover in brain phospholipids. J Neurochem. 2007; 101:201–11. https://doi.org/10.1111/j.1471-4159.2006.04357.x PMID:17250657

61. Ingram TL, Shephard F, Sarmad S, Ortori CA, Barrett DA, Chakrabarti L. Sex specific inflammatory profiles of cerebellar mitochondria are attenuated in Parkinson's disease. Aging (Albany NY). 2020; 12:17713–37. https://doi.org/10.18632/aging.103937 PMID:32855358

62. Lipton SA, Kim WK, Choi YB, Kumar S, D'Emilia DM, Rayudu PV, Arnelle DR, Stamler JS. Neurotoxicity associated with dual actions of homocysteine at the N-methyl-D-aspartate receptor. Proc Natl Acad Sci USA. 1997; 94:5923–28. https://doi.org/10.1073/pnas.94.11.5923 PMID:9159176

63. Müller T, Werne B, Fowler B, Kuhn W. Nigral endothelial dysfunction, homocysteine, and Parkinson's disease. Lancet. 1999; 354:126–27. https://doi.org/10.1016/s0140-6736(99)01660-8 PMID:10408491

64. Duan W, Ladenheim B, Cutler RG, Kruman II, Cadet JL, Mattson MP. Dietary folate deficiency and elevated homocysteine levels endanger dopaminergic neurons in models of Parkinson's disease. J Neurochem. 2002; 80:101–10. https://doi.org/10.1046/j.0022-3042.2001.00676.x PMID:11796748

65. Martignoni E, Tassorelli C, Nappi G, Zangaglia R, Pacchetti C, Blandini F. Homocysteine and Parkinson's disease: a dangerous liaison? J Neurol Sci. 2007; 257:31–37. https://doi.org/10.1016/j.jns.2007.01.028 PMID:17336337

66. Mayer O, Filipovský J, Hromádka M, Svobodová V, Racek J, Mayer O Jr, Stehlík P, Trefil L, Zárybnická M. Treatment of hyperhomocysteinemia with folic acid: effects on homocysteine levels, coagulation status, and oxidative stress markers. J Cardiovasc Pharmacol. 2002; 39:851–57. https://doi.org/10.1097/00005344-200206000-00010 PMID:12021579

67. Maron BA, Loscalzo J. The treatment of hyperhomocysteinemia. Annu Rev Med. 2009; 60:39–54. https://doi.org/10.1146/annurev.med.60.041807.123308 PMID:18729731

68. Shen L. Associations between B Vitamins and Parkinson's Disease. Nutrients. 2015; 7:7197–208. https://doi.org/10.3390/nu7095333 PMID:26343714

69. Xie Y, Feng H, Peng S, Xiao J, Zhang J. Association of plasma homocysteine, vitamin B12 and folate levels with cognitive function in Parkinson's disease: A meta-analysis. Neurosci Lett. 2017; 636:190–95. https://doi.org/10.1016/j.neulet.2016.11.007 PMID:27840145

70. Shen Y, Dong ZF, Pan PL, Xu G, Huang JY, Liu CF. Association of homocysteine, folate, and white matter hyperintensities in Parkinson's patients with different motor phenotypes. Neurol Sci. 2019; 40:1855–63. https://doi.org/10.1007/s10072-019-03906-3 PMID:31055730

71. Dong B, Wu R. Plasma homocysteine, folate and vitamin B12 levels in Parkinson's disease in China: A meta-analysis. Clin Neurol Neurosurg. 2020; 188:105587. https://doi.org/10.1016/j.clineuro.2019.105587 PMID:31733593

72. Liu S, Lu B. Reduction of protein translation and activation of autophagy protect against PINK1 pathogenesis in Drosophila melanogaster. PLoS Genet. 2010; 6:e1001237. https://doi.org/10.1371/journal.pgen.1001237 PMID:21151574

73. Morel E, Chamoun Z, Lasiecka ZM, Chan RB, Williamson RL, Vetanovetz C, Dall'Armi C, Simoes S, Point Du Jour KS, McCabe BD, Small SA, Di Paolo G. Phosphatidylinositol-3-phosphate regulates sorting and processing of amyloid precursor protein through the endosomal system. Nat Commun. 2013; 4:2250. https://doi.org/10.1038/ncomms3250 PMID:23907271

74. Khadilkar RJ, Rodrigues D, Mote RD, Sinha AR, Kulkarni V, Magadi SS, Inamdar MS. ARF1-GTP regulates Asrij to provide endocytic control of Drosophila blood cell homeostasis. Proc Natl Acad Sci USA. 2014; 111:4898–903. https://doi.org/10.1073/pnas.1303559111 PMID:24707047

75. Li X, Wang L, Cykowski M, He T, Liu T, Chakranarayan J, Rivera A, Zhao H, Powell S, Xia W, Wong ST. OCIAD1 contributes to neurodegeneration in Alzheimer's disease by inducing mitochondria dysfunction, neuronal vulnerability and synaptic damages. EBioMedicine. 2020; 51:102569. https://doi.org/10.1016/j.ebiom.2019.11.030 PMID:31931285

76. Shetty DK, Kalamkar KP, Inamdar MS. OCIAD1 Controls Electron Transport Chain Complex I Activity to Regulate Energy Metabolism in Human Pluripotent Stem Cells. Stem Cell Reports. 2018; 11:128–41. https://doi.org/10.1016/j.stemcr.2018.05.015 PMID:29937147

77. Cherwinski HM, Cohn RG, Cheung P, Webster DJ, Xu YZ, Caulfield JP, Young JM, Nakano G, Ransom JT. The immunosuppressant leflunomide inhibits lymphocyte proliferation by inhibiting pyrimidine biosynthesis. J Pharmacol Exp Ther. 1995; 275: 1043–49. PMID:7473131

78. Miret-Casals L, Sebastián D, Brea J, Rico-Leo EM, Palacín M, Fernández-Salguero PM, Loza MI, Albericio F, Zorzano A. Identification of New Activators of Mitochondrial Fusion Reveals a Link between Mitochondrial Morphology and Pyrimidine Metabolism. Cell Chem Biol. 2018; 25:268–78.e4. https://doi.org/10.1016/j.chembiol.2017.12.001 PMID:29290623

79. Fang J, Uchiumi T, Yagi M, Matsumoto S, Amamoto R, Takazaki S, Yamaza H, Nonaka K, Kang D. Dihydro-orotate dehydrogenase is physically associated with the respiratory complex and its loss leads to mitochondrial dysfunction. Biosci Rep. 2013; 33:e00021. https://doi.org/10.1042/BSR20120097 PMID:23216091

80. Tufi R, Gandhi S, de Castro IP, Lehmann S, Angelova PR, Dinsdale D, Deas E, Plun-Favreau H, Nicotera P, Abramov AY, Willis AE, Mallucci GR, Loh SH, Martins LM. Enhancing nucleotide metabolism protects against mitochondrial dysfunction and neurodegeneration in a PINK1 model of Parkinson's disease. Nat Cell Biol. 2014; 16:157–66. https://doi.org/10.1038/ncb2901 PMID:24441527

81. Cheedipudi SM, Hu J, Fan S, Yuan P, Karmouch J, Czernuszewicz G, Robertson MJ, Coarfa C, Hong K, Yao Y, Campbell H, Wehrens X, Gurha P, Marian AJ. Exercise restores dysregulated gene expression in a mouse model of arrhythmogenic cardiomyopathy. Cardiovasc Res. 2020; 116:1199–213. https://doi.org/10.1093/cvr/cvz199 PMID:31350552

82. Piazza N, Gosangi B, Devilla S, Arking R, Wessells R. Exercise-training in young Drosophila melanogaster reduces age-related decline in mobility and cardiac performance. PLoS One. 2009; 4:e5886. https://doi.org/10.1371/journal.pone.0005886 PMID:19517023

SUPPLEMENTARY MATERIALS

Ingram counter-balanced exerciser

Our bespoke Ingram Counter-balanced Exercise (ICE) machine was adapted from the PT design of Piazza et al., by Mr. John Ingram (TI's father) [82]. The exerciser fits into an incubator with internal dimensions of 48 x 48 x 35cm and provides a vertically moving tray measuring 30 x 34cm. A solenoid-powered counterbalanced lever causes the tray to be lifted 3cm. The tray is lifted and immediately dropped every 15 seconds.

Counterbalancing the lever are a series of springs, which can be adjusted to allow lifts of up to 3.0kg. Springs efficiently store and release energy enabling a more rapid drop than would be the case if weights were used. They also reduce the size and overall weight of the device.

Lift is provided by a solenoid wound onto a nylon core and fixed to the body of the exerciser. The steel armature passing through the solenoid is attached to the counterbalanced lever. Activation of the solenoid causes the armature to rise which lifts the lever.

Solenoid activation is controlled by an astable timer. This triggers a relay to pulse the applied AC voltage. Two capacitors acting as a loss-less resistor allow the voltage to be reduced without producing excess heat, before it is rectified, smoothed and finally applied to the solenoid. Powering with DC current causes less vibration and heat generation in the solenoid but, as the capacitors and the solenoids both work more efficiently at lower temperatures, any excess heat is subsequently dissipated by proximate fans. Using a pulse of current as described rather than the discharge from a large capacitor to activate the solenoid saves space, it is also safer as there is far less stored energy.

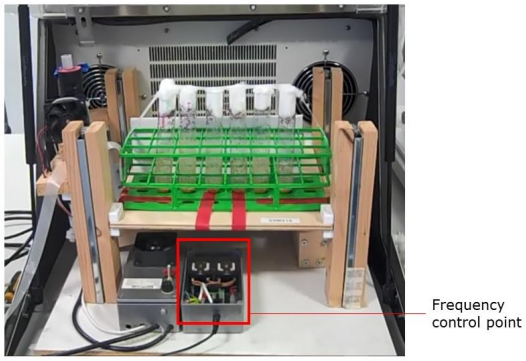

Supplementary Figure

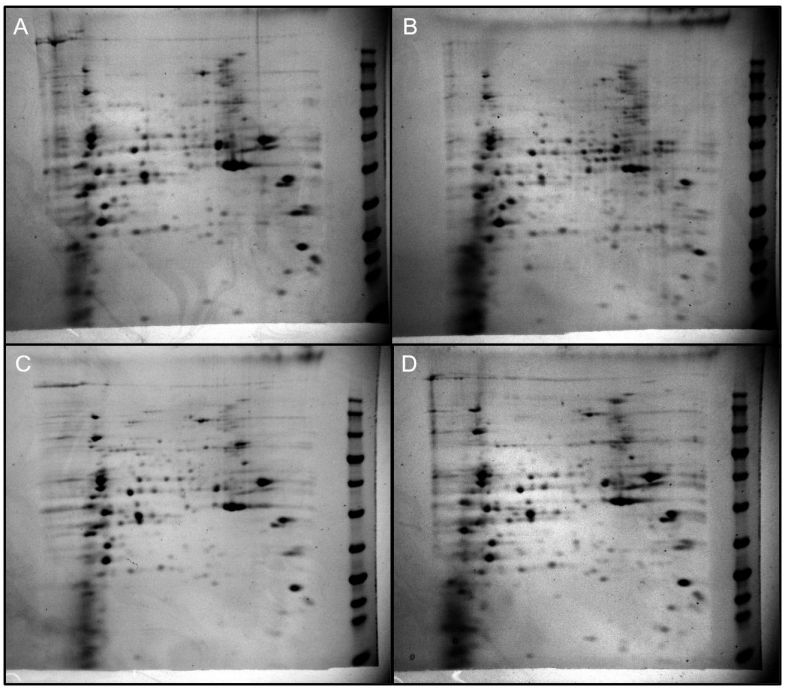

Supplementary Figure 1. Representative 2DE gels of (**A**) exercised Pink1, (**B**) non-exercised Pink1, (**C**) exercised wildtype, (**D**) non-exercised wildtype *Drosophila melanogaster*.

Supplementary Tables

Please browse Full Text version to see the data of Supplementary Tables 1–5.

Supplementary Table 1. Label-free MS identified 516 proteins from the mitochondrial fractions of *Pink1*$^{-}$ and WT *D. melanogaster.*

Supplementary Table 2. Label-free MS identified 105 proteins with different abundance when comparing non-exercised *Pink1*$^{-}$ and wildtype flies.

Supplementary Table 3. Label-free MS identified 57 proteins with altered abundance between exercised and non-exercised *Pink1*$^{-}$ flies, 55 of which had decreased abundance.

Supplementary Table 4. Label-free MS identified 56 proteins with different abundance when comparing exercised *Pink1*$^{-}$ and exercised WT flies.

Supplementary Table 5. Label-free MS identified 55 proteins with different abundance when comparing exercised *Pink1*$^{-}$ and non-exercised WT flies.

PLOS ONE

RESEARCH ARTICLE

Sequence and structure comparison of ATP synthase F_0 subunits 6 and 8 in notothenioid fish

Gunjan Katyal[1], Brad Ebanks[1], Magnus Lucassen[2], Chiara Papetti[3], Lisa Chakrabarti[1,4]*

1 School of Veterinary Medicine and Science, University of Nottingham, Sutton Bonington, United Kingdom, **2** Alfred Wegener Institute, Bremerhaven, Germany, **3** Biology Department, University of Padova, Padova, Italy, **4** MRC-Versus Arthritis Centre for Musculoskeletal Ageing Research, Nottingham, United Kingdom

* lisa.chakrabarti@nottingham.ac.uk

OPEN ACCESS

Citation: Katyal G, Ebanks B, Lucassen M, Papetti C, Chakrabarti L (2021) Sequence and structure comparison of ATP synthase F_0 subunits 6 and 8 in notothenioid fish. PLoS ONE 16(10): e0245822. https://doi.org/10.1371/journal.pone.0245822

Editor: Benedetta Ruzzenente, Imagine Institute for genetic diseases, FRANCE

Received: January 7, 2021

Accepted: September 9, 2021

Published: October 6, 2021

Peer Review History: PLOS recognizes the benefits of transparency in the peer review process; therefore, we enable the publication of all of the content of peer review and author responses alongside final, published articles. The editorial history of this article is available here: https://doi.org/10.1371/journal.pone.0245822

Data Availability Statement: All relevant data are within the manuscript and its Supporting information files.

Funding: Gunjan Katyal was supported by Vice Chancellor's International Scholarship for Research

Abstract

Mitochondrial changes such as tight coupling of the mitochondria have facilitated sustained oxygen and respiratory activity in haemoglobin-less icefish of the Channichthyidae family. We aimed to characterise features in the sequence and structure of the proteins directly involved in proton transport, which have potential physiological implications. ATP synthase subunit a (*ATP6*) and subunit 8 (*ATP8*) are proteins that function as part of the F_0 component (proton pump) of the F_0F_1complex. Both proteins are encoded by the mitochondrial genome and involved in oxidative phosphorylation. To explore mitochondrial sequence variation for ATP6 and ATP8 we analysed sequences from *C. gunnari* and *C. rastrospinosus* and compared them with their closely related red-blooded species and eight other vertebrate species. Our comparison of the amino acid sequence of these proteins reveals important differences that could underlie aspects of the unique physiology of the icefish. In this study we find that changes in the sequence of subunit a of the icefish *C. gunnari* at position 35 where there is a hydrophobic alanine which is not seen in the other notothenioids we analysed. An amino acid change of this type is significant since it may have a structural impact. The biology of the haemoglobin-less icefish is necessarily unique and any insights about these animals will help to generate a better overall understanding of important physiological pathways.

Introduction

The oceans which surround Antarctica, and their sub-zero temperatures provide a home to fish of the suborder Notothenioidei—a prime example of a marine species flock.

Notothenioids are renowned for their physiological adaptations to cold temperatures. This includes the ability to synthesise antifreeze glycoproteins (AFGP) and antifreeze-potentiating proteins (AFPP) [1]. The capacity to synthesise antifreeze glycopeptides (AFGPs) is a biochemical adaptation that enabled the Notothenioidei to colonize and thrive in the extreme polar environment [2]. These proteins are largely composed of a Thr-Ala-Ala repeat with a

Excellence, University of Nottingham (2018-2021) https://www.nottingham.ac.uk/. Brad E Banks was supported by the Biotechnology and Biological Sciences Research Council https://bbsrc.ukri.org/ [grant number BB/J014508/1. The funders had no role in study design, data collection and analysis, decision to publish, or preparation of the manuscript.

Competing interests: The authors have declared that no competing interests exist.

conjugated disaccharide via the hydroxyl group of the Thr residue and reduce the freezing point of the animals internal fluids [3,4].

Channichthyidae, contained within the Notothenioid suborder, are remarkable due to the absence of haemoglobin and, in some species, myoglobin too [5–7]. The sub-zero temperatures of the water they inhabit allow the highest levels of oxygen solubility, which is suggested to facilitate their survival despite the loss of globin proteins [7].

Myoglobin is absent in the oxidative skeletal muscle in all icefish, but the absence of myoglobin in cardiac muscle has been reported in only six of the species of the Channichthyinae [8,9]. While the molecular genetics of how myoglobin expression has been lost have been studied, the physiological differences between those that express and those that do not express myoglobin are not fully understood. Small intracellular diffusion distances to mitochondria and a greater percentage of cell volume occupied by mitochondria are two evolutionary adaptations that might compensate for the absence of myoglobin [10,11]. In the particular case of *Champsocephalus gunnari*, the mRNA transcript of myoglobin is present in the cardiac tissue but a 5-bp frameshift insertion hinders the synthesis of protein from the mRNA transcript [8,12].

Notothenioidei have high densities of mitochondria in muscle cells, versatility in mitochondrial biogenesis and a unique lipidomic profile [13–15]. These features have also been hypothesised to facilitate sustained oxygen consumption and respiratory activity in the absence of haemoglobin and myoglobin.

Complex V of the electron transport chain, ATP synthase, is responsible for the production of intracellular ATP from ADP and inorganic phosphate. Composed of an F_0 and F_1 component, the F_0 component is responsible for channelling protons from the intermembrane space across the inner mitochondrial membrane and into the mitochondrial matrix [16–18]. The rotation of the c-ring in F_0, and with this the γ-subunit of the central stalk, facilitates the translocation of protons across the inner mitochondrial membrane that ultimately drives the catalytic mechanism of the F_1 component [19,20].

The motor unit F_0, embedded in the inner membrane of mitochondria, is composed of subunits b, OSCP (oligomycin sensitivity conferring protein), d, e, f, g, h, i/j, k which are encoded by nuclear genes and subunits a (ATP6) and 8 (ATP8), which are encoded by mitochondrial genes [21]. Despite the structure of the complex having been first resolved decades ago, and hypotheses of the chemical mechanism were developed over half a century ago, significant breakthroughs continue to be made in our understanding of both the structure and function of the enzyme and its F_0 component [22–25].

Both ATP synthase subunit a (ATP6) and subunit 8 (ATP8) are proteins that function as part of the F_0 component of ATP synthase, encoded by genes that overlap within the mitochondrial genome [26]. This overlap is over a short, but variable between species, base pair sequence where the translation initiation site of subunit 8 is contained within the coding region of subunit 6.

The peripheral stalk is a crucial component of the F_0 component forming a physical connection between the membrane sector of the complex and the catalytic core. It provides flexibility, aids in the assembly and stability of the complex, and forms the dimerization interface between ATP synthase pairs [27]. ATP8 is an integral transmembrane component of the peripheral stalk, serving an important role in the assembly of the complex [28]. The C-terminus of ATP8 extends 70 Å from the surface of the makes contacts with subunits b, d and F_6, while the N-terminus has been reported to make connections with subunits b, f and 6 in the intermembrane space [29,30]. Subunit 8 is also known to play a role in the activity of the enzyme complex [31].

ATP6 is an α-helical protein embedded within the inner mitochondrial membrane and it interacts closely with the c-ring of F_0, providing aqueous half-channels that shuttle protons to and from the rotating c-ring [17,32]. It has previously been reported that ATP6 has at least five hydrophobic transmembrane spanning α helices domain, where two of the helices h4 and h5 are well conserved across many species [33].

Proteins coded by mitochondrial DNA (mtDNA) are involved in oxidative phosphorylation and can directly influence the metabolic performance of this pathway. Evaluating the selective pressures acting on these proteins can provide insights in their evolution, where mutations in the mtDNA can be favourable, neutral, or harmful. The amino acid changes can cause inefficiencies in the electron transfer chain, causing oxidative damage by excess production of reactive oxygen species and eventually interrupting the production of mitochondrial energy. Due to the tight coupling of icefish mitochondria relative to their red-blooded relatives, any changes in the structure of ATP Synthase subunits, particularly those directly involved in the transport of protons across the membrane, could result in significant physiological outcomes [34].

In this work, we combine sequence analyses and secondary structure prediction analyses to explore mitochondrial genetic variation for ATP6 and ATP8 in the Notothenioidei suborder species as well as other vertebrate species. The species considered include *Champsocephalus gunnari*, *Chionodraco rastrospinosus* and *Chaenocephalus aceratus* from the Channichthyidae family, *Notothenia coriiceps* and *Trematomus bernacchii* from the Nototheniidae family and the sub-Antarctic *Eleginops maclovinus* from family Eleginopsidae, all the broader Notothenioidei suborder. The species of suborder Notothenioidei are further compared with the following eight vertebrates: *Homo sapiens* (family: Hominidae), *Nothobranchius furzeri* (family: Nothobranchiidae), *Danio rerio* (family: Cyprinidae), *Anolis carolinensis* (family: Dactyloidae), *Cavia porcellus* (family: Caviidae), *Balaena mysticetus* (family: Balaenidae), *Heterocephalus glaber* (family: Heterocephalidae), and Lasiurus *borealis* (family: Vespertilionidae) to shed light on the changes of these proteins in the notothenioid species by comparing them to better characterised diverse vertebrate species. These species choices help us decipher amino acid changes specific to notothenioids and those that are potentially species specific (S1 Fig).

Methodology

Extraction of gene and protein sequences of ATP8 and ATP6 suborder Notothenioidei and other vertebrates

The list of complete coding sequences (CDS) and protein sequences of the proteins were obtained from the National Centre for Biotechnology Information (NCBI) protein database search, we chose only the Refseq (provides a comprehensive, integrated, non-redundant, well-annotated set of sequences, including genomic DNA, transcripts, and proteins) sequence queries (https://www.ncbi.nlm.nih.gov/ lMSast searched:17th August 2020). Though these sequences have been taken from highly reliable Refseq database [35] validated by different sources it is important to recognise they could still be prone to error.

Multiple protein sequence alignment (MSA)

(-/-) indicates absence of both haemoglobin and myoglobin genes, whereas (-/+) indicate absence of haemoglobin but presence of myoglobin. The sequences for the Notothenioidei suborder species *C. gunnari* (-/-), *C. rastrospinosus* (-/+), *C. aceratus* (-/-), *N. coriiceps* (+/+), *T. bernacchii*, *E. maclovinus* (+/+), and eight other vertebrate species, *N. furzeri*, *D. rerio*, *A. carolinensis*, *C. porcellus*, *B. mysticetus*, *H. glaber*, *L. borealis*, *H. sapiens* were aligned using Clustal

omega [36] to prepare the initial alignment of ATP6 protein under the criteria of the presence and the absence of haemoglobin and myoglobin proteins in the species, the alignments were also verified using the other two progressive methods, MAFFT [37] and MUSCLE [36]. The same method was applied for protein ATP8. The MSA was visualised and edited using JALVIEW [38]. The eight vertebrate species were selected as well known and sequenced representative of different groups under vertebrate: fish (*N. furzeri* and *D. rerio*), reptiles (*A. carolinesis*), mammals (*C. porcellus*, *H. glaber*, *L. borealis*, *H. sapiens*, *B. mysticetus*). *H.sapiens* sequences have been included in our analyses since much of what is known about these proteins has previously been characterised in humans. The selection of these different species shows the conservation of these mitochondrial proteins across vertebrate species, including *H. sapiens*.

Codon alignment

Complete nucleotide coding sequences for genes *ATP6* and *ATP8* from the fourteen vertebrate species were retrieved from NCBI GenBank database (see Table 1). The sequences were aligned using Clustal omega [36] and were manually edited and visualised as codons using MATLAB version R2018b (9.5.0).

Comparison of properties of amino acids among the sequence from the above-mentioned species

Using the ExPASy [39] tool ProtScale [40], different amino acid properties such as the molecular weight of amino acids across the sequence, hydrophobicity trend of amino acids, α—helix forming amino acids, average flexibility trend and mutability for the protein ATP6 were compared graphically among the seven fish species (5 Antarctic, 1 sub-Antarctic, *D. rerio* and *N. furzeri*) (https://web.expasy.org/protscale/).

Structure prediction for protein sequences

The MSA was structurally validated using the structure prediction tool I-TASSER [41] (Iterative Threading ASSEmbly Refinement) a hierarchical approach to protein structure and function prediction, to generate the protein structure for AT6 from different species (https://zhanglab.ccmb.med.umich.edu/I-TASSER/). The structures were validated using SAVES v6.0 (https://saves.mbi.ucla.edu/), using ERRAT [42], PROCHECK [43,44] and ProSA-web [45]. (Figures in supplementary files).

Figures

Protein structure images were produced with PyMOL v. 2.3.2. (The PyMOL Molecular Graphics System, Version 2.0 Schrödinger, LLC.) Graphs were produced with MATLAB version R2018b (9.5.0). Sequence logos were created using the webserver WebLogo using alignment of 5947 vertebrate (NCBI:txid7742) protein sequences for the protein ATP6 (http://weblogo.threeplusone.com/). Using RefSeq sequences with custom range of sequence length of 224–231 to obtain full sequences only (searched: 3rd May 2021).

Results

Codon alignment

MSA of all the sequences of ATP8 (see Fig 1) and ATP6 (see Fig 2) from the different vertebrate species (see Table 1) for both nucleotide (codon) and proteins identified several

Table 1. Features of nucleotide and protein sequences for ATP synthase F_0 subunit 6 and 8.

Species/Features	*C. gunnari*	*C. rastrospinosus*	*C. aceratus*	*N. corriceps*	*T. bernacchii*	*E. maclovinus*	*N. furzeri*	*D. rerio*	*A. carolinensis*	*L. borealis*	*H. glaber*	*C. porcellus*	*B. mysticetus*	*H. sapiens*
Common Name	Mackerel Icefish	Ocellated icefish	Blackfin Icefish	Marbled rockcod	Emerald rockcod	Rockcod	Killifish	Zebra fish	Lizard	Eastern red bat	Naked mole rat	Guinea Pig	Bowhead Whale	Humans
Accession No. ATP6 (protein)	YP_006575887.1	YP_009519992.1	AEH05456.1	BBC27483.1	ANN44664.1	YP_009340798.1	YP_002456261.1	NP_059336.1	ACD81888.2	YP_005255233.1	YP_004222617.1	QIQ22938.1	AWM99473.1	YP_003024031.1
Accession No. ATP6 (nucleotide)	NC_018340.1	NC_039543.1	NC_015654.1	NC_015653.1	KU166863	NC_033386.1	NC_011814.1	NC_002333.2	NC_016873.1	NC_001573.1	NC_015112.1	NC_000884.1	NC_005268.1	NC_012920.1
Accession No. ATP8 (protein)	YP_006575886.1	YP_009519991.1	YP_004581501.1	YP_004581488.1	ANN44663.1	YP_009340797.1	YP_002456260.1	NP_059335.1	ACD81887.2	YP_005255232.1	YP_004222616.1	NP_008755.1	NP_944611.1	NC_012920.1
Haemoglobin	-	-	-	+	+	+	+	+	+	+	+	+	+	+
Myoglobin	-	+	-	+	+	+	+	+	+	+	+	+	+	+
Length of nucleotide ATP6	683	695	695	695	695	695	682	683	680	683	680	680	680	680
5' flanking region ATP8	74 nt	75nt	75nt	75nt	75nt	75nt	74nt	73nt	67nt-trn-Lysine	71nt	73nt	68nt	71nt	71nt
ATP6-Start codon	atg	gtg	gtg	gtg	atg	gtg	atg	atg	atg	atg	atg	atg	atg	atg
4_nucleotides at 5'end	-	+ GTG-AAC-CTG-ACC	+ GTG-AAC-CTG-ACC	+ GTG-GTC-CTG-ACC	+ ATG-AAC-TTG-GCC	+ GTG-AAC-CTG-ACC	-	-	-	-	-	-	-	-
4_amino acid at 5'end	-	+MNLT	+MNLT	+MVLT	+MNLA	+MNLT	-	-	-	-	-	-	-	-
Codon aligning at position 35/39 (nucleotide)	GCT	TCT	TCT	TCT	TCC	TCT	CTT	ACA	AAT	ACC	CCC	CCC	CCA	CCA
Residue Aligning at position 35/39 (protein)	Alanine	Serine	Serine	Serine	Serine	Serine	Leucine	Threonine	Asparagine	-	-	-	-	-
Residues at positions 38–39 aligned to 42–43 residues	Valine-Isoleucine	Valine-Isoleucine	Valine-Isoleucine	Valine-Isoleucine	Valine-Valine	Valine-Valine	Tryptophan-Leucine	Tryptophan-Isoleucine	Leucine-Valine	Isoleucine-Asparagine	Isoleucine-Asparagine	Isoleucine-Asparagine	Isoleucine-Asparagine	Isoleucine-Asparagine
Properties of substitution	Non-Polar	Non-Polar	Non-Polar	Non-Polar	Non-Polar	Non-Polar	Non-polar aromatic AA -Hydrophobic branched AA	Non-polar aromatic AA -Hydrophobic branched AA	Hydrophobic AA	Hydrophobic AA—Polar, non-charged AA	Hydrophobic AA—Polar, non-charged AA	Hydrophobic AA—Polar, non-charged AA	Hydrophobic AA—Polar, non-charged AA	Hydrophobic AA—Polar, non-charged AA
Structural change at position 38–39 aligned to 42–43 residues	strand-strand	coil-coil	coil-coil	coil-coil	strand-strand	strand-strand	strand-strand	strand-strand	strand-strand	coil-coil	coil-coil	coil-coil	coil-coil	coil-coil

https://doi.org/10.1371/journal.pone.0245822.t001

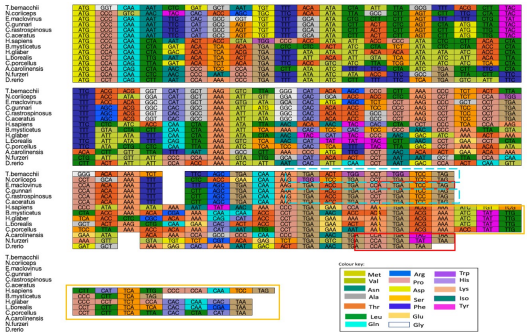

Fig 1. Multiple sequence alignment for nucleotide sequences of ATP synthase subunit 8. Multiple codon alignment of nucleotide sequences of ATP synthase subunit 8 was created using the Clustal omega alignment of nucleotides we screened five Antarctic and one sub-Antarctic fish species and eight vertebrate outgroups same as ATP6 MSA (See Fig 1 for colour key). The highlighted boxes show the overlap of the ATP8 and ATP6 sequences for different species where different colour of the boxes correspond to the different lengths of overlap.

https://doi.org/10.1371/journal.pone.0245822.g001

conserved codons and amino acid residues. The sequence knowledge was gathered from curated entries in RefSeq which nevertheless could be subject to error.

Five of the six Antarctic fish species have twelve nucleotides (four codons) at the 5' end of the gene sequence which are not found in the other eight vertebrate species. The codon alignment ATP6 for species *E. maclovinus*, *N. coriiceps*, *C. rastrospinosus* and *C. aceratus* show that GTG codes for methionine, as the start codon for the protein. GTG which is originally known for coding the amino acid valine has been accepted as a mitochondrion start codon for invertebrate mitogenomes [46–48]. A common feature with the species that have GTG as a start codon is that *N. coriiceps*, *E. maclovinus*, *C. rastrospinosus* have genes coding for myoglobin, where the latter is devoid of haemoglobin. *C. aceratus* do not express myoglobin due to a 15 bp sequence insertion, other than that difference, their myoglobin gene sequence is identical to that of *C. rastrospinosus* [9]. The only exception to this is the red-blooded species *T. bernacchii*, but this may be attributed to the unverified source of its sequence submission.

Another trend that has been observed through sequence alignment is that the species that are more similar and have the same amino acid for a particular position also have codons with the same nucleotide (nt) at the third position. 'TGA' codons or 'stop codons' are found within the translated sequence, here these code for tryptophan, as seen in human and yeast mitochondria [49]. A variation in the length of the sequences was observed, with an average length for *ATP6* nt sequence of 683 and 74 nt for *ATP8* gene sequences. The *ATP6* sequence ends with a TAA stop codon in all species except the two red blooded Antarctic fish species, *N. coriiceps* and *E. maclovinus*.

Overlapping genes

The overlap between genes is encoded on the same strand (Table 1). The length of overlap was 22 nt in ATP8-ATP6 for the five of the six species of Notothenioidei suborder, that is excluding

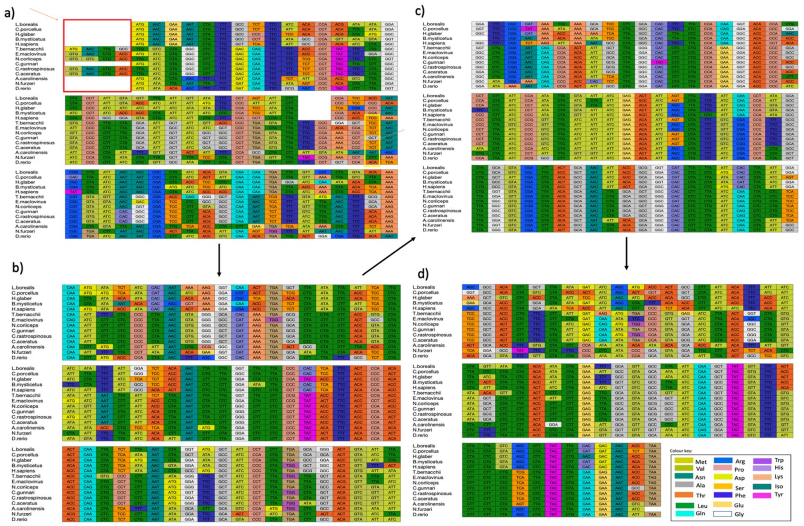

Fig 2. (a-d) Multiple sequence alignment for nucleotide sequences of ATP synthase subunit 6. Multiple codon alignment of nucleotide sequences of ATP synthase subunit 6 was created using the Clustal omega alignment of nucleotides for five Antarctic and one sub-Antarctic fish species and eight vertebrate outgroups and visualised) using MATLAB. The colour of the codon boxes corresponds to the respective amino acid (See colour key).

https://doi.org/10.1371/journal.pone.0245822.g002

icefish *C. gunnari* where the overlap was of 10nt. Species *H. sapiens*, *H. glaber*, *L. borealis* and *C. porcellus* had an overlap of 43nt between ATP6 and ATP8. The shortest overlap between the two genes were observed in the species *A. carolinesis* has an overlap of 10nt and *N. furzeri* and *D. rerio*, have an overlap of 7nts.

Protein alignment and structural changes in ATP6

The complete amino acid sequences for ATP8 and ATP6 were aligned separately for the fourteen vertebrate species (see Figs 3 & 4). Protein sequence alignment showed conserved residues across the species based on identity and similarity. Four Antarctic fish species, *N. coriiceps*, *T. bernacchii*, *C. rastrospinosus*, *C. aceratus* and the sub-Antarctic *E. maclovinus* have four amino acids at the N-terminal with a total of 231 residues. As previously mentioned, the only exception to this, is the species *C. gunnari* with 227 residues similar to that of other fish species, *N. furzeri* and *D. rerio*. Species *H. sapiens*, *A. carolinesis*, *L. borealis*, *H. glaber* and *C. porcellus* have 226 residues and *B. mysticetus* has 225 residues. The protein ATP6 in vertebrates is known to have 226–228 residues. In humans, four point mutations in the ATP6 gene account for 82% of disease associated with this gene, suggesting point mutations could have physiological relevance [50,51]. Common features in all fourteen species were as follows: (1) several hydrophobic amino acids (light pink) were observed to be conserved across the sequences in

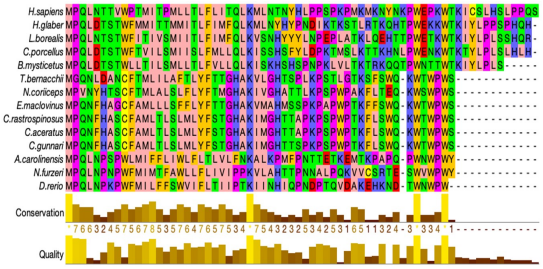

Fig 3. Multiple sequence alignment of ATP8 protein sequences. The ATP8 protein sequences were aligned using Clustal omega and edited using zappo colour scheme in JalView. Notothenioidei are grouped together in blue; all species are displayed to the colour corresponding to their phylogenetic closeness. (Colours according to physio-chemical properties of amino acids; Aliphatic/hydrophobic-A, I, L, M, V- light pink; Aromatic-F, W, Y- mustard; Conformationally special- Glycine, P- magenta; C-yellow; Hydrophilic- N, Q, S, Q, T- light green; Negatively charged/D,E-Red; Positively charged/R,H,K-Blue) in jalview. The bar-graphs below represent a quantitative measure of conservation at each position. The figure was created using JalView.

https://doi.org/10.1371/journal.pone.0245822.g003

the species, (2) insertions and deletions of amino acids occurred more frequently near N-termini, and (3) the C-terminal of the protein sequence is hydrophilic. Dashes in the amino acid sequence represent gaps which may be an insertion or deletion of a residue. The gap in the alignment is observed for the species *H. sapiens*, *L. borealis*, *C. porcellus*, *B. mysticetus* and *H. glaber* at position 35, and at the C-terminal end for *A. carolinesis* and *B. mysticetus*, at position 226 and 225 respectively.

The amino acid at position 35 has predominantly hydrophilic residues except in the two species *C. gunnari* and *N. furzeri*, where it is substituted with alanine or leucine respectively.

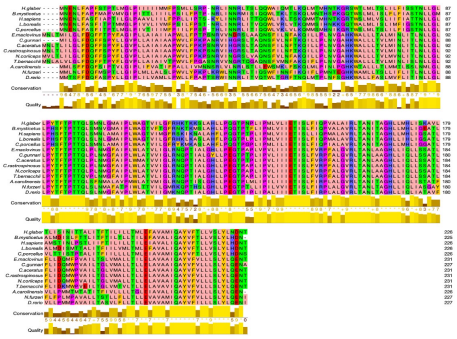

Fig 4. Multiple sequence alignment for protein sequences of ATP synthase F_0 subunit 6. The ATP6 protein sequences were aligned using Clustal omega and edited using zappo colour scheme.

https://doi.org/10.1371/journal.pone.0245822.g004

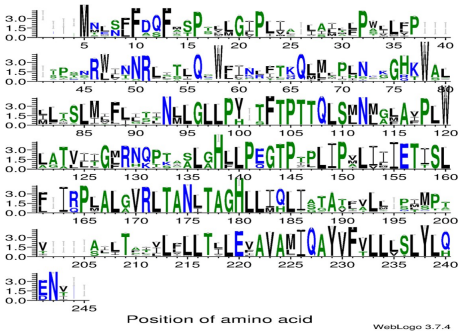

Fig 5. Sequence logos displaying conservation of residues created for all aligned blocks of the MSA for protein ATP synthase F_0 subunit 6 for 5947 vertebrate species from NCBI using webserver WebLogo (http://weblogo.threeplusone.com/) the y axis represents probability of the residue occurring at that position from the MSA.

https://doi.org/10.1371/journal.pone.0245822.g005

All the Antarctic species except *C. gunnari*, the sub-Antarctic species, *E. maclovinus* and surprisingly *H. sapiens* from the mammalian species have a serine at this position. When we look at the codon alignment of the ATP6 gene, serine is encoded by codon TCT predominantly at position 39 for all the species except *T. bernacchii* and *H. sapiens* and the alanine for the species *C. gunnari* is encoded by GCT (see Fig 2).

The logo (see Fig 5) displays the conserved amino acids in the protein ATP6 for a particular position for 5947 vertebrate species. The protein is overall very conserved in the vertebrates, and position 38–39 show conservation for amino acids serine and threonine as also seen in the Antarctic species (except *C. gunnari*) and *E. maclovinus*.

A similar pattern was found in the amino acid alignment of ATP8, where the species, *H. sapiens*, *B. mysticetus*, *H. glaber*, *C. porcellus* and *L. borealis*, that showed a gap in the previous alignment have hydrophilic residues whereas the other species have a gap at the position 47. This observation could be attributed to the overlapping nature of the nucleotide sequences coding for the two proteins. The protein sequence of ATP6 was observed to be more conserved than ATP8. The amino acid sequences at the N- terminal are more diverse, and the methionine residues are usually followed by amino acids with short polar side chains [52]. Alanine is a non-polar amino acid whereas serine is a polar amino acid. The hydrophobicity plot, average flexibility, mutability, and coil prediction across the sequences has shown that *T. bernacchii* and *E. maclovinus* show similar trends in their physico-chemical properties across the sequence. *Notothenia coriiceps*, *C. aceratus* and *C. rastrospinosus* follow this trend. *Champsocephalus gunnari* is the only species out of the seven fish species compared, that is different from the others (see Fig 6).

Protein structure differences were predicted at position 38–39 for species *C. gunnari* (icefish), *N. furzeri*, *D. rerio* and *A. carolinesis*, where a strand-strand structure is found at that position. All other species have coil structures at those positions (see Fig 7). For species *T. bernacchii* and *E. maclovinus* there is also a prediction for a strand structure at positions 42–43.

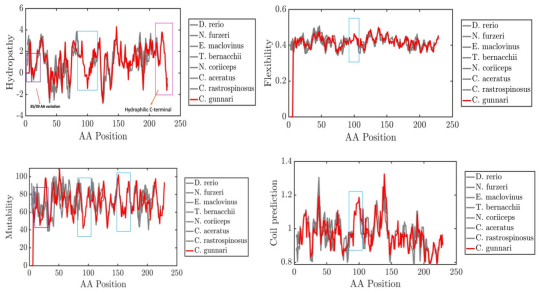

Fig 6. Primary sequence features of ATP Synthase F_0 subunit 6 in species *C. gunnari* (red), *C. rastrospinosus*, *C. aceratus*, *N. coriiceps*, *T. bernacchii*, *E. maclovinus*, *N. furzeri* and *D. rerio*. Red Box: N-terminal property changes, Purple Box: Changes in properties observed at 35/39 variation, blue box: Conserved regions 90–170 (Active site 160–169), Pink Box: C-terminal low hydrophobicity. A difference in the peaks have been observed for different properties (highlighted) such as molecular weight and hydrophobicity of amino acid residues across the sequence and other properties such as tendency of amino acid residues towards beta-sheet, bulkiness and flexibility.

https://doi.org/10.1371/journal.pone.0245822.g006

Discussion

We present our analyses highlighting differences in sequence and structure observed in the two proteins of complex V, ATP8 and ATP6, encoded by mtDNA between the red- and white blooded species of suborder Notothenioidei. Our analyses are based on the current genome annotation available which is subject to change as more information becomes available. We have only selected *RefSeq* sequences as these are reviewed by NCBI and represent a compilation of the current knowledge of a gene and protein products and is synthesised using information integrated from multiple sources. *RefSeq* is used as a reference standard for a variety of purposes such as genome annotation and reporting locations of sequence variation. It is important to acknowledge however that database information is regularly updated and may change. Currently, the RefSeq and GenBank entries available for a ATP6 sequences for the Antarctic/sub-Antarctic fish, NC_015653.1, AP006021.1 (*N. coriiceps*), NC_039543.1, MF622064.1 (*C. rastrospinosus*), NC_033386.1, KY038381.1 (*E. maclovinus*), NC_015654.1, YP_004581502.1 (*C. aceratus*), which are submitted by different authors, have the start codon as GTG for the five species of Notothenioidei suborder. The protein length of ATP6 has been consistent in all the entries, 231 amino acids.

It has previously been shown that mitochondria from icefish are more tightly coupled than those of their red-blooded counterparts [34]. Mitochondria that are tightly coupled usually have competent membranes and protons can only get into the matrix by passing through complex V. The red-blooded species *N. coriiceps*, *E. maclovinus*, *T. bernacchii*, the two icefish *C. rastrospinosus* (devoid of hb, have mb), *C. aceratus* (devoid of hb, do not express mb but have a nearly identical gene to that of C. rastrospinosus for mb), have an additional 12 nucleotides at the N-terminal. The only exception to this is the icefish *C. gunnari* which is completely devoid of both hb and mb. Since *C. gunnari* is the extreme of all the species of Notothenioidei suborder in question in terms of loss of globins, the change observed could be an altered variation for the gene.

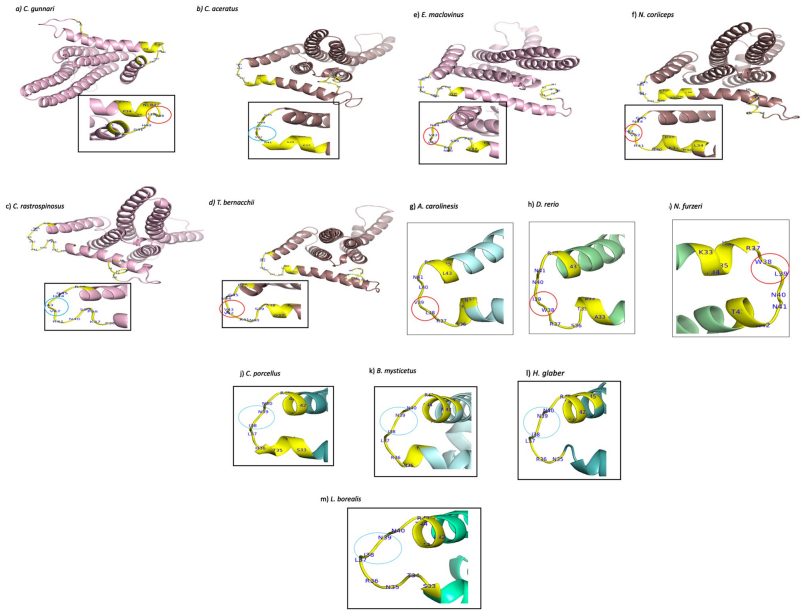

Fig 7. Representative structures of ATP synthase F_0 subunit 6 for the fourteen vertebrate species created using I-TASSER [41] suite and visualised and edited using PyMOL v. 2.3.2. a) *C. gunnari*(-/-) residues 38 (valine) and 39 (isoleucine) shows strand structure b) *C. aceratus*(-/-) residues 42(valine) and 43 coil (isoleucine), aligning with 38/39 in MSA, show a coil structure c) *C. rastrospinosus*(-/+) residues 42-Valine and 43-Isoleucine has a coil structure d) *T. bernacchii*(+/+) residues 42-Valine and 43-Valine show a strand structure e) *E. maclovinus* (+/+) residues 42 -Valine and 43-Valine show a strand structure f) *N. coriiceps*(+/+) residues 42 (Valine) 43 (isoleucine) has a coil structure. g) *A. carolinesis* residues 38 (Leucine) and 39(Valine) show a strand structure h) *D. rerio* residues 38 (tryptophan) and 39(Isoleucine) show a strand structure i) *N. furzeri* residues 38 (Tryptophan) and 39 (Leucine) show a strand structure. j) *C. porcellus* residues 38 (Isoleucine) and 39 (Asparagine) show a coil structure k) *B. mysticetus* residues 38 (Isoleucine) and 39 (Asparagine) show a coil structure. l) *H. glaber* residues 38 (Isoleucine) and 39 (Asparagine) show a coil structure—m) *L. borealis* residues 38 (Isoleucine) and 39 (Asparagine) show a coil structure.

https://doi.org/10.1371/journal.pone.0245822.g007

GTG as an alternative start codon

The biosynthesis of proteins encoded by their respective mRNA requires an initiation codon for their translation. ATG is the usual initiation codon but GTG has been reported as initiation codon in some lower organisms, the frequency of annotated alternate codon in higher organisms is found to be less than 1% [53]. An *in-vitro* study of GTG-mediated translation of enhanced green fluorescent protein suggested that initiation with GTG codon regulates expression of lower levels of the protein and a similar observation was made for the protein endopin 2B-2 [54]. It has also been observed in a few human diseases that a mutation of the ATG initiation codon to a GTG are associated with diseases such as beta-thalassemia and Norrie disease, where GTG mutation leads to inactivation of the gene [55,56]. Another example is

a disruption caused by GTG as the initiation codon in the gene CYP2C19, which resulted in poor metabolism of a drug, mephenytoin, when compared to the gene with an ATG initiation codon [57]. Numerous studies on bacteria and lower organisms show GTG as a start codon, where the non-methionine codon is initially coded for, however, when they act as a start codon the initial amino acid is substituted with a methionine [54,58]. There is only a single report of a vertebrate species, rat, where GTG is the start codon in mtDNA [59]. An ATG to GTG exchange in human gene *FRMD7* (FERM Domain Containing 7) has been found as a first base transversion of the start codon that accounts for a mutation, causing morphological changes in the optic nerve head [60]. The level of corresponding protein expression has been shown to be lower when initiated using an alternative codon such as GTG rather than ATG [54,61]. GTG was observed as a start codon for ATP8 in fish *Philomycus bilineatus*, which adds onto the show GTG as an acceptable start codon [62].

A few but increasing number of mammalian genes have been found to give rise to an alternative initiation codon in regulatory proteins such as transcription factors, growth factors and a few kinases in humans and rats. The finding in all these studies have shown a similar trend of a lower level of protein production when compared to an ATG start codon [63–65]. It has been shown that the fish inhabiting colder climates had undergone stronger selective constraints in order to avoid deleterious mutations [66,67]. MtDNA coding genes such as ATP6, could be placed under selective pressures by low environmental temperatures. A larger ratio of substitution for different sites could indicate proteins undergoing adaptations [68]. A decrease in ATP6 activity previously reported, shows incomplete ATPase complexes that are capable of ATP hydrolysis but not ATP synthesis. ATPase complexes completely lacking subunit a, were capable of maintaining structural interactions between F1 and F0 parts of the enzyme but the interactions were found to be weaker [69].

The GTG initiation for protein ATP6 in these fish species could suggest a common parallel evolution of the translation machinery. The favouring of GTG as a start codon could also mean a higher stability of the protein as GC base pair has higher thermal stability when compared to the AT base pair which is attributed from stronger stacking interaction between GC bases and a presence of triple bond compared to that of AT double bond [70].

Overlap of ATP8 and ATP6 genes

Protein coding genes ATP8 and ATP6 are located adjacent to each other and are overlapping on the same strand in humans and other vertebrates, with an overlap of 44 nt (NCBI: NC_012920.1) observed in the humans for the gene. It has been previously reported that ATP8-ATP6 overlap is generally of 10 nt in the fish genome [71]. Species *T. bernacchii*, *E. maclovinus*, *N. coriiceps*, *C. rastrospinosus* and *C. aceratus* show an overlap of 22 nts and *C. gunnari* has a 10 nt overlap, as reported previously in other fish genomes mentioned above. The overlap for the four out of six species of suborder Notothenioidei start from the third nucleotide for codon AAG coding for amino acid lysine whereas for the other two species, *T. bernacchii* and *C. gunnari*, it is encoded by AAA. It is hypothesised that overlaps are a mechanism for reduction of genome size and regulation of gene expression [72,73], which is seen in the species *C. gunnari* and the eight vertebrate outgroups.

The gene coding ATP8 ends with the stop codon TAG for all species of suborder Notothenioidei and TAA for the other vertebrate species, a single exception to this was *H. glaber* that ends with a TAG stop codon. It has been previously hypothesised that TAG is a sub-optimal stop codon which is less likely to be selected. A study showed that the protein encoding genes that end with TAA stop codons are, on average more abundant than those with genes ending with TGA or TAG and further shows that a switch of stop codon TAG from TGA might pass

through the mutational path of TAA stop codon which could be subject to positive selection in several groups [74].

Protein alignment and structural changes in ATP6

The four Antarctic fish species, *N. coriiceps*, *T. bernacchii*, *C. rastrospinosus*, *C. aceratus* and the sub-Antarctic *E. maclovinus* have four amino acids at the N-terminal of ATP6 and a total of 231 residues. As previously mentioned, the only exception to this is the species *C. gunnari* with 227 residues similar to *N. furzeri* and *D. rerio*. N-terminal addition of amino acids can influence the properties of the protein, as it can change the molecular weight of the protein, the charge, hydrophobicity, and this has been seen in the yeast meta-caspase prion protein Mca1 [75].

Amino acid position 35 is populated with predominantly hydrophilic residues, apart for the two species *C. gunnari* and *N. furzeri*, where respectively, alanine and leucine are found. All the other Antarctic fish species and *E. maclovinus* have a serine at this position. When we look at the codon alignment of the ATP6 gene, serine is encoded by codon TCT at position 39 for all the species except *T. bernacchii* (encoded by TCC) and the alanine for the species *C. gunnari* is encoded by GCT. Serine is the only amino acid that is encoded by two codon sets. A common example of a missense mutation is where the single base pair can alter the corresponding codon to a different amino acid. This base substitution even though affecting a single codon can still have a significant effect on the protein production. It has been recently discovered that serine at a highly conserved position is more often encoded in TCN fashion and will tend to substitute non-synonymously to proline and alanine, which shows that codon for which serine is coded indicate different types of selection for amino acid and its acceptable substitutions [76]. This may be suggested as a reason for the presence of hydrophobic alanine observed in *C. gunnari* at position 35.

The weblogo for protein ATP6 shows overall conservation across the sequence for the vertebrates where the C-terminal of the protein is more conserved than the N-terminal. High conservation is observed from residues 85–112 and 165–185, as also seen in our MSA for the fourteen species. The position 35 is seen to be conserved preferably for threonine or serine as in the weblogo (Fig 5).

The hydrophobicity plot, average flexibility, mutability, and coil prediction across the sequences highlights differences in the physiochemical properties across the sequence of protein ATP6 in the species *C. gunnari*.

The secondary structure of a protein is the way in which protein molecules are coiled and folded in a certain way according to the primary sequence. Beta-strands give stability to the structure of a protein, its intrinsic flexibility can sometimes return it to coil configuration in order for the protein to perform other functions. Structural changes were observed at position 38–39 for species *C. gunnari*, *N. furzeri*, *D. rerio* and *A. carolinesis*, where strand-strand structure was predicted at that position. All other species are predicted to have coil structures at those positions (Figs 6 & 7). Species *T. bernacchii* and *E. maclovinus* are predicted to have strand structures at positions 42–43.

Protein structure, dynamics and function are all interlinked and it is vital to understand the structure of a protein in relation to function to comprehend molecular processes [77]. We have used the unique biology of the icefish to gain a better understanding of the variability of ATP6 and ATP8 sequence and structure which has importance for mitochondrial function.

Conclusions

In this study we suggest that mitochondrial encoded protein ATP6 has an alternative start codon GTG in the species of suborder Notothenioidei except for the hb-less *C. gunnari*. This

could be related to a higher thermal stability with altered expression of this protein. Another striking difference observed only in *C. gunnari* for the protein, was a substitution of hydrophilic amino acid serine (TCT) to hydrophobic amino acid alanine (GCT). This could be a base substitution for thymine to guanine at N1 position of the codon that might have a structural impact on the protein. Our predictions based on the available curated sequence data now point to the need for targeted experimentation to understand the full physiological impact of our findings.

Supporting information

S1 Fig. A pictographic representation of the relatedness of 'ATP6 protein' sequence for notothenioids to other species using NJ-phylogenetic tree (Clustal omega[35]) analysed by taking alignment data that shows similarity in the amino acid composition of the protein for different vertebrate species (pictures source: Wikipedia.com, human skull: Bonesclones.com, naked mole rat: Wikiwand.com, *E. maclovinus*: Scanndposters.com).
(DOCX)

S2 Fig. Protein structure evaluations of ATP6 for fish species C. aceratus, C. gunnari, C. rastrospinosus, E. maclovinus, N. corriceps, T. bernacchii, D. rerio and N. furzeri (A-I) using SAVES v6.0 (https://saves.mbi.ucla.edu/), using ERRAT[41], PROCHECK[42,43] and ProSA-web[44].
(DOCX)

Author Contributions

Conceptualization: Gunjan Katyal, Magnus Lucassen, Chiara Papetti, Lisa Chakrabarti.

Data curation: Gunjan Katyal, Brad Ebanks.

Formal analysis: Gunjan Katyal.

Funding acquisition: Lisa Chakrabarti.

Investigation: Gunjan Katyal.

Methodology: Gunjan Katyal, Lisa Chakrabarti.

Resources: Magnus Lucassen, Chiara Papetti.

Supervision: Lisa Chakrabarti.

Writing – original draft: Gunjan Katyal, Brad Ebanks, Lisa Chakrabarti.

Writing – review & editing: Gunjan Katyal, Brad Ebanks, Magnus Lucassen, Chiara Papetti, Lisa Chakrabarti.

References

1. Duman JG. Animal ice-binding (antifreeze) proteins and glycolipids: An overview with emphasis on physiological function. J Exp Biol. 2015; 218: 1846–1855. https://doi.org/10.1242/jeb.116905 PMID: 26085662
2. Devries AL. Role of glycopeptides and peptides in inhibition of crystallization of water in polar fishes. Philos Trans R Soc London B, Biol Sci. 1984; 304: 575–588. https://doi.org/10.1098/rstb.1984.0048
3. Chen L, Devries AL, Cheng CHC. Evolution of antifreeze glycoprotein gene from a trypsinogen gene in Antarctic notothenioid fish. Proc Natl Acad Sci U S A. 1997; 94: 3811–3816. https://doi.org/10.1073/pnas.94.8.3811 PMID: 9108060

4. Harding MM, Anderberg PI, Haymet ADJ. "Antifreeze" glycoproteins from polar fish. European Journal of Biochemistry. 2003. pp. 1381–1392. https://doi.org/10.1046/j.1432-1033.2003.03488.x PMID: 12653993
5. Ruud Johan T. Vertebrates without Erythrocytes and Blood Pigment. Nature. 1954; 173: 848–850. https://doi.org/10.1038/173848a0 PMID: 13165664
6. Hamoir G. Biochemical adaptation of the muscles of the channichthyidae to their lack in hemoglobin and myoglobin. Comp Biochem Physiol—Part B Biochem. 1988; 90: 557–559. https://doi.org/10.1016/0305-0491(88)90295-7
7. Sidell BD, O'Brien KM. When bad things happen to good fish: The loss of hemoglobin and myoglobin expression in Antarctic icefishes. J Exp Biol. 2006; 209: 1791–1802. https://doi.org/10.1242/jeb.02091 PMID: 16651546
8. Sidell BD, Vayda ME, Small DJ, Moylan TJ, Londraville RL, Yuan ML, et al. Variable expression of myoglobin among the hemoglobinless Antarctic icefishes. Proc Natl Acad Sci U S A. 1997; 94: 3420–3424. https://doi.org/10.1073/pnas.94.7.3420 PMID: 9096409
9. Small DJ, Moylan T, Vayda ME, Sidell BD. The myoglobin gene of the Antarctic icefish, Chaenocephalus aceratus, contains a duplicated TATAAAA sequence that interferes with transcription. J Exp Biol. 2003; 206: 131–139. https://doi.org/10.1242/jeb.00067 PMID: 12456703
10. O'Brien KM, Xue H, Sidell BD. Quantification of diffusion distance within the spongy myocardium of hearts from antarctic fishes. Respir Physiol. 2000; 122: 71–80. https://doi.org/10.1016/s0034-5687(00)00139-0 PMID: 10936602
11. O'Brien KM, Sidell BD. The interplay among cardiac ultrastructure, metabolism and the expression of oxygen-binding proteins in Antarctic fishes. J Exp Biol. 2000; 203: 1287–1297. PMID: 10729278
12. Small DJ, Vayda ME, Sidell BD. A novel vertebrate myoglobin gene containing three A+T-rich introns is conserved among antarctic teleost species which differ in myoglobin expression. J Mol Evol. 1998; 47: 156–166. https://doi.org/10.1007/pl00006372 PMID: 9694664
13. Archer SD, Johnston IA. Density of Cristae and Distribution of Mitochondria in the Slow Muscle Fibers of Antarctic Fish. Physiol Zool. 1991; 64: 242–258. https://doi.org/10.1086/physzool.64.1.30158522
14. O'Brien KM. Mitochondrial biogenesis in cold-bodied fishes. J Exp Biol. 2011; 214: 275–285. https://doi.org/10.1242/jeb.046854 PMID: 21177947
15. Biederman AM, Kuhn DE, O'Brien KM, Crockett EL. Mitochondrial membranes in cardiac muscle from Antarctic notothenioid fishes vary in phospholipid composition and membrane fluidity. Comp Biochem Physiol Part—B Biochem Mol Biol. 2019; 235: 46–53. https://doi.org/10.1016/j.cbpb.2019.05.011 PMID: 31176865
16. Dimroth P. Operation of the F0 motor of the ATP synthase. Biochimica et Biophysica Acta—Bioenergetics. 2000. pp. 374–386. https://doi.org/10.1016/S0005-2728(00)00088-8
17. Angevine CM, Fillingame RH. Aqueous access channels in subunit a of rotary ATP synthase. J Biol Chem. 2003; 278: 6066–6074. https://doi.org/10.1074/jbc.M210199200 PMID: 12473663
18. Aksimentiev A, Balabin IA, Fillingame RH, Schulten K. Insights into the Molecular Mechanism of Rotation in the F o Sector of ATP Synthase. Biophys J. 2004; 86: 1332–1344. https://doi.org/10.1016/S0006-3495(04)74205-8 PMID: 14990464
19. Noji H, Yasuda R, Yoshida M, Kinosita K. Direct observation of the rotation of F1-ATPase. Nature. 1997; 386: 299–302. https://doi.org/10.1038/386299a0 PMID: 9069291
20. Ma J, Flynn TC, Cui Q, Leslie AGW, Walker JE, Karplus M. A dynamic analysis of the rotation mechanism for conformational change in F1-ATPase. Structure. 2002; 10: 921–931. https://doi.org/10.1016/s0969-2126(02)00789-x PMID: 12121647
21. Artika IM. Current understanding of structure, function and biogenesis of yeast mitochondrial ATP synthase. J Bioenerg Biomembr. 2019; 51: 315–328. https://doi.org/10.1007/s10863-019-09809-4 PMID: 31418131
22. Mitchell P. Coupling of phosphorylation to electron and hydrogen transfer by a chemi-osmotic type of mechanism. Nature. 1961; 191: 144–148. https://doi.org/10.1038/191144a0 PMID: 13771349
23. Abrahams JP, Leslie AGW, Lutter R, Walker JE. Structure at 2.8 Å resolution of F1-ATPase from bovine heart mitochondria. Nature. 1994; 370: 621–628. https://doi.org/10.1038/370621a0 PMID: 8065448
24. Klusch N, Murphy BJ, Mills DJ, Yildiz Ö, Kühlbrandt W. Structural basis of proton translocation and force generation in mitochondrial ATP synthase. Elife. 2017; 6: 1–16. https://doi.org/10.7554/eLife.33274 PMID: 29210357
25. Kubo S, Niina T, Takada S. Molecular dynamics simulation of proton-transfer coupled rotations in ATP synthase FO motor. Sci Rep. 2020; 10: 1–16.

26. Fearnley IM, Walker JE. Two overlapping genes in bovine mitochondrial DNA encode membrane components of ATP synthase. EMBO J. 1986; 5: 2003–2008. https://doi.org/10.1002/j.1460-2075.1986.tb04456.x PMID: 2875870

27. Colina-Tenorio L, Dautant A, Miranda-Astudillo H, Giraud MF, González-Halphen D. The peripheral stalk of rotary ATPases. Front Physiol. 2018; 9: 1–19.

28. Devenish RJ, Papakonstantinou T, Galanis M, Law RH, Linnane AW, Nagley P. Structure/function analysis of yeast mitochondrial ATP synthase subunit 8. Ann N Y Acad Sci. 1992; 671: 403–14. https://doi.org/10.1111/j.1749-6632.1992.tb43814.x PMID: 1288337

29. Stephens AN, Khan MA, Roucou X, Nagley P, Devenish RJ. The molecular neighborhood of subunit 8 of yeast mitochondrial F1F0-ATP synthase probed by cysteine scanning mutagenesis and chemical modification. J Biol Chem. 2003; 278: 17867–17875. https://doi.org/10.1074/jbc.M300967200 PMID: 12626501

30. Lee J, Ding SJ, Walpole TB, Holding AN, Montgomery MG, Fearnley IM, et al. Organization of subunits in the membrane domain of the bovine F-ATPase revealed by covalent cross-linking. J Biol Chem. 2015; 290: 13308–13320. https://doi.org/10.1074/jbc.M115.645283 PMID: 25851905

31. Grandier-Vazeille X, Ouhabi R, Guérin M. Antibodies against subunits of F0 sector of ATP synthase from Saccharomyces cerevisiae Stimulation of ATP synthase by subunit-8-reactive antibodies and inhibition by subunit-9-reactive antibodies. Eur J Biochem. 1994; 223: 521–528. https://doi.org/10.1111/j.1432-1033.1994.tb19021.x PMID: 8055922

32. Allegretti M, Klusch N, Mills DJ, Vonck J, Kühlbrandt W, Davies KM. Horizontal membrane-intrinsic α-helices in the stator a-subunit of an F-type ATP synthase. Nature. 2015; 521: 237–240. https://doi.org/10.1038/nature14185 PMID: 25707805

33. Gu J, Zhang L, Zong S, Guo R, Liu T, Yi J, et al. Cryo-EM structure of the mammalian ATP synthase tetramer bound with inhibitory protein IF1. 2019; 1075: 1068–1075.

34. Mueller IA, Grim JM, Beers JM, Crockett EL, O'Brien KM. Inter-relationship between mitochondrial function and susceptibility to oxidative stress in red-And white-blooded Antarctic notothenioid fishes. J Exp Biol. 2011; 214: 3732–3741. https://doi.org/10.1242/jeb.062042 PMID: 22031737

35. O'Leary NA, Wright MW, Brister JR, Ciufo S, Haddad D, McVeigh R, et al. Reference sequence (RefSeq) database at NCBI: Current status, taxonomic expansion, and functional annotation. Nucleic Acids Res. 2016; 44: D733–D745. https://doi.org/10.1093/nar/gkv1189 PMID: 26553804

36. Madeira F, Park YM, Lee J, Buso N, Gur T, Madhusoodanan N, et al. The EMBL-EBI search and sequence analysis tools APIs in 2019. Nucleic Acids Res. 2019; 47: W636–W641. https://doi.org/10.1093/nar/gkz268 PMID: 30976793

37. Rozewicki J, Li S, Amada KM, Standley DM, Katoh K. MAFFT-DASH: Integrated protein sequence and structural alignment. Nucleic Acids Res. 2019; 47: W5–W10. https://doi.org/10.1093/nar/gkz342 PMID: 31062021

38. Waterhouse AM, Procter JB, Martin DMA, Clamp M, Barton GJ. Jalview Version 2-A multiple sequence alignment editor and analysis workbench. Bioinformatics. 2009; 25: 1189–1191. https://doi.org/10.1093/bioinformatics/btp033 PMID: 19151095

39. Gasteiger E, Gattiker A, Hoogland C, Ivanyi I, Appel RD, Bairoch A. ExPASy: The proteomics server for in-depth protein knowledge and analysis. Nucleic Acids Res. 2003; 31: 3784–3788. https://doi.org/10.1093/nar/gkg563 PMID: 12824418

40. Gasteiger E, Hoogland C, Gattiker A, Duvaud S, Wilkins MR, Appel RD, et al. The Proteomics Protocols Handbook. Proteomics Protoc Handb. 2005; 571–608. https://doi.org/10.1385/1592598900

41. Yang J, Zhang Y. I-TASSER server: New development for protein structure and function predictions. Nucleic Acids Res. 2015; 43: W174–W181. https://doi.org/10.1093/nar/gkv342 PMID: 25883148

42. Colovos C, Yeates TO. Verification of protein structures: Patterns of nonbonded atomic interactions. Protein Sci. 1993; 2: 1511–1519. https://doi.org/10.1002/pro.5560020916 PMID: 8401235

43. Laskowski RA, MacArthur MW, Moss DS, Thornton JM. PROCHECK: a program to check the stereochemical quality of protein structures. J Appl Crystallogr. 1993; 26: 283–291. https://doi.org/10.1107/s0021889892009944

44. Sippl MJ. Recognition of errors in three-dimensional structures of proteins. Proteins Struct Funct Bioinforma. 1993; 17: 355–362. https://doi.org/10.1002/prot.340170404 PMID: 8108378

45. Wiederstein M, Sippl MJ. ProSA-web: Interactive web service for the recognition of errors in three-dimensional structures of proteins. Nucleic Acids Res. 2007; 35: 407–410. https://doi.org/10.1093/nar/gkm290 PMID: 17517781

46. Guo J, Yang H, Zhang C, Xue H, Xia Y, Zhang JE. Complete mitochondrial genome of the apple snail Pomacea diffusa (Gastropoda, Ampullariidae) with phylogenetic consideration. Mitochondrial DNA Part B Resour. 2017; 2: 865–867. https://doi.org/10.1080/23802359.2017.1407683 PMID: 33474014

47. Lin GM, Xiang P, Sampurna BP, Der Hsiao C. Genome skimming yields the complete mitogenome of Chromodoris annae (Mollusca: Chromodorididae). Mitochondrial DNA Part B Resour. 2017; 2: 609–610. https://doi.org/10.1080/23802359.2017.1372715 PMID: 33473918

48. Yang T, Xu G, Gu B, Shi Y, Mzuka HL, Shen H. The complete mitochondrial genome sequences of the Philomycus bilineatus (Stylommatophora: Philomycidae) and phylogenetic analysis. Genes (Basel). 2019; 10: 1–13. https://doi.org/10.3390/genes10030198 PMID: 30841657

49. Fox TD. Five TGA "stop" codons occur within the translated sequence of the yeast mitochondrial gene for cytochrome c oxidase subunit II. Proc Natl Acad Sci U S A. 1979; 76: 6534–6538. https://doi.org/10.1073/pnas.76.12.6534 PMID: 230513

50. Verny C, Guegen N, Desquiret V, Chevrollier A, Prundean A, Dubas F, et al. Hereditary spastic paraplegia-like disorder due to a mitochondrial ATP6 gene point mutation. Mitochondrion. 2011; 11: 70–75. https://doi.org/10.1016/j.mito.2010.07.006 PMID: 20656066

51. Pfeffer G, Frcpc CM, Blakely EL, Alston CL, Boggild M, Horvath R, et al. Europe PMC Funders Group Adult-onset spinocerebellar ataxia syndromes due to MTATP6 mutations. 2014; 83: 883–886.

52. Arnesen T, Van Damme P, Polevoda B, Helsens K, Evjenth R, Colaert N, et al. Proteomics analyses reveal the evolutionary conservation and divergence of N-terminal acetyltransferases from yeast and humans. Proc Natl Acad Sci U S A. 2009; 106: 8157–8162. https://doi.org/10.1073/pnas.0901931106 PMID: 19420222

53. Donath A, Jühling F, Al-Arab M, Bernhart SH, Reinhardt F, Stadler PF, et al. Improved annotation of protein-coding genes boundaries in metazoan mitochondrial genomes. Nucleic Acids Res. 2019; 47: 10543–10552. https://doi.org/10.1093/nar/gkz833 PMID: 31584075

54. Hwang SR, Garza CZ, Wegrzyn JL, Hook VYH. Demonstration of GTG as an alternative initiation codon for the serpin endopin 2B-2. Biochem Biophys Res Commun. 2005; 327: 837–844. https://doi.org/10.1016/j.bbrc.2004.12.053 PMID: 15649421

55. Villalobos-ar AR, Casas-casta M, Guti E, Perea FJ, Thein SL, Ibarra B. Globin gene haplotypes in Mexican mestizos. 1997; 498–500. PMID: 9262381

56. Isashiki Y, Ohba N, Yanagita T, Hokita N, Doi N, Nakagawa M, et al. Novel mutation at the initiation codon in the Norrie disease gene in two Japanese families. Hum Genet. 1995; 95: 105–108. https://doi.org/10.1007/BF00225085 PMID: 7814011

57. Ferguson RJ, De Morais SMF, Benhamou S, Bouchardy C, Blaisdell J, Ibeanu G, et al. A new genetic defect in human CYP2C19: Mutation of the initiation codon is responsible for poor metabolism of S-mephenytoin. J Pharmacol Exp Ther. 1998; 284: 356–361. PMID: 9435198

58. Kitamoto T, Wang W, Salvaterra PM. Structure and organization of the Drosophila cholinergic locus. J Biol Chem. 1998; 273: 2706–2713. https://doi.org/10.1074/jbc.273.5.2706 PMID: 9446576

59. Gadaleta G, Pepe G, De Candia G, Quagliariellol C, Sbisa E, Saccone C, et al. Nucleic Acids Research Nucleotide sequence of rat nitochondrial NADH dehydrogenase subunit 1. GTG, a new initiator codon in vertebrate mitochondrial genome We have determined the nucleotide sequence of cloned fragments that contain with ATT. However th. 1988;22: 6233.

60. Choi JH, Shin JH, Seo JH, Jung JH, Choi KD. A start codon mutation of the FRMD7 gene in two Korean families with idiopathic infantile nystagmus. Sci Rep. 2015; 5: 5–10. https://doi.org/10.1038/srep13003 PMID: 26268155

61. Panicker IS, Browning GF, Markham PF. The effect of an alternate start codon on heterologous expression of a PhoA fusion protein in mycoplasma gallisepticum. PLoS One. 2015; 10: 1–10. https://doi.org/10.1371/journal.pone.0127911 PMID: 26010086

62. Yang T, Xu G, Gu B, Shi Y, Mzuka HL, Shen H. The complete mitochondrial genome sequences of the Philomycus bilineatus (Stylommatophora: Philomycidae) and phylogenetic analysis. Genes (Basel). 2019; 10: 1–14. https://doi.org/10.3390/genes10030198 PMID: 30841657

63. Short JD, Pfarr CM. Translational regulation of the JunD messenger RNA. J Biol Chem. 2002; 277: 32697–32705. https://doi.org/10.1074/jbc.M204553200 PMID: 12105216

64. Claus P, Döring F, Gringel S, Müller-Ostermeyer F, Fuhlrott J, Kraft T, et al. Differential intranuclear localization of fibroblast growth factor-2 isoforms and specific interaction with the survival of motoneuron protein. J Biol Chem. 2003; 278: 479–485. https://doi.org/10.1074/jbc.M206056200 PMID: 12397076

65. Rhee S, Yang SJ, Lee SJ, Park D. βPix-bL, a novel isoform of βPix, is generated by alternative translation. Biochem Biophys Res Commun. 2004; 318: 415–421. https://doi.org/10.1016/j.bbrc.2004.04.039 PMID: 15120616

66. Silva G, Lima FP, Martel P, Castilho R. Thermal adaptation and clinal mitochondrial DNA variation of European anchovy. Proc R Soc B Biol Sci. 2014; 281. https://doi.org/10.1098/rspb.2014.1093 PMID: 25143035

67. Sun YB, Shen YY, Irwin DM, Zhang YP. Evaluating the roles of energetic functional constraints on teleost mitochondrial-encoded protein evolution. Mol Biol Evol. 2011; 28: 39–44. https://doi.org/10.1093/molbev/msq256 PMID: 20924083

68. Deng Z, Wang X, Xu S, Gao T, Han Z. Population genetic structure and selective pressure on the mitochondrial ATP6 gene of the Japanese sand lance Ammodytes personatus Girard. J Mar Biol Assoc United Kingdom. 2019; 99: 1409–1416. https://doi.org/10.1017/S0025315419000225

69. Ješina P, Tesařová M, Fornůsková D, Vojtíšková A, Pecina P, Kaplanová V, et al. Diminished synthesis of subunit a (ATP6) and altered function of ATP synthase and cytochrome c oxidase due to the mtDNA 2 bp microdeletion of TA at positions 9205 and 9206. Biochem J. 2004; 383: 561–571. https://doi.org/10.1042/BJ20040407 PMID: 15265003

70. Yakovchuk P, Protozanova E, Frank-Kamenetskii MD. Base-stacking and base-pairing contributions into thermal stability of the DNA double helix. Nucleic Acids Res. 2006; 34: 564–574. https://doi.org/10.1093/nar/gkj454 PMID: 16449200

71. Satoh TP, Miya M, Mabuchi K, Nishida M. Structure and variation of the mitochondrial genome of fishes. BMC Genomics. 2016; 17. https://doi.org/10.1186/s12864-016-3054-y PMID: 27604148

72. Krakauer DC. Evolutionary Principles of Genomic Compression. Comments Theor Biol. 2002; 7: 215–236.

73. Johnson ZI, Chisholm SW. Properties of overlapping genes are conserved across microbial genomes. Genome Res. 2004; 14: 2268–2272. https://doi.org/10.1101/gr.2433104 PMID: 15520290

74. Belinky F, Babenko VN, Rogozin IB, Koonin EV. Purifying and positive selection in the evolution of stop codons. Sci Rep. 2018; 8: 1–11.

75. Erhardt M, Wegrzyn RD, Deuerling E. Extra N-terminal residues have a profound effect on the aggregation properties of the potential yeast prion protein Mca1. PLoS One. 2010; 5. https://doi.org/10.1371/journal.pone.0009929 PMID: 20360952

76. Schwartz GW, Shauli T, Linial M, Hershberg U. Serine substitutions are linked to codon usage and differ for variable and conserved protein regions. Sci Rep. 2019; 9: 1–9.

77. Garcia-Manero Guillermo, Yang Hui, Kuang Shao-Qing, O'Brien Susan, Thomas Deborah and K H. 基因的改变NIH Public Access. Bone. 2005; 23: 1–7.

BEC BIOENERGETICS COMMUNICATIONS Bioenerg Commun 2021.2 doi:10.26124/bec:2021-0002
Open Access

Review

Cite
Krako Jakovljevic N, Ebanks B, Katyal G, Chakrabarti L, Markovic I, Moisoi N (2021) Mitochondrial homeostasis in cellular models of Parkinson's disease. Bioenerg Commun 2021.2. doi:10.26124/bec:2021-0002

Author contributions
Data collection and evaluation was performed by NKJ, BE, NM. GK performed protein network analysis. All authors wrote the manuscript. IM and NM designed the framework of the review.

Conflicts of interest
The authors declare they have no conflict of interest.

Academic editor
Pablo Garcia-Roves, University of Barcelona and Bellvitge Biomedical Research Institute, ES

Copy editors
Erich Gnaiger, Luiza HD Cardoso

Received 2021-02-19
Reviewed 2021-04-05
Resubmitted 2021-06-25
Reviewed 2021-07-20
Resubmitted 2021-09-01
Accepted 2021-09-27

Published 2021-10-06

Editorial and peer review record
doi:10.26124/bec:2021-0002

Preprint
MitoFit Preprints 2021.4
doi:10.26124/mitofit:2021-0004

Supplementary files
doi:10.26124/bec:2021-0002

Mitochondrial homeostasis in cellular models of Parkinson's disease

Nina Krako Jakovljevic[1], Brad Ebanks[2], Gunjan Katyal[2], Lisa Chakrabarti[2,3], Ivanka Markovic[4*], Nicoleta Moisoi[5*]

1 Clinic for Endocrinology, Diabetes and Metabolic Diseases, University Clinical Center of Serbia, Faculty of Medicine, University of Belgrade Dr Subotica 13, 11000 Belgrade, Serbia
2 School of Veterinary Medicine and Science, University of Nottingham, Sutton Bonington, LE12 5RD, UK.
3 MRC Versus Arthritis Centre for Musculoskeletal Ageing Research, UK
4 Institute for Medical and Clinical Biochemistry, Faculty of Medicine, University of Belgrade, Pasterova 2, 11000 Belgrade, Serbia
5 Leicester School of Pharmacy, Leicester Institute for Pharmaceutical Innovation, De Montfort University, The Gateway, Leicester LE1 9BH

* Corresponding authors: nicoleta.moisoi@dmu.ac.uk, ivanka.markovic@med.bg.ac.rs

Abstract

Mitochondrial function is an important factor in maintaining cellular homeostasis and its dysregulation has become a hallmark for multiple disease conditions. This review aims to synthesise the current knowledge by analysing changes of mitochondrial physiology parameters in Parkinson's disease (PD) and to evaluate the contribution of cellular models of PD in the field. We present a platform for further elucidation of mitochondrial function parameters that may potentiate disease progression.

Keywords - mitochondrial homeostasis, mitochondrial respiration, Parkinson's disease, cellular models of Parkinson's, qualitative analysis

1. Mitochondria and Parkinson's disease

Mitochondria comprise a dynamic organellar network with a central position in maintaining eukaryotic homeostasis. Besides their role in cellular bioenergetics, namely adenosine triphosphate (ATP) synthesis, these organelles support essential metabolic processes, regulation of calcium and reactive oxygen species (ROS) homeostasis as well as a multitude of signalling cascades. The mitochondrial compartments host functional molecular groups which coordinate protein import and sorting, transport of metabolites, mitochondrial DNA (mtDNA) replication and expression, oxidative phosphorylation (OXPHOS) respiratory system, metabolic enzymes protein and organelle quality control mechanisms as well as fusion and fission regulators. Dysfunction in these mitochondrial components leads to impaired homeostasis and has been linked to diseases, of which we shall focus here on Parkinson's disease.

Parkinson's disease (PD) is a progressive neurodegenerative disease characterised primarily by loss of dopaminergic neurons in the nigrostriatal pathway, presenting motor and non-motor clinical phenotypes. It is the most prevalent cause of parkinsonism, a broader clinical syndrome with motor features that include: hypokinesia, bradykinesia, muscle rigidity, joint stiffness, resting tremor, shuffling gait, expressionless face and micrography. Non-motor features comprise constipation, anxiety and depression, REM-sleep behaviour, and olfactory deficits (Poewe et al 2017). The neuropathological hallmark of PD are intracellular protein inclusions called Lewy bodies, consisting predominantly of α-Synuclein. Ageing, environment, and genetic susceptibility are implicated in PD and cellular defects leading to dopaminergic dysfunction are connected with defects in proteostasis, mitochondrial function, vesicle trafficking and lysosomal activity (Figure 1). The distinctiveness of these interactions gives rise to a spectrum of PD neuronal phenotypes that can be unique to individual patients, making development of suitable disease models challenging.

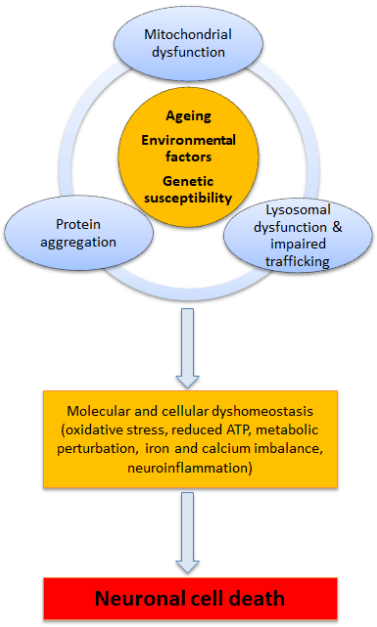

Figure 1. Key cellular defects in PD.

1.1. Respiratory physiology dysfunction as a key feature of PD

The investigation of mitochondria in PD began in early eighties when independent reports revealed that 1-methyl-4-phenyl-1,2,3,6-tetrahydropyridine (MPTP), was the likely cause of permanent parkinsonism in several patients. The parkinsonism phenotype was associated with degeneration of nigrostriatal dopaminergic neurons (Burns et al 1983; Langston et al 1983) and appearance of Lewy bodies in the Substantia Nigra (SN) (Davis et al 1979). It was found that the MPTP metabolite 1-methyl-4-phenylpyridinium (MPP+) can be taken up by dopaminergic transporters (DAT), and inhibit Complex I (CI) of the mitochondrial electron transfer system (ETS) resulting in nigrostriatal degeneration (Ramsay, Singer 1986; Ramsay et al 1986; Salach et al 1984; Vyas et al 1986). Subsequently, it was shown that CI activity was reduced by 20–30% in the SN of patients with sporadic PD (Schapira 2007; Schapira et al 1990), with reports of enzyme complex dysfunction that may affect other tissues as well (Bindoff et al 1989; Mortiboys et al 2008; Müftüoglu et al 2004; Parker et al 1989). In addition, mitochondria from post-mortem tissue, show greater age-dependent accumulation of mtDNA deletions and somatic mosaicism, compared to control subjects (Coxhead et al 2015; Dölle et al 2016; Giannoccaro et al 2017; Grünewald et al 2016).

1.2. Dissecting mitochondrial dysfunction in PD

Parkinsonism is a consistent and predominant feature in 23 monogenic disorders (Klein et al 2018; Marras et al 2016). Many of the identified genes encode proteins that have strong links to mitochondrial function as summarised in Table 1.

Table 1. Key genes linked to mitochondrial dysfunction in PD

Gene	Key biomolecular functions	Key effects of PD mutations on mitochondrial function and cellular homeostasis	References
PINK1 Recessive	**PTEN induced serine/threonine protein kinase 1** - Phosphorylates mitochondrial proteins; - Mediates activation and translocation of Parkin during mitophagy	- Reduced activity of Complexes CI, CII, and CIV - Impaired respiration in the striatum - Decreased respiration and membrane potential - Decreased ATP level and increased ROS - Impaired mitophagy - Impaired synaptic transmission	Amo et al 2011; Clark et al 2006; Gautier et al 2008; Ge et al 2020; Liu et al 2020; Liu et al 2011; Matsumine et al 1997; Morais et al 2009; Park et al 2006; Temelie et al 2018; Valente et al 2001; Yuan et al 2010

PRKN (Parkin) Recessive	**E3 ubiquitin protein ligase Parkin** - Ubiquitinates multiple substrates for proteasome-dependent protein degradation; - Regulates mitophagy by ubiquitination of mitochondrial proteins	- Reduced activity of Complexes CI and CII - Impaired mitophagy	Damiano et al 2014; Lehmann et al 2016
DJ-1 Recessive	**Parkinson's disease protein 7** Multifunctional protein protecting against oxidative stress and regulating mitochondrial homeostasis - Protein and nucleotide glycase; - Cysteine protease -Redox regulated chaperone - Parkin S-nitrosylation	- Reduced ATP synthesis and respiration - Increased ROS, reduced membrane potential, higher transition-pore opening (cell death) - Respiratory Complex stability, mitochondrial quality control, maintenance of cell redox balance; - Accelerates accumulation and aggregation of α-Synuclein in mice	Bonifati et al 2003; Giaime et al 2012; Klein, Lohmann-Hedrich 2007; Ozawa et al 2020; Xu et al 2017
LRRK2 Dominant	**Leucine rich repeat serine/threonine protein kinase 2** - Serine threonine protein kinase which phosphorylates a broad range of proteins. - GTPase activity - Scaffolding protein	- Decreased mitochondrial membrane potential and cellular ATP level - Modulates mitochondrial dynamics - Modulates cellular trafficking	Abeliovich, Gitler 2016; Mortiboys et al 2010; Xinglong Wang et al 2012
SNCA (α-Synuclein) Dominant	**Alpha-Synuclein** - Cellular trafficking - Roles in synaptic vesicle formation, docking and neurotransmitter release	- Impairment of CI-dependent respiration - Inhibition of mitochondrial protein import, - Mitochondrial membrane depolarisation - Mitochondrial fragmentation	Ludtmann et al 2018; Shahmoradian et al 2019; Wang et al 2019; Zambon et al 2019

VPS35 Dominant	**Vacuolar protein sorting-associated protein 35** - Component of the retromer cargo selective complex involved in endosomal trafficking and lysosomal degradation pathway	- Impaired mitochondrial dynamics and function - Mitochondrial fragmentation - Enhanced turnover of the mitochondrial DRP1 complexes - Defects in the CI and supercomplex assembly - Bioenergetic deficits - Impaired autophagy	Wang et al 2016; Zhou et al 2017
ATP13A2 Recessive	**Polyamine-transporting ATPase 13A2** - Lysosomal ATPase (P-type) - Regulates cellular homeostasis of cations	- Increased cellular sensitivity to extracellular zinc - Decreased ATP synthesis rates, - Higher frequency of mitochondrial DNA lesions - Increased respiration - Increased fragmentation of the mitochondrial network	Grünewald et al 2012
FBXO7 Recessive	**F-box only protein 7** - E3 ubiquitin protein ligase - Parkin recruitment to mitochondria	- Impaired mitochondrial clearance, - Proteasomal malfunctioning - Increased ROS and PARP overactivation (cell death)	Burchell et al 2013; Delgado-Camprubi et al 2017; Ilyin et al 2000; Shojaee et al 2008
CHCHD2 Dominant	**Coiled-coil-helix-coiled-coil-helix (CHCH) domain – containing protein 2** - Transcription factor - Proposed role in OXPHOS regulation, - Modulates cell death signalling	- Modifies mitochondrial reticular morphology Reduced oxidative phosphorylation - Apoptosis induction via cytochrome *c* destabilization - Impaired respiration - Increased mitochondrial ROS production	Cornelissen et al 2020; Lee et al 2018; Meng et al 2017

To illustrate how the proteins encoded by these genes interact with each other and the respiratory Complexes we have created a visual network for protein-protein interactions (Figure 2).

The network was built using input protein products for the genes in Table 1 PINK1, Parkin (PARK2), DJ-1 (PARK7), LRRK2, SNCA, VPS35, ATP13A2, FBXO7 and *CHCHD2*. The protein products of the genes in Table 1 were uploaded to InnateDB (Breuer et al 2013) (http://www.innatedb.com) pathway analysis tool and mapped to Pathway ID-2912,

source database: KEGG, $p < 1.0E-5$. The other genes (139) that were part of the Pathway ID-2912, were then used as an input for STRINGdb with the initial 9 genes, organism *Homo sapiens*, to generate the protein-protein interaction network. This protein network illustrated the complexity of interaction between the proteins linked to mitochondrial homeostasis found to be mutated in PD and the mitochondrial respiratory Complexes. Thus, the relevant PD mutations are likely to impact on many aspects of mitochondrial physiology. The PD models that we are discussing further will be instrumental in detailing these interactions and their effects on mitochondrial dysfunction in PD.

Genome Wide Association Studies (GWAS) have uncovered increasing numbers of PD risk alleles which remain to be studied in detail (Blauwendraat et al 2020; Chang et al 2017; Nalls et al 2014). As we go forward, idiopathic PD samples including primary fibroblasts, iPSc and iPSc derived neurons are more readily available to elucidate etiopathological roles of the mitochondria in PD providing a test-bed for potential therapeutic strategies.

To provide a platform for ongoing and future work we have reviewed and compared studies of mitochondrial physiology in cellular PD models and compared these with animal models of PD to identify common features that may be investigated as PD risk factors.

2. Mitochondrial homeostasis parameters

Given the importance of consolidating and disseminating protocols for mitochondrial homeostasis dysfunction and neurodegeneration (Burbulla, Krüger 2012; Fang et al 2017; Joshi, Bakowska 2011; Lampl et al 2015), here we have considered parameters that are typically used to assess PD phenotypes and we have summarised common assays employed for these analyses.

2.1. Mitochondrial respiration

Oxygen consumption by the mitochondria is one of the physiological parameters used to characterise the health status of mitochondrial preparations from cell models or tissue samples from animal models. Mitochondrial respiratory physiology has mostly been interrogated with two platforms, the Oroboros O2k (Doerrier et al 2018) and Seahorse XF (Gu et al 2021) whose advantages and experimental capabilities have been previously compared (Horan et al 2012; Zdrazilova et al 2021; Gnaiger 2021). By permeabilization of cells, purification of mitochondria and specific combinations of respiration substrates and inhibitors these allow detailed dissection of mitochondrial physiology states (Gnaiger et al 2020) as well as differentiating between oxidative phosphorylation and glycolysis. Typically, mitochondrial function is assessed through basal respiration, response to endogenous substrates (ROUTINE) in saturating substrate and ADP conditions (OXPHOS), respiration uncoupled from ATP synthesis (LEAK) and residual oxygen capacity (*Rox*) (Gnaiger 2020).

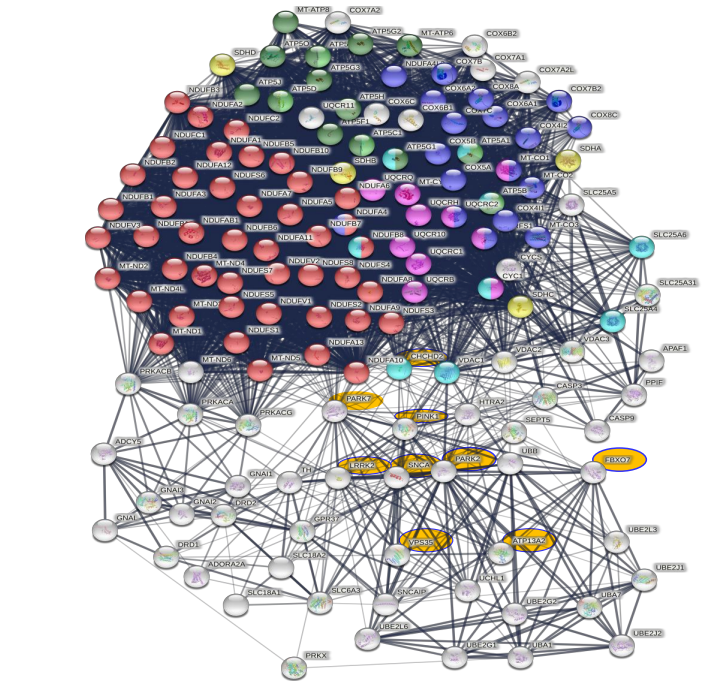

Figure 2. Protein interaction network (medium interaction confidence 0.400, PPI enrichment $p < 1.0e-16$; nodes: 147; edges: 4341; organism: *Homo sapiens*) of PINK1, PARK2, PARK7, LRRK2, SNCA, VPS35, ATP13A2, FBXO7, CHCHD2 (highlighted in orange) and related mitochondrial proteins using the STRING database (Szklarczyk et al 2019). Red nodes: Complex I proteins, Yellow nodes: Complex II protein, pink nodes: Complex III proteins, purple: Complex IV, green: Complex V, light blue: mitochondrial transport proteins. GO:Cellular components was used for functional enrichment of the proteins. GO:0005747- mitochondrial respiratory Complex I; GO:0045277- Complex IV; GO:0045261-proton-transporting ATP synthase complex; GO:0005749- Complex II; GO:0005750- Complex III; GO:0005753- ATP synthase and Reactome pathways, HSA-1268020- mitochondrial protein import.

In PD models a decrease in oxygen consumption is typically connected with the disease. However, sometimes the disease condition is linked to enhanced respiration and oxygen consumption (see analysis below and attached tables). Biochemical assays can be used to measure individual mitochondrial complexes' activities (Barrientos et al 2009) however, respirometry is now the gold standard to evaluate mitochondrial function.

2.2. Adenosine triphosphate

Adenosine triphosphate (ATP) measurement is important to assess mitochondrial function for *in vivo* and *in vitro* models. A variety of colorimetric, fluorometric and luminescence assays are used for these measurements (Fujikawa, Yoshida 2010). These provide information about the total ATP in the sample and can't distinguish the ATP produced from glycolysis versus oxidative phosphorylation. More recently developed genetically-encoded fluorescent reporters are able to detect changes in ATP at the mitochondrial level (Imamura et al 2009).

2.3. Mitochondrial membrane potential

Mitochondrial membrane potential describes the difference in charge across the mitochondrial inner membrane, regulating ion transport and protein import. Together with the pH gradient across the inner membrane, it is the driving force of ATP synthesis during the oxidative phosphorylation process. Fluctuations in mitochondrial potential need to be interpreted in conjunction with other mitochondrial physiology parameters, e.g. respiration, in order to address mitochondrial health (Nicholls, Budd 2000). However significant membrane depolarisation is typically correlated with cellular death (Bock, Tait 2020). The mitochondrial potential is determined by using membrane permeable fluorescent probes which accumulate in the mitochondrial matrix proportionally to the mitochondrial potential Fluorophores employed for this purpose include TMRM, JC-1, TMRE, Rhodamine 123, which can be evaluated using flow cytometry, fluorometry and fluorescence microscopy for detailed subcellular and temporal changes in mitochondrial potential

2.4. Mitochondrial dynamics

Mitochondria are dynamic organelles that regulate their structure-function through fission, fusion, exchange of components, transport, biogenesis and degradation. The bioenergetic and metabolic status of the mitochondria are intertwined with these processes (Picard et al 2013; Van Laar, Berman 2013) and have been associated with disease in both cellular and animal models of PD.

Mitochondrial morphology is typically assessed alongside mitochondrial number and size and more recently branching and elongation states are evaluated through form factor and aspect ratio measurements (Antony et al 2020; Burbulla, Krüger 2012).

2.5. Reactive oxygen species

Reactive oxygen species (ROS) produced in oxidative metabolism have a two-sided contribution to mitochondria and cellular homeostasis. They can act as physiological signalling molecules and at the same time their excess presents a significant challenge to

which the mitochondria can respond with a range antioxidant defences (Andreyev et al 2015; Andreyev et al 2005). Mitochondrial stress including oxidative damage itself can cause an imbalance between ROS production and removal. This can give rise to net ROS production with consequent increase in lipid, protein and DNA oxidation products and connects with neurodegenerative disease etiopathology (Lin, Beal 2006). Measurements of mitochondrial reactive oxygen species are typically undertaken with superoxide redox-sensitive probes (mito-HEt, MitoSOX, Dihydrorhodamine 123) or redox sensitive fluorescent proteins targeted to mitochondria (e.g. reduction-oxidation-sensitive GFP probes). Membrane permeable fluorescent probes present difficulties in specific measurement of mitochondrially derived ROS rather than general cellular ROS, whereas the main challenges of GFP probes are linked to their redox and pH related sensitivity.

3. Mitochondrial homeostasis in animal models of PD

3.1. Toxicological models

6-hydroxydopamine (6-OHDA), or oxidopamine, is a product of the dopamine metabolism which can be taken up by dopaminergic neurons via the DAT receptors and has also been found at elevated levels in the urine of PD patients (Andrew et al 1993). As a synthetic neurotoxin it is widely used to generate rodent models of Parkinson's disease (PD). Unilateral injection of 6-OHDA in SN and medial forebrain bundle (MFB) in rat (Costall et al 1976; Simmonds, Uretsky 1970; Tieu 2011; Ungerstedt 1968) and mouse (Thiele et al 2012) causes dopaminergic neuronal death and motor behaviour defects including ipsilateral circling behaviour. Mechanistically, 6-OHDA is understood to cause the death of dopaminergic neurons in rats through inhibition of the mitochondrial ETS Complexes CI and CIV and through the production of free radicals (Ferger et al 2001; Glinka, Youdim 1995). High-resolution respirometry data from mitochondria in the SN of male Sprague-Dawley rats which had been injected with 6-OHDA in the MFB found that CI activity was decreased along with the respiratory control ratio (RCR) in a time-dependent manner (Kupsch et al 2014). These observations tally with the finding that 6-OHDA caused oxidative stress in the striatum (Smith, Cass 2007) in agreement with evidence for oxidative stress as a common feature in PD patients.

Since its discovery as a PD inducing toxin, **MPTP** has been used to develop animal models of disease. While rats have been largely resistant to MPTP toxicity, MPTP animal models that have been successfully used in PD research include mice and non-human primates such as squirrel monkeys and macaques (Riachi et al 1990). In mouse models, the inhibition of CI in brain mitochondria resulted in reduced ATP levels, an in increase in oxidative stress and the loss of DA neurons in the SN (Nicklas et al 1985; Petroske et al 2001).

Rotenone is a widely used pesticide in aquatic environments. Like MPTP it is highly lipophilic, enabling its transport across the blood brain barrier (BBB). Like MPTP it also inhibits the catalytic activity of the mitochondrial CI enzyme, a characteristic pathology in PD patients (Betarbet et al 2000; Parker et al 1989; Schapira et al 1990), although there is now evidence for a CI independent activity of rotenone (Choi et al 2008). Alongside CI inhibition, rotenone administration to rats also resulted in decreased levels of DA and its

metabolites in the striata (Heikkila et al 1985). However, damage to brain regions not including the SN had also been recorded, suggesting that rotenone may be unsuitable for producing animal models of PD (Ferrante et al 1997; Höglinger et al 2003). Another significant issue with rotenone rat models was the inconsistent response to the toxin, which often resulted in high rates of mortality (Antkiewicz-Michaluk et al 2003; Fleming et al 2004). However as a systemic inhibitor of mitochondrial function it is capable of inducing PD-like pathology across several animal models (Cicchetti et al 2010; Greenamyre et al 2010).

Paraquat is a herbicide that was first suggested as a toxin that could induce PD due to the structural similarities that it shares with MPP+. Investigations into paraquat as an environmental risk factor for PD have largely used mice as the animal model. It was shown in mice that paraquat treatment can cause a dose- and age-dependent decrease of DA neuron numbers in the SN, and a decline in the density of striatal DA nerve terminals (Brooks et al 1999; McCormack et al 2002). Paraquat mice models have replicated increased presence of α-Synuclein fibrils, the up-regulation of α-Synuclein protein levels and the formation of aggregates that contain α-Synuclein (Manning-Bog et al 2002). In striatal mitochondria isolated from paraquat-treated Sprague-Dawley rats LEAK (state 4) respiration was significantly increased while the respiratory control ratio was significantly decreased in comparison with control rats (Czerniczyniec et al 2015).

The most significant drawback of toxicologic models of PD are that they are acute models of disease contrary to the typical evolution of PD which takes place over many years, the high variability of the results between different murine strains that are administered the toxins (Fornai et al 2005) and the variability in reproducing PD features including loss of DA neurons (Miller 2007), appearance of Lewy bodies and motor and non-motor behavioural changes (Meredith, Rademacher 2011; Vingill et al 2018). Although animal toxicological models are still in use for studying various aspects of PD etiopathology, they focus less on mitochondrial homeostasis.

3.2. Transgenic models

The discoveries in the genetics of PD have led to development of genetic murine models harbouring genetic modifications related to PD. However, these models do not fully recapitulate the PD characteristics and present rather mild phenotypes (Airavaara et al 2020; Terzioglu, Galter 2008). To complement these, other animal models of PD, particularly using *D. melanogaster*, have been successfully employed to address mitochondrial homeostasis alongside behavioural and other mechanistic PD characteristics (Hewitt, Whitworth 2017).

Much of the work done to elucidate the mitophagy pathway, within which **PINK1** is a crucial enzyme, was completed using *D. melanogaster* (Clark et al 2006; Park et al 2006; Yang et al 2006). These first studies reported that in *D. melanogaster Pink1* loss of function mutants present the PD phenotypes of dysfunctional mitochondria and locomotive defects associated with DA neurons degeneration. Further studies have reported impaired synaptic transmission, defects in mitochondrial fission and decreased ATP levels arising from reduced Complex I and Complex IV(CIV) activity (Liu et al 2011; Morais et al 2009). When *Pink1* models of PD in mice have been investigated, the fidelity

of the phenotype to PD in humans has had mixed results. RNAi silencing of the *Pink1* gene in mice aged 6 months failed to cause a significant decrease in the number of TH-positive neurons in the SN (Zhou et al 2007). Building upon this, it has been reported that the *Pink1* null mice had no changes to the number of DA neurons or striatal DA content, but there was a significant decrease in the evoked release of DA (Kitada et al 2009). Impaired mitochondrial respiration was observed in the striatum of *Pink1* null mice (Gautier et al 2008) and similarly to *D. melanogaster Pink1* mutants which present reduced respiratory activity linked to Complex I and Complex II (Liu et al 2020). Interestingly the *Pink1* loss of function accelerates in vivo neurodegenerative phenotypes induced by mitochondrial stress triggered by the expression of an unfolded protein in the mitochondrial matrix, namely a truncated form of ornithine transcarbamylase (deltaOTC) (Moisoi et al 2014).

Investigations into the role of the ***Parkin*** gene, in PD were also first conducted in *D. melanogaster*, concurrently with the *Pink1* studies (Clark et al 2006; Greene et al 2003; Park et al 2006; Yang et al 2006). Many of the studies that have investigated *Parkin* loss of function mutants as a model of PD in *D. melanogaster* have observed mitochondrial dysfunction. *Parkin* loss-of-function *D. melanogaster* had significantly decreased CI and CII activity when measured as a function of oxygen flux by high resolution respirometry (Lehmann et al 2016). In mitochondria isolated from the striata of 9 months old *Parkin* null mice OXPHOS (state 3) respiration was significantly decreased while in 24 months old mice respiratory reserve was instead significantly decreased on Complex I substrates, both as detected by high resolution respirometry (Damiano et al 2014).

Multiple studies have reported motor defects in **DJ-1** loss of function murine models of PD as well as altered DA metabolism, however a loss of DA neurons and formation of Lewy bodies has been more difficult to replicate (Chen et al 2005; Goldberg et al 2005; Kim et al 2005; Rousseaux et al 2012). A recent study reported that DJ-1 deficiency in mice accelerated the accumulation and aggregation of the key Lewy body component, α-Synuclein (Xu et al 2017). In mitochondria isolated from the cortex of DJ-1 null mice aged either 3 months or 24 – 26 months, there were no significant differences in OXPHOS or LEAK respiration for Complex I, Complex II or Complex III/IV (Giaime et al 2012).

Murine models addressing **α-Synuclein** pathology range from transgenic mice overexpressing human α-Synuclein with PD relevant mutations, overexpression of human α-Synuclein mutants, through viral delivery of transgenes directly to the brain and more recently, delivery to the brain of exogenous human α-Synuclein in oligomeric or preformed fibrils (PFF) forms (Airavaara et al 2020; Carta et al 2020; Terzioglu, Galter 2008). In transgenic mice, A53T α-Synuclein mutant induces defects in the autophagic clearance of mitochondria (Chen et al 2015). Other mitochondrial roles for α-Synuclein in PD have been derived mainly from cellular models, as detailed below, and are consistent with the finding that Lewy bodies from patients with PD contained fragmented mitochondria crowded with lipids and lysosomes as well as α-Synuclein (Shahmoradian et al 2019).

Additional PD murine models have mutations affecting mitochondrial function and molecular quality control. Loss of function of the mitochondrial protease HtrA2, situated in the intermembrane space, induces a reduction in mitochondrial respiration,

accumulation of oxidative stress markers and accumulation of unfolded proteins in the mitochondria. These correlate with sustained upregulation of the integrated stress signalling specifically in the brain, which contributes to neurodegeneration (Moisoi et al 2009). Mitochondrial protein quality control is an important emerging area of interest, addressed throughout the toxicological and genetic models with an aim to identify how quality control mechanisms contribute to PD etiopathogenesis and may be targeted to ameliorate disease phenotypes (Hu et al 2019; Lautenschläger et al 2020).

An interesting transgenic model to address mitochondrial homeostasis in PD is represented by the 'MitoPark' mouse model with deletion of the mitochondrial transcription factor A (TFAM) in dopaminergic neurons. Although the model does not present a mutation of a PD gene, it is inducing mitochondrial dysfunction and PD phenotypes rendering the model as a tool to further etiopathology mechanistic studies in the field (Beckstead, Howell 2021; Ekstrand et al 2007; Ekstrand, Galter 2009; Galter et al 2010).

Despite the differences in how the murine models are being developed which will influence the interpretation of the results, these are still being employed to investigate 'whole body' aspects of PD etiopathology and responses to treatments.

4. Mitochondrial homeostasis in cellular models of PD

Given the experimental challenges and the extensive time required for use of animal models to study mechanistic details of mitochondrial dysfunction in PD, an extensive range of cellular PD models has been developed. These comprise cell lines as well as primary neuronal and iPSc neuronal models undergoing combinations of PD related toxin treatments as well as relevant genetic manipulations.

PD treatments (Enogieru et al 2019; Fonseca-Fonseca et al 2019; Iglesias-González et al 2012; Imamura et al 2006; Ma et al 2019) While in animal models MPTP itself is used as an inducer of PD etiopathology, in cellular models of dopaminergic neurons presenting the DAT transporter, like SH-SY5Y, its metabolite MPP+ is employed. In addition, inhibitors of mitochondrial function particularly those demonstrated to induce PD phenotypes in animal models, e.g. rotenone, are also employed as PD relevant toxins in cellular models. MPP+ and rotenone are primarily linked to inducing a dysfunction in the CI linked respiration. However, some studies have shown that these drugs are toxic in the absence of CI functionality (Choi et al 2008). Whether CI inhibition leads to compensatory mechanisms that are influenced by MPP+ and Rotenone is not fully addressed.

6-OHDA is successfully employed as a PD-relevant toxin in cellular models, both for its dopaminergic link as well as its oxidative stress-inducing properties. Generic oxidative stressors like H_2O_2 have also been used in cellular PD models.

More recently models of α-Synuclein seeding/exposure to oligomers or preformed fibrils (PFFs) have been developed to address the mitochondrial toxicity of the different types of protein structures (Mahul-Mellier et al 2020; Tapias et al 2017; Zambon et al 2019).

PD phenotypes are evaluated by a wide range of assays determining cell viability (e.g. MTS MTT, Alamar Blue), accumulation of ROS and redox profile (ROS-DCF-DA,

Amplex red, reduced glutathione content, malondialdehyde, carbonylated proteins, catalase and superoxide dismutase activities), autophagy/mitophagy markers, formation of protein aggregates, electrophysiological properties of neuronal cells, Ca^{2+} /Mg^{2+} imaging, alongside the mitochondrial homeostasis parameters specified above.

4.1. Murine primary neurons

Primary neuronal cultures from mice and rats offer unique possibilities to study molecular mechanisms of neurodegeneration given their neurochemical properties correlated to the specific cell type. Primary neuronal cultures can be derived from selected brain regions leading to development of specific cellular models, e.g. dopaminergic neurons, cortical neurons, striatal neurons, hippocampus neurons. A strong advantage of these cultures is that they can be derived from transgenic animals providing homogenous genetic cellular models. However, primary neuronal cultures have disadvantages including the limited number of cells that can be obtained in one preparation, while the preparation and maintenance of the cultures are not trivial Moreover, numerous potential variations in preparation may affect the neuronal physiology including the mitochondrial homeostasis leading to heterogeneity in the experimental results. In addition, the primary neuronal cultures are typically derived from embryonic stage or newly born animals questioning their appropriateness for age related neurodegenerative diseases.

Despite these drawbacks, primary neuronal cultures are a common and very useful tool for PD studies including for analysis of mitochondrial function parameters and provide valuable information on mitochondrial physiology.

Thus, treatment with rotenone of dopaminergic neurons induces decreased respiration, enhanced ROS and decreased mitochondrial potential (Radad et al 2006, 2015; Zhu et al 2019). The decrease in mitochondrial respiration following rotenone treatment is also reported in cortical cultures. Interestingly, loss of Parkin induces a decrease in mitochondrial respiration in striatal neurons but not cortical neurons (Damiano et al 2014).

More recently primary neurons have been used in the context of α-Synuclein pathology analysis using exogenous addition of α-Synuclein. Contrary to monomeric α-Synuclein, pathological α-Synuclein forms (oligomeric, dopamine-modified and phosphorylated), bind with high affinity to mitochondria, resulting in mitochondrial membrane depolarisation and impaired cellular respiration (Di Maio et al 2016; Wang et al 2019). Models of α-Synuclein seeding/exposure to preformed fibrils (PFFs) demonstrated that mitochondrial dysfunction develops as a consequence of the interaction between the newly formed α-Synuclein aggregates and mitochondria, resulting in reduced basal and maximal respiration, coupled with diminished spare respiratory capacity (Mahul-Mellier et al 2020; Tapias et al 2017; Zambon et al 2019). However, it appears that the effects of α-Synuclein pathology on mitochondrial respiration occur primarily at later stages of LB formation and maturation (Burtscher et al 2020; Mahul-Mellier et al 2020).

4.2. SH-SY5Y

SH-SY5Y have gained ground as a popular cell model for PD (Xicoy et al 2017). Developed from a metastatic neuroblastoma the cell line (Biedler, Schachner 1978) has been shown to present tyrosine hydroxylase activity (Ross, Biedler 1985) and consequent dopaminergic phenotypes. The cell line is broadly used as a PD model in differentiated or nondifferentiated conditions. A variety of protocols have been reported for culturing of the cells as well as for differentiation (Xicoy et al 2017), which makes it difficult to cross-compare data between studies.

MPP+ treatment in differentiated SH-SY5Y (Risiglione et al 2020) has demonstrated a profound effect on decreasing coupled respiration and increasing the LEAK respiration indicating significant damage at the level of the inner membrane. However, the study did not account for loss of mitochondrial mass. Treatment of SH-SY5Y with 6-OHDA is shown to reduce NADH-linked mitochondrial respiration but detailed characterisation of mitochondrial physiological changes under 6-OHDA has not been performed (Iglesias-González et al 2012). A protective effect for antioxidant enzymes was correlated with increasing ROS, a result of 6-OHDA treatment, thereby uncoupling respiration and phosphorylation.

In SH-SY5Y PINK1/Parkin downregulation and overexpression of loss of function disease mutations are the most relevant genetic transformations employed for this model (Supplementary File 1). Also in SH-SY5Y, the R492X mutation overexpression appears to have a dominant effect in inducing mitochondrial dysfunction and oxidative stress, particularly in the presence of MPP+ (Yuan et al 2010). Although DJ-1 has multiple roles in maintaining cellular function there is now evidence for a role in S-nitrosylation of Parkin. Thus, denitrosylation of Parkin due to DJ-1 loss of function has negative consequences on mitochondrial function reducing ATP synthesis and respiration (Ozawa et al 2020). PD-associated mutations in F-box only protein (FBXO7) have been linked to disruption in mitochondrial homeostasis. SH-SY5Y genetically modified to achieve FBXO7 loss of function have been used to demonstrate that FBXO7 deficiency is linked to mitochondrial dysfunction increased ROS and consequent PARP overactivation which contributes to cell death (Delgado-Camprubi et al 2017).

SH-SY5Ys are also used to produce cybrids by fusing dopaminergic cells depleted of mtDNA with human platelets from PD patients. The cybrids recapitulate mitochondrial dysfunction observed in PD human samples providing an additional model to study PD (Cronin-Furman et al 2019; Keeney et al 2006).

4.3. Mouse embryonic fibroblasts

Immortalised mouse embryonic fibroblasts (MEF) offer the opportunity of high numbers of cells to employ in parallel for different experimental approaches.

Pink1 KO MEF have been used to demonstrate that mitochondrial dysfunction in PD is not due to proton leak but defects of the electron transfer system with consequences on decreased mitochondrial potential, ATP levels and increased ROS production. Mitochondrial impairments are more pronounced when the cells were grown in galactose rather than glucose medium (Amo et al 2011). We have also shown independently in MEF

that *Pink1* KO results in impaired respiration, reduced ATP levels, increased ROS and decreased mitochondrial potential (Temelie et al 2018). However, the individual activity of the respiratory Complexes did not appear to be affected by *Pink1* loss of function (Heeman et al 2011). The data in MEF are consistent with results on mitochondrial impairment in the brains of *Pink1* KO mice (Gispert et al 2009).

DJ-1 loss of function in KO primary MEF, does not appear to affect mitochondrial respiration but increases ROS production, contributes to reduced mitochondrial potential and leads to higher mitochondrial transition-pore opening, rendering the cells more susceptible to death following oxidative stress (Giaime et al 2012). The DJ-1 effect on mitochondrial physiology has shown some differences in immortalised MEF, with reduced respiration in the DJ1-KO while the other mitochondrial features were consistent with data in the primary cells (Krebiehl et al 2010).

Lrrk2 mutant MEF have been obtained through genetic manipulation *in vitro* rather than from transgenic mice and shows the Lrrk2 kinase activity sustains mitochondrial function via tethering of mitochondria to the ER (Toyofuku et al 2020).

4.4. Human fibroblasts

A number of studies have reported decreased respiratory activity in fibroblasts from PD patients with *Parkin* mutations (Mortiboys et al 2008; Pacelli et al 2011). In contrast, some studies reported higher mitochondrial respiratory rates in *Parkin*-mutant fibroblasts, while exhibiting more fragmented mitochondrial networks and ultrastructural abnormalities (Haylett et al 2016). Zanelatti et al reported higher respiratory activity, reduced ATP levels and mitochondrial potential. While the mitochondrial size did not appear affected, a peculiar mitochondrial network with "chain-like" structures was observed in mutant fibroblasts (Zanellati et al 2015). In human fibroblasts (HF) with *Parkin* mutations, Grunewald et al observed an overall decrease in the ATP level, increased oxidative stress associated with enhanced mitochondrial mass and higher sensitivity to oxidative stress (Grünewald et al 2010). The high variability between the different fibroblast lines made it difficult to find significant differences between controls and PD (González-Casacuberta et al 2019). Respiratory system dysfunction is also identified in fibroblasts from patients with *PINK1* mutations (Hoepken et al 2007).

The impaired ETS Complex assembly in genetic PD together with reduced mitochondrial potential has been reported in samples with *DJ-1* mutation (Di Nottia et al 2017; Krebiehl et al 2010). *VPS35* mutations result in defective mitochondrial function (Wang et al 2016; Zhou et al 2017), whereas inefficient response to mitochondrial challenges was seen in fibroblasts with *LRRK2* mutation G2019S, suggesting compromised bioenergetic function (Juárez-Flores et al 2018). Fibroblasts from non-manifesting carriers of *LRRK2* mutation showed an increase in mitochondrial network in standard growing conditions (glucose) and an improvement of mitochondrial dynamics under mitochondrial challenging conditions (galactose), while in PD patients carrying the same mutation, mitochondrial dynamic pattern is similar to controls (glucose condition)

and there were less branched networks and shorter mitochondria with galactose (Juárez-Flores et al 2018).

CHCHD2 encodes a protein that modulates mitochondrial function in conjunction with the ALS/FTD-associated gene CHCHD10. CHCHD2 accumulates in damaged mitochondria and regulates CHCHD10 oligomerisation and has been linked to PD (Huang et al 2018; Liu et al 2020). The *CHCHD2* disease-causing mutations in PD patient fibroblasts induce fragmentation of the mitochondrial reticular morphology and results in reduced activity of Complexes CI and CIV (Lee et al 2018), as well as accumulation in an insoluble form in the intermembrane space and apoptosis induction via cytochrome *c* destabilization, impaired respiration and increased mitochondrial ROS production (Cornelissen et al 2020; Meng et al 2017).

Studies have focussed on idiopathic PD (IPD) patient stratification based on identification of pathological mechanisms linked to mitochondrial homeostasis in peripheral tissues using dermal fibroblasts. These demonstrate high variability in mitochondrial parameters between patients. Thus only a small number of IPD samples present significant mitochondrial dysfunction in skin fibroblasts (Carling et al 2020) as reflected in ATP production, IPD mitochondria present morphometric changes leading to reduced depolarisation by FCCP (Antony et al 2020) and mitochondrial bioenergetics are changed more significantly by metabolic stress in IPD cases versus control (Milanese et al 2019). Deus et al have shown that idiopathic PD fibroblasts present hyperpolarised mitochondria associated with reduced ATP and enhanced ROS (Deus et al 2020), while Ambrosi et al demonstrated proteolytic and bioenergetic deficits in IPD fibroblasts (Ambrosi et al 2014).

Human fibroblasts show a circadian mitochondrial and glycolytic activity (Pacelli et al 2019). This has impacted on how mitochondrial function appears in PD versus control samples. Thus, human fibroblasts with mutated *Parkin* present mitochondrial dysfunction and reduced respiration that is evident when the cell culture is synchronised, while these differences are not evident under basal asynchronous conditions. This may explain some of the difficulties in observing significant differences in patient primary fibroblasts.

Baltimore Longitudinal Study of Aging (BLSA) clearly indicated that, if health status and biopsy conditions are controlled, the replicative lifespan of fibroblasts in culture does not correlate with donor age (Cristofalo et al 1998). Despite the fact that mitochondrial dysfunction has been listed as one of nine hallmarks of ageing (López-Otín et al 2013), to our knowledge there is no study dedicated to investigate the effect of age of donor on mitochondrial dysfunction in HF PD. Antony et al recently included age and gender of PD patients as variables in their morphometric analysis, showing no significant covariates affecting TMRM fluorescence, and no significant difference in mitochondrial branching between male and female subjects (Antony et al 2020). A recent study of healthy subjects provided evidence for a functional specialization of human dermal fibroblasts and identifies the partial loss of cellular identity as an important age-related change in the human dermis (Solé-Boldo et al 2020). More studies to come may focus on potential correlation of mitochondrial dysfunction in HF with age of PD patients as well as with severity of the disease.

4.5. iPSc derived neurons

In recent years iPSc technologies have allowed the development of human neuronal models to avoid the impact of the genetic differences between murine animal models and human neurons. These have been developed either from fibroblasts of patients with idiopathic PD or with characterised mutations through genetic modifications approaches including CRISP-R-Cas9 editing to produce KO lines.

iPSc derived dopaminergic neurons with *α-Synuclein A53T* mutation as well as *α-Synuclein* triplication cause impairment in several mitochondrial function parameters, including respiration (basal, maximal, spare capacity), reduction in mitochondrial potential and change in mitochondrial morphology associated with decreased DRP1 phosphorylation (Zambon et al 2019). Interestingly non-differentiated iPSc did not present the mitochondrial respiration dysfunction. Additional mechanistic findings from this study were perturbation of lipid biology, enhanced ER stress and autophagic dysfunction in the PD models. iPSc derived neuroepithelial cells genetically engineered to harbour *α-Synuclein A53T* and *α-Synuclein A30P* mutations also present reduced energy performance, reflected in lower basal respiration and ATP level (Arias-Fuenzalida et al 2017).

iPSc derived dopaminergic neurons with Parkin loss of function show no change in respiration with glucose as a substrate, but reduced respiration with lactate (Bogetofte et al 2019). Interestingly iPSc derived neurons show strong mitochondrial dysfunction phenotypes at the end stage of differentiation, when the metabolic shift from glycolysis to oxidative phosphorylation has completed, consisting of decreased ATP levels, decreased mitochondrial potential, increased mitochondrial fragmentation, and increased mitochondrial ROS production (Schwartzentruber et al 2020).

LRRK2 G2019S iPSc-derived neurons analysis has demonstrated that dopaminergic neurons present an enhanced number of mitochondrial abnormalities when compared with glutamatergic and sensory neurons including decreased respiration, and trafficking abnormalities (Schwab et al 2017). Decreased respiration in LRRK2 iPSc neurons has been observed in another independent study which reported an increase in respiratory activity in iPSc derived neurons harbouring *PINK1 Q456X* mutation (Cooper et al 2012). Mutation of another component of the vesicle trafficking machinery VPS35 has been found to lead to decreased respiration and mitochondrial potential, increased ROS and defective trafficking and consequent impaired mitophagy (Hanss et al 2020).

5. Qualitative analysis of mitochondrial homeostasis parameters

Here we evaluated mitochondrial parameters in cellular PD models and compared them with those obtained in animal PD models to address to which extent the data converge. Mitochondrial homeostasis is assessed and reported differently by different research groups. Therefore, we have employed a scoring system to compare and classify data from experimental studies relative to controls in each study. For mitochondrial respiration parameters, ATP, ROS and mitochondrial potential we have scored '1' for an increase in the disease model versus control, '-1' for a decrease in the disease model

versus control and '0' for no change. For mitochondrial fragmentation we have scored '-1' for more fragmented or damaged mitochondrial network '1' for less fragmented and higher mitochondrial network. The controls have a score of '0'.

We have focused on studies that present mitochondrial respiration data and we have considered that mitochondrial respiration was changed (reduced or enhanced) if one mitochondrial parameter out of the several studied in the original publication presented a significant change. The papers considered for the analysis were searched in PUBMED using combinations of the keywords 'mouse embryonic fibroblasts', 'SH-SY5Y', 'human fibroblasts', 'iPSc neurons', 'primary neurons' 'Parkinson's disease' 'Parkinson's models', 'mitochondria', 'mitochondrial respiration'. The main inclusion criterion was that the study had analysed mitochondrial respiration. Studies bringing additional data on the key selected models have been added to strengthen the characterisation of these models. The scores are recorded in the Supplementary File 1. The data were processed with GraphPad Prism.

Our qualitative summary of mitochondrial homeostasis parameters shows that the parameters analysed most often in PD murine brains are mitochondrial respiratory activity, ATP level and accumulation of oxidative species. These show a consistent decrease of respiratory activity, reduced ATP and increased oxidative species (Figure 3A). For primary neuronal cultures studies analysing mitochondrial respiration, have also addressed oxidative stress markers and mitochondrial potential (Figure 3B). SH-SY5Y models of PD show consistent decrease of respiratory activity, reduced ATP and increased oxidative species. These are accompanied by mitochondrial potential reduction and mitochondrial fragmentation (Figure 3C).

Mitochondrial homeostasis parameters show that in MEFs PD models there is consistent decrease of respiratory activity, reduced ATP and increased oxidative species. These are accompanied by mitochondrial potential reduction and mitochondrial fragmentation (Figure 3D)

The qualitative analysis of mitochondrial parameters in HF follows the same pattern as in other cellular models of PD (Figure 3E and F). However, there is much higher variability in the data and increasingly the mitochondrial properties of these samples are observed in parallel in glucose versus galactose conditions to highlight the impact of the disease mutation or treatment in predominantly glycolytic versus oxidative phosphorylation metabolic conditions. When galactose is used instead of glucose, to create mitochondria-challenging conditions, HF showed stronger decrease in the mitochondrial parameters respiration (González-Casacuberta et al 2019; Milanese et al 2019), and mitochondrial membrane potential (Lee et al 2018), as well as stronger increase in fragmentation (Juárez-Flores et al 2018; Lee et al 2018) and ROS production (Juárez-Flores et al 2018). This data might suggest that PD derived HF have lower oxidative capacity to cope with an extra metabolic requirement such as the galactose condition as compared to HF from healthy individuals. In addition, the direction of the change in mitochondrial parameters depends also of the protein mutated, thus for example the loss-of function mutations in Parkin, impact not only the process of mitophagy but can also affect the physiological regulation of mitochondrial dynamics,

which can influence mitochondrial activity, e.g. augmented fusion of mitochondrial network resulting in increased respiratory activity (Zanellati et al 2015).

iPSc derived PD models appear to have generally higher sensitivity to cellular stressors affecting mitochondrial activity or to PD toxins (Cooper et al 2012) while the details of mitochondrial function present much higher variability and appear to be strongly dependent on the PD mutation as well as the neuronal type the iPSc have been processed into (Figure 3G). The increase in respiration in one study was explained as compensation for decreased mitochondrial inner membrane integrity, evidenced by increased proton leakage, in attempt to compensate for less efficient ATP production (Harjuhaahto et al 2020).

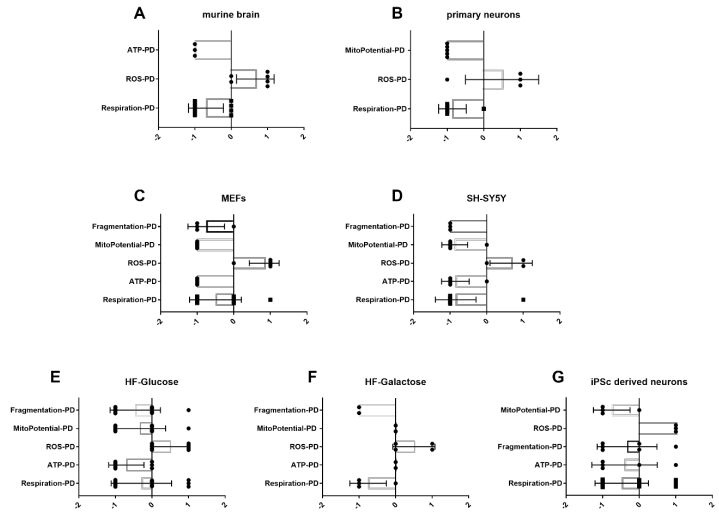

Figure 3. Variation of mitochondrial homeostasis parameters in models of PD represented as mean+/-SD versus the 'zero' line as control. The analysis includes data from (A) murine brain (15 studies), (B) primary neurons (9 studies) (C) SH-SY5Y (13 studies), (D) mouse embryonic fibroblast (MEF) (7 studies) (E) human fibroblasts in glucose media (17 studies) (F) human fibroblast in galactose media (4 studies) and (G) iPSc derived neurons (9 studies).

Information provided by different disease models has largely been complementary and has offered a panoramic prospective on the mitochondrial contribution to mechanisms of dysfunction in PD. The direction of change for these parameters in a PD context is fairly consistent between the different models. However, the results present variability given that most models have their own experimental characteristics which include cell type, passage (even subcloning) status, culture media, treatment variations, diverse methods of genetic manipulations even for the same gene etc. The variability in mitochondrial parameters has also been addressed in the literature, with different explanations or comments. One of plausible explanations is that, in most cell types, mitochondria perform at the basal respiratory levels, and that subtle changes can be observed only when they need to use their "reserve respiratory capacity" to increase substrate oxidation and/or ATP synthesis (e.g. mitochondria challenging conditions) (Rossignol et al 2003). It is also possible that the presence of variability in our analysis could be a result of the activation of different compensatory mechanisms that may depend on the model or mutation type (e.g. increased respiration to compensate for decreased coupling and inefficient ATP production, increase in mitophagy/ autophagy). Consequently, employing more than one model for the study of a particular condition may give complementary answers to the specific research question.

In modelling PD, immortalised cell lines offer the advantage of being able to use large amounts of cells that can be manipulated genetically and pharmacologically to address mechanistic details of disease and to investigate novel pharmacological approaches to tackle cellular dysfunction. Despite differences between individual studies, the data indicate that PD models present reduced mitochondrial respiration activity, reduced ATP levels, reduced mitochondrial potential and enhanced ROS typically together with mitochondria fragmentation. The qualitative analysis presented here indicates that SH-SY5Ys and MEF provide relatively consistent results which correlate well with the data obtained in the brain of murine PD models. Human fibroblasts from PD patients whether idiopathic or harbouring genetic mutation reflect best the high individual variability of mitochondrial function parameters. Similarly, the results of iPSc derived neurons reflect the variability of the models and present additional experimental challenges to maintain, rendering the experiments expensive.

6. Perspectives

Mitochondrial dysfunction plays a central, multifaceted role in PD pathogenesis, and the number of models, described herein, provided valuable information on the role of mitochondrial dysfunction in PD. However, to date, the findings obtained in a variety of PD models failed to result in the development of successful treatment strategies targeting mitochondrial pathways, and clinical trials targeting mitochondrial dysfunction and oxidative stress have not yet demonstrated significant beneficial effects. One of the reasons may be that it seems unlikely that any model can fully recapitulate the complexity of the human disease. For instance, cultured cells, as reduced systems, can be used to provide an answer to specific questions, clarify signalling pathways and resolve mechanistic details. Cellular PD models have significant disadvantages in studying mitochondrial function, due to the high rate of glycolytic metabolism (cell lines) or mixed

Information provided by different disease models has largely been complementary and has offered a panoramic prospective on the mitochondrial contribution to mechanisms of dysfunction in PD. The direction of change for these parameters in a PD context is fairly consistent between the different models. However, the results present variability given that most models have their own experimental characteristics which include cell type, passage (even subcloning) status, culture media, treatment variations, diverse methods of genetic manipulations even for the same gene etc. The variability in mitochondrial parameters has also been addressed in the literature, with different explanations or comments. One of plausible explanations is that, in most cell types, mitochondria perform at the basal respiratory levels, and that subtle changes can be observed only when they need to use their "reserve respiratory capacity" to increase substrate oxidation and/or ATP synthesis (e.g. mitochondria challenging conditions) (Rossignol et al 2003). It is also possible that the presence of variability in our analysis could be a result of the activation of different compensatory mechanisms that may depend on the model or mutation type (e.g. increased respiration to compensate for decreased coupling and inefficient ATP production, increase in mitophagy/ autophagy). Consequently, employing more than one model for the study of a particular condition may give complementary answers to the specific research question.

In modelling PD, immortalised cell lines offer the advantage of being able to use large amounts of cells that can be manipulated genetically and pharmacologically to address mechanistic details of disease and to investigate novel pharmacological approaches to tackle cellular dysfunction. Despite differences between individual studies, the data indicate that PD models present reduced mitochondrial respiration activity, reduced ATP levels, reduced mitochondrial potential and enhanced ROS typically together with mitochondria fragmentation. The qualitative analysis presented here indicates that SH-SY5Ys and MEF provide relatively consistent results which correlate well with the data obtained in the brain of murine PD models. Human fibroblasts from PD patients whether idiopathic or harbouring genetic mutation reflect best the high individual variability of mitochondrial function parameters. Similarly, the results of iPSc derived neurons reflect the variability of the models and present additional experimental challenges to maintain, rendering the experiments expensive.

6. Perspectives

Mitochondrial dysfunction plays a central, multifaceted role in PD pathogenesis, and the number of models, described herein, provided valuable information on the role of mitochondrial dysfunction in PD. However, to date, the findings obtained in a variety of PD models failed to result in the development of successful treatment strategies targeting mitochondrial pathways, and clinical trials targeting mitochondrial dysfunction and oxidative stress have not yet demonstrated significant beneficial effects. One of the reasons may be that it seems unlikely that any model can fully recapitulate the complexity of the human disease. For instance, cultured cells, as reduced systems, can be used to provide an answer to specific questions, clarify signalling pathways and resolve mechanistic details. Cellular PD models have significant disadvantages in studying mitochondrial function, due to the high rate of glycolytic metabolism (cell lines) or mixed

glycolytic and oxidative metabolism (primary fibroblasts), which is different from neurons. Furthermore, more complex models (iPSCs-derived neurons), even though they recapitulate PD pathogenicity at an individual basis, including genetic and epigenetic factors, such as aging and environmental insults, fail in the assessment of the contribution of non-neuronal cell populations to the pathogenic process. The use of animal models (toxic or genetic) has strengths in reproducing the complex interplay between different neural and non-neural cells in disease pathogenesis. Unfortunately, animal models also have limitations. Thus, toxin-induced models fail to replicate the chronic course of the disease in the aged animals, whereas genetic models fail to reproduce some of the important hallmarks of PD including the influence of aging, epigenetic, and disease-modifying factors characteristic of PD etiopathology. Choosing a 'best model' to recapitulate disease particularly for a disease with multifactorial etiopathology like PD is still challenging as each of them offers advantages and disadvantages. Nevertheless, each model can contribute to deciphering the mechanisms that play a role of mitochondrial dysfunction in PD pathogenesis and help identify the relevant pieces of the puzzle of mitochondria-triggered neuronal demise. It is worth mentioning that, in recent years, several targets for therapeutic interventions have been recognized — specific organelles (e.g. mitochondria or lysosomes), or disease — associated proteins (e.g. β-glucocerebrosidase or LRRK2). This concept, may, in the future, result in the approach where specific subgroups of patients with PD could be identified, enabling a more personalized therapeutic approach.

Thus, establishing mechanistic details in cell lines and validating such data in patient HF or iPSc derived neurons can perhaps give an integrated view on the disease aspect that is investigated. Addressing the disease condition and pharmacological approaches at whole body level may still require the use of animal models. However, we have seen now significant development of human cellular models, including patient derived, to be able to include more of these in PD studies. Despite the fact that none of the models can fully reproduce the complex pattern of *in vivo* human PD, it can be still stated that they can provide better understanding of molecular mechanisms and risk factors responsible for neuronal demise in PD and help identify reliable markers of the disease process. Therefore, for the time being, studies in animal models still have a valuable role in PD research, although the knowledge gained with cellular models, especially those derived from iPSCs that would allow a more personalized approach, may help to develop better targeted disease-modifying therapeutic strategies.

Acknowledgements

This study is a contribution to COST Action CA15203 MitoEAGLE. This work was supported by the Biotechnology and Biological Sciences Research Council [grant number BB/J014508/1], via a doctoral training partnership award to BE and the Grant No 451-03-68/2020-14/200110 to NKJ and IM from the Ministry of Education, Science and Technological Development of the Republic of Serbia.

References

Abeliovich A, Gitler AD (2016) Defects in trafficking bridge Parkinson's disease pathology and genetics. Nature 539:207–16. doi:10.1038/nature20414

Airavaara M, Parkkinen I, Konovalova J, Albert K, Chmielarz P, Domanskyi A (2020) Back and to the Future: From Neurotoxin-Induced to Human Parkinson's Disease Models. Curr Protoc Neurosci 91:1–33. doi:10.1002/cpns.88

Ambrosi G, Ghezzi C, Sepe S, Milanese C, Payan-Gomez C, Bombardieri CR, Armentero MT, Zangaglia R, Pacchetti C, Mastroberardino PG, Blandini F (2014) Bioenergetic and proteolytic defects in fibroblasts from patients with sporadic Parkinson's disease. Biochim Biophys Acta - Mol Basis Dis 1842:1385–94. doi:10.1016/j.bbadis.2014.05.008

Amo T, Sato S, Saiki S, Wolf AM, Toyomizu M, Gautier CA, Shen J, Ohta S, Hattori N (2011) Mitochondrial membrane potential decrease caused by loss of PINK1 is not due to proton leak, but to respiratory chain defects. Neurobiol Dis 41:111–8. doi:10.1016/j.nbd.2010.08.027

Andrew R, Watson DG, Best SA, Midgley JM, Wenlong H, Petty RKH (1993) The determination of hydroxydopamines and other trace amines in the urine of Parkinsonian patients and normal controls. Neurochem Res 18:1175–7. doi:10.1007/BF00978370

Andreyev AY, Kushnareva YE, Murphy AN, Starkov AA (2015) Mitochondrial ROS metabolism: 10 Years later. Biochemistry (Mosc) 80:517–31. doi:10.1134/S0006297915050028

Andreyev AY, Kushnareva YE, Starkov AA (2005) Mitochondrial metabolism of reactive oxygen species. Biochemistry (Mosc) 70:246–64. doi:10.1007/s10541-005-0102-7

Antkiewicz-Michaluk L, Karolewicz B, Romańska I, Michaluk J, Bojarski AJ, Vetulani J (2003) 1-Methyl-1,2,3,4-tetrahydroisoquinoline protects against rotenone-induced mortality and biochemical changes in rat brain. Eur J Pharmacol 466:263–9. doi:10.1016/S0014-2999(03)01565-6

Antony PMA, Kondratyeva O, Mommaerts K, Ostaszewski M, Sokolowska K, Baumuratov AS, Longhino L, Poulain JF, Grossmann D, Balling R, Krüger R, Diederich NJ (2020) Fibroblast mitochondria in idiopathic Parkinson's disease display morphological changes and enhanced resistance to depolarization. Sci Rep 10:1–10. doi:10.1038/s41598-020-58505-6

Arias-Fuenzalida J, Jarazo J, Qing X, Walter J, Gomez-Giro G, Nickels SL, Zaehres H, Schöler HR, Schwamborn JC (2017) FACS-Assisted CRISPR-Cas9 Genome Editing Facilitates Parkinson's Disease Modeling. Stem Cell Reports 9:1423–31. doi:10.1016/j.stemcr.2017.08.026

Barrientos A, Fontanesi F, Díaz F (2009) Evaluation of the mitochondrial respiratory Chain and oxidative phosphorylation system using polarography and spectrophotometric enzyme assays. Curr Protoc Hum Genet 63:1–14. doi:10.1002/0471142905.hg1903s63

Beckstead MJ, Howell RD (2021) Progressive parkinsonism due to mitochondrial impairment: Lessons from the MitoPark mouse model. Exp Neurol 341:113707. doi:10.1016/j.expneurol.2021.113707

Betarbet R, Sherer TB, MacKenzie G, Garcia-Osuna M, Panov A V., Greenamyre JT (2000) Chronic systemic pesticide exposure reproduces features of Parkinson's disease. Nat Neurosci 3:1301–6. doi:10.1038/81834

Biedler JL, Schachner M (1978) Multiple Neurotransmitter Synthesis by Human Neuroblastoma Cell Lines and Clones. Cancer Res 38:3751–7.

Bindoff LA, Birch-Machin M, Cartlidge NEF, Parker WD, Turnbull DM (1989) Mitochondrial Function in Parkinson's Disease. Lancet 334:49. doi:10.1016/S0140-6736(89)90291-2

Blauwendraat C, Nalls MA, Singleton AB (2020) The genetic architecture of Parkinson's disease. Lancet Neurol 19:170–8. doi:10.1016/S1474-4422(19)30287-X

Bock FJ, Tait SWG (2020) Mitochondria as multifaceted regulators of cell death. Nat Rev Mol Cell Biol 21:85–100. doi:10.1038/s41580-019-0173-8

Bogetofte H, Jensen P, Ryding M et al (2019) PARK2 mutation causes metabolic disturbances and impaired survival of human iPSC-derived neurons. Front Cell Neurosci 13:1–14. doi:10.3389/fncel.2019.00297

Bonifati V, Rizzu P, Van Baren MJ, Schaap O, Breedveld GJ, Krieger E, Dekker MCJ, Squitieri F, Ibanez P, Joosse M, Van Dongen JW, Vanacore N, Van Swieten JC, Brice A, Meco G, Van Duijn CM, Oostra BA, Heutink P (2003) Mutations in the DJ-1 gene associated with autosomal recessive early-onset parkinsonism. Science (80-) 299:256–9. doi:10.1126/science.1077209

Breuer K, Foroushani AK, Laird MR, Chen C, Sribnaia A, Lo R, Winsor GL, Hancock REW, Brinkman FSL, Lynn DJ (2013) InnateDB: Systems biology of innate immunity and beyond - Recent updates and continuing curation. Nucleic Acids Res 41:1228–33. doi:10.1093/nar/gks1147

Brooks A., Chadwick C., Gelbard H., Cory-Slechta D., Federoff H. (1999) Paraquat elicited neurobehavioral syndrome caused by dopaminergic neuron loss. Brain Res 823:1–10. doi:10.1016/S0006-8993(98)01192-5

Burbulla LF, Krüger R (2012) The use of primary human fibroblasts for monitoring mitochondrial phenotypes in the field of Parkinson's disease. J Vis Exp 68:1–6. doi:10.3791/4228

Burchell VS, Nelson DE, Sanchez-Martinez A et al (2013) The Parkinson's disease-linked proteins Fbxo7 and Parkin interact to mediate mitophagy. Nat Neurosci 16:1257–65. doi:10.1038/nn.3489

Burns RS, Chiueh CC, Markey SP, Ebert MH, Jacobowitz DM, Kopin IJ (1983) A primate model of parkinsonism: Selective destruction of dopaminergic neurons in the pars compacta of the substantia nigra by N-methyl-4-phenyl-1,2,3,6-tetrahydropyridine. Proc Natl Acad Sci U S A 80:4546–50. doi:10.1073/pnas.80.14.4546

Burtscher J, Copin JC, Sandi C, Lashuel HA (2020) Pronounced a-synuclein pathology in a seeding-based mouse model is not sufficient to induce mitochondrial respiration deficits in the striatum and amygdala. 7:1–13. doi:10.1523/ENEURO.0110-20.2020

Carling PJ, Mortiboys H, Green C et al (2020) Deep phenotyping of peripheral tissue facilitates mechanistic disease stratification in sporadic Parkinson's disease. Prog Neurobiol 187:101772. doi:10.1016/j.pneurobio.2020.101772

Carta AR, Boi L, Pisanu A, Palmas MF, Carboni E, De Simone A (2020) Advances in modelling alpha-synuclein-induced Parkinson's diseases in rodents: Virus-based models versus inoculation of exogenous preformed toxic species. J Neurosci Methods 338:108685. doi:10.1016/j.jneumeth.2020.108685

Chang D et al — International Parkinson's Disease Genomics Consortium (2017) A meta-analysis of genome-wide association studies identifies 17 new Parkinson's disease risk loci. Nat Genet 49:1511–6. doi:10.1038/ng.3955

Chen L, Cagniard B, Mathews T, Jones S, Koh HC, Ding Y, Carvey PM, Ling Z, Kang UJ, Zhuang X (2005) Age-dependent Motor Deficits and Dopaminergic Dysfunction in DJ-1 Null Mice. J Biol Chem 280:21418–26. doi:10.1074/jbc.M413955200

Chen L, Xie Z, Turkson S, Zhuang X (2015) A53T human α-synuclein overexpression in transgenic mice induces pervasive mitochondria macroautophagy defects preceding dopamine neuron degeneration. J Neurosci 35:890–905. doi:10.1523/JNEUROSCI.0089-14.2015

Choi WS, Kruse SE, Palmiter RD, Xia Z (2008) Mitochondrial complex I inhibition is not required for dopaminergic neuron death induced by rotenone, MPP+, or paraquat. Proc Natl Acad Sci U S A 105:15136–41. doi:10.1073/pnas.0807581105

Cicchetti F, Drouin-Ouellet J, Gross RE (2010) Viability of the rotenone model in question. Trends Pharmacol Sci 31:142–3. doi:10.1016/j.tips.2009.12.008

Clark IE, Dodson MW, Jiang C, Cao JH, Huh JR, Seol JH, Yoo SJ, Hay BA, Guo M (2006) Drosophila pink1 is required for mitochondrial function and interacts genetically with parkin. Nature 441:1162–6. doi:10.1038/nature04779

Cooper O, Seo H, Andrabi S et al (2012) Pharmacological rescue of mitochondrial deficits in iPSC-derived neural cells from patients with familial Parkinson's disease. Sci Transl Med 4:141ra90. doi:10.1126/scitranslmed.3003985

Cornelissen T, Spinazzi M, Martin S, Imberechts D, Vangheluwe P, Bird M, De Strooper B, Vandenberghe W (2020) CHCHD2 harboring Parkinson's disease-linked T61I mutation precipitates inside mitochondria and induces precipitation of wild-type CHCHD2. Hum Mol Genet 29:1096–106. doi:10.1093/hmg/ddaa028

Costall B, Naylor RJ, Pycock C (1976) Non-specific supersensitivity of striatal dopamine receptors after 6-hydroxydopamine lesion of the nigrostriatal pathway. Eur J Pharmacol 35:275–83. doi:10.1016/0014-2999(76)90229-6

Coxhead J, Kurzawa-Akanbi M, Hussain R, Pyle A, Chinnery P, Hudson G (2015) Somatic mtDNA variation is an important component of Parkinson's disease. Neurobiol Aging 38:217.e1-217.e6. doi:10.1016/j.neurobiolaging.2015.10.036

Cristofalo VJ, Allen RG, Pignolo RJ, Martin BG, Beck JC (1998) Relationship between donor age and the replicative lifespan of human cells in culture: A reevaluation. Proc Natl Acad Sci U S A 95:10614–9. doi:10.1073/pnas.95.18.10614

Cronin-Furman EN, Barber-Singh J, Bergquist KE, Yagi T, Trimmer PA (2019) Differential effects of yeast NADH dehydrogenase (Ndi1) expression on mitochondrial function and inclusion formation in a cell culture model of sporadic parkinson's disease. Biomolecules 9:1–23. doi:10.3390/biom9040119

Czerniczyniec A, Lanza EM, Karadayian AG, Bustamante J, Lores-Arnaiz S (2015) Impairment of striatal mitochondrial function by acute paraquat poisoning. J Bioenerg Biomembr 47:395–408. doi:10.1007/s10863-015-9624-x

Damiano M, Gautier CA, Bulteau AL et al (2014) Tissue- and cell-specific mitochondrial defect in Parkin-deficient mice. PLoS One 9:e99898. doi:10.1371/journalpone.0099898

Davis GC, Williams AC, Markey SP, Ebert MH, Caine ED, Reichert CM, Kopin IJ (1979) Chronic parkinsonism secondary to intravenous injection of meperidine analogues. Psychiatry Res 1:249–54. doi:10.1016/0165-1781(79)90006-4

Delgado-Camprubi M, Esteras N, Soutar MP, Plun-Favreau H, Abramov AY (2017) Deficiency of Parkinson's disease-related gene Fbxo7 is associated with impaired mitochondrial metabolism by PARP activation. Cell Death Differ 24:120–31. doi:10.1038/cdd.2016.104

Deus CM, Pereira SP, Cunha-Oliveira T, Pereira FB, Raimundo N, Oliveira PJ (2020) Mitochondrial remodeling in human skin fibroblasts from sporadic male Parkinson's disease patients uncovers metabolic and mitochondrial bioenergetic defects. Biochim Biophys Acta - Mol Basis Dis 1866:165615. doi:10.1016/j.bbadis.2019.165615

Di Maio R, Barrett PJ, Hoffman EK, Barrett CW, Zharikov A, Borah A, Hu X, McCoy J, Chu CT, Burton EA, Hastings TG, Greenamyre JT (2016) α-synuclein binds to TOM20 and inhibits mitochondrial protein import in Parkinson's disease. Sci Transl Med 8:1–15. doi:10.1126/scitranslmed.aaf3634

Di Nottia M, Masciullo M, Verrigni D, Petrillo S, Modoni A, Rizzo V, Di Giuda D, Rizza T, Niceta M, Torraco A, Bianchi M, Santoro M, Bentivoglio AR, Bertini E, Piemonte F, Carrozzo R, Silvestri G (2017) DJ-1 modulates mitochondrial response to oxidative stress: clues from a novel diagnosis of PARK7. Clin Genet 92:18–25. doi:10.1111/cge.12841

Doerrier C, Garcia-Souza LF, Krumschnabel G, Wohlfarter Y, Mészáros AT, Gnaiger E (2018) High-Resolution FluoRespirometry and OXPHOS protocols for human cells, permeabilized fibers from small biopsies of muscle, and isolated mitochondria. Methods Mol Biol 1782:31-70. doi: 10.1007/978-1-4939-7831-1_3

Dölle C, Fløgnes I, Nido GS, Miletic H, Osuagwu N, Kristoffersen S, Lilleng PK, Larsen JP, Tysnes OB, Haugarvoll K, Bindoff LA, Tzoulis C (2016) Defective mitochondrial DNA homeostasis in the substantia nigra in Parkinson disease. Nat Commun 7:13548. doi:10.1038/ncomms13548

Ekstrand MI, Galter D (2009) The MitoPark Mouse - An animal model of Parkinson's disease with impaired respiratory chain function in dopamine neurons. Park Relat Disord 15:S185–8. doi:10.1016/S1353-8020(09)70811-9

Ekstrand MI, Terzioglu M, Galter D et al (2007) Progressive parkinsonism in mice with respiratory-chain-deficient dopamine neurons. Proc Natl Acad Sci U S A 104:1325–30. doi:10.1073/pnas.0605208103

Enogieru AB, Haylett WL, Miller HC, van der Westhuizen FH, Hiss DC, Ekpo OE (2019) Attenuation of Endoplasmic Reticulum Stress, Impaired Calcium Homeostasis, and Altered Bioenergetic Functions in MPP+-Exposed SH-SY5Y Cells Pretreated with Rutin. Neurotox Res 36:764–76. doi:10.1007/s12640-019-00048-4

Fang EF, Palikaras K, Sun N et al (2017) In vitro and in vivo detection of mitophagy in human cells, *C. Elegans*, and mice. J Vis Exp 129:e56301. doi:10.3791/56301

Ferger B, Rose S, Jenner A, Halliwell B, Jenner P (2001) 6-Hydroxydopamine increases hydroxyl free radical production and DNA damage in rat striatum. Neuroreport 12:1155–9. doi:10.1097/00001756-200105080-00021

Ferrante RJ, Schulz JB, Kowall NW, Beal MF (1997) Systemic administration of rotenone produces selective damage in the striatum and globus pallidus, but not in the substantia nigra. Brain Res 753:157–62. doi:10.1016/S0006-8993(97)00008-5

Fleming SM, Zhu C, Fernagut PO, Mehta A, DiCarlo CD, Seaman RL, Chesselet MF (2004) Behavioral and immunohistochemical effects of chronic intravenous and subcutaneous infusions of varying doses of rotenone. Exp Neurol 187:418–29. doi:10.1016/j.expneurol.2004.01.023

Fonseca-Fonseca LA, Wong-Guerra M, Ramírez-Sánchez J, Montano-Peguero Y, Padrón Yaquis AS, Rodríguez AM, da Silva VDA, Costa SL, Pardo-Andreu GL, Núñez-Figueredo Y (2019) JM-20, a novel hybrid molecule, protects against rotenone-induced neurotoxicity in experimental model of Parkinson's disease. Neurosci Lett 690:29–35. doi:10.1016/j.neulet.2018.10.008

Fornai F, Schluter OM, Lenzi P, Gesi M, Ruffoli R, Ferrucci M, Lazzeri G, Busceti CL, Pontarelli F, Battaglia G, Pellegrini A, Nicoletti F, Ruggieri S, Paparelli A, Sudhof TC (2005) Parkinson-like syndrome induced by continuous MPTP infusion: Convergent roles of the ubiquitin-proteasome system and -synuclein. Proc Natl Acad Sci U S A 102:3413–8. doi:10.1073/pnas.0409713102

Fujikawa M, Yoshida M (2010) A sensitive, simple assay of mitochondrial ATP synthesis of cultured mammalian cells suitable for high-throughput analysis. Biochem Biophys Res Commun 401:538–43. doi:10.1016/j.bbrc.2010.09.089

Galter D, Pernold K, Yoshitake T, Lindqvist E, Hoffer B, Kehr J, Larsson NG, Olson L (2010) MitoPark mice mirror the slow progression of key symptoms and L-DOPA response in Parkinson's disease. Genes, Brain Behav 9:173–81. doi:10.1111/j.1601-183X.2009.00542.x

Gautier CA, Kitada T, Shen J (2008) Loss of PINK1 causes mitochondrial functional defects and increased sensitivity to oxidative stress. Proc Natl Acad Sci U S A 105:11364–9. doi:10.1073/pnas.0802076105

Ge P, Dawson VL, Dawson TM (2020) PINK1 and Parkin mitochondrial quality control: A source of regional vulnerability in Parkinson's disease. Mol Neurodegener 15:1–18. doi:10.1186/s13024-020-00367-7

Giaime E, Yamaguchi H, Gautier CA, Kitada T, Shen J (2012) Loss of DJ-1 does not affect mitochondrial respiration but increases ROS production and mitochondrial permeability transition pore opening. PLoS One 7:e40501. doi:10.1371/journalpone.0040501

Giannoccaro MP, La Morgia C, Rizzo G, Carelli V (2017) Mitochondrial DNA and primary mitochondrial dysfunction in Parkinson's disease. Mov Disord 32:346–63. doi:10.1002/mds.26966

Gispert S, Ricciardi F, Kurz A et al (2009) Parkinson phenotype in aged PINK1-deficient mice is accompanied by progressive mitochondrial dysfunction in absence of neurodegeneration. PLoS One 4:e5777. doi:10.1371/journalpone.0005777

Glinka YY, Youdim MBH (1995) Inhibition of mitochondrial complexes I and IV by 6-hydroxydopamine. Eur J Pharmacol Environ Toxicol 292:329–32. doi:10.1016/0926-6917(95)90040-3

Gnaiger E (2020) Mitochondrial pathways and respiratory control. An introduction to OXPHOS analysis. 5th ed. Bioenerg Commun 2020.2:114 pp. doi:10.26124/bec:2020-0002

Gnaiger E (2021) Bioenergetic cluster analysis – mitochondrial respiratory control in human fibroblasts. MitoFit Preprints 2021.8. doi:10.26124/mitofit:2021-0008

Gnaiger E et al — MitoEAGLE Task Group (2020) Mitochondrial physiology. Bioenerg Commun 2020.1:1–44. doi:10.26124/bec:2020-0001.v1

Goldberg MS, Pisani A, Haburcak M et al (2005) Nigrostriatal dopaminergic deficits and hypokinesia caused by inactivation of the familial Parkinsonism-linked gene DJ-1. Neuron 45:489–96. doi:10.1016/j.neuron.2005.01.041

González-Casacuberta I, Juárez-Flores DL, Ezquerra M et al (2019) Mitochondrial and autophagic alterations in skin fibroblasts from Parkinson disease patients with Parkin mutations. Aging (Albany NY) 11:3750–67. doi:10.18632/aging.102014

Greenamyre JT, Cannon JR, Drolet R, Mastroberardino PG (2010) Lessons from the rotenone model of Parkinson's disease. Trends Pharmacol Sci 31:141–2. doi:10.1016/j.tips.2009.12.006

Greene JC, Whitworth AJ, Kuo I, Andrews LA, Feany MB, Pallanck LJ (2003) Mitochondrial pathology and apoptotic muscle degeneration in Drosophila parkin mutants. Proc Natl Acad Sci U S A 100:4078–83. doi:10.1073/pnas.0737556100

Grünewald A, Arns B, Seibler P, Rakovic A, Münchau A, Ramirez A, Sue CM, Klein C (2012) ATP13A2 mutations impair mitochondrial function in fibroblasts from patients with Kufor-Rakeb syndrome. Neurobiol Aging 33:1843.e1-1843.e7. doi:10.1016/j.neurobiolaging.2011.12.035

Grünewald A, Rygiel KA, Hepplewhite PD, Morris CM, Picard M, Turnbull DM (2016) Mitochondrial DNA depletion in respiratory chain-deficient Parkinson disease neurons. Ann Neurol 79:366–78. doi:10.1002/ana.24571

Grünewald A, Voges L, Rakovic A et al (2010) Mutant parkin impairs mitochondrial function and morphology in human fibroblasts. PLoS One 5:e12962. doi:10.1371/journalpone.0012962

Gu X, Ma Y, Liu Y, Wan Q (2021) Measurement of mitochondrial respiration in adherent cells by Seahorse XF96 Cell Mito Stress Test. STAR Protoc 2:100245. doi:10.1016/j.xpro.2020.100245

Hanss Z, Larsen SB, Antony P, Mencke P, Massart F, Jarazo J, Schwamborn JC, Barbuti PA, Mellick GD, Krüger R (2020) Mitochondrial and clearance impairment in p.D620N VPS35 patient-derived neurons. Mov Disord 36:704–15. doi:10.1002/mds.28365

Harjuhaahto S, Rasila TS, Molchanova SM et al (2020) ALS and Parkinson's disease genes CHCHD10 and CHCHD2 modify synaptic transcriptomes in human iPSC-derived motor neurons. Neurobiol Dis 141:104940. doi:10.1016/j.nbd.2020.104940

Haylett W, Swart C, Van Der Westhuizen F, Van Dyk H, Van Der Merwe L, Van Der Merwe C, Loos B, Carr J, Kinnear C, Bardien S (2016) Altered mitochondrial respiration and other features of mitochondrial function in parkin-mutant fibroblasts from Parkinson's disease patients. Parkinsons Dis 2016:1819209. doi:10.1155/2016/1819209

Heeman B, Van den Haute C, Aelvoet SA, Valsecchi F, Rodenburg RJ, Reumers V, Debyser Z, Callewaert G, Koopman WJH, Willems PHGM, Baekelandt V (2011) Depletion of PINK1 affects mitochondrial metabolism, calcium homeostasis and energy maintenance. J Cell Sci 124:1115–25. doi:10.1242/jcs.078303

Heikkila RE, Nicklas WJ, Vyas I, Duvoisin RC (1985) Dopaminergic toxicity of rotenone and the 1-methyl-4-phenylpyridinium ion after their stereotaxic administration to rats: Implication for the mechanism of 1-methyl-4-phenyl-1,2,3,6-tetrahydropyridine toxicity. Neurosci Lett 62:389–94. doi:10.1016/0304-3940(85)90580-4

Hewitt VL, Whitworth AJ (2017) Mechanisms of Parkinson's Disease: Lessons from Drosophila. In Current Topics in Developmental Biology (1st ed, Vol 121) Elsevier Inc. doi:10.1016/bs.ctdb.2016.07.005

Hoepken HH, Gispert S, Morales B et al (2007) Mitochondrial dysfunction, peroxidation damage and changes in glutathione metabolism in PARK6. Neurobiol Dis 25:401–11. doi:10.1016/j.nbd.2006.10.007

Höglinger GU, Féger J, Prigent A, Michel PP, Parain K, Champy P, Ruberg M, Oertel WH, Hirsch EC (2003) Chronic systemic complex I inhibition induces a hypokinetic multisystem degeneration in rats. J Neurochem 84:491–502. doi:10.1046/j.1471-4159.2003.01533.x

Horan MP, Pichaud N, Ballard JWO (2012) Review: Quantifying mitochondrial dysfunction in complex diseases of aging. Journals Gerontol - Ser A Biol Sci Med Sci 67 A:1022–35. doi:10.1093/gerona/glr263

Hu D, Sun X, Liao X, Zhang X, Zarabi S, Schimmer A, Hong Y, Ford C, Luo Y, Qi X (2019) Alpha-synuclein suppresses mitochondrial protease ClpP to trigger mitochondrial oxidative damage and neurotoxicity. Acta Neuropathol :939–60. doi:10.1007/s00401-019-01993-2

Huang X, Wu BP, Nguyen D, Liu YT, Marani M, Hench J, Bénit P, Kozjak-Pavlovic V, Rustin P, Frank S, Narendra DP (2018) CHCHD2 accumulates in distressed mitochondria and facilitates oligomerization of CHCHD10. Hum Mol Genet 27:3881–900. doi:10.1093/hmg/ddy270

Iglesias-González J, Sánchez-Iglesias S, Méndez-Álvarez E, Rose S, Hikima A, Jenner P, Soto-Otero R (2012) Differential toxicity of 6-hydroxydopamine in SH-SY5Y human neuroblastoma cells and rat brain mitochondria: Protective role of catalase and superoxide dismutase. Neurochem Res 37:2150–60. doi:10.1007/s11064-012-0838-6

Ilyin GP, Rialland M, Pigeon C, Guguen-Guillouzo C (2000) cDNA cloning and expression analysis of new members of the mammalian F- box protein family. Genomics 67:40–7. doi:10.1006/geno.2000.6211

Imamura H, Huynh Nhat KP, Togawa H, Saito K, Iino R, Kato-Yamada Y, Nagai T, Noji H (2009) Visualization of ATP levels inside single living cells with fluorescence resonance energy transfer-based genetically encoded indicators. Proc Natl Acad Sci U S A 106:15651–6. doi:10.1073/pnas.0904764106

Imamura K, Takeshima T, Kashiwaya Y, Nakaso K, Nakashima K (2006) D-β-hydroxybutyrate protects dopaminergic SH-SY5Y cells in a rotenone model of Parkinson's disease. J Neurosci Res 84:1376–84. doi:10.1002/jnr.21021

Joshi DC, Bakowska JC (2011) Determination of mitochondrial membrane potential and reactive oxygen species in live rat cortical neurons. J Vis Exp 51:2–5. doi:10.3791/2704

Juárez-Flores DL, González-Casacuberta I, Ezquerra M et al (2018) Exhaustion of mitochondrial and autophagic reserve may contribute to the development of LRRK2 G2019S -Parkinson's disease. J Transl Med 16:1–13. doi:10.1186/s12967-018-1526-3

Keeney PM, Xie J, Capaldi RA, Bennett JP (2006) Parkinson's disease brain mitochondrial complex I has oxidatively damaged subunits and is functionally impaired and misassembled. J Neurosci 26:5256–64. doi:10.1523/JNEUROSCI.0984-06.2006

Kim RH, Smith PD, Aleyasin H et al (2005) Hypersensitivity of DJ-1-deficient mice to 1-methyl-4-phenyl-1,2,3,6-tetrahydropyrindine (MPTP) and oxidative stress. Proc Natl Acad Sci U S A 102:5215–20. doi:10.1073/pnas.0501282102

Kitada T, Pisani A, Karouani M, Haburcak M, Martella G, Tscherter A, Platania P, Wu B, Pothos EN, Shen J (2009) Impaired dopamine release and synaptic plasticity in the striatum of *Parkin*−/− mice. J Neurochem 110:613–21. doi:10.1111/j.1471-4159.2009.06152.x

Klein C, Hattori N, Marras C (2018) MDSGene: Closing data gaps in genotype-phenotype correlations of monogenic Parkinson's disease. J Parkinsons Dis 8:S25–30. doi:10.3233/JPD-181505

Klein C, Lohmann-Hedrich K (2007) Impact of recent genetic findings in Parkinson's disease. Curr Opin Neurol 20:453–64. doi:10.1097/WCO.0b013e3281e6692b

Krebiehl G, Ruckerbauer S, Burbulla LF et al (2010) Reduced basal autophagy and impaired mitochondrial dynamics due to loss of Parkinson's disease-associated protein DJ-1. PLoS One 5:e9367. doi:10.1371/journalpone.0009367

Kupsch A, Schmidt W, Gizatullina Z, Debska-Vielhaber G, Voges J, Striggow F, Panther P, Schwegler H, Heinze HJ, Vielhaber S, Gellerich FN (2014) 6-Hydroxydopamine impairs mitochondrial function in the rat model of Parkinson's disease: respirometric, histological, and behavioral analyses. J Neural Transm 121:1245–57. doi:10.1007/s00702-014-1185-3

Lampl T, Crum JA, Davis TA, Milligan C, Moore VDG (2015) Isolation and functional analysis of mitochondria from cultured cells and mouse tissue. J Vis Exp 2015:1–9. doi:10.3791/52076

Langston J, Ballard P, Tetrud J, Irwin I (1983) Chronic Parkinsonism in humans due to a product of meperidine-analog synthesis. Science 219:979–80. doi:10.1126/science.6823561

Lautenschläger J, Wagner-Valladolid S, Stephens AD, Fernández-Villegas A, Hockings C, Mishra A, Manton JD, Fantham MJ, Lu M, Rees EJ, Kaminski CF, Schierle GSK (2020) Intramitochondrial proteostasis is directly coupled to α-synuclein and amyloid β1-42 pathologies. J Biol Chem 295:10138–52. doi:10.1074/jbc.RA119.011650

Lee RG, Sedghi M, Salari M, Shearwood A-MJ, Stentenbach M, Kariminejad A, Goullee H, Rackham O, Laing NG, Tajsharghi H, Filipovska A (2018) Early-onset Parkinson disease caused by a mutation in CHCHD2 and mitochondrial dysfunction. Neurol Genet 4:e276. doi:10.1212/nxg.0000000000000276

Lehmann S, Costa AC, Celardo I, Loh SHY, Martins LM (2016) Parp mutations protect against mitochondrial dysfunction and neurodegeneration in a PARKIN model of Parkinson's disease. Cell Death Dis 7:1–7. doi:10.1038/cddis.2016.72

Lin MT, Beal MF (2006) Mitochondrial dysfunction and oxidative stress in neurodegenerative diseases. Nature 443:787–95. doi:10.1038/nature05292

Liu M, Yu S, Wang J, Qiao J, Liu Y, Wang S, Zhao Y (2020) Ginseng protein protects against mitochondrial dysfunction and neurodegeneration by inducing mitochondrial unfolded protein response in Drosophila melanogaster PINK1 model of Parkinson's disease. J Ethnopharmacol 247:112213. doi:10.1016/j.jep.2019.112213

Liu W, Acin-Perez R, Geghman KD, Manfredi G, Lu B, Li C (2011) Pink1 regulates the oxidative phosphorylation machinery via mitochondrial fission. Proc Natl Acad Sci 108:12920–4. doi:10.1073/pnas.1107332108

López-Otín C, Blasco MA, Partridge L, Serrano M, Kroemer G (2013) The hallmarks of aging. Cell 153(6):1194-217. doi:10.1016/j.cell.2013.05.039

Ludtmann MHR, Angelova PR, Horrocks MH et al (2018) α-synuclein oligomers interact with ATP synthase and open the permeability transition pore in Parkinson's disease. Nat Commun 9:2293. doi:10.1038/s41467-018-04422-2

Ma H, Liu Y, Tang L, Ding H, Bao X, Song F, Zhu M, Li W (2019) Echinacoside selectively rescues complex I inhibition-induced mitochondrial respiratory impairment via enhancing complex II activity. Neurochem Int 125:136–43. doi:10.1016/j.neuint.2019.02.012

Mahul-Mellier AL, Burtscher J, Maharjan N, Weerens L, Croisier M, Kuttler F, Leleu M, Knott GW, Lashuel HA (2020) The process of Lewy body formation, rather than simply α-synuclein fibrillization, is one of the major drivers of neurodegeneration. Proc Natl Acad Sci U S A 117:4971–82. doi:10.1073/pnas.1913904117

Manning-Bog AB, McCormack AL, Li J, Uversky VN, Fink AL, Di Monte DA (2002) The herbicide paraquat causes up-regulation and aggregation of α-synuclein in mice. J Biol Chem 277:1641–4. doi:10.1074/jbc.C100560200

Marras C, Lang A, van de Warrenburg BP et al (2016) Nomenclature of genetic movement disorders: Recommendations of the international Parkinson and movement disorder society task force. Mov Disord 31:436–57. doi:10.1002/mds.26527

Matsumine H, Saito M, Shimoda-Matsubayashi S et al (1997) Localization of a gene for an autosomal recessive form of juvenile parkinsonism to chromosome 6q25.2-27. Am J Hum Genet 60:588–96.

McCormack AL, Thiruchelvam M, Manning-Bog AB, Thiffault C, Langston JW, Cory-Slechta DA, Di Monte DA (2002) Environmental risk factors and Parkinson's disease: selective degeneration of nigral dopaminergic neurons caused by the herbicide paraquat. Neurobiol Dis 10:119–27. doi:10.1006/nbdi.2002.0507

Meng H, Yamashita C, Shiba-Fukushima K, Inoshita T, Funayama M, Sato S, Hatta T, Natsume T, Umitsu M, Takagi J, Imai Y, Hattori N (2017) Loss of Parkinson's disease-associated protein CHCHD2 affects mitochondrial crista structure and destabilizes cytochrome *c*. Nat Commun 8:1–18. doi:10.1038/ncomms15500

Meredith GE, Rademacher DJ (2011) MPTP mouse models of Parkinson's disease: An update. J Parkinson's Disease 1:19–33. doi:10.3233/JPD-2011-11023

Milanese C, Payán-Gómez C, Galvani M, González NM, Tresini M, Abdellah SN, van Roon-Mom WMC, Figini S, Marinus J, van Hilten JJ, Mastroberardino PG (2019) Peripheral mitochondrial function correlates with clinical severity in idiopathic Parkinson's disease. Mov Disord 34:1192–202. doi:10.1002/mds.27723

Miller GW (2007) Paraquat: the red herring of Parkinson's disease research. Toxicol Sci 100:1–2. doi:10.1093/toxsci/kfm223

Moisoi N, Klupsch K, Fedele V et al (2009) Mitochondrial dysfunction triggered by loss of HtrA2 results in the activation of a brain-specific transcriptional stress response. Cell Death Differ 16:449–64. doi:10.1038/cdd.2008.166

Moisoi N, Fedele V, Edwards J, Martins LM (2014) Loss of PINK1 enhances neurodegeneration in a mouse model of Parkinson's disease triggered by mitochondrial stress. Neuropharmacology 77:350–7. doi:10.1016/j.neuropharm.2013.10.009

Morais VA, Verstreken P, Roethig A, Smet J, Snellinx A, Vanbrabant M, Haddad D, Frezza C, Mandemakers W, Vogt-Weisenhorn D, Van Coster R, Wurst W, Scorrano L, De Strooper B (2009) Parkinson's disease mutations in PINK1 result in decreased Complex I activity and deficient synaptic function. EMBO Mol Med 1:99–111. doi:10.1002/emmm.200900006

Mortiboys H, Johansen KK, Aasly JO, Bandmann O (2010) Mitochondrial impairment in patients with Parkinson disease with the G2019S mutation in LRRK2. Neurology 75:2017–20. doi:10.1212/WNL.0b013e3181ff9685

Mortiboys H, Thomas KJ, Koopman WJH, Klaffke S, Abou-Sleiman P, Olpin S, Wood NW, Willems PHGM, Smeitink JAM, Cookson MR, Bandmann O (2008) Mitochondrial function and morphology are impaired in parkin-mutant fibroblasts. Ann Neurol 64:555–65. doi:10.1002/ana.21492

Müftüoglu M, Elibol B, Dalmizrak Ö, Ercan A, Kulaksiz G, Ögüs H, Dalkara T, Özer N (2004) Mitochondrial complex I and IV activities in leukocytes from patients with parkin mutations. Mov Disord 19:544–8. doi:10.1002/mds.10695

Nalls MA et al — International Parkinson's Disease Genomics Consortium et al (2014) Large-scale meta-analysis of genome-wide association data identifies six new risk loci for Parkinson's disease. Nat Genet 46:989–93. doi:10.1038/ng.3043

Nicholls DG, Budd SL (2000) Mitochondria and neuronal survival Physiol Rev 80:315–60. doi:10.1152/physrev.2000.80.1.315

Nicklas W J, Vyas I, Heikkila RE (1985) Inhibition of NADH-linked oxidation in brain mitochondria by 1086 1-methyl-4-phenyl-pyridine, a metabolite of the neurotoxin, 1-methyl-4-phenyl-1,2,5,6-1087 tetrahydropyridine. Life Sci 36 (26):2503–8. doi:10.1016/0024-3205(85)90146-8

Ozawa K, Tsumoto H, Miura Y, Yamaguchi J, Iguchi-Ariga SMM, Sakuma T, Yamamoto T, Uchiyama Y (2020) DJ-1 is indispensable for the S-nitrosylation of Parkin, which maintains function of mitochondria. Sci Rep 10:1–11. doi:10.1038/s41598-020-61287-6

Pacelli C, De Rasmo D, Signorile A et al (2011) Mitochondrial defect and PGC-1α dysfunction in parkin-associated familial Parkinson's disease. Biochim Biophys Acta - Mol Basis Dis 1812:1041–53. doi:10.1016/j.bbadis.2010.12.022

Pacelli C, Rotundo G, Lecce L et al (2019) Parkin mutation affects clock gene-dependent energy metabolism. Int J Mol Sci 20:2772. doi:10.3390/ijms20112772

Park J, Lee SB, Lee S, Kim Y, Song S, Kim S, Bae E, Kim J, Shong M, Kim JM, Chung J (2006) Mitochondrial dysfunction in Drosophila PINK1 mutants is complemented by parkin. Nature 441:1157–61. doi:10.1038/nature04788

Parker WD, Boyson SJ, Parks JK (1989) Abnormalities of the electron transport chain in idiopathic parkinson's disease. Ann Neurol 26:719–23. doi:10.1002/ana.410260606

Petroske E, Meredith GE, Callen S, Totterdell S, Lau YS (2001) Mouse model of Parkinsonism: A comparison between subacute MPTP and chronic MPTP/probenecid treatment. Neuroscience 106:589–601. doi:10.1016/S0306-4522(01)00295-0

Picard M, Shirihai OS, Gentil BJ, Burelle Y (2013) Mitochondrial morphology transitions and functions: Implications for retrograde signaling? Am J Physiol - Regul Integr Comp Physiol 304:R393–406. doi:10.1152/ajpregu.00584.2012

Poewe W, Seppi K, Tanner CM, Halliday GM, Brundin P, Volkmann J, Schrag AE, Lang AE (2017) Parkinson disease. Nat Rev Dis Prim 3:1–21. doi:10.1038/nrdp.2017.13

Radad K, Moldzio R, Rausch WD (2015) Rapamycin protects dopaminergic neurons against rotenone-induced cell death in primary mesencephalic cell culture. Folia Neuropathol 53:250–61. doi:10.5114/fn.2015.54426

Radad K, Rausch WD, Gille G (2006) Rotenone induces cell death in primary dopaminergic culture by increasing ROS production and inhibiting mitochondrial respiration. Neurochem Int 49:379–86. doi:10.1016/j.neuint.2006.02.003

Ramsay RR, Singer TP (1986) Energy-dependent uptake of N-methyl-4-phenylpyridinium, the neurotoxic metabolite of 1-methyl-4-phenyl-1,2,3,6-tetrahydropyridine, by mitochondria. J Biol Chem 261:7585–7.

Ramsay RR, Salach JI, Dadgar J, Singer TP (1986) Inhibition of mitochondrial NADH dehydrogenase by pyridine derivatives and its possible relation to experimental and idiopathic parkinsonism. Biochem Biophys Res Commun 135:269–75. doi:10.1016/0006-291X(86)90972-1

Riachi NJ, Dietrich WD, Harik SI (1990) Effects of internal carotid administration of MPTP on rat brain and blood-brain barrier. Brain Res 533:6–14. doi:10.1016/0006-8993(90)91788-I

Risiglione P, Leggio L, Cubisino SAM, Reina S, Paternò G, Marchetti B, Magrì A, Iraci N, Messina A (2020) High-resolution respirometry reveals mpp+ mitochondrial toxicity mechanism in a cellular model of parkinson's disease. Int J Mol Sci 21:1–15. doi:10.3390/ijms21217809

Ross RA, Biedler JL (1985) Presence and Regulation of Tyrosinase Activity in Human Neuroblastoma Cell Variants in Vitro. Cancer Res 45:1628–32.

Rossignol R, Faustin B, Rocher C, Malgat M, Mazat JP, Letellier T (2003) Mitochondrial threshold effects. Biochem J 370:751–62. doi:10.1042/BJ20021594

Rousseaux MWC, Marcogliese PC, Qu D, Hewitt SJ, Seang S, Kim RH, Slack RS, Schlossmacher MG, Lagace DC, Mak TW, Park DS (2012) Progressive dopaminergic cell loss with unilateral-to-bilateral progression in a genetic model of Parkinson disease. Proc Natl Acad Sci U S A 109:15918–23. doi:10.1073/pnas.1205102109

Salach JI, Singer TP, Castagnoli N, Trevor A (1984) Oxidation of the neurotoxic amine 1-methyl-4-phenyl-1,2,3,6-tetrahydropyridine (MPTP) by monoamine oxidases A and B and suicide inactivation of the enzymes by MPTP. Biochem Biophys Res Commun 125:831–5. doi:10.1016/0006-291X(84)90614-4

Schapira AHV (2007) Mitochondrial dysfunction in Parkinson's disease. Cell Death Differ 14:1261–6. doi:10.1038/sj.cdd.4402160

Schapira AHV, Cooper JM, Dexter D, Clark JB, Jenner P, Marsden CD (1990) Mitochondrial Complex I Deficiency in Parkinson's Disease. J Neurochem 54:823–7. doi:10.1111/j.1471-4159.1990.tb02325.x

Schwab AJ, Sison SL, Meade MR, Broniowska KA, Corbett JA, Ebert AD (2017) Decreased sirtuin deacetylase activity in LRRK2 G2019S iPSC-derived dopaminergic neurons. Stem Cell Reports 9:1839–52. doi:10.1016/j.stemcr.2017.10.010

Schwartzentruber A, Boschian C, Lopes FM, Myszczynska MA, New EJ, Beyrath J, Smeitink J, Ferraiuolo L, Mortiboys H (2020) Oxidative switch drives mitophagy defects in dopaminergic parkin mutant patient neurons. Sci Rep 10:1–14. doi:10.1038/s41598-020-72345-4

Shahmoradian SH, Lewis AJ, Genoud C et al (2019) Lewy pathology in Parkinson's disease consists of crowded organelles and lipid membranes. Nat Neurosci 22:1099–109. doi:10.1038/s41593-019-0423-2

Shojaee S, Sina F, Banihosseini SS, Kazemi MH, Kalhor R, Shahidi GA, Fakhrai-Rad H, Ronaghi M, Elahi E (2008) Genome-wide Linkage Analysis of a Parkinsonian-Pyramidal Syndrome Pedigree by 500 K SNP Arrays. Am J Hum Genet 82:1375–84. doi:10.1016/j.ajhg.2008.05.005

Simmonds MA, Uretsky NJ (1970) Central effects of 6-hydroxydopamine on the body temperature of the rat. Br J Pharmacol 40:630–8. doi:10.1111/j.1476-5381.1970.tb10643.x

Smith MP, Cass WA (2007) Oxidative stress and dopamine depletion in an intrastriatal 6-hydroxydopamine model of Parkinson's disease. Neuroscience 144:1057–66. doi:10.1016/j.neuroscience.2006.10.004

Solé-Boldo L, Raddatz G, Schütz S, Mallm JP, Rippe K, Lonsdorf AS, Rodríguez-Paredes M, Lyko F (2020) Single-cell transcriptomes of the human skin reveal age-related loss of fibroblast priming. Commun Biol 3:1–12. doi:10.1038/s42003-020-0922-4

Szklarczyk D, Gable AL, Lyon D, Junge A, Wyder S, Huerta-Cepas J, Simonovic M, Doncheva NT, Morris JH, Bork P, Jensen LJ, Von Mering C (2019) STRING v11: Protein-protein association networks with increased coverage, supporting functional discovery in genome-wide experimental datasets. Nucleic Acids Res 47:D607–13. doi:10.1093/nar/gky1131

Tapias V, Hu X, Luk KC, Sanders LH, Lee VM, Greenamyre JT (2017) Synthetic alpha-synuclein fibrils cause mitochondrial impairment and selective dopamine neurodegeneration in part via iNOS-mediated nitric oxide production. Cell Mol Life Sci 74:2851–74. doi:10.1007/s00018-017-2541-x

Temelie M, Savu DI, Moisoi N (2018) Intracellular and intercellular signalling mechanisms following DNA damage are modulated by PINK1. Oxid Med Cell Longev 2018:1391387. doi:10.1155/2018/1391387

Terzioglu M, Galter D (2008) Parkinson's disease: Genetic versus toxin-induced rodent models. FEBS J 275:1384–91. doi:10.1111/j.1742-4658.2008.06302.x

Thiele SL, Warre R, Nash JE (2012) Development of a unilaterally-lesioned 6-OHDA mouse model of Parkinson's disease. J Vis Exp 60:3234. doi:10.3791/3234

Tieu K (2011) A Guide to Neurotoxic Animal Models of Parkinson's Disease. Cold Spring Harb Perspect Med 1:a009316. doi:10.1101/cshperspect.a009316

Toyofuku T, Okamoto Y, Ishikawa T, Sasawatari S, Kumanogoh A (2020) LRRK 2 regulates endoplasmic reticulum–mitochondrial tethering through the PERK -mediated ubiquitination pathway . EMBO J 39:1–19. doi:10.15252/embj.2018100875

Ungerstedt U (1968) 6-Hydroxy-dopamine induced degeneration of central monoamine neurons. Eur J Pharmacol 5:107–10. doi:10.1016/0014-2999(68)90164-7

Valente EM, Bentivoglio AR, Dixon PH, Ferraris A, Lalongo T, Frontali M, Albanese A, Wood NW (2001) Localization of a novel locus for autosomal recessive early-onset parkinsonism, PARK6, on human chromosome 1p35-p36. Am J Hum Genet 68:895–900. doi:10.1086/319522

Van Laar VS, Berman SB (2013) The interplay of neuronal mitochondrial dynamics and bioenergetics: implications for Parkinson's disease. Neurobiol Dis 51:43–55. doi:10.1016/j.nbd.2012.05.015

Vingill S, Connor-Robson N, Wade-Martins R (2018) Are rodent models of Parkinson's disease behaving as they should? Behav Brain Res 352:133–41. doi:10.1016/j.bbr.2017.10.021

Vyas I, Heikkila RE, Nicklas WJ (1986) Studies on the neurotoxicity of 1-methyl-4-phenyl-1,2,3,6-tetrahydropyridine: inhibition of NAD-linked substrate oxidation by its metabolite, 1-methyl-4-phenylpyridinium. J Neurochem 46:1501–7. doi:10.1111/j.1471-4159.1986.tb01768.x

Wang W, Wang X, Fujioka H, Hoppel C, Whone AL, Caldwell MA, Cullen PJ, Liu J, Zhu X (2016) Parkinson's disease-associated mutant VPS35 causes mitochondrial dysfunction by recycling DLP1 complexes. Nat Med 22:54–63. doi:10.1038/nm.3983

Wang X, Yan MH, Fujioka H, Liu J, Wilson-Delfosse A, Chen SG, Perry G, Casadesus G, Zhu X (2012) LRRK2 regulates mitochondrial dynamics and function through direct interaction with DLP1. Hum Mol Genet 21:1931–44. doi:10.1093/hmg/dds003

Wang, Becker K, Levine N, Zhang M, Lieberman AP, Moore DJ, Ma J (2019) Pathogenic alpha-synuclein aggregates preferentially bind to mitochondria and affect cellular respiration. Acta Neuropathol Commun 7:41. doi:10.1186/s40478-019-0696-4

Xicoy H, Wieringa B, Martens GJM (2017) The SH-SY5Y cell line in Parkinson's disease research: a systematic review. Mol Neurodegener 12:1–11. doi:10.1186/s13024-017-0149-0

Xu CY, Kang WY, Chen YM, Jiang TF, Zhang J, Zhang LN, Ding JQ, Liu J, Chen SD (2017) DJ-1 inhibits α-synuclein aggregation by regulating chaperone-mediated autophagy. Front Aging Neurosci 9:1–13. doi:10.3389/fnagi.2017.00308

Yang Y, Gehrke S, Imai Y, Huang Z, Ouyang Y, Wang JW, Yang L, Beal MF, Vogel H, Lu B (2006) Mitochondrial pathology and muscle and dopaminergic neuron degeneration caused by inactivation of Drosophila Pink1 is rescued by Parkin. Proc Natl Acad Sci U S A 103:10793–8. doi:10.1073/pnas.0602493103

Yuan XL, Guo JF, Shi ZH, Xiao ZQ, Yan XX, Zhao BL, Tang BS (2010) R492X mutation in PTEN-induced putative kinase 1 induced cellular mitochondrial dysfunction and oxidative stress. Brain Res 1351:229–37. doi:10.1016/j.brainres.2010.06.005

Zambon F, Cherubini M, Fernandes HJR et al (2019) Cellular α-synuclein pathology is associated with bioenergetic dysfunction in Parkinson's iPSC-derived dopamine neurons. Hum Mol Genet 28:2001–13. doi:10.1093/hmg/ddz038

Zanellati MC, Monti V, Barzaghi C, Reale C, Nardocci N, Albanese A, Valente EM, Ghezzi D, Garavaglia B (2015) Mitochondrial dysfunction in Parkinson disease: evidence in mutant PARK2 fibroblasts. Front Genet 6:78. doi:10.3389/fgene.2015.00078

Zdrazilova L, Hansikova H, Gnaiger E (2021) Comparable respiratory activity in attached and suspended human fibroblasts. MitoFit Preprints 2021.7. doi:10.26124/mitofit:2021-0007

Zhou H, Falkenburger BH, Schulz JB, Tieu K, Xu Z, Xia XG (2007) Silencing of the Pink1 gene expression by conditional RNAi does not induce dopaminergic neuron death in mice. Int J Biol Sci 3:242–50. doi:10.7150/ijbs.3.242

Zhou L, Wang W, Hoppel C, Liu J, Zhu X (2017) Parkinson's disease-associated pathogenic VPS35 mutation causes complex I deficits. Biochim Biophys Acta - Mol Basis Dis 1863:2791–5. doi:10.1016/j.bbadis.2017.07.032

Zhu JL, Wu YY, Wu D, Luo WF, Zhang ZQ, Liu CF (2019) SC79, a novel Akt activator, protects dopaminergic neuronal cells from MPP+ and rotenone. Mol Cell Biochem 461:81–9. doi:10.1007/s11010-019-03592-x

International Journal of
Molecular Sciences

MDPI

Article

Exercising *D. melanogaster* Modulates the Mitochondrial Proteome and Physiology. The Effect on Lifespan Depends upon Age and Sex

Brad Ebanks [1,†], Ying Wang [1,2,†], Gunjan Katyal [1], Chloe Sargent [3], Thomas L. Ingram [1], Antonia Bowman [1], Nicoleta Moisoi [4] and Lisa Chakrabarti [1,5,*]

[1] School of Veterinary Medicine and Science, University of Nottingham, Nottingham NG7 2RD, UK; mbybdpo@exmail.nottingham.ac.uk (B.E.); Wangying03@tyut.edu.cn (Y.W.); gunjan.katyal@nottingham.ac.uk (G.K.); Thomas.Ingram@md.catapult.org.uk (T.L.I.); svyab6@exmail.nottingham.ac.uk (A.B.)
[2] College of Biomedical Engineering, Taiyuan University of Technology, Taiyuan 030024, China
[3] School of Bioscience, University of Nottingham, Nottingham NG7 2RD, UK; stxcs17@exmail.nottingham.ac.uk
[4] Leicester School of Pharmacy, Leicester Institute for Pharmaceutical Innovation, De Montfort University, The Gateway, Leicester LE1 9BH, UK; nicoleta.moisoi@dmu.ac.uk
[5] MRC Versus Arthritis Centre for Musculoskeletal Ageing Research, Nottingham NG7 2RD, UK
* Correspondence: lisa.chakrabarti@nottingham.ac.uk
† These authors contributed equally to this work.

Citation: Ebanks, B.; Wang, Y.; Katyal, G.; Sargent, C.; Ingram, T.L.; Bowman, A.; Moisoi, N.; Chakrabarti, L. Exercising *D. melanogaster* Modulates the Mitochondrial Proteome and Physiology. The Effect on Lifespan Depends upon Age and Sex. *Int. J. Mol. Sci.* **2021**, *22*, 11606. https://doi.org/10.3390/ijms222111606

Academic Editor: Anna Atlante

Received: 24 September 2021
Accepted: 25 October 2021
Published: 27 October 2021

Publisher's Note: MDPI stays neutral with regard to jurisdictional claims in published maps and institutional affiliations.

Abstract: Ageing is a major risk factor for many of the most prevalent diseases, including neurodegenerative diseases, cancer, and heart disease. As the global population continues to age, behavioural interventions that can promote healthy ageing will improve quality of life and relieve the socioeconomic burden that comes with an aged society. Exercise is recognised as an effective intervention against many diseases of ageing, but we do not know the stage in an individual's lifetime at which exercise is most effective at promoting healthy ageing, and whether or not it has a direct effect on lifespan. We exercised w^{1118} *Drosophila melanogaster*, investigating the effects of sex and group size at different stages of their lifetime, and recorded their lifespan. Climbing scores at 30 days were measured to record differences in fitness in response to exercise. We also assessed the mitochondrial proteome of w^{1118} *Drosophila* that had been exercised for one week, alongside mitochondrial respiration measured using high-resolution respirometry, to determine changes in mitochondrial physiology in response to exercise. We found that age-targeted exercise interventions improved the lifespan of both male and female *Drosophila*, and grouped males exercised in late life had improved climbing scores when compared with those exercised throughout their entire lifespan. The proteins of the electron transport chain were significantly upregulated in expression after one week of exercise, and complex-II-linked respiration was significantly increased in exercised *Drosophila*. Taken together, our findings provide a basis to test specific proteins, and complex II of the respiratory chain, as important effectors of exercise-induced healthy ageing.

Keywords: mitochondria; ageing; exercise; *Drosophila*; respirometry; lifespan; proteomics

1. Introduction

The dramatic ageing of the global population is a well-documented phenomenon. The World Health Organisation estimates that there are currently over 900 million people over the age of 60, and by 2050 this is set to increase to 2 billion [1]. With this demographic transformation, there will be huge economic costs incurred due to the health and social care needs of this group, in particular with the increased occurrence of non-communicable diseases. Within the EU, it has been estimated that over-65s already account for over 40% of healthcare spending—a figure that will increase as this demographic continues to

expand [2]. It is therefore paramount that we develop a comprehensive understanding of the biology of ageing, and of how we can increase the healthspan of individuals as lifespans continue to rise.

Lifespan can be defined as the length of time between the birth and death of an individual; however, the definition of healthspan is different. One common definition of healthspan is 'healthspan is the period of life spent in good health, free from the chronic diseases and disabilities of ageing'; the potential pitfalls of this definition are clear [3]. In humans, females live longer average lifespans in populations with both shorter and longer life expectancies [4]. Furthermore, lifestyle considerations can also influence the outcomes of lifespan and healthspan, and these can include whether an individual lives a solitary or social lifestyle. When considering the sociality of animals and lifespan, those that are obligately social tend to have greater lifespans when they have more associates and stronger social bonds with those associates [5–8]; however, this benefit is not universal, and in particular there are differences for species with facultative sociality [9–11].

The biology of ageing itself is a complex picture, but has characteristic hallmarks: genomic instability, telomere attrition, epigenetic alterations, loss of proteostasis, deregulated nutrient sensing, mitochondrial dysfunction, cellular senescence, stem cell exhaustion, and altered intercellular communication [12]. Due to the central role that functional mitochondria play in metabolism and intracellular signaling [13–17], the regulation of apoptosis [18], and their well-documented dysfunction in a broad range of age-related pathologies [19–21], a fundamental understanding of their role in the ageing process will anchor developments in the field.

Exercise is recognised as being pivotal in the fight to keep individuals healthier for longer. While exercise has long been advocated as a broad-spectrum remedy against ill health, many of the molecular details that underpin this have remained elusive. However, as the weight of evidence for exercise as a protective strategy accumulates, our comprehension of how exercise extends lifespan is increasing [22]. These molecular changes are now known to include exercise-induced oxidative stress, in line with mitohormesis [23,24].

Drosophila are a viable model for both ageing and lifespan studies, as well as mitochondrial studies [25,26]. This is due to their well-understood genetics, the high proportion of homologous genes that they share with *H. sapiens*—including those implicated in disease—and their relative ease in husbandry. Examples of lifespan assays in *Drosophila* include their use to explore the effects of D-GADD45, Cu/ZnSOD, and MnSOD overexpression, as well as survival outcomes [27,28]. However, lifespan assays have more traditionally been used in human and mammalian studies. Landmark mitochondrial studies in *Drosophila* were those that presented mechanistic evidence of PINK1 and parkin dysfunction in Parkinson's disease [29–31].

Proteomics is the study of the entire complement of proteins present within a biological sample [32,33]. In this instance, we focused on the proteome of the mitochondrion, facilitating a deep evaluation of the physiology of the mitochondrion in both health and disease.

While it is recognised that exercise is an effective means of delaying the onset of certain hallmarks of ageing, and in preventing the onset of diseases of ageing, there is less certainty around how exercise should be applied as an intervention, or which molecular mechanisms are modulated to influence the ageing process. In this study, we explored exercise interventions at different stages of life for *Drosophila*, and recorded how this affected their probability of survival, plotting Kaplan–Meier survival curves with log-rank test analysis. To assess sex differences and the effects of a grouped or solitary lifestyle, we exercised female and male flies that were housed singly, as well as in groups of females and males. Climbing assay scores at 30 days were also measured to assess age-associated fitness correlated with exercise. To understand the molecular changes that are associated with differences in survival outcomes, we assessed the mitochondrial proteome via 2D gel electrophoresis coupled with mass spectrometry (2DE-MS) and label-free mass spectrometry of *Drosophila* that had been exercised for one week. We measured

mitochondrial fitness via high-resolution respirometry to specifically reveal mitochondrial responses to exercise.

2. Materials and Methods

2.1. Fly Husbandry

We used the *Drosophila melanogaster* strain w^{1118}. Fly food (Quick Mix Medium, Blades Biological) was added to the vial, to a depth of 1 cm, and 3 mL of distilled water was added; it was left for one minute, and then a small sprinkle of yeast was added. The singly housed *Drosophila* from further trials were given the same amount of food as those kept in groups. *Drosophila* were transferred to new food once a week, and were kept in an incubator at 25 °C. Food was kept hydrated with 150 µL of distilled water every day. When food became dry or the flies laid eggs, they were moved to a new vial and transferred back following food rehydration. The light cycle varied depending on when lights were turned off/on in the laboratory, but was generally a 12-h cycle. The study was reviewed and approved by the University of Nottingham SVMS local area ethics committee (#3091 200203 10 February 2020).

2.2. Fly Separation

Flies in glass vials were cooled on ice for 5–10 min, placed under a microscope to determine sex, and then placed into vials accordingly. The groups consisted of 20 flies in each vial. These were labelled GF/GM for exercised group females/males. Ten individual flies of known sex were placed in separate vials, labelled SF/SM for single females/males. Two cohorts of flies were exercised in independent experiments, and the datasets for the two cohorts were then pooled for the statistical analysis of the lifespan assay.

2.3. Exercise Regime

The methodology for the exercise regime was modified from the protocol used by Tinkerhess et al. [34]. The exercise machine utilised a power tower strategy that taps the flies down every 15 s to induce negative geotaxis behaviour. The flies were exercised within a 25 °C incubator. The flies were transferred to empty vials during the exercise sessions. Flies were exercised at 10:30 a.m. for 10 min on Mondays, Wednesdays, and Fridays, with a two-day rest on Saturdays and Sundays.

For lifespan assay, flies were subjected to one of the following five exercise regimes: lifetime exercise (weeks 1–6 of life), early-life exercise (weeks 1–2 of life), middle-life exercise (weeks 3–4 of life), late-life exercise (weeks 5–6 of life), or no exercise.

For proteomic analysis, mixed-sex flies that were 1–4 days post-eclosion were placed in vials of 20 flies and exercised for one week before being euthanized by freezing at −80 °C, one hour after the final exercise period.

2.4. Mortality

Deaths were recorded throughout the experiment. Mortality was analysed using GraphPad Prism 8 by inputting data into Kaplan–Meier survival graphs. Log-rank tests ($p < 0.05$) were carried out between groups of interest.

2.5. Climbing Assay

A modified power tower protocol was used to perform a 'RING assay' [35]. Flies were moved into empty vials, and images were taken 4 s after the frame had been tapped down. A climbing index score was calculated by multiplying the number of flies per quadrant score and dividing by the number of flies in the vial. Movie Player Classic was used to create frames to analyse, edited in Microsoft Paint to add lines and distinguish the 4 quadrants. A mean was calculated ($n = 6$), and unpaired *t*-tests were performed between means of different groups 30 days into their lifespan, using GraphPad Prism.

2.6. Tissue Preparation for HRR

High-resolution respirometry (HRR) analysis was carried out on the sixth day after the start of the exercise or control treatment. To prepare the tissue, flies were cooled on ice. before five were randomly chosen and mechanically homogenised in 500 µL of MiR05 buffer (Oroboros Instruments; 0.5 mM EGTA, 3 mM $MgCl_2$, 60 mM lactobionic acid, 20 mM taurine, 10 mM KH_2PO_4, 20 mM HEPES, 110 mM D-sucrose, 1 g/L BSA, pH 7.1). The homogenate was briefly spun, and only the supernatant was used in order to exclude non-cellular debris. The sample was kept on ice until HRR analysis.

2.7. High-Resolution Respirometry

HRR was carried out using the Oroboros Oxygraph-2k (Oroboros® Instruments, Innsbruck, Austria). The electrodes were calibrated daily to ensure that oxygen consumption was consistent, and analysis was carried out at 20 °C. A total of 100 µL of the fly homogenate was added to each chamber before the following substrates were added: (1) 5 µL and 10 µL of the complex I substrates, pyruvate and malate, respectively (5 mM and 2 mM, respectively); (2) 20 µL of 10 mM succinate—a complex II substrate; (3) 1 µL titrations of 0.5 µM CCCP; and, finally, (4) 1 µL of 2.5 µM antimycin A—a complex III inhibitor.

2.8. Mitochondrial Preparation

Flies were placed in 250 µL of mitochondrial isolation buffer, and then subjected to 5 min of manual homogenisation with a 1.2–2.0 mL Eppendorf micropestle. Fractions were obtained using protocols described previously [36].

2.9. 2D Gel Electrophoresis (2D–PAGE)

Drosophila mitochondrial fractions and whole-fly homogenates were subjected to isoelectric focusing using the ZOOM IPG system and pH 3–10 (non-linear) ZOOM IPG strips following the manufacturer's protocol (Life Technologies, Carlsbad, CA, USA). Gels were stained and imaged before analysis with SameSpots software (one-way ANOVA). Spots identified with SameSpots were excised from the gel for proteomic analysis.

2.10. Matrix-Assisted Laser Desorption Ionization Tandem Time-of-Flight Mass Spectrometry (MALDI–TOF/MS)

Samples identified with SameSpots were excised from the 2D gel, and were analysed at the Centre of Excellence in Mass Spectrometry at the University of York. Proteins were reduced and alkylated, followed by in-gel digestion with trypsin. MALDI–TOF/MS was used to analyse the samples. The generated tandem MS data were compared against the NCBI database using the MASCOT search program to identify the proteins. De novo sequence interpretation for individual peptides was inferred from peptide matches.

2.11. Liquid Chromatography Tandem Mass Spectrometry (LC–MS/MS)

Following separation with SDS-PAGE (NuPAGE™ 4 to 12%, Bis-Tris, 1.0 mm, Mini Protein Gel, 12-well) according to the manufacturer's protocols, the gel-resolved mitochondrial fractions were analysed at the Centre of Excellence in Mass Spectrometry at the University of York. Proteins were reduced and alkylated, followed by in-gel digestion with trypsin. LC–MS/MS was used to analyse the samples. Resulting LC–MS/MS data were imported in PEAKS Studio X for peak picking, peptide identification, and precursor-intensity-based relative protein quantification. Extracted tandem MS data were searched against the combined *D. melanogaster* and *S. cerevisiae* subsets of the UniProt database. Protein identifications were filtered to achieve a <1% false discovery rate (FDR), and to require a minimum of two unique peptides per protein group.

For relative label-free quantification, extracted ion chromatograms for identified peptides were extracted and integrated for all samples. Protein abundances were normalised between samples on the basis of the total area of identified peptide ions. Significance was established using the PEAKSX interpretation of the significance of the B model. The

multiple tests corrected FDR thresholds. A −log10 p value > 23.52 (1% FDR) was deemed significant using the model.

2.12. Bioinformatic Analyses

To state that a protein had significant changes in abundance between the exercised and non-exercised groups, we developed the following criteria: the protein must be quantified in all three biological replicates, and the relative abundance ratios (RAR (exercise/non-exercise)) must be either <0.67 or >1.5 and have a −log10 p value > 23.52. Proteins that were not quantified in more than one biological triplicate in only one of the treatment groups were also noted as being of interest.

Two representative heatmaps were developed: one for proteins with increased abundance (RAR > 1.5), and one for proteins with decreased abundance (RAR < 0.67) post-exercise. All three biological replicates for each group were included, with relative abundances depicted using a red-to-blue (high-to-low relative abundance) colour gradient. Proteins were further analysed using the STRING database v.11.0 to examine functional relationships between proteins significantly different in abundance between the exercised and non-exercised groups. The platform was used to create two protein–protein interaction (PPI) networks. To narrow down proteins of interest, those with no associated interactions in the network were hidden, and protein nodes were coloured based on their biological process, molecular function, and cellular component designation as per Gene Ontology (GO) and UniProt annotation.

3. Results

3.1. In Males, Late-Life Exercise Has the Most Beneficial Effect, and Exercise throughout Life Is Detrimental in Comparison

Male *Drosophila* exercised throughout their lifetime had worse survival outcomes when compared with groups of males exercised at any other age or not exercised at all.

Grouped male *Drosophila* that were exercised throughout their lifetime had a worse probability of survival than those that were exercised in early life, middle life, or late life, as well as those that were not exercised at all (Figure 1A–D). Grouped male *Drosophila* that were exercised in middle life had an improved probability of survival compared with those that were not exercised at all (Figure 1E). Only single male *Drosophila* that were exercised during late life had an improved survival probability compared with those exercised throughout their lives (Figure 1F), which was also observed in the grouped male flies.

In groups of female Drosophila, age-targeted exercise was more beneficial than lifetime exercise; late-life exercise extended lifespan in individually housed female individuals.

Grouped female *Drosophila* exercised in early, middle, and late life had an increased probability of survival compared with those that were exercised throughout their lives (Figure 2A–C). As observed in male *Drosophila*, the single females that were exercised in late life also had an improved probability of survival compared with those that were exercised throughout their lives (Figure 2D). Single females that were not exercised at all also had an increased probability of survival compared with flies that were exercised throughout their lifetimes (Figure 2E), as well as those exercised in early life (Figure 2F).

When the climbing scores at 30 days were assessed for the *Drosophila* lifespan assay data in Figures 1 and 2, we found that there were significant differences in climbing score outcomes (Figure 3). Flies that were exercised in the middle of their lives, along with flies not exercised at all, had lower climbing scores than flies that been exercised throughout their lifetimes. However, flies exercised in late life had improved climbing scores compared with those exercised throughout their lifetimes, correlating with the improved lifespan assay outcomes.

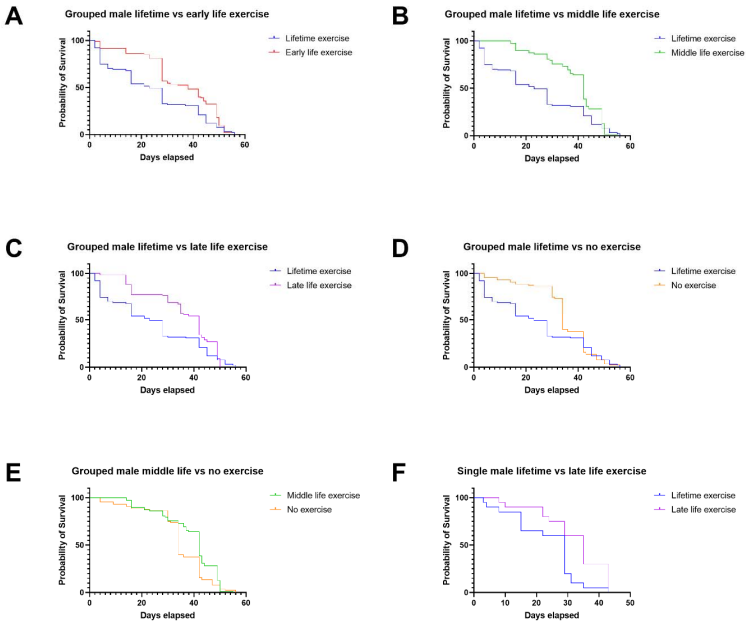

Figure 1. Percentage probability of survival for grouped and single male flies: (**A**) Grouped male flies' lifetime exercise vs. early-life exercise (n = 93, 95, respectively) (log-rank test p = 0.0011). (**B**) Grouped male lifetime vs. middle-life exercise (n = 93, 78, respectively) (log-rank test p = 0.0014). (**C**) Grouped male lifetime vs. late-life exercise (n = 93, 121, respectively) (log-rank test p = 0.0050). (**D**) Grouped male lifetime vs. no exercise (n = 93, 87, respectively) (log-rank test p = 0.0237). (**E**) Grouped male middle-life vs. no exercise (n = 78, 87, respectively) (log-rank test p = 0.0125). (**F**) Single male lifetime vs. late-life exercise (n = 20, 20, respectively) (log-rank test p = 0.0053).

3.2. High-Resolution Respirometry of Exercised Drosophila

The flux control ratio (FCR) is an internal normalization of a given respiratory rate; It takes the ratio of the measured respiratory rate and the maximal uncoupled electron transport (ET) capacity of the mitochondria. We found a significant difference in the mean FCR of exercised and non-exercised flies when succinate—a complex II substrate—was added after the addition of pyruvate and malate (0.32 and 0.13, respectively; student's *t*-test *p*-value = 0.025). Furthermore, the mean ET capacity was significantly greater in non-exercised flies compared to the exercised flies (42.55 and 14.27, respectively; Student's *t*-test *p*-value = 0.002) (Figure 4, Table 1).

The spare respiratory capacity (SRC) is calculated as a relative value by (ET capacity specific flux)/(Routine specific flux * 100), where the SRC for non-exercised and exercised flies is 0.39 and 0.26, respectively.

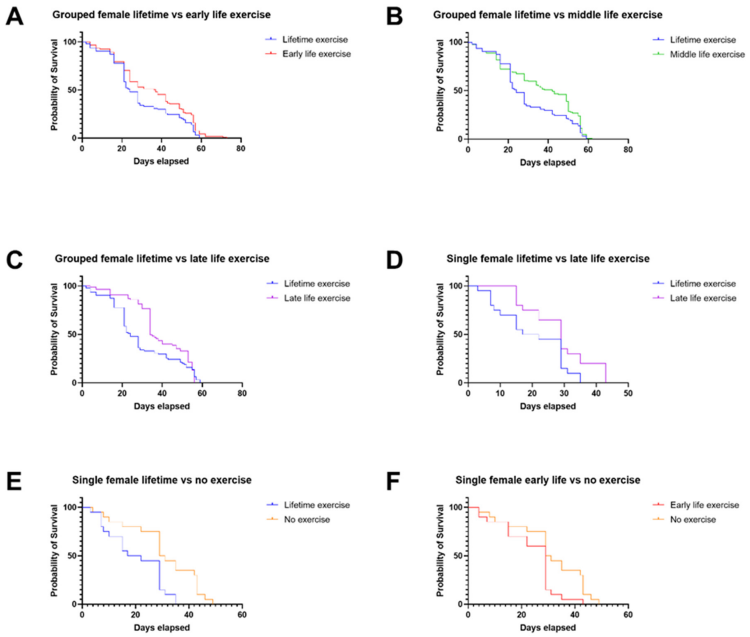

Figure 2. Percentage probability of survival for grouped and single female flies: (**A**) Grouped female lifetime vs. early-life exercise (n = 94, 121, respectively) (log-rank test p = 0.0094). (**B**) Grouped female lifetime vs. middle-life exercise (n = 94, 127, respectively) (log-rank test p = 0.0141). (**C**) Grouped female lifetime vs. late-life exercise (n = 94, 85, respectively) (log-rank test p = 0.0241). (**D**) Single female lifetime vs. late-life exercise (n = 20, 20, respectively) (log-rank test p = 0.0202). (**E**) Single female lifetime vs. no exercise (n = 20, 20, respectively) (log-rank test p = 0.0025). (**F**) Single female early-life vs. no exercise (n = 20, 20, respectively) (log-rank test p = 0.0202).

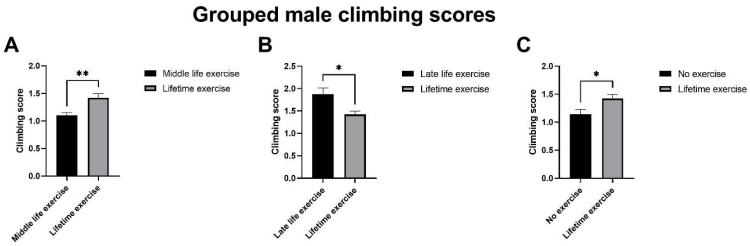

Figure 3. Grouped male Drosophila under different exercise regimens produced different climbing scores when compared with lifetime exercise: (**A**) Lifetime exercise vs. middle-life exercise (n = 6) (unpaired t-test, p = 0.0051, ** = <0.01). (**B**) Lifetime exercise vs. late-life exercise (n = 6) (unpaired t-test, p = 0.0183, * = < 0.05). (**C**) Lifetime exercise vs. no exercise (n = 6) (unpaired t-test, p = 0.0344, * = < 0.05).

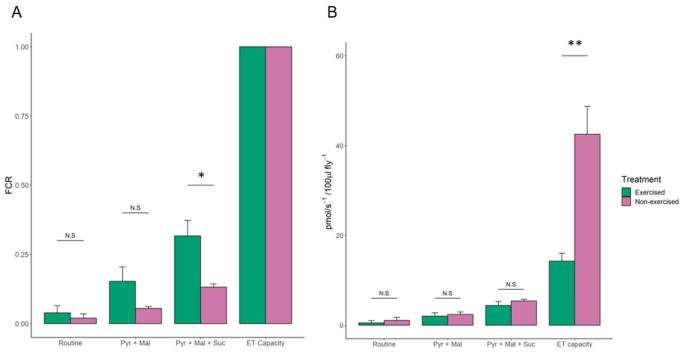

Figure 4. (**A**) Flux control ratio (FCR), in exercised and non-exercised male *D. melanogaster*; and (**B**) specific flux oxygen consumption in exercised and non-exercised male *D. melanogaster* (n = 3). Significant p-values: (**A**) succinate p-value = 0.025; (**B**) ET capacity p-value = 0.002. N.S = >0.05, * = <0.05, ** = < 0.01.

Table 1. Mean values of the specific flux and flux control ratio in exercised and non-exercised male *D. melanogaster* seen in Figure 4 (n = 3, * = p < 0.05; ** = p < 0.01). p-values from unpaired Student's t-tests.

Stage	Exercised n = 5 Mean (s.e)	Non-Exercised n = 4 Mean (s.e)	p-Value
Routine			
Specific flux	0.55 (0.48)	1.08 (0.70)	0.537
FCR	0.04 (0.03)	0.02 (0.02)	0.58
Pyruvate & Malate			
Specific flux	2.04 (0.70)	2.41 (0.54)	0.699
FCR	0.15 (0.05)	0.05 (0.01)	0.143
Succinate			
Specific flux	4.40 (0.89)	5.39 (0.35)	0.381
FCR	0.32 (0.06)	0.13 (0.01)	0.025 *
ET capacity			
Specific flux	14.27 (1.77)	42.55 (6.19)	0.002 **

3.3. There Is Increased Expression of Many Proteins in Response to Exercise, including Those of the Electron Transport Chain

The 2DE-MS method was used as a scoping technique to identify proteins of interest based on changes in their expression in response to exercise, as well as considering the effects of group size and sex of the flies (Supplementary Tables S1 and S2). Label-free mass spectrometry was then used to determine differences in the expression of mitochondrial proteins after *Drosophila* had been exercised for one week. A total of 515 proteins were identified and quantified in relation to the whole sample.

Of the 515 proteins identified, 424 had significant differences in abundance between the groups that were analysed (>23.52 −log10P, >1% FDR). A total of 337 proteins were quantified in all three replicates of the exercised and non-exercised fly groups. It should be noted that one biological replicate from the exercised *Drosophila* group had less total protein than the other samples, but normalisation procedures compensated for this, and there was no notable effect on the results. Of the 337 commonly identified proteins, 51 had

increased expression (RAR > 1.5) in response to exercise, with some intra-replica variation observed (Figure 5).

Using UniProt and Gene Ontology (GO) annotation for cellular component assignment, we found that 27 of the 51 proteins with increased expression in response to exercise localise to the mitochondria. The other proteins were from either the cytoplasm or other membrane-bound organelles, with likely close association with mitochondria resulting in their presence in the mitochondrial isolates.

Of the 27 mitochondrial proteins identified by GO:CC enrichment analysis, 24 are associated with the electron transport chain: 14 from complex I, 3 from complex III, 6 from complex IV, and 1 from cytochrome c-2 (Table 2).

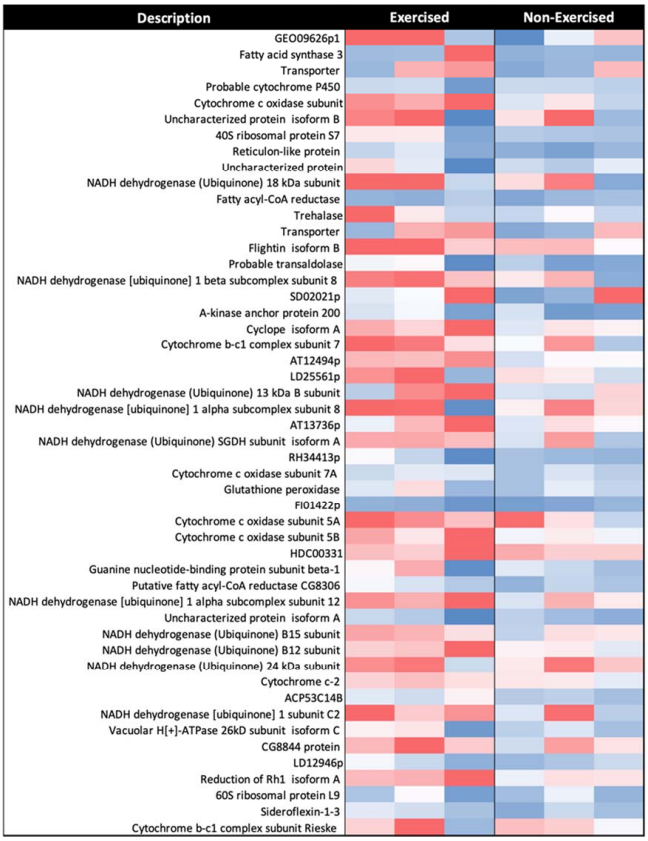

Figure 5. Representative heatmap of mitochondrial proteins with increased abundance (RAR of >1.5) after 1 week of exercise in *D. melanogaster* ($n = 3$). Red-to-blue colour gradient represents high-to-low relative protein abundance. The proteomic approach used was label-free mass spectrometry. All proteins listed were classified as significant as per the criteria described in the results.

Table 2. Electron transport chain proteins increased in abundance in response to one week of exercise in *D. melanogaster* (n = 3). Enrichment analysis used Gene Ontology cellular component allocation from STRING database v.11.0. RAR: relative abundance ratio; FC: fold change.

Description		Accession	Significance (−log10P)	RAR	Log2 FC
Complex I					
NADH dehydrogenase (ubiquinone)	1Subunit C2	Q9VQM2	200	1.53	0.61
	1 Beta subcomplex subunit 8 mitochondrial	Q9W3X7	133.11	1.85	0.89
	1 Alpha subcomplex subunit 8	Q9W125	142.39	1.68	0.74
	1 Alpha subcomplex subunit 12	Q9VQD7	200	1.57	0.65
	SGDH subunit isoform A	Q9VTU2	86.17	1.64	0.71
	B15 subunit	Q6IDF5	36.57	1.56	0.64
	B12 subunit isoform A	Q9W2E8	88.95	1.55	0.64
	24 kDa subunit isoform A	Q9VX36	65.53	1.54	0.63
	18 kDa subunit	Q9VWI0	200	2.05	1.04
	13 kDa Bsubunit	Q9VTB4	78.35	1.69	0.76
	GEO09626p1	Q8SYJ2	26.03	2.92	1.55
	EG:152A3.7 protein	O97418	29.75	1.9	0.93
	CG8844 protein	Q9VQR2	200	1.53	0.61
	AT12494p	Q9VJZ4	70.67	1.7	0.77
Complex III					
Cytochrome b-c1 complex	Subunit Rieske mitochondrial	Q9VQ29	80.35	1.5	0.59
	Subunit 7	Q9VXI6	200	1.73	0.79
	AT13736p	Q9VVH5	129.49	1.65	0.72
Complex IV					
	Cyclope isoform A	Q9VMS1	200	1.78	0.83
Cytochrome C oxidase	Cytochrome C oxidase subunit	Q8IQW2	200	2.14	1.1
	Subunit 7A mitochondrial	Q9VHS2	82.59	1.61	0.69
	Subunit 5A mitochondrial	Q94514	110.61	1.6	0.68
	Subunit 5B isoform A	Q9VMB9	140.51	1.59	0.67
	GEO09626p1	Q8SYJ2	26.03	2.92	1.55
Other OXPHOS proteins					
	HDC00331	Q6IHY5	200	1.58	0.66
	Uncharacterized protein isoform A	Q0KHZ6	93.18	1.56	0.64
	Cytochrome c-2	P84029	38.14	1.54	0.62

3.4. A Subset of Mitochondrial Proteins Decreased in Response to One Week of Exercise in D. melanogaster

Of the 337 commonly identified proteins from the mitochondrial fraction, across all replicates from the exercise and non-exercise fly groups, there were 36 proteins that had significantly decreased expression in response to exercise (RAR < 0.67) (Figure 6).

Gene Ontology biological process (GO:BP) enrichment analysis with the STRING database v.11.0. identified that, among the proteins with significantly decreased expression in response to exercise, there was enrichment of a diverse range of metabolic pathways (Table 3). These pathways included the ATP metabolic process, the TCA cycle, the pyruvate metabolic process, the cellular amino acid metabolic process, the carboxylic acid metabolic process, and chaperone-mediated protein folding.

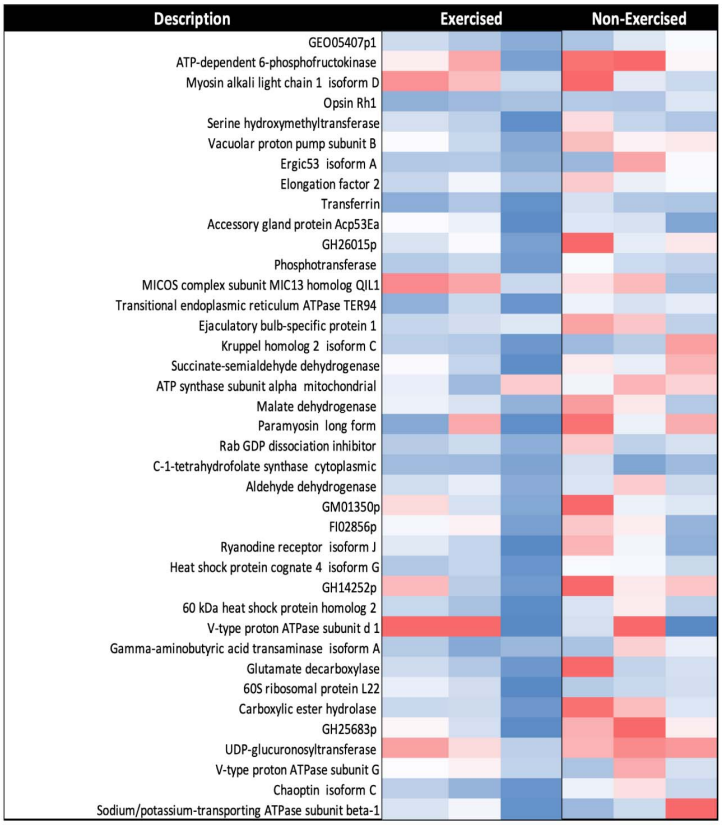

Figure 6. Representative heatmap of mitochondrial proteins with decreased abundance (RAR < 0.67) in response to one week of exercise in *D. melanogaster* ($n = 3$). Red-to-blue colour gradient represents high-to-low relative protein abundance. Proteomic analysis was conducted using label-free mass spectrometry. All proteins listed were classified as significant as per the criteria described in the results.

Table 3. Proteins identified from the mitochondrial fraction with decreased expression in response to exercise, with Gene Ontology biological process enrichment, as determined by STRING database v.11.0. analysis. Enrichment of a diverse range of metabolic processes was identified among the proteins with decreased expression. RAR: relative abundance ratio; FC: fold change.

Description	Accession	Significance (−log10P)	RAR	Log2 FC
ATP metabolic process				
ATP synthase subunit alpha mitochondrial	P35381	84.91	0.62	−0.68

Table 3. *Cont.*

Description	Accession	Significance (−log10P)	RAR	Log2 FC
TCA cycle				
GM01350p	Q9VGQ1	32.66	0.58	−0.78
Malate dehydrogenase	Q9VKX2	56.18	0.62	−0.68
Pyruvate metabolic process				
Aldehyde dehydrogenase	Q9VLC5	38.53	0.59	−0.76
Cellular amino acid metabolic process				
Succinate-semialdehyde dehydrogenase	Q9VBP6	77.81	0.63	−0.67
Gamma-aminobutyric acid transaminase isoform A	Q9VW68	200	0.52	−0.94
Serine hydroxymethyltransferase	Q9W457	200	0.66	−0.59
Carboxylic acid metabolic process				
GM01350p	Q9VGQ1	32.66	0.58	−0.78
Aldehyde dehydrogenase	Q9VLC5	38.53	0.59	−0.76
Malate dehydrogenase	Q9VKX2	56.18	0.62	−0.68
Serine hydroxymethyltransferase	Q9W457	200	0.66	−0.59
Succinate-semialdehyde dehydrogenase	Q9VBP6	77.81	0.63	−0.67
Gamma-aminobutyric acid transaminase isoform A	Q9VW68	200	0.52	−0.94
Chaperone-mediated protein folding				
Heat shock protein cognate 4 isoform G	C7LA75	153.53	0.58	−0.8
60 kDa heat shock protein homolog 2 mitochondrial	Q9VMN5	200	0.55	−0.87
Other mitochondrial proteins				
MICOS complex subunit MIC60	A0A0B4KGN2	27.65	0.64	−0.65

4. Discussion

4.1. Lifetime Exercise Has Worse Outcomes Than Targeted Exercise Interventions in Male and Female Drosophila

A consistent theme in our findings was the poor lifespan outcomes for both male and female *Drosophila* that were exercised throughout their lifetimes, as opposed to targeted interventions (Figure 1A–C,F and Figure 2A–D), or in some instances no exercise at all (Figures 1D and 2E). It could be suggested that lifetime exercise of the flies could produce injury or exhaustion, leading to early mortality. In the case of single female flies, where no exercise at all had better lifespan outcomes than lifetime exercise, this theory is worth consideration.

Mechanistically, it is well understood that acute exercise induces oxidative stress through the generation of reactive oxygen species (ROS), which according to the mitohormetic explanation induce healthy levels of activity in cellular antioxidant responses [37]. The field has now moved away from the idea of oxidative stress being only detrimental with regards to ageing, with a more nuanced argument around low levels of oxidative stress and ageing [38]. However, it is also recognised that excessive levels of oxidative stress can contribute to the ageing process, so it may be the case that over-exercise—in this instance, lifetime exercise—results in detrimental levels of oxidative stress being produced as a cellular response, ultimately contributing to the early mortality of these flies [39,40]. As with every drug, the dose makes the poison.

It is noteworthy that, at 30 days in the lifespan assay, there was a large difference in the probability of survival for grouped male and female flies that were exercised throughout their lifetimes, compared with those that were subjected to targeted exercise interventions (Figure 1A–C and Figure 2A–C). This suggests that excessive, lifetime exercise can increase the risk of early mortality in the flies. Then, from the 30-day mark onward, the probability of

survival in these groups falls to similar levels, which indicates that many of the detrimental effects of consistent exercise take place early in the lifespans of the flies.

4.2. Late-Life Exercise Produces a Rapid Improvement in Climbing Assay Scores Compared with Life-Time Exercise for Grouped Male Drosophila

Middle-life exercise, late-life exercise, and no exercise all produced significantly different climbing assay scores compared with lifetime exercise for grouped male *Drosophila* (Figure 3). When the difference seen between the 'late life vs. lifetime' and 'no exercise vs. lifetime' graphs is considered, it is striking given that the 'late-life exercise group' had only been subject to three days of exercise to this point. One possible explanation for this large swing in climbing scores in response to just three days of exercise is that there is a rapid, adaptive response to exercise. It has previously been observed that male *Drosophila* have a greater adaptive response to exercise than females, in age-matched 5-day-old flies [41]. It could be the case that the male flies exercised later in life also exhibit a rapid adaptive response to a similar, short amount of exercise training, which is no longer obvious after longer term exercise.

4.3. Succinate-Linked Respiration Is Elevated in Exercised Flies

We found that daily exercise in *D. melanogaster* significantly increases oxygen flux when succinate is supplied, compared with non-exercised flies (Figure 4). Succinate—a complex II substrate—is less efficient in producing ATP than complex-I-associated substrates (pyruvate and malate), as complex II does not pump protons that contribute to the electrochemical gradient. However, when ATP demand is high—such as during exercise—succinate may be an important substrate to help increase the ETC efficiency, due to complex I substrates being more rapidly diminished.

Succinate has been previously shown to be a respiratory substrate utilised during stress [42,43]. In the bumblebee, *Bombus terrestris*, succinate oxidation has been shown to cause a twofold increase in flight muscle mitochondria after a one-hour flight [42]. It is well established that exercise can induce an acute stress response; this resonates with our findings and the association between exercise, increased succinate oxidation, and complex II activity.

4.4. Reduced Spare Respiratory Capacity in Exercised Drosophila May Promote Longevity

Exercised flies had a significantly lower maximum electron transport chain capacity (ET capacity) compared to non-exercised flies (p-value = 0.002). Furthermore, the spare respiratory capacity (SRC)—described as the mitochondrial capacity to produce ATP beyond routine respiration—was higher in the non-exercised flies [44]. This suggests that non-exercised flies use a lower percentage of their maximum respiratory capacity to maintain routine respiration. This is in contrast to the findings of previous studies, as exercise is acknowledged to improve mitochondrial function [45].

One explanation for the lower SRC in the exercised flies could be due to acute stress induced by exercise, as low SRC has been associated with poor adaptation to stress and an inability to meet ATP demands [44]. However, the ability to meet the energetic requirements of the cell by utilising oxidative phosphorylation to the fullest extent before resorting to anaerobic means could be considered advantageous later in life, in that 'if you don't use it, you lose it'. Measurements are needed of acute and longer term exercise cohorts, for purposes of comparison.

4.5. Proteins from the Electron Transport Chain Are Significantly Upregulated in Response to Exercise

Proteomic analysis of mitochondria from flies that had been exercised for one week, 1–4 days post-eclosion, showed higher quantities of mitochondrial electron transport chain proteins (Table 2 and Supplementary Figure S1). This could be a means of maximising the efficiency of the aerobic respiration that initially takes place during exercise during the transition to anaerobic respiration [46]. Enzymatic activities of the electron transport chain

are decreased during the ageing process as markers of oxidative stress increase [47]. This may be a simplistic view, since Tavallaie et al. reported that administration of a moderate inhibitor of complex IV promoted mitochondrial fitness in C57BL/6J mice, suggesting that this may be used to mitigate metabolic syndromes of ageing in humans [48]. It is possible that an upregulated electron transport chain corresponds to greater mitochondrial fitness, which would be beneficial in the context of ageing.

4.6. Multiple Metabolic Pathways Are Downregulated in Response to Exercise

Enrichment analysis of proteins that were downregulated in the mitochondrial fraction after exercise pointed to a broad range of metabolic pathways (Table 3 and Figure S2). While it is difficult to suggest a direct link between these pathways and their decreased activity in exercise, the variety of pathways identified could simply reflect the cellular conservation and resource redirection that takes place during exercise-induced stress. The enrichment of chaperone-mediated protein folding proteins—specifically heat shock protein cognate 4 isoform G, and 60 kDa heat shock protein homolog 2 mitochondrial—may reflect a reduced rate of protein synthesis, which would also support this hypothesis. The identification of heat shock proteins is interesting, as these are connected with failed proteostasis—one of the hallmarks of ageing [12,49].

5. Conclusions

We found that targeted exercise, as opposed to lifetime exercise, produces better survival outcomes in male and female *Drosophila*. Exercise has a rapid and significant effect on mitochondrial physiology, as seen through changes in the ETC of fruit flies. Through proteomic analysis, we found that components of the electron transport chain are upregulated in response to exercise, while a variety of other metabolic pathways show decreased expression. We suggest that exercise causes increased utilisation of mitochondrial pathways, thus leading to better healthspan.

Supplementary Materials: The following are available online at https://www.mdpi.com/article/10.3390/ijms222111606/s1.

Author Contributions: B.E. and Y.W. performed data analysis, performed the experiments, and wrote the manuscript; T.L.I. performed experimental work and helped prepare the manuscript; G.K. performed STRING analyses and helped prepare the manuscript; A.B. conducted the initial proteomics analyses; C.S. generated respirometry data and helped with writing; N.M. generated the flies used for these experiments, and was consulted on all aspects of the fly work; L.C. directed the research, supervised experiments, provided reagents, and prepared the manuscript. All authors have read and agreed to the published version of the manuscript.

Funding: This work was supported by the Biotechnology and Biological Sciences Research Council (grant number BB/J014508/1), via awards to B.E. and T.L.I. G.K. is supported by a University of Nottingham Vice Chancellor's International Scholarship award. C.S. is supported by a University of Nottingham and Rothamsted Institute 'Future Foods' doctoral scholarship. Y.W. is supported by China Scholarship Fund (CSC201806935060). N.M. and L.C. are funded by HEFCE.

Institutional Review Board Statement: Not applicable.

Informed Consent Statement: This proposal has been reviewed by the School's Committee for Animal Research and Ethics (CARE) and responses have been received from at least four members of the panel. No ethical issues were raised by the panel and I confirm the ethical approval of this work (assigned #.3091 200203).

Data Availability Statement: Please contact corresponding author.

Acknowledgments: We are grateful to John R Ingram for the construction of the ICE exercise machine which was used to exercise the flies and has been described in a previous manuscript. We would like to thank Hannah Belli and Michalis Borakis for their initial efforts towards statistical analysis of the lifespan and climbing assays.

Conflicts of Interest: The authors declare they have no conflict of interest.

References

1. Mitchell, E.; Walker, R. Global ageing: Successes, challenges and opportunities. *Br. J. Hosp. Med.* **2020**, *81*, 1–9. [CrossRef]
2. Marešová, P.; Mohelská, H.; Kuča, K. Economics Aspects of Ageing Population. *Procedia Econ. Financ.* **2015**, *23*, 534–538. [CrossRef]
3. Kaeberlein, M. How healthy is the healthspan concept? *GeroScience* **2018**, *40*, 361–364. [CrossRef] [PubMed]
4. Austad, S.N. Sex Differences in Longevity and Aging. In *Handbook of the Biology of Aging*; Elsevier: Amsterdam, The Netherlands, 2011; pp. 479–495.
5. Brent, L.J.N.; Ruiz-Lambides, A.; Platt, M.L. Family network size and survival across the lifespan of female macaques. *Proc. R. Soc. B Boil. Sci.* **2017**, *284*, 20170515. [CrossRef]
6. Stanton, M.A.; Mann, J. Early Social Networks Predict Survival in Wild Bottlenose Dolphins. *PLoS ONE* **2012**, *7*, e47508. [CrossRef]
7. Silk, J.B.; Beehner, J.; Bergman, T.J.; Crockford, C.; Engh, A.L.; Moscovice, L.R.; Wittig, R.M.; Seyfarth, R.M.; Cheney, D.L. Strong and Consistent Social Bonds Enhance the Longevity of Female Baboons. *Curr. Biol.* **2010**, *20*, 1359–1361. [CrossRef]
8. Holt-Lunstad, J.; Smith, T.B.; Layton, J.B. Social Relationships and Mortality Risk: A Meta-analytic Review. *PLoS Med.* **2010**, *7*, e1000316. [CrossRef] [PubMed]
9. Brouwer, L.; Richardson, D.S.; Eikenaar, C.; Komdeur, J. The role of group size and environmental factors on survival in a cooperatively breeding tropical passerine. *J. Anim. Ecol.* **2006**, *75*, 1321–1329. [CrossRef] [PubMed]
10. Gager, Y.; Gimenez, O.; O'Mara, M.T.; Dechmann, D.K.N. Group size, survival and surprisingly short lifespan in socially foraging bats. *BMC Ecol.* **2016**, *16*, 2. [CrossRef]
11. Blumstein, D.T.; Williams, D.M.; Lim, A.N.; Kroeger, S.; Martin, J. Strong social relationships are associated with decreased longevity in a facultatively social mammal. *Proc. R. Soc. B Boil. Sci.* **2018**, *285*, 20171934. [CrossRef]
12. López-Otín, C.; Blasco, M.A.; Partridge, L.; Serrano, M.; Kroemer, G. The Hallmarks of Aging. *Cell* **2013**, *153*, 1194–1217. [CrossRef]
13. Spinelli, J.B.; Haigis, M.C. The multifaceted contributions of mitochondria to cellular metabolism. *Nat. Cell Biol.* **2018**, *20*, 745–754. [CrossRef]
14. Giorgi, C.; Marchi, S.; Pinton, P. The machineries, regulation and cellular functions of mitochondrial calcium. *Nat. Rev. Mol. Cell Biol.* **2018**, *19*, 713–730. [CrossRef]
15. Ward, D.M.; Cloonan, S.M. Mitochondrial Iron in Human Health and Disease. *Annu. Rev. Physiol.* **2019**, *81*, 453–482. [CrossRef]
16. Martínez-Reyes, I.; Chandel, N.S. Mitochondrial TCA cycle metabolites control physiology and disease. *Nat. Commun.* **2020**, *11*, 102. [CrossRef]
17. Letts, J.; Fiedorczuk, K.; Sazanov, L. The architecture of respiratory supercomplexes. *Nat. Cell Biol.* **2016**, *537*, 644–648. [CrossRef]
18. Wang, C.; Youle, R.J. The Role of Mitochondria in Apoptosis. *Annu. Rev. Genet.* **2009**, *43*, 95–118. [CrossRef]
19. Ebanks, B.; Ingram, T.L.; Chakrabarti, L. ATP synthase and Alzheimer's disease: Putting a spin on the mitochondrial hypothesis. *Aging* **2020**, *12*, 16647–16662. [CrossRef]
20. Butterfield, D.A.; Halliwell, B. Oxidative stress, dysfunctional glucose metabolism and Alzheimer disease. *Nat. Rev. Neurosci.* **2019**, *20*, 148–160. [CrossRef]
21. Poewe, W.; Seppi, K.; Tanner, C.M.; Halliday, G.M.; Brundin, P.; Volkmann, J.; Schrag, A.E.; Lang, A.E. Parkinson disease. *Nat. Rev. Dis. Primers* **2017**, *3*, 1–21. [CrossRef]
22. Chen, X.; Yi, Z.; Wong, G.T.; Hasan, K.M.M.; Kwan, J.S.; Ma, A.C.; Chang, R.C. Is exercise a senolytic medicine? A systematic review. *Aging Cell* **2021**, *20*, e13294. [CrossRef]
23. Ristow, M.; Zarse, K.; Oberbach, A.; Klöting, N.; Birringer, M.; Kiehntopf, M.; Stumvoll, M.; Kahn, C.R.; Blüher, M. Antioxidants prevent health-promoting effects of physical exercise in humans. *Proc. Natl. Acad. Sci. USA* **2009**, *106*, 8665–8670. [CrossRef]
24. Bárcena, C.; Mayoral, P.; Quirós, P.M. Mitohormesis, an Antiageing Paradigm. *Int. Rev. Cell Mol. Biol.* **2018**, *340*, 35–77.
25. Sun, Y.; Yolitz, J.; Wang, C.; Spangler, E.; Zhan, M.; Zou, S. Aging Studies in *Drosophila melanogaster*. *Methods Mol. Biol.* **2013**, *1048*, 77–93. [CrossRef]
26. Fernández-Moreno, M.A.; Farr, C.L.; Kaguni, L.S.; Garesse, R. *Drosophila melanogaster* as a Model System to Study Mitochondrial Biology. *Methods Mol. Biol.* **2007**, *372*, 33–49. [CrossRef]
27. Plyusnina, E.N.; Shaposhnikov, M.V.; Moskalev, A.A. Increase of *Drosophila melanogaster* lifespan due to D-GADD45 overexpression in the nervous system. *Biogerontology* **2010**, *12*, 211–226. [CrossRef]
28. Sun, J.; Molitor, J.; Tower, J. Effects of simultaneous over-expression of Cu/ZnSOD and MnSOD on *Drosophila melanogaster* life span. *Mech. Ageing Dev.* **2004**, *125*, 341–349. [CrossRef]
29. Yang, Y.; Gehrke, S.; Imai, Y.; Huang, Z.; Ouyang, Y.; Wang, J.; Yang, L.; Beal, M.F.; Vogel, O.H.; Lu, B. Mitochondrial pathology and muscle and dopaminergic neuron degeneration caused by inactivation of Drosophila Pink1 is rescued by Parkin. *Proc. Natl. Acad. Sci. USA* **2006**, *103*, 10793–10798. [CrossRef]
30. Clark, I.E.; Dodson, M.W.; Jiang, C.; Cao, J.H.; Huh, J.R.; Seol, J.H.; Yoo, S.J.; Hay, B.A.; Guo, M. Drosophila pink1 is required for mitochondrial function and interacts genetically with parkin. *Nat. Cell Biol.* **2006**, *441*, 1162–1166. [CrossRef]
31. Park, J.; Lee, S.B.; Lee, S.; Kim, Y.; Song, S.; Kim, S.; Bae, E.; Kim, J.; Shong, M.; Kim, J.-M.; et al. Mitochondrial dysfunction in Drosophila PINK1 mutants is complemented by parkin. *Nat. Cell Biol.* **2006**, *441*, 1157–1161. [CrossRef]
32. Kasarda, D.D.; Tao, H.P.; Evans, P.K.; Adalsteins, A.E.; Yuen, S.W. Sequencing of Protein from a Single Spot of a 2-D Gel Pattern: N-Terminal Sequence of a Major Wheat LMW-Glutenin Subunit. *J. Exp. Bot.* **1988**, *39*, 899–906. [CrossRef]

33. Zhu, W.; Smith, J.W.; Huang, C.-M. Mass Spectrometry-Based Label-Free Quantitative Proteomics. *J. Biomed. Biotechnol.* **2009**, *2010*, 840518. [CrossRef]
34. Tinkerhess, M.J.; Healy, L.; Morgan, M.; Sujkowski, A.; Matthys, E.; Zheng, L.; Wessells, R. The Drosophila PGC-1α Homolog spargel Modulates the Physiological Effects of Endurance Exercise. *PLoS ONE* **2012**, *7*, e31633. [CrossRef]
35. Gargano, J.W.; Martin, I.; Bhandari, P.; Grotewiel, M.S. Rapid iterative negative geotaxis (RING): A new method for assessing age-related locomotor decline in Drosophila. *Exp. Gerontol.* **2005**, *40*, 386–395. [CrossRef]
36. Shephard, F.; Greville-Heygate, O.; Liddell, S.; Emes, R.; Chakrabarti, L. Analysis of Mitochondrial haemoglobin in Parkinson's disease brain. *Mitochondrion* **2016**, *29*, 45–52. [CrossRef]
37. Fisher-Wellman, K.; Bloomer, R.J. Acute exercise and oxidative stress: A 30 year history. *Dyn. Med.* **2009**, *8*, 1. [CrossRef]
38. Hekimi, S.; Lapointe, J.; Wen, Y. Taking a "good" look at free radicals in the aging process. *Trends Cell Biol.* **2011**, *21*, 569–576. [CrossRef]
39. Golden, T.R.; Hinerfeld, D.A.; Melov, S. Oxidative stress and aging: Beyond correlation. *Aging Cell* **2002**, *1*, 117–123. [CrossRef]
40. Liguori, I.; Russo, G.; Curcio, F.; Bulli, G.; Aran, L.; DELLA Morte, D.; Gargiulo, G.; Testa, G.; Cacciatore, F.; Bonaduce, D.; et al. Oxidative stress, aging, and diseases. *Clin. Interv. Aging* **2018**, *13*, 757–772. [CrossRef]
41. Sujkowski, A.; Ramesh, D.; Brockmann, A.; Wessells, R. Octopamine Drives Endurance Exercise Adaptations in Drosophila. *Cell Rep.* **2017**, *21*, 1809–1823. [CrossRef]
42. Gorbacheva, T.M.; Syromyatnicov, M.Y.; Popov, V.N.; Lopatin, A.V.; Eprintsev, A.T.; Fedorin, D.N. Characteristics of functioning of succinate dehydrogenase from flight muscles of the bumblebee *Bombus terrestris* (L.). *Biol. Bull.* **2013**, *40*, 429–434. [CrossRef]
43. Zakharchenko, M.V.; Zakharchenko, A.; Khunderyakova, N.; Tutukina, M.; Simonova, M.; Vasilieva, A.; Romanova, O.; Fedotcheva, N.; Litvinova, E.; Maevsky, E.; et al. Burst of succinate dehydrogenase and α-ketoglutarate dehydrogenase activity in concert with the expression of genes coding for respiratory chain proteins underlies short-term beneficial physiological stress in mitochondria. *Int. J. Biochem. Cell Biol.* **2012**, *45*, 190–200. [CrossRef]
44. Marchetti, P.; Fovez, Q.; Germain, N.; Khamari, R.; Kluza, J. Mitochondrial spare respiratory capacity: Mechanisms, regulation, and significance in non-transformed and cancer cells. *FASEB J.* **2020**, *34*, 13106–13124. [CrossRef]
45. Silva, L.A.; Pinho, C.A.; Scarabelot, K.S.; Fraga, D.B.; Volpato, A.M.J.; Boeck, C.R.; De Souza, C.T.; Streck, E.L.; Pinho, R.A. Physical exercise increases mitochondrial function and reduces oxidative damage in skeletal muscle. *Eur. J. Appl. Physiol.* **2009**, *105*, 861–867. [CrossRef]
46. Skinner, J.S.; McLellan, T.H. The Transition from Aerobic to Anaerobic Metabolism. *Res. Q. Exerc. Sport* **1980**, *51*, 234–248. [CrossRef]
47. Tatarková, Z.; Kuka, S.; Račay, P.; Lehotsky, J.; Dobrota, D.; Mištuna, D.; Kaplan, P. Effects of Aging on Activities of Mitochondrial Electron Transport Chain Complexes and Oxidative Damage in Rat Heart. *Physiol. Res.* **2011**, *60*, 281–289. [CrossRef]
48. Tavallaie, M.; Voshtani, R.; Deng, X.; Qiao, Y.; Jiang, F.; Collman, J.P.; Fu, L. Moderation of mitochondrial respiration mitigates metabolic syndrome of aging. *Proc. Natl. Acad. Sci. USA* **2020**, *117*, 9840–9850. [CrossRef]
49. Sabath, N.; Levy-Adam, F.; Younis, A.; Rozales, K.; Meller, A.; Hadar, S.; Soueid-Baumgarten, S.; Shalgi, R. Cellular proteostasis decline in human senescence. *Proc. Natl. Acad. Sci. USA* **2020**, *117*, 31902–31913. [CrossRef]

frontiers in Molecular Biosciences

MINI REVIEW
published: 14 February 2022
doi: 10.3389/fmolb.2022.854321

Mitochondrial ATP Synthase is a Target of Oxidative Stress in Neurodegenerative Diseases

Brad Ebanks[1]* *and Lisa Chakrabarti*[1,2]

[1]School of Veterinary Medicine and Science, University of Nottingham, Nottingham, United Kingdom, [2]MRC Versus Arthritis Centre for Musculoskeletal Ageing Research, Nottingham, United Kingdom

The mitochondrial ATP synthase is responsible for the production of cellular ATP, and it does so by harnessing the membrane potential of the mitochondria that is produced by the sequential oxidation of select cellular metabolites. Since the structural features of ATP synthase were first resolved nearly three decades ago, significant progress has been made in understanding its role in health and disease. Mitochondrial dysfunction is common to neurodegeneration, with elevated oxidative stress a hallmark of this dysfunction. The patterns of this oxidative stress, including molecular targets and the form of oxidative modification, can vary widely. In this mini review we discuss the oxidative modifications of ATP synthase that have been observed in Alzheimer's disease, Parkinson's disease, and Huntington's disease. Oxidative modifications of ATP synthase in Alzheimer's disease are well-documented, and there is a growing body of knowledge on the subject in Parkinson's disease. The consideration of ATP synthase as a pharmacological target in a variety of diseases underlines the importance of understanding these modifications, both as a potential target, and also as inhibitors of any pharmacological intervention.

Keywords: mitochondria, ATP synthase, oxidative stress, neurodegenarative disease, oxidative phoshorylation

OPEN ACCESS

Edited by:
Fabrizio Gentile,
University of Molise, Italy

Reviewed by:
Katarzyna Kaczynska,
Mossakowski Medical Research Centre (PAN), Poland

***Correspondence:**
Brad Ebanks
mbybdpo@nottingham.ac.uk

Specialty section:
This article was submitted to Cellular Biochemistry, a section of the journal Frontiers in Molecular Biosciences

Received: *13 January 2022*
Accepted: *26 January 2022*
Published: *14 February 2022*

Citation:
Ebanks B and Chakrabarti L (2022) Mitochondrial ATP Synthase is a Target of Oxidative Stress in Neurodegenerative Diseases. Front. Mol. Biosci. 9:854321. doi: 10.3389/fmolb.2022.854321

INTRODUCTION

Neurodegenerative Diseases

Neurodegeneration is the process of progressive atrophy and loss of functional neurons in the central nervous system, and in particular the brain. The neurodegenerative process is not uniform, distinctions between which brain regions undergo atrophy, and by what molecular mechanisms the atrophy can be characterised, lead to the different neurodegenerative diseases that we now recognise (Damier et al., 1999; Sabuncu, 2011; Dugger and Dickson, 2017).

The most prevalent neurodegenerative disease is Alzheimer's disease (AD), a form of dementia that is lived with by over 20 million people around the world, and in 2016 was the fifth largest cause of death at 2.4 million people (Nichols, 2019). As global population demographics shift towards older ages, the prevalence of the disease will increase, creating a huge health and social care as well as an economic burden (Castro et al., 2010; Marasco, 2020). The pathophysiology of AD is best characterised by three main characteristics: the aggregation of the amyloid beta (Aβ) protein into plaques (Selkoe and Hardy, 2016; Makin, 2018), the formation of neurofibrillary tangles by the tau protein (Braak and Braak, 1991; Gao et al., 2018), and the dysfunction of mitochondria (Moreira et al., 2006; Swerdlow, 2018), the cell's bioenergetic and signalling hubs.

Parkinson's disease (PD) is the second most prevalent neurodegenerative disease seen today. Characterised by classical motor symptoms of resting tremor and bradykinesia, much of this is due to the degeneration of the dopaminergic neurons of the substantia nigra (Hirsch et al., 1988). There are many genetic risk factors for PD, such as mutations to the *SNCA* gene that lead to the formation of α-synuclein aggregates known as Lewy bodies (Schulz-Schaeffer, 2010; Mahul-Mellier et al., 2020), as well as mutations to the *PINK1* and *parkin* genes that lead to failed mitophagy (the managed intracellular degradation of dysfunctional mitochondria), neuronal defects and even apoptosis (Goldberg et al., 2003; Palacino et al., 2004; Wood-Kaczmar et al., 2008).

Other less frequent forms of neurodegenerative disease include amyotrophic lateral sclerosis (ALS), ataxia, and Huntington's disease. Huntington's disease (HD) is caused by an excessive number of CAG repeats in the *Htt* gene, resulting in PolyQ repeats near the amino terminus. Accumulation of the mutant Huntingtin protein, as well as protein fragments, leads to the formation of toxic inclusion bodies that impact cell physiology, in particular proteostatic function (Bates et al., 2015). Mitochondrial dysfunction in the form of impaired complex II activity and decreased membrane potential have also been widely discussed in HD (Damiano et al., 2010). Atrophy of the medium spiny GABAergic neurons of the striatum is the classical neurodegenerative process observed in the disease (Rikani, 2014), and the major clinical presentations include involuntary movements and bradykinesia (Roos, 2010). With higher prevalence in people of European heritage, it is shown that around one in 7,300 from this demographic are affected (Bates et al., 2015).

Redox Stress in Ageing and Neurodegenerative Disease

One common feature of neurodegenerative disease is the observation of high levels of oxidative stress within the cells of affected tissues (Lin and Beal, 2006; Smith and Cass, 2007; Sorolla, 2008; Wang, 2014; Liguori, 2018). This is in a large part due to the dysfunction of mitochondria that seems ubiquitous in these conditions. Mitochondria are the primary consumers of oxygen, they use molecular oxygen as the terminal electron acceptor at complex IV (cytochrome c oxidase) of the electron transport chain, reducing it to water (Kadenbach, 2021). This flow of electrons, provided by oxidised metabolites, facilitates the pumping of protons across the inner mitochondrial membrane and into the inter membrane space, generating a proton gradient. The activity of complexes I–IV of the electron transport chain is coupled to the activity of the enzyme ATP synthase, which harnesses the flow of protons from the inter membrane space back into the mitochondrial matrix to drive its rotary function, which ultimately provides the energy for the enzyme's ATP synthesising catalytic activity (Gnaiger, 2020).

However, variations in this collective process leads to the production of oxygen based free radicals that are thought to be important signalling molecules (Zhang, 2016; Bárcena et al., 2018), but that can be harmful in excess (Perry et al., 1998; Redza-Dutordoir and Averill-Bates, 2016; Nissanka and Moraes, 2018). The endogenous production of free radicals largely occurs due to the leak or slip of electrons from complexes I and III, before their arrival at the catalytic site of complex IV, producing reactive oxygen species such as superoxide ($O_2^{\cdot}$) (Chen et al., 2003; Balaban et al., 2005; Hirst et al., 2008).

Forms of Protein Oxidation

The oxygen based free radicals such as superoxide and the hydroxyl radical, if not detoxified by antioxidants such as superoxide dismutase and catalase, go on to produce a variety of downstream radical species. In turn these species can modify the structure and function of proteins within the cell, and ultimately alter cellular physiology. While the radicals are capable of interacting with proteins directly (Stadtman and Levine, 2006), they are also known to lead to the modification of proteins through lipid peroxidation (Ayala et al., 2014), carbonylation (Fedorova et al., 2014), and also nitration (Ischiropoulos, 2009). These covalent modifications lead to often irreversible modifications to the proteins structure and therefore function, which often has detrimental outcomes. In order to determine the presence of these modifications, highly sensitive and specific assays can indicate the presence of a type of a modification within a sample (Shacter, 2000), while methods of liquid chromatography coupled with mass spectrometry can determine the presence of that modification to a specific protein (Hawkins and Davies, 2019).

ATP Synthase Structure and Function

The ATP synthase enzyme itself is a large, two component enzyme that provides many targets for oxidative species to covalently modify. The insoluble F_O component is contained within the inner mitochondrial membrane and channels the protons from the intermembrane space to the mitochondrial matrix *via* its c-ring (composed of multiple subunit c peptides and subunit a) (Kühlbrandt and Davies, 2016). The movement of protons through the F_O component drives its rotary function, with the protruding central stalk (composed of the γ, δ, and ε subunits) stimulating conformational changes in the α and β subunits of the aqueous F_1 component, which undertake the catalytic process of ATP synthesis from ADP and P_i (Abrahams et al., 1994; Noji et al., 1997; Stock et al., 1999; Von Ballmoos et al., 2009).

The aqueous component of ATP synthase is a target for the oxidative species produced by mitochondria, due to the proximity to the sites of radical production and the surface exposure of the aqueous F_1 component. In one model of ageing the tryptophan-503 amino acid of the α subunit was identified as frequently oxidised in the *P. anserina* model of ageing (Rexroth, 2012). Reversible thiol oxidation of the α-subunit in the oocytes of *X. laevis* has also been observed to impact the function of the enzyme's catalytic activity (Cobley et al., 2020). Other studies have also presented ATP synthase as a target of carbonylation and 4-hydroxy-2-nonenal (HNE) modification (Prokai et al., 2007; Jeong, 2008; Guo, 2011).

Alzheimer's Disease

Oxidative stress is widely observed in AD and is a defining characteristic of the mitochondrial hypothesis (Swerdlow, 2018; Butterfield and Halliwell, 2019). Within this hypothesis, it is described how oxidative stress is generated by intramitochondrial Aβ mediated dysfunction of the electron transport chain (Casley, 2002; Manczak, 2006). The original mitochondrial cascade hypothesis of AD describes how a gradual accumulation of oxidative damage to mitochondrial DNA, RNA, lipids, and proteins through dysfunctional electron transport chain activity contributes to disease pathology (Swerdlow and Khan, 2004). An updated consideration of this hypothesis considers how mitochondrial dysfunction can lead to oxidative stress, independent of intramitochondrial Aβ (Swerdlow, 2018). Aβ is also recognised as a source of neuroinflammation and oxidative stress in AD through its extracellular deposition in the brain that leads to the activation of microglia, the CNS macrophage (Colton et al., 2000; Koenigsknecht-Talboo and Landreth, 2005; Joshi, 2014; Zhong, 2018). Activated microglia contribute to the oxidative stress environment through the activity of the membrane-bound NADPH oxidase, and its release of the superoxide radical (Wilkinson and Landreth, 2006).

With mitochondria being a primary site of endogenous free-radical production and oxidative stress, the modification of ATP synthase by oxidative species is not unexpected. One of the first studies to identify the oxidation of ATP synthase in an AD context used *C. elegans* that overexpressed an aggregating form of GFP (as a proxy for protein aggregates observed in AD), and ATP synthase subunit *α* was identified as an oxidised protein (Boyd-Kimball, 2006). Since this preliminary observation, more detailed analyses of ATP synthase oxidation in AD have been produced.

Lipid peroxidation is a common hallmark of the oxidative stress that is observed in AD. The complex chemical interaction between ROS and polyunsaturated fatty acids leads to the production of reactive aldehydes, such as HNE, which can covalently modify proteins, modulating their structure and function. The first observation of HNE modified ATP synthase in the context of AD was from both the hippocampus and inferior parietal lobule (IPL) of mild cognitive impairment (MCI) patient brains, where ATP synthase subunit *α* was identified as excessively HNE modified (Reed, 2008). ATP synthase enzymatic activity was also reduced in both tissue types.

The Butterfield research group reported that the ATP synthase subunit *α* was again HNE modified in the IPL of early AD patients, considered to be the intermediate between MCI and AD (Reed et al., 2009a). ATP synthase was identified as HNE modified when the IPL of AD patients were studied, and this was again coupled with the observation that ATP synthase catalytic activity was reduced (Perluigi, 2009). A study of the entorhinal cortex from patients at Braak stages I/II observed the HNE oxidation of the ATP synthase subunit *α*, and the activity of the ATP synthase enzyme from the AD patient samples was found to be significantly decreased, while there was no observed decrease in activity of the major electron transport chain enzyme Complex I (Terni et al., 2010). At the earliest stages of AD, HNE modification of ATP synthase and subsequent downregulation of its activity has been observed. However, enzyme activity assays have suggested that this decrease in ATP synthase activity is not concordant with a decrease in Complex I activity, which suggests that a decrease in mitochondrial ATP output in early AD might be specifically dependent upon inhibited ATP synthase activity.

The frontal cortex of AD patient brains at Braak stages V/VI was assessed for a variety of oxidative protein modifications, and a four-fold increase in N^{ϵ}-(malondialdehyde)-lysine (MDAL) modification of mitochondrial ATP synthase subunit *β* (Pamplona, 2005). However, when the entorhinal cortices of AD patients at Braak stages V/VI were assessed for variations in protein expression and for the presence of protein carbonylation, it was reported that while ATP synthase subunit β had upregulated protein expression, there were no significant differences in the carbonylation of the protein when compared with age-matched controls (Korolainen, 2006). When considered alongside the previously discussed studies that reported HNE modification of ATP synthase subunit α, this suggests that the oxidative modifications are specific to ATP synthase subunit α, and that changes in the oxidation state of the protein could be modified throughout disease progression.

Linked to the oxidative stress that characterises AD is the production of highly reactive peroxynitrite from nitrate and superoxide radicals (Radi, 2018). ATP synthase subunit *α* was identified as excessively nitrated in the hippocampus of AD patients (Sultana, 2006). When the IPL of early AD patients were measured, H^+-transporting ATPase had excessive levels of nitration which was also coupled with a significantly reduced ATP synthase catalytic activity (Reed et al., 2009b).

A study of the APP23 transgenic mouse model of AD in the pre-symptomatic stage considered the carbonylation of proteins that were extracted from cortex tissue (Hartl, 2012). The carbonylated forms of ATP synthase subunit *α*, ATP synthase subunit β, ATP synthase subunit b, ATP synthase subunit O, and the ADP/ATP translocase 1 were all more abundant in the APP23 transgenic mouse model than in the control. Primary cortical neurons of the APP23 mice were cultured and were found to have a significantly decreased ADP/ATP ratio than controls, pointing to a disrupted energy metabolism that appears at the very earliest stages of the disease. The observed oxidative modifications of ATP synthase in AD are summarised in **Figure 1**, adapted from Spikes et al. (2020).

Huntington's Disease

While oxidative stress is a common feature of both PD and HD, there are fewer observations of ATP synthase being a target of oxidative modifications in these diseases. However, a study of the oxidised proteins from the striatum of HD patients reported that ATP synthase subunit *α* is significantly carbonylated in comparison with age-matched controls (Sorolla, 2010). Enriched mitochondrial fractions were taken from the patient striatum samples and assessed ATP synthase catalytic activity, which was also significantly lower in comparison with controls.

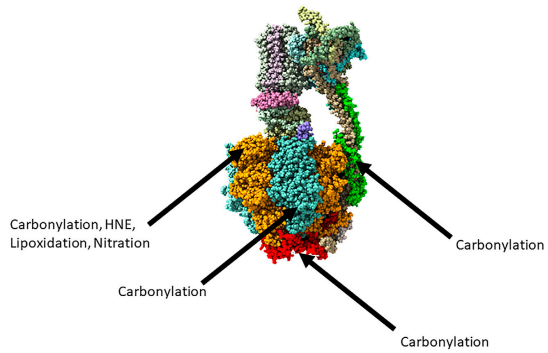

FIGURE 1 | The reported oxidative modifications of ATP synthase in Alzheimer's disease. Adapted from https://www.rcsb.org/structure/6ZPO. Subunit α represented in orange, subunit β represented in blue, subunit O represented in red, subunit D represented in green.

TABLE 1 | The different oxidative modifications of ATP synthase reported in Alzheimer's disease, Parkinson's disease, and Huntington's disease.

Disease	Protein				
	ATP5A	ATP5B	Subunit d	Subunit O	ADP/ATP translocase
Alzheimer's	Carbonylation, HNE, Lipoxidation, Nitration	Carbonylation	Carbonylation	Carbonylation	Carbonylation
Parkinson's	Carbonylation	Carbonylation			
Huntington's	Carbonylation				

Parkinson's Disease

Rotenone is a well-characterised inhibitor of the mitochondrial complex I that is used in studies of PD (Greenamyre et al., 2010). Complex I dysfunction is a major pathophysiological component of PD, and its inhibition by rotenone is utilised widely in both cell and animal disease models (KrakoJakovljevic, 2021). A study of dopaminergic PC12 cells exposed to rotenone observed that both ATP synthase subunit α and ATP synthase subunit β were carbonylated, to which the authors suggest could contribute to a reduced ATP output (Chiaradia, 2019). Mutations in the *SNCA* gene that encodes α-synuclein are also a feature of PD, as the aggregation of the protein leads to the formation of toxic oligomers and fibrils (Schulz-Schaeffer, 2010; Mahul-Mellier et al., 2020). Rat neuronal co-cultures treated with oligomers of α-synuclein showed a co-localisation of the oligomers with ATP synthase, which resulted in high levels of oxidised ATP synthase subunit β (Ludtmann, 2018). There is evidence of mitochondrial permeability transition pore (mPTP) opening in response to α-synuclein oligomer induced oxidative stress and compromised bioenergetics, and the role of ATP synthase as a structural component of mPTP is now increasingly better understood (Angeli, 2021).

D. melanogaster with *parkin* mutations are also a well-characterised disease model for PD (Greene, 2003). Studies have reported reduced Glutathione S-Transferase Omega (GSTO) in these mutants, which may result in increased susceptibility to oxidative stress due to the protective role of S-Glutathionylation against the irreversible oxidation of protein thiols (Song, 2014). When *parkin* mutants of *D. melanogaster* had GSTO1 restored, as it is downregulated in *parkin* mutants, the levels of S-Glutathionylation of ATP synthase subunit β increased, along with the catalytic activity of the ATP synthase enzyme (Kim et al., 2012).

CONCLUSION AND PERSPECTIVES

The mitochondrion is a primary site of free radical production in the cell, and thus a site of high levels of oxidative stress. This mitochondrial dysfunction that leads to oxidative stress has come to characterise many neurodegenerative diseases. The protein targets of this oxidative stress are varied but distinct to given diseases, and so in order to better understand the disease process, a comprehension of the oxidised proteins is required.

Proper functioning of the ATP synthase enzyme is essential to metazoan life, and in *H. sapiens*, its dysfunction is widely

implicated in disease (Dautant, 2018). Here we have discussed the published evidence of ATP synthase modification by processes of oxidation in different neurodegenerative diseases, with a summary of these modification presented in **Table 1**. A more complete understanding of ATP synthase oxidation is presented in AD, largely based upon the work of the D. Allan Butterfield lab, but there is still more to be understood about this process.

Much less information is available in PD and HD but given that oxidative stress is a major feature in the pathophysiology of both diseases, effort should be directed toward understanding the oxidised proteome in both diseases, and in particular the oxidation of the ATP synthase enzyme. Other neurodegenerative conditions such not be overlooked in these investigations either, protein oxidation has long being understood to characterise ALS, but information regarding the specific proteins which are modified is lacking (Beal, 1997; Andrus et al., 1998).

Given the progression of the candidate drug J147, which targets ATP synthase, to clinical trial as a potential treatment for AD (Goldberg, 2018), as well as the deeper consideration of the enzyme as a target in anti-cancer therapies (Wang et al., 2021), a deeper understanding of the frequency, type, and location of the oxidative modifications of the mitochondrial ATP synthase enzyme should allow for the development of candidate drugs to treat these diseases in the future.

AUTHOR CONTRIBUTIONS

BE and LC co-wrote the manuscript.

FUNDING

BE is supported by the Biotechnology and Biological Sciences Research Council (grant number BB/J014508/1).

REFERENCES

Abrahams, J. P., Leslie, A. G. W., Lutter, R., and Walker, J. E. (1994). Structure at 2.8 Å Resolution of F1-ATPase from Bovine Heart Mitochondria. *Nature* 370, 621–628. doi:10.1038/370621a0

Andrus, P. K., Fleck, T. J., Gurney, M. E., and Hall, E. D. (1998). Protein Oxidative Damage in a Transgenic Mouse Model of Familial Amyotrophic Lateral Sclerosis. *J. Neurochem.* 71, 2041–2048. doi:10.1046/j.1471-4159.1998.71052041.x

Angeli, S. (2021). The Mitochondrial Permeability Transition Pore Activates the Mitochondrial Unfolded Protein Response and Promotes Aging. *Elife* 10, 1–23. doi:10.7554/elife.63453

Ayala, A., Muñoz, M. F., and Argüelles, S. (2014). Lipid Peroxidation: Production, Metabolism, and Signaling Mechanisms of Malondialdehyde and 4-Hydroxy-2-Nonenal. *Oxid. Med. Cel. Longev.* 2014, 1. doi:10.1155/2014/360438

Balaban, R. S., Nemoto, S., and Finkel, T. (2005). Mitochondria, Oxidants, and Aging. *Cell* 120, 483–495. doi:10.1016/j.cell.2005.02.001

Bárcena, C., Mayoral, P., and Quirós, P. M. (2018). Mitohormesis, an Antiaging Paradigm. *Int. Rev. Cell Mol. Biol.* 340, 35–77.

Bates, G. P., Dorsey, R., Gusella, J. F., Hayden, M. R., Kay, C., Leavitt, B. R., et al. (2015). Huntington Disease. *Nat. Rev. Dis. Primers* 1, 15005–15021. doi:10.1038/nrdp.2015.5

Beal, M. F. (1997). Increased 3-nitrotyrosine in Both Sporadic and Familial Amyotrophic Lateral Sclerosis. *Ann. Neurol.* 42, 644–654. doi:10.1002/ana.410420416

Boyd-Kimball, D. (2006). Proteomic Identification of Proteins Specifically Oxidized in *Caenorhabditis elegans* Expressing Human Aβ(1-42): Implications for Alzheimer's Disease. *Neurobiol. Aging* 27, 1239–1249. doi:10.1016/j.neurobiolaging.2005.07.001

Braak, H., and Braak, E. (1991). Neuropathological Stageing of Alzheimer-Related Changes. *Acta Neuropathol.* 82, 239–259. doi:10.1007/bf00308809

Butterfield, D. A., and Halliwell, B. (2019). Oxidative Stress, Dysfunctional Glucose Metabolism and Alzheimer Disease. *Nat. Rev. Neurosci.* 20, 148–160. doi:10.1038/s41583-019-0132-6

Casley, C. S. (2002). β-Amyloid Fragment 25-35 Causes Mitochondrial Dysfunction in Primary Cortical Neurons. *Neurobiol. Dis.* 10, 258–267. doi:10.1006/nbdi.2002.0516

Castro, D. M., Dillon, C., Machnicki, G., and Allegri, R. F. (2010). The Economic Cost of Alzheimer's Disease: Family or Public-Health burden? *Dement. Neuropsychol.* 4, 262–267. doi:10.1590/s1980-57642010dn40400003

Chen, Q., Vazquez, E. J., Moghaddas, S., Hoppel, C. L., and Lesnefsky, E. J. (2003). Production of Reactive Oxygen Species by Mitochondria: Central Role of Complex III. *J. Biol. Chem.* 278, 36027–36031. doi:10.1074/jbc.m304854200

Chiaradia, E. (2019). Protein Carbonylation in Dopaminergic Cells Exposed to Rotenone. *Toxicol. Lett.* 309, 20–32. doi:10.1016/j.toxlet.2019.04.002

Cobley, J., Noble, A., Bessell, R., Guille, M., and Husi, H. (2020). Reversible Thiol Oxidation Inhibits the Mitochondrial ATP Synthase in Xenopus Laevis Oocytes. *Antioxidants* 9, 1. doi:10.3390/antiox9030215

Colton, C. A., Chernyshev, O. N., Gilbert, D. L., and Vitek, M. P. (2000). Microglial Contribution to Oxidative Stress in Alzheimer's Disease. *Ann. N. Y. Acad. Sci.* 899, 292–307. doi:10.1111/j.1749-6632.2000.tb06195.x

Damiano, M., Galvan, L., Déglon, N., and Brouillet, E. (2010). Mitochondria in Huntington's Disease. *Biochim. Biophys. Acta (Bba) - Mol. Basis Dis.* 1802, 52–61. doi:10.1016/j.bbadis.2009.07.012

Damier, P., Hirsch, E. C., Agid, Y., and Graybiel, A. M. (1999). The Substantia Nigra of the Human Brain. *Brain* 122, 1437–1448. doi:10.1093/brain/122.8.1437

Dautant, A. (2018). ATP Synthase Diseases of Mitochondrial Genetic Origin. *Front. Physiol.* 9, 329. doi:10.3389/fphys.2018.00329

Dugger, B. N., and Dickson, D. W. (2017). Pathology of Neurodegenerative Diseases. *Cold Spring Harb Perspect. Biol.* 9, a028035. doi:10.1101/cshperspect.a028035

Fedorova, M., Bollineni, R. C., and Hoffmann, R. (2014). Protein Carbonylation as a Major Hallmark of Oxidative Damage: Update of Analytical Strategies. *Mass. Spectrom. Rev.* 33, 79–97. doi:10.1002/mas.21381

Gao, Y.-L., Wang, N., Sun, F.-R., Cao, X.-P., Zhang, W., and Yu, J.-T. (2018). Tau in Neurodegenerative Disease. *Ann. Transl. Med.* 6, 175. doi:10.21037/atm.2018.04.23

Gnaiger, E. (2020). *Mitochondrial Pathways and Respiratory Control: An Introduction to OXPHOS Analysis*. Innsbruck, Austria: Bioenergetic Communications, 5.

Goldberg, J. (2018). The Mitochondrial ATP Synthase Is a Shared Drug Target for Aging and Dementia. *Aging Cell* 17, e12715. doi:10.1111/acel.12715

Goldberg, M. S., Fleming, S. M., Palacino, J. J., Cepeda, C., Lam, H. A., Bhatnagar, A., et al. (2003). Parkin-deficient Mice Exhibit Nigrostriatal Deficits but Not Loss of Dopaminergic Neurons. *J. Biol. Chem.* 278, 43628–43635. doi:10.1074/jbc.m308947200

Greenamyre, J. T., Cannon, J. R., Drolet, R., and Mastroberardino, P. G. (2010). Lessons from the Rotenone Model of Parkinson's Disease. *Trends Pharmacol. Sci.* 31, 141–142. doi:10.1016/j.tips.2009.12.006

Greene, J. C. (2003). Mitochondrial Pathology and Apoptotic Muscle Degeneration in Drosophila Parkin Mutants. *Proc. Natl. Acad. Sci.* 100, 4078–4083. doi:10.1073/pnas.0737556100

Guo, J. (2011). Protein Targets for Carbonylation by 4-Hydroxy-2-Nonenal in Rat Liver Mitochondria. *J. Proteomics* 74, 2370–2379. doi:10.1016/j.jprot.2011.07.009

Hartl, D. (2012). Presymptomatic Alterations in Energy Metabolism and Oxidative Stress in the APP23 Mouse Model of Alzheimer Disease. *J. Proteome Res.* 11, 3295–3304. doi:10.1021/pr300021e

Hawkins, C. L., and Davies, M. J. (2019). Detection, Identification, and Quantification of Oxidative Protein Modifications. *J. Biol. Chem.* 294, 19683–19708. doi:10.1074/jbc.rev119.006217

Hirsch, E., Graybiel, A. M., and Agid, Y. A. (1988). Melanized Dopaminergic Neurons Are Differentially Susceptible to Degeneration in Parkinson's Disease. *Nature* 334, 345–348. doi:10.1038/334345a0

Hirst, J., King, M. S., and Pryde, K. R. (2008). The Production of Reactive Oxygen Species by Complex I. *Biochem. Soc. Trans.* 36, 976–980. doi:10.1042/bst0360976

Ischiropoulos, H. (2009). Protein Tyrosine Nitration-An Update. *Arch. Biochem. Biophys.* 484, 117–121. doi:10.1016/j.abb.2008.10.034

Jeong, H. J. (2008). Mitochondrial ATP Synthase Is a Target for TNBS-Induced Protein Carbonylation in XS-106 Dendritic Cells. *Proteomics* 8, 2384–2393. doi:10.1002/pmic.200700962

Joshi, P. (2014). Microglia Convert Aggregated Amyloid-β into Neurotoxic Forms through the Shedding of Microvesicles. *Cell Death Differ* 21, 582–593. doi:10.1038/cdd.2013.180

Kadenbach, B. (2021). Complex IV – the Regulatory center of Mitochondrial Oxidative Phosphorylation. *Mitochondrion* 58, 296–302. doi:10.1016/j.mito.2020.10.004

Kim, K., Kim, S. H., Kim, J., Kim, H., and Yim, J. (2012). Glutathione S-Transferase omega 1 Activity Is Sufficient to Suppress Neurodegeneration in a Drosophila Model of Parkinson Disease. *J. Biol. Chem.* 287, 6628–6641. doi:10.1074/jbc.m111.291179

Koenigsknecht-Talboo, J., and Landreth, G. E. (2005). Microglial Phagocytosis Induced by Fibrillar β-amyloid and IgGs Are Differentially Regulated by Proinflammatory Cytokines. *J. Neurosci.* 25, 8240–8249. doi:10.1523/jneurosci.1808-05.2005

Korolainen, M. A. (2006). Oxidative Modification of Proteins in the Frontal Cortex of Alzheimer's Disease Brain. *Neurobiol. Aging* 27, 42–53. doi:10.1016/j.neurobiolaging.2004.11.010

Krako Jakovljevic, N. (2021). Mitochondrial Homeostasis in Cellular Models of Parkinson's Disease. *Bioenerg. Commun.* 2021, 1–31.

Kühlbrandt, W., and Davies, K. M. (2016). Rotary ATPases: A New Twist to an Ancient Machine. *Trends Biochem. Sci.* 41, 106–116.

Liguori, I. (2018). Oxidative Stress, Aging, and Diseases. *Clin. Interv. Aging* 13, 757–772. doi:10.2147/cia.s158513

Lin, M. T., and Beal, M. F. (2006). Mitochondrial Dysfunction and Oxidative Stress in Neurodegenerative Diseases. *Nature* 443, 787–795. doi:10.1038/nature05292

Ludtmann, M. H. R. (2018). α-Synuclein Oligomers Interact with ATP Synthase and Open the Permeability Transition Pore in Parkinson's Disease. *Nat. Commun.* 9, 1. doi:10.1038/s41467-018-04422-2

Mahul-Mellier, A.-L., Burtscher, J., Maharjan, N., Weerens, L., Croisier, M., Kuttler, F., et al. (2020). The Process of Lewy Body Formation, rather Than Simply α-synuclein Fibrillization, Is One of the Major Drivers of Neurodegeneration. *Proc. Natl. Acad. Sci. USA* 117, 4971–4982. doi:10.1073/pnas.1913904117

Makin, S. (2018). The Amyloid Hypothesis on Trial. *Nature* 559, S4–S7. doi:10.1038/d41586-018-05719-4

Manczak, M. (2006). Mitochondria Are a Direct Site of Aβ Accumulation in Alzheimer's Disease Neurons: Implications for Free Radical Generation and Oxidative Damage in Disease Progression. *Hum. Mol. Genet.* 15, 1437–1449. doi:10.1093/hmg/ddl066

Marasco, R. A. (2020). Economic burden of Alzheimer Disease and Managed Care Considerations. *Am. J. Manag. Care* 26, S177–S183.

Moreira, P. I., Cardoso, S. M., Santos, M. S., and Oliveira, C. R. (2006). The Key Role of Mitochondria in Alzheimer's Disease. *Jad* 9, 101–110. doi:10.3233/jad-2006-9202

Nichols, E. (2019). Global, Regional, and National burden of Alzheimer's Disease and Other Dementias, 1990-2016: a Systematic Analysis for the Global Burden of Disease Study 2016. *Lancet Neurol.* 18, 88–106. doi:10.1016/S1474-4422(18)30403-4

Nissanka, N., and Moraes, C. T. (2018). Mitochondrial DNA Damage and Reactive Oxygen Species in Neurodegenerative Disease. *FEBS Lett.* 592, 728–742. doi:10.1002/1873-3468.12956

Noji, H., Yasuda, R., Yoshida, M., and Kinosita, K. (1997). Direct Observation of the Rotation of F1-ATPase. *Nature* 386, 299–302. doi:10.1038/386299a0

Palacino, J. J., Sagi, D., Goldberg, M. S., Krauss, S., Motz, C., Wacker, M., et al. (2004). Mitochondrial Dysfunction and Oxidative Damage in Parkin-Deficient Mice. *J. Biol. Chem.* 279, 18614–18622. doi:10.1074/jbc.m401135200

Pamplona, R. (2005). Proteins in Human Brain Cortex Are Modified by Oxidation, Glycoxidation, and Lipoxidation: Effects of Alzheimer Disease and Identification of Lipoxidation Targets. *J. Biol. Chem.* 280, 21522–21530. doi:10.1074/jbc.m502255200

Perluigi, M. (2009). Redox Proteomics Identification of 4-hydroxynonenalmodified Brain Proteins in Alzheimer's Disease: Role of Lipid Peroxidation in Alzheimer's Disease Pathogenesis. *Proteomics - Clin. Appl.* 3, 682–693. doi:10.1002/prca.200800161

Perry, G., Castellani, R. J., Hirai, K., and Smith, M. A. (1998). Reactive Oxygen Species Mediate Cellular Damage in Alzheimer Disease. *J. Alzheimer's Dis.* 1, 45–55. doi:10.3233/jad-1998-1103

Prokai, L., Yan, L. J., Vera-Serrano, J. L., Stevens, S. M., and Forster, M. J. (2007). Mass Spectrometry-Based Survey of Age-Associated Protein Carbonylation in Rat Brain Mitochondria. *J. Mass. Spectrom.* 42, 1583–1589. doi:10.1002/jms.1345

Radi, R. (2018). Oxygen Radicals, Nitric Oxide, and Peroxynitrite: Redox Pathways in Molecular Medicine. *Proc. Natl. Acad. Sci. U. S. A.* 115, 5839–5848. doi:10.1073/pnas.1804932115

Redza-Dutordoir, M., and Averill-Bates, D. A. (2016). Activation of Apoptosis Signalling Pathways by Reactive Oxygen Species. *Biochim. Biophys. Acta - Mol. Cell Res.* 1863, 2977–2992. doi:10.1016/j.bbamcr.2016.09.012

Reed, T. (2008). Redox Proteomic Identification of 4-Hydroxy-2-Nonenal-Modified Brain Proteins in Amnestic Mild Cognitive Impairment: Insight into the Role of Lipid Peroxidation in the Progression and Pathogenesis of Alzheimer's Disease. *Neurobiol. Dis.* 30, 107–120. doi:10.1016/j.nbd.2007.12.007

Reed, T. T., Pierce, W. M., Markesbery, W. R., and Butterfield, D. A. (2009). Proteomic Identification of HNE-Bound Proteins in Early Alzheimer Disease: Insights into the Role of Lipid Peroxidation in the Progression of AD. *Brain Res.* 1274, 66–76. doi:10.1016/j.brainres.2009.04.009

Reed, T. T., Pierce, W. M., Turner, D. M., Markesbery, W. R., and Allan Butterfield, D. (2009). Proteomic Identification of Nitrated Brain Proteins in Early Alzheimer's Disease Inferior Parietal Lobule. *J. Cel. Mol. Med.* 13, 2019–2029. doi:10.1111/j.1582-4934.2008.00478.x

Rexroth, S. (2012). Reactive Oxygen Species Target Specific Tryptophan Site in the Mitochondrial ATP Synthase. *Biochim. Biophys. Acta - Bioenerg.* 1817, 381–387. doi:10.1016/j.bbabio.2011.11.006

Rikani, A. A. (2014). The Mechanism of Degeneration of Striatal Neuronal Subtypes in Huntington Disease. *Ann. Neurosci.* 21, 112–114. doi:10.5214/ans.0972.7531.210308

Roos, R. A. (2010). Huntington's Disease: a Clinical Review. *Orphanet J. Rare Dis.* 5, 40. doi:10.1186/1750-1172-5-40

Sabuncu, M. R. (2011). The Dynamics of Cortical and Hippocampal Atrophy in Alzheimer Disease. *Arch. Neurol.* 68, 1040–1048. doi:10.1001/archneurol.2011.167

Schulz-Schaeffer, W. J. (2010). The Synaptic Pathology of α-synuclein Aggregation in Dementia with Lewy Bodies, Parkinson's Disease and Parkinson's Disease Dementia. *Acta Neuropathol.* 120, 131–143. doi:10.1007/s00401-010-0711-0

Selkoe, D. J., and Hardy, J. (2016). The Amyloid Hypothesis of Alzheimer's Disease at 25 Years. *EMBO Mol. Med.* 8, 595–608. doi:10.15252/emmm.201606210

Shacter, E. (2000). Quantification and Significance of Protein Oxidation in Biological Samples. *Drug Metab. Rev.* 32, 307–326. doi:10.1081/dmr-100102336

Smith, M. P., and Cass, W. A. (2007). Oxidative Stress and Dopamine Depletion in an Intrastriatal 6-hydroxydopamine Model of Parkinson's Disease. *Neuroscience* 144, 1057–1066. doi:10.1016/j.neuroscience.2006.10.004

Song, J. (2014). Glutathione Protects Brain Endothelial Cells from Hydrogen Peroxide-Induced Oxidative Stress by Increasing Nrf2 Expression. *Exp. Neurobiol.* 23, 93–103. doi:10.5607/en.2014.23.1.93

Sorolla, M. A. (2010). Protein Oxidation in Huntington Disease Affects Energy Production and Vitamin B6 Metabolism. *Free Radic. Biol. Med.* 49, 612–621. doi:10.1016/j.freeradbiomed.2010.05.016

Sorolla, M. A. (2008). Proteomic and Oxidative Stress Analysis in Human Brain Samples of Huntington Disease. *Free Radic. Biol. Med.* 45, 667–678. doi:10.1016/j.freeradbiomed.2008.05.014

Spikes, T. E., Montgomery, M. G., and Walker, J. E. (2020). Structure of the Dimeric ATP Synthase from Bovine Mitochondria. *Proc. Natl. Acad. Sci. U. S. A.* 117 (38), 23519–23526. doi:10.1073/pnas.2013998117

Stadtman, E. R., and Levine, R. L. (2006). Oxidatively Modified Proteins Proteins by Reactive Oxygen Species. *Redox Proteomics Protein Modif. Cel. Dysfunct. Dis.* 32 (9), 797–803. doi:10.1002/0471973122.ch1

Stock, D., Leslie, A. G. W., and Walker, J. E. (1999). Molecular Architecture of the Rotary Motor in ATP Synthase. *Science (80-.)* 286, 1700–1705. doi:10.1126/science.286.5445.1700

Sultana, R. (2006). Identification of Nitrated Proteins in Alzheimer's Disease Brain Using a Redox Proteomics Approach. *Neurobiol. Dis.* 22, 76–87. doi:10.1016/j.nbd.2005.10.004

Swerdlow, R. H., and Khan, S. M. (2004). A 'mitochondrial cascade Hypothesis' for Sporadic Alzheimer's Disease. *Med. Hypotheses* 63, 8–20. doi:10.1016/j.mehy.2003.12.045

Swerdlow, R. H. (2018). Mitochondria and Mitochondrial Cascades in Alzheimer's Disease. *Jad* 62, 1403–1416. doi:10.3233/jad-170585

Terni, B., Boada, J., Portero-Otin, M., Pamplona, R., and Ferrer, I. (2010). Mitochondrial ATP-Synthase in the Entorhinal Cortex Is a Target of Oxidative Stress at Stages I/II of Alzheimer's Disease Pathology. *Brain Pathol.* 20, 222–233. doi:10.1111/j.1750-3639.2009.00266.x

Von Ballmoos, C., Wiedenmann, A., and Dimroth, P. (2009). Essentials for ATP Synthesis by F1F0 ATP Synthases. *Annu. Rev. Biochem.* 78, 649–672. doi:10.1146/annurev.biochem.78.081307.104803

Wang, T., Ma, F., and Qian, H. (2021). Defueling the Cancer: ATP Synthase as an Emerging Target in Cancer Therapy. *Mol. Ther. - Oncolytics* 23, 82–95. doi:10.1016/j.omto.2021.08.015

Wang, X. (2014). Oxidative Stress and Mitochondrial Dysfunction in Alzheimer's Disease. *Biochim. Biophys. Acta - Mol. Basis Dis.* 1842, 1240–1247. doi:10.1016/j.bbadis.2013.10.015

Wilkinson, B. L., and Landreth, G. E. (2006). The Microglial NADPH Oxidase Complex as a Source of Oxidative Stress in Alzheimer's Disease. *J. Neuroinflammation* 3, 1–12. doi:10.1186/1742-2094-3-30

Wood-Kaczmar, A., Gandhi, S., Yao, Z., Abramov, A. S. Y., Miljan, E. A., Keen, G., et al. (2008). PINK1 Is Necessary for Long Term Survival and Mitochondrial Function in Human Dopaminergic Neurons. *PLoS One* 3, e2455. doi:10.1371/journal.pone.0002455

Zhang, J. (2016). ROS and ROS-Mediated Cellular Signaling. *Oxid. Med. Cel. Longev.* 2016, 1. doi:10.1155/2016/4350965

Zhong, L. (2018). Amyloid-beta Modulates Microglial Responses by Binding to the Triggering Receptor Expressed on Myeloid Cells 2 (TREM2). *Mol. Neurodegener.* 13, 1–12. doi:10.1186/s13024-018-0247-7

Conflict of Interest: The authors declare that the research was conducted in the absence of any commercial or financial relationships that could be construed as a potential conflict of interest.

Publisher's Note: All claims expressed in this article are solely those of the authors and do not necessarily represent those of their affiliated organizations, or those of the publisher, the editors and the reviewers. Any product that may be evaluated in this article, or claim that may be made by its manufacturer, is not guaranteed or endorsed by the publisher.

biology

MDPI

Article

Quantitative Proteomics and Network Analysis of Differentially Expressed Proteins in Proteomes of Icefish Muscle Mitochondria Compared with Closely Related Red-Blooded Species

Gunjan Katyal [1], Brad Ebanks [1], Adam Dowle [2], Freya Shephard [1], Chiara Papetti [3], Magnus Lucassen [4] and Lisa Chakrabarti [1,5,*]

[1] School of Veterinary Medicine and Science, University of Nottingham, Sutton Bonington LE12 5RD, UK; gunjan.katyal@nottingham.ac.uk (G.K.); brad.ebanks@nottingham.ac.uk (B.E.); freya.shephard@nottingham.ac.uk (F.S.)
[2] Department of Biology, Bioscience Technology Facility, University of York, York YO10 5DD, UK; adam.dowle@york.ac.uk
[3] Biology Department, University of Padova, Via U. Bassi, 58/b, 35121 Padova, Italy; chiara.papetti@unipd.it
[4] Alfred Wegener Institute, 27570 Bremerhaven, Germany; magnus.lucassen@awi.de
[5] MRC-Versus Arthritis Centre for Musculoskeletal Ageing Research, Liverpool L7 8TX, UK
* Correspondence: lisa.chakrabarti@nottingham.ac.uk

Simple Summary: Antarctic icefish are unusual in that they are the only vertebrates that survive without the protein haemoglobin. One way to try and understand the biological processes that support this anomaly is to record how proteins are regulated in these animals and to compare what we find to closely related Antarctic fish that do still retain haemoglobin. The part of the cell that most clearly utilises oxygen, which is normally transported by haemoglobin, is the mitochondrion. Therefore, we chose to catalogue all the proteins and their relative quantities in the mitochondria (pl.) from two different muscle types in two species of icefish and two species of red-blooded notothenioids. We used an approach called mass spectrometry to reveal relative amounts of the proteins from the muscles of each fish. We present analysis that shows how the connections and relative quantities of proteins differ between these species.

Abstract: Antarctic icefish are extraordinary in their ability to thrive without haemoglobin. We wanted to understand how the mitochondrial proteome has adapted to the loss of this protein. Metabolic pathways that utilise oxygen are most likely to be rearranged in these species. Here, we have defined the mitochondrial proteomes of both the red and white muscle of two different icefish species (*Champsocephalus gunnari* and *Chionodraco rastrospinosus)* and compared these with two related red-blooded Notothenioids (*Notothenia rossii*, *Trematomus bernacchii*). Liquid Chromatography-Mass spectrometry (LC-MS/MS) was used to generate and examine the proteomic profiles of the two groups. We recorded a total of 91 differentially expressed proteins in the icefish red muscle mitochondria and 89 in the white muscle mitochondria when compared with the red-blooded related species. The icefish have a relatively higher abundance of proteins involved with Complex V of oxidative phosphorylation, RNA metabolism, and homeostasis, and fewer proteins for striated muscle contraction, haem, iron, creatine, and carbohydrate metabolism. Enrichment analyses showed that many important pathways were different in both red muscle and white muscle, including the citric acid cycle, ribosome machinery and fatty acid degradation. Life in the Antarctic waters poses extra challenges to the organisms that reside within them. Icefish have successfully inhabited this environment and we surmise that species without haemoglobin uniquely maintain their physiology. Our study highlights the mitochondrial protein pathway differences between similar fish species according to their specific tissue oxygenation idiosyncrasies.

Keywords: icefish; proteomics; mitochondria; muscle; network analysis; notothenioid

check for updates

Citation: Katyal, G.; Ebanks, B.; Dowle, A.; Shephard, F.; Papetti, C.; Lucassen, M.; Chakrabarti, L. Quantitative Proteomics and Network Analysis of Differentially Expressed Proteins in Proteomes of Icefish Muscle Mitochondria Compared with Closely Related Red-Blooded Species. *Biology* **2022**, *11*, 1118. https://doi.org/10.3390/biology11081118

Academic Editors: Francesco Bellanti and Ansgar Poetsch

Received: 16 May 2022
Accepted: 19 July 2022
Published: 26 July 2022

1. Introduction

Mitochondria are crucial organelles that produce ATP via oxidative phosphorylation, a process that involves the transfer of electrons between multi-subunit complexes (I to IV) of the electron transport chain (ETC), resulting in the reduction of molecular oxygen. These organelles are also known for their involvement in many vital cellular activities such as apoptosis, calcium homeostasis, and regulation of cell homeostasis. Due to this, there has been an increasing interest in the structure and function of mitochondrial proteins [1–4]. Efforts have been made to decipher the structure, assembly process, coupling mechanism, and associated pathologies of respiratory chain complexes [5,6].

Haemoglobin (Hb) synthesis requires a coordinated production of both haem and globin. Hb is a multi-subunit globular molecule made up of four polypeptide subunits, two alpha and two beta subunits. Each of the four subunits has a haem moiety that contains iron [7]. The prosthetic group haem is synthesised in a series of steps shuttling between the mitochondrion and the cytosol of immature erythrocytes [8]. To understand the role of haemoglobin, it can be useful to examine eukaryotic systems that express this important protein at different levels. There is a wide range of evidence that suggests Hb has dynamic locations in cell, neurons, endothelial cells, mitochondria, and vascular expression [9–13]. Previously, we have shown that haemoglobin proteins are located in the mitochondrion and both direct and indirect links have been established between mitochondria function and Hb expression [10,14,15].

Interestingly, a group of vertebrates known as Antarctic icefish are "null-mutants" for haemoglobin that have some likely relevant cellular modifications, including a high mitochondrial density [16]. Antarctic icefish/white-blooded fish, (subfamily Channichthyidae, family Notothenioidei, suborder Notothenioidei [17]) are the only known vertebrates that do not possess functional haemoglobin genes and red blood cells (RBCs), in stark contrast to all the others that depend upon Hb to get oxygen to tissues and cells, via RBCs [18–20]. The loss of Hb in the Antarctic icefish is postulated to be a mutational process, resulting in the loss of the β-globin (hbb) gene and partial omission of the α-globin (hba) gene from α-/β-globin, causing the locus to become functionally inactive. Fifteen out of the sixteen icefish species are known to retain only a 3′ fragment of an α-globin gene [21]. The sixteenth species, *Neopagetopsis ionah*, retains an intact but unexpressed hba gene fused to two β-globin pseudogenes [22].

As might be expected, some proteins have been shown to be altered in icefish and reasons have been suggested for these differences. Previously, studies have shown changes in the iron transporting proteins such as transferrin, ceruloplasmin, and ferritin [23]. Not all notothenioid species express myoglobin (Mb), an intracellular oxygen-binding protein in the muscle. In total, six of the sixteen icefish species do not express Mb in their heart ventricles, a loss that occurred through four different mutational events [24]. Icefish have large hearts [25], which do not contain the mitochondrial creatine kinase [26]. They also have high mitochondrial densities, which is postulated to counter the effects of cold temperature [27]. The high density of mitochondria rich in lipids serves as a pathway that enhances oxygen storage and diffusion, which compensates for the lack of Hb and Mb [28]. An observed increase in mitochondrial phospholipids may be due to an upregulation in the glycerol-lipid synthesis pathway. There is still a lot to be learned about protein networks and pathways in icefish [29].

Proteomics can be used to identify protein-protein interactions, which in turn influence protein expression or regulation [30]. In silico methods and web servers have been developed to predict the function and structure of proteins [31]. Although large-scale mitochondrial comparative proteomic data have been accumulated, mitochondrial proteomics still faces the challenge of how to investigate the functions of the identified mitochondrial proteins and how to build mitochondria specific signalling networks. An integrative network analysis approach can accommodate information from PPIs and proteomics and bridge the gap between the two. Hence, using an interactive network approach could lay the foundation for a better understanding of mitochondrial changes in icefish [32].

Here, we establish for the first time the proteomes of red muscle mitochondria (RMM) and white muscle mitochondria (WMM) from four species of the suborder Notothenioidei: two icefish, *Champsocephalus gunnari* (*C. gunnari*) devoid of Hb and Mb (the loss of Hb and Mb completely) and *Chionodraco rastrospinosus* (*C. rastrospinosus*), devoid of Hb but with tissue specific expression of Mb that is only expressed in the hearts of these species, are compared to their closely related red-blooded species *Notothenia rossii* (*N. rossii*) and *Trematomus bernacchii* (*T. bernacchii*), both the species belonging to the Nototheniidae, expressing Hb, and having tissue specific expression of Mb only in heart ventricles. Mammalian skeleton muscles are mainly composed of two kinds of fibres, white-fast twitch type that makes the white muscle and red-slow twitch type that makes the red muscle [33]. White muscle requires a greater capacity for anaerobic energy production to meet the demands of the fast-twitch fibres [34]. In contrast to mammalian white muscle tissue, the central regions of icefish red muscle contain numerous mitochondria [16]. In establishing these proteomes, we can understand how the mitochondrial proteome has adapted to the loss of this protein and potentially understand the role and interaction pathways of haemoglobin in the context of mitochondrial biology.

2. Methodology

Antarctic Fish Muscle tissue: SVMS Clinical Ethical Review, University of Nottingham, (ref # 2744 190509). White and red muscle samples of Antarctic notothenioid fish, *N. rossii*, *T. bernacchii* (red-blooded species—Cruise PS112, Weddell Sea in 2013–2014), *C. gunnari* and *C. rastrospinosus* [icefish species—Cruise ANTXXVIII (PS79), Antarctic Peninsula in 2012]. *N. rossii* and *T. bernacchii* have 30–45% of haematocrit and 18–28% haematocrit respectively.

Ethics Statement: The proposal for the Antarctic Fish project was approved by Veterinary School's Clinical Ethical Review panel, University of Nottingham, with responses from at least four members of the panel. No ethical issues were raised by the panel. The Ethical project Number issued: 2744 190509.

Subcellular fractionation: The white and red muscle tissues were stored at −80 °C and while obtaining the fractions were put on ice throughout. The tissues were cut with a sterile blade and then homogenised using Dounce homogeniser, in 2 mL mitochondria extraction buffer (50 mM Tris-Cl pH 7.4, 100 mM KCl, 1.5 mM MgCl2, 1 mM EGTA, 50 mM HEPES and 100 mM sucrose). The homogenized mixture was centrifuged at 800 rpm for 10 min at 4 °C to remove the insoluble fraction, and the first supernatant was centrifuged at 1000 rpm to pellet nuclear fraction. The supernatant obtained from the second centrifuge, was centrifuged at 10,500 rpm at 4 °C for 30 min to obtain the mitochondrial fraction. The supernatant which contained the cytosolic fraction was transferred into a separate tube and the pellet contained the mitochondrial fraction. The quality of the crude fractions was confirmed using standard western blotting techniques with nuclear, mitochondrial and cytoplasmic markers (Histone H3, ab1791 (Abcam) Rb pAB; COX IV ab16056 (Abcam) Rb Ab; and GAPDH, Sigma G9545 Rb respectively) as described previously specific blots or this study can be found [15]. A majority of the proteins identified are associated with mitochondrial processes, confirming the successful fractionation.

Liquid Chromatography-Mass spectroscopy proteomic analysis (LC-MS/MS): Complete mass spectrometry data sets and proteomic identifications are available to download from MassIVE (MSV000089644), [doi:10.25345/C5PZ51Q9F] and ProteomeXchange (PXD034498).

Red Muscle: The extracted mitochondrial fractions of three specimens per species (*C. gunnari:* samples 639, 673, 690; *C. rastrospinosus*: sample 1005, 1020, 1355; *N. rossii*: 4–10, 4–27, 5–14; *T. bernacchii*: samples 7–23, 7–56, 8–24) were captured in gel and sent to the Metabolomics and Proteomics Lab (University of York, York, UK) for Liquid Chromatography-Mass spectroscopy (D-100) proteomic analysis. A label-free, intensity-based quantification for comparing relative protein amounts between samples approach was used. Mass spectrometry data were analysed using PEAKSX software. The mapped ion areas were used

as metric for significance testing for changes in the abundances between groups by using the PEAKSQ interpretation of the significance of the B model. These were converted into relative percent of the total ion area for analysis. The PEAKSQ significance values have been multiply-test-corrected using the Hochberg and Benjamin FDR approach ($q < 0.01$).

Protein identification: The spectra from PEAKSX studio were searched against the combined NCBI deposited proteins from *Notothenia coriiceps* (32,361 sequences; 15,554,893 residues), *Chaenocephalus aceratus* (223 sequences; 59,314 residues), *Dissostichus mawsoni* (210 sequences; 61,335 residues) and *Eleginops maclovinus* (193 sequences; 53,595 residues), in addition to 115 common proteomic contaminant proteins. Protein identifications were filtered to achieve <1% false discovery rate (FDR) as assessed against a reverse database. Identifications were further filtered to require a minimum of two unique peptide identifications per protein group.

White Muscle: The extracted mitochondrial fractions of three specimens per species (*C. gunnari:* 675, 708, 641 samples; *C. rastrospinosus*: 1006, 1021, 1386 samples; *T. bernacchii*: 7–37, 7–54, 8–22 samples; *N. rossii*: 4–25, 4–42, 4–59 samples) were captured in gel and sent to the Metabolomics and Proteomics Lab (University of York, UK) for Liquid Chromatography-Mass spectroscopy (D-270) proteomic analysis. The same approach was applied for analysing the mass spectrometry data for the white muscle mitochondria samples and was matched against the previously mentioned NCBI deposited proteins.

From the proteomic data, we used 'number of spectral matches' as it shows the best metric for the presence and absence of a predicted protein. For the quantitative analysis of the changes in protein proportions, we used the relative percent of total ion map area for comparison of the proteins.

Proteins that were individually low in abundance or higher in abundance for each species were characterised using the number of spectral matches and Ion Map Area (Supplementary Tables S1–S12). The proteins from those lists present in species-specific quantities were grouped and used for comparing the abundance of proteins in red-blooded species (*N. rossii* & *T. bernacchii*) samples and with icefish species (*C. gunnari* & *C. rastrospinosus*) samples. This also took in account the proteins that followed a similar trend in their amounts, i.e., more in abundance in icefish in comparison to red-blooded species and vice versa.

There is no proteomic or genomic data available for these samples so searching against other species was the only option. To help ameliorate issues such as the case of divergent sequences of proteins or/and quantification data of identified peptides, three rounds of searches were performed—initially against Notothenia coriiceps, Chaenocephalus aceratus, Dissostichus mawsoni, and Eleginops maclovinus, which were publicly available using conventional parameters; subsequently, searching was expanded to include 313 common PTMs and single point amino acid substitutions. The inclusion of single point substitution can allow for better coverage between non-identical species. The similarity in mitochondrial proteins between these species and this coupled strategy helps elevate that issue. The similarity in mitochondrial proteins between these species, coupled with the search strategy applied, means that this divergence in species does not appear to be too dramatic in these samples

STRING Network analysis and Clustering: The list of proteins that were found to follow a definite pattern in the proteome of the icefish in comparison to the red-blooded fish were checked as separate groups in the STRING database (http://string-db.org; accessed on 20 February 2021). The protein IDs of the selected protein was extracted from the proteomics data and the respective FASTA sequences were extracted. The multiple FASTA sequence of the proteins was searched against the closest available species on the STRING db, *Danio rerio* (zebrafish) using the multiple sequence. The STRING networks were generated with a medium confidence (0.400) and 5% FDR. Network analyses were visualised in Cytoscape_v3.8.0 [35] and to obtain the top hub proteins, a molecular complex detection plug-in (MCODE) was used to obtain the modules. The criteria used were Degree cut-off = 2, node score cut-off = 0.2, k-core = 2 and max Depth = 100 [36]. The top modules (score > 4) were selected for graphical representation. The hub nodes (proteins) in the

PPI were also analysed by their topological relevance using the Cytoscape plugin CentiScaPe [37] (Supplementary Figures S2, S3, S5 and S6) with default options. The plots were generated using the plot by node option and supports the importance of those highlighted hubs, specifically pointing out the shortest path betweenness and centroid values.

Cytoscape with the GeneMANIA plugin was used to identify the genes most related to the groups of gene sets to form a network of functional genes based on their interaction, such as co-expression, physical-interaction, and shared protein domains. GeneMANIA, a plug-in for Cytoscape, predicts the function of the identified gene sets by using a 'guilt-by-association' approach informed by functional networks from multiple organisms [38]. The gene symbols for the proteins were inputted with default parameters using in-built *D. rerio* gene information, which have been collected from GEO, BioGRID and organism-specific functional genomic data sets. The pathway enrichment was analysed for GO terms 'biological significance' and 'associated metabolic pathways in KEGG'. The enrichment database fishENRICHR was run using gene symbols (Tables 1–4); these were sorted according to the p values ($p < 0.05$, probability of any gene belonging to any set) [39,40].

Graphical representation: R package ggplot2 v.3.5.1. was used for generating heatmaps and volcano plots.

Table 1. Differentially expressed proteins (DEPs) among the four species in RMM—higher abundance in icefish.

S. No.	Protein Abundance—Higher in Icefish (Red Muscle Mitochondria)			Relative Percent of Total Ion Area (Mapped)—Converted from Total Sum of Ion Area to Relative Percent of Total Ion Area				
	Protein Name	**Gene Name**	**Quant Significance H&B Multiple Test Corrected q-Value**	***N. rossii***	***T. bernacchii***	***C. rastrospinosus***	***C. gunnari***	**Accession Number**
1	26S protease regulatory subunit 4 isoform X1 & X2	psmc1a	1.25×10^{-6}	4.9	6.6	7	81.4	XP_010780333.1
2	Apolipoprotein B-100-like partial	apobb	3.76×10^{-19}	3.2	3.3	27.9	65.6	XP_010781933.1
3	NAD(P) transhydrogenase mitochondrial-like	nnt	2.95×10^{-19}	5.5	5.8	29.6	59.2	XP_010786020.1
4	Hyaluronan and proteoglycan link protein 1	hapln1	7.26×10^{-20}	9.1	5.2	30	55.7	XP_010767902.1
5	Sarcolemmal membrane-associated protein-like isoform X1 & X2	slmapa	9.73×10^{-3}	15.2	15.7	24	45.1	XP_010782086.1
6	ADP/ATP translocase 2-like	slc25a5	1.03×10^{-18}	13	6.2	36.5	44.3	XP_010765274.1
7	Dihydrolipoyllysine-residue acetyltransferase component of pyruvate dehydrogenase complex	dlat	9.09×10^{-12}	15.9	16.3	27.3	40.5	XP_010773292.1
8	Alpha-2-macroglobulin-like partial	a2ml	1.23×10^{-4}	14.7	22.1	23.1	40.1	XP_010771939.1
9	Inter-alpha-trypsin inhibitor heavy chain H4-like	itih3a.2	1.37×10^{-11}	12.1	12.7	35.9	39.3	XP_010793736.1
10	Stress-70 protein mitochondrial-like	hspa9	1.58×10^{-5}	20	18.3	33.7	28.1	XP_010766277.1
11	Epoxide hydrolase 1	ephx1l	3.79×10^{-20}	10.2	21.6	31.1	37.1	XP_010790338.1
12	Sorting and assembly machinery component 50 homolog	samm50	1.65×10^{-19}	17.4	8.9	37.3	36.4	XP_010773400.1
13	Calcium-binding mitochondrial carrier protein Aralar1	slc25a12	1.21×10^{-19}	23	7.8	32.8	36.4	XP_010768357.1
14	Long chain fatty acyl CoA synthetase	acsl1a	5.88×10^{-7}	2.6	19.1	42.1	36.1	AAK07470.1
15	Malonyl-CoA decarboxylase mitochondrial	mlycd	3.73×10^{-20}	10.9	18.7	34.7	35.6	XP_010792494.1
16	NADH dehydrogenase [ubiquinone] 1 beta subcomplex subunit 8 mitochondrial	ndufb8	6.625×10^{-7}	13.1	19.5	31.9	35.6	XP_010779169.1
17	60S ribosomal protein L27a isoform X1 & X2	rpl27a	5.17×10^{-20}	10.7	14.8	38.9	35.6	XP_010790259.1
18	Fatty acid binding protein H8-isoform	fabp3	2.43×10^{-19}	2.4	25.6	37.2	34.8	AAC60356.1
19	ATP-dependent 6-phosphofructokinase muscle type-like	pfkm	2.02×10^{-10}	22.3	12.5	31	34.2	XP_010794434.1
20	Carnitine/acylcarnitine carrier protein	slc25a20	1.2×10^{-19}	20	9.9	36.2	33.9	XP_010773584.1
21	ATP synthase subunit O	atp5o	4.06×10^{-8}	24.6	13.4	29.1	32.9	XP_010772138.1
22	Proliferation-associated protein 2G4-like	pa2g4b	4.31×10^{-3}	19	21.8	27.3	32	XP_010782747.1

Table 1. *Cont.*

S. No.	Protein Abundance—Higher in Icefish (Red Muscle Mitochondria)			Relative Percent of Total Ion Area (Mapped)—Converted from Total Sum of Ion Area to Relative Percent of Total Ion Area				
	Protein Name	**Gene Name**	**Quant Significance H&B Multiple Test Corrected q-Value**	***N. rossii***	***T. bernacchii***	***C. rastrospinosus***	***C. gunnari***	**Accession Number**
23	ATP synthase subunit g mitochondrial	atp5l	2.26×10^{-7}	23.1	10.6	34.4	31.9	XP_010779232.1
24	Voltage-dependent anion-selective channel protein 3	vdac3	4.6×10^{-19}	13.2	12.1	43.2	31.6	XP_010782516.1
25	ATP synthase subunit alpha mitochondrial	atp5fa1	7.02×10^{-9}	22.2	14.9	31.7	31.2	XP_010779868.1
26	ATP synthase subunit beta mitochondrial	zgc:163069	1.07×10^{-8}	24.7	13.4	31.1	30.8	XP_010765728.1
27	ATP synthase subunit gamma mitochondrial isoform X1	atp5g	2.53×10^{-14}	18.3	10	41.5	30.1	XP_010778067.1
28	60S ribosomal protein L35	rpl35	2.93×10^{-15}	14.9	15.2	40.2	29.6	XP_010790499.1
29	ATP synthase F(0) complex subunit B1 mitochondrial	atp5pb	1.54×10^{-15}	23	11.6	36	29.5	XP_010786327.1
30	ATP synthase subunit delta mitochondrial	atp5d	6.63×10^{-3}	18.8	23.4	28.4	29.4	XP_010775450.1
31	Prothrombin partial	f2	7.41×10^{-20}	14.3	23.2	33.2	29.3	XP_010786167.1
32	ADP/ATP translocase 3	slc25a6	5.06×10^{-12}	23.5	13.6	33.9	29	XP_010784438.1
33	60S ribosomal protein L18a-like	rpl18a	3.97×10^{-8}	18.2	18.8	34.1	28.9	XP_010774792.1
34	ATP synthase subunit d mitochondrial	atp5pd	8.44×10^{-20}	25.2	8.6	37.5	28.7	XP_010766730.1
35	Malate dehydrogenase cytoplasmic-like partial	mdh1aa	7.88×10^{-16}	13.2	16.9	42.1	27.8	XP_010766317.1
36	Cytochrome c oxidase subunit 5A mitochondrial isoform X2	cox5a	5.67×10^{-20}	16.5	9.2	46.4	27.8	XP_010766309.1
37	60S ribosomal protein L23	rpl23	1.13×10^{-12}	15.9	20.4	37	26.7	XP_010783746.1
38	Prohibitin	phb	2.72×10^{-6}	18.1	18.4	39.1	24.5	XP_010773724.1
39	Ubiquinone biosynthesis protein COQ9	coq9	8.44×10^{-11}	17.2	17.6	42.1	23	XP_010793356.1
40	26S proteasome non-ATPase regulatory subunit 6	psmd6	3.76×10^{-2}	8.5	15	28.3	48.1	XP_010773228.1
41	Fragile X mental retardation syndrome-related protein 2	fxr2	7.06×10^{-2}	9.6	10.5	16.4	63.5	XP_010770797.1
42	Reticulon-4-interacting protein 1 homolog mitochondrial-like	rtn4ip1	1.04×10^{-1}	19.8	20.5	28.7	31	XP_010790805.1
43	Kininogen-1	kng1	1.28×10^{-1}	13.7	16.6	25.8	43.8	XP_010787469.1

Table 2. DEPs between WMM with increased abundance in icefish specifically seen upregulated in icefish *Champsocephalus gunnari*.

Protein Abundance—Higher in Icefish (White Muscle)				Relative Percent of Total Ion Area (Mapped)—Converted from Total Sum of Ion Area to Relative Percent of Total Ion Area				
S. No.	**Protein Name**	**Gene Name**	**Quant Significance H&B Multiple Test Corrected *q*-Value**	***N. rossii***	***T. bernacchii***	***C. rastrospinosus***	***C. gunnari***	**Accession Number**
1	Myosin regulatory light chain 2 skeletal muscle isoform-like	mylpfb	3.42×10^{-19}	1	2.2	2.3	94.4	XP_010770965.1
2	Myozenin-1 isoform X1 & X2	myoz1b	1.54×10^{-7}	0	7.8	13.3	78.9	XP_010791910.1
3	Heat shock protein beta 1	hspb1	9.48×10^{-5}	9.9	4.1	11.5	74.6	XP_010788098.1
4	60S ribosomal protein L35	rpl35	4.58×10^{-20}	3.4	7.9	32.7	56	XP_010790499.1
5	40S ribosomal protein S16 isoform X1	rps16	9.29×10^{-3}	12.3	16.9	17.9	52.8	XP_010773777.1
6	60S ribosomal protein L7	rpl7	1.08×10^{-6}	6.9	7.8	33.1	52.3	XP_010770361.1
7	Fragile X mental retardation syndrome-related protein 2	fxr2	6.55×10^{-4}	4.6	11.6	32.2	51.6	XP_010770797.1
8	40S ribosomal protein S12	rps12	1.13×10^{-4}	8.4	13.8	27	50.8	XP_010783785.1
9	60S ribosomal protein L30	rpl30	8.33×10^{-5}	3.1	22.6	24	50.3	XP_010765856.1
10	60S ribosomal protein L12 isoform X2	rpl12	5.13×10^{-20}	9.9	11.7	28.5	49.8	XP_010779104.1
11	Reticulon	rtn1a	5.51×10^{-20}	14.9	13	22.7	49.4	XP_010790870.1
12	Palladin-like	palld	1.07×10^{-14}	2.7	15.9	32.1	49.2	XP_010785200.1
13	60S ribosomal protein L9	rpl9	4.70×10^{-20}	4.2	3.4	43.7	48.7	XP_010776310.1
14	AMP deaminase 1 isoform X1 & X2	ampd1	1.65×10^{-19}	18.6	10.9	22.8	48.4	XP_010793467.1
15	ADP/ATP translocase 3	slc25a5	3.22×10^{-10}	7.8	10.6	33.7	47.8	XP_010784438.1
16	40S ribosomal protein S13	rps13	9.87×10^{-4}	13.1	10.6	29.1	47.3	XP_010794693.1
17	40S ribosomal protein S8-like partial	rps8	2.91×10^{-10}	9.1	11.8	33	46	XP_010787537.1
18	Alpha-actinin-2	actn2	1.42×10^{-8}	12.1	18.2	23.6	46	XP_010791686.1
19	Kelch-like protein 41b	klhl41b	5.57×10^{-20}	4.2	11.6	38.5	45.7	XP_010791686.1
20	60S ribosomal protein L6	rpl6	4.536×10^{-20}	7	11.3	36.3	45.4	XP_010774286.1
21	40S ribosomal protein S5	rps5	7.75×10^{-4}	17	12.2	25.5	45.3	XP_010782543.1
22	Cytochrome c oxidase subunit II	mt-co2	5.91×10^{-13}	2.6	26.8	25.9	44.7	XP_010783741.1
23	40S ribosomal protein S25	rps25	6.64×10^{-3}	13	14.5	28.4	44.2	YP_004581500.1
24	60S ribosomal protein L11	rpl11	4.98×10^{-20}	15.6	11.7	29.1	43.7	XP_010776714.1

Table 2. *Cont.*

Protein Abundance—Higher in Icefish (White Muscle)				Relative Percent of Total Ion Area (Mapped)—Converted from Total Sum of Ion Area to Relative Percent of Total Ion Area				
S. No.	**Protein Name**	**Gene Name**	**Quant Significance H&B Multiple Test Corrected *q*-Value**	***N. rossii***	***T. bernacchii***	***C. rastrospinosus***	***C. gunnari***	**Accession Number**
25	Voltage-dependent anion-selective channel protein 2	vdac2	8.76×10^{-7}	15.6	10.6	30.4	43.5	XP_010779161.1
26	40S ribosomal protein S4	rps4x	6.41×10^{-20}	7.5	16	33.6	43	XP_010767141.1
27	40S ribosomal protein S2	rps2	5.4×10^{-20}	6.8	11.4	39	42.8	XP_010792965.1
28	60S ribosomal protein L10a	rp10a	2.26×10^{-14}	14.8	15.1	29.7	40.4	XP_010783756.1
29	40S ribosomal protein S9	rps9	4.40×10^{-8}	12.5	17.9	29.3	40.3	XP_010791484.1
30	ATP synthase subunit g	atp5l	4.66×10^{-20}	18.7	11.6	32.7	37	XP_010786813.1
31	Vinculin	vcla	1.15×10^{-7}	18.7	11.6	32.7	37	XP_010794136.1
32	60S ribosomal protein L13	rpl13	5.51×10^{-11}	8.2	16	39.4	36.5	XP_010787927.1
33	Fructose-1 6-bisphosphatase isozyme 2-like	fbp2	5.63×10^{-20}	9.8	26	28.1	36.1	XP_010789836.1
34	40S ribosomal protein SA isoform X2	rpsa	6.10×10^{-20}	10	17.7	37.1	35.3	XP_010781656.1
35	Succinyl-CoA ligase	suclg1	6.66×10^{-11}	5.5	10.2	49.4	35	XP_010768032.1
36	Tubulin alpha chain-like isoform X1 & X2	tuba8l2	4.49×10^{-4}	11.3	23.9	29.9	34.9	XP_010778226.1
37	60S ribosomal protein L23a	rpl23a	5.29×10^{-8}	3.5	9.8	56.9	34.8	XP_010766070.1
38	NADH-ubiquinone oxidoreductase	mt-nd1	8.21×10^{-7}	3.5	9.8	51.9	34.7	XP_010791811.1
39	Alpha-enolase-like	eno1a	4.27×10^{-4}	13	22.3	30.3	34.5	XP_010777506.1
40	Isocitrate dehydrogenase	idh1	1.22×10^{-19}	20.6	11	35.7	32.6	XP_010765339.1
41	26S proteasome non-ATPase regulatory subunit 12	psmd12	1.19×10^{-3}	10	11.8	47.6	30.6	XP_010791048.1
42	ATP synthase F(0) complex subunit B1	atp5pb	2.06×10^{-10}	19	6.4	44.2	30.2	XP_010777584.1
43	Peptidyl-prolyl cis-trans isomerase-like	pplb	1.02×10^{-3}	8	27.2	35.3	29.5	XP_010786327.1
44	Malate dehydrogenase	mdh1aa	1.71×10^{-19}	15.1	9	46.6	29.4	XP_010790691.1
45	ATP synthase subunit O	atp5o	5.16×10^{-4}	16.1	9.4	45.9	28.6	XP_010780749.1
46	NAD(P) transhydrogenase	nnt	5.81×10^{-8}	15.9	16.7	39	28.3	XP_010772138.1
47	Glycogen phosphorylase muscle form-like	pygma	8.47×10^{-6}	17.7	25.3	30	26.9	XP_010776087.1
48	Ubiquitin carboxyl-terminal hydrolase 5 isoform X1	usp5	4.8×10^{-4}	9.3	19.1	44.8	26.7	XP_010788355.1

Table 2. *Cont.*

Protein Abundance—Higher in Icefish (White Muscle)				Relative Percent of Total Ion Area (Mapped)—Converted from Total Sum of Ion Area to Relative Percent of Total Ion Area				
S. No.	**Protein Name**	**Gene Name**	**Quant Significance H&B Multiple Test Corrected *q*-Value**	***N. rossii***	***T. bernacchii***	***C. rastrospinosus***	***C. gunnari***	**Accession Number**
49	Cytochrome b-c1 complex subunit 2	uqcrfs1	4.32×10^{-4}	11.7	10.4	52.9	25	XP_010769500.1
50	ATP synthase subunit gamma	atp5g	1.41×10^{-12}	13.4	12.3	49.6	24.7	XP_010784571.1
51	ATP synthase subunit beta	zgc:163069	9.98×10^{-16}	17.5	12.4	46.2	23.8	XP_010778067.1
52	Pyruvate kinase PKM	pkma	5.13×10^{-19}	11	10.3	56	22.7	XP_010765728.1
53	Vitellogenin-1-like	vtg2	1.38×10^{-2}	0	2	93.6	4.4	XP_010766216.1
54	Proteasome subunit alpha type-7-like	psma8	1.96×10^{-2}	9.6	11.7	55.1	23.6	XP_010779640.1
55	Guanine nucleotide-binding protein subunit beta-2-like 1	gnb2l1	1.57×10^{-2}	13.2	21	29.6	36.2	XP_010783619.1
56	ATP-dependent 6-phosphofructokinase muscle type-like	pfkmb	1.84×10^{-2}	16.7	17.3	26.1	39.9	XP_010780163.1
57	Inter-alpha-trypsin inhibitor heavy chain H3-like	zgc:110377	1.92×10^{-2}	0	14.4	46.5	39.1	XP_010782695.1

Table 3. DEPs in RMM with decreased abundance in icefish specifically seen downregulated in icefish *Champsocephalus gunnari*.

Protein Abundance—Lower in Icefish (Red Muscle)				Relative Percent of Total Ion Area (Mapped)—Converted from Total Sum of Ion Area to Relative Percent of Total Ion Area				
S. No.	**Protein Name**	**Gene Name**	**Quant Significance H&B Multiple Test Corrected *q*-Value**	***N. rossii***	***T. bernacchii***	***C. rastrospinosus***	***C. gunnari***	**Accession Number**
1	Hemoglobin subunit alpha-1	hbae1	1.88×10^{-19}	60	38.7	0.8	0.5	NP_001290227.1
2	Calsequestrin-1	casq1	6.08×10^{-20}	33.3	44.4	18.6	3.7	XP_010782377.1
3	Perilipin-3	plin3	1.53×10^{-19}	48.8	35.6	11.1	4.5	XP_010778108.1
4	creatine kinase S-type mitochondrial-like	ckmt2a	4.35×10^{-19}	71.4	22.4	1.4	4.8	XP_010772488.1
5	Transferrin	tfa	8.36×10^{-20}	34	54.2	17.3	5.5	CAI.92189.1
6	Dehydrogenase/reductase SDR family member 7C	dhrs7cb	3.01×10^{-9}	68.9	18.2	7.1	5.7	XP_010784042.1
7	Myosin-binding protein H-like	mybpha	$9.09 \times 10\text{-}^{20}$	66.6	20.7	5.9	6.8	XP_010764981.1
8	Band 3 anion transport protein	slc4a1	1.91×10^{-8}	39	52	2.1	6.9	XP_010785995.1

Table 3. *Cont.*

Protein Abundance—Lower in Icefish (Red Muscle)				Relative Percent of Total Ion Area (Mapped)—Converted from Total Sum of Ion Area to Relative Percent of Total Ion Area				
S. No.	**Protein Name**	**Gene Name**	**Quant Significance H&B Multiple Test Corrected *q*-Value**	***N. rossii***	***T. bernacchii***	***C. rastrospinosus***	***C. gunnari***	**Accession Number**
9	Cytochrome c oxidase subunit 4 isoform 2 mitochondrial-like	cox4i2	5.79×10^{-20}	60.1	22.5	9.6	7.7	XP_010770791.1
10	Titin-like	ttna	2.47×10^{-11}	50.9	21.6	19.4	8.1	XP_010787367.1
11	Glutaryl-CoA dehydrogenase mitochondrial-like	gcdh	4.92×10^{-20}	34	28.8	28.2	9	XP_010795730.1
12	Fibrillin-1-like isoform X1	fbn2a	5.14×10^{-20}	67.5	17.5	6	9	XP_010767938.1
13	heme oxygenase 2	hmox1	1.18×10^{-4}	48.5	20.6	21.3	9.7	XP_010786435.1
14	NADP-dependent malic enzyme	me1	1.29×10^{-19}	33.9	40.3	16	9.8	XP_010776993.1
15	Pyruvate dehydrogenase phosphatase regulatory subunit	pdpr	8.30×10^{-9}	24.9	48.6	15.4	11.1	XP_010773093.1
16	Dolichyl-diphosphooligosaccharide–protein glycosyltransferase subunit 1	rpn1	7.17×10^{-12}	38.5	30.1	20.2	11.2	XP_010777725.1
17	CDGSH iron-sulfur domain-containing protein 1	zgc:110843	4.54×10^{-20}	41	36	11.6	11.5	XP_010767760.1
18	Glutamate dehydrogenase	gdh	3.06×10^{-19}	29.9	48.6	11.1	11.9	P82264.1
19	Thioredoxin-dependent peroxide reductase mitochondrial	prdx3	6.46×10^{-20}	31.2	29.5	27.2	12.1	XP_010779546.1
20	malate dehydrogenase	mdh	1.178×10^{-12}	32.5	37	18.4	12.1	XP_010765488.1
21	Cytochrome c	cycsb	5.55×10^{-20}	42.8	28.7	16.1	12.5	XP_010792793.1
22	Troponin T fast skeletal muscle isoforms-like isoform X1 to X3	tnnt3a	4.89×10^{-20}	37.2	29.6	20.5	12.7	XP_010784864.1
23	Superoxide dismutase [Mn] mitochondrial	sod2	1.01×10^{-10}	42	33.4	11.5	13.1	XP_010771234.1
24	Carnitine O-acetyltransferase	crat	6.46×10^{-13}	29.1	38.8	19	13.1	XP_010795330.1
25	PDZ and LIM domain protein 7	ENSDARG00000030638	1.44×10^{-8}	45.5	21	20.3	13.3	XP_010765699.1
26	Protein FAM162B-like	fam162a	4.13×10^{-4}	41.5	32	13	13.6	XP_010783349.1
27	Aconitate hydratase mitochondrial	aco1	4.14×10^{-19}	45.3	26.8	14	14	XP_010781940.1
28	Retinol dehydrogenase 13-like isoform X1 & X2	wu:fd55e03	2.59×10^{-13}	42.1	26.2	17.6	14.1	XP_010791045.1
29	Myosin-binding protein C slow-type isoform X1 to X17	mybpc	2.39×10^{-3}	39.8	27.3	18.8	14.1	XP_010774860.1
30	Lumican	lum	2.21×10^{-7}	47.8	26.9	11.3	14.1	XP_010795529.1
31	Retinol dehydrogenase 13-like isoform X1	rdh13	2.59×10^{-13}	26.2	42.1	17.6	14.1	XP_010791045.1
32	PDZ and LIM domain protein 7-like isoform X2	ENSDARG00000030638	4.70×10^{-20}	40.6	26.1	18.9	14.4	XP_010785930.1

Table 3. *Cont.*

Protein Abundance—Lower in Icefish (Red Muscle)				Relative Percent of Total Ion Area (Mapped)—Converted from Total Sum of Ion Area to Relative Percent of Total Ion Area				
S. No.	**Protein Name**	**Gene Name**	**Quant Significance H&B Multiple Test Corrected *q*-Value**	***N. rossii***	***T. bernacchii***	***C. rastrospinosus***	***C. gunnari***	**Accession Number**
33	Glycogen phosphorylase	pygm	7.81×10^{-20}	30.6	44.1	10.9	14.4	XP_010788472.1
34	Alpha-aminoadipic semialdehyde dehydrogenase	aldh7a1	1.25×10^{-19}	36.3	28.9	20	14.7	XP_010772035.1
35	Myozenin-1-like	myoz1a	7.07×10^{-20}	46.5	26.8	12	14.7	XP_010764663.1
36	Collagen alpha-1(I) chain-like	col1a1a	9.40×10^{-20}	52.6	27.3	5.3	14.8	XP_010768975.1
37	Peroxiredoxin-5 mitochondrial	prdx5	8.32×10^{-7}	30.5	28.9	25.2	15.4	XP_010783999.1
38	Short-chain specific acyl-CoA dehydrogenase mitochondrial	acads	4.54×10^{-8}	32.5	26.7	25.1	15.8	XP_010779541.1
39	Troponin alpha-3 chain-like	tnnt3b	1.56×10^{-19}	36.9	35.9	11	16.1	XP_010771394.1
40	Creatine kinase M-type	ckmb	4.11×10^{-5}	34.8	25.6	23.3	16.3	XP_010791917.1
41	Glycerol-3-phosphate dehydrogenase mitochondrial	gpd2	1.13×10^{-10}	42.6	23.5	17	16.9	XP_010791177.1
42	electron transfer flavoprotein subunit beta	etfb	2.38×10^{-5}	33.9	24.8	24.2	17.1	XP_010791064.1
43	1 4-alpha-glucan-branching enzyme	gbe1b	2.20×10^{-10}	28.1	44.4	10.4	17.1	XP_010775191.1
44	Ubiquitin carboxyl-terminal hydrolase 5 isoform X1 & X2	usp5	8.40×10^{-5}	34.9	25.9	21.1	18	XP_010769508.1
45	Methylmalonyl-CoA mutase mitochondrial	mut	2.48×10^{-4}	33.7	26.7	21.5	18	XP_010784587.1
46	probable acyl-CoA dehydrogenase 6	zgc:85777	1.82×10^{-3}	31.3	26.9	23.2	18.6	XP_010772948.1
47	Alpha-actinin-3	actn3b	5.52×10^{-19}	39.5	28.5	13.3	18.7	XP_010784415.1
48	Carbonic anhydrase 1	ca1	7.88×10^{-20}	49.4	20	10.9	19.6	XP_010765900.1

Table 4. DEPs between WMM with decreased abundance in the icefish.

Protein Abundance—Lower in Icefish (White Muscle)				Relative Percent of Total Ion Area (Mapped)—Converted from Total Sum of Ion Area to Relative Percent of Total Ion Area				
S. No.	**Protein Name**	**Gene Name**	**Quant Significance H&B Multiple Test Corrected *q*-Value**	***N. rossii***	***T. bernacchii***	***C. rastrospinosus***	***C. gunnari***	**Accession Number**
1	Calreticulin	calr	5.72×10^{-3}	75.4	4.7	19.8	0	XP_010773398.1
2	Creatine kinase S-type mitochondrial-like	ckmt2a	1.19×10^{-19}	78.2	14.8	6.4	0.7	XP_010772488.1
3	Myosin heavy chain fast skeletal 13	zgc:66156	3.68×10^{-3}	37.8	34.7	26.6	0.9	XP_010791001.1
4	Prothrombin partial	f2	7.77×10^{-4}	37.3	30.3	31.2	1.1	XP_010786167.1
5	Fibronectin	fn1a	1.33×10^{-5}	33.1	30.2	34.9	1.8	XP_010794764.1
6	Transmembrane protease serine 2-like	LOC571565	6.81×10^{-3}	81.2	16.8	0	2	XP_010778161.1
7	Hemoglobin subunit zeta	hbz	2.98×10^{-4}	80.5	16.4	0.3	2.5	XP_010778322.1
8	Fibrinogen alpha chain-like	fga	2.67×10^{-5}	51.4	39.8	5.2	2.8	XP_010771898.1
9	Alpha globin	hbaa1	7.77×10^{-20}	79.6	16.5	0.4	3.3	AAC25100.1
10	Beta-globin	ba-1	7.45×10^{-9}	87.5	9.1	0	3.4	AAC60372.1
11	Haemoglobin	hb	7.33×10^{-9}	87.5	9.1	0	3.4	NP_001290226.1
12	Ryanodine receptor 1-	ryr1a	3.16×10^{-4}	54.5	19.7	21.1	4.5	XP_010787188.1
13	Keratin type I cytoskeletal 19-like	zgc:153629	8.84×10^{-20}	54.7	31.8	8.9	4.6	XP_010787448.1
14	Myosin heavy chain fast skeletal muscle-like	myhb	4.58×10^{-12}	46.7	27.6	19.2	6.5	NP_001290213.1
15	Malate dehydrogenase cytoplasmic	mdh1aa	5.56×10^{-7}	54.8	24.1	13.3	7.8	XP_010765488.1
16	Apolipoprotein A	apoa1	1.282×10^{-19}	54.4	20	16.1	9.3	XP_010792180.1
17	Myomesin-1-like	myom1	1.31×10^{-19}	31.1	29.8	21.8	17.3	XP_010789743.1
18	Betaine-homocysteine S-methyltransferase 1-like	bhmt	7.32×10^{-20}	53.1	20.8	14.4	11.6	XP_010794476.1
19	Collagen alpha-1(I) chain-like	col1a1b	6.56×10^{-4}	37.2	34.6	15.8	12.4	XP_010768975.1
20	Hemopexin	zgc:152945	3.14×10^{-6}	40.7	26.6	19.7	13	XP_010788340.1
21	T-complex protein 1 subunit theta	cct8	3.34×10^{-6}	60.6	18.2	7.4	13.9	NP_001290219.1
22	Transitional endoplasmic reticulum ATPase-like	vcp	3.10×10^{-3}	51.4	20.5	12.7	15.4	XP_010770092.1
23	40S ribosomal protein S11	rps11	8.261×10^{-4}	43.2	32.7	8.7	15.5	XP_010791578.1
24	Titin-like partial	ttna	1.66×10^{-3}	32.9	28.7	21.1	17.2	XP_010790363.1

Table 4. *Cont.*

Protein Abundance—Lower in Icefish (White Muscle)				Relative Percent of Total Ion Area (Mapped)—Converted from Total Sum of Ion Area to Relative Percent of Total Ion Area				
S. No.	**Protein Name**	**Gene Name**	**Quant Significance H&B Multiple Test Corrected *q*-Value**	***N. rossii***	***T. bernacchii***	***C. rastrospinosus***	***C. gunnari***	**Accession Number**
25	Calmodulin	calm1a	1.197×10^{-10}	36.2	30.9	14	18.9	XP_010768524.1
26	40S ribosomal protein S3a	rps3a	9.93×10^{-12}	35.1	30.1	15.3	19.5	XP_010773841.1
27	Obscurin isoform X2	obscnb	2.1×10^{-2}	36.8	30.2	14.9	18.1	XP_010790854.1
28	Transferrin	tfa	3.14×10^{-2}	36.3	33.5	22.7	7.6	CAL92189.1
29	Collagen alpha 1(XII) chain isoform X1, X2, X3, X4 & X5	col12a1a	8.53×10^{-2}	68.8	18.2	8.5	4.5	XP_010777236.1
30	Nebulin-like isoform X4	neb	2.23×10^{-1}	54.2	23.8	9.2	12.7	XP_010772593.1
31	Myosin-binding protein C slow-type isoform X1 to X17	mybpc3	1.31×10^{-1}	45.6	26.9	12.6	14.9	XP_010774870.1
32	Collagen alpha-2(I) chain isoform X1	col1a2	2.91×10^{-1}	54.6	20.8	9.6	14.9	XP_010772950.1

3. Results

3.1. LC/LC-MS Data for RMM and WMM

The purpose of the study was to identify mitochondrial and mitochondrial-associated proteins in icefish and to understand how the loss of haemoglobin affects the proteome. LC-MS/MS data were analysed using PEAKSX for reliable matching to the available sequence database and the data were filtered to a 1% false discovery rate by at least two unique peptides for each protein group (Figure 1(A1,B1)). For red muscle mitochondria (RMM), 1148 proteins were identified belonging to unique protein groups; this contrasts with white muscle mitochondria (WMM), where 429 proteins were identified. Haemoglobin α, β and γ were only identified in the red-blooded fish confirming sample specificity. The two types of muscle are faced with very different energetic demands; however, previously it has been shown that there are no large differences in mitochondrial protein expression when surveying different porcine muscle tissues [41].

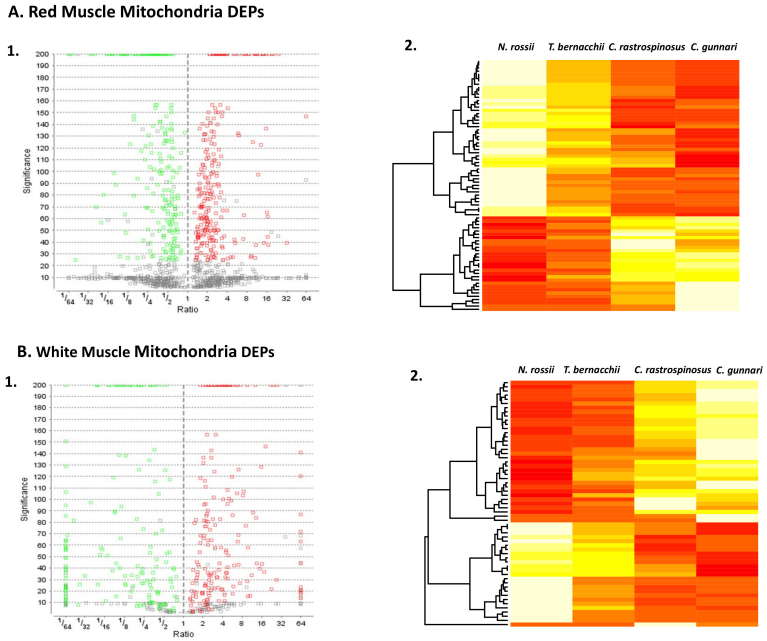

Figure 1. Volcano Plot and Heat Map of DEPs for the two tissue types. Volcano plot for differentially expressed proteins (**A1**,**B1**). The x axis depicts log fold change and y axis depicts FDR; the lower genes are low p values, less significant. Genes that are upregulated are on the right side of the graph and those that down regulate are on the left side of the graph (FDR > 0.01). DEPs in red muscle mitochondria (**A2**) and white muscle mitochondria (**B2**) for the four species (Red is significantly more highly expressed). The heat maps are produced using the relative percent of total ion area that is used for comparing the change in abundance for the same protein from different samples. A clear distinction in the expression of the protein abundance among different species can be seen, red being more abundant and yellow being less (List of proteins Tables 1–4).

Group 1 consisted of the proteins that were significantly more abundant, and group 2 consisted of less abundant proteins in the two icefish species when compared with the red-blooded species (Tables 1–4). The reported significance value is the –log10 p value, with the null hypothesis being that the protein is of equal abundance in all samples. The higher the significance value the greater the probability that the protein is not equal in abundance in all groups. The volcano plot distinctively shows the significant differentially expressed proteins (DEPs) ($q < 0.05$) that were downregulated (green) and upregulated (red). The WMM had fewer proteins that were not significant when compared to the RMM. A heat map that includes the differentially expressed proteins (DEPs) in red muscle (Figure 1(A2)) and white muscle (Figure 1(B2)) mitochondria illustrates that protein expression profiles are characteristic for the haemoglobin-less species when compared with red-blooded groups. The mapped ion areas were converted to relative percent values by weighting each protein equally to point out differences between groups.

There was a common increase in abundance in the complex V proteins and a group of ribosomal proteins (more evidently in the white muscle) in the icefish in both the muscle mitochondria tissues. A few mitochondrial import proteins were also seen to be increased such as ADP/ATP translocases, voltage-dependent anion channels, and heat shock proteins. A common decrease in abundance in the proteins for the icefish were seen in Hb and haem/Hb-associated proteins such as cytochrome c, transferrin, haem oxygenase 2 and hemopexin. Apart from those, a decrease in the abundance was seen in muscle proteins such as creatine kinase, troponin, titin, and myosin heavy chain.

The two groups of proteins from both the tissues RMM and WMM were mapped into protein-protein interaction (PPI) networks constructed using STRINGdb. The enrichment p-value for each of the three PPI networks is lesser than10^{-16}, indicating that proteins share more interactions than would be expected for a random set of proteins of similar size drawn from the proteome and suggesting at least partial biological connection as a group [42]. The network was retrieved and analysed using Cytoscape software, which allowed us to visualize and analyse molecular interaction networks [43] (Figures 2 and 4) [38].

3.2. Analysis of Proteins More in Abundance in Icefish

Forty-three proteins were differentially expressed with higher abundance in the RMM of the two icefishes compared to the red-blooded nonfamilial species. Fifty-seven proteins were significantly higher expressed in the WMM (Tables 1 and 2). Most proteins that were seen upregulated in both RMM and WMM were found to be part of the complex V, ribosomal and proteosome machineries in addition to a common upregulated expression of malate dehydrogenase and Fragile X mental retardation isoform 2 protein. In RMM, components of complex V of the electron transport chain and proteins involved in transportation across mitochondria were observed. The upregulated proteins of WMM were involved in the citrate cycle and carbon metabolism.

GeneMANIA (based on zebrafish) analysis for interactions of the proteins with increased abundance in icefish produced one network per each muscle tissue (Figure 2A,B). In RMM, co-expression occupied 98.66% of the interactions seen in the network; shared protein domains occupied 1.13%; physical interaction, 0.21%. The network showed shared domains among proteins slc25a5, slc25a6, slc25a20, vdac3 and slc25a12, and, between atp5a1 and atp5b. The network showed physical interactions between atp5a1, atp5o, predicted cyc1 and coq9. In WMM, co-expression occupied 98.46% of the interactions seen in the network; physical interactions occupied 1.431%; and shared protein domains occupied 0.11%. The network showed physical interactions between ribosomal proteins and separately also between proteasome proteins.

Figure 2. Gene interaction networks for DEPs with increased abudance in icefish. (**A**) RMM Analysis and (**B**) WMM Analysis. A GeneMANIA gene–gene interaction network for protein abundance following the pattern *N. rossii* (+/+), *T. bernacchii* (+/+), *C. rastrospinosus* (−/+) and *C. gunnari* (−/−) in increasing order of their protein abundance, laid out and visualised with Cytoscape, showing interaction strength (edge thickness), interaction type (colour-bottom right), multiple edges between nodes, and protein score (node size). Black nodes indicate query proteins, and grey nodes are neighboring proteins with interactions as co-expressed, physical, or shared protein domains.

Figure 3A shows the PPI network generated using the FASTA sequences (corresponding NCBI IDs) for the proteins using STRING. The 43 identified DEPs that were more abundant in RMM were analysed and connected with a PPI enrichment p-value $< 1.0 \times 10^{-16}$, with 42 nodes (proteins RPL27 was not identified for organism *D. rerio*), 143 edges, and an average node-degree of 6.8. Four of forty-two DEPs (RTN4IP1, PFKMA, FRX2 and HAPLN1b) did not connect to any type of network (STRING interaction score = 0.4). Thirty-eight of the remaining DEPs were connected to networks by complex relationships. RPL23, MDH1AA, ATP5B, and VDAC3 showed network hubs highly associated with other nodes in PPI. (Supplementary Figure S2). A single network was formed between DEPs ITIH4, A2ML, KNG1, F2 and APOBB. The highly connected proteins are majorly involved in energy metabolism and protein metabolism. Three distinctive clusters were seen for RMM upregulated proteins. Cluster 1 had proteins involved in ETC and oxidative phosphorylation, Cluster 2, proteins involved in cell signalling, and Cluster 3, proteins involved in fatty acid biosynthesis (Supplementary Figure S1).

Functional enrichment analysis (FDR $< 1.9 \times 10^{-2}$) showed proteins involved in the TCA cycle, oxidative phosphorylation, degradation of RNA, cristae formation, mitochondrial protein import, and carbon metabolism (See Figure 3A), using the STRINGdb information provided under KEGG and Reactome pathways.

Using FishENRICHR [39,40], the most used GO Terms for different biological processes were: GO:0019674, NAD metabolic process; GO:0070306 lens fibre cell differentiation; GO:0006754 ATP biosynthesis; GO:0006839 mitochondrial transport; GO:0045898 regulation of RNA polymerase II transcriptional pre-initiation complex assembly. (See Figure 3(C1,C2)).

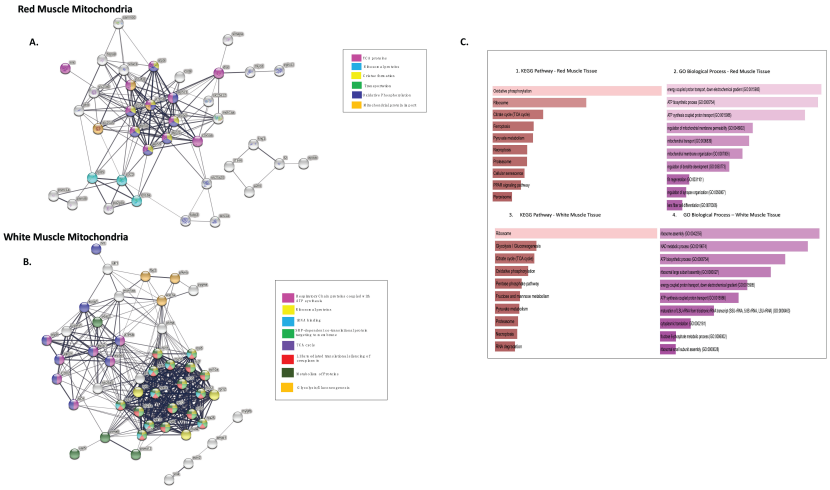

Figure 3. Network analysis of more highly abundant proteins in icefish mitochondria compared with closely related red-blooded species. (**A**) RMM DEPs, number of nodes 42 with 143 edges, the average node degree is 6.8 and (**B**) WMM, number of nodes 56 with 382 edges with an average node degree of 13.6. Network analysed using STRINGdb. The network highlights proteins involved in different pathways curated by STRINGdb from KEGG and Reactome databases. Nodes are coloured according to pathways. The edge shows type of interactions, experimentally determined interactions derived from databases, predicted interactions such as gene neighbourhood, gene co-occurrence, and gene fusions, respectively, co-expression interactions, text-mining interactions, and homology; the thicker the edge, the higher the confidence obtained by the mentioned sources. (**C**) Using FishEnrichr [39,40] analyser KEGG Pathways and GO terms for Biological process showed proteins in different pathways. The length of the bar represents the significance of that specific gene-set or term. Brighter colours are highly significant.

Using the same steps as for RMM, a PPI network was generated for WMM DEPs (Figure 3B). As for the WMM, the intra network connections were strongest (PPI enrichment p-value $< 1.0 \times 10^{-16}$, with fifty-six nodes, 382 edges, and an average node-degree of 13.6). Nine of the fifty-six DEPs did not connect to any network (RTNA1, MYOZ1B, HSPB1, KLH41B, TUBA8L2, VTG2, ZGC:110377, PALLD, and FXR2- Table 2).

The remaining forty-seven of the differentially expressed proteins were connected to networks where differentially expressed proteins ATP5B, GNB2L1, RPL11, RPL13, RPSA, and PKMA are the major protein-hubs (See Supplementary Figure S3). A single network was formed between DEPs MYLPFB, AMPD, ACTN2, and VCLA.

Three distinctive clusters were seen for WMM upregulated proteins similar to RMM. Cluster 1 had proteins of ribosome machinery, Cluster 2 proteins involved in ETC and TCA, and Cluster 3 proteins involved in fatty acid biosynthesis (Supplementary Figure S1).

Functional enrichment analysis (FDR $< 1.4 \times 10^{-2}$) showed proteins involved in TCA, ribosomal proteins, downstream signalling events of B cell receptors, and L13a-mediated translational silencing of ceruloplasmin. The fishENRICHR identified, GO:0000463: "maturation of LSU-rRNA", GO:0045727 and GO:0000470: "positive regulation of translation", GO:0000027 and GO:0042273: "ribosomal large subunit assembly" as most common GO terms. Enriched KEGG pathways included ribosome, glycolysis, and gluconeogenesis, and

the pentose pathway (pathways sorted according to *p*-values) (Figure 3(C3,C4)). The proteins involved in gluconeogenesis have previously been reported altered in their expression in rainbow trout. The study goes on to show an increase in the enzyme FB2, a key enzyme of gluconeogenesis to be increased in red muscle of the fish. On contrary we see FB2 to be increased fourfold in the white muscle tissue for icefish rather than the red muscle [44].

The protein networks between RMM and WMM differ. In RMM, there is one quite dense cluster with some weak "satellites" and another cluster with similar connectivity as seen in WMM. In WMM there are three separate clusters with good and quite similar connections.

3.3. Proteins with Lower Abundance in Icefish

Forty-eight proteins were found in lower quantities in RMM (ENSDARG00000030638, ca1, casq, gdh, mdh, pygm, rdh13, wu:fd55e03 were not recognised by GENEmania) and thirty-two proteins were differentially expressed in WMM in icefish compared to their red-blooded relatives (Tables 3 and 4). As before, GeneMANIA was used to analyse the interactions and produced one network per tissue (Figure 4A,B). In RMM, co-expression accounted for 96.14% of the total interactions seen in the network; and shared protein domains occupied 3.86%. In WMM, co-expression occupied 94.76%; physical interactions occupied 5.02%; and shared protein domains occupied 0.21%. The network showed physical interactions between ribosomal proteins and nebulin and this was predicted for the neighbouring protein tropomodulin.

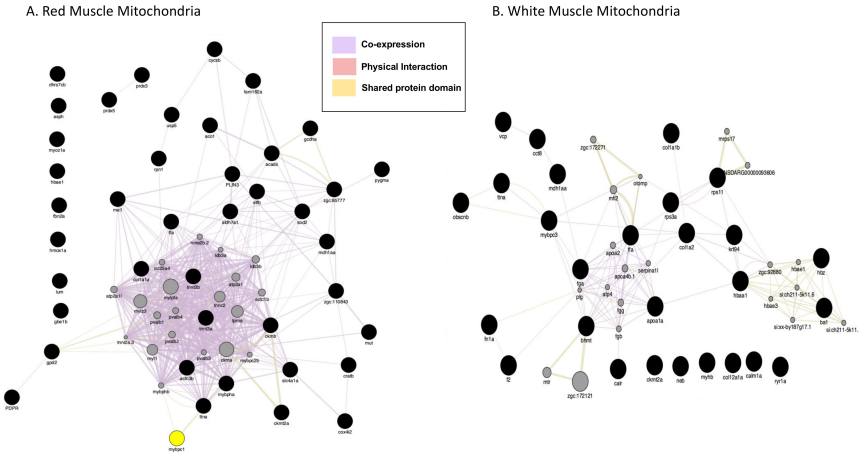

Figure 4. Gene interaction network for proteins with lower abundance in icefish (**A**) RMM and (**B**) WMM. (**A**) GeneMANIA gene–gene interaction network for protein abundance following the pattern *N. rossii* (+/+), *T. bernacchii* (+/+), *C. rastrospinosus* (−/+) and *C. gunnari* (−/−) in decreasing order of their protein abundance, laid out and visualised with Cytoscape, showing interaction strength (edge thickness), interaction type (colour-bottom right), multiple edges between nodes, protein score (node size) Black dots indicate query proteins, and grey dots depict neighbouring proteins.

In RMM, PPI networks include forty-eight protein nodes (Figure 5A), nine proteins (MUT, RPN1, CKMT2A, PDPR, DHRS7CB, ALDH7A1, WU:FD55e03, USP5, PLIN3) did not connect to any type of network (STRING interaction score = 0.4). The PPI enrichment

(p-value < 1.0×10^{-16}) had thirty-nine nodes, fifty-three edges, and an average node degree of 2.52. The rest of the DEPs were connected to networks by complex relationships, where proteins ACTN3B, TTNA, CKMB, MYBPC1, TTNT3B, and CYCSB showed network hubs highly associated with many proteins (Supplementary Figure S5). Single networks were observed between FBN2A and TFA, SLC4A1A and HBAE1. Two distinctive clusters were seen for RMM. Cluster 1 had proteins involved in striated muscle contraction, and Cluster 2 proteins involved in oxidative stress (Supplementary Figure S4).

In WMM, six (ZGC:153629, HBZ, HBAA1, MYOM1A, EVA1BA and, MDH1AA) out of the thirty-two protein nodes in the network did not connect to any type of network (Figure 5B). Proteins FGA, TFA, and TTNA represent network hubs, highly associated with other proteins (Supplementary Figure S6). The PPI enrichment (p-value < 3.49×10^{-12}) gave thirty-two nodes with forty-five edges and an average node-degree of 2.58. Three distinctive clusters were seen for WMM downregulated proteins. Cluster 1 had proteins of actin filament regulation, Cluster 2, proteins involved in muscle contraction, and Cluster 3, proteins involved with collagen (Supplementary Figure S4).

The functional enrichment analysis (FDR < 3.8×10^{-3}) for RMM reduced proteins in icefish were involved in striated muscle contraction, erythrocytes absorbing oxygen, fibrin clot formation hemostasias, and haem-associated proteins (Figure 5A). The following GO terms for biological processes were found overrepresented: GO:0006941 and GO:0006936: "striated muscle contraction" and GO:0045214: "sarcomere organisation". The following KEGG pathways were affected: amino acid metabolism, fatty acid degradation, and peroxisome, glyoxylate, and dicarboxylate metabolism (Figure 5(C1,C2)).

The functional enrichment analysis (FDR < 2.5×10^{-4}) for white muscle downregulated proteins in icefish identified multiple pathways, including translational silencing proteins and signal-recognition particle SRP-dependent co-translational protein targeting, the latter being involved in binding to the endoplasmic reticulum (ER) (Figure 5B).

Based on fishENRICHR analysis, the most used GO Terms for different biological processes were: GO:0019674 NAD metabolic process, GO:0060956 endocardial cell differentiation, GO:0020027 haemoglobin metabolic process, and GO:1903512 endoplasmic reticulum to cytosol transport (Figure 5(C4)). AGE-RAGE signalling pathway metabolism, glyoxylate and dicarboxylate metabolism, amino acid metabolism, ECM-receptor interaction, and focal adhesion were identified by KEGG pathway analysis (See Figure 5(C3)).

(p-value < 1.0×10^{-16}) had thirty-nine nodes, fifty-three edges, and an average node degree of 2.52. The rest of the DEPs were connected to networks by complex relationships, where proteins ACTN3B, TTNA, CKMB, MYBPC1, TTNT3B, and CYCSB showed network hubs highly associated with many proteins (Supplementary Figure S5). Single networks were observed between FBN2A and TFA, SLC4A1A and HBAE1. Two distinctive clusters were seen for RMM. Cluster 1 had proteins involved in striated muscle contraction, and Cluster 2 proteins involved in oxidative stress (Supplementary Figure S4).

In WMM, six (ZGC:153629, HBZ, HBAA1, MYOM1A, EVA1BA and, MDH1AA) out of the thirty-two protein nodes in the network did not connect to any type of network (Figure 5B). Proteins FGA, TFA, and TTNA represent network hubs, highly associated with other proteins (Supplementary Figure S6). The PPI enrichment (p-value < 3.49×10^{-12}) gave thirty-two nodes with forty-five edges and an average node-degree of 2.58. Three distinctive clusters were seen for WMM downregulated proteins. Cluster 1 had proteins of actin filament regulation, Cluster 2, proteins involved in muscle contraction, and Cluster 3, proteins involved with collagen (Supplementary Figure S4).

The functional enrichment analysis (FDR < 3.8×10^{-3}) for RMM reduced proteins in icefish were involved in striated muscle contraction, erythrocytes absorbing oxygen, fibrin clot formation hemostasias, and haem-associated proteins (Figure 5A). The following GO terms for biological processes were found overrepresented: GO:0006941 and GO:0006936: "striated muscle contraction" and GO:0045214: "sarcomere organisation". The following KEGG pathways were affected: amino acid metabolism, fatty acid degradation, and peroxisome, glyoxylate, and dicarboxylate metabolism (Figure 5(C1,C2)).

The functional enrichment analysis (FDR < 2.5×10^{-4}) for white muscle downregulated proteins in icefish identified multiple pathways, including translational silencing proteins and signal-recognition particle SRP-dependent co-translational protein targeting, the latter being involved in binding to the endoplasmic reticulum (ER) (Figure 5B).

Based on fishENRICHR analysis, the most used GO Terms for different biological processes were: GO:0019674 NAD metabolic process, GO:0060956 endocardial cell differentiation, GO:0020027 haemoglobin metabolic process, and GO:1903512 endoplasmic reticulum to cytosol transport (Figure 5(C4)). AGE-RAGE signalling pathway metabolism, glyoxylate and dicarboxylate metabolism, amino acid metabolism, ECM-receptor interaction, and focal adhesion were identified by KEGG pathway analysis (See Figure 5(C3)).

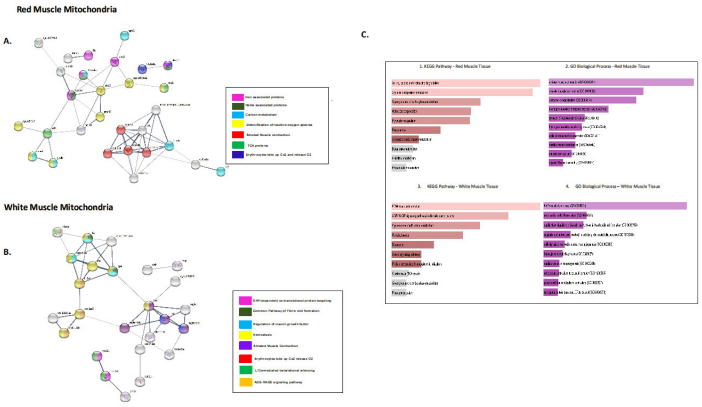

Figure 5. Network analysis of proteins lower expressed in icefish in comparison to closely related red-blooded species. (**A**) RMM DEPs, number of nodes 48 with 53 edges, the average node degree is 2.52 and (**B**) WMM, number of nodes 32 with 45 edges, the average node degree is 2.5. Network analysed using STRINGdb. The network highlights proteins involved in different pathways curated by string from Reactome database. The nodes are coloured according to the pathways determined with Reactome Pathway Database. The edge shows type of interactions, experimentally determined interactions derived from databases, predicted interactions such as gene neighbourhood, gene co-occurrence, and gene fusions, respectively, co-expression interactions, text-mining interactions and homology, thicker the edge higher the confidence obtained the mentioned sources. (**C**) Using FishEnrichr analyser KEGG Pathway and GO terms for biological process showed proteins involved in different pathways.

4. Discussion

The paper presents the comparative analysis of the mitochondrial proteomes of white (WMM) and red muscle (RMM) of icefish that do not express haemoglobin protein and closely related red-blooded species. We wanted to understand how the mitochondrial proteome has adapted to the loss of this protein. The differentially expressed proteins are identified using the LC/LC-MS technique. The network built using the STRING database provided unbiased identification of network hubs as it builds all the networks entirely on external information. Network enrichment analysis provided several KEGG pathways that were linked to protein machinery, amino acid metabolism, energy production, and fatty acid metabolism.

4.1. Proteins Involved in Energy Metabolism

The RMM and WMM tissues had a few proteins following a similar trend in their protein abundance in the icefish. The proteins involved in the ribosomal machinery and cellular hypoxia were found to be commonly increased in the icefish (RMM: ATP5O, ATP5D ATP5B1, ATP5G; WMM: PSMD12, PSMA8). In cluster 1 of the red muscle tissue, apart from involvement in hypoxia, some were also involved in ETC, oxidative phosphorylation, and the TCA cycle (Figure 3A; increased abundance in icefish). ATP synthase subunit O (ATP5O), stress 70 protein (HSPA9), and malate dehydrogenase (MDH1AA) were found to be highly connected to the other nodes, and changes in any highly connected network proteins are likely to be lethal for an organism [45–47]. ATP5O is a component of the multi-subunit enzyme ATP synthase (complex V of the electron transport chain), which is located in the stalk that connects the catalytic core (F_1) to the membrane proton channel (F_O) [48]. The protein is known to influence the proton conductance by conformational changes [48]. ATP5O has also been found to interact directly with sirtuin 3 (SIRT3), which is significantly involved in energy production and stress responses [49]. ATP5O may contribute to the age-associated decline in association with SIRT3, mitochondria dysfunction, and diseases linked to mitochondrial homeostasis under hypoxia [49,50]. Another component of complex V, ATP synthase subunit gamma (ATPγ), which is also a part of the central stalk, was comparably high in the icefish cohort. ATPγ helps in the binding change mechanism by helping in the rotation of the β subunit. Icefish have been previously reported to show an increased coupling of proton transport and ATP synthase compared with red-blooded notothenioids [51] and this could be correlated to the increase in the specific subunits of complex V that are directly involved in proton translocation. Previously, we have shown the ATP synthase subunit 6 of complex V to be sequentially and structurally different in the icefish *C. gunnari* when compared to its red-blooded related species [52].

One of the proteins densely connected in RMM (a hub node) in cluster 1 also involved in the TCA was the dihydrolipoyllysine-residue acetyltransferase component (DLAT). The increase in the abundance of this protein subunit, a component of the pyruvate dehydrogenase complex (PDH), involved in the breakdown of pyruvate to acetyl-CoA that requires converting NAD^+ to NADH, in icefish could be a response to moderate pyruvate levels. This could be to prevent pyruvate being converted into acetyl-CoA for TCA and instead be used to meet muscle energetic demands via anaerobic respiration [53,54]. The skeletal muscle is known to have metabolic flexibility in meeting the energy demands of the tissue and responding and adapting to environmental changes [53,55]. The hearts and skeletal muscle of icefish have been suggested to have a dual oxidative-anaerobic metabolism to maintain ATP levels [56–59]. An increase in the metabolites of fatty acid metabolism in icefish have also been suggested previously [59]. This could further suggest that the increase in DLAT is to maintain pyruvate levels, which could be converted to oxaloacetate for fatty acid cholesterol biosynthesis via the glycolytic pathway [53]. PDH has been seen to be involved in metabolic rate depression in vertebrates, which is a common element of anaerobiosis [60]. The regeneration of NAD^+ either happens aerobically via OxPhos or anaerobically by fermentation wherein lactate dehydrogenase (LDH) converts pyruvate to lactate. The LDH enzyme has previously been reported to be highly increased in the

icefish myocardium, which indicates involvement of anaerobic energetics in the icefish heart muscle [57] LDH is regulated by the relative concentrations of its substrates, and an increase in pyruvate could inhibit the enzyme [61–63].

4.2. Muscle-Contraction Proteins

A common decrease in the expression in icefish of the proteins associated with biological processes of striated muscle contraction (RMM: MYBPC1, MYBPHA, NEB, TNA3, TTN3A, TNNT3A; WMM: MYBPC1, MYHB, MYBPC2A, MYBPC2B, MYBPC3, TTNA), creatine metabolism (RMM: CKMT2A, CKMB; WMM: CKMT2A), and amino acid/protein metabolism (RMM: GCDH, OGDHA, BCKDHA, PSME2, CKMT2A; WMM: CCT8, VCP, TFA, RPS11, RPS3A) was observed in both RMM and WMM. Creatine kinase (CK), which has previously been shown by Western blot to be absent in the hearts of icefish, did not appear in our protein lists from skeletal muscle mitochondria [26]. The mitochondria are enlarged in the oxidative muscle of icefish, which decreases the distance for the diffusion of oxygen and for ATP between mitochondria and myofibrils, which might reduce the demand for CK [29]. Mitochondrial CK helps maintain flux through the respiratory chain by maintaining low ATP levels [64]. This is coherent with our observation of an increase in the abundance of proteins of complex V. Notothenioids lacking mtCK may compensate by increasing levels of ADP/ATP nucleotide translocases and voltage dependent anion-selective channel proteins (VDACs), as observed in our proteomics study as well, where VDAC3 is selectively seen higher. The lower levels or absence of this enzyme has previously also been reported to be an example of a 'paedomorphic trait', a juvenile trait that persists into adulthood. This trait observed as a result of delayed development has been seen as a common feature in icefish; whether this is energetically efficient or not is still debatable [26,65].

A common muscle protein that was found to be downregulated both in RMM and WMM tissues is myosin binding protein C isoforms (MYBPC), which encodes myosin binding protein C. MYBPC is a thick filament associated protein that has both structural and regulatory roles in sarcomere assembly [66]. The protein was seen to decrease four- fold in the icefish *C. gunnari* when compared to the red-blooded species, but the amount was comparable in the icefish *C. rastrospinosus*. MYBPC mutations have been shown to increase the energetic cost of contraction in the muscle, and usually are found to act by reducing the protein content [67–69]. The downregulation of this protein in icefish is in contrast to a study that has shown significant upregulation of MYBPC in colder temperatures, which is consistent with the observation of the amount of this protein seen in their closely related red-blooded species [70]. Previously, mutations in MYBPC were seen to be involved in increased cardiac oxidative stress in the mouse model [71]. The other sarcomere protein that was seen significantly less in abundance in icefish was myosin heavy chain b (MYBPH); the activity of this protein has been used as a model to explain the mechanism underlying alterations in skeletal muscle contraction [72]. The ATPase reaction of a muscle fibre is determined by its myosin heavy chain composition, which might be altered with ageing, as seen previously in human skeletal muscle [73]. An impaired sarcomere energetics such as mutations in muscle contractions protein can cause mitochondrial dysfunction due to a Ca^{2+} imbalance or ROS accumulation impairing oxidative phosphorylation capacity [74]. The other proteins that were connected to MYBPH were titin, nebulin, and CK. Titin, nebulin, and CK proteins have previously been seen to be downregulated under long term exposure to hypoxia in the zebrafish model [75]. Chaperonin proteins, T-complex protein 1 encoded by CCT8 are known for their role in the folding of cytoskeleton proteins upon ATP hydrolysis and changes in the protein can cause defects in the functioning of the cytoskeleton and mitosis arrest. A study with *C. elegans* showed CCT8 as a candidate to sustain proteostasis during organismal ageing [76]. The decrease in the level of the protein is observed in human brain ageing and neurodegenerative diseases [77].

4.3. Redox

The proteins GCDH- glutaryl-CoA dehydrogenase and Aldh7a1- Alpha aminoadipic semialdehyde dehydrogenase were remarkedly seen lower in the icefish *C. gunnari*, specifically in WMM tissue. GCDH is a mitochondrial enzyme necessary for the metabolism of lysine/tryptophan and hydroxylysine. The absence of this enzyme is known to result in mitochondrial dysfunction. ALDH7A1 is an enzyme that metabolises betaine aldehyde to betaine, which is an important cellular osmolyte and methyl donor that helps in protecting the cell from oxidative stress. The enzyme is seen to be involved in lysine catabolism and helps in maintaining the cellular nitrogen pool [78]. The changes in expression of these proteins might indicate the red-muscle tissue of *N. rossii* and *T. bernacchii* and even *C. rastrospinosus* (that has the expression mb) has enhanced defences against oxidative stress, which is consistent with the previous observation made in the cardiac mitochondrial protein expression data [79]. In WMM, we see that transmembrane protease serine 2-like is very reduced and perhaps missing in icefish. This protein has not been investigated very much to date and has not been reported as absent in these fish previously; the higher levels of it in the red-blooded fish suggest this difference may be of biological relevance.

4.4. Haem-Associated Proteins

Consistent with all the studies of icefish, haemoglobin alpha and beta were solely identified in red-blooded species. We also show that hemopexin (Hx) protein is reduced in the WMM of icefish. It was previously shown that Hx transcription occurs at levels comparable to those in the red-blooded notothenioids; however, it seems possible that there is a discrepancy between transcript and protein levels of Hx [80]. Cytochrome c oxidase (CO) is an important haem-containing protein just like haemoglobin and in our study was also found to be much reduced in icefish RMM. As this protein performs a multitude of functions, including cell apoptosis and energy metabolism, it remains to be seen what this reduced level means for the physiology of this tissue [81,82]. The oxygen-carrying capacity of their blood is only 10% compared to that of red-blooded species. Cytochrome c oxidase is at first the terminal electron carrier of the respiratory chain, so lower protein expression may indicate a modification in redox metabolism in icefish. Previously, it has also been shown that maximal capacities of CO and activities of another mitochondrial enzyme, citrate synthase, to be higher in red-blooded fish species in comparison to icefish [83]. Transferrin was another protein that was found to be significantly reduced (five-fold) in the WMM of the icefish *C. gunnari*.

4.5. Ribosome Machinery in WMM

Overall, a striking finding in the samples we interrogated is the numbers of 26S, 40S and 60S ribosome proteins that are differentially (mostly) upregulated in icefish. There have been extensive studies on close interaction between mitochondria and the endoplasmic reticulum [84]. FXR2P, a ribosomal binding protein, was also measured at much higher levels in icefish muscle; it would be interesting to probe the connections between ribosome and mitochondrial biology in these organisms. FXR2P protein has not been found to be present in mammalian muscle and therefore its role in icefish muscle remains to be elucidated [85].

With this study, we have established biological pathways and proteins that can be used to understand the unique 'haemoglobin-free' biology of icefish. We analysed samples directly taken from the field in the late summer season, ensuring that the pressures of a captive environment are not a factor. We show that muscle mitochondrial proteomes are distinct between fish with different quantities of haemoglobin. We expect our contribution will direct researchers in this field to focus on the identified proteins and pathways that allow these remarkable and unique fish to survive and thrive in Antarctic waters.

Supplementary Materials: The following supporting information can be downloaded at: https://www.mdpi.com/article/10.3390/biology11081118/s1, Figure S1: Top modules obtained from the PPI network using Cytoscape's plugin MCODE for Red muscle tissue network (C) and white

muscle tissue network (D) for upregulated proteins in the icefish, Figure S2: Highly connected protein nodes for RMM PPI using CentiScaPe, Cytoscape plugin, Figure S3: Highly connected protein nodes for WMM PPI, Figure S4: Top modules obtained from the PPI network using Cytoscape's plugin MCODE for Red muscle tissue network (C) and white muscle tissue network (D) for upregulated proteins in the icefish, Figure S5: Highly connected protein nodes for RMM PPI, Figure S6: Highly connected protein nodes for WMM PPI; Table S1: Proteins higher in abundance in *N. rossii* (RMM), Table S2: Proteins lower in abundance in *N. rossii* (RMM), Table S3: Proteins higher in abundance in *C. rastrospinosus* (RMM), Table S4: Proteins lower in abundance in *C. rastrospinosus* (RMM), Table S5: Proteins more in abundance in *C. gunnari* (RMM), Table S6: Proteins less in abundance in *C. gunnari* (RMM), Table S7: Proteins higher in abundance in *N. rossii* (WMM), Table S8: Proteins lower in abundance in *N. rossii* (WMM), Table S9: Proteins higher in abundance in *C. rastrospinosus* (WMM), Table S10: Proteins lower in abundance in *C. rastrospinosus* (WMM), Table S11: Proteins more in abundance in *C. gunnari* (WMM), Table S12: Proteins less in abundance in *C. gunnari* (WMM).

Author Contributions: Conceptualization: L.C., C.P. and M.L.; Methodology: A.D., L.C. and G.K.; Software: A.D. and G.K.; Validation: A.D., G.K., B.E. and L.C.; Formal analysis: G.K., B.E., A.D. and L.C.; Investigation: G.K., B.E., A.D., C.P., M.L., L.C. and F.S.; Resources: C.P., M.L. and C.P.; Data Curation: G.K., B.E., A.D. and L.C.; Writing- original draft preparation: G.K., B.E. and L.C.; Writing review and editing: G.K., B.E., A.D. and L.C.; Visualization: G.K., B.E. and A.D.; Supervision: L.C.; Project administration: L.C.; Funding acquisition: L.C. All authors have read and agreed to the published version of the manuscript.

Funding: Gunjan Katyal was supported by Vice Chancellor's International Scholarship for Research Excellence, University of Nottingham (2018–2021). Brad Ebanks was supported by the Biotechnology and Biological Sciences Research Council [grant number BB/J014508/1]. This collaboration was made possible by a University of Nottingham International Research Collaboration Fund award.

Institutional Review Board Statement: The animal study protocol was approved by the Institutional Review Board (or Ethics Committee) of University of Nottingham SVMS (ref # 2744 190509).

Data Availability Statement: Complete mass spectrometry data sets and proteomic identifications are available to download from MassIVE (MSV000089644), [doi:10.25345/C5PZ51Q9F] and ProteomeXchange (PXD034498).

Acknowledgments: The York Centre of Excellence in Mass Spectrometry was created thanks to a major capital investment through Science City York, supported by Yorkshire Forward with funds from the Northern Way Initiative, and subsequent support from EPSRC (EP/K039660/1; EP/M028127/1). The authors would like to thank Nils Koschnick (Alfred Wegener Institute Helmholtz Centre for Polar and Marine Research, AWI, Bremerhaven, Germany) and the ship crew for their help in collecting samples on board the R/V Polarstern.

Conflicts of Interest: The authors declare that they have no conflict of interest.

References

1. Giorgi, C.; Agnoletto, C.; Bononi, A.; Bonora, M.; de Marchi, E.; Marchi, S.; Missiroli, S.; Patergnani, S.; Poletti, F.; Rimessi, A.; et al. Mitochondrial calcium homeostasis as potential target for mitochondrial medicine. *Mitochondrion* **2012**, *12*, 77–85. [CrossRef] [PubMed]
2. Murphy, M.P. How mitochondria produce reactive oxygen species. *Biochem. J.* **2009**, *417*, 1–13. [CrossRef]
3. Tait, S.W.; Green, D.R. Mitochondrial regulation of cell death. *Cold Spring Harb. Perspect. Biol.* **2013**, *53*, a008706. [CrossRef] [PubMed]
4. Chu, Q.; Martinez, T.F.; Novak, S.W.; Donaldson, C.J.; Tan, D.; Vaughan, J.M.; Chang, T.; Diedrich, J.K.; Andrade, L.; Kim, A.; et al. Regulation of the ER stress response by a mitochondrial microprotein. *Nat. Commun.* **2019**, *10*, 4883. [CrossRef] [PubMed]
5. Azuma, K.; Ikeda, K.; Inoue, S. Functional mechanisms of mitochondrial respiratory chain supercomplex assembly factors and their involvement in muscle quality. *Int. J. Mol. Sci.* **2020**, *21*, 3182. [CrossRef]
6. Guo, R.; Gu, J.; Zong, S.; Wu, M.; Yang, M. Structure and mechanism of mitochondrial electron transport chain. *Biomed. J.* **2018**, *41*, 9–20. [CrossRef] [PubMed]
7. Perutz, M.; Rossmann, M.; Cullis, A.F.; Muirhead, H.; Will, G.; North, A.C.T. Structure of hoemoglobin. *Nature* **1960**, *185*, 416–422. [CrossRef] [PubMed]
8. Heinemann, I.U.; Jahn, M.; Jahn, D. The biochemistry of heme biosynthesis. *Arch. Biochem. Biophys.* **2008**, *474*, 238–251. [CrossRef]

9. Straub, A.C.; Butcher, J.T.; Billaud, M.; Mutchler, S.M.; Artamonov, M.V.; Nguyen, A.T.; Johnson, T.; Best, A.K.; Miller, M.P.; Palmer, L.A.; et al. Hemoglobin α/eNOS coupling at myoendothelial junctions is required for nitric oxide scavenging during vasoconstriction. *Arterioscler. Thromb. Vasc. Biol.* **2014**, *34*, 2594–2600. [CrossRef]
10. Shephard, F.; Greville-Heygate, O.; Marsh, O.; Anderson, S.; Chakrabarti, L. A mitochondrial location for haemoglobins—Dynamic distribution in ageing and Parkinson's disease. *Mitochondrion* **2014**, *14*, 64–72. [CrossRef] [PubMed]
11. Brown, N.; Alkhayer, K.; Clements, R.; Singhal, N.; Gregory, R.; Azzam, S.; Li, S.; Freeman, E.; McDonough, J. Neuronal Hemoglobin Expression and Its Relevance to Multiple Sclerosis Neuropathology. *J. Mol. Neurosci.* **2016**, *59*, 1–17. [CrossRef] [PubMed]
12. Lechauve, C.; Butcher, J.T.; Freiwan, A.; Biwer, L.A.; Keith, J.M.; Good, M.E.; Ackerman, H.; Tillman, H.S.; Kiger, L.; Isakson, B.E.; et al. Endothelial cell α-globin and its molecular chaperone α-hemoglobin-stabilizing protein regulate arteriolar contractility. *J. Clin. Investig.* **2018**, *128*, 5073–5082. [CrossRef]
13. Corliss, B.A.; Delalio, L.J.; Stevenson Keller, T.C.; Keller, A.S.; Keller, D.A.; Corliss, B.H.; Beers, J.M.; Peirce, S.M.; Isakson, B.E. Vascular Expression of Hemoglobin Alpha in Antarctic Icefish Supports Iron Limitation as Novel Evolutionary Driver. *Front. Physiol.* **2019**, *10*, 1389. [CrossRef]
14. Chuang, J.Y.; Lee, C.W.; Shih, Y.H.; Yang, T.; Yu, L.; Kuo, Y.M. Interactions between amyloid-β and hemoglobin: Implications for amyloid plaque formation in alzheimer's disease. *PLoS ONE* **2012**, *7*, e33120. [CrossRef]
15. Shephard, F.; Greville-Heygate, O.; Liddell, S.; Emes, R.; Chakrabarti, L. Analysis of Mitochondrial haemoglobin in Parkinson's disease brain. *Mitochondrion* **2016**, *29*, 45–52. [CrossRef]
16. Archer, S.D.; Johnston, I.A. Density of Cristae and Distribution of Mitochondria in the Slow Muscle Fibers of Antarctic Fish. *Physiol. Zool.* **1991**, *64*, 242–258. [CrossRef]
17. Duhamel, G.; Hulley, P.A.; Causse, R.; Koubbi, P.; Vacchi, M.; Pruvost, P.; Vigetta, S.; Irisson, J.-O.; Mormède, S.; Belchier, M.; et al. Chapter 7. Biogeographic Patterns of Fish. In *Biogeographic Atlas of the Southern Ocean*; Scientific Communitte on Antarctic Research: Cambridge, UK, 2014; ISBN 9780948277283.
18. Johan, T. Ruud Vertebrates without Erythrocytes and Blood Pigment. *Nature* **1954**, *173*, 848–850.
19. Kim, B.M.; Amores, A.; Kang, S.; Ahn, D.H.; Kim, J.H.; Kim, I.C.; Lee, J.H.; Lee, S.G.; Lee, H.; Lee, J.; et al. Antarctic blackfin icefish genome reveals adaptations to extreme environments. *Nat. Ecol. Evol.* **2019**, *3*, 469–478. [CrossRef] [PubMed]
20. Beers, J.M.; Jayasundara, N. Antarctic notothenioid fish: What are the future consequences of "losses" and "gains" acquired during long-term evolution at cold and stable temperatures? *J. Exp. Biol.* **2015**, *218*, 1834–1845. [CrossRef] [PubMed]
21. Di Prisco, G.; Cocca, E.; Parker, S.K.; Detrich, H.W. Tracking the evolutionary loss of hemoglobin expression by the white-blooded Antarctic icefishes. *Gene* **2002**, *295*, 185–191. [CrossRef]
22. Near, T.J.; Parker, S.K.; Detrich, H.W. A genomic fossil reveals key steps in hemoglobin loss by the Antarctic icefishes. *Mol. Biol. Evol.* **2006**, *23*, 2008–2016. [CrossRef] [PubMed]
23. Scudiero, R.; Trinchella, F.; Riggio, M.; Parisi, E. Structure and expression of genes involved in transport and storage of iron in red-blooded and hemoglobin-less antarctic notothenioids. *Gene* **2007**, *97*, 1–11. [CrossRef] [PubMed]
24. Borley, K.A.; Sidell, B.D. Evolution of the myoglobin gene in Antarctic Icefishes (Channichthyidae). *Polar Biol.* **2011**, *34*, 659–665. [CrossRef]
25. Wujcik, J.M.; Wang, G.; Eastman, J.T.; Sidell, B.D. Morphometry of retinal vasculature in Antarctic fishes is dependent upon the level of hemoglobin in circulation. *J. Exp. Biol.* **2007**, *210*, 815–824. [CrossRef] [PubMed]
26. O'Brien, K.M.; Mueller, I.A.; Orczewska, J.I.; Dullen, K.R.; Ortego, M. Hearts of some Antarctic fishes lack mitochondrial creatine kinase. *Comp. Biochem. Physiol. Part A Mol. Integr. Physiol.* **2014**, *178*, 30–36. [CrossRef]
27. Sidell, B.D.; O'Brien, K.M. When bad things happen to good fish: The loss of hemoglobin and myoglobin expression in Antarctic icefishes. *J. Exp. Biol.* **2006**, *209*, 1791–1802. [CrossRef]
28. Sidell, B.D. Intracellular oxygen diffusion: The roles of myoglobin and lipid at cold body temperature. *J. Exp. Biol.* **1998**, *201*, 1119–1128. [CrossRef] [PubMed]
29. O'Brien, K.M.; Mueller, I.A. The unique mitochondrial form and function of antarctic channichthyid icefishes. *Integr. Comp. Biol.* **2010**, *50*, 993–1008. [CrossRef] [PubMed]
30. Lu, H.; Zhou, Q.; He, J.; Jiang, Z.; Peng, C.; Tong, R.; Shi, J. Recent advances in the development of protein–protein interactions modulators: Mechanisms and clinical trials. *Signal Transduct. Target. Ther.* **2020**, *5*, 213. [CrossRef]
31. Rachlin, J.; Cohen, D.D.; Cantor, C.; Kasif, S. Biological context networks: A mosaic view of the interactome. *Mol. Syst. Biol.* **2006**, *2*, 66. [CrossRef] [PubMed]
32. Marín, M.; Esteban, F.J.; Ramírez-Rodrigo, H.; Ros, E.; Sáez-Lara, M.J. An integrative methodology based on protein-protein interaction networks for identification and functional annotation of disease-relevant genes applied to channelopathies. *BMC Bioinformatics* **2019**, *20*, 565. [CrossRef]
33. Baldwin, K.M.; Winder, W.W.; Terjung, R.L.; Holloszy, J.O. Glycolytic enzymes in different types of skeletal muscle: Adaptation to exercise. *Am. J. Physiol. Content* **1973**, *225*, 962–966. [CrossRef] [PubMed]
34. Huang, Y.C.; Dennis, R.G.; Baar, K. Cultured slow vs. fast skeletal muscle cells differ in physiology and responsiveness to stimulation. *Am. J. Physiol. Cell Physiol.* **2006**, *291*, 11–17. [CrossRef]
35. Shannon, P.; Markiel, A.; Ozier, O.; Baliga, N.S.; Wang, J.T.; Ramage, D.; Amin, N.; Schwikowski, B.; Ideker, T. Cytoscape: A Software Environment for Integrated Models of Biomolecular Interaction Networks. *Genome Res.* **2003**, *13*, 2498–2504. [CrossRef]

36. Pruitt, K.D.; Hogue, C.W.; Groll, M.; Hartmann, C.; Huber, R.; Fields, S. Mcode. *Nucleic Acids Res.* **2001**, *29*, 137–140. [CrossRef]
37. Scardoni, G.; Petterlini, M.; Laudanna, C. Analyzing biological network parameters with CentiScaPe. *Bioinformatics* **2009**, *25*, 2857–2859. [CrossRef]
38. Franz, M.; Rodriguez, H.; Lopes, C.; Zuberi, K.; Montojo, J.; Bader, G.D.; Morris, Q. GeneMANIA update 2018. *Nucleic Acids Res.* **2018**, *46*, W60–W64. [CrossRef]
39. Chen, E.Y.; Tan, C.M.; Kou, Y.; Duan, Q.; Wang, Z.; Meirelles, G.V.; Clark, N.R.; Ma'ayan, A. Enrichr: Interactive and collaborative HTML5 gene list enrichment analysis tool. *BMC Bioinformatics* **2013**, *14*, 128. [CrossRef]
40. Kuleshov, M.V.; Jones, M.R.; Rouillard, A.D.; Fernandez, N.F.; Duan, Q.; Wang, Z.; Koplev, S.; Jenkins, S.L.; Jagodnik, K.M.; Lachmann, A.; et al. Enrichr: A comprehensive gene set enrichment analysis web server 2016 update. *Nucleic Acids Res.* **2016**, *44*, W90–W97. [CrossRef]
41. Glancy, B.; Balaban, R.S. Protein composition and function of red and white skeletal muscle mitochondria. *Am. J. Physiol. Cell Physiol.* **2011**, *300*, C1280–C1290. [CrossRef]
42. Szklarczyk, D.; Gable, A.L.; Lyon, D.; Junge, A.; Wyder, S.; Huerta-Cepas, J.; Simonovic, M.; Doncheva, N.T.; Morris, J.H.; Bork, P.; et al. STRING v11: Protein–protein association networks with increased coverage, supporting functional discovery in genome-wide experimental datasets. *Nucleic Acids Res.* **2019**, *47*, D607–D613. [CrossRef] [PubMed]
43. Doncheva, N.T.; Assenov, Y.; Domingues, F.S.; Albrecht, M. Topological analysis and interactive visualization of biological networks and protein structures. *Nat. Protoc.* **2012**, *7*, 670–685. [CrossRef]
44. Magnoni, L.J.; Crespo, D.; Ibarz, A.; Blasco, J.; Fernández-Borràs, J.; Planas, J.V. Effects of sustained swimming on the red and white muscle transcriptome of rainbow trout (Oncorhynchus mykiss) fed a carbohydrate-rich diet. *Comp. Biochem. Physiol. A Mol. Integr. Physiol.* **2013**, *166*, 510–521. [CrossRef]
45. Raman, K.; Damaraju, N.; Joshi, G.K. The organisational structure of protein networks: Revisiting the centrality-lethality hypothesis. *Syst. Synth. Biol.* **2014**, *8*, 73–81. [CrossRef]
46. He, X.; Zhang, J. Why do hubs tend to be essential in protein networks? *PLoS Genet.* **2006**, *2*, 0826–0834. [CrossRef]
47. Zotenko, E.; Mestre, J.; O'Leary, D.P.; Przytycka, T.M. Why do hubs in the yeast protein interaction network tend to be essential: Reexamining the connection between the network topology and essentiality. *PLoS Comput. Biol.* **2008**, *4*, e1000140. [CrossRef]
48. Devenish, R.J.; Prescott, M.; Boyle, G.M.; Nagley, P. The oligomycin axis of mitochondrial ATP synthase: OSCP and the proton channel. *J. Bioenerg. Biomembr.* **2000**, *32*, 507–515. [CrossRef]
49. Yang, W.; Nagasawa, K.; Münch, C.; Xu, Y.; Satterstrom, K.; Jeong, S.; Hayes, S.D.; Jedrychowski, M.P.; Vyas, F.S.; Zaganjor, E.; et al. Mitochondrial Sirtuin Network Reveals Dynamic SIRT3-Dependent Deacetylation in Response to Membrane Depolarization. *Cell* **2016**, *167*, 985–1000.e21. [CrossRef]
50. Okada, H.; Goldhaber, J.I.; Ross, R.S.; Okada, H.; Lai, N.C.; Kawaraguchi, Y.; Liao, P.; Copps, J.; Sugano, Y.; Okada-maeda, S.; et al. Integrins protect cardiomyocytes from ischemia/reperfusion injury Find the latest version : Integrins protect cardiomyocytes from ischemia/reperfusion injury. *J. Clin. Investig.* **2013**, *123*, 4294–4308. [CrossRef]
51. Mueller, I.A.; Grim, J.M.; Beers, J.M.; Crockett, E.L.; O'Brien, K.M. Inter-relationship between mitochondrial function and susceptibility to oxidative stress in red-And white-blooded Antarctic notothenioid fishes. *J. Exp. Biol.* **2011**, *214*, 3732–3741. [CrossRef]
52. Katyal, G.; Ebanks, B.; Lucassen, M.; Papetti, C. Sequence and structure comparison of ATP synthase F0 subunits 6 and 8 in notothenioid fish. *PLoS ONE* **2021**, *16*, e0245822. [CrossRef] [PubMed]
53. Zhang, S.; Hulver, M.W.; McMillan, R.P.; Cline, M.A.; Gilbert, E.R. The pivotal role of pyruvate dehydrogenase kinases in metabolic flexibility. *Nutr. Metab.* **2014**, *11*, 10. [CrossRef] [PubMed]
54. Guderley, H.; Storey, K.B.; Fields, J.H.A.; Hochachka, P.W. Pyruvate kinase from Oplophorus gracilirostris muscle. *Comp. Biochem. Physiol. Part B Comp. Biochem.* **1976**, *55*, 475–478. [CrossRef]
55. Goodpaster, B.H.; Sparks, L.M. Metabolic Flexibility in Health and Disease. *Cell Metab.* **2017**, *25*, 1027–1036. [CrossRef] [PubMed]
56. Feller, G.; Goessens, G.; Gerday, C.; Bassleer, R. Heart structure and ventricular ultrastructure of hemoglobin- and myoglobin-free icefish Channichthys rhinoceratus. *Cell Tissue Res.* **1985**, *242*, 669–676. [CrossRef] [PubMed]
57. Feller, G.; Gerday, C. Metabolic pattern of the heart of haemoglobin- and myoglobin-free Antarctic fish Channichthys rhinoceratus. *Polar Biol.* **1987**, *7*, 225–229. [CrossRef]
58. Feller, G.; Pauly, J.-P.; Smal, A.; O'Carra, P.; Gerday, C. The lactate dehydrogenase of the icefish heart: Biochemical adaptations to hypoxia tolerance. *Biochim. Biophys. Acta-Protein Struct. Mol. Enzymol.* **1991**, *1079*, 343–347. [CrossRef]
59. Feller, G.; Gerday, C. Adaptations of the hemoglobinless Antarctic icefish (Channichthyidae) to hypoxia tolerance. *Comp. Biochem. Physiol.-A Physiol.* **1997**, *118*, 981–987. [CrossRef]
60. Storey, K.B.; Storey, J.M. Metabolic rate depression in animals: Transcriptional and translational controls. *Biol. Rev. Camb. Philos. Soc.* **2004**, *79*, 207–233. [CrossRef]
61. June, F.L. Volume 3, number 5 FEBS LETTERS June 1969. *FEBS Lett.* **2000**, *3*, 3–7.
62. Hewitt, C.O.; Eszes, C.M.; Sessions, R.B.; Moreton, K.M.; Dafforn, T.R.; Takei, J.; Dempsey, C.E.; Clarke, A.R.; Holbrook, J.J. A general method for relieving substrate inhibition in lactate dehydrogenases. *Protein Eng.* **1999**, *12*, 491–496. [CrossRef] [PubMed]
63. Soler, J.; de Arriaga, D.; Cadenas, Q.; Cadenas, E. Substrate inhibition of lactate dehydrogenase fromPhycomyces blakesleeanus: NADH dependence. *Exp. Mycol.* **1981**, *5*, 357–362. [CrossRef]

64. Wallimann, T.; Wyss, M.; Brdiczka, D.; Nicolay, K.; Eppenberger, H.M. Intracellular compartmentation, structure and function of creatine kinase isoenzymes in tissues with high and fluctuating energy demands: The "phosphocreatine circuit" for cellular energy homeostasis. *Biochem. J.* **1992**, *281*, 21–40. [CrossRef] [PubMed]
65. Albertson, R.C.; Yan, Y.L.; Titus, T.A.; Pisano, E.; Vacchi, M.; Yelick, P.C.; Detrich, H.W.; Postlethwait, J.H. Molecular pedomorphism underlies craniofacial skeletal evolution in Antarctic notothenioid fishes. *BMC Evol. Biol.* **2010**, *10*, 4. [CrossRef] [PubMed]
66. Kraker, J.; Viswanathan, S.K.; Knöll, R.; Sadayappan, S. Recent advances in the molecular genetics of familial hypertrophic cardiomyopathy in South Asian descendants. *Front. Physiol.* **2016**, *7*, 499. [CrossRef] [PubMed]
67. Witjas-Paalberends, E.R.; Güclü, A.; Germans, T.; Knaapen, P.; Harms, H.J.; Vermeer, A.M.C.; Christiaans, I.; Wilde, A.A.M.; Dos-Remedios, C.; Lammertsma, A.A.; et al. Gene-specific increase in the energetic cost of contraction in hypertrophic cardiomyopathy caused by thick filament mutations. *Cardiovasc. Res.* **2014**, *103*, 248–257. [CrossRef]
68. Barefield, D.; Kumar, M.; de Tombe, P.P.; Sadayappan, S. Contractile dysfunction in a mouse model expressing a heterozygous MYBPC3 mutation associated with hypertrophic cardiomyopathy. *Am. J. Physiol.-Heart Circ. Physiol.* **2014**, *306*, 807–815. [CrossRef]
69. Van Dijk, S.J.; Dooijes, D.; Dos Remedios, C.; Michels, M.; Lamers, J.M.J.; Winegrad, S.; Schlossarek, S.; Carrier, L.; Cate, F.J.T.; Stienen, G.J.M.; et al. Cardiac myosin-binding protein C mutations and hypertrophic ardiomyopathy haploinsufficiency, deranged phosphorylation, and cardiomyocyte dysfunction. *Circulation* **2009**, *119*, 1473–1483. [CrossRef]
70. Dimitriadi, A.; Beis, D.; Arvanitidis, C.; Adriaens, D.; Koumoundouros, G. Developmental temperature has persistent, sexually dimorphic effects on zebrafish cardiac anatomy. *Sci. Rep.* **2018**, *8*, 8125. [CrossRef] [PubMed]
71. Lynch, T.L.; Sivaguru, M.; Velayutham, M.; Cardounel, A.J.; Michels, M.; Barefield, D.; Govindan, S.; Dos Remedios, C.; Van Der Velden, J.; Sadayappan, S. Oxidative Stress in Dilated Cardiomyopathy Caused by MYBPC3 Mutation. *Oxid. Med. Cell. Longev.* **2015**, *2015*, 424751. [CrossRef] [PubMed]
72. Han, Y.S.; Proctor, D.N.; Geiger, P.C.; Sieck, G.C. Reserve capacity for ATP consumption during isometric contraction in human skeletal muscle fibers. *J. Appl. Physiol.* **2001**, *90*, 657–664. [CrossRef] [PubMed]
73. Klitgaard, H.; Zhou, M.; Schiaffino, S.; Betto, R.; Salviati, G.; Saltin, B. Ageing alters the myosin heavy chain composition of single fibres from human skeletal muscle. *Acta Physiol. Scand.* **1990**, *140*, 55–62. [CrossRef] [PubMed]
74. Van Der Velden, J.; Tocchetti, C.G.; Varricchi, G.; Bianco, A.; Sequeira, V.; Hilfiker-Kleiner, D.; Hamdani, N.; Leite-Moreira, A.F.; Mayr, M.; Falcao-Pires, I.; et al. Metabolic changes in hypertrophic cardiomyopathies: Scientific update from the working group of myocardial function of the European Society of Cardiology. *Cardiovasc. Res.* **2018**, *114*, 1273–1280. [CrossRef] [PubMed]
75. Marques, I.J.; Leito, J.T.D.; Spaink, H.P.; Testerink, J.; Jaspers, R.T.; Witte, F.; Van Den Berg, S.; Bagowski, C.P. Transcriptome analysis of the response to chronic constant hypoxia in zebrafish hearts. *J. Comp. Physiol. B Biochem. Syst. Environ. Physiol.* **2008**, *178*, 77–92. [CrossRef] [PubMed]
76. Noormohammadi, A.; Khodakarami, A.; Gutierrez-Garcia, R.; Lee, H.J.; Koyuncu, S.; Konig, T.; Schindler, C.; Saez, I.; Fatima, A.; Dieterich, C.; et al. Somatic increase of CCT8 mimics proteostasis of human pluripotent stem cells and extends C. elegans lifespan. *Nat. Commun.* **2016**, *7*, 13649. [CrossRef] [PubMed]
77. Brehme, M.; Voisine, C.; Rolland, T.; Wachi, S.; Soper, J.H.; Zhu, Y.; Orton, K.; Villella, A.; Garza, D.; Vidal, M.; et al. A chaperome subnetwork safeguards proteostasis in aging and neurodegenerative disease. *Cell Rep.* **2014**, *9*, 1135–1150. [CrossRef]
78. Brocker, C.; Lassen, N.; Estey, T.; Pappa, A.; Cantore, M.; Orlova, V.V.; Chavakis, T.; Kavanagh, K.L.; Oppermann, U.; Vasiliou, V. Aldehyde dehydrogenase 7A1 (ALDH7A1) is a novel enzyme involved in cellular defense against hyperosmotic stress. *J. Biol. Chem.* **2010**, *285*, 18452–18463. [CrossRef]
79. O'Brien, K.M.; Rix, A.S.; Egginton, S.; Farrell, A.P.; Crockett, E.L.; Schlauch, K.; Woolsey, R.; Hoffman, M.; Merriman, S. Cardiac mitochondrial metabolism may contribute to differences in thermal tolerance of red- and white-blooded Antarctic notothenioid fishes. *J. Exp. Biol.* **2018**, *221*, jeb177816. [CrossRef]
80. Bilyk, K.T.; Zhuang, X.; Murphy, K.R.; Christina Cheng, C.H. A tale of two genes: Divergent evolutionary fate of haptoglobin and hemopexin in hemoglobinless Antarctic icefishes. *J. Exp. Biol.* **2019**, *222*, jeb188573. [CrossRef]
81. Cai, J.; Yang, J.; Jones, D.P. Mitochondrial control of apoptosis: The role of cytochrome c. *Biochim. Biophys. Acta-Bioenerg.* **1998**, *1366*, 139–149. [CrossRef]
82. Santucci, R.; Sinibaldi, F.; Cozza, P.; Polticelli, F.; Fiorucci, L. Cytochrome c: An extreme multifunctional protein with a key role in cell fate. *Int. J. Biol. Macromol.* **2019**, *136*, 1237–1246. [CrossRef] [PubMed]
83. O'Brien, K.M.; Skilbeck, C.; Sidell, B.D.; Egginton, S. Muscle fine structure may maintain the function of oxidative fibres in haemoglobinless Antarctic fishes. *J. Exp. Biol.* **2003**, *206*, 411–421. [CrossRef] [PubMed]
84. Marchi, S.; Patergnani, S.; Pinton, P. The endoplasmic reticulum-mitochondria connection: One touch, multiple functions. *Biochim. Biophys. Acta-Bioenerg.* **2014**, *1837*, 461–469. [CrossRef]
85. Bakker, C.E.; De Diego Otero, Y.; Bontekoe, C.; Raghoe, P.; Luteijn, T.; Hoogeveen, A.T.; Oostra, B.A.; Willemsen, R. Immunocytochemical and biochemical characterization of FMRP, FXR1P, and FXR2P in the mouse. *Exp. Cell Res.* **2000**, *258*, 162–170. [CrossRef] [PubMed]

7 Bibliography

1. Taylor, K. Mighty mitochondria and neurodegenerative diseases. *Science in the News* https://sitn.hms.harvard.edu/flash/2012/issue111/ (2012).

2. Mitchell, P. Coupling of phosphorylation to electron and hydrogen transfer by a chemi-osmotic type of mechanism. *Nature* **191**, 144–148 (1961).

3. Krebs, H. A. & Johnson, W. A. The role of citric acid in intermediate metabolism in animal tissues. *FEBS Lett.* **117**, K2–K10 (1980).

4. Wilson, B. A., Schisler, J. C. & Willis, M. S. Sir Hans Adolf Krebs: Architect of metabolic cycles. *Lab. Med.* **41**, 377–380 (2010).

5. Abrahams, J. P., Leslie, A. G. W., Lutter, R. & Walker, J. E. Structure at 2.8 Â resolution of F1-ATPase from bovine heart mitochondria. *Nature* **370**, 621–628 (1994).

6. Margulis, L. On the origin of mitosing cells. *J. Theor. Biol.* **14**, 255–74 (1967).

7. Gray, M. W., Burger, G. & Lang, B. F. Mitochondrial evolution. *Science (80-.).* **283**, 1476–1481 (1999).

8. Martin, W. F., Garg, S. & Zimorski, V. Endosymbiotic theories for eukaryote origin. *Philos. Trans. R. Soc. B Biol. Sci.* **370**, (2015).

9. Adams, K. L., Qiu, Y. L., Stoutemyer, M. & Palmer, J. D. Punctuated evolution of mitochondrial gene content: High and variable rates of mitochondrial gene loss and transfer to the nucleus during angiosperm evolution. *Proc. Natl. Acad. Sci. U. S. A.* **99**, 9905–9912 (2002).

10. Adams, K. L. & Palmer, J. D. Evolution of mitochondrial gene content: Gene loss and transfer to the nucleus. *Mol. Phylogenet. Evol.* **29**, 380–

395 (2003).

11. Timmis, J. N., Ayliff, M. A., Huang, C. Y. & Martin, W. Endosymbiotic gene transfer: Organelle genomes forge eukaryotic chromosomes. *Nat. Rev. Genet.* **5**, 123–135 (2004).

12. Ku, C. *et al.* Endosymbiotic origin and differential loss of eukaryotic genes. *Nature* **524**, 427–432 (2015).

13. Anderson, S. *et al.* Sequence and organization of the human mitochondrial genome. *Nature* **290**, 457–465 (1981).

14. Chacinska, A. *et al.* Essential role of Mia40 in import and assembly of mitochondrial intermembrane space proteins. *EMBO J.* **23**, 3735–3746 (2004).

15. Wiedemann, N. *et al.* Machinery for protein sorting and assembly in the mitochondrial outer membrane. *Nature* **424**, 565–571 (2003).

16. Kovermann, P. *et al.* Tim22, the essential core of the mitochondrial protein insertion complex, forms a voltage-activated and signal-gated channel. *Mol. Cell* **9**, 363–373 (2002).

17. Bauer, M. F., Sirrenberg, C., Neupert, W. & Brunner, M. Role of Tim23 as voltage sensor and presequence receptor in protein import into mitochondria. *Cell* **87**, 33–41 (1996).

18. Esaki, M. *et al.* Tom40 protein import channel binds to non-native proteins and prevents their aggregation. *Nat. Struct. Biol.* **10**, 988–994 (2003).

19. Wiedemann, N. *et al.* Biogenesis of the protein import channel Tom40 of the mitochondrial outer membrane: Intermembrane space components are involved in an early stage of the assembly pathway. *J. Biol. Chem.* **279**, 18188–18194 (2004).

20. Humphries, A. D. *et al.* Dissection of the mitochondrial import and assembly pathway for human Tom40. *J. Biol. Chem.* **280**, 11535–11543

(2005).

21. Yao, C. H. *et al.* Mitochondrial fusion supports increased oxidative phosphorylation during cell proliferation. *Elife* **8**, 1–19 (2019).

22. Zanna, C. *et al.* OPA1 mutations associated with dominant optic atrophy impair oxidative phosphorylation and mitochondrial fusion. *Brain* **131**, 352–367 (2008).

23. Otera, H., Ishihara, N. & Mihara, K. New insights into the function and regulation of mitochondrial fission. *Biochim. Biophys. Acta - Mol. Cell Res.* **1833**, 1256–1268 (2013).

24. Cordova, L. T. & Alper, H. S. Central metabolic nodes for diverse biochemical production. *Curr. Opin. Chem. Biol.* **35**, 37–42 (2016).

25. Ward, D. M. & Cloonan, S. M. Mitochondrial Iron in Human Health and Disease. *Annu. Rev. Physiol.* **81**, 453–482 (2019).

26. Giorgi, C., Marchi, S. & Pinton, P. The machineries, regulation and cellular functions of mitochondrial calcium. *Nature Reviews Molecular Cell Biology* vol. 19 713–730 (2018).

27. Mammucari, C. *et al.* The Mitochondrial Calcium Uniporter Controls Skeletal Muscle Trophism In Vivo. *Cell Rep.* **10**, 1269–1279 (2015).

28. McCormack, J. G., Halestrap, A. P. & Denton, R. M. Role of calcium ions in regulation of mammalian intramitochondrial metabolism. *Physiol. Rev.* **70**, 391–425 (1990).

29. De Stefani, D., Patron, M. & Rizzuto, R. Structure and function of the mitochondrial calcium uniporter complex. *Biochim. Biophys. Acta - Mol. Cell Res.* **1853**, 2006–2011 (2014).

30. Denton, R. M. Regulation of mitochondrial dehydrogenases by calcium ions. *Biochim. Biophys. Acta - Bioenerg.* **1787**, 1309–1316 (2009).

31. Maekawa, H. *et al.* Mitochondrial Damage Causes Inflammation via

cGAS-STING Signaling in Acute Kidney Injury. *Cell Rep.* **29**, 1261-1273.e6 (2019).

32. Guo, Y. *et al.* Mitochondrial DNA drives noncanonical inflammation activation via cGAS–STING signaling pathway in retinal microvascular endothelial cells. *Cell Commun. Signal.* **18**, 1–12 (2020).

33. Martinou, J. C., Desagher, S. & Antonsson, B. Cytochrome c release from mitochondria: All or nothing. *Nat. Cell Biol.* **2**, 41–43 (2000).

34. Ott, M., Robertson, J. D., Gogvadze, V., Zhivotovsky, B. & Orrenius, S. Cytochrome c release from mitochondria proceeds by a two-step process. *Proc. Natl. Acad. Sci. U. S. A.* **99**, 1259–1263 (2002).

35. Garrido, C. *et al.* Mechanisms of cytochrome c release from mitochondria. *Cell Death Differ.* **13**, 1423–1433 (2006).

36. Ryan, M. T. & Hoogenraad, N. J. Mitochondrial-nuclear communications. *Annu. Rev. Biochem.* **76**, 701–722 (2007).

37. Zhu, D., Li, X. & Tian, Y. Mitochondrial-to-nuclear communication in aging: an epigenetic perspective. *Trends Biochem. Sci.* **47**, 645–659 (2022).

38. Eigentler, A., Draxl, A. & Wiethüchter, A. Laboratory protocol: citrate synthase a mitochondrial marker enzyme. *Mitochondrial Physiol. Netw.* **04**, 1–11 (2015).

39. Shi, L. & Tu, B. P. Acetyl-CoA and the regulation of metabolism: Mechanisms and consequences. *Curr. Opin. Cell Biol.* **33**, 125–131 (2015).

40. Hirst, J. Mitochondrial Complex I. *Annu. Rev. Biochem.* **82**, 551–575 (2013).

41. Henriques, B. J., Katrine Jentoft Olsen, R., Gomes, C. M. & Bross, P. Electron transfer flavoprotein and its role in mitochondrial energy metabolism in health and disease. *Gene* **776**, (2021).

42. Watmough, N. J. & Frerman, F. E. The electron transfer flavoprotein: Ubiquinone oxidoreductases. *Biochim. Biophys. Acta - Bioenerg.* **1797**, 1910–1916 (2010).

43. Mráček, T., Drahota, Z. & Houštěk, J. The function and the role of the mitochondrial glycerol-3-phosphate dehydrogenase in mammalian tissues. *Biochim. Biophys. Acta - Bioenerg.* **1827**, 401–410 (2013).

44. Pallag, G. *et al.* Proline Oxidation Supports Mitochondrial ATP Production When Complex I Is Inhibited. *Int. J. Mol. Sci.* **23**, 5111 (2022).

45. Gnaiger, E. *Mitochondrial pathways and respiratory control. An introduction to OXPHOS analysis. Bioenergetic Communications* vol. 5th (2020).

46. Chandel, N. S., Budinger, G. R. S. & Schumacker, P. T. Molecular oxygen modulates cytochrome c oxidase function. *J. Biol. Chem.* **271**, 18672–18677 (1996).

47. Michel, H., Behr, J., Harrenga, A. & Kannt, A. Cytochrome c oxidase: Structure and spectroscopy. *Annu. Rev. Biophys. Biomol. Struct.* **27**, 329–356 (1998).

48. Mitchell, P. Chemiosmotic coupling in oxidative and photosynthetic phosphorylation. *Biol. Rev. Camb. Philos. Soc.* **41**, 445–502 (1966).

49. Boyer, P. D., Cross, R. L. & Momsen, W. A New Concept for Energy Coupling in Oxidative Phosphorylation Based on a Molecular Explanation of the Oxygen Exchange Reactions. *Proc. Natl. Acad. Sci.* **70**, 2837–2839 (1973).

50. Sakamoto, J. Identification of the nucleotide-binding site for ATP synthesis and hydrolysis in mitochondrial soluble F1-ATPase. *J. Biochem.* **96**, 475–481 (1984).

51. Diez, M. *et al.* Proton-powered subunit rotation in single membrane-

bound F 0F1-ATP synthase. *Nat. Struct. Mol. Biol.* **11**, 135–141 (2004).

52. Stincone, A. *et al.* The return of metabolism: Biochemistry and physiology of the pentose phosphate pathway. *Biol. Rev.* **90**, 927–963 (2015).

53. Moon, S. J., Dong, W., Stephanopoulos, G. N. & Sikes, H. D. Oxidative pentose phosphate pathway and glucose anaplerosis support maintenance of mitochondrial NADPH pool under mitochondrial oxidative stress. *Bioeng. Transl. Med.* **5**, 1–18 (2020).

54. Hardie, D. G. AMPK: Positive and negative regulation, and its role in whole-body energy homeostasis. *Curr. Opin. Cell Biol.* **33**, 1–7 (2015).

55. Houtkooper, R. H., Cantó, C., Wanders, R. J. & Auwerx, J. The secret life of NAD+: An old metabolite controlling new metabolic signaling pathways. *Endocr. Rev.* **31**, 194–223 (2010).

56. López-Otín, C., Blasco, M. A., Partridge, L., Serrano, M. & Kroemer, G. The hallmarks of aging. *Cell* (2013) doi:10.1016/j.cell.2013.05.039.

57. Tatarková, Z. *et al.* Effects of aging on activities of mitochondrial electron transport chain complexes and oxidative damage in rat heart. *Physiol. Res.* **60**, 281–289 (2011).

58. Trounce, I., Byrne, E. & Marzuki, S. Decline in Skeletal Muscle Mitochondrial Respiratory Chain Function: Possible Factor in Ageing. *Lancet* **333**, 637–639 (1989).

59. Yen, T.-C., Chen, Y.-S., King, K.-L., Yeh, S.-H. & Wei, Y.-H. Liver mitochondrial respiratory functions decline with age. *Biochem. Biophys. Res. Commun.* **165**, 994–1003 (1989).

60. Turrens, J. F. Mitochondrial formation of reactive oxygen species. *J. Physiol.* **552**, 335–344 (2003).

61. Trifunovic, A. & Larsson, N. G. Mitochondrial dysfunction as a cause of ageing. *J. Intern. Med.* **263**, 167–178 (2008).

62. Kauppila, T. E. S., Kauppila, J. H. K. & Larsson, N. G. Mammalian Mitochondria and Aging: An Update. *Cell Metab.* **25**, 57–71 (2017).

63. Corsetti, G. *et al.* Morphometric Changes Induced by Amino Acid Supplementation in Skeletal and Cardiac Muscles of Old Mice. *Am. J. Cardiol.* **101**, (2008).

64. Calkins, M. J., Manczak, M., Mao, P., Shirendeb, U. & Reddy, P. H. Impaired mitochondrial biogenesis, defective axonal transport of mitochondria, abnormal mitochondrial dynamics and synaptic degeneration in a mouse model of Alzheimer's disease. *Hum. Mol. Genet.* **20**, 4515–4529 (2011).

65. Sheng, B. *et al.* Impaired mitochondrial biogenesis contributes to mitochondrial dysfunction in Alzheimer's disease. *J. Neurochem.* **120**, 419–429 (2012).

66. Murphy, M. P. How mitochondria produce reactive oxygen species. *Biochem. J.* **417**, 1–13 (2009).

67. Harman, D. Aging: A Theory Based on Free Radical and Radiation Chemistry. *J. Gerontol.* **11**, 298–300 (1956).

68. Harman, D. Free radical theory of aging: Consequences of mitochondrial aging. *Age (Omaha).* **6**, 86–94 (1983).

69. Harman, D. Free radical theory of aging. *Mutat. Res. DNAging* **275**, 257–266 (1992).

70. Hekimi, S., Lapointe, J. & Wen, Y. Taking a 'good' look at free radicals in the aging process. *Trends in Cell Biology* (2011) doi:10.1016/j.tcb.2011.06.008.

71. Matsuzaki, S., Szweda, P. A., Szweda, L. I. & Humphries, K. M. Regulated production of free radicals by the mitochondrial electron transport chain: Cardiac ischemic preconditioning. *Adv. Drug Deliv. Rev.* **61**, 1324–1331 (2009).

72. Bárcena, C., Mayoral, P. & Quirós, P. M. Mitohormesis, an Antiaging Paradigm. *Int. Rev. Cell Mol. Biol.* **340**, 35–77 (2018).

73. Vermulst, M. *et al.* Mitochondrial point mutations do not limit the natural lifespan of mice. *Nat. Genet.* **39**, 540–543 (2007).

74. Khrapko, K. & Vijg, J. Mitochondrial DNA mutations and aging: a case closed? *Nat. Genet.* **39**, 445–446 (2007).

75. Park, C. B. & Larsson, N. G. Mitochondrial DNA mutations in disease and aging. *J. Cell Biol.* **193**, 809–818 (2011).

76. Kauppila, T. E. S. *et al.* Mutations of mitochondrial DNA are not major contributors to aging of fruit flies. *Proc. Natl. Acad. Sci. U. S. A.* **115**, E9620–E9629 (2018).

77. Wolf, A. M. MtDNA mutations and aging—not a closed case after all? *Signal Transduct. Target. Ther.* **6**, 2020–2021 (2021).

78. Austad, S. N. & Hoffman, J. M. Is antagonistic pleiotropy ubiquitous in aging biology? *Evol. Med. Public Heal.* **2018**, 287–294 (2018).

79. Soukas, A. A., Hao, H. & Wu, L. Metformin as Anti-Aging Therapy: Is It for Everyone? *Trends Endocrinol. Metab.* **30**, 745–755 (2019).

80. Hamer, M., Lavoie, K. L. & Bacon, S. L. Taking up physical activity in later life and healthy ageing: The English longitudinal study of ageing. *Br. J. Sports Med.* **48**, 239–243 (2014).

81. Viña, J. *et al.* Mitochondrial biogenesis in exercise and in ageing. *Adv. Drug Deliv. Rev.* **61**, 1369–1374 (2009).

82. Hoene, M. *et al.* Exercise prevents fatty liver by modifying the compensatory response of mitochondrial metabolism to excess substrate availability. *Mol. Metab.* **54**, 1–17 (2021).

83. Granata, C. *et al.* High-intensity training induces non-stoichiometric changes in the mitochondrial proteome of human skeletal muscle

without reorganisation of respiratory chain content. *Nat. Commun.* **12**, 7056 (2021).

84. Ebanks, B. *et al.* Exercising D. melanogaster Modulates the Mitochondrial Proteome and Physiology. The Effect on Lifespan Depends upon Age and Sex. *Int. J. Mol. Sci.* **22**, 11606 (2021).

85. Sreekumar, R. *et al.* Effects of caloric restriction on mitochondrial function and gene transcripts in rat muscle. *Am. J. Physiol. - Endocrinol. Metab.* **283**, 38–43 (2002).

86. López-Lluch, G. *et al.* Calorie restriction induces mitochondrial biogenesis and bioenergetic efficiency. *Proc. Natl. Acad. Sci. U. S. A.* **103**, 1768–1773 (2006).

87. Civitarese, A. E. *et al.* Calorie restriction increases muscle mitochondrial biogenesis in healthy humans. *PLoS Med.* **4**, 485–494 (2007).

88. Lanza, I. R. *et al.* Chronic caloric restriction preserves mitochondrial function in senescence without increasing mitochondrial biogenesis. *Cell Metab.* **16**, 777–788 (2012).

89. Sparks, L. M. *et al.* Effects of 12 months of caloric restriction on muscle mitochondrial function in healthy individuals. *J. Clin. Endocrinol. Metab.* **102**, 111–121 (2017).

90. Wallace, D. C. Mitochondria and cancer. *Nat. Rev. Cancer* **12**, 685–698 (2012).

91. Moreira, P. I., Carvalho, C., Zhu, X., Smith, M. A. & Perry, G. Mitochondrial dysfunction is a trigger of Alzheimer's disease pathophysiology. *Biochim. Biophys. Acta - Mol. Basis Dis.* **1802**, 2–10 (2010).

92. Park, J. S., Davis, R. L. & Sue, C. M. Mitochondrial Dysfunction in Parkinson's Disease: New Mechanistic Insights and Therapeutic

Perspectives. *Current Neurology and Neuroscience Reports* vol. 18 (2018).

93. Swerdlow, R. H. Mitochondria and Mitochondrial Cascades in Alzheimer's Disease. *Journal of Alzheimer's Disease* vol. 62 1403–1416 (2018).

94. Yang, Y. *et al.* Mitochondrial pathology and muscle and dopaminergic neuron degeneration caused by inactivation of Drosophila Pink1 is rescued by Parkin. *Proc. Natl. Acad. Sci. U. S. A.* **103**, 10793–10798 (2006).

95. Park, J. *et al.* Mitochondrial dysfunction in Drosophila PINK1 mutants is complemented by parkin. *Nature* **441**, 1157–1161 (2006).

96. Clark, I. E. *et al.* Drosophila pink1 is required for mitochondrial function and interacts genetically with parkin. *Nature* **441**, 1162–1166 (2006).

97. Gautier, C. A., Kitada, T. & Shen, J. Loss of PINK1 causes mitochondrial functional defects and increased sensitivity to oxidative stress. *Proc. Natl. Acad. Sci.* **105**, 11364–11369 (2008).

98. Wood-Kaczmar, A. *et al.* PINK1 is necessary for long term survival and mitochondrial function in human dopaminergic neurons. *PLoS One* **3**, (2008).

99. Valente, E. M. *et al.* Hereditary early-onset Parkinson's disease caused by mutations in PINK1. *Science (80-.).* **304**, 1158–1160 (2004).

100. Betarbet, R. *et al.* Chronic systemic pesticide exposure reproduces features of Parkinson's disease. *Nat. Neurosci.* **3**, 1301–1306 (2000).

101. Glinka, Y., Gassen, M. & Youdim, M. B. H. Mechanism of 6-hydroxydopamine neurotoxicity. *Journal of Neural Transmission, Supplement* 55–66 (1997) doi:10.1007/978-3-7091-6842-4_7.

102. Pizzorno, J. Mitochondria-fundamental to life and health. *Integr. Med.*

13, 8–15 (2014).

103. Ma, J. *et al.* A dynamic analysis of the rotation mechanism for conformational change in F1-ATPase. *Structure* **10**, 921–931 (2002).

104. Stock, D., Leslie, A. G. W. & Walker, J. E. Molecular architecture of the rotary motor in ATP synthase. *Science (80-.).* **286**, 1700–1705 (1999).

105. He, J. *et al.* Assembly of the membrane domain of ATP synthase in human mitochondria. *Proc. Natl. Acad. Sci. U. S. A.* **115**, 2988–2993 (2018).

106. Noji, H., Yasuda, R., Yoshida, M. & Kinosita, K. Direct observation of the rotation of F1-ATPase. *Nature* **386**, 299–302 (1997).

107. Allegretti, M. *et al.* Horizontal membrane-intrinsic α-helices in the stator a-subunit of an F-type ATP synthase. *Nature* **521**, 237–240 (2015).

108. Ebanks, B., Ingram, T. L. & Chakrabarti, L. ATP synthase and Alzheimer's disease: putting a spin on the mitochondrial hypothesis. *Aging (Albany. NY).* **12**, 1–16 (2020).

109. Braig, K., Menz, R. I., Montgomery, M. G., Leslie, A. G. & Walker, J. E. Structure of bovine mitochondrial F1-ATPase inhibited by Mg2+ADP and aluminium fluoride. *Structure* **8**, 567–573 (2000).

110. Kagawa, R., Montgomery, M. G., Braig, K., Leslie, A. G. W. & Walker, J. E. The structure of bovine F1-ATPase inhibited by ADP and beryllium fluoride. *EMBO J.* **23**, 2734–2744 (2004).

111. Bowler, M. W., Montgomery, M. G., Leslie, A. G. W. & Walker, J. E. Ground state structure of F1-ATPase from bovine heart mitochondria at 1.9 Å resolution. *J. Biol. Chem.* **282**, 14238–14242 (2007).

112. Itoh, H. *et al.* Mechanically driven ATP synthesis by F1-ATPase. *Nature* **427**, 465–468 (2004).

113. Rondelez, Y. *et al.* Highly coupled ATP synthesis by F1-ATPase single molecules. *Nature* **433**, 773–777 (2005).

114. Masaike, T., Koyama-Horibe, F., Oiwa, K., Yoshida, M. & Nishizaka, T. Cooperative three-step motions in catalytic subunits of F 1-ATPase correlate with 80° and 40° substep rotations. *Nat. Struct. Mol. Biol.* **15**, 1326–1333 (2008).

115. Adachi, K. *et al.* Coupling of Rotation and Catalysis in F1-ATPase Revealed by Single-Molecule Imaging and Manipulation. *Cell* **130**, 309–321 (2007).

116. Nishizaka, T. *et al.* Chemomechanical coupling in F1-ATPase revealed by simultaneous observation of nucleotide kinetics and rotation. *Nat. Struct. Mol. Biol.* **11**, 142–148 (2004).

117. Menz, R. I., Walker, J. E. & Leslie, A. G. W. Structure of bovine mitochondrial F1-ATPase with nucleotide bound to all three catalytic sites: Implications for the mechanism of rotary catalysis. *Cell* **106**, 331–341 (2001).

118. Rees, D. M., Montgomery, M. G., Leslie, A. G. W. & Walker, J. E. Structural evidence of a new catalytic intermediate in the pathway of ATP hydrolysis by F1-ATPase from bovine heart mitochondria. *Proc. Natl. Acad. Sci. U. S. A.* **109**, 11139–11143 (2012).

119. Li, C. B., Ueno, H., Watanabe, R., Noji, H. & Komatsuzaki, T. ATP hydrolysis assists phosphate release and promotes reaction ordering in F1 -ATPase. *Nat. Commun.* **6**, 10223 (2015).

120. Walker, J. E. & Dickson, V. K. The peripheral stalk of the mitochondrial ATP synthase. *Biochim. Biophys. Acta - Bioenerg.* **1757**, 286–296 (2006).

121. He, J. *et al.* Assembly of the peripheral stalk of ATP synthase in human mitochondria. *Proc. Natl. Acad. Sci. U. S. A.* **117**, 29602–29608 (2020).

122. Guo, H. & Rubinstein, J. L. Structure of ATP synthase under strain during catalysis. *Nat. Commun.* **13**, 2–10 (2022).

123. Cabezón, E., Runswick, M. J., Leslie, A. G. W. & Walker, J. E. The structure of bovine IF1, the regulatory subunit of mitochondrial F-ATPase. *EMBO J.* **20**, 6990–6996 (2001).

124. Gledhill, J. R., Montgomery, M. G., Leslie, A. G. W. & Walker, J. E. How the regulatory protein, IF1, inhibits F1-ATPase from bovine mitochondria. *Proc. Natl. Acad. Sci. U. S. A.* **104**, 15671–15676 (2007).

125. Galber, C. *et al.* The mitochondrial inhibitor IF1 binds to the ATP synthase OSCP subunit and protects cancer cells from apoptosis. *Cell Death Dis.* **14**, (2023).

126. Shah, D. I. *et al.* Mitochondrial Atpif1 regulates haem synthesis in developing erythroblasts. *Nature* **491**, 608–612 (2012).

127. Chen, W. W. *et al.* Inhibition of ATPIF1 ameliorates severe mitochondrial respiratory chain dysfunction in mammalian cells. *Cell Rep.* **7**, 27–34 (2014).

128. García-Bermúdez, J. *et al.* PKA Phosphorylates the ATPase Inhibitory Factor 1 and Inactivates Its Capacity to Bind and Inhibit the Mitochondrial H+-ATP Synthase. *Cell Rep.* **12**, 2143–2155 (2015).

129. Flygaard, R. K., Mühleip, A., Tobiasson, V. & Amunts, A. Type III ATP synthase is a symmetry-deviated dimer that induces membrane curvature through tetramerization. *Nat. Commun.* **11**, (2020).

130. Domínguez-Zorita, S., Romero-Carramiñana, I., Cuezva, J. M. & Esparza-Moltó, P. B. The ATPase Inhibitory Factor 1 is a Tissue-Specific Physiological Regulator of the Structure and Function of Mitochondrial ATP Synthase: A Closer Look Into Neuronal Function. *Front. Physiol.* **13**, 1–11 (2022).

131. Ebanks, B. & Chakrabarti, L. Mitochondrial ATP Synthase is a Target

of Oxidative Stress in Neurodegenerative Diseases. *Front. Mol. Biosci.* **9**, 1–7 (2022).

132. Wang, T., Ma, F. & Qian, H. Defueling the cancer: ATP synthase as an emerging target in cancer therapy. *Mol. Ther. - Oncolytics* **23**, 82–95 (2021).

133. Perutz, M. F. *et al. Structure of Hæmoglobin: A three-dimensional fourier synthesis at 5.5-. resolution, obtained by X-ray analysis*. *Nature* vol. 185 (1960).

134. Kendrew, J. C. *et al.* A Three-Dimensional Model of the Myoglobin Molecule Obtained by X-Ray Analysis. *Nature* **181**, 662–666 (1958).

135. KENDREW, J. C. *et al.* Structure of Myoglobin: A Three-Dimensional Fourier Synthesis at 2 Å. Resolution. *Nature* **185**, 422–427 (1960).

136. Monod, J., Wyman, J. & Changeux, J. P. On the nature of allosteric transitions: A plausible model. *J. Mol. Biol.* **12**, 88–118 (1965).

137. Ogata, R. T. & McConnell, H. M. Mechanism of cooperative oxygen binding to hemoglobin (spin-labeled triphosphate-concerted transition model-hemoglobin chesapeake). *Proc. Natl. Acad. Sci. U. S. A.* **69**, 335–339 (1972).

138. Wittenberg, J. B. & Wittenberg, B. A. Myoglobin function reassessed. *J. Exp. Biol.* **206**, 2011–2020 (2003).

139. Keppner, A. *et al.* Lessons from the post-genomic era: Globin diversity beyond oxygen binding and transport. *Redox Biol.* **37**, 101687 (2020).

140. Burmester, T., Ebner, B., Weich, B. & Hankeln, T. Cytoglobin: A novel globin type ubiquitously expressed in vertebrate tissues. *Mol. Biol. Evol.* **19**, 416–421 (2002).

141. Schmidt, M. *et al.* Cytoglobin Is a Respiratory Protein in Connective Tissue and Neurons, Which Is Up-regulated by Hypoxia. *J. Biol. Chem.* **279**, 8063–8069 (2004).

142. Fordel, E. *et al.* Cytoglobin expression is upregulated in all tissues upon hypoxia: An in vitro and in vivo study by quantitative real-time PCR. *Biochem. Biophys. Res. Commun.* **319**, 342–348 (2004).

143. Liu, X. *et al.* Characterization of the function of cytoglobin as an oxygen-dependent regulator of nitric oxide concentration. *Biochemistry* **51**, 5072–5082 (2012).

144. Corti, P. *et al.* Globin X is a six-coordinate globin that reduces nitrite to nitric oxide in fish red blood cells. *Proc. Natl. Acad. Sci.* **113**, 8538–8543 (2016).

145. Dröge, J. & Makałowski, W. Phylogenetic analysis reveals wide distribution of globin X. *Biol. Direct* **6**, 3–7 (2011).

146. Hoffmann, F. G., Storz, J. F., Kuraku, S., Vandewege, M. W. & Opazo, J. C. Whole-Genome Duplications and the Diversification of the Globin-X Genes of Vertebrates. *Genome Biol. Evol.* **13**, 1–13 (2021).

147. Koch, J. & Burmester, T. Membrane-bound globin X protects the cell from reactive oxygen species. *Biochem. Biophys. Res. Commun.* **469**, 275–280 (2016).

148. Liu, J. *et al.* Effects of neuroglobin overexpression on mitochondrial function and oxidative stress following hypoxia/reoxygenation in cultured neurons. *J. Neurosci. Res.* **87**, 164–170 (2009).

149. Yu, Z. *et al.* Mitochondrial distribution of neuroglobin and its response to oxygen-glucose deprivation in primary-cultured mouse cortical neurons. *Neuroscience* **218**, 235–242 (2012).

150. Lechauve, C. *et al.* Neuroglobin involvement in respiratory chain function and retinal ganglion cell integrity. *Biochim. Biophys. Acta - Mol. Cell Res.* **1823**, 2261–2273 (2012).

151. Nishi, H. *et al.* Hemoglobin is expressed by mesangial cells and reduces oxidant stress. *J. Am. Soc. Nephrol.* **19**, 1500–1508 (2008).

152. Liu, W., Baker, S. S., Baker, R. D., Nowak, N. J. & Zhu, L. Upregulation of hemoglobin expression by oxidative stress in hepatocytes and its implication in nonalcoholic steatohepatitis. *PLoS One* **6**, 1–7 (2011).

153. Dassen, H. *et al.* Haemoglobin expression in human endometrium. *Hum. Reprod.* **23**, 635–641 (2008).

154. Russo, R. *et al.* Hemoglobin is present as a canonical α2β2 tetramer in dopaminergic neurons. *Biochim. Biophys. Acta - Proteins Proteomics* **1834**, 1939–1943 (2013).

155. Biagioli, M. *et al.* Unexpected expression of α- and β-globin in mesencephalic dopaminergic neurons and glial cells. *Proc. Natl. Acad. Sci. U. S. A.* **106**, 15454–15459 (2009).

156. Codrich, M. *et al.* Neuronal hemoglobin affects dopaminergic cells' response to stress. *Cell Death Dis.* **8**, e2538–e2538 (2017).

157. Richter, F., Meurers, B. H., Zhu, C., Medvedeva, V. P. & Chesselet, M. F. Neurons express hemoglobin α- and β-chains in rat and human brains. *J. Comp. Neurol.* **515**, 538–547 (2009).

158. Saha, D. *et al.* Hemoglobin Expression in Nonerythroid Cells: Novel or Ubiquitous? *Int. J. Inflam.* **2014**, (2014).

159. Cassanova, N., O'Brien, K. M., Stahl, B. T., McClure, T. & Poyton, R. O. Yeast flavohemoglobin, a nitric oxide oxidoreductase, is located in both the cytosol and the mitochondrial matrix: Effects of respiration, anoxia, and the mitochondrial genome on its intracellular level and distribution. *J. Biol. Chem.* **280**, 7645–7653 (2005).

160. Shephard, F., Greville-Heygate, O., Marsh, O., Anderson, S. & Chakrabarti, L. A mitochondrial location for haemoglobins-Dynamic distribution in ageing and Parkinson's disease. *Mitochondrion* **14**, 64–72 (2014).

161. Yang, W., Li, X., Li, X., Li, X. & Yu, S. Neuronal hemoglobin in mitochondria is reduced by forming a complex with a-synuclein in aging monkey brains. *Oncotarget* **7**, 7441–7454 (2016).

162. Shephard, F., Greville-Heygate, O., Liddell, S., Emes, R. & Chakrabarti, L. Analysis of Mitochondrial haemoglobin in Parkinson's disease brain. *Mitochondrion* **29**, 45–52 (2016).

163. Brown, N. *et al.* Neuronal Hemoglobin Expression and Its Relevance to Multiple Sclerosis Neuropathology. *J. Mol. Neurosci.* **59**, 1–17 (2016).

164. Brunyanszki, A. *et al.* Upregulation and mitochondrial sequestration of hemoglobin occur in circulating leukocytes during critical illness, conferring a cytoprotective phenotype. *Mol. Med.* **21**, 666–675 (2015).

165. Basile, A. J., Kirkton, S. D., Hedrick, M. S., Carey, H. V. & Sweazea, K. L. Defining comparative physiology: results from an online survey and systematic review. *Am. J. Physiol. - Regul. Integr. Comp. Physiol.* **320**, R938–R944 (2021).

166. Krogh, A. The progress of physiology. *Science (80-.).* **70**, 200–204 (1929).

167. Burmester, T. & Hankeln, T. A globin gene of Drosophila melanogaster. *Mol. Biol. Evol.* **16**, 1809–1811 (1999).

168. Hankeln, T. *et al.* Characterization of Drosophila hemoglobin. Evidence for hemoglobin-mediated respiration in insects. *J. Biol. Chem.* **277**, 29012–29017 (2002).

169. Burmester, T., Storf, J., Hasenjäger, A., Klawitter, S. & Hankeln, T. The hemoglobin genes of Drosophila. *FEBS J.* **273**, 468–480 (2006).

170. Gleixner, E., Herlyn, H., Zimmerling, S., Burmester, T. & Hankeln, T. Testes-specific hemoglobins in Drosophila evolved by a combination of sub- and neofunctionalization after gene duplication. *BMC Evol. Biol.* **12**, 1–12 (2012).

171. Gleixner, E. *et al.* Knockdown of Drosophila hemoglobin suggests a role in O2 homeostasis. *Insect Biochem. Mol. Biol.* **72**, 20–30 (2016).

172. Burmester, T. *et al.* Divergent roles of the Drosophila melanogaster globins. *J. Insect Physiol.* **106**, 224–231 (2018).

173. Ruud, J. T. Vertebrates without erythrocytes and blood pigment. *Nature* **173**, 848–850 (1954).

174. Sidell, B. D. *et al.* Variable expression of myoglobin among the hemoglobinless Antarctic icefishes. *Proc. Natl. Acad. Sci. U. S. A.* **94**, 3420–3424 (1997).

175. Cocca, E. *et al.* Do the hemoglobinless icefishes have globin genes? *Comp. Biochem. Physiol. - A Physiol.* **118**, 1027–1030 (1997).

176. Di Prisco, G., Cocca, E., Parker, S. K. & Detrich, H. W. Tracking the evolutionary loss of hemoglobin expression by the white-blooded Antarctic icefishes. *Gene* **295**, 185–191 (2002).

177. Small, D. J., Vayda, M. E. & Sidell, B. D. A novel vertebrate myoglobin gene containing three A+T-rich introns is conserved among antarctic teleost species which differ in myoglobin expression. *J. Mol. Evol.* **47**, 156–166 (1998).

178. Small, D. J., Moylan, T., Vayda, M. E. & Sidell, B. D. The myoglobin gene of the Antarctic icefish, Chaenocephalus aceratus, contains a duplicated TATAAAA sequence that interferes with transcription. *J. Exp. Biol.* **206**, 131–139 (2003).

179. Grove, T. J., Hendrickson, J. W. & Sidell, B. D. Two species of antarctic icefishes (genus Champsocephalus) share a common genetic lesion leading to the loss of myoglobin expression. *Polar Biol.* **27**, 579–585 (2004).

180. Laptikhovsky, V. White blood of the antarctic icefish: Why? *Mar. Ecol. Prog. Ser.* **626**, 227–231 (2019).

181. Devries, A. L. Role of glycopeptides and peptides in inhibition of crystallization of water in polar fishes. *Philos. Trans. R. Soc. London. B, Biol. Sci.* **304**, 575–588 (1984).

182. Ahlgren, J. A. & DeVries, A. L. Comparison of antifreeze glycopeptides from several Antarctic fishes. *Polar Biol.* **3**, 93–97 (1984).

183. Archer, S. D. & Johnston, I. A. Density of Cristae and Distribution of Mitochondria in the Slow Muscle Fibers of Antarctic Fish. *Physiol. Zool.* **64**, 242–258 (1991).

184. O'Brien, K. M., Xue, H. & Sidell, B. D. Quantification of diffusion distance within the spongy myocardium of hearts from antarctic fishes. *Respir. Physiol.* **122**, 71–80 (2000).

185. Celis, A. I. & DuBois, J. L. Making and breaking heme. *Curr. Opin. Struct. Biol.* **59**, 19–28 (2019).

186. Thomas, C. & Lumb, A. B. Physiology of haemoglobin. *Contin. Educ. Anaesthesia, Crit. Care Pain* **12**, 251–256 (2012).

187. Rouault, T. A. & Tong, W. H. Iron-sulphur cluster biogenesis and mitochondrial iron homeostasis. *Nat. Rev. Mol. Cell Biol.* **6**, 345–351 (2005).

188. Johnson, D. C., Dean, D. R., Smith, A. D. & Johnson, M. K. Structure, function, and formation of biological iron-sulfur clusters. *Annu. Rev. Biochem.* **74**, 247–281 (2005).

189. Winterbourn, C. C. Toxicity of iron and hydrogen peroxide: the Fenton reaction. *Toxicol. Lett.* **82**–**83**, 969–974 (1995).

190. Hentze, M. W., Muckenthaler, M. U., Galy, B. & Camaschella, C. Two to Tango: Regulation of Mammalian Iron Metabolism. *Cell* **142**, 24–38 (2010).

191. Kakhlon, O. & Cabantchik, Z. I. The labile iron pool: Characterization, measurement, and participation in cellular processes. *Free Radic. Biol.*

Med. **33**, 1037–1046 (2002).

192. Cabantchik, Z. I. Labile iron in cells and body fluids: Physiology, pathology, and pharmacology. *Front. Pharmacol.* **5 MAR**, 1–11 (2014).

193. Konijn, A. M. *et al.* The cellular labile iron pool and intracellular ferritin in K562 cells. *Blood* **94**, 2128–2134 (1999).

194. Kawabata, H. Transferrin and transferrin receptors update. *Free Radic. Biol. Med.* **133**, 46–54 (2019).

195. Jaeger, J. L., Shimizu, N. & Gitlin, J. D. Tissue-specific ceruloplasmin gene expression in the mammary gland. *Biochem. J.* **280**, 671–677 (1991).

196. Klomp, L. W. J., Farhangrazi, Z. S., Dugan, L. L. & Gitlin, J. D. Ceruloplasmin gene expression in the murine central nervous system. *J. Clin. Invest.* **98**, 207–215 (1996).

197. Miyajima, H. Aceruloplasminemia, an iron metabolic disorder. in *Neuropathology* vol. 23 345–350 (2003).

198. Patel, B. N., Dunn, R. J. & David, S. Alternative RNA Splicing Generates a Glycosylphosphatidylinositol-anchored Form of Ceruloplasmin in Mammalian Brain. *J. Biol. Chem.* **275**, 4305–4310 (2000).

199. Jeong, S. Y. & David, S. Glycosylphosphatidylinositol-anchored ceruloplasmin is required for iron efflux from cells in the central nervous system. *J. Biol. Chem.* **278**, 27144–27148 (2003).

200. Roeser, H. P., Lee, G. R., Nacht, S. & Cartwright, G. E. The role of ceruloplasmin in iron metabolism. *J. Clin. Invest.* **49**, 2408–2417 (1970).

201. Gitlin, J. D. Transcriptional regulation of ceruloplasmin gene expression during inflammation. *J. Biol. Chem.* **263**, 6281–6287 (1988).

202. Fleming, R. E., Whitman, I. P. & Gitlin, J. D. Induction of ceruloplasmin gene expression in rat lung during inflammation and hyperoxia. *Am. J. Physiol. - Lung Cell. Mol. Physiol.* **260**, 68–74 (1991).

203. Sarkar, J., Seshadri, V., Tripoulas, N. A., Ketterer, M. E. & Fox, P. L. Role of Ceruloplasmin in Macrophage Iron Efflux during Hypoxia. *J. Biol. Chem.* **278**, 44018–44024 (2003).

204. Qian, Z. M. & Ke, Y. Rethinking the role of ceruloplasmin in brain iron metabolism. *Brain Res. Rev.* **35**, 287–294 (2001).

205. Harned, J. *et al.* Ceruloplasmin alters intracellular iron regulated proteins and pathways: Ferritin, transferrin receptor, glutamate and hypoxia-inducible factor-1α. *Exp. Eye Res.* **97**, 90–97 (2012).

206. Eid, C., Hémadi, M., Ha-Duong, N. T. & El Hage Chahine, J. M. Iron uptake and transfer from ceruloplasmin to transferrin. *Biochim. Biophys. Acta - Gen. Subj.* **1840**, 1771–1781 (2014).

207. De Domenico, I. *et al.* Ferroxidase activity is required for the stability of cell surface ferroportin in cells expressing GPI-ceruloplasmin. *EMBO J.* **26**, 2823–2831 (2007).

208. Vroegindeweij, L. H. P. *et al.* Aceruloplasminemia presents as Type 1 diabetes in non-obese adults: A detailed case series. *Diabet. Med.* **32**, 993–1000 (2015).

209. Dunaief, J. L. *et al.* Macular degeneration in a patient with aceruloplasminemia, a disease associated with retinal iron overload. *Ophthalmology* **112**, 1062–1065 (2005).

210. Pelucchi, S. *et al.* Phenotypic heterogeneity in seven Italian cases of aceruloplasminemia. *Park. Relat. Disord.* **51**, 36–42 (2018).

211. Piperno, A. & Alessio, M. Aceruloplasminemia: Waiting for an Efficient Therapy. *Front. Neurosci.* **12**, 1–8 (2018).

212. Vasin, A. V. *et al.* Mitochondrial ceruloplasmin of mammals. *Mol. Biol.*

39, 42–52 (2005).

213. Miyajima, H., Kono, S., Takahashi, Y. & Sugimoto, M. Increased lipid peroxidation and mitochondrial dysfunction in aceruloplasminemia brains. *Blood Cells. Mol. Dis.* **29**, 433–438 (2002).

214. Boddaert, N. *et al.* Selective iron chelation in Friedreich ataxia: Biologic and clinical implications. *Blood* **110**, 401–408 (2007).

215. Bartzokis, G. *et al.* In vivo evaluation of brain iron in Alzheimer disease using magnetic resonance imaging. *Arch. Gen. Psychiatry* **57**, 47–53 (2000).

216. Thomas, G. E. C. *et al.* Brain iron deposition is linked with cognitive severity in Parkinson's disease. *J. Neurol. Neurosurg. Psychiatry* **91**, 418–425 (2020).

217. Schapira, A. H. V. *et al.* Mitochondrial Complex I Deficiency in Parkinson's Disease. *Lancet* **333**, 1269 (1989).

218. Parker, W. D. Cytochrome oxidase deficiency in Alzheimer's disease. *Ann. N. Y. Acad. Sci.* **640**, 59–64 (1991).

219. Doni, D. *et al.* The displacement of frataxin from the mitochondrial cristae correlates with abnormal respiratory supercomplexes formation and bioenergetic defects in cells of Friedreich ataxia patients. *FASEB J.* **35**, 1–14 (2021).

220. Ruiz, L. M., Libedinsky, A. & Elorza, A. A. Role of Copper on Mitochondrial Function and Metabolism. *Front. Mol. Biosci.* **8**, 1–17 (2021).

221. Adeloye, D. *et al.* Global, regional, and national prevalence of, and risk factors for, chronic obstructive pulmonary disease (COPD) in 2019: a systematic review and modelling analysis. *Lancet Respir. Med.* **10**, 447–458 (2022).

222. Buist, A. S. *et al.* International variation in the prevalence of COPD

(The BOLD Study): a population-based prevalence study. *Lancet* **370**, 741–750 (2007).

223. Hersh, C. P. *et al.* Family history is a risk factor for COPD. *Chest* **140**, 343–350 (2011).

224. Hall, R., Hall, I. P. & Sayers, I. Genetic risk factors for the development of pulmonary disease identified by genome-wide association. *Respirology* **24**, 204–214 (2019).

225. Janciauskiene, S. M. *et al.* The discovery of α1-antitrypsin and its role in health and disease. *Respir. Med.* **105**, 1129–1139 (2011).

226. Burney, P., Jarvis, D. & Perez-Padilla, R. The global burden of chronic respiratory disease in adults. *Int. J. Tuberc. Lung Dis.* **19**, 10–20 (2015).

227. Lõpez-Campos, J. L., Tan, W. & Soriano, J. B. Global burden of COPD. *Respirology* **21**, 14–23 (2016).

228. Hogg, J. C. & Timens, W. The pathology of chronic obstructive pulmonary disease. *Annu. Rev. Pathol. Mech. Dis.* **4**, 435–459 (2009).

229. Tsiligianni, I. & Kocks, J. W. H. Daytime symptoms of chronic obstructive pulmonary disease: a systematic review. *npj Prim. Care Respir. Med.* **30**, (2020).

230. Calverley, P. M. A. Respiratory failure in chronic obstructive pulmonary disease. *Eur. Respir. Journal, Suppl.* **22**, 26–30 (2003).

231. Kent, B. D., Mitchell, P. D. & Mcnicholas, W. T. Hypoxemia in patients with COPD: Cause, effects, and disease progression. *Int. J. COPD* **6**, 199–208 (2011).

232. Wiegman, C. H. *et al.* Oxidative stress-induced mitochondrial dysfunction drives inflammation and airway smooth muscle remodeling in patients with chronic obstructive pulmonary disease. *J. Allergy Clin. Immunol.* **136**, 769–780 (2015).

233. Even, B. *et al.* Heme oxygenase-1 induction attenuates senescence in chronic obstructive pulmonary disease lung fibroblasts by protecting against mitochondria dysfunction. *Aging Cell* **17**, (2018).

234. Maremanda, K. P., Sundar, I. K. & Rahman, I. Role of inner mitochondrial protein OPA1 in mitochondrial dysfunction by tobacco smoking and in the pathogenesis of COPD. *Redox Biol.* **45**, 102055 (2021).

235. Gilkerson, R., De La Torre, P. & St. Vallier, S. Mitochondrial OMA1 and OPA1 as Gatekeepers of Organellar Structure/Function and Cellular Stress Response. *Front. Cell Dev. Biol.* **9**, 1–7 (2021).

236. Haji, G. *et al.* Mitochondrial dysfunction in airways and quadriceps muscle of patients with chronic obstructive pulmonary disease. *Respir. Res.* **21**, 1–11 (2020).

237. Agustí, A. G. N. *et al.* Systemic effects of chronic obstructive pulmonary disease. *Eur. Respir. J.* **21**, 347–360 (2003).

238. Rabinovich, R. A. *et al.* Mitochondrial dysfunction in COPD patients with low body mass index. *Eur. Respir. J.* **29**, 643–650 (2007).

239. Puente-Maestu, L. *et al.* Abnormal mitochondrial function in locomotor and respiratory muscles of COPD patients. *Eur. Respir. J.* **33**, 1045–1052 (2009).

240. Clark, L. C., Wolf, R., Granger, D. & Taylor, Z. Continuous Recording of Blood Oxygen Tensions by Polarography. *J. Appl. Physiol.* **6**, 189–193 (1953).

241. Chance, B. & Williams, G. R. A simple and rapid assay of oxidative phosphorylation. *Nature* **175**, 1120–1121 (1955).

242. Chance, B. & Williams, G. R. A method for the localization of sites for oxidative phosphorylation. *Nature* **176**, 250–254 (1955).

243. CHANCE, B. & WILLIAMS, G. R. Respiratory enzymes in oxidative

phosphorylation. II. Difference spectra. *J. Biol. Chem.* **217**, 409–427 (1955).

244. CHANCE, B. & WILLIAMS, G. R. Respiratory enzymes in oxidative phosphorylation. III. The steady state. *J. Biol. Chem.* **217**, 409–427 (1955).

245. Li, Z. & Graham, B. H. Measurement of mitochondrial oxygen consumption using a Clark electrode. *Methods Mol. Biol.* **837**, 63–72 (2012).

246. Rogers, G. W. *et al.* High throughput microplate respiratory measurements using minimal quantities of isolated mitochondria. *PLoS One* **6**, (2011).

247. Yépez, V. A. *et al.* OCR-Stats: Robust estimation and statistical testing of mitochondrial respiration activities using seahorse xf analyzer. *PLoS One* **13**, 1–18 (2018).

248. Gu, X., Ma, Y., Liu, Y. & Wan, Q. Measurement of mitochondrial respiration in adherent cells by Seahorse XF96 Cell Mito Stress Test. *STAR Protoc.* **2**, 100245 (2021).

249. Gnaiger, E. Mitochondrial physiology. *Bioenerg. Commun.* **1**, 1–44 (2020).

250. Schmidt, C. A. *et al.* Aglycemic growth enhances carbohydrate metabolism and induces sensitivity to menadione in cultured tumor-derived cells. *Cancer Metab.* **9**, 1–21 (2021).

251. McWilliams, T. G. *et al.* Phosphorylation of Parkin at serine 65 is essential for its activation in vivo. *Open Biol.* **8**, (2018).

252. Dorigatti, J. D., Thyne, K. M., Ginsburg, B. C. & Salmon, A. B. Beta-guanidinopropionic acid has age-specific effects on markers of health and function in mice. *GeroScience* **43**, 1497–1511 (2021).

253. Correa Soares, J. B. R., Gaviraghi, A. & Oliveira, M. F. Mitochondrial

physiology in the major arbovirus vector Aedes aegypti: Substrate preferences and sexual differences define respiratory capacity and superoxide production. *PLoS One* **10**, 1–35 (2015).

254. Leo, E., Dahlke, F. T., Storch, D., Pörtner, H. O. & Mark, F. C. Impact of Ocean Acidification and Warming on the bioenergetics of developing eggs of Atlantic herring Clupea harengus. *Conserv. Physiol.* **6**, 1–10 (2018).

255. Mahmood, T. & Yang, P. C. Western blot: Technique, theory, and trouble shooting. *N. Am. J. Med. Sci.* **4**, 429–434 (2012).

256. Lin, J.-S. & Lai, E.-M. Protein–Protein Interactions: Co-Immunoprecipitation. in *Methods in Molecular Biology* vol. 1615 211–219 (2017).

257. Maccarrone, G., Bonfiglio, J. J., Silberstein, S., Turck, C. W. & Martins-de-Souza, D. Characterization of a Protein Interactome by Co-Immunoprecipitation and Shotgun Mass Spectrometry. in *Methods in Molecular Biology* vol. 1546 223–234 (2017).

258. Frese, C. K. *et al.* Quantitative Map of Proteome Dynamics during Neuronal Differentiation. *Cell Rep.* **18**, 1527–1542 (2017).

259. Szklarczyk, D. *et al.* STRING v11: Protein-protein association networks with increased coverage, supporting functional discovery in genome-wide experimental datasets. *Nucleic Acids Res.* **47**, D607–D613 (2019).

260. Costerllo, A. J. R., Marshall, W. E., Omachi, A. & Henderson, T. O. Interactions between hemoglobin and organic phosphates investigated with 31P nuclear magnetic resonance spectroscopy and ultrafiltration. *BBA - Protein Struct.* **427**, 481–491 (1976).

261. Nie, X. & Hill, R. D. Mitochondrial respiration and hemoglobin gene expression in barley aleurone tissue. *Plant Physiol.* **114**, 835–840 (1997).

262. Eastman, J. T. & Eakin, R. R. Checklist of the species of notothenioid fishes. *Antarct. Sci.* **33**, 273–280 (2021).

263. Matschiner, M. *et al.* The adaptive radiation of notothenioid fishes in the waters of antarctica. in *Extremophile Fishes: Ecology, Evolution, and Physiology of Teleosts in Extreme Environments* 35–57 (Springer International Publishing, 2015). doi:10.1007/978-3-319-13362-1_3.

264. Eastman, J. T. The buoyancy-based biotope axis of the evolutionary radiation of Antarctic cryonotothenioid fishes. *Polar Biol.* **43**, 1217–1231 (2020).

265. Bowen, B. W. *et al.* Species Radiations in the Sea: What the Flock? *J. Hered.* **111**, 70–83 (2020).

266. Duman, J. G. Animal ice-binding (antifreeze) proteins and glycolipids: An overview with emphasis on physiological function. *J. Exp. Biol.* **218**, 1846–1855 (2015).

267. Hamoir, G. Biochemical adaptation of the muscles of the channichthyidae to their lack in hemoglobin and myoglobin. *Comp. Biochem. Physiol. Part B Comp. Biochem.* **90**, 557–559 (1988).

268. Sidell, B. D. & O'Brien, K. M. When bad things happen to good fish: The loss of hemoglobin and myoglobin expression in Antarctic icefishes. *Journal of Experimental Biology* vol. 209 1791–1802 (2006).

269. O'Brien, K. M. & Mueller, I. A. The unique mitochondrial form and function of antarctic channichthyid icefishes. in *Integrative and Comparative Biology* vol. 50 993–1008 (2010).

270. O'Brien, K. M. Mitochondrial biogenesis in cold-bodied fishes. *J. Exp. Biol.* **214**, 275–285 (2011).

271. Biederman, A. M., Kuhn, D. E., O'Brien, K. M. & Crockett, E. L. Mitochondrial membranes in cardiac muscle from Antarctic notothenioid fishes vary in phospholipid composition and membrane

fluidity. *Comp. Biochem. Physiol. Part - B Biochem. Mol. Biol.* **235**, 46–53 (2019).

272. Herrmann, J. M., Westermann, B. & Neupert, W. Analysis of protein-protein interactions in Mitochondria by coimmunoprecipitation and chemical cross-linking. *Methods Cell Biol.* **65**, 217–230 (2001).

273. Chen, R. *et al.* Identification of a novel mitochondrial interacting protein of C1QBP using subcellular fractionation coupled with CoIP-MS. *Anal. Bioanal. Chem.* **408**, 1557–1564 (2016).

274. Markham, K., Bai, Y. & Schmitt-Ulms, G. Co-immunoprecipitations revisited: An update on experimental concepts and their implementation for sensitive interactome investigations of endogenous proteins. *Anal. Bioanal. Chem.* **389**, 461–473 (2007).

275. Neilson, K. A. *et al.* Less label, more free: Approaches in label-free quantitative mass spectrometry. *Proteomics* **11**, 535–553 (2011).

276. Schneider, C. A., Rasband, W. S. & Eliceiri, K. W. NIH Image to ImageJ: 25 years of image analysis. *Nat. Methods* **9**, 671–675 (2012).

277. Centre for Excellence in Mass Spectrometry. FAQs - Biology, The University of York. (2019).

278. O'Brien, K. M. *et al.* Cardiac mitochondrial metabolism may contribute to differences in thermal tolerance of red- and white-blooded Antarctic notothenioid fishes. *J. Exp. Biol.* **221**, (2018).

279. Katyal, G., Ebanks, B., Lucassen, M., Papetti, C. & Chakrabarti, L. Sequence and structure comparison of ATP synthase F0 subunits 6 and 8 in notothenioid fish. *PLoS One* **16**, e0245822 (2021).

280. Yamada, T. *et al.* Myoglobin and the regulation of mitochondrial respiratory chain complex IV. *J. Physiol.* **594**, 483–495 (2016).

281. Yamada, T. *et al.* Interaction between myoglobin and mitochondria in rat skeletal muscle. *J. Appl. Physiol.* **114**, 490–497 (2013).

282. O'Brien, K. M. & Sidell, B. D. The interplay among cardiac ultrastructure, metabolism and the expression of oxygen-binding proteins in Antarctic fishes. *J. Exp. Biol.* **203**, 1287–1297 (2000).

283. Seelert, H. & Dencher, N. A. ATP synthase superassemblies in animals and plants: Two or more are better. *Biochim. Biophys. Acta - Bioenerg.* **1807**, 1185–1197 (2011).

284. Wittig, I. & Schägger, H. Supramolecular organization of ATP synthase and respiratory chain in mitochondrial membranes. *Biochim. Biophys. Acta - Bioenerg.* **1787**, 672–680 (2009).

285. Liu, F., Lössl, P., Rabbitts, B. M., Balaban, R. S. & Heck, A. J. R. The interactome of intact mitochondria by cross-linking mass spectrometry provides evidence for coexisting respiratory supercomplexes. *Mol. Cell. Proteomics* **17**, 216–232 (2018).

286. Schweppe, D. K. *et al.* Mitochondrial protein interactome elucidated by chemical cross-linking mass spectrometry. *Proc. Natl. Acad. Sci. U. S. A.* **114**, 1732–1737 (2017).

287. Ikwegbue, P. C., Masamba, P., Oyinloye, B. E. & Kappo, A. P. Roles of heat shock proteins in apoptosis, oxidative stress, human inflammatory diseases, and cancer. *Pharmaceuticals* **11**, 1–18 (2018).

288. Fan, F. *et al.* Deletion of heat shock protein 60 in adult mouse cardiomyocytes perturbs mitochondrial protein homeostasis and causes heart failure. *Cell Death Differ.* **27**, 587–600 (2020).

289. Wang, S. B., Murray, C. I., Chung, H. S. & Van Eyk, J. E. Redox Regulation of Mitochondrial ATP Synthase. *Trends Cardiovasc. Med.* **23**, 14 (2013).

290. Martínez-Reyes, I. & Cuezva, J. M. The H+-ATP synthase: A gate to ROS-mediated cell death or cell survival. *Biochim. Biophys. Acta - Bioenerg.* **1837**, 1099–1112 (2014).

291. Mueller, I. A., Grim, J. M., Beers, J. M., Crockett, E. L. & O'Brien, K. M. Inter-relationship between mitochondrial function and susceptibility to oxidative stress in red-And white-blooded Antarctic notothenioid fishes. *J. Exp. Biol.* **214**, 3732–3741 (2011).

292. Mueller, I. A. *et al.* Exposure to critical thermal maxima increases oxidative stress in hearts of whitebut not red-blooded Antarctic notothenioid fishes. *J. Exp. Biol.* **215**, 3655–3664 (2012).

293. Mueller, I., Hoffman, M., Dullen, K. & O'Brien, K. Moderate elevations in temperature do not increase oxidative stress in oxidative muscles of antarctic notothenioid fishes. *Polar Biol.* **37**, 311–320 (2013).

294. O'Brien, K. M. *et al.* The loss of hemoglobin and myoglobin does not minimize oxidative stress in Antarctic icefishes. *J. Exp. Biol.* **221**, (2018).

295. Mazumder, B. *et al.* Regulated release of L13a from the 60S ribosomal subunit as a mechanism of transcript-specific translational control. *Cell* **115**, 187–198 (2003).

296. Orzheshkovskyi, V. V. & Trishchynska, M. A. Ceruloplasmin: Its Role in the Physiological and Pathological Processes. *Neurophysiology* **51**, 141–149 (2019).

297. Scudiero, R., Trinchella, F., Riggio, M. & Parisi, E. Structure and expression of genes involved in transport and storage of iron in red-blooded and hemoglobin-less antarctic notothenioids. *Gene* **397**, 1–11 (2007).

298. Kuhn, D. E., O'Brien, K. M. & Crockett, E. L. Expansion of capacities for iron transport and sequestration reflects plasma volumes and heart mass among white-blooded notothenioid fishes. *Am. J. Physiol. - Regul. Integr. Comp. Physiol.* **311**, R649–R657 (2016).

299. Benesch, R. & Benesch, R. E. The effect of organic phosphates from the human erythrocyte on the allosteric properties of hemoglobin. *Biochem.*

Biophys. Res. Commun. **26**, 162–167 (1967).

300. Benesch, R., Benesch, R. E. & Yu, C. I. Reciprocal binding of oxygen and diphosphoglycerate by human hemoglobin. *Proc. Natl. Acad. Sci. U. S. A.* **59**, 526–532 (1968).

301. Greaney, G. S., Hobish, M. K. & Powers, D. A. The effects of temperature and pH on the binding of ATP to carp (Cyprinus carpio) deoxyhemoglobin. *J. Biol. Chem.* **255**, 445–453 (1980).

302. Mathai, C., Jourd'heuil, F. L., Lopez-Soler, R. I. & Jourd'heuil, D. Emerging perspectives on cytoglobin, beyond NO dioxygenase and peroxidase. *Redox Biol.* **32**, 101468 (2020).

303. Burmester, T. & Hankeln, T. What is the function of neuroglobin? *J. Exp. Biol.* **212**, 1423–1428 (2009).

304. Keppner, A. *et al.* Lessons from the post-genomic era: Globin diversity beyond oxygen binding and transport. *Redox Biol.* **37**, 101687 (2020).

305. Xie, L. K. & Yang, S. H. Brain globins in physiology and pathology. *Medical Gas Research* vol. 6 154–163 (2016).

306. Russo, R. *et al.* Hemoglobin is present as a canonical α2β2 tetramer in dopaminergic neurons. *Biochim. Biophys. Acta - Proteins Proteomics* (2013) doi:10.1016/j.bbapap.2013.05.005.

307. Freed, J. & Chakrabarti, L. Defining a role for hemoglobin in Parkinson's disease. *npj Park. Dis.* **2**, 16021 (2016).

308. Codrich, M. *et al.* Neuronal hemoglobin affects dopaminergic cells' response to stress. *Cell Death Dis.* **8**, (2017).

309. Chen, L., Devries, A. L. & Cheng, C. H. C. Evolution of antifreeze glycoprotein gene from a trypsinogen gene in Antarctic notothenioid fish. *Proc. Natl. Acad. Sci. U. S. A.* **94**, 3811–3816 (1997).

310. Chen, L., Devries, A. L. & Cheng, C. H. C. Convergent evolution of

antifreeze glycoproteins in Antarctic notothenioid fish and Arctic cod. *Proc. Natl. Acad. Sci. U. S. A.* **94**, 3817–3822 (1997).

311. Harding, M. M., Anderberg, P. I. & Haymet, A. D. J. 'Antifreeze' glycoproteins from polar fish. *European Journal of Biochemistry* vol. 270 1381–1392 (2003).

312. Near, T. J. *et al.* Ancient climate change, antifreeze, and the evolutionary diversification of Antarctic fishes. *Proc. Natl. Acad. Sci. U. S. A.* **109**, 3434–3439 (2012).

313. Yeo, E. J. Hypoxia and aging. *Exp. Mol. Med.* **51**, (2019).

314. Solaini, G., Baracca, A., Lenaz, G. & Sgarbi, G. Hypoxia and mitochondrial oxidative metabolism. *Biochim. Biophys. Acta - Bioenerg.* **1797**, 1171–1177 (2010).

315. Lee, P., Chandel, N. S. & Simon, M. C. Cellular adaptation to hypoxia through hypoxia inducible factors and beyond. *Nat. Rev. Mol. Cell Biol.* **21**, 268–283 (2020).

316. Schito, L. & Rey, S. Cell-Autonomous Metabolic Reprogramming in Hypoxia. *Trends Cell Biol.* **28**, 128–142 (2018).

317. O'Brien, K. A. *et al.* Enhanced hepatic respiratory capacity and altered lipid metabolism support metabolic homeostasis during short-term hypoxic stress. *BMC Biol.* **19**, 265 (2021).

318. Horscroft, J. A. *et al.* Inorganic nitrate, hypoxia, and the regulation of cardiac mitochondrial respiration—probing the role of PPARα. *FASEB J.* **33**, 7563–7577 (2019).

319. O'Brien, K. A. *et al.* PPARα-independent effects of nitrate supplementation on skeletal muscle metabolism in hypoxia. *Biochim. Biophys. Acta - Mol. Basis Dis.* **1865**, 844–853 (2019).

320. Zhang, P. *et al.* Mitochondrial Energy-Regulating Effect of Atractyloside Inhibits Hepatocellular Steatosis Through the Activation

of Autophagy. *Front. Pharmacol.* **11**, 1–11 (2020).

321. de Araújo, M. E. G., Lambert, G. & Huber, L. A. Homogenization of mammalian cells. *Cold Spring Harb. Protoc.* **2015**, 1009–1012 (2015).

322. Han, Y., Ma, B. & Zhang, K. Spider: Software for protein identification from sequence tags with de novo sequencing error. *J. Bioinform. Comput. Biol.* **3**, 697–716 (2005).

323. Pettersen, E. F. *et al.* UCSF Chimera - A visualization system for exploratory research and analysis. *J. Comput. Chem.* **25**, 1605–1612 (2004).

324. Schneidman-Duhovny, D., Inbar, Y., Nussinov, R. & Wolfson, H. J. PatchDock and SymmDock: Servers for rigid and symmetric docking. *Nucleic Acids Res.* **33**, 363–367 (2005).

325. Andrusier, N., Nussinov, R. & Wolfson, H. J. FireDock: Fast interaction refinement in molecular docking. *Proteins Struct. Funct. Bioinforma.* **69**, 139–159 (2007).

326. Laskowski, R. A., Jabłońska, J., Pravda, L., Vařeková, R. S. & Thornton, J. M. PDBsum: Structural summaries of PDB entries. *Protein Sci.* **27**, 129–134 (2018).

327. Yan, Y., Tao, H., He, J. & Huang, S. Y. The HDOCK server for integrated protein–protein docking. *Nat. Protoc.* **15**, 1829–1852 (2020).

328. Desta, I. T., Porter, K. A., Xia, B., Kozakov, D. & Vajda, S. Performance and Its Limits in Rigid Body Protein-Protein Docking. *Structure* **28**, 1071-1081.e3 (2020).

329. Weiner, S. J. *et al.* A New Force Field for Molecular Mechanical Simulation of Nucleic Acids and Proteins. *J. Am. Chem. Soc.* **106**, 765–784 (1984).

330. Aliev, A. E. *et al.* Motional timescale predictions by molecular dynamics simulations: Case study using proline and hydroxyproline

sidechain dynamics. *Proteins Struct. Funct. Bioinforma.* **82**, 195–215 (2014).

331. Janson, G., Zhang, C., Prado, M. G. & Paiardini, A. PyMod 2.0: Improvements in protein sequence-structure analysis and homology modeling within PyMOL. *Bioinformatics* **33**, 444–446 (2017).

332. Galeazzi, R. *et al.* Protein-protein interactions of human glyoxalase II: findings of a reliable docking protocol. *Org. Biomol. Chem.* **16**, 5167–5177 (2018).

333. Notredame, C., Higgins, D. G. & Heringa, J. T-coffee: A novel method for fast and accurate multiple sequence alignment. *J. Mol. Biol.* **302**, 205–217 (2000).

334. Pettersen, E. F. *et al.* UCSF ChimeraX: Structure visualization for researchers, educators, and developers. *Protein Sci.* **30**, 70–82 (2021).

335. Fermi, G., Perutz, M. F., Shaanan, B. & Fourme, R. The crystal structure of human deoxyhaemoglobin at 1.74 Å resolution. *J. Mol. Biol.* **175**, 159–174 (1984).

336. De Sanctis, D. *et al.* Bishistidyl heme hexacoordination, a key structural property in Drosophila melanogaster hemoglobin. *J. Biol. Chem.* **280**, 27222–27229 (2005).

337. Lindorff-Larsen, K. *et al.* Improved side-chain torsion potentials for the Amber ff99SB protein force field. *Proteins Struct. Funct. Bioinforma.* **78**, 1950–1958 (2010).

338. Khacho, M. *et al.* Acidosis overrides oxygen deprivation to maintain mitochondrial function and cell survival. *Nat. Commun.* **5**, 3550 (2014).

339. Zhu, M. Y., Zhang, D. L., Zhou, C. & Chai, Z. Mild Acidosis Protects Neurons during Oxygen-Glucose Deprivation by Reducing Loss of Mitochondrial Respiration. *ACS Chem. Neurosci.* **10**, 2489–2497 (2019).

340. Devaux, J. B. L. *et al.* Acidosis maintains the function of brain mitochondria in hypoxia-tolerant triplefin fish: A strategy to survive acute hypoxic exposure? *Front. Physiol.* **10**, 1–14 (2019).

341. Richardson, R. S., Noyszewski, E. A., Kendrick, K. F., Leigh, J. S. & Wagner, P. D. Myoglobin O2 desaturation during exercise: Evidence of limited O2 transport. *J. Clin. Invest.* **96**, 1916–1926 (1995).

342. Lundby, C., Calbet, J. A. L. & Robach, P. The response of human skeletal muscle tissue to hypoxia. *Cell. Mol. Life Sci.* **66**, 3615–3623 (2009).

343. Liu, G., Roy, J. & Johnson, E. A. Identification and function of hypoxia-response genes in Drosophila melanogaster. *Physiol. Genomics* **25**, 134–141 (2006).

344. Van Voorhies, W. A. Metabolie function in Drosophila melanogaster in response to hypoxia and pure oxygen. *J. Exp. Biol.* **212**, 3132–3141 (2009).

345. GOLD. Global Strategy for Prevention, Diagnosis and Management of COPD. 177 (2022).

346. Barnes, P. J. *et al.* Chronic obstructive pulmonary disease. *Nat. Rev. Dis. Prim.* **1**, 1–22 (2015).

347. Wüst, R. C. I. & Degens, H. Factors contributing to muscle wasting and dysfunction in COPD patients. *Int. J. COPD* **2**, 289–300 (2007).

348. Lee, H., Smith, S. B. & Yoon, Y. The short variant of the mitochondrial dynamin OPA1 maintains mitochondrial energetics and cristae structure. *J. Biol. Chem.* **292**, 7115–7130 (2017).

349. Calverley, P. M. A. Exercise and dyspnoea in COPD. *Eur. Respir. Rev.* **15**, 72–79 (2006).

350. Nicholas, J. J., Gilbert, R., Gabe, R. & Auchincloss, J. H. Evaluation of an exercise therapy program for patients with chronic obstructive

pulmonary disease. *Am. Rev. Respir. Dis.* **102**, 1–9 (1970).

351. Ward, T. J. C. *et al.* Submaximal Eccentric Cycling in People With COPD: Acute Whole-Body Cardiopulmonary and Muscle Metabolic Responses. *Chest* **159**, 564–574 (2021).

352. Joschtel, B. *et al.* Effects of exercise training on physical and psychosocial health in children with chronic respiratory disease: A systematic review and meta-analysis. *BMJ Open Sport Exerc. Med.* **4**, 1–11 (2018).

353. Padulo, J., Laffaye, G., Chamari, K. & Concu, A. Concentric and Eccentric: Muscle Contraction or Exercise? *Sports Health* **5**, 306 (2013).

354. Dufour, S. P. *et al.* Eccentric cycle exercise: Training application of specific circulatory adjustments. *Med. Sci. Sports Exerc.* **36**, 1900–1906 (2004).

355. Rocha Vieira, D. S. *et al.* Eccentric cycle exercise in severe COPD: Feasibility of application. *COPD J. Chronic Obstr. Pulm. Dis.* **8**, 270–274 (2011).

356. Hody, S., Croisier, J. L., Bury, T., Rogister, B. & Leprince, P. Eccentric muscle contractions: Risks and benefits. *Front. Physiol.* **10**, 1–18 (2019).

357. Rattray, B., Caillaud, C., Ruell, P. A. & Thompson, M. W. Heat exposure does not alter eccentric exercise-induced increases in mitochondrial calcium and respiratory dysfunction. *Eur. J. Appl. Physiol.* **111**, 2813–2821 (2011).

358. MacMillan, N. J. *et al.* Eccentric ergometer training promotes locomotor muscle strength but not mitochondrial adaptation in patients with severe chronic obstructive pulmonary disease. *Front. Physiol.* **8**, 1–14 (2017).

359. Touron, J., Costes, F., Coudeyre, E., Perrault, H. & Richard, R. Aerobic

Metabolic Adaptations in Endurance Eccentric Exercise and Training: From Whole Body to Mitochondria. *Front. Physiol.* **11**, 1–14 (2021).

360. Isner-Horobeti, M. E. *et al.* Effect of eccentric versus concentric exercise training on mitochondrial function. *Muscle and Nerve* **50**, 803–811 (2014).

361. Yang, M. *et al.* Proteomic profiling of lung immune cells reveals dysregulation of phagocytotic pathways in female-dominated molecular COPD phenotype. *Respir. Res.* **19**, 1–11 (2018).

362. Zhang, Y. H. *et al.* Lung proteomic biomarkers associated with chronic obstructive pulmonary disease. *Am. J. Physiol. - Lung Cell. Mol. Physiol.* **321**, L1119–L1130 (2021).

363. Bai, S. *et al.* Identification of Proteomic Signatures in Chronic Obstructive Pulmonary Disease Emphysematous Phenotype. *Front. Mol. Biosci.* **8**, 1–13 (2021).

364. Kim, S. H. *et al.* A proteomics-based analysis of blood biomarkers for the diagnosis of COPD acute exacerbation. *Int. J. COPD* **16**, 1497–1508 (2021).

365. Ebanks, B. *et al.* The dysregulated Pink1 - drosophila mitochondrial proteome is partially corrected with exercise. *Aging (Albany. NY).* **13**, 14709–14728 (2021).

366. David, D. C. *et al.* Proteomic and functional analyses reveal a mitochondrial dysfunction in P301L tau transgenic mice. *J. Biol. Chem.* **280**, 23802–23814 (2005).

367. Walls, K. C. *et al.* Swedish Alzheimer mutation induces mitochondrial dysfunction mediated by HSP60 mislocalization of Amyloid Precursor Protein (APP) and beta-amyloid. *J. Biol. Chem.* **287**, 30317–30327 (2012).

368. Broadwater, L. *et al.* Analysis of the mitochondrial proteome in multiple

sclerosis cortex. *Biochim. Biophys. Acta - Mol. Basis Dis.* **1812**, 630–641 (2011).

369. Geiger, T., Cox, J. & Mann, M. Proteomics on an orbitrap benchtop mass spectrometer using all-ion fragmentation. *Mol. Cell. Proteomics* **9**, 2252–2261 (2010).

370. Zubarev, R. A. & Makarov, A. Orbitrap mass spectrometry. *Anal. Chem.* **85**, 5288–5296 (2013).

371. Kanehisa, M., Furumichi, M., Tanabe, M., Sato, Y. & Morishima, K. KEGG: New perspectives on genomes, pathways, diseases and drugs. *Nucleic Acids Res.* **45**, D353–D361 (2017).

372. Krueger, F. & Andrews, S. R. Bismark: A flexible aligner and methylation caller for Bisulfite-Seq applications. *Bioinformatics* **27**, 1571–1572 (2011).

373. Voisin, S., Eynon, N., Yan, X. & Bishop, D. J. Exercise training and DNA methylation in humans. *Acta Physiol.* **213**, 39–59 (2015).

374. Plaza-Diaz, J. *et al.* Impact of Physical Activity and Exercise on the Epigenome in Skeletal Muscle and Effects on Systemic Metabolism. *Biomedicines* **10**, 1–29 (2022).

375. Pollard, A., Shephard, F., Freed, J., Liddell, S. & Chakrabarti, L. Mitochondrial proteomic profiling reveals increased carbonic anhydrase II in aging and neurodegeneration. *Aging (Albany. NY).* **8**, 2425–2436 (2016).

376. Leung, C. L., Green, K. J. & Liem, R. K. H. Plakins: A family of versatile cytolinker proteins. *Trends Cell Biol.* **12**, 37–45 (2002).

377. Winter, L. & Wiche, G. The many faces of plectin and plectinopathies: Pathology and mechanisms. *Acta Neuropathol.* **125**, 77–93 (2013).

378. Reipert, S. *et al.* Association of mitochondria with plectin and desmin intermediate filaments in striated muscle. *Exp. Cell Res.* **252**, 479–491

(1999).

379. Appaix, F. *et al.* Possible role of cytoskeleton in intracellular arrangement and regulation of mitochondria. *Exp. Physiol.* **88**, 175–90 (2003).

380. Winter, L., Abrahamsberg, C. & Wiche, G. Plectin isoform 1b mediates mitochondrion - Intermediate filament network linkage and controls organelle shape. *J. Cell Biol.* **181**, 903–911 (2008).

381. Winter, L. *et al.* Plectin isoform P1b and P1d deficiencies differentially affect mitochondrial morphology and function in skeletal muscle. *Hum. Mol. Genet.* **24**, 4530–4544 (2015).

382. Rainteau, D., Mansuelle, P., Rochat, H. & Weinman, S. Characterization and ultrastructural localization of annexin VI from mitochondria. *FEBS Lett.* **360**, 80–84 (1995).

383. Chlystun, M. *et al.* Regulation of Mitochondrial Morphogenesis by Annexin A6. *PLoS One* **8**, (2013).

384. Mukherjee, I., Ghosh, M. & Meinecke, M. MICOS and the mitochondrial inner membrane morphology – when things get out of shape. *FEBS Lett.* **595**, 1159–1183 (2021).

385. Anand, R. *et al.* MIC26 and MIC27 cooperate to regulate cardiolipin levels and the landscape of OXPHOS complexes. *Life Sci. Alliance* **3**, 1–17 (2020).

386. He, F. & DiMario, P. J. Drosophila delta-1-pyrroline-5-carboxylate dehydrogenase (P5CDh) is required for proline breakdown and mitochondrial integrity-Establishing a fly model for human type II hyperprolinemia. *Mitochondrion* **11**, 397–404 (2011).

387. Anand, R., Strecker, V., Urbach, J., Wittig, I. & Reichert, A. S. Mic13 is essential for formation of crista junctions in mammalian cells. *PLoS One* **11**, 1–19 (2016).

388. Bortoluzzi, S., D'Alessi, F., Romualdi, C. & Danieli, G. A. Differential expression of genes coding of ribosomal proteins in different human tissues. *Bioinformatics* **17**, 1152–1157 (2002).

389. Sasikumar, A. N., Perez, W. B. & Kinzy, T. G. The many roles of the eukaryotic elongation factor 1 complex. *Wiley Interdiscip. Rev. RNA* **3**, 543–555 (2012).

390. Gold, V. A., Chroscicki, P., Bragoszewski, P. & Chacinska, A. Visualization of cytosolic ribosomes on the surface of mitochondria by electron cryo-tomography. *EMBO Rep.* **18**, 1786–1800 (2017).

391. Shah, G. N. *et al.* Mitochondrial carbonic anhydrase CA VB: Differences in tissue distribution and pattern of evolution from chose of CA VA suggest distinct physiological roles. *Proc. Natl. Acad. Sci. U. S. A.* **97**, 1677–1682 (2000).

392. Vullo, D., Nishimori, I., Innocenti, A., Scozzafava, A. & Supuran, C. T. Carbonic anhydrase activators: An activation study of the human mitochondrial isoforms VA and VB with amino acids and amines. *Bioorganic Med. Chem. Lett.* **17**, 1336–1340 (2007).

393. Torella, D. *et al.* Carbonic anhydrase activation is associated with worsened pathological remodeling in human ischemic diabetic cardiomyopathy. *J. Am. Heart Assoc.* **3**, 1–16 (2014).

394. Antunes, M. A., Lopes-Pacheco, M. & Rocco, P. R. M. Oxidative Stress-Derived Mitochondrial Dysfunction in Chronic Obstructive Pulmonary Disease: A Concise Review. *Oxid. Med. Cell. Longev.* **2021**, (2021).

395. Ristow, M. *et al.* Antioxidants prevent health-promoting effects of physical exercise in humans. *Proc. Natl. Acad. Sci. U. S. A.* **106**, 8665–8670 (2009).

396. Shabihkhani, M. *et al.* The procurement, storage, and quality assurance of frozen blood and tissue biospecimens in pathology, biorepository,

and biobank settings. *Clin. Biochem.* **47**, 258–266 (2014).

397. Fleming, M. D. & Hamza, I. Mitochondrial heme: An exit strategy at last. *J. Clin. Invest.* **122**, 4328–4330 (2012).

398. Bock, F. J. & Tait, S. W. G. Mitochondria as multifaceted regulators of cell death. *Nat. Rev. Mol. Cell Biol.* **21**, 85–100 (2020).

399. Cecchini, G. Function and structure of complex II of the respiratory chain. *Annu. Rev. Biochem.* **72**, 77–109 (2003).

400. Von Ballmoos, C., Wiedenmann, A. & Dimroth, P. Essentials for ATP synthesis by F1F0 ATP synthases. *Annu. Rev. Biochem.* **78**, 649–672 (2009).

401. Pesta, D. & Gnaiger, E. High-Resolution Respirometry: OXPHOS Protocols for Human Cells and Permeabilized Fibers from Small Biopsies of Human Muscle. in *Mitochondrial Bioenergetics: Methods and Protocols (Methods in Molecular Biology, vol. 810)* (eds. Palmeira, C. M. & Moreno, A. J.) vol. 810 25–58 (Humana Press, 2012).

402. Doerrier, C. *et al.* High-resolution fluorespirometry and oxphos protocols for human cells, permeabilized fibers from small biopsies of muscle, and isolated mitochondria. in *Methods in Molecular Biology* vol. 1782 31–70 (2018).

403. Araki, T. Freezing injury in mitochondrial membranes. I. Susceptible components in the oxidation systems of frozen and thawed rabbit liver mitochondria. *Cryobiology* **14**, 144–150 (1977).

404. Thebud, R. & Santarius, K. A. Effects of freezing on isolated plant mitochondria. *Planta* **152**, 242–247 (1981).

405. Štětina, T., Des Marteaux, L. E. & Koštál, V. Insect mitochondria as targets of freezing-induced injury: Mitochondria and freeze tolerance. *Proc. R. Soc. B Biol. Sci.* **287**, (2020).

406. Pollard, A. K., Craig, E. L. & Chakrabarti, L. Mitochondrial complex 1

activity measured by spectrophotometry is reduced across all brain regions in ageing and more specifically in neurodegeneration. *PLoS One* **11**, 1–13 (2016).

407. García-Roche, M. *et al.* Respiratory analysis of coupled mitochondria in cryopreserved liver biopsies. *Redox Biol.* **17**, 207–212 (2018).

408. Acin-Perez, R. *et al.* A novel approach to measure mitochondrial respiration in frozen biological samples. *EMBO J.* **39**, 1–18 (2020).

409. Nukala, V. N., Singh, I. N., Davis, L. M. & Sullivan, P. G. Cryopreservation of brain mitochondria: A novel methodology for functional studies. *J. Neurosci. Methods* **152**, 48–54 (2006).

410. Yamaguchi, R. *et al.* Mitochondria frozen with trehalose retain a number of biological functions and preserve outer membrane integrity. *Cell Death Differ.* **14**, 616–624 (2007).

411. Thebud, R. & Santarius, K. A. Effects of freezing on isolated plant mitochondria. *Planta* **152**, 242–7 (1981).

412. Rule, C. S., Patrick, M. & Sandkvist, M. Measuring in vitro ATPase activity for enzymatic characterization. *J. Vis. Exp.* **2016**, 3–7 (2016).

413. Zuccolotto-dos-Reis, F. H. *et al.* Acetyl-CoA-driven respiration in frozen muscle contributes to the diagnosis of mitochondrial disease. *Eur. J. Clin. Invest.* **51**, 1–10 (2021).

414. Gu, J. *et al.* Cryo-EM structure of the mammalian ATP synthase tetramer bound with inhibitory protein IF1. *Science (80-.).* **364**, 1068–1075 (2019).

415. Spikes, T. E., Montgomery, M. G. & Walker, J. E. Structure of the dimeric ATP synthase from bovine mitochondria. *Proc. Natl. Acad. Sci. U. S. A.* (2020) doi:10.1073/pnas.2013998117.

416. Pinke, G., Zhou, L. & Sazanov, L. A. Cryo-EM structure of the entire mammalian F-type ATP synthase. *Nat. Struct. Mol. Biol.* (2020)

doi:10.1038/s41594-020-0503-8.

417. Chen, R., Runswick, M. J., Carroll, J., Fearnley, I. M. & Walker, J. E. Association of two proteolipids of unknown function with ATP synthase from bovine heart mitochondria. *FEBS Lett.* **581**, 3145–3148 (2007).

418. Meyer, B., Wittig, I., Trifilieff, E., Karas, M. & Schägger, H. Identification of two proteins associated with mammalian ATP synthase. *Mol. Cell. Proteomics* **6**, 1690–1699 (2007).

419. He, J. *et al.* Assembly of the membrane domain of ATP synthase in human mitochondria. *Proc. Natl. Acad. Sci. U. S. A.* **115**, 2988–2993 (2018).

420. Ko, Y. H., Bianchet, M., Amzel, L. M. & Pedersen, P. L. Novel insights into the chemical mechanism of ATP synthase. Evidence that in the transition state the γ-phosphate of ATP is near the conserved alanine within the P-loop of the β-subunit. *J. Biol. Chem.* **272**, 18875–18881 (1997).

421. Kamga, C., Krishnamurthy, S. & Shiva, S. Myoglobin and mitochondria: A relationship bound by oxygen and nitric oxide. *Nitric Oxide - Biol. Chem.* **26**, 251–258 (2012).

422. Scudiero, R., Trinchella, F. & Parisi, E. Iron metabolism genes in Antarctic notothenioids: A review. *Mar. Genomics* **1**, 79–85 (2008).

423. Marchi, G., Busti, F., Zidanes, A. L., Castagna, A. & Girelli, D. Aceruloplasminemia: A severe neurodegenerative disorder deserving an early diagnosis. *Frontiers in Neuroscience* vol. 13 (2019).

424. Saha, D., Koli, S., Patgaonkar, M. & Reddy, K. V. R. Expression of hemoglobin-α and β subunits in human vaginal epithelial cells and their functional significance. *PLoS One* **12**, 1–26 (2017).

425. Hernansanz-Agustín, P. *et al.* Acute hypoxia produces a superoxide burst in cells. *Free Radic. Biol. Med.* **71**, 146–156 (2014).

426. Jenner, P. *et al.* Oxidative stress in Parkinson's disease. *Ann. Neurol.* **53**, S26–S38 (2003).

427. Reed, T. *et al.* Redox proteomic identification of 4-Hydroxy-2-nonenal-modified brain proteins in amnestic mild cognitive impairment: Insight into the role of lipid peroxidation in the progression and pathogenesis of Alzheimer's disease. *Neurobiol. Dis.* **30**, 107–120 (2008).

428. Chiaradia, E. *et al.* Protein carbonylation in dopaminergic cells exposed to rotenone. *Toxicol. Lett.* **309**, 20–32 (2019).

429. Sorolla, M. A. *et al.* Protein oxidation in Huntington disease affects energy production and vitamin B6 metabolism. *Free Radic. Biol. Med.* **49**, 612–621 (2010).

430. Gnaiger, E. Mitochondrial respiratory states and rates. *MitoFit* **19**, 5–8 (2019).